AD-A034 172 BOEING AEROSPACE CO SEATTLE WASH F/G 21/5
INTEGRATED PROPULSION CONTROL SYSTEM (IPCS) VOLUME III. FLIGHT --ETC(U)
AUG 76 W J HASTINGS, C M CARLIN F33615-73-C-2035
UNCLASSIFIED AFAPL-TR-76-61-VOL-3 NL

1 OF 4
AD A034172

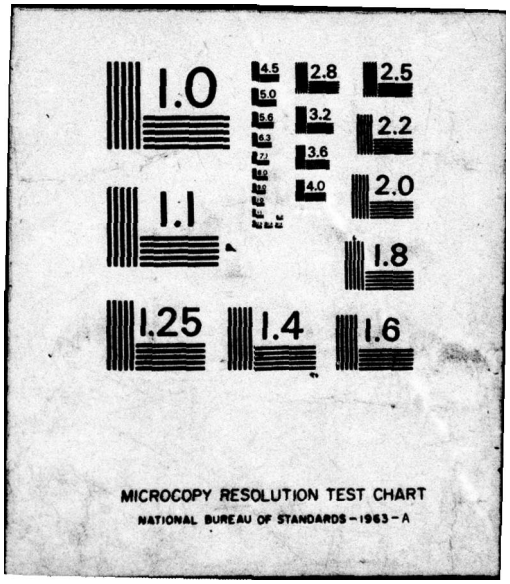
1.0
1.1
1.25
1.4
1.6
1.8
2.0
2.2
2.5
2.8
3.2
3.6
4.0
4.5
5.0
5.6
6.3
7.1
MICROCOPY RESOLUTION TEST CHART
NATIONAL BUREAU OF STANDARDS-1963-A

ADA034172

AFAPL-TR-76-61
VOLUME III

INTEGRATED PROPULSION CONTROL SYSTEM (IPCS)
FINAL REPORT
VOLUME III
FLIGHT TEST REPORT

BOEING AEROSPACE COMPANY
P.O. BOX 3999
SEATTLE, WA. 98124

AUGUST 1976

TECHNICAL REPORT AFAPL-TR-76-61 VOLUME III
FINAL REPORT FOR PERIOD 1 MARCH 1973 - 30 AUGUST 1976

Approved for public release; distribution unlimited

DDC
RECEIVED
11 1977
D

COPY AVAILABLE TO DDC DOES NOT
PERMIT FULLY LEGIBLE PRODUCTION

AIR FORCE AERO-PROPULSION LABORATORY
AIR FORCE WRIGHT AERONAUTICAL LABORATORIES
AIR FORCE SYSTEMS COMMAND
WRIGHT-PATTERSON AIR FORCE BASE, OHIO 45433

NOTICE

When Government drawings, specification, or other data are used for any purpose other than in connection with a definitely related Government procurement operation, the United States Government thereby incurs no responsibility nor any obligation whatsoever; and the fact that the government may have formulated, furnished or in any way supplied the said drawings, specifications, or other data, is not to be regarded by implication or otherwise as in any manner licensing the holder or any other person or corporation, or conveying any rights or permission to manufacture, use, or sell any patented invention that may in any way be related thereto.

This final report was submitted by Boeing Aerospace Company, under contract F33615-73-C-2035. The effort was sponsored by the Air Force Aero Propulsion Laboratory, Air Force Systems Command, Wright-Patterson AFB, Ohio under Project Number 3066, Task Number 03 and Work Unit Number 42 with Joseph J. Batka, AFAPL/TBC as Project Engineer. Mr. G. W. N. Lampard of Boeing Aerospace Company was technically responsible for the work.

This report has been reviewed by the Information Office, (ASD/OIP) and is releasable to the National Technical Information Service (NTIS). At NTIS, it will be available to the general public, including foreign nations.

This technical report has been reviewed and is approved for publication.

Joseph J. Batka

JOSEPH J. BATKA
Project Engineer

FOR THE COMMANDER

Charles E. Bentz

CHARLES E. BENTZ
Technical Area Manager - Controls

Copies of this report should not be returned unless return is required by security considerations, contractual obligations, or notice on a specific document.

AIR FORCE - 22 NOVEMBER 76 - 100

UNCLASSIFIED

SECURITY CLASSIFICATION OF THIS PAGE (When Data Entered)

REPORT DOCUMENTATION PAGE

READ INSTRUCTIONS BEFORE COMPLETING FORM

1. REPORT NUMBER: AFAPL-TR-76-61-Vol III	2. GOVT ACCESSION NO.
3. RECIPIENT'S CATALOG NUMBER	
4. TITLE (and Subtitle): Integrated Propulsion Control System (IPCS) Volume III, FLIGHT TEST RESULTS	5. TYPE OF REPORT & PERIOD COVERED: Final Technical Report (Final) 1 March 1973-30 August 1976
	6. PERFORMING ORG. REPORT NUMBER
7. AUTHOR(s): William J. Hastings, Christopher M. Carlin	8. CONTRACT OR GRANT NUMBER(s): F33615-73-C-2035
9. PERFORMING ORGANIZATION NAME AND ADDRESS: Boeing Aerospace Company, P. O. Box 3999, Seattle, WA 98124	10. PROGRAM ELEMENT, PROJECT, TASK AREA & WORK UNIT NUMBERS: P.E. 62203F, PROJ 3066, Task 306603, W.U. 30660342
11. CONTROLLING OFFICE NAME AND ADDRESS: Air Force Aero-Propulsion Laboratory (AFAPL/TBC), Air Force System Command, Wright Patterson AFB OH 45433	12. REPORT DATE: August 1976
	13. NUMBER OF PAGES: 323 (328)
14. MONITORING AGENCY NAME & ADDRESS (if different from Controlling Office)	15. SECURITY CLASS. (of this report): UNCLASSIFIED
	15a. DECLASSIFICATION/DOWNGRADING SCHEDULE

V1 A032 439 77-3 CB

V4 A033 062 MT

16. DISTRIBUTION STATEMENT (of this Report)

Approved for Public Release; Distribution Unlimited.

17. DISTRIBUTION STATEMENT (of the abstract entered in Block 20, if different from Report)

18. SUPPLEMENTARY NOTES

19. KEY WORDS (Continue on reverse side if necessary and identify by block number)

Gas turbine testing, digital controls, propulsion controls, F-111, TF30, flight testing, integrated control

20. ABSTRACT

The Integrated Propulsion Control System (IPCS) program was conducted to pursue and demonstrate the advantages of integrated propulsion controls. The program encompassed the design, build, flight qualification, and flight testing of control modes, software, and hardware. The flight test vehicle was an F-111E. The left inlet and TF30-P-9 engine were modified to operate under control of an HDC-601 computer. Two sets of hardware were built or modified and two sets of software were developed; one implemented the bill-of-materials control laws and one implemented control laws developed under contract. Fifteen flights were conducted to evaluate the IPCS. The testing demonstrated that integrated digital propulsion control is effective. This document describes the flight test program and flight test results.

DD FORM 1 JAN 73 1473 EDITION OF 1 NOV 65 IS OBSOLETE

UNCLASSIFIED

SECURITY CLASSIFICATION OF THIS PAGE (When Data Entered)

059 610

White Section
Buff Section
Dist. AVAIL. and/or SPL

Contents

Section			Page
ILLUSTRATIONS			5
TABLES			9
NOMENCLATURE			10
SUMMARY			14
1.0	INTRODUCTION AND SUMMARY		15
2.0	OBJECTIVES		19
3.0	PROCEDURES		20
3.1	TEST OPERATION		20
3.2	SPECIFIC TEST PROCEDURES		20
3.2.1	Seal Saver Turn (SST)		21
3.2.2	Yaw to β Limit		21
3.2.3	Throttle Transients - Snap and Bodies		21
3.2.4	Expand Cone to Stall		21
3.2.5	AFBIAS		21
3.2.6	Stable Throttle Conditions		23
3.2.7	Autothrottle		23
3.2.8	650 KT Climbing Acceleration		23
3.2.9	500 KT Climbing Acceleration		23
3.2.10	Buzz		23
3.2.11	Noise		23
3.3	SOFTWARE CONTROL PROCEDURES		23
3.3.1	SFCO Generation Procedure		24
3.3.2	Patch Tape Generation and Loading Procedure		24
3.3.3	IPCS DPCU Software Configuration Control Procedures Prior to Flight		24
3.4	SOFTWARE TEST PROCEDURES		28
3.4.1	Formal Testing		28
3.4.2	Informal Testing		29
4.0	TEST CONFIGURATION		30
4.1	IPCS HARDWARE INSTALLATION		30
4.1.1	Cockpit Installation		30
4.1.2	Inlet Hardware		30
4.1.3	Engine Hardware		30
4.1.4	DPCU Hardware		30
4.2	BASELINE CONTROL CONFIGURATION		42
4.2.1	Inlet Control		42
4.2.2	Gas Generator Control		42
	4.2.2.1	N2 Governing - Loop 7	42
	4.2.2.2	Minimum Airflow - Loop 8	42
	4.2.2.3	Low Compressor Exit Mach Number (Mach 22) - Loop 9	42
	4.2.2.4	Minimum Fuel Flow/Burner Pressure (Wf/Pb) - Loop 10	45
	4.2.2.5	Buzz Loop - Loop 11	45
	4.2.2.6	High Compressor Exit (Mach 3) - Loop 1	45
	4.2.2.7	Trubine Inlet Temperature (T4) - Loop 2	45
	4.2.2.8	Maximum Airflow - Loop 3	45
	4.2.2.9	Maximum N1 - Loop 4	45
	4.2.2.10	Maximum N2 - Loop 5	45
	4.2.2.11	Maximum Fuel Flow/Burner Pressure (Wf/Pb) - Loop 6	45
	4.2.2.12	Select Logic	45
	4.2.2.13	Fuel Flow Command	46

4.2.3 Afterburner Control 46
4.2.3.1 Light Off and Blow Out Detection 46
4.2.3.2 PLAP Control Logic 46
4.2.3.3 Suppression Control 48

5.0 INSTRUMENTATION 49
5.1 NASA INSTRUMENTATION 49
5.1.1 Airplane 49
5.1.2 Inlet 49
5.1.3 Engine 49
5.1.4 Exhaust Profile Rake 49
5.2 CONTROL INSTRUMENTATION 49
5.3 DATA ACQUISITION AND PROCESSING 57
5.3.1 Data Acquisition 57
5.3.2 On-Site PCM Processing 57
5.3.3 Contractor Processing of PCM Data 61
5.3.4 High Response Data Processing 61
5.3.5 Data Processing Evaluation 61
5.4 MEASUREMENT COMPARISONS 66
5.4.1 Engine Pressure Transducers 66
5.4.1.1 Ground Calibration 66
5.4.1.2 Flight Comparisons 66
5.4.2 Thermocouples 81
5.4.2.1 T2S Performance History 81
5.4.2.2 T3S and T22 Performance 86
5.4.3 Fuel Flow, WFGS 86
5.4.4 Synthesized Turbine Inlet Temperature 91
5.4.4.1 Steady-State Comparison 91
5.4.4.2 T4SYN Transient Response 96
5.4.5 IPCS Pressure and Temperature Probes 96
5.5 HIGH LEVEL ANALOG TRANSDUCERS 100
5.6 DIGITAL SENSOR PERFORMANCE 100
5.6.1 Tachometers - N1, N2 100
5.6.2 Inlet Pressure Transducers 100

6.0 RESULTS 111
6.1 INLET 111
6.1.1 BOM Inlet Control 111
6.1.2 Afterburner Anticipation 111
6.2 GAS GENERATOR 111
6.2.1 Steady State Gas Generator Governing 111
6.2.2 Engine Health 117
6.2.3 Gas Generator Transients 117
6.2.3.1 IPCS Accelerations 117
6.2.3.2 IPCS Decelerations 164
6.2.3.3 BOMDIG Accelerations 167
6.3 AFTERBURNING 174
6.3.1 Steady State A/B 174
6.3.1.1 Fan Suppression 174
6.3.1.2 Afterburner Fuel Scheduling 178
6.3.2 Afterburning Transient Operation 181
6.3.2.1 Light Off Detection 181
6.3.2.2 Blow Out Detection 185
6.3.2.3 Afterburner Accel Time Comparisons 185
6.3.2.4 Afterburner Decel Time Comparisons 192
6.3.2.5 Suppression Control During Afterburner Transients 197
6.3.3 DPCU Disengagement During Afterburning 202
6.4 IDLE/MAX OPERATION 202
6.5 IPCS SPECIAL LOOPS 207
6.5.1 Buzz Loop Performance 207
6.5.2 Distortion Control of Bleeds 217
6.5.3 AFBIAS 229
6.5.4 Stall and Recovery Detection Loop 229
6.5.5 Autothrottle 237

6.6 NOISE TESTING 237
6.6.1 Background 237
6.6.2 Configuration and Procedures 243
6.6.3 Testing 244
6.6.4 Results 246

7.0 HARDWARE PERFORMANCE 248
7.1 INTERFACE UNIT (IFU) 248
7.1.1 Auto-disengage 248
7.1.2 Core Location Changes 248
7.1.3 T2S Noise 248
7.2 ENGINE TEMPERATURE HARNESS 248
7.3 DCU V2 MEMORY MALFUNCTIONS 250
7.4 PAROSCIENTIFIC TRANSDUCERS 252
7.5 N1 TACHOMETER 254
7.6 FLIGHT 28 TEMPERATURE MEASUREMENT FAILURE 255

8.0 SOFTWARE 257
8.1 CONFIGURATION HISTORY 257
8.1.1 Stall Detection 257
8.1.2 Acceleration Loop Control Modifications 257
8.1.3 Schedule Changes and Minor Revisions 269
8.1.4 Hardware Adaptions 269
8.1.4.1 Noise Filters 269
8.1.4.2 Pulse Code Modulation Data Output 276
8.1.4.3 Memory Restoration 276
8.1.4.4 Paroscientific Transducers 276
8.1.4.5 Autodisengage 276
8.1.5 Functional Additions to IPCS 278
8.1.5.1 Noise Reduction 278
8.1.5.2 Thrust Calculation 278
8.1.5.3 Autothrottle 282
8.2 SOFTWARE CHANGE ANALYSIS 282
8.3 PROGRAM SEQUENCE 286
8.3.1 Executive Operation 286
8.3.2 Failure Response 286

9.0 CONCLUSIONS AND RECOMMENDATIONS 288

9.1 CONCLUSIONS 288
9.2 RECOMMENDATIONS 289

10.0 REFERENCES 291

APPENDIX A - CONFIGURATION CHANGES AND TEST EVENTS 292

A.1 Preflight Engine Runs 292
A.2 Flight 14 - September 4, 1975 292
A.2.1 Hardware Configuration 292
A.2.2 Software Configuration - BOMDIG 292
A.2.3 Event Summary 292
A.3 Flight 15 - November 6, 1975 295
A.3.1 Hardware Configuration 295
A.3.2 Software Configuration - BOMDIG 295
A.3.3 Events Summary 295
A.4 Flight 16 - November 10, 1975 296
A.4.1 Hardware Configuration 296
A.4.2 Software Configuration - BOMDIG 296
A.4.3 Events Summary 296
A.5 Flight 17 - November 17, 1975 297
A.5.1 Hardware Configuration 297
A.5.2 Software Configuration - IPCS 297
A.5.3 Events Summary 297
A.6 Flight 18 - December 2, 1975 298
A.6.1 Hardware Configuration 298
A.6.2 Software Configuration - IPCS 298
A.6.3 Event Summary 298
A.7 Flight 19 - December 2, 1975 299
A.7.1 Hardware Configuration 299
A.7.2 Software Configuration 299
A.7.3 Event Summary 299

A.8 Flight 20 - December 5, 1975 299
A.8.1 Hardware Configuration 299
A.8.2 Software Configuration - BOMDIG 299
A.8.3 Event Summary 299
A.9 Flight 21 - December 23, 1975 300
A.9.1 Hardware Configuration 300
A.9.2 Software Configuration - IPCS 300
A.9.3 Event Summary 301
A.10 Engine Run 20 - December 19, 1975 301
A.11 Flight 22 - January 7, 1976 302
A.11.1 Hardware Configuration 302
A.11.2 Software Configuration - IPCS 302
A.11.3 Event Summary 302
A.12 Flight 23 - January 12, 1976 302
A.12.1 Hardware Configuration 302
A.12.2 Software Configuration - IPCS 302
A.12.3 Event Summary 303
A.13 Autodisengage Engine Runs 303
A.14 Flight 24 - January 22, 1976 304
A.14.1 Hardware Configuration 304
A.14.2 Software Configuration - IPCS 304
A.14.3 Event Summary 305
A.15 Flight 25 - January 23, 1976 305
A.15.1 Hardware Configuration 305
A.15.2 Software Configuration - IPCS 305
A.15.3 Event Summary 305
A.16 Engine Run 26 - January 27, 1976 306
A.17 Engine Run 27 - February 5, 1976 306
A.17.1 Hardware Configuration 306
A.17.2 Software Configuration - IPCS 306
A.17.3 Event Summary 307
A.18 Engine Run 28 - February 6, 1976 307
A.19 Flight 26 - February 20, 1976 307
A.19.1 Hardware Configuration 307
A.19.2 Software Configuration - IPCS 307
A.19.3 Event Summary 307
A.20 Flight 27 - February 27, 1976 308
A.20.1 Hardware Configuration 308
A.20.2 Software Configuration - IPCS 309
A.20.3 Event Summary 309
A.21 Flight 28 - February 27, 1976 309
A.21.1 Hardware Configuration 309
A.21.2 Software Configuration 309
A.21.3 Event Summary 309
A.22 Engine Run 34 - March 4, 1975 310
A.23 Engine Run 35 - March 5, 1976 310

Appendix B - Preflight Procedures 311

Appendix C - Suggested IFU Hardware Revisions 318

C.1 Restrict DMA Addresses to Locations 400 - 577 318
C.2 Transfer BITE Data to Discrete Input Word 318
C.3 Modify N1, N2 Converters to Clear Prior to Each Sample 318

ILLUSTRATIONS

Figure		Page
1.0-1	F-111 Test Airplane	16
1.0-2	IPCS Program Test Points	17
3.3-1	Software Change Procedure	25
3.3-2	SFCO Form	26
3.3-3	IPCS Patch Tape Record Form	27
4.1-1	IPCS Installation on F-111	32
4.1-2	IPCS Signal Paths	33
4.1-3	Computer Monitor Unit	34
4.1-4	Manual Inlet Control	35
4.1-5	Distortion Probe - Rake, Modification	36
4.1-6	Compressor Face Rake	37
4.1-7	Engine Installation	38
4.1-8	Station 3 Probes	39
4.1-9	Signal Lines	40
4.1-10	DPCU Installation	41
4.2-1	Inlet Control Configuration	43
4.2-2	Gas Generator Control Configuration	44
4.2-3	Afterburner Control Configuration	47
5.1-1	Compressor Face Distortion Rake	52
5.1-2	Aft View of Exhaust Profile Rake Installation	53
5.1-3	Side View of Exhaust Profile Rake Installation	54
5.1-4	Exhaust Survey Probes Before Testing	55
5.1-5	Exhaust Survey Probes After Testing	56
5.3-1	Data Recording Flow	59
5.3-2	IPCS NASA/DFRC Data Flow	60
5.3-3	Off Site PCM Processing	62
5.3-4	FM Analog Data Flow	63
5.3-5	Typical Distortion Time Histories	64
5.3-6	PCM Processing Times	65
5.4-1	P6MS and ΔP3S Preflight Transducer Calibrations	67
5.4-2	PS22S Ground Calibrations	68
5.4-3	P22S Ground Calibrations	69
5.4-4	ΔP22S Ground Calibrations	70
5.4-5	PS3S Ground Calibrations	71
5.4-6	P3S Ground Calibrations	72
5.4-7	ΔP3S Ground Calibrations	73
5.4-8	P6MS Ground Calibration	74
5.4-9	Comparison of NASA and DPCU PS3	75
5.4-10	PS3 Difference as a Function of T2	76
5.4-11	Comparison of NASA and DPCU PS22	77
5.4-12	PS22 Difference as a Function of T2	78
5.4-13	Comparison of NASA and DPCU P6M	79
5.4-14	P6M Difference as a Function of T2	80
5.4-15	Transducer Box Configuration	82
5.4-16	Comparison of NASA and DPCU T2, IPCS Harness	83
5.4-17	Comparison of NASA and DPCU T2, Con Ohmic References	84
5.4-18	Comparison of NASA and DPCU T2, Hanger and Flights 26 and 28	85
5.4-19	Unfiltered T2 Noise	87
5.4-20	T2 Noise - Filtered and IFU V2	88
5.4-21	T3 Comparison for Flight 24 Autothrottle Accel	88
5.4-22	Gas Generator Fuel Flow Calibration	89
5.4-23	Idle-Mil Wf/Pb Plot, BOMDIG, HMC	90
5.4-24	T4SYN Calibration	92
5.4-25	T4 Comparison for Flight 24 Autothrottle Accel	93
5.4-26	T4SYN Noise Contributions	94
5.4-27	Comparison of T4SYN and T4H for Idle-Mil Snap	97
5.4-28	Operation on the T4 Loop	98

5.4-29	Temperature Time History During Stall	99
5.6-1	Tachometer Systems	101
5.6-2	EPR Variations - T2 Locked	102
5.6-3	EPR Variations - T3 Locked	102
5.6-4	EPR Variations - P2 Locked	103
5.6-5	N1 Noise Comparison at Mil	104
5.6-6	N1 Noise Comparison in A/B	105
5.6-7	N1 Tachometer Steady State Performance	106
5.6-8	N2 Tachometer Steady State Performance	107
5.6-9	Paroscientific Transducer Calibrations	108
5.6-10	Paroscientific Transducer Long Term Stability	109
6.1-1	Inlet System Positioning Error	112
6.1-2	A/B Anticipation Logic	113
6.1-3	A/B Anticipation at Mach 1.4	114
6.1-4	A/B Anticipation at Mach 1.6	115
6.2-1	Idle Power Setting Comparison - HMC, BOMDIG, IPCS	118
6.2-2	Military Power Setting Comparison - HMC, IPCS	119
6.2-3	Installed Performance Calibrations	120
6.2-4	Compressor Exit Mach Number Control	126
6.2-5	Idle-Mil Accel Time Comparison - IPCS, HMC	128
6.2-6	Accel Comparison - 2K, 0 MN	129
6.2-7	Accel Comparison - 10K, .5 MN	130
6.2-8	Accel Comparison - 10K, .7 MN	131
6.2-9	Accel Comparison - 10K, .9 MN	132
6.2-10	Accel Comparison - 30K, .8 MN	133
6.2-11	Accel Comparison - 41K, 1.4 MN	135
6.2-12	Accel Comparison - 45K, 1.9 MN	136
6.2-13	Accel Comparison - 50K, 1.4 MN	137
6.2-14	Idle-Mil Time History Comparison HMC, IPCS, Engine Run 35	138
6.2-15	Idle-MIL Wf/Pb Comparison - HMC, IPCS	140
6.2-16	Idle-Mil MN3 IPCS	141
6.2-17	MN3 Tracking - Integral MN3 Control, Nominal Gain	143
6.2-18	MN3 Tracking - Integral MN3 Control, High Gain	144
6.2-19	Minor Cycle Sample MN3 Accel	145
6.2-20	Effect of 7th Stage Bleed and Secondary Manifold on MN3 Undershoots	146
6.2-21	Effect of Nozzle, Bleeds and ECS on ($\Delta P/P$)3 Value	148
6.2-22	Dynamic Simulation Results Idle-Mil Accel	149
6.2-23	High Compressor Map - BOMDIG Bodie	150
6.2-24	Wf/Pb Plot - BOMDIG Bodie	151
6.2-25	High Compressor Map - IPCS Bodie	152
6.2-26	Wf/Pb Plot - IPCS Bodie	153
6.2-27	MN3 During IPCS Bodie	154
6.2-28	Predicted and Measured HPC Inlet and Discharge Temperature During Cold Accel and Bodie	157
6.2-29	Dynamic Simulation MN3 Control of Cold Accel and Bodie	158
6.2-30	Dynamic Simulation MN3 Control of Cold Accel and Bodie - High Compressor Map	158
6.2-31	Altitude Test Bodie High Compressor Map	159
6.2-32	High Compressor Excursion During Bodie and Cold Accel	159
6.2-33	Comparison of High Pressure Compressor Temperatures During Bodie and Cold Accel	161
6.2-34	Wf/Pb Plot for Stall	162
6.2-35	MN3 History after Stall	163
6.2-36	High Compressor Map after Stall	165
6.2-37	Decel Time Comparison Mil-Idle	166
6.2-38	Decel Airflow Time History - 45K, 1.9 MN	168
6.2-39	Decel Airflow Time History - 50K, 1.4 MN	169
6.2-40	Decel High Rotor Speed Time History - 50K, 1.4 MN	170
6.2-41	Low Compressor Map During Mil-Idle Decel	171
6.2-42	MN22 During Mil-Idle Decel	172
6.2-43	Idle-Mil Accel Time Comparison - BOMDIG, HMC	173
6.3-1	Suppression Control Comparison - IPCS vs BOMDIG	175
6.3-2	Exhaust Nozzle Control Time Curve	176

6.3-3	A/B Suppression Schedule Changes to Eliminate A/B Roughness	177
6.3-4	A/B Fuel Flow Scheduling - BOMDIG, IPCS	179
6.3-5	IPCS Mil-Max Nozzle Overshoot	180
6.3-6	Response of Core A/B Zones to Stall	182
6.3-7	Response of Duct A/B Zones to Stall	183
6.3-8	Afterburner Lightoff Attempt at .9 MN, 45K	184
6.3-9	BOMDIG Stall	186
6.3-10	IPCS SST Stall and Blowout Protection	187
6.3-11	Accel Time Comparisons Mil-Max	191
6.3-12	BOMDIG, IPCS A/B Acceleration	193
6.3-13	Manifold Fill Comparison, BOMDIG, IPCS	194
6.3-14	Fuel Flow and Nozzle Area Transient with 51°/Second PLAP Rate	195
6.3-15	EPR Transient with 51°/Second PLAP Rate	196
6.3-16	Decel Time Comparisons Max-Mil	198
6.3-17	Nozzle Area Transient for Max-Mil Transient, IPCS, BOMDIG	199
6.3-18	Suppression During Max-Mil Transient, IPCS, BOMDIG	200
6.3-19	IPCS Base Area Schedule	201
6.3-20	Fan Suppression Comparison During Mil to Max	203
6.3-21	Fan Suppression Comparison During Max to Mil	204
6.3-22	Max A/B Disengage	205
6.4-1	Speed Comparison for Serial and Parallel Max-Idle Decel	208
6.4-2	Suppression Comparison for Serial and Parallel Max-Idle Decel	209
6.4-3	Accel Time Comparison Idle-Max	210
6.4-4	Decel Time Comparison Max-Idle	211
6.5-1	Buzz Loop Block Diagram	213
6.5-2	Mach 1.9 Buzz Loop Evaluation	214
6.5-3	Mach 2.3 Buzz Loop Evaluation	215
6.5-4	Buzz Loop Laboratory Test	216
6.5-5	Engine Distortion Tolerance Computation	218
6.5-6	Bleed Logic	219
6.5-7	Distortion Control of Bleeds During 650 KT Acceleration	220
6.5-8	Distortion Control of Bleeds with 300 KD Hysteresis	221
6.5-9	Effect of 7th Stage Bleed During 500 Knot Climb to Maximum Altitude	222
6.5-10	650 Knot Acceleration Comparison	223
6.5-11	Engine Inlet Temperature Variation During 650 Knot Acceleration	224
6.5-12	Manual Cone Induced Distortion	226
6.5-13	Bleed Cycling in Response to Distortion	227
6.5-14	Rapid Cone Expansion to Stall	228
6.5-15	AFBIAS Control Loop	230
6.5-16	AFBIAS Response at Mach 1.4	231
6.5-17	AFBIAS Response at Mach 1.9	232
6.5-18	Compressor Stall Detection Threshold	233
6.5-19	Compressor Stall Recovery	234
6.5-20	PS3S Decay Rate Following Stall	235
6.5-21	Stall Detection	236
6.5-22	Stall Recovery Detection	238
6.5-23	Autothrottle Performance	239
6.6-1	Afterburner Configuration	241
6.6-2	Velocity Profile Comparisons	242
6.6-3	Exahust Velocity Profiles	247
7.1-1	IFU Noise Comparison	249
7.4-1	Paroscientific Transducer Installation	253
7.6-1	Thermocouple Harness Interfaces	256
8.1-1	BOMDIG SFCO Summary	258
8.1-2	IPCS SFCO Summary	260
8.1-3	ICD (IPCS C) Stall Detector	266
8.1-4	Revised Stall Detector	267
8.1-5a	Baseline Accel Limiting	268
8.1-5b	Non-Linear MN3 Control	268
8.1-6	Downstream Wf/Pb Limiting	270
8.1-7	High Rate Sampling Non-Linear MN3 Control	271
8.1-8a	N2 Governing Schedule Changes	272
8.1-8b	MN3 Loop Schedule Changes	274

8.1-8c	MN3 Loop Configuration Changes	275
8.1-9	PCM Interrupt Processing Logic	277
8.1-10	Thrust Calculation Block Diagram	279
8.1-11	Thrust Data Correlation	281
8.1-12	Autothrottle System	283
8.2-1	SFCO Summary - Revision C CPCEIs	284
8.3-1	Program Execution Sequence	287
C-1	Restrict DMA Addressed to 400-577	319
C-2	Output BITE Data to DISIN1	320
C-3	N1/N2 Converter Modification to Clear Converter Prior to Each Sample	322

Tables

		Page
3.2-1	Engine Performance Variables	22
3.2-2	Transient Stabilization Times	22
4.1-1	CMU Light Functions	31
4.1-2	Major Engine IPCS Components	31
5.1-1	NASA Airplane Instrumentation	50
5.1-2	NASA Engine Instrumentation	50
5.2-1	DPCU Output Variables	51
5.3-1	FM Channel Assignments	58
6.6-1	Noise Test Procedures	243
6.6-2	A/B Configurations for Engine Run 33 Noise Data	245
6.6-3	A/B Configurations for Noise Flight	245
7.3-1	DCU V2 Vibration Test Anomalies	251
8.1-1	Thrust Calucation Approximations	278
A-1	Engine Run Summary	293
A-2	Software Configuration for Preflight Engine Runs	294
B-1	Paros Voltage Check	314
B-2	Transducer Preflight Calibration Check Form	316
B-3	Transducer Preflight Calibration Check Form - Octal	317

IPCS NOMENCLATURE

A/B	Afterburner
ABPERM	Afterburner Permission Logical Flag
ABC1-ABC8	Afterburner Control Scheduled Functions in BOMDIG
AFBIAS	Difference Between Optimum and Actual Inlet Airflow
AJ	Nozzle Area
AJPS	Nozzle Area Feedback Pulley Position
A/D	Analog-to-Digital
ATP	Acceptance Test Procedure
B/C	Bleed Closed
BITE	Built In Test Equipment
BLFT	Baseline Flight Test
B/O	Bleed Open
BOM	Bill-of-Materials
BOMDIG	Bill-of-Material Digital Control
BOTRIG	Blowout Logical Flag
CADC	Central Air Data Computer
CCU	Computer Control Unit
CDR	Critical Design Review
CFE	Contractor Furnished Equipment
CLBT	Closed-Loop Bench Test
CMD	Command
CMU	Computer Monitor Unit
CPC	Computer Program Component
CPCEI	Computer Program Contract End Item
CPU	Central Processor Unit
D/A	Digital-to-Analog
dB	Decibel
DCS	Digital Computer System
DCU	Digital Computer Unit
DEM	Diffuser Exit Mach Number
DFRC	Dryden Flight Research Center
DIB	Discrete Input Buffers
DIO	Direct Input/Output Channel
DMA	Direct Memory Access Channel
DOB	Discrete Output Buffers
DPCU	Digital Propulsion Control Unit
DPLAP	Time Rate of Change of PLAP
DS	Design Specifications
ECS	Environmental Control System
EIB	Engine Interface Box
ENC	Exhaust Nozzle Control
ENC1-ENC8	Exhaust Nozzle Scheduled Control Functions in BOMDIG
EPR	Engine Pressure Ratio, P6M/P2
EX	Excitation
FAT	Flight Assurance Test
FBCANG	Feedback Cam Angle
F/D	Frequency to Digital
FM	Frequency Modulation
FMEA	Failure Mode & Effect Analysis
FMECA	Failure Mode, Effect, and Criticality Analysis
FPM	Feet per Minute
FPS	Feet per Second
FT	Feet
GFE	Government Furnished Equipment
GSE	Ground Support Equipment
HPC	High Pressure Compressor
HSPT	High Speed Paper Tape Punch & Reader
HMC	Hydromechanical Control
Hz	Hertz (= cycles per second)
I.C.	Initial Control
ICD	Interface Control Document
Idle	Idle Power Setting
IFU	Interface Unit
I/O	Input/Output
IPCS	Advanced Control System
KD	Distortion Index

LLMUX	Low Level Multiplexer
LM	Local Mach Number
LPC	Low Pressure Compressor
LRD	Lamp and Relay Drivers
LVDT	Linear Variable Differetial Transformer
KT	Knot Indicated Airspeed
L/H	Left Hand
Max	Maximum Airburning Power Setting
MEDIC	Communication and Debugging Program
MFC	Main Fuel Control
MFC1-MFC7	Scheduled Functions in the BOM fuel Control, Represented by Tables or Polynominal Curve Fits in BOMDIG
Mil	Military Power Setting (Maximum Non-afterburning Thrust)
MN	Airplane Mach Number
MN3	Mach Number Station 3
MN22	Mach Number Station 22
MSB	Most Significant Bit
MTBF	Mean Time Between Failures
MUX	Multiplex or Mulitplexer
NSP	Non Standard Part
N1	Low Pressure Rotor Speed, RPM
N2	High Pressure Rotor Speed, RPM
OCV	Oscillator Controlled Voltage Circuits Demodulators
P	Pressure, See Illustration next page for Station Designations
Pb	Burner Static Pressure
Pb	Time Rate of Change of Burner Pressure
PC	Programmable Clock
P/C	Printed Circuit
PCM	Pulse Code Modulation
PDEM	Inlet Control Duct Exit Mach Pressure
PDR	Preliminary Design Review
PIL	Priority Interrupt Lines
PKDA-PKDD	Inlet Distortion Pressures (Figure 5.1-1)
PLA	Power Lever Angle
PLAP	Logically Constrained PLA
PLM	Inlet Control Local Mach Pressure
P/N	Part Number
POT	Potentiometer
PPH	Pounds Per Hour
PPS	Pounds Per Second
PRBC	Pressure Ratio Bleed Control (12th Stage Bleed)
PRI	Power Recovery Interrupt
PSDEM	Inlet Control Duct Exit Mach Static Pressure
PSLM	Inlet Control Local Mach Static Pressure
PSU	Power Supply Unit
P6M	Turbine Discharge Pressure, Average of Core and Fan Streams
RAM	Random Access Memory
RFD	Recycling Frequency-to-Digital Converters
R/H	Right Hand
RMS	Root Mean Square
ROM	Read Only Memory
RNI	Reynolds Number Index, $\delta/\theta^{1.24}$
RSS	Root Sum Square
RTC	Real Time Clock
RTD	Recycling Time-to-Digital Converters
Sec	Second
Sense Switch	Sense Switch Number - Generated by weighting the CMU Sense Switches 10, 4, 2, 1 per switch from the left
SFC	Specific Fuel Consumption (Fuel Flow/Thrust)
SFCO	Software Field Change Order
S&H	Sample and Hold
SIA	Simulation Interface Adapter
SLS	Sea Level Static

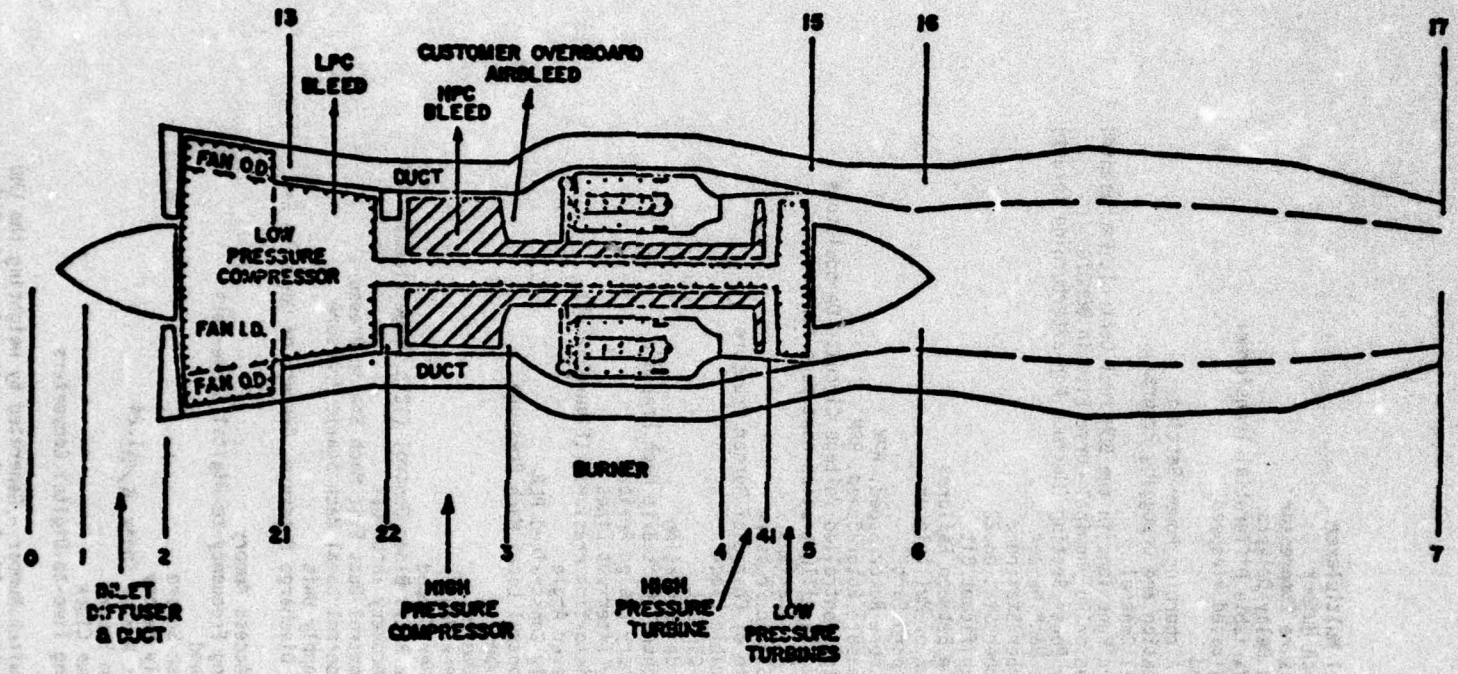

Station Identification

SMD	Stepping Motor Drivers
SMITE	P&WA Technique for Iterative Solutions in Digital Simulation Program
S/N	Serial No.
SOAPP	P&WA Modular Program Assembly Procedure
SOD	Solenoid Drivers
SPS	Samples per Second
SST	Seal Saver Turn
STE	Special Test Equipment
SOVi	Afterburner Fuel Shutoff Valve, ith zone, i=1,...,5
T	Temperature
T/A	Turnaround
T/C	Thermocouple
THETA	Inlet Cone Angle
TIGT	Turbine Inlet Gas Temperature
TSU	Test Set Unit
TTY	Teletype
T2H	Total Temperature Station 2
T4H	Total Temperature Station 4
T4SYN	Synthesized Turbine Inlet Temperature
VCO	Voltage Controlled Oscillator
Vex	Sensor Excitation Voltage
Vo	Sensor Output Voltage
W	Airflow Rate, lb/second
WAT2SX	Corrected Air Flow Rate at Station 2
Wf	Fuel Flow Rate, Gas Generator, lb/hr.
WFAB	Total Afterburner Fuel Flow
WFG	Commanded Fuel Flow Rate, Gas Generator
WFGS	Sensed Gas Generator Fuel Flow
WFZi	Commanded Afterburner Fuel Flow, ith zone, i=1,...,5
XZJP	Resolver Angle on Nozzle Position Feedback
XAJV	Nozzle Control Pilot Valve Position
XCON	Cone Actuator Position
XLOOP	IPCS Control Loop Indicator
XOO	Afterburner Control Power Piston Position
XSPK (XORLS)	Spike Position (normalized spike position)
XPOLE	Primary Real Root of the Open Loop Engine Transfer Function
α	Angle of Attack
β	Angle of Yaw
ΔP	Total Minus Static Pressure
δ	P/14.7
θ	T/518.69

A suffix "S" indicates a variable sensed by the DPCU

A suffix "H" indicates a variable obtained from the BOM harness and processed by the aircraft instrumentation system.

Summary

The purpose of the flight test program was to demonstrate the feasibility of digital propulsion control in a flight environment. The control hardware and software had been evaluated and refined through a series of tests including closed loop bench testing and engine testing at sea level and simulated altitude conditions prior to installation on the airplane. Engine ground runs were conducted after installation to eliminate any airplane interface related problems.

The flight test program consisted of 15 flights in which both BOMDIG and IPCS were tested to the Mach number and altitude limits of the airplane. BOMDIG was established as a valid representation of the hydromechanical control. A number of new control concepts were evaluated during the IPCS testing. Generally they were designed to use direct control of the relevant variables, such as turbine inlet temperature and inlet distortion.

During the later part of the program, testing was conducted to evaluate the effect of exhaust velocity profile on noise. Modifications were made to the IPCS software to produce profiles of interest. Ground testing included the measurement of thrust, noise, and exhaust velocity profiles. Preliminary results indicate that the desired profiles were approximated and some noise reduction was observed. Flight tests at 400 feet altitude and 250 KTS were conducted to evaluate the effect of airplane velocity on noise production.

Many detailed conclusions are drawn from the test results but three major conclusions relating to the overall system stand out.

1. The testing demonstrated that digital propulsion control is effective. The following operational advantages were demonstrated in the flight test program:
   - Faster engine acceleration for both gas generator and afterburner operation
   - Better thrust and SFC at many flight conditions
   - Reduced flight idle thrust
   - Accurate, stable trim set points which compensate for engine deterioration
   - Extended service ceiling
   - Automatic stall detection and stall recovery detection providing "hands off" return to the original power setting.
2. Software flexibility is essential during the flight test program. The software control procedures developed on IPCS were effective at maintaining control while still permitting the required ability to make field changes in response to test results.
3. Sixteen hour turnaround of printed and plotted data is needed to take advantage of the flexibility of the digital controller and to run a test program efficiently. Most current installations do not approach this performance. Dedicated, on-site data processing equipment appears to be a practical way to provide such capability.

Specific recommendations have been made in the areas of data processing, software control, and hardware modifications.

1.0 INTRODUCTION AND SUMMARY

This document reports on the IPCS Flight Test Program conducted from 4 September 1975 to 5 March 1976. It is submitted to the government in partial fulfillment of CDRL Item A007, of contract F33615-73-C-2035. The report contains discussions of the hardware and software configuration, test conditions, and results of the flight tests and engine runs associated with those flight tests. The testing was supported by a team of engineers from the Boeing Aerospace Company (BAC), Honeywell, Inc. (HI) and Pratt and Whitney Aircraft (P&WA TM), and the NASA Dryden Flight Research Center (NASA/DFRC).

The bill-of-materials hydromechanical inlet and engine controls were modified to interface with the digital propulsion control unit (DPCU). The DPCU and modified engine and inlet were installed in an F-111E airplane for flight testing (Figure 1.0-1). Two digital control systems had been developed, a digital implementation of the bill of materials control (BOMDIG) and a control incorporating a number of advanced concepts to be evaluated in the flight test (IPCS). These controls, together with the backup hydromechanical gas generator control, had been evaluated in a series of tests prior to the flight test program. This test series began with a closed loop bench test, was followed by a sea level static test on the TF30 engine and an engine test under simulated altitude conditions at NASA/LeRC. Thus the hardware and software were relatively well developed prior to entering the flight test program.

The flight test was the last in this series of tests to evaluate integrated digital control of the propulsion system. Its purpose was to demonstrate the feasibility of digital propulsion control in a flight environment. The flight test program consisted of 15 flights in which both BOMDIG and IPCS were tested to the Mach number and altitude limits of the airplane. Comparisons were made between the hydromechanical control, BOMDIG, and IPCS at flight conditions throughout the flight envelope (Figure 1.0-2).

A series of engine ground runs were conducted on each control mode prior to flight testing. These tests served to document the system static performance, identify and correct any problems, check out the data systems, and demonstrate the flight worthiness of the DPCU installed in the airplane. As a result of the previous testing, most of the preflight testing was routine. The problems were largely confined to data system interfaces, control room displays, etc. The flight test program was designed to progress from the relatively easy tasks to the more difficult. The initial testing was performed on BOMDIG. The first few IPCS flights documented the IPCS performance with a baseline control configuration without many of the special control loops enabled. In this way system flight experience was gained prior to beginning the more difficult tests.

The testing demonstrated that digital propulsion control is effective. The following operational advantages were demonstrated in the flight test program.

- Faster engine acceleration for both gas generator and afterburner operation
- Better thrust and SFC at many flight conditions
- Reduced flight idle thrust
- Accurate, stable trim set points which compensate for engine deterioration
- Extended service ceiling
- Automatic stall detection and stall recovery detection providing "hands off" return to the original power setting.

The initial flight testing established that the BOMDIG control of the engine was comparable to hydromechanical control. The early IPCS flights showed that the baseline IPCS without the special loops enabled worked properly. This testing also demonstrated the advantages of the IPCS afterburner control. The manifold prefill logic anticipated the need to open the fuel shutoff valves eliminating the dead time associated with manifold filling. This resulted in a 15% to 44% reduction in acceleration time relative to HMC for the Mil to Max transient. This was accomplished without any degradation in fan stall margin. During decelerations IPCS had more fan stall margin due to the deliberate lagging of nozzle area relative to fuel flow.

(28084)

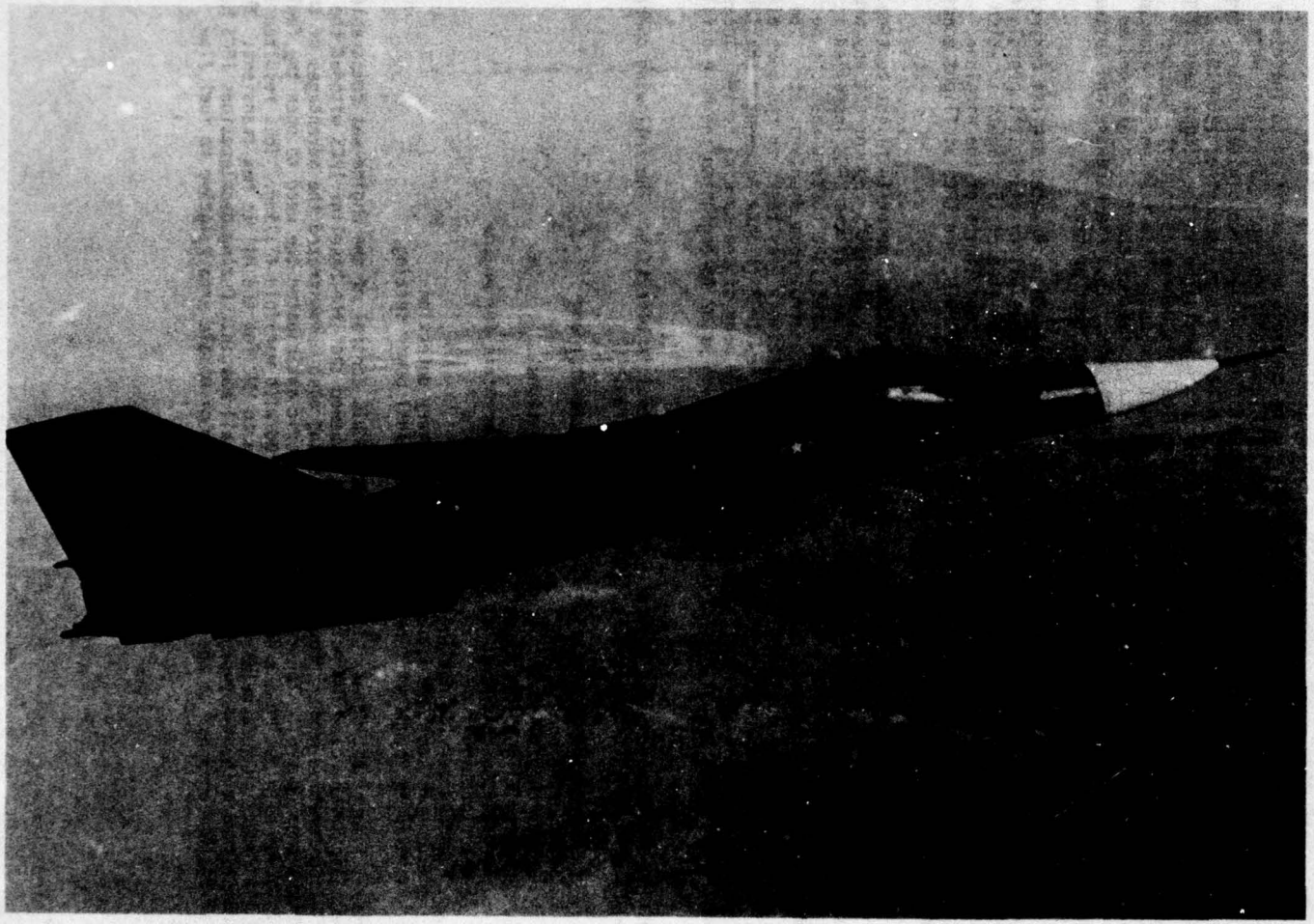

Figure 1.0-1 F-111 Test Airplane

IPCS Program Test Points

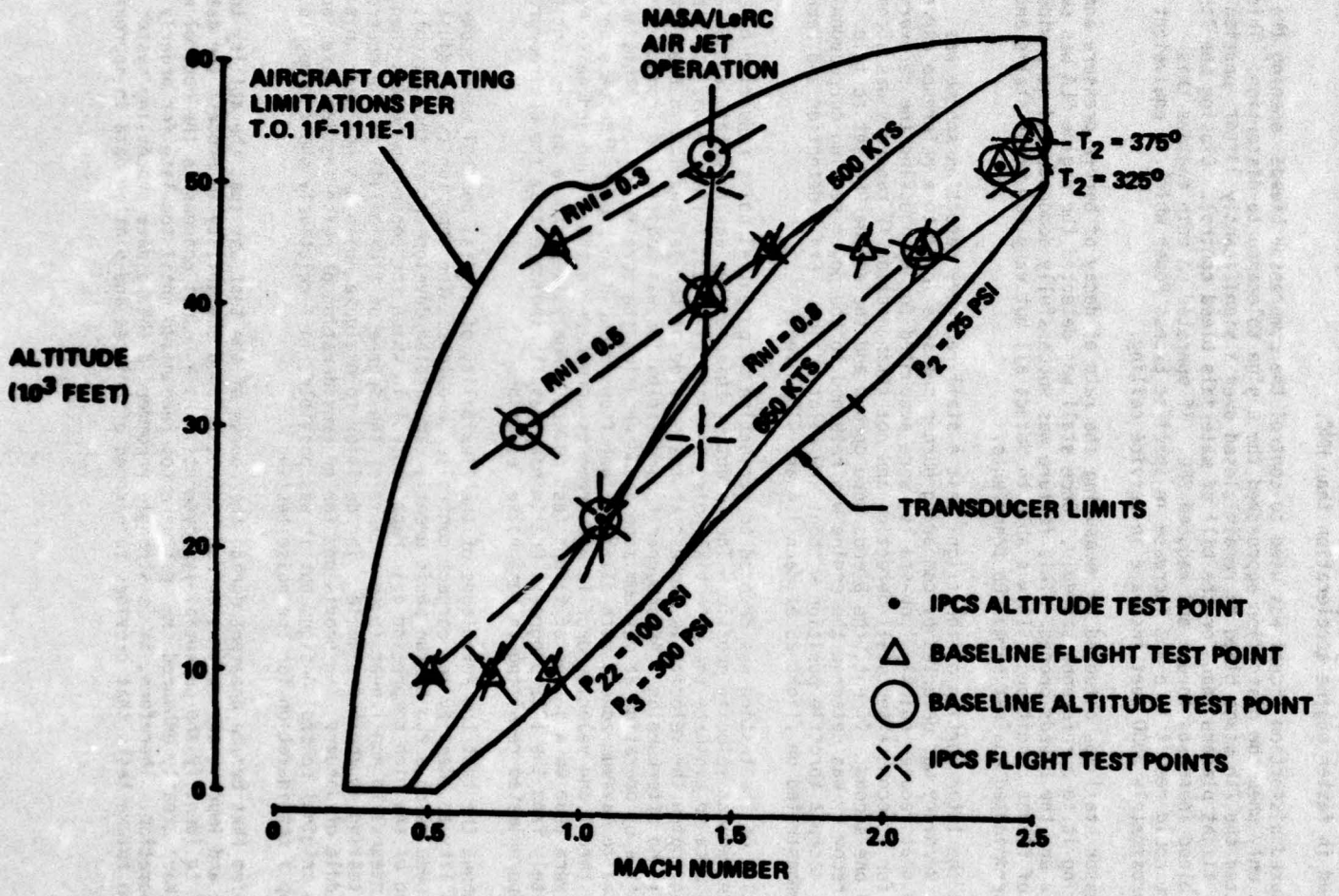

Figure 1.0-2 IPCS Program Test Points

During the later flights (21-28) the special IPCS loops were evaluated. In addition a number of changes were made to the high compressor exit Mach number, MN3, control to reduce gas generator acceleration time. Four variations of MN3 control were tested: the basic integral control, the integral control with higher gain (ground test only), a non-linear control operating at the major cycle rate (33 Hz), and the non-linear control operating at the minor cycle rate (200 Hz). The results of these tests indicate that the MN3 control is a viable alternative to Wf/Pb control although it does not solve all the gas generator control problems. Operation with MN3 control resulted in faster engine acceleration than HMC.

A measured distortion signal was used to control the compressor bleeds, opening the bleeds only when the distortion approached the engine tolerance to distortion. This permitted the 7th stage bleed to remain closed over a significantly larger portion of the flight placard than for the bill of materials bleed control. Closing the 7th stage bleed increases thrust and reduced SFC. If operated on both engines this feature could result in a 35% increase in Specific Excess Power which is equivalent to approximately 3000 feet increase in service ceiling.

Compressor stall was detected by measuring the rate of decay of burner pressure and comparing it to a reference schedule. Once stall was detected the engine PLA was set to idle and the bleeds opened. This feature was successfully demonstrated at a wide range of flight conditions. It was able to detect all but very low power stalls and it discriminated against normal Pb transients.

During the later portion of the flight test a stall recovery detection scheme was added. Recovery was detected by comparing burner pressure level to a reference curve. Stalls that recover quickly (pop-stalls) were accounted for by checking the recovery curve for 1 second after stall detection and not taking action if recovery was accomplished within one second. If not, the bleeds were opened and the engine PLA set to idle. Once stall recovery was detected the engine was returned to the power setting corresponding to the cockpit throttle position without any pilot action. Stall detection and recovery was demonstrated on flight 25 at Mach 1.4 and 41000 feet.

A portion of the testing was devoted to evaluation of potential noise reduction by controlling the exhaust velocity profile. The intent of this testing was to obtain static and flight data to evaluate the potential noise benefits of a duct burning engine.In a duct burning engine the velocity is highest at the outside of the jet and low in the core where there is no afterburning. Afterburner fuel distribution was modified to produce this type of profile by operating at maximum zone 4 and reducing the core fuel flow. This was compared to maximum zone 5 with all zone fuel flows reduced to produce the same thrust. Noise, thrust and velocity profile measurements were made on the ground and noise measurements were made on a series of flight test points. Analysis of these data is continuing separately from the IPCS program. Preliminary results indicate that the desired profiles were approximated resulting in some noise reduction.

Throughout the test the advantages of the flexibility of digital control were apparent in the ability to identify and correct controller problems. The opportunity to adjust gains and schedules on a run by run basis greatly facilitated development of the control. The testing of the high compressor exit Mach control in which the control mode was changed from integral to non-linear is an example of the degree of flexibility of the control. Noise testing is another example. The decision to evaluate noise was not made unitl the middle of January. No provisions for or consideration of noise testing were included in the original control design, but it was possible, in a relatively short time, to develop a configuration for the noise testing.

A problem that became apparent during the course of the test was that the ability to refine and improve the controller had far outstripped the ability to process the data needed to identify the potential improvements. As a result changes to the control which might have greatly enhanced the test were not recognized until too late for orderly incorporation. Therefore, it is strongly recommended that a data processing system be used in future tests that provides turnaround of printed and plotted data in approximately 16 hours.

2.0 OBJECTIVES

The overall objective of the flight test program was to demonstrate the feasibility of digital propulsion control in a flight environment. More specifically the objectives included:

1. Demonstration that the digital implementation of the hydromechanical control (BOMDIG) would produce control operation comparable to that of the hydromechanical control.
2. Evaluation of advanced control modes through the use of the IPCS program, e.g., compressor exit Mach number, stall detection, distortion control of bleeds, buzz, and airflow control.
3. Demonstration of the advantages of the flexibility of digital control to improve the control development program.
4. Demonstration of the reliability and effectiveness of the DPCU hardware operating in a flight environment.

New objectives added toward the end of the test warranted a program extension.

1. Measurement of jet noise, thrust, and velocity profiles for a flat velocity profile and an inverted velocity profile, similar to that generated by a duct burning engine.
2. Flight evaluation of a Mach hold autothrottle.
3. On-line thrust calculation in the DPCU.

3.0 PROCEDURES

This section deals both with the specific procedures used in the tests and with the way in which NASA and contractor engineers worked to plan and conduct the tests.

3.1 TEST OPERATION

The test plan document (Reference 1) provided the basic framework for planning the majority of the flights. Three revisions were made to the document during the test program to reflect significant changes to the overall test plan, priorities, etc. These changes were coordinated among the contractors and then discussed with NASA prior to implementation. The discussions took place in meetings in which the contractors, NASA Operations, NASA Research, NASA IPCS Project Office , and the pilots were represented. The implications of the changes were discussed in terms of technical reasons for the changes, effect on pilot workload, and potential schedule impact. Modifications to the revisions were made during the course of the meeting and the resulting changes incorporated in the document. Changes to the scope of the testing during the later portion of the test were coordinated in a similar manner.

Prior to each flight or engine run the on-site contractor engineers identified a tentative software configuration and specific test events. These were coordinated with engineers at BAC and P&WA to provide a single set of requirements to NASA. Contractor engineers then worked with the NASA IPCS Project Engineer to produce a set of event cards for the run. From this point engine runs and flights were handled somewhat differently.

Prior to each flight a technical briefing was held to discuss the flight. Representatives from NASA Flight Safety, Operations, Research, and the IPCS Project Office attended in addition to the pilots and engineers directly involved in the flight. The discussions covered the condition of all airplane systems, the status of data processing, and the availability of the control room and related equipment for the desired flight date. All modifications to the IPCS hardware and software were discussed. The specific events for the flight were discussed in detail and modified as necessary based on pilot inputs.

The day before the flight or day of the flight a crew briefing was held to review the flight events. Changes were made to the events, as necessary, to take into consideration analysis which was not available at the time of the Tech briefing. No changes were made to the flight plan after the crew briefing. When lack of time required, the two briefings were held together.

During the flight, strip charts were monitored by contractor and NASA engineers. All the engineers were able to communicate with each other via an intercom. When it was necessary to repeat or modify events during the flight, the requirements were coordinated by the NASA IPCS Project Engineer and relayed to the pilot by the Flight Controller, who was the only person able to talk to the pilot.

Formal pre-run briefings were not generally held for the engine runs. If the procedures for a particular run were complicated, such as the noise measurement runs, briefings were conducted prior to the run. During a ground run the attention of the crew can be devoted entirely to the operation of one engine and the DPCU. As a result a greater degree of flexibility of test events could be maintained. Changes were made to the run cards up to the point of crew entry into the airplane and a great deal of flexibility existed during the run for event changes. As with the flight test a single NASA Operations Engineer conducted the test; however, the crew and all engineers monitoring the run were on the same radio.

After an engine run or flight a data request was prepared from the on-line data stripouts by contractor engineers. This request was approved by the NASA IPCS Project Office prior to the initiation of data processing to coordinate other requirements for data.

3.2 SPECIFIC TEST PROCEDURES

The specific procedures used for individual events are discussed in this section to assist in understanding the test results. A series of maneuvers was developed to explore the operational limits of the propulsion system. Obviously there were quite a number of different events. There is no attempt to discuss each one, but the more significant events are covered. The test variables which affect the engine operation are listed

in Table 3.2-1 along with a definition of how each was controlled during the flight test program. Four sense switches in the cockpit mounted Computer Monitor Unit, CMU, were used to select data output, control modes, etc. Sense switch numbers were specified in terms of an actal number (10, 4, 2, 1 per switch from the left).

3.2.1 Seal Saver Turn (SST)

The SST was designed to subject the inlet to gradually increasing angle of attack up to the airplane limit. It was defined as the following: an approximately 60° bank turn with increasing positive pitch (back stick) at a rate of approximately two g's per second, holding for about two seconds at the alpha or normal load factor limit, whichever occurred first.

3.2.2 Yaw to β Limit

Yaw tests were conducted to subject the engine to different distortion pattersn. Baseline flight testing indicated that the distortion was more severe if the inlet was on the leeward side of the airplane. Thus the yaw transient consisted of a nose left sideslip to the beta limit as defined in TO 1F111E-1. Rate of increase of sideslip was approximately 0.5°/sec.

3.2.3 Throttle Transients - Snaps and Bodies

Snap transients and bodies consume a large amount of surge margin. A snap throttle transient was a single direction throttle movement from first to second PLA at a rate corresponding to less than one second from ground idle to mil. Conditions at the second PLA were stabilized prior to the next snap transient. Stabilization is defined as follows:

Mil-Max Max-Mil Idle-Max	Nozzle area and fuel flow are stable
Mil-Idle Idle-Mil Max-Idle	Wait X seconds before next transient, X is defined in Table 3.2-2

A BODIE is defined as a transient involving two throttle directions, i.e., MIL-IDLE-MIL, in which the engine is not stabilized at the intermediate throttle setting.

3.2.4 Expand Cone to Stall

Manual inlet control was used to evaluate the distortion control of bleeds and stall detection features of the IPCS control. Sense switch 12 was used to activate the stall detection and stall recovery detection loop. The cone angle was increased until the increasing distortion caused compressor surge. Following surge the inlet was returned to automatic control to clear the distortion. The specific procedure was as follows:

a. Select sense switch 12
b. When stabilized on condition, set spike and cone potentiometers to auto settings
c. Select MANUAL on cockpit mounted manual inlet control panel
d. Expand cone (02) slowly until stall occurs
e. Select AUTO on control panel as soon as stall occurs
f. Leave PLA for 30-45 seconds

3.2.5 Airflow Bias

The airflow bias control, AFBIAS, was also tested using the manual inlet control. The cone angle was increased to mismatch the inlet relative to engine airflow and sense switch 10 selected to activate the airflow bias loop:

a. When stabilized on condition, set spike and cone potentiometers to auto settings
b. Select MANUAL on control panel
c. Increase cone angle by 1 unit (~ 2°)
d. Sense switch to 10, hold PLA for 15 seconds and observe N2 change.

Table 3.2-1 ENGINE PERFORMANCE VARIABLES

Variable	Control
Flight Condition-Altitude, Mach	Specified on Test Event Cards
Angle of Attack	Nominal Cruise α unless Specified on Test Event Cards
Yaw	Zero unless Specified on Test Event Cards
T2	Uncontrolled
CADC	On
Power Takeoff	Both Generators On
Bleed Control	
ECS	Right Hand Engine Only
7th	Auto Unless Specified on Test Event Cards
Throttle	Specified on Test Event Cards
Inlet Control	Auto unless Specified on Test Event Cards
DPCU Operation Power	Turned on At Time Specified In Test Event Cards, Left On Unless Specified in Test Event Cards
Engage Select	Specified in Test Event Cards
Sense Switches	Specified in Test Event Cards

Table 3.2-2 TRANSIENT STABILIZATION TIMES

		X-STABILIZATION TIME ~ SEC		
MN	Alt (FT)	Mil-Idle	Idle-Mil	Max-Idle
0.5, 0.7, 0.9	10000	7	7	7
0.8	30000	8	8	8
0.9	45000	8	35	8
1.4	50000	8	35	8
1.4	30000, 41000	8	8	8
1.06	22000	5	5	6
1.6	45000	5	5	6
1.9	45000	4	4	4
2.1	45000	4	4	4
2.3	50000	-	-	4
2.47	54000	-	-	4

3.2.6 Stable Throttle Conditions

For the following events the L/H throttle was held steady throughout the transient:

Event	Throttle
SST (para 3.2.1)	MIL or above
YAW (para 3.2.2)	MIL or above
STALL (para 3.2.4)	MIL or above
AFBIAS (para 3.2.5)	Less than MIL

The right hand engine was set as required to maintain Mach/Altitude. If sufficient thrust was not available to hold a flight condition, the event was conducted by starting at a higher Mach number and slowing down to the desired condition.

3.2.7 Autothrottle

All autothrottle events were conducted either 1) by setting the cone pot on the manual inlet control (Mn command) to a desired value, switching to sense switch 11 and stabilizing the airplane or 2) by switching to sense switch 11, stabilizing the airplane, changing the cone pot setting and stabilizing the airplane again.

3.2.8 650 KT Climbing Acceleration

This airplane acceleration was conducted to evaluate the effect of bleed control on the time to reach maximum Mach number.

a. Both PLA to Max. A/B
b. Accelerate the airplane at 650 KTS indicated airspeed from Mach 1.6 to a Mach number where the airplane does not accelerate or an engine stalls (2.4).

3.2.9 500 KT Climbing Acceleration

The 500 knot climbing acceleration was conducted to evaluate bleed control at high altitude conditions.

a. Both PLA to Max
b. Climb at 500 KTS indicated airspeed to altitude limit defined as the point where the rate of climb was small in the pilot's opinion.

3.2.10 Buzz

Inlet buzz occurs at low airflow. For sense switch 12 the normal minimum airflow loop was disabled to permit low enough airflow to encounter buzz. In flight 21 the R/H engine was used to attempt to hold the flight condition. On subsequent flights both engines were retarded to idle to provide a more representative buzz transient.

Flight 21
a. Sense switch 16
b. L/H throttle to Idle, hold for 30 sec
c. Use R/H PLA to attempt to maintain flight condition

Other flights
a. Sense switch 16
b. Both throttles to Idle, hold for 30 sec

3.2.11 Noise

The procedures used in the noise testing are described in Section 6.6.

3.3 SOFTWARE CONTROL PROCEDURES

Revisions C of both BOMDIG and IPCS were completed on 23 June 1975. Documentation of this software has been provided to the government as CDRL A00J. The resulting punched paper object tapes were checked out in the last week of Altitude Test. Software Field Change Orders (SFCO) required to make the released object tapes operable were defined

during this checkout. During the Flight Test these SFCO's and those defined during Ground and Flight Test were incorporated into the 601 core contents in accordance with the procedure defined in the following paragraphs. Figure 3.3-1 shows the sequence of events leading to incorporation of an SFCO in the software.

3.3.1 SFCO Generation Procedure

SFCO's were generated to document any desired change to program software. The changes corrected anomalies, tested new control designs, or output different data. The requirements for a change were identified by contractor or NASA engineers. Change requirements were coordinated by the Contractor System Engineer. The Senior Contractor Engineer and NASA/DFRC Flight Systems Engineer reviewed requests for changes and determined those to be coded. The Contractor System Engineer coded the change and documented it on an SFCO form (Figure 3.3-2) including an engineering description of the function of the change.

The Senior Contractor Engineer and NASA/DFRC Flight Systems Engineer reviewed and approved the SFCO for technical content and coding. As necessary, use was made of contractor engineers at P&WA, HI, and BAC for consultation. The SFCO was loaded intc memory using the teletype (TTY) and the TTY printed record was annotated with the SFCO number, date, time, initials of operator and other comments. Open and/or closed loop testing as deemed appropriate was conducted to verify operation of each SFCO. Within four working days of incorporation, copies of SFCO's were forwarded to engineers at P&WA, HI and BAC for review.

3.3.2 Patch Tape Generation and Loading Procedure

The Contractor System Engineer reviewed the Contractor Engineering Log and SFCO file to determine which SFCO's were to be included in the patch tape. The Senior Contractor Engineer and NASA/DFRC Flight Systems Engineer reviewed and approved the selection of SFCO's. The selected SFCO's were documented by SFCO number and core location on an IPCS PATCH TAPE RECORD FORM, Figure 3.3-3. The documentation was verified by the Senior Contractor Engineer and NASA Flight Systems Engineer.

The following were loaded into core by the Contractor Systems Engineer or designated NASA personnel; the current program (IPCS or BOMDIG) and the communication and debugging program, MEDIC, using punched paper tape and the high speed paper tape reader, and the contents of the SFCO's by TTY as described in the SFCO generation procedure. The memory locations specified in the Patch Tape Record were verified correct per the SFCO File by comparison. A patch tape was punched per the Patch Tape Record by the Contractor Systems Engineer or by designated NASA personnel. The memory was cleared, the patch tape loaded and the Contractor Systems Engineer and designated NASA personnel verified the locations specified in the Patch Tape Record line for line with the SFCO's. The Contractor System Engineer incorporated SFCO's in the Software Maintenance Listing, and documented the tape punching in the engineer log and the IPCS Inter-flight Worksheet and Removal Record. The tape leader was identified with the patch tape number from the Patch Tape Record. The Senior Contractor Engineer and designated NASA personnel verified that the correct number was on the tape leader.

The contractors maintained workbooks - 1 for IPCS, 1 for BOMDIG containing the original SFCO's relevant to each program in numerical order and the original IPCS Patch Tape Record Forms.

3.3.3 IPCS DPCU Software Configuration Control Procedure Prior to Flight

This procedure provided for configuration control of the contents of the IPCS Digital Propulsion Control Unit (DPCU) core memory.

Two modes of operation of the DPCU were recognized. TROUBLE-SHOOTING and FLIGHT. In both modes of operation it was the responsibility of the computer operator to log DPCU activities in the DPCU Supplement to the Aircraft Log and to date and annotate the DPCU teletype output in a cogent manner. Any anomalies observed in DPCU operation, either software or hardware related, were logged as squawks in the DPCU Supplement to the Aircraft Log and resolved per standard NASA/DFRC procedure.

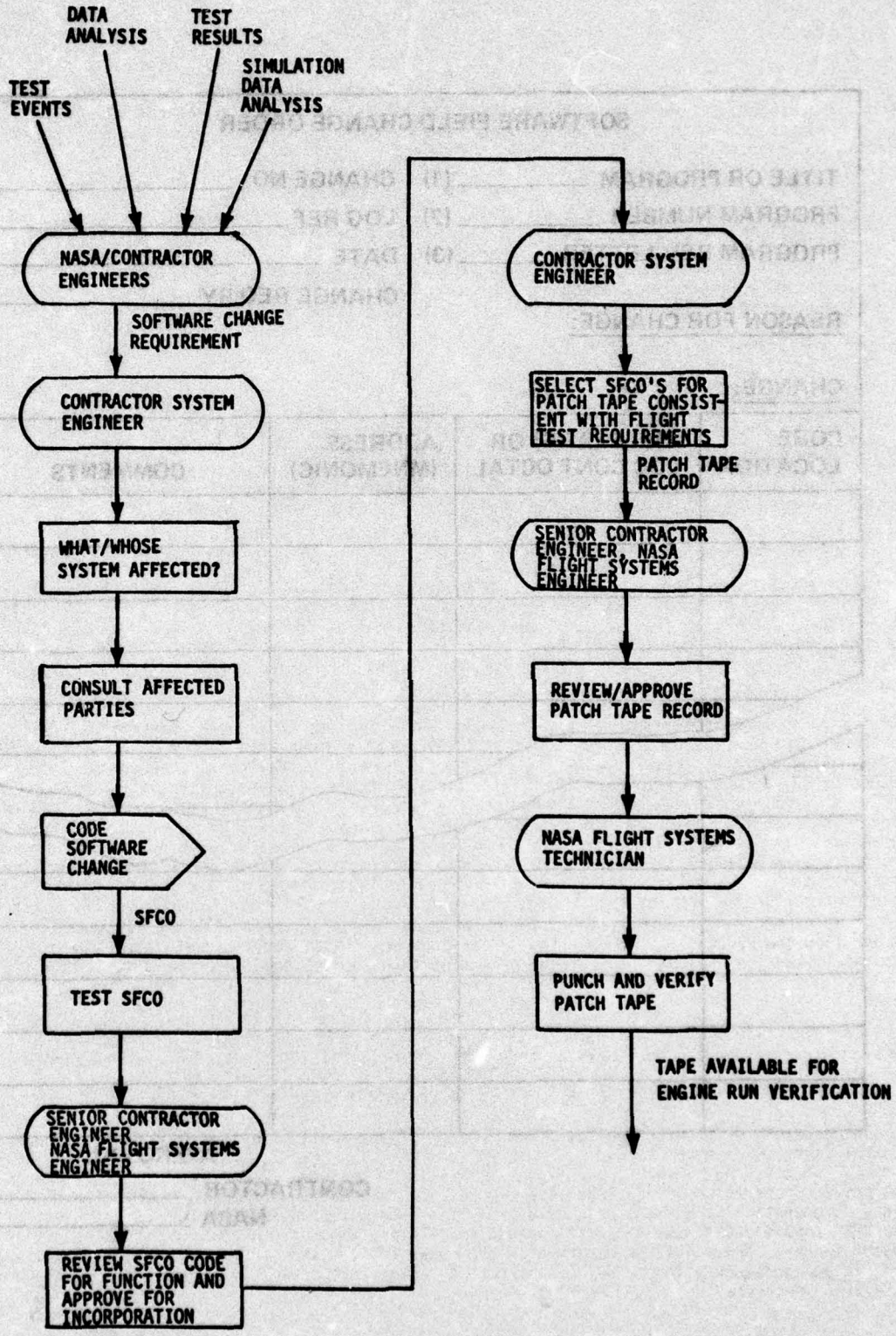

Figure 3.3-1 Software Change Procedure

SOFTWARE FIELD CHANGE ORDER

TITLE OR PROGRAM _____ (1) CHANGE NO. _____ (4)

PROGRAM NUMBER _____ (2) LOG REF _____ (5)

PROGRAM REV LETTER _____ (3) DATE _____ (6)

CHANGE REQ BY _____

REASON FOR CHANGE:

CHANGE:

CORE LOCATION	INSTR (ARG) OR LOC CONT OCTAL	ADDRESS (MNEMONIC)	COMMENTS

APPROVAL

CONTRACTOR _____

NASA _____

Figure 3.3-2 SFCO Form

IPCS PATCH TAPE RECORD

PROGRAM NAME:

REV. LETTER:

PROGRAM #:

TAPE #:

DATE:

TAPE COMPILED BY:

TAPE PUNCHED BY:

COMMENTS/PURPOSE

TAPE CONTENTS

SFCO	LOCATIONS PUNCHED	LOC CONT VERIF.	LOC PUNCHED

Figure 3.3-3 IPCS Patch Tape Record Form

In addition to these general responsibilities the procedures described below were followed in preparing the DPCU for flight.

The flight mode started when the Senior Contractor Engineer, the NASA DFRC Operations Engineer, Project Engineer, and Flight Systems Engineer had established a flight preparation schedule for the flight. The flight preparation schedule included milestones for completion of software load, completion of DPCU checkout, preflight engine proof run, and flight.

The Senior Contractor Engineer verified with the Systems Engineer that all software required for the proposed flight was incorporated on verified patch tapes or in the basic software release.

The Systems Engineer or designated NASA personnel performed the following:

1. Cleared core using MEDIC, resident diagnostic utility routine
2. Loaded Basic Released Tape (e.g., BOMDIG or IPCS)
3. Loaded MEDIC
4. Loaded verified Patch Tapes in sequence of generation

With the exception of MEDIC all tapes were required to read smoothly and cease reading at the last punched location. The MEDIC tape read through to the end of the paper tape. A load failure of any tape aborted the process. In case of a load failure the process was restarted with step 1. Load failures were logged. The loading sequence was logged in the DPCU supplement and the aircraft log and witnessed by NASA DFRC Quality Assurance. A verified load of tapes resulted when a HI released tape and one or more patch tapes generated per Patch Tape Generation Procedure were loaded per the Flight Mode load procedure without failure indication.

Final verification of flight software was then achieved by running the sequence of hanger and engine run pad tests described in Section 3.4.

The trouble-shooting mode was entered anytime the flight mode was broken by either breaking the tape load sequence or the reconnecting the Computer Control Unit, CCU, after disconnecting it in the flight mode sequence.

In trouble-shooting mode the systems engineer or his designate modified core contents to any configuration suitable to the test activity underway. Test activities were coordinated with the Senior Contractor Engineer and NASA Operations, Systems, and Project organizations.

In the trouble-shooting mode documentation of core contents was maintained by writing SFCO's defining all modifications to the control program (IPCS or BOMDIG) with the exception of temporary changes to small numbers of locations (less than 3). The teletype printout, comprising a complete record of activities, was dated and frequently annotated with time of day and explanatory remarks. All SFCO's incorporated were identified by number. All activities were recorded in the Boeing Log. Squawks, in addition, were recorded in the DPCU supplement to the aircraft log. Flight mode was only entered from trouble-shooting mode at Step 1 of the flight mode procedure.

3.4 SOFTWARE TEST PROCEDURES

Software test procedures fell into two categories:

1. Formal system testing following a flight mode load of the software,
2. Informal testing used to open loop verify software modification prior to formal system testing.

3.4.1 Formal Testing

Formal system testing was performed following completion of a formal flight mode load of the program. If the configuration loaded was one already verified by an engine verification run the standard preflight procedure was performed in the hanger. This verified correct operation of all DPCU I/O systems and transducers. After pilot entry and left hand engine start the DPCU was engaged and the following series of engine transients was performed to assure safe operation of the engine during take-off:

Idle → Mil
Mil → Idle
Mil → Zone 3
Mil → Max
Max → Mil
Idle → Max
Max → Idle
Manual disengage in afterburning

If the configuration loaded was not already verified by an engine verification run, a brief series of DPCU health checks was performed in the hanger verifying DCU ability to track and engage, and reasonable behavior of all inputs and outputs. Where possible new functions incorporated in the software were rechecked at this time. The airplane was then taken to an engine run pad and all new functions testable on the ground were demonstrated with the engine running and DPCU engaged. After completion of these tests the standard set of engine transients tabulated above was performed to verify correct engine operation during takeoff. In addition, trim at idle, mil, and max was checked by comparison to previous ground run data.

After return to the hanger the software was completely reloaded and the procedure described above for use with verified software was followed. Thus, in addition to on line review of engine verification run data, a period of time was available for detailed review of these data prior to flight.

3.4.2 Informal Testing

Informal testing was performed on SFCO's prior to their inclusion in patch tapes to verify their correct function. This testing was based on a review of the SFCO functional requirements. Open loop tests were devised to verify changes in schedules, with table checks, etc., appropriate to the SFCO. As the lab DPCU/TSU setup became available after repair of the DCU V2 these tests became both more sophisticated and easier to perform. As a result, more ambitious changes were possible with less risk to airplane hardware and less interference with aircraft test activities.

4.0 TEST CONFIGURATION

The following paragraphs describe the hardware and control configuration at the beginning of the flight test program. Appendix A defines the changes on a flight by flight basis.

4.1 IPCS HARDWARE INSTALLATION

The IPCS system was installed in an F-111E for the flight test (Figure 4.1-1). Figure 4.1-2 shows the interconnection between the IPCS components and the airplane. The configuration is defined in detail in Reference 3.

4.1.1 Cockpit Installation

The DPCU was controlled from the cockpit with the computer monitor unit (CMU), (Figure 4.1-3). The CMU is used to select either the IPCS or the backup hydromechanical control. Lights display control information (see Table 4.1-1). Four sense switches and three pots supply on line information to the computer. The pots were used initially to provide the trim functions in the IPCS and BOMDIG mode which are normally performed in the hydromechanical control. During the noise testing (section 6.6) these pots were used to vary control parameters on-line.

The manual inlet control panel (Figure 4.1-4) provided additional on-line input to the computer. A switch selected manual or automatic inlet operation. In manual the two pots supplied commands for the inlet control. The guages displayed inlet position regardless of the switch position. During the later portion of the test program the pots were used to vary control parameters such as the Mach number command to the autothrottle and bias to the MN3 loop.

4.1.2 Inlet Hardware

The hydromechanical inlet controller was replaced with an electromechanical module. The hydromechanical inlet pressure ratio and position feedback sensors were replaced with electrical transducers. Four distortion probes were added to the 40 probe compressor face instrumentation rake system (Figures 4.1-5 and 4.1-6). The installation of the pressure transducers and the required changes to that installation are discussed in section 7.4. One of the 40 Kulite miniature transducers in the rake was used to provide buzz and turbulence signals to the DPCU.

4.1.3 Engine Hardware

The major engine modifications were made to the diffuser and fan case for incorporation of the four (4) new P3 total pressure probes and four (4) PS3 static pressure ports. In addition to the actual engine modifications, which included the necessary plumbing for the above probes, external hardware was also modified or added to the basic engine. This included a P22-T22 combination probe installed in the existing borescope hole at the exit from the low compressor, two (2) tachometers for measurement of the low (N1) and high (N2) compressor speeds, the modified main and afterburner fuel controls and the transducer box assembly used to house the pressure transducers and thermocouple cold reference junction probes.

The IPCS components and their part numbers which were tested on the engine are noted in Table 4.1-2. Figures 4.1-7, 4.1-8 and 4.1-9 show the engine installed in the airplane.

4.1.4 DPCU Hardware

In addition to the CMU, the DPCU consisted of the power supply (PSU V1) the digital computer (DCU V1) and the interface unit (IFU V1). These units were installed in an insulated box which was shock mounted in the weapons bay (Figure 4.1-10) alongside the NASA instrumentation package.

Table 4.1-1 CMU LIGHT FUNCTIONS

Light	Function
PWR	DPCU Power On
TRACK	DPCU control meets requirements for engaging
ENGAGE SEL	Pilot has selected DPCU control
DPCU ENGAGE	DPCU is in control
BACKUP	One sensor has failed, synthesized signal is being used
FAULT	The DPCU has failed specific tests such as two sensor failures or PLA > 69° when not engaged (Volume II , Table 2.3-3 defines the failures which cause a fault light). When the fault light is set the DPCU cannot be engaged. If it is engaged it will disengage.

Table 4.1-2 MAJOR ENGINE IPCS COMPONENTS

IPCS Components	P-676627 Engine
CJ-U1 Main Fuel Control	P/N 749008 S/N 200874
AA-R1 Afterburner and Exhaust Nozzle Control	P/N 749009 S/N 1874
Transducer Box Assembly	P/N 724790
P3 Pressure Probes	P/N 724786-300
N1 Tachometer	P/N 751103
N2 Tachometer	P/N 751103
P22-T22 Combination Probe	P/N 724784-300
Electrical Harnesses	
Main Fuel Control	P/N 724792
Transducer Box	P/N 751168
Afterburner Control	P/N 751169
Thermocouple	P/N 751170
N1 Tachometer	P/N 751240
Afterburner Control	P/N 751302

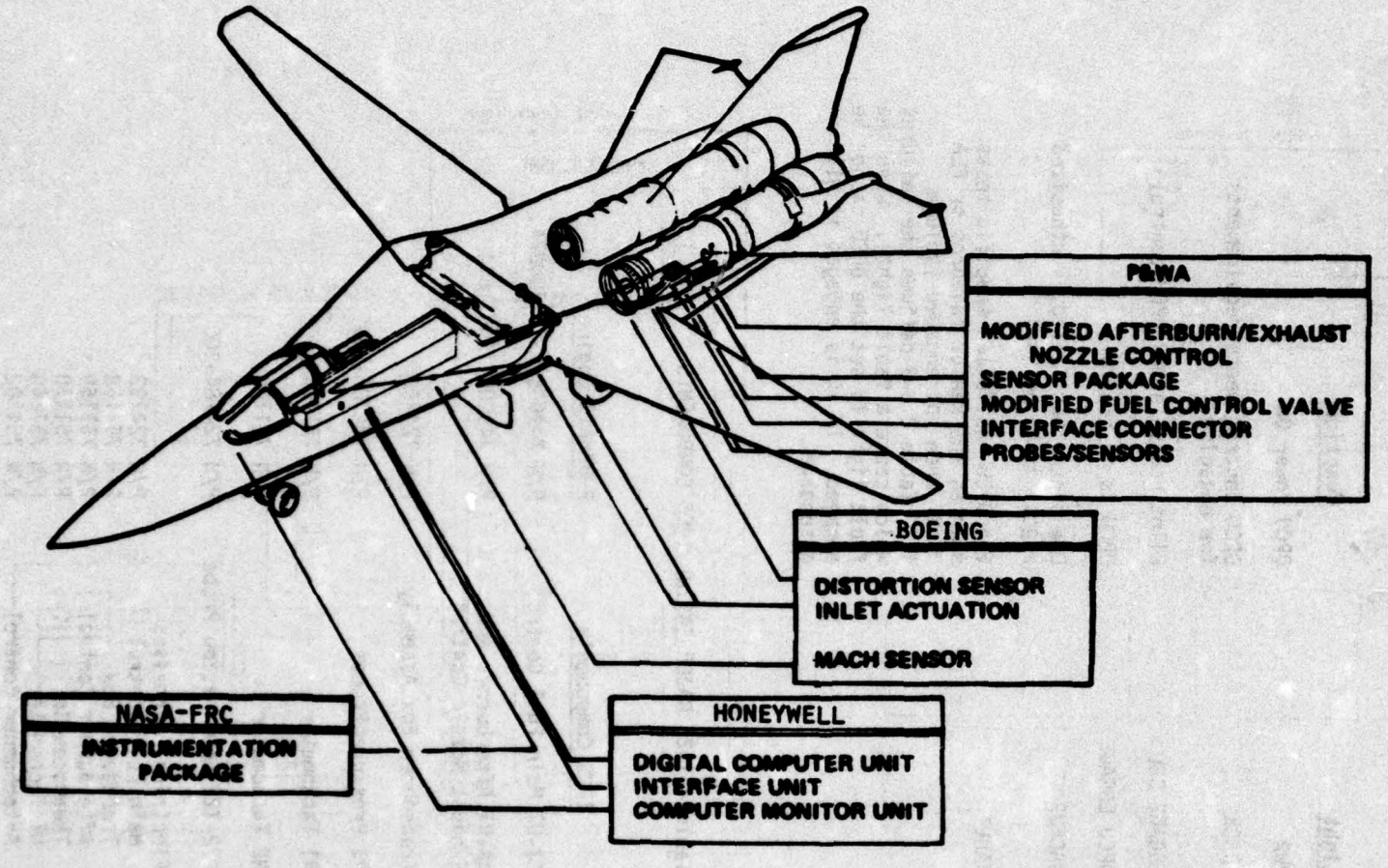

Figure 4.1-1 IPCS Installation on F-111

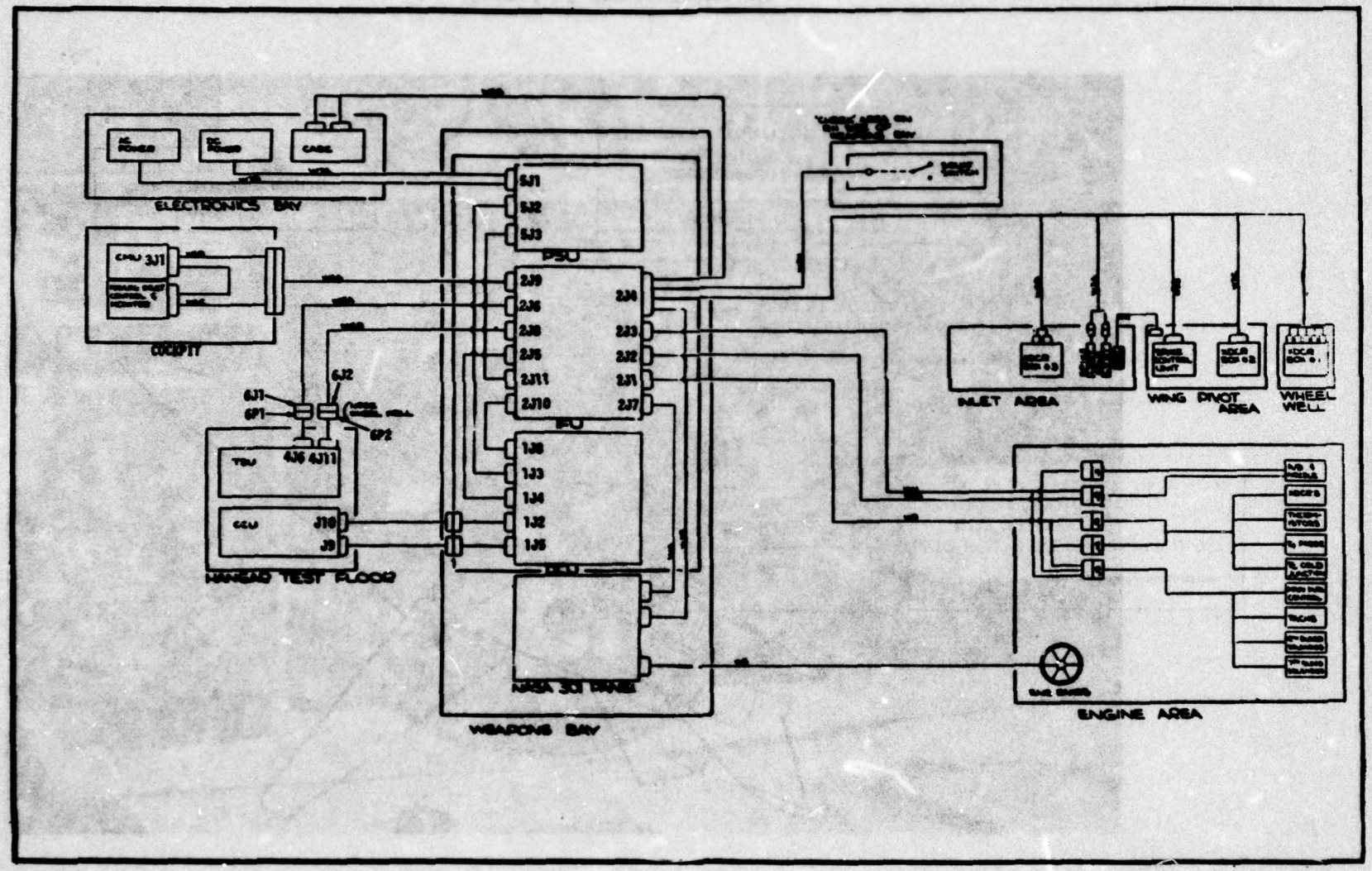

Figure 4.1-2 IPCS Signal Paths

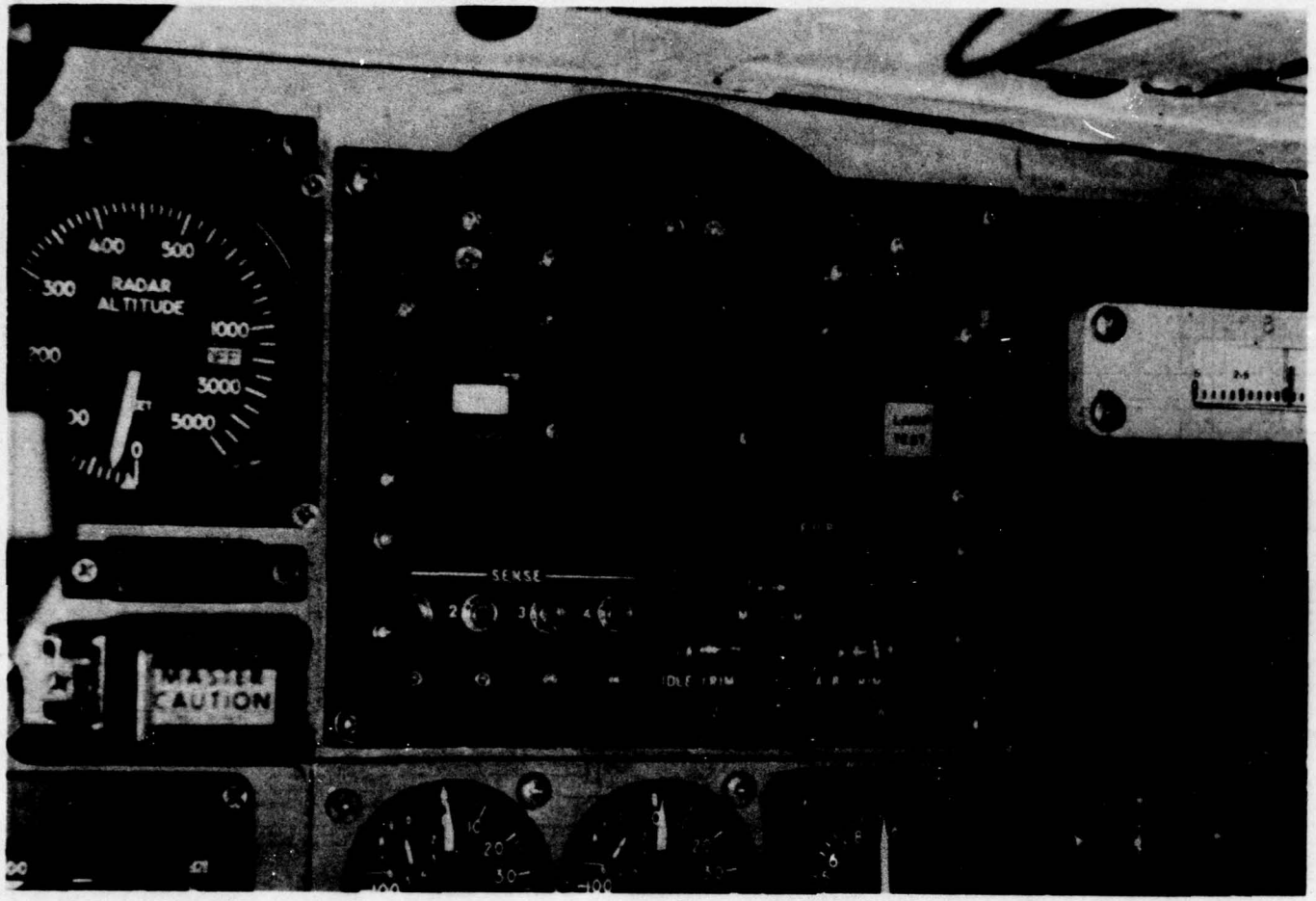

Figure 4.1-3 Computer Monitor Unit

(29617)

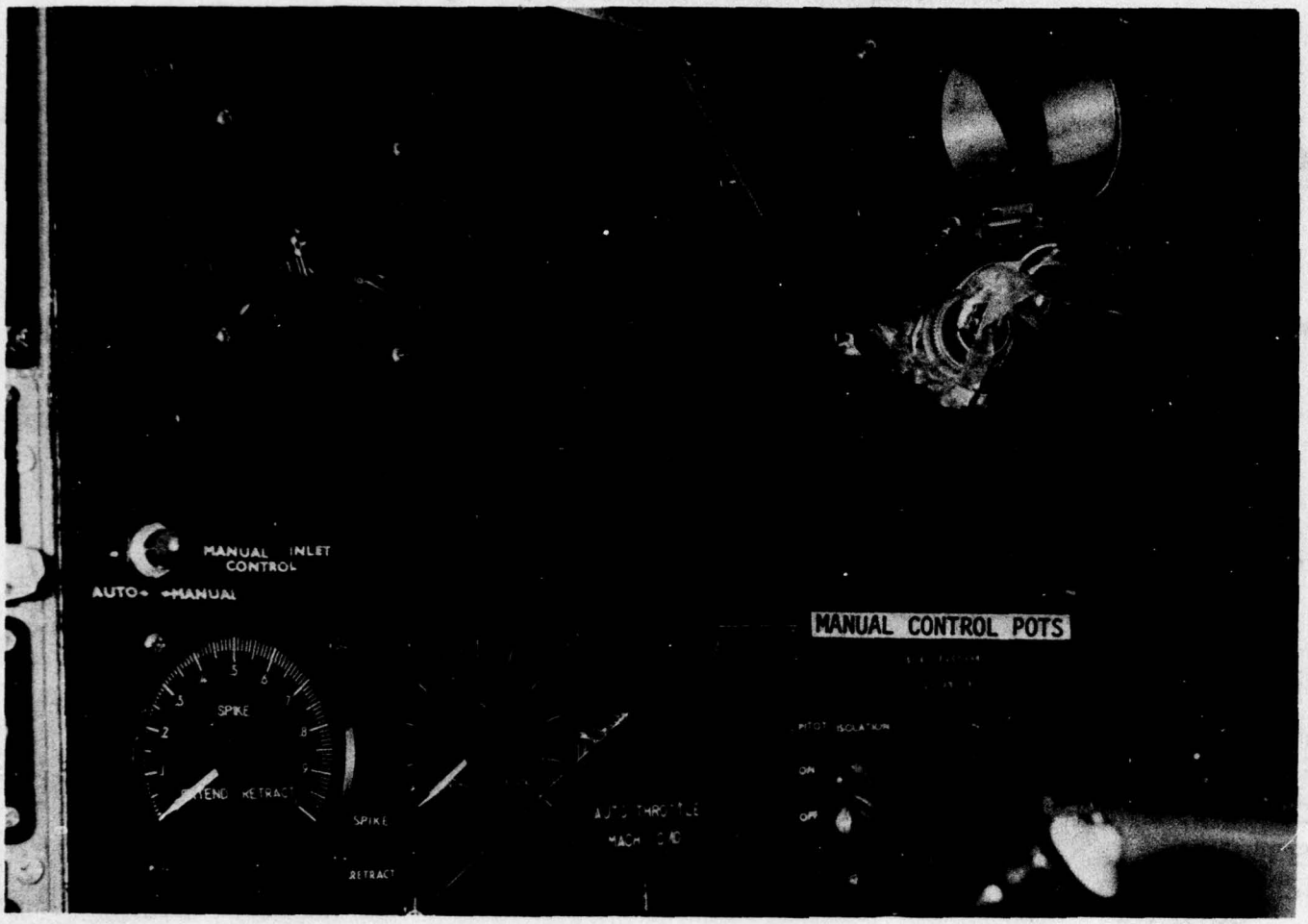

Figure 4.1-4 Manual Inlet Control

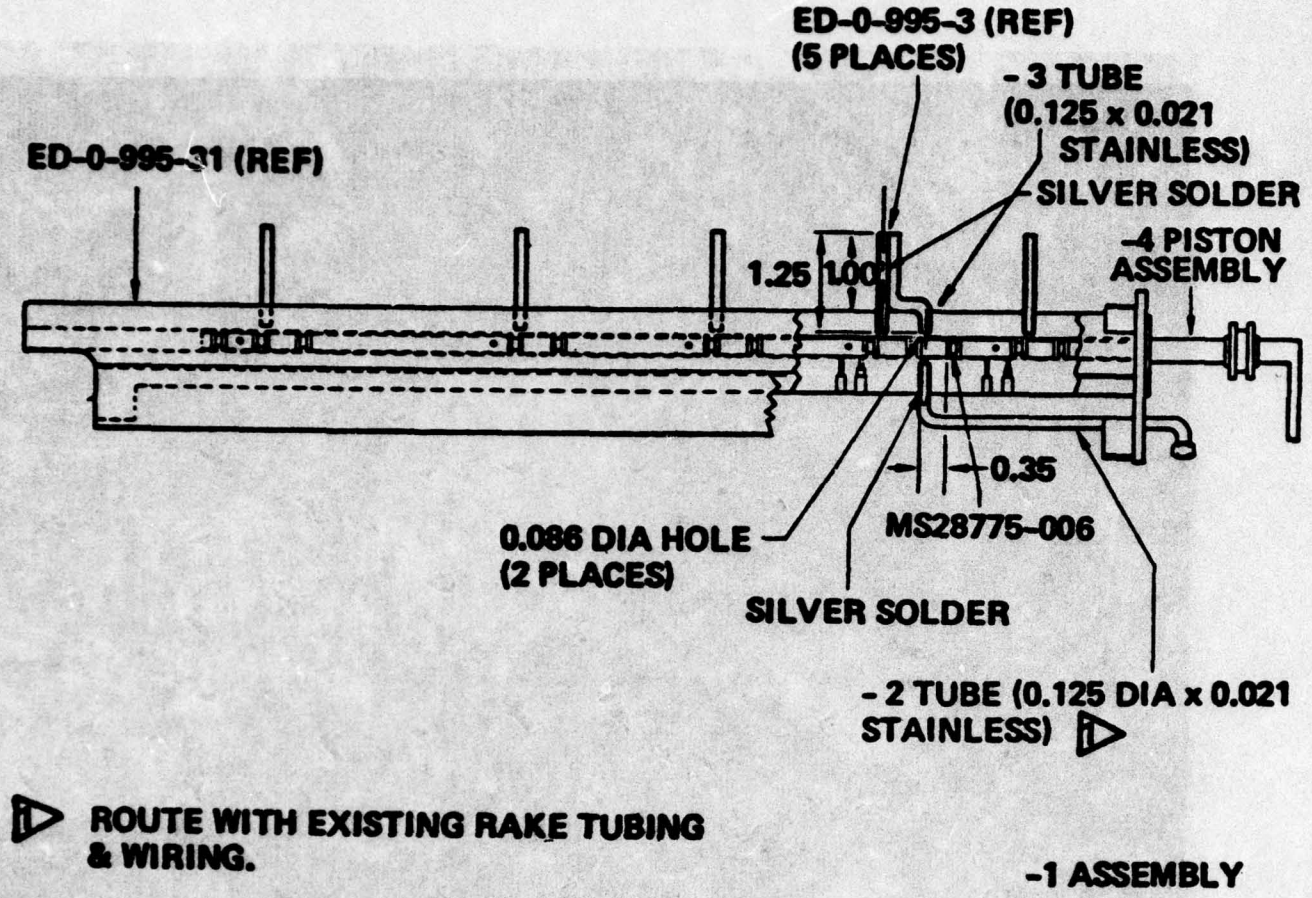

Figure 4.1-5 Distortion Probe - Rake Modification

(28405)

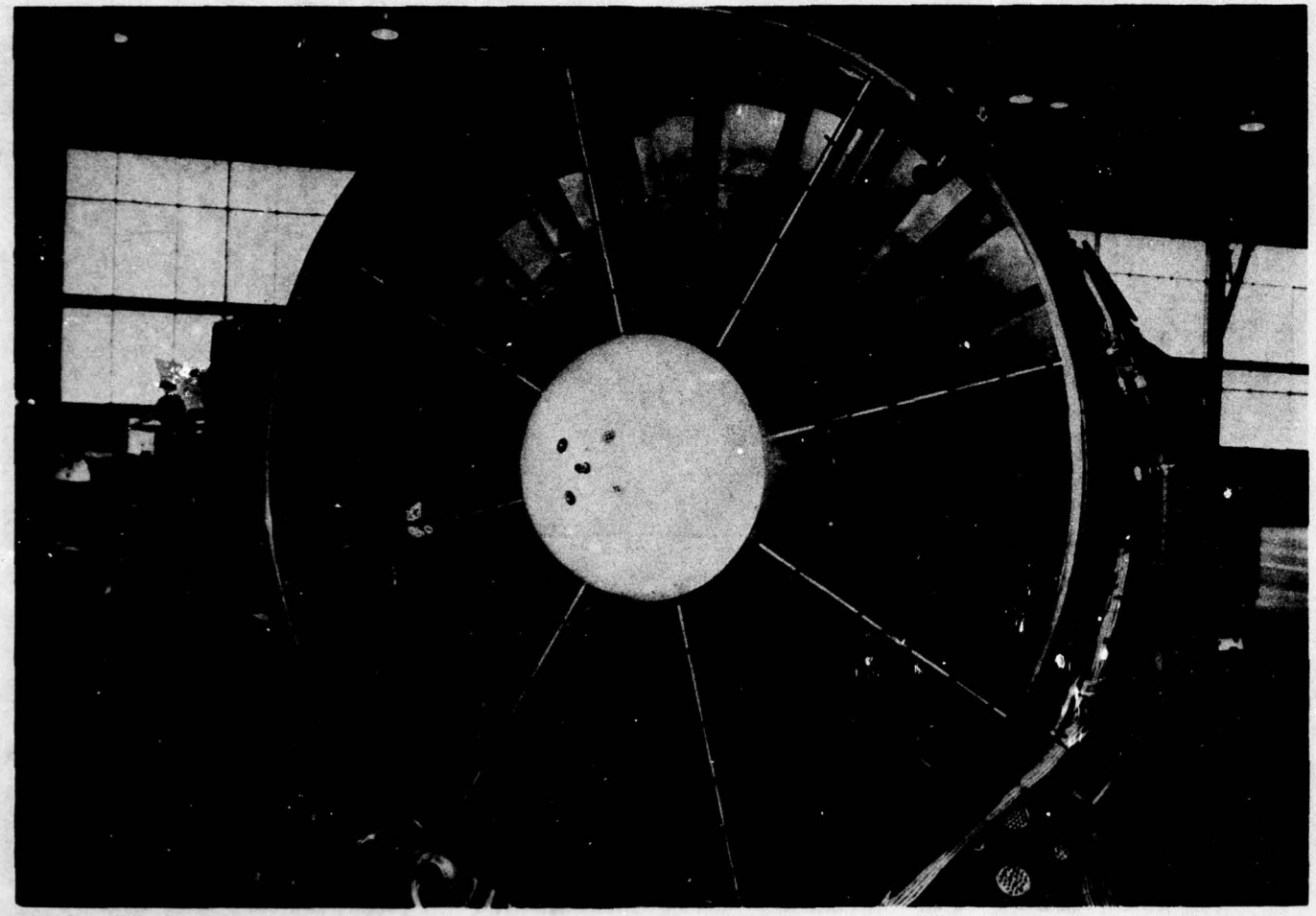

Figure 4.1-6 Compressor Face Rake

(29665)

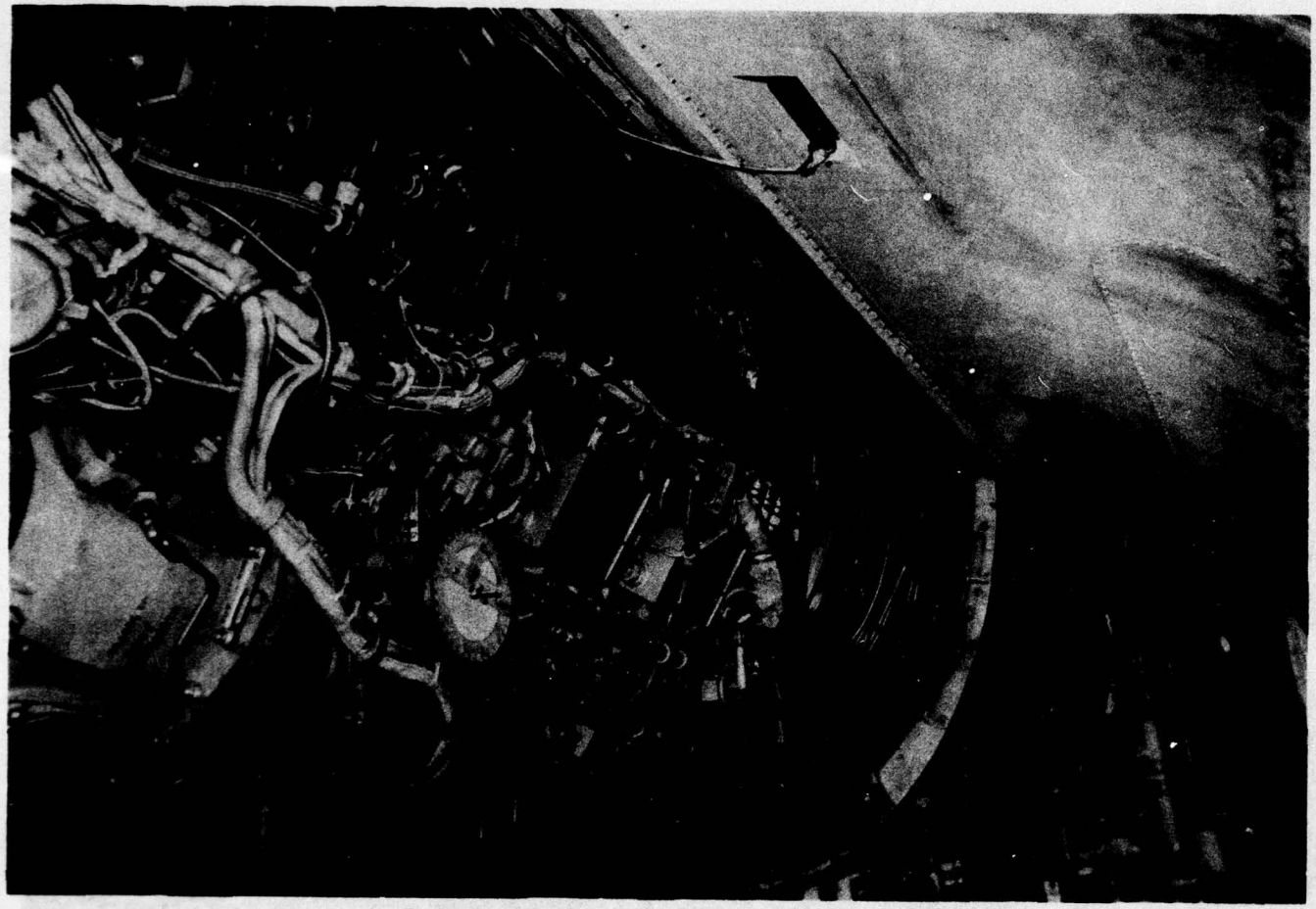

Figure 4.1-7 Engine Installation

(29608)

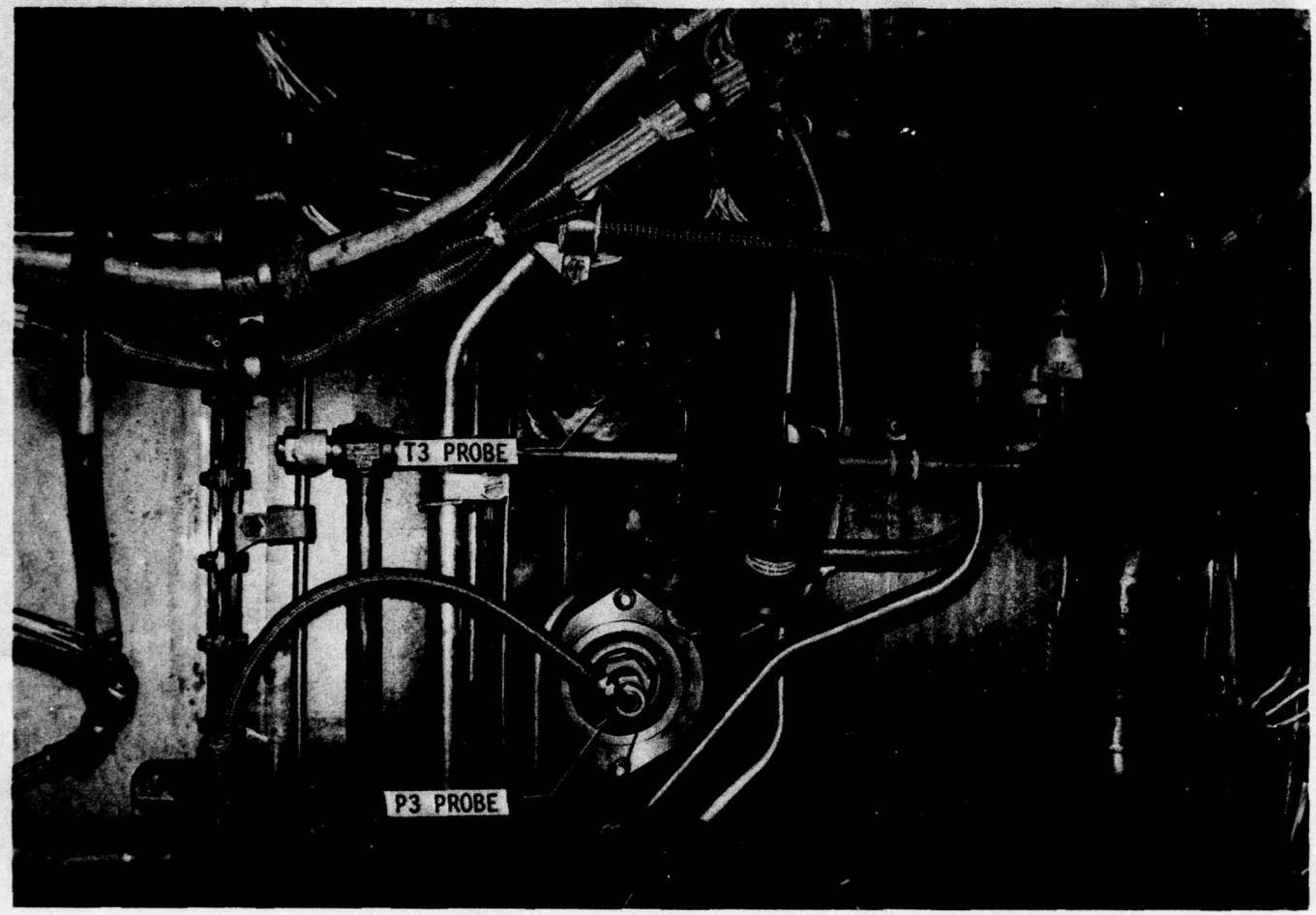

Figure 4.1-8 Station 3 Probes

(29607)

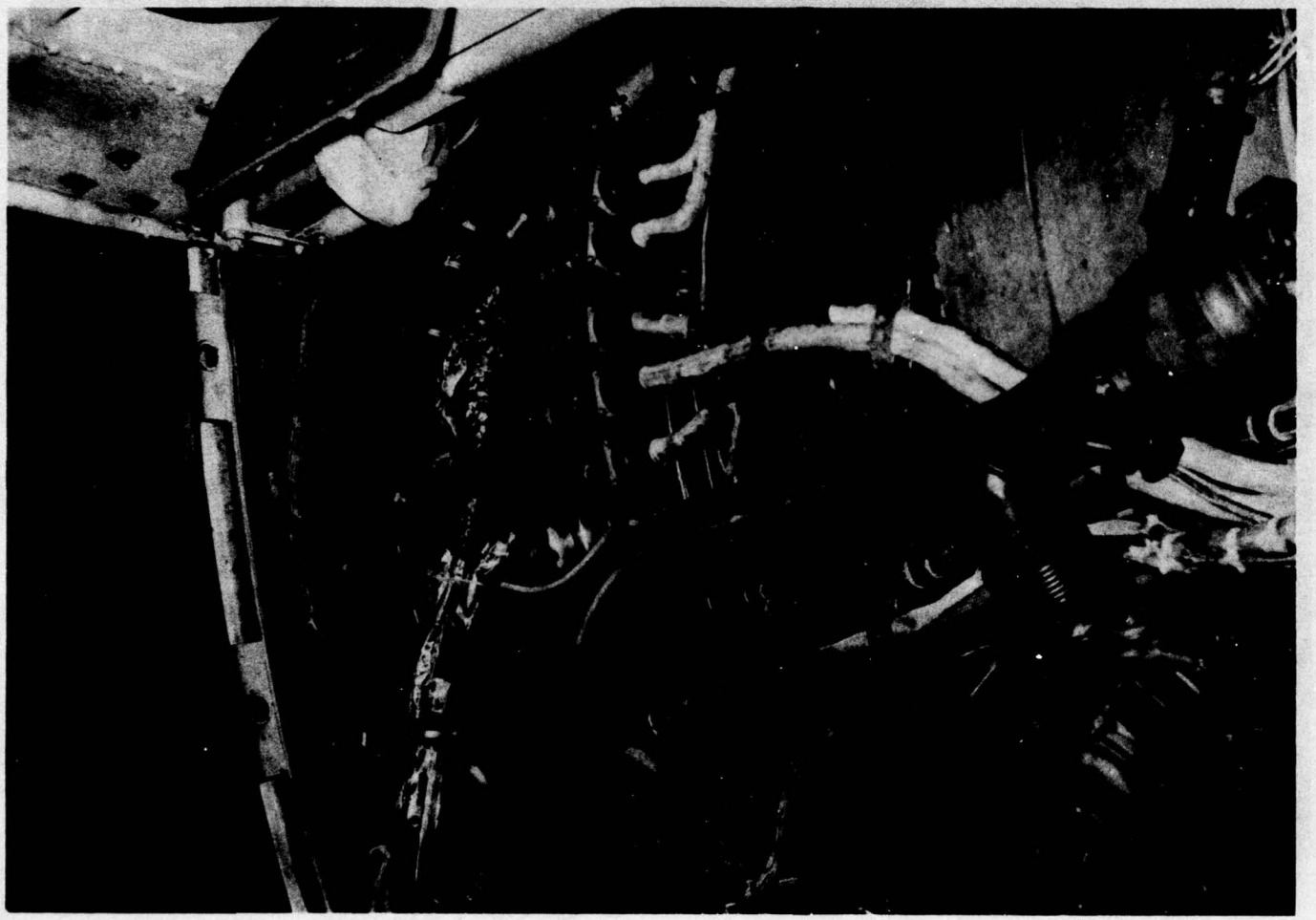

Figure 4.1-9 Signal Lines

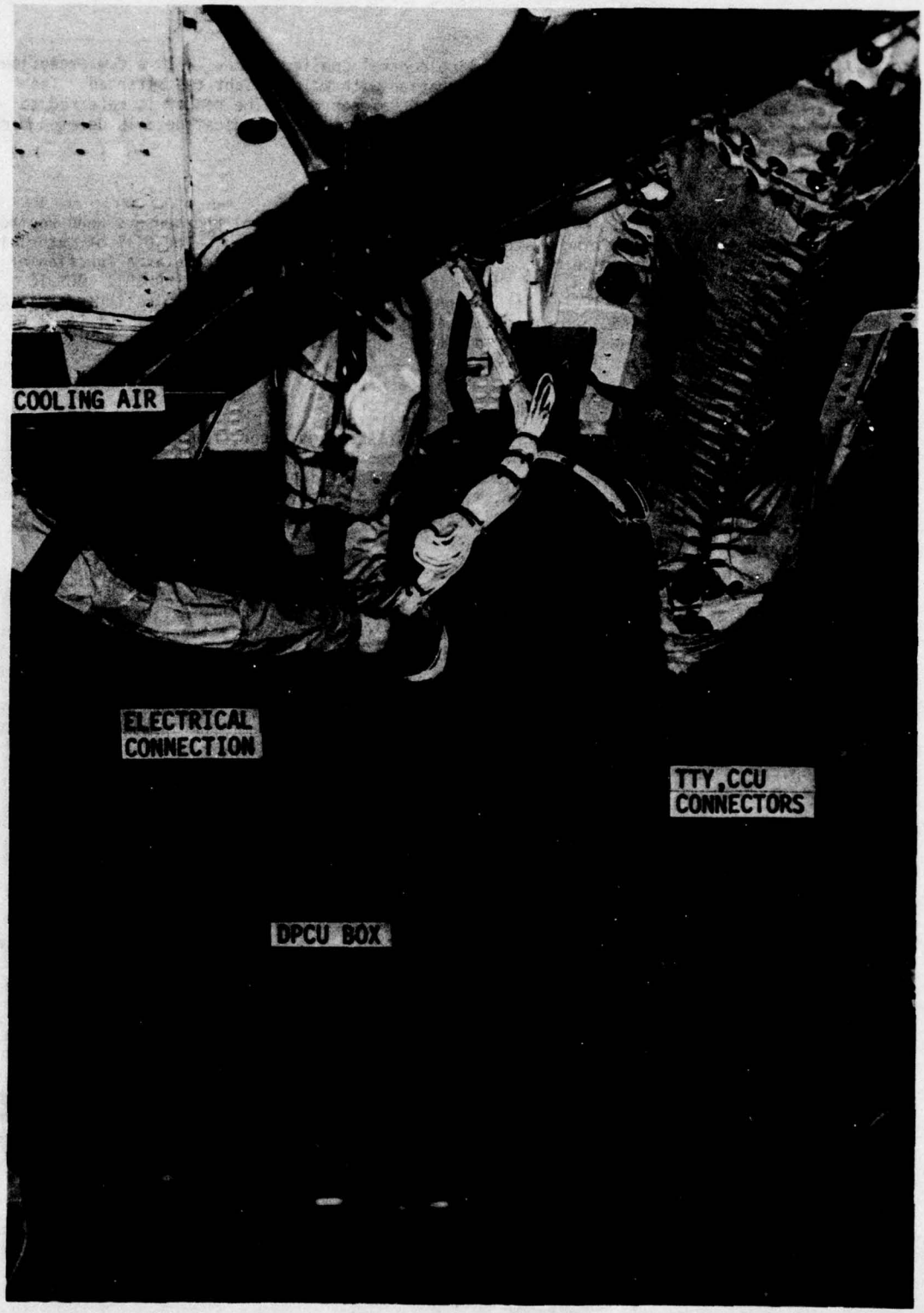

(29612)

Figure 4.1-10 DPCU Installation

4.2 BASELINE CONTROL CONFIGURATION

Figure 4.2-1, -2, and -3 depict the IPCS baseline control configuration. With a few exceptions, discussed below, this corresponds to the configuration with which flight test started. The drawings are derived from those in the Honeywell ICD, Reference 2. The reader is referred to that document for detailed schedule data and for computational and logical details deleted here in the interests of clarity.

4.2.1 Inlet Control

As described in Reference 2 (HI ICD) the hydromechanical inlet control and sensors were replaced with IPCS components. The resulting system is depicted in Figure 4.2-1. The bill of materials (BOM) inlet control consisted of open loop positioning of the spike and cone as a function of the local Mach pressure ratio (PRLM) and the duct exit Mach pressure ratio (PRDEM). BOMDIG duplicates this control. The IPCS inlet control included the BOM control plus three additional modes, A/B anticipation, AFBIAS, and distortion adjustment to inlet positioning. Of these modes, only A/B anticipation was active during the flight test program. Both the BOM control modes and A/B anticipation functioned correctly.

4.2.2 Gas Generator Control

The IPCS control is an isochronous, integral, high rotor speed governor, feedback limited by various parameters. Control errors for high rotor speed and the limiting parameters are computed and compared in the select logic. The select logic identifies the appropriate control error and inputs it to a series integrator, isochronous control, whose output is gas generator fuel flow command. The following paragraphs describe the control modules depicted in Figure 4.2-2.

4.2.2.1 N2 Governing - Loop 7

Base N2 request is a function of PLA. Provision is made to automatically set N2 request to idle in case of blowout or stall. The base N2 request is modified as a function of compressor face pressure and temperature. Different schedules are provided for dry and augmented operation. The resulting N2 request is compared to a minimum (idle) N2, scheduled as a function of airplane Mach number and compressor face total temperature, and the greater of the two is selected as requested N2. Requested N2 is differenced with actual N2 and the resulting N2 error is compensated by a first order 10 to 1 lead lag whose pole location is scheduled on burner pressure, effectively cancelling the open loop real pole associated with the high rotor. The resulting compensated error is input to the loop selector switch, see Section 4.2.2.11. A normalized N2 error, CERN2, is also generated and input to the select logic for control of the loop select switch.

4.2.2.2 Minimum Airflow - Loop 8

The minimum airflow loop is a governing loop intended to control flight idle, primarily to maintain inlet airflow above the buzz threshold. The idle N2 schedule in the N2 control is lowered relative to that in the BOM control to permit operation on the minimum airflow loop. Engine total airflow corrected at station 2 is computed based on N1 corrected to station 2, EPR, and Reynolds Index. This parameter, used elsewhere in the control, is differenced with a minimum airflow request scheduled on airplane Mach number. The resulting error is normalized for input to the select logic and multiplied by a gain scheduled on burner pressure for input to the loop select switch.

4.2.2.3 Low Compressor Exit Mach Number (Mach 22) - Loop 9

The Mach 22 loop is intended to prevent flameout during engine deceleration due to excessive fuel reduction requested by the N2 loop. Station 22 Mach number is computed from the differential to static pressure ratio at station 22 and differenced with a reference scheduled on low rotor speed corrected to station 2 and Reynolds index. A bias is provided for operation following an A/B blowout. The resulting error is normalized for use in the select logic and multiplied by a gain scheduled on burner pressure to provide a control error for input to the loop select switch.

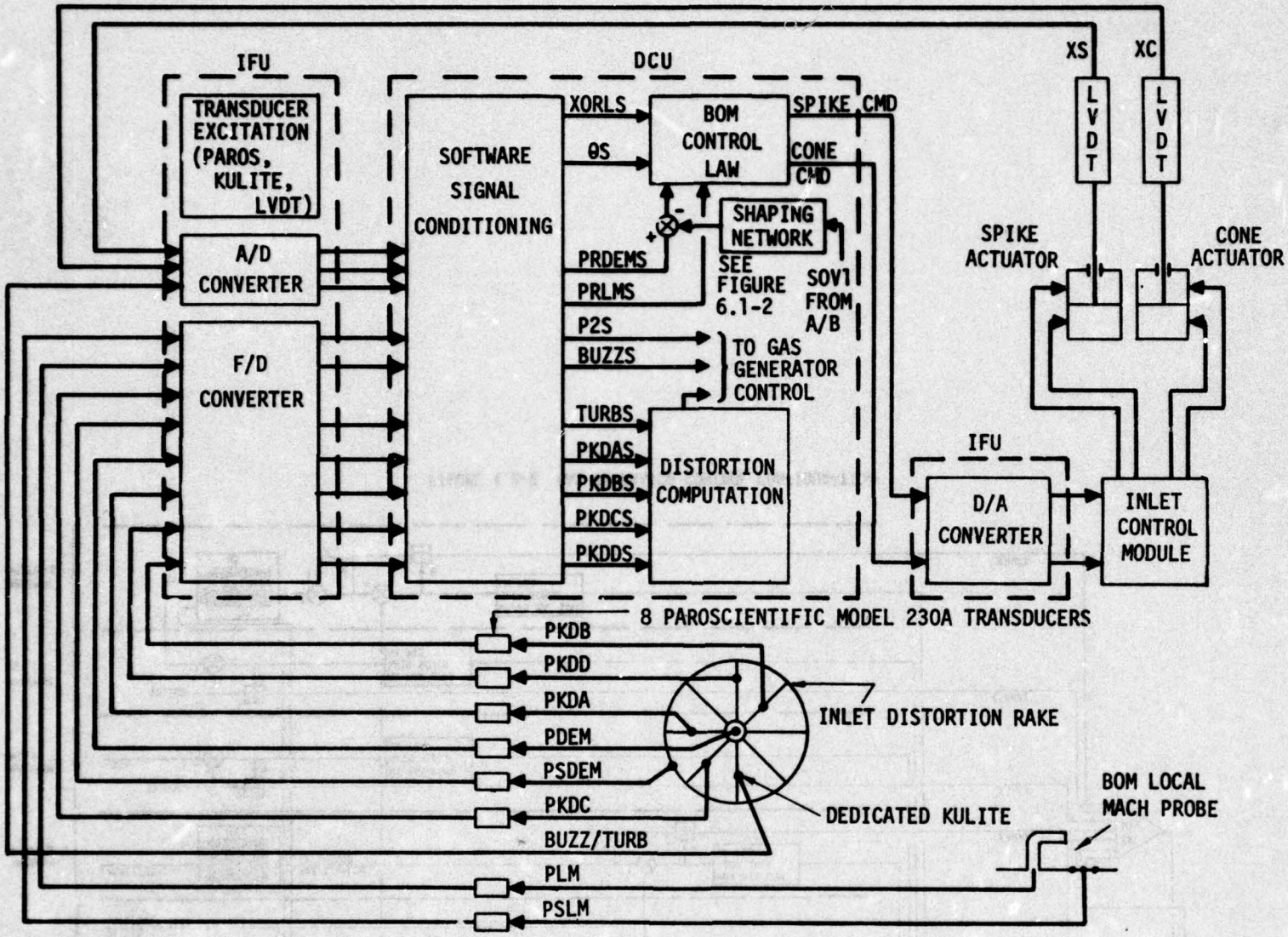

Figure 4.2-1 Inlet Control Configuration

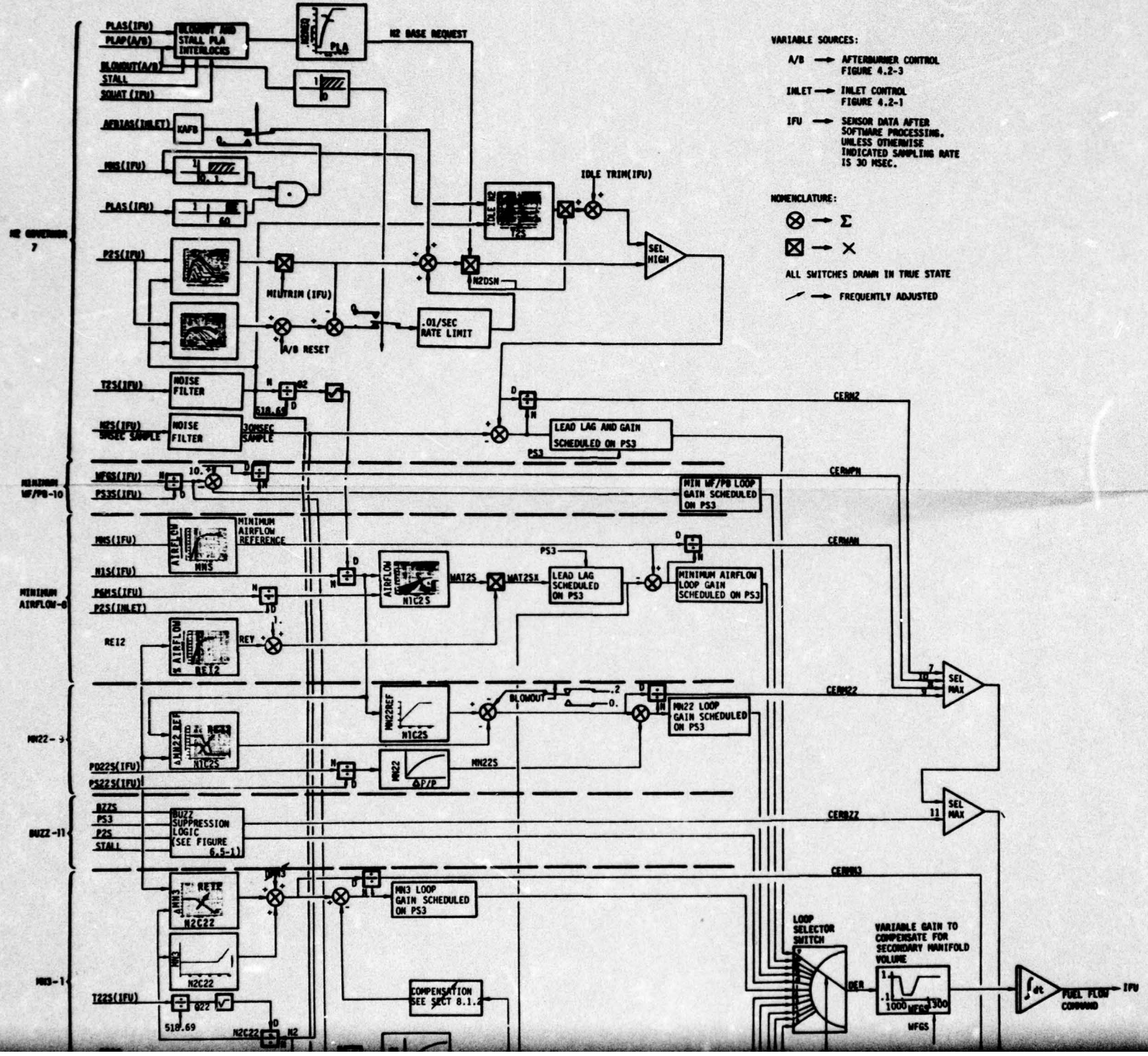
VARIABLE SOURCES:
A/B → AFTERBURNER CONTROL FIGURE 4.2-3
INLET → INLET CONTROL FIGURE 4.2-1
IFU → SENSOR DATA AFTER SOFTWARE PROCESSING. UNLESS OTHERWISE INDICATED SAMPLING RATE IS 30 MSEC.
NOMENCLATURE:
⊗ → Σ
⊠ → ×
ALL SWITCHES DRAWN IN TRUE STATE
FREQUENTLY ADJUSTED
N2 GOVERNOR 7
MINIMUM WF/PB-10
MINIMUM AIRFLOW-8
MN22-9
BUZZ-11
MN3-1
PLAS(IFU)
PLAP(A/B)
BLOWOUT(A/B)
STALL
SQUAT (IFU)
AFBIAS(INLET)
MNS(IFU)
PLAS(IFU)
P2S(IFU)
T2S(IFU)
N2S(IFU) 30MSEC SAMPLE
WFGS(IFU)
PS3S(IFU)
MNS(IFU)
N1S(IFU)
PSMS(IFU)
P2S(INLET)
RE12
PD22S(IFU)
PS22S(IFU)
BZZS
PS3
P2S
STALL
T22S(IFU)
N2 BASE REQUEST
IDLE TRIM(IFU)
SEL HIGH
N2DSN
MEUTRIM (IFU)
A/B RESET
.01/SEC RATE LIMIT
NOISE FILTER
30MSEC SAMPLE
LEAD LAG AND GAIN SCHEDULED ON PS3
CERN2
MIN WF/PB LOOP GAIN SCHEDULED ON PS3
CERWPN
MINIMUM AIRFLOW REFERENCE
LEAD LAG SCHEDULED ON PS3
MINIMUM AIRFLOW LOOP GAIN SCHEDULED ON PS3
CERWAN
MN22 LOOP GAIN SCHEDULED ON PS3
CERN22
SEL MAX
BUZZ SUPPRESSION LOGIC (SEE FIGURE 6.5-1)
CERBZZ
MN3 LOOP GAIN SCHEDULED ON PS3
CERMN3
LOOP SELECTOR SWITCH
VARIABLE GAIN TO COMPENSATE FOR SECONDARY MANIFOLD VOLUME
WFGS
FUEL FLOW COMMAND
IFU
COMPENSATION SEE SECT 8.1.2

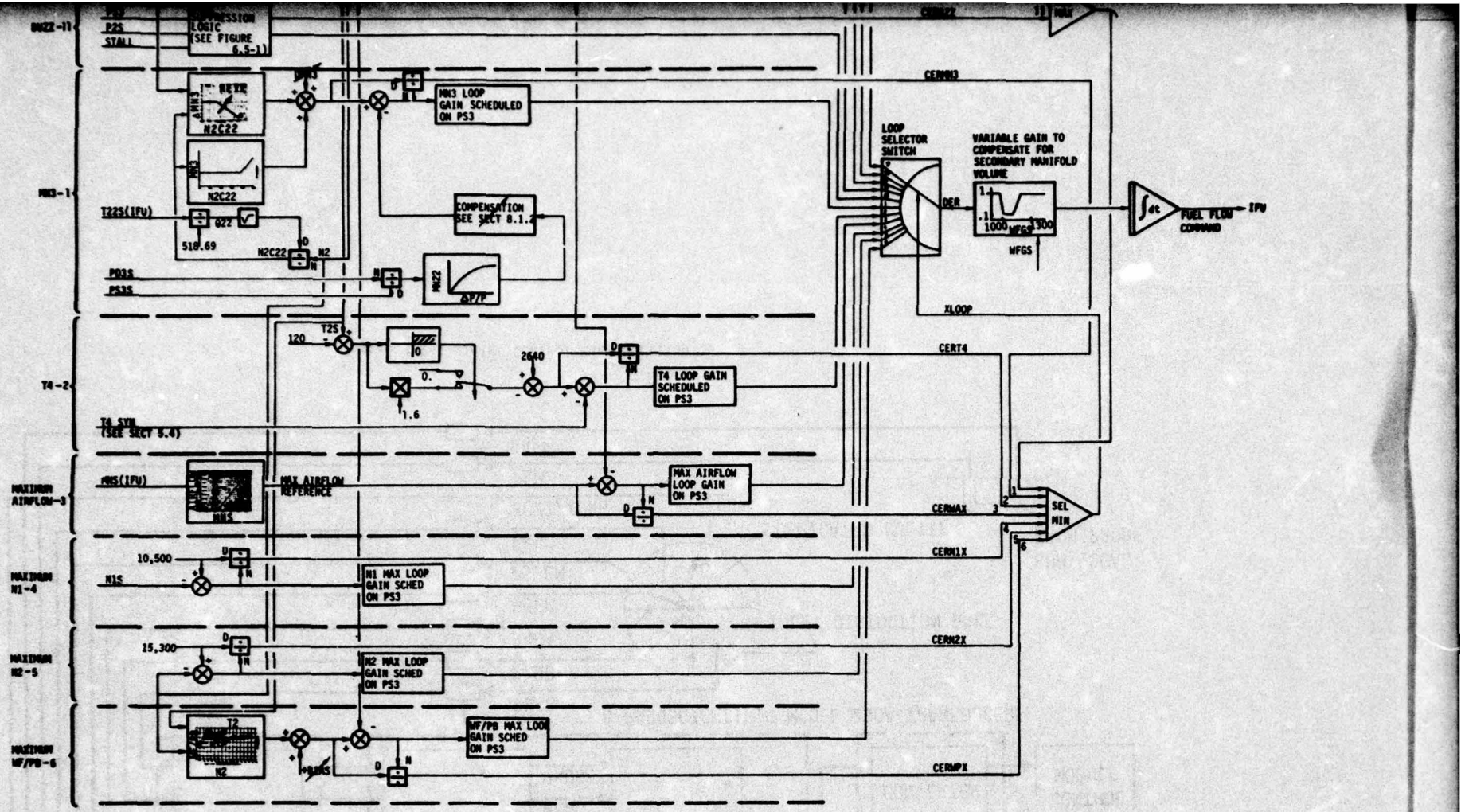

FIGURE 4.2-2 GAS GENERATOR CONTROL CONFIGURATION

4.2.2.4 Minimum Fuel Flow/Burner Pressure (Wf/Pb) - Loop 10

The minimum Wf/Pb control serves the same function as the Mach 22 control, deceleration transient limiting. The set point of 10 RU, the same as used in BOM control, is differenced with actual Wf/Pb and the resulting error processed into the select logic as in the other loops.

4.2.2.5 Buzz Loop - Loop 11

The buzz loop acts as another decel limiting loop using the logic described in Paragraph 6.5.1.

4.2.2.6 High Compressor Exit (Mach 3) - Loop 1

The Mach 3 loop, the first of six so called topping loops, limits fuel flow during acceleration transients to prevent engine (high compressor) stalls. Mach number at the high compressor exit, determined from differential and static pressure at station 3, is differenced with a reference scheduled on N2 corrected at station 22 and Reynolds index. The schedule is selected, ideally at least, to parallel the stall line with sufficient offset to prevent stalls due to controller error. In practice the baseline Wf/Pb schedule, see Section 4.2.2.11 below, prevented approach to the stall line so that operation on the MN3 loop was achieved by moving either the Wf/Pb reference or MN3 reference. The MN3 control error, once generated, is normalized and amplified in the same manner as other loop for use in the select logic.

4.2.2.7 Turbine Inlet Temperature (T4) - Loop 2

The T4 loop limits T4 during both accels and steady state operation to protect against engine overtemperature. The loop error is formed from T4 synthesized, calculated from T2, T3, WFGS, and MN3, and a T4 reference computed from the engine dynamic temperature limit, 2640°R, corrected for inlet temperature. Again, the error is processed into the select logic in the same manner as the other loops.

4.2.2.8 Maximum Airflow - Loop 3

The control limits engine airflow to prevent high airflow creating excessive inlet distortion. The maximum allowable corrected airflow scheduled on airplane Mach number is differenced with corrected airflow already computed for use in the minimum airflow loop and the resulting error is processed as indicated in Figure 4.2-2 for use in the select logic.

4.2.2.9 Maximum N1 - Loop 4

The maximum N1 loop protects engine structural integrity by controlling N1 to the T.O. limit. N1 is differenced with the T.O. limit, 10,500 RPM, and processed for use in the select logic. XPOLE compensation on the control error stabilizes the loop.

4.2.2.10 Maximum N2 - Loop 5

This loop is identical to maximum N1 except N2 is controlled to its T.O. limit of 15,300 RPM. Both the N1 and N2 max loops are overdamped by design to prevent overspeeds.

4.2.2.11 Maximum Fuel Flow/Burner Pressure (Wf/Pb) - Loop 6

The BOM control limits Wf/Pb open loop during engine accels to prevent stalls and limit transient turbine inlet temperature. The IPCS control uses the BOM schedules in a closed loop mode. The Wf/Pb reference is scheduled on N2 and T2 and shifted by a fixed bias. The bias was used to match IPCS and BOM results and shift the Wf/Pb maximum loop relative to the MN3 loop. The reference is differenced with sensed Wf/Pb and the error processed into the select logic in the same manner as the other loop errors.

4.2.2.12 Select Logic

The select logic determines which of the 11 loop errors commands engine fuel flow. The selection is based on the relative magnitude of the normalized uncompensated control errors. The first select maximum compares the N2 normalized error to the normalized errors of the bottoming loops in order to establish a lower error constraint. This error is then compared to that for buzz, see Section 6.5.1. The resulting lower constraint is compared to the topping loop errors in the select minimum checking for upper contraints on the control. The loop selected by this process is identified by number and output as XLOOP. XLOOP controls the selector switch to set the control error, DER, equal to the error associated with the selected loop.

4.2.2.13 Fuel Flow Command

The control error, DER, is passed through a variable gain, reducing gain by an order of magnitude in the secondary manifold transition region in order to improve stability margin, to the fuel flow command integrator. Fuel is delivered through two sequenced manifolds. The primary flows at all delivery rates, the secondary transistions on between 1000 and 1300 pph. The volume of the secondary manifold creates a variable time delay in manifold response when fuel flows are in the 1000 to 1300 pph range. The variable gain was removed, in order to improve accel performance, without incurring any significant stability penalty. When the DPCU is not engaged the output of the fuel command integrator is set equal to the current sensed fuel flow to provide smooth engage transients.

4.2.3 Afterburner Control

The afterburner control maintains suppression, P6M/P2, through modulation of zone fuel flows and nozzle area. Fuel flow and nozzle area are open loop scheduled on PLAP, a rate limited and logically constrained variable linearly related in steady state to PLA. Suppression errors relative to the nominal map are corrected by a proportional plus integral control modulating nozzle area, or fuel flow if nozzle area is saturated. Prefill and sequencing logic, depending upon the fixed rate advance of PLAP, opens zone control solenoids in anticipation of entering the relevant zone during snap accels, thus permitting more rapid transients.

4.2.3.1 Light Off and Blow Out Detection

Differencing the airflow request, scheduled on P6M/P2, with corrected airflow and normalizing by the request creates a normalized airflow error W2ERQ. The derivative of this variable is used as an indicator of sharp A/B perturbations, light off and blow out, by comparison to references scheduled on fan corrected speed. LOPERM, the light off indicator, is tripped by the W2ERQ pulse and latches provided the zone 1 solenoid, SOV1, is on. BOTRIG, the blowout indicator, is tripped by the W2ERQ pulse, provided LOPERM is true, and latches if either SOV1 or ABPERM, see Section 4.2.3.2, is true.

4.2.3.2 PLAP Control Logic

The intermediate variable PLAR, from which PLAP is generated, is held equal to zero by ABPERM, until gas generator operations approach steady state mil. ABPERM is set if N2 is within 5% of set point, the control is operating on a steady state governing loop, and PLA is greater than 69°. Setting ABPERM permits PLAR and thus PLAP, through the rate limited tracking lag, to advance to 1° opening the zone 1 solenoid and initiating lightoff provided BOTRIG is false. LOPERMD follows LOPERM by a .24 second delay to permit the nozzle to unlock. LOPERMD going true switches the PLA input from 1. to PLA-69° and engages the prefill and sequence logic which sequences PLAP to 51° subject to various constraints. If at any time BOTRIG is set PLAP retards to 0. at 51°/sec due to the combined action of BOTRIG and LOPERMD. Note that LOPERMD introduces a delay on the 0 to 1 transition only.

The prefill logic computes the time required to fill the zone manifold based on the engine airflow and the fuel/air schedules and, recognizing that DPLAP is 15°/second, computes the zone advance angle to permit prefilling the manifold. The logical variables KZ2 and LZ2 identify respectively that PLAP has passed the zone threshold, and that PLAP or PLAR has passed the zone threshold and that PLAP plus the zone advance has passed the zone threshold.

The sequencing logic opens the zone 2 solenoid if LZ2 is true then checks KZ2 to determine whether the solenoid was opened due to prefill requirements or not. If prefill requirements are not involved PLAPA is advanced to 15.3° if PLAP is greater than or equal to 15.3° or set equal to PLAR if PLAR is within zone 2. If prefill requirements are involved, KZ2,false, the elapsed time filling zone 2, Z2T, is computed by integration and the logical variable DR is set if Z2T is greater than the manifold fill time and PLAP is up to the zone 2 threshold. Until this test is passed PLAPA holds at or below 7.6° (zone 1). Once the test is passed PLAPA is allowed to respond to PLAR. If LZ2 is false the zone solenoid command is reset and MFT2, FIOF11, and Z2T are initialized and PLAPA is limited to 7.6°.

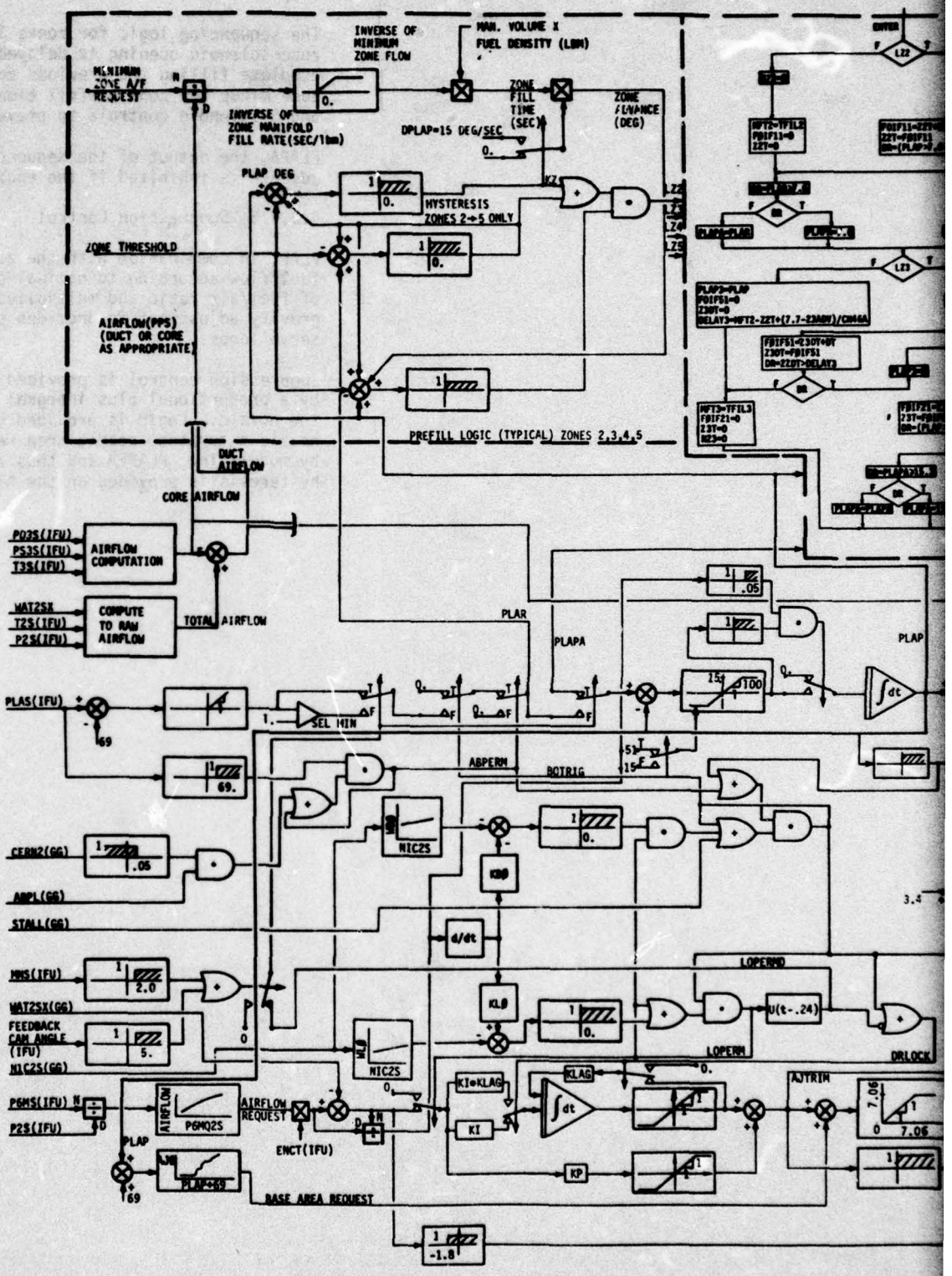
INVERSE OF MINIMUM ZONE FLOW
MAN. VOLUME X FUEL DENSITY (LBM)
MINIMUM ZONE A/F REQUEST
INVERSE OF ZONE MANIFOLD FILL RATE(SEC/lbm)
DPLAP=15 DEG/SEC
ZONE FILL TIME (SEC)
ZONE ADVANCE (DEG)
PLAP DEG
HYSTERESIS ZONES 2→5 ONLY
ZONE THRESHOLD
AIRFLOW(PPS) (DUCT OR CORE AS APPROPRIATE)
PREFILL LOGIC (TYPICAL) ZONES 2,3,4,5
DUCT AIRFLOW
CORE AIRFLOW
P03S(IFU)
PS3S(IFU)
T3S(IFU)
AIRFLOW COMPUTATION
WAT2SX
T2S(IFU)
P2S(IFU)
COMPUTE TO RAW AIRFLOW
TOTAL AIRFLOW
PLAR
PLAPA
PLAP
PLAS(IFU)
SEL MIN
ABPERM
BOTRIG
NIC2S
CERN2(GG)
AMPL(GG)
STALL(GG)
d/dt
LOPERMD
MNS(IFU)
WAT2SX(GG)
FEEDBACK CAM ANGLE (IFU)
N1C2S(GG)
LOPERM
DRLOCK
AJTRIM
P6MS(IFU)
P2S(IFU)
P6MQ2S
AIRFLOW REQUEST
ENCT(IFU)
KI*KLAG
KLAG
KI
KP
PLAP+69
BASE AREA REQUEST

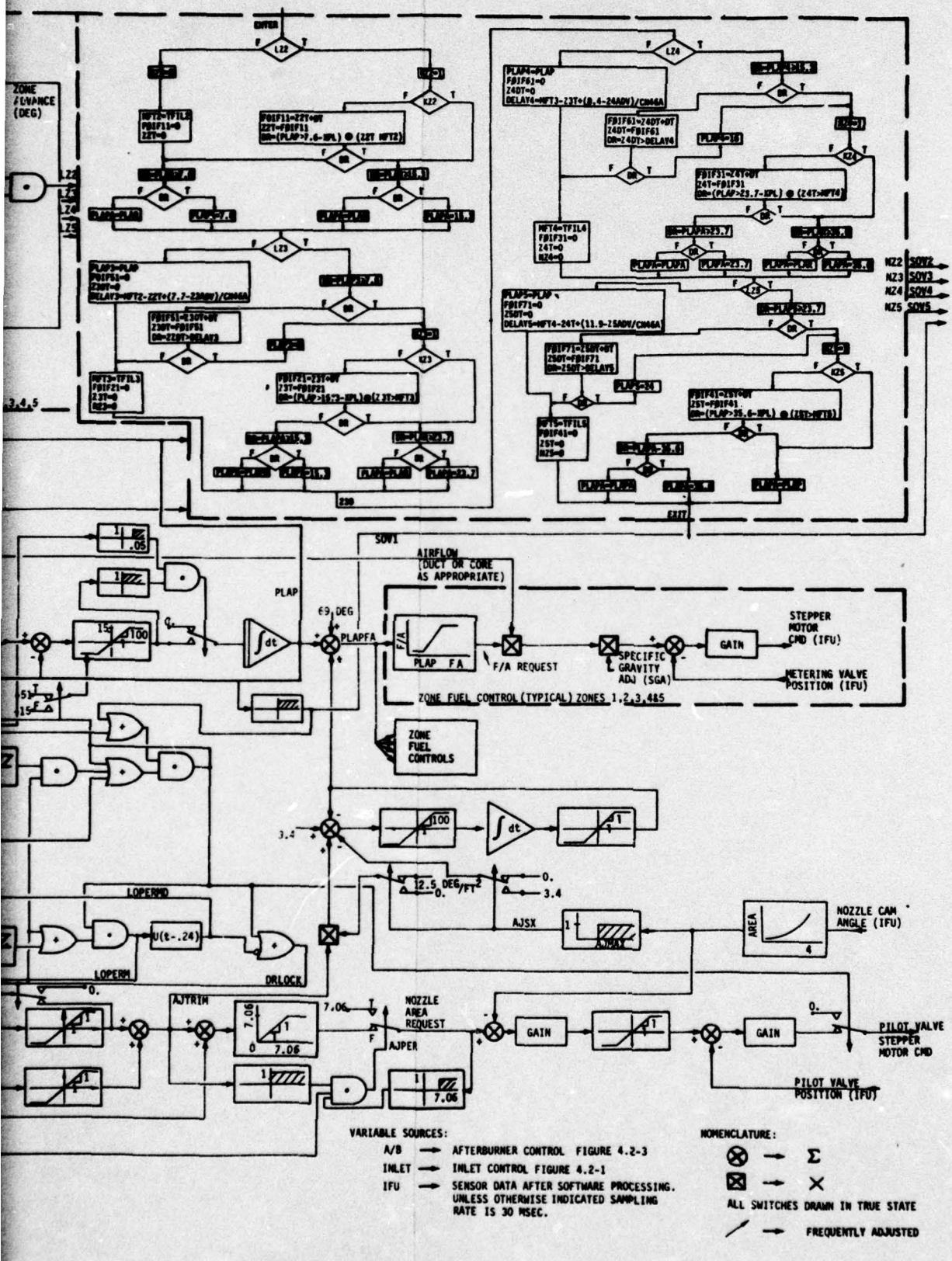

VARIABLE SOURCES:

A/B → AFTERBURNER CONTROL FIGURE 4.2-3

INLET → INLET CONTROL FIGURE 4.2-1

IFU → SENSOR DATA AFTER SOFTWARE PROCESSING. UNLESS OTHERWISE INDICATED SAMPLING RATE IS 30 MSEC.

NOMENCLATURE:

⊗ → Σ

⊠ → ×

ALL SWITCHES DRAWN IN TRUE STATE

↗ → FREQUENTLY ADJUSTED

FIGURE 4.2-3 AFTERBURNER CONTROL CONFIGURATION

The sequencing logic for zones 3, 4, 5, is similar to that for zone 2 except that the zone solenoid opening is delayed by an amount, DELAY i, equal to the time required to complete filling the previous zone plus the time for PLAP to advance across the previous zone minus the zone prefill time. One degree hysteresis is provided on Zone 2, 3, 4, and 5 solenoid controls to prevent limit cycles at the zone boundaries.

PLAPA, the output of the sequencing logic, drives PLAP through a rate limited lag. PLAP advance is inhibited if the engine is oversuppressed, W2ERQ > .05.

4.2.3.3 Suppression Control

PLAP, in combination with the zone solenoids, opens the exhaust nozzle and increases A/B fuel flow according to nominal open loop schedules. Fuel commands are scheduled in terms of fuel/air ratio and multiplied by core or duct airflow as appropriate. A specific gravity adjustment is provided prior to the error summation for the fuel metering valve servo loops.

Suppression control is provided by control of airflow error,WA2ERR. WA2ERR is conditioned by a proportional plus integral network and added to the base area request to modulate the nozzle. Logic is provided to reset the integrator during dry operation. When the nozzle saturates, nozzle area request greater than AJ MAX suppression control is provided by modulating PLAPFA and thus zone fuel flow through a rate limited lag. One degree hysteresis is provided on the AJMAX comparison to prevent limit cycles.

5.0 INSTRUMENTATION

Two different data sources were used throughout the flight test program these were the DPCU and NASA instrumentation largely originating with the baseline flight test.

5.1 NASA INSTRUMENTATION

5.1.1 Airplane

A primary purpose of the NASA instrumentation was to determine the airplane condition for each test event. Table 5.1-1 lists the airplane variables recorded. In addition to the items on the list, various power supply voltages were monitored as well as electronics temperatures and the main airplane 400 Hz power.

5.1.2 Inlet

The inlet instrumentation consisted of distortion measured by a 40 probe high response compressor face rake system. Inlet geometric position was measured by the DPCU. Figure 5.1-1 shows the location of the compressor face probes. Each probe has a closed coupled Kulite ΔP transducer. One transducer is isolated from the NASA instrumentation system for turbulence and buzz sensing. It is both energised and monitored by the DPCU. The remaining 39 transducers are energised by NASA instrumentation, their outputs are recorded for offline distortion computation and are input to an on-line, on board distortion computer which calculates and outputs ring KD for each of the five (5) rings and total KD (reference 3).

The rake is designed to compensate for the transducer zero shift due to temperature (Reference 4). The rake mechanically switches the reference pressure to both sides of the transducer to provide zero ΔP. The zero correction is applied to the pressure levels in the off-line data processing program and in the distortion computer. The rake zero was normally operated every minute for approximately 2 seconds using an automatic zeroing system. The pilot also had the capability of manually activating the rake zero.

5.1.3 Engine

The airplane previously had been instrumented for baseline testing in which the DPCU was not available as a source of engine data. Thus a substantial amount of NASA engine instrumentation was available. Table 5.1-2 lists the engine variables being measured. The only instrumentation on the right hand engine was N1, N2, and EPR.

5.1.4 Exhaust Profile Rake

As part of the noise testing (Section 6.6) the exhaust total pressure and total temperature profiles were measured using a NASA/LeRC rake. The rake mounted behind the airplane (Figures 5.1-2 and 5.1-3) and traversed across the nozzle. Most of the measurements were made at the vertical centerline. Measurements were also made at +6 inches from the centerline. The rake as used at NASA/LeRC consisted of a gas sample probe, three unshielded rhodium/iridium thermocouples, and a total pressure probe. In an effort to provide more accurate total temperature data a platinum shield was placed over one of the thermocouples and a shielded platinum/iridium thermocouple was placed in the gas sample probe (Figure 5.1-4). As expected,neither of the shielded thermocouples functioned for long, but data were recorded to use as a calibration for the unshielded thermocouples. Heat damage occurred to all the probes (Figure 5.1-5). The short probe above the gas sample probe is the total pressure probe. The unshielded thermocouples at the top and bottom continued to function throughout the test as did the total pressure probe.

5.2 CONTROL INSTRUMENTATION

The DPCU serves as a large source of data on inlet and engine operation. In addition to the output of control sensors, the DPCU was capable of providing calculated variables from the controller. These data were used as the major information for control evaluation. A total of 59 variables were output at 20 samples per second (SPS). Table 5.2-1 lists the variables for the early flights. Those variables listed as sensed are the output of control sensors while the remainder are calculated in the DPCU. Certain variables are different between the BOMDIG and IPCS control modes as identified in the table. During the later flights it became necessary to modify the list of data output from the DPCU for special testing, but most of the initial 59 variables were output for the entire test program. In addition to 59 variables 11 channels of analog data were available. The analog data were updated in the DPCU at 33 SPS and recorded on the PCM main com at 200 SPS. These data were used primarily for online stripouts. The variables output on the analog channels were controlled with the CMU sense switches. The variable list associated with each sense switch was changed periodically to provide data of interest for a particular test.

Table 5.1-1 NASA AIRPLANE INSTRUMENTATION

Angle of Attack, α

Yaw Angle, β

Altitude

Airspeed

Freestream Total Pressure

Freestream Total Temperature

Wing Sweep

Fuel Quantity - Forward, Aft, Total

Table 5.1-2 NASA ENGINE INSTRUMENTATION

L/H Engine

Low Compressor Exit Static Pressure, PS22
High Compressor Exit Static Pressure, PS3
Turbine Discharge Pressure, P6M
Power Level Angle, PLA
Low Rotor Speed, N1
High Rotor Speed, N2
Engine Pressure Ratio, EPR
Engine Fuel Flow, Wfe
Total Fuel Flow, Wft
Nozzle Area, Aj
Compressor Face Temperature*, T2
High Compressor Exit Temperature*, T3
Computed Turbine Inlet Temperature*, T4
Turbine Exit Temperature*, T5
Fuel Temperature
7th, 12th, and 16th Stage Bleed Position
A/B Fuel Manifold Pressures

R/H Engine

Engine Pressure Ratio, EPR
Low Rotor Speed, N1
High Rotor Speed, N2

*From the BOM Harness

Table 5.2-1 DPCU OUTPUT VARIABLES

Sensed Low Rotor Speed, N1S
Sensed High Rotor Speed, N2S
Sensed Turbine Exit Pressure, P6MS
Sensed High Compressor Exit Static Pressure, PS3S
Sensed High Compressor Exit Total Pressure, P3S
Sensed High Compressor Exit Differential Pressure (P-PS)3S
Sensed Low Compressor Exit Static Pressure, PS22S
Sensed Low Compressor Exit Total Pressure, P22S
Sensed Low Compressor Exit Differential Pressure (P-PS)22S
Sensed High Compressor Exit Total Temperature, T3S
Commanded Fuel Flow, WFG (Channel not used in BOMDIG)
Sensed Compressor Face Total Temperature, T2S
Sensed Low Compressor Exit Total Temperature, T22S
Sensed Transducer Box Temperature, TJBS2A
Sensed Nozzle Area Feedback Pulley Position, AJPS
Sensed Main Fuel Valve Position, WFGS
Sensed A/B Metering Valve Positions (5 Zones), WFZ1-WFZ5
Sensed Nozzle Servo Valve Position, AJPSV
Sensed Power Lever Angle, PLAS
Sensed Distortion Pressures (4), PKDAS-PKDDS
Sensed DEM Total Pressure, PDEMS
Sensed DEM Static Pressure, PSDEMS
Sensed LM Total Pressure, PLMS
Sensed LM Static Pressure, PSLMS
Sensed Spike Position, XORLS
Sensed Cone Position, THETAS
Buzz Indicator, IFU BUZZ
Commanded Spike Position, SPKCOM
Commanded Cone Position, CONCOM
Commanded Main Fuel Flow Rate of Change, DER (Commanded Fuel Flow, WFG in BOMDIG)
High Compressor Exit Mach No., MN3S (Δ P/P in BOMDIG)
Low Compressor Exit Mach No., MN22S (Δ P/P in BOMDIG)
Steady-State Distortion, ZKDS (Not Available in BOMDIG)
Airflow Bias, AFBIAS (Not Available in BOMDIG)
Compressor Face Corrected Airflow, WAT2SX (Approximate Corrected Flow in BOMDIG)
Turbulence, TUS
Control Loop Number, XLOOP (Not Available in BOMDIG)
Airplane Mach Number from CADC, MNS
Angle of Attack from CADC, ALPHAS
Discrete Word #1, DISO1
Discrete Word #2, DISO2
Discrete Word #3, DISIN1
Synthesized Turbine Inlet Temperature, T4SYN (Not Available in BOMDIG)
Distortion Tolerance, MAXTOL (Not Available in BOMDIG)
Compressor Face Total Pressure, P2S
Power Supply Tolerance Flags, DVT1
Transducer Failure Flags, DVT2
Total Afterburner Fuel Flow, WFAB
Corrected Low Rotor Speed, N1/ $\sqrt{\theta 2}$
Corrected High Rotor Speed, N2/ $\sqrt{\theta 22}$ (Corrected to Station 2 in BOMDIG, N2/ $\sqrt{\theta 2}$)
Gas Generator Ratio Units, WFGS/PS3
Rumble Detector, IFU RUMBLE

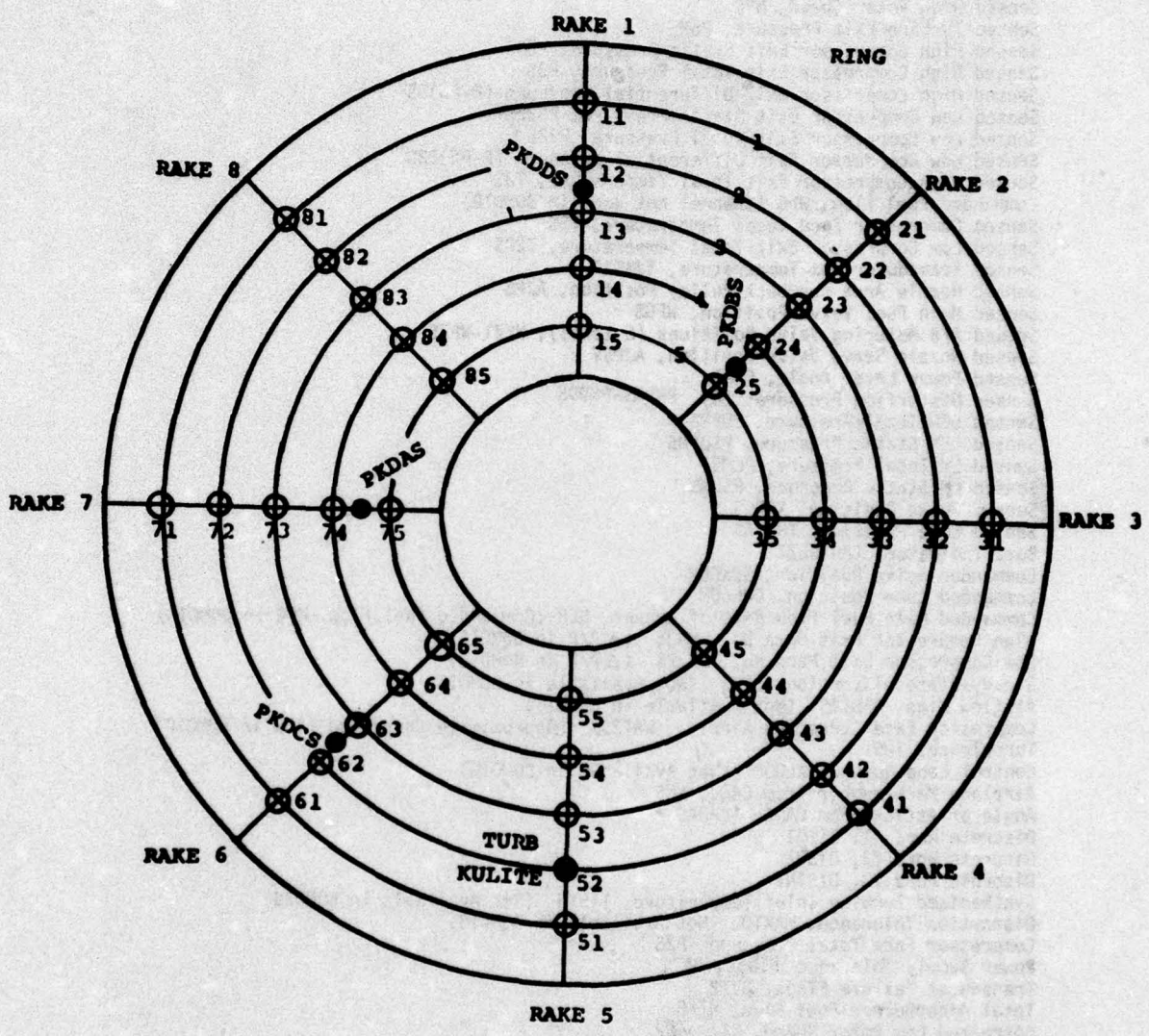

View Looking Downstream

Figure 5.1-1 Compressor Face Distortion Rake

(29627)

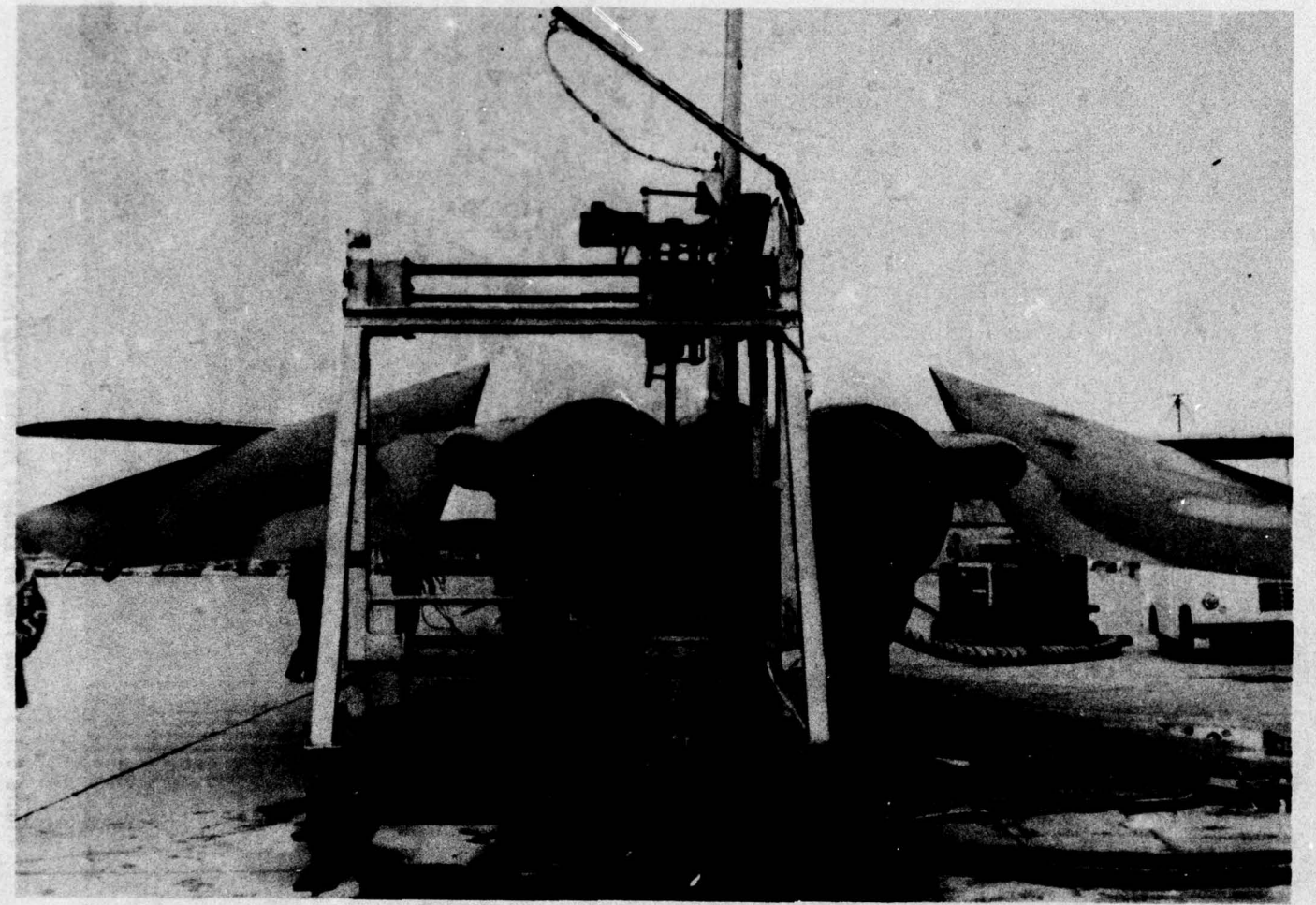

Figure 5.1-2 Aft View of Exhaust Profile Rake Installation

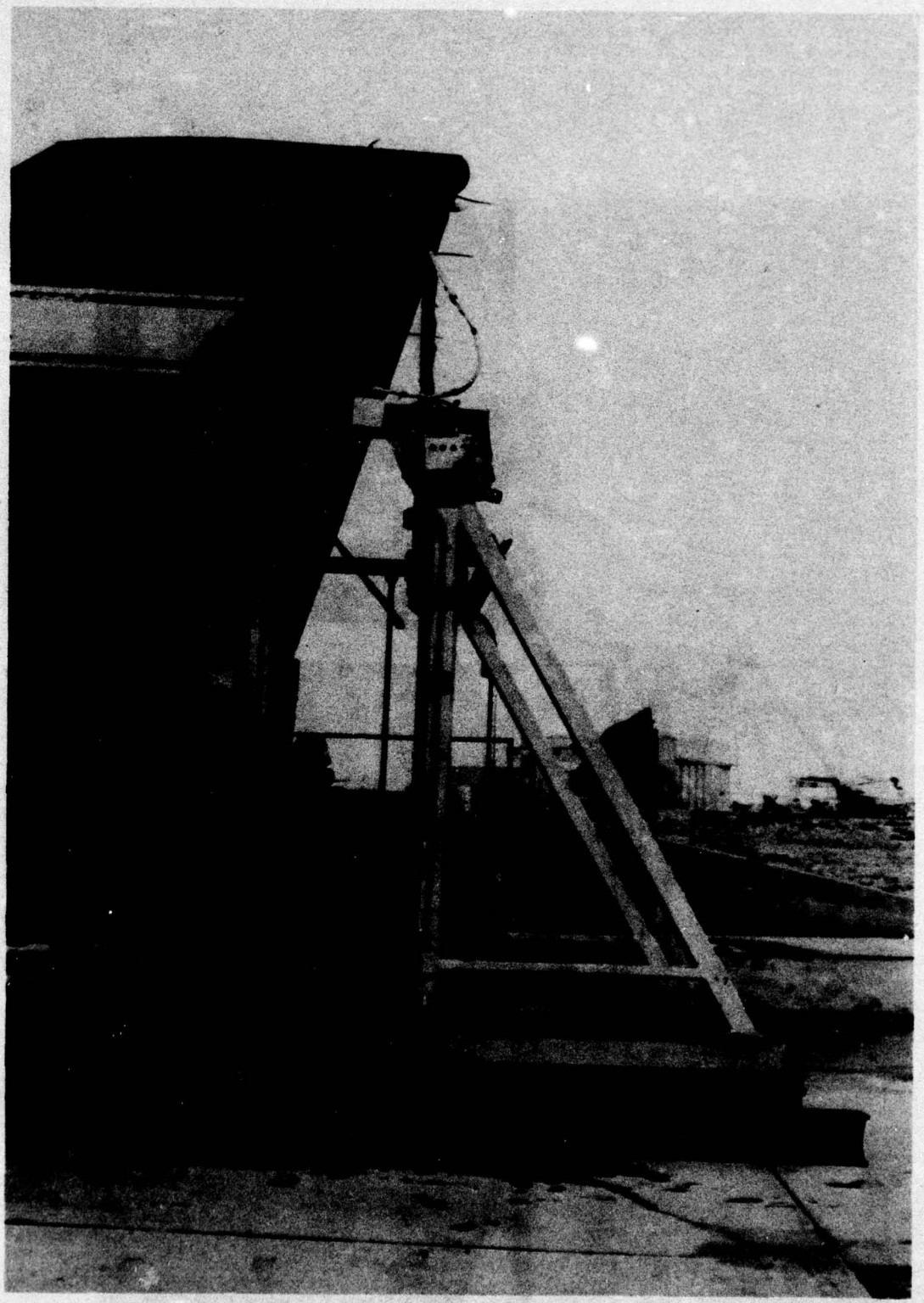

(29624)

Figure 5.1-3 Side View of Exhaust Profile Rake Installation

(30060)

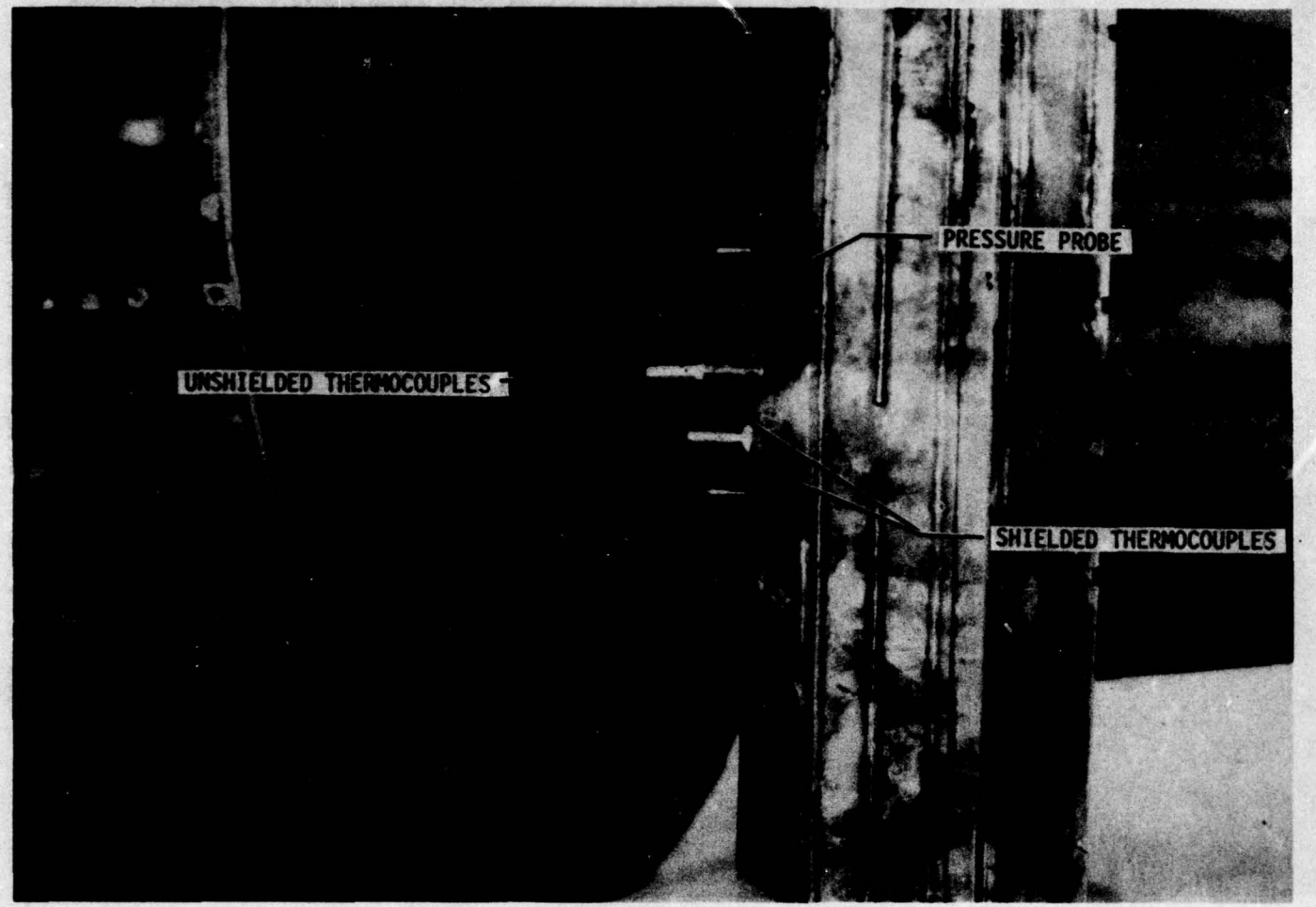

Figure 5.1-4 Exhaust Survey Probes Before Testing

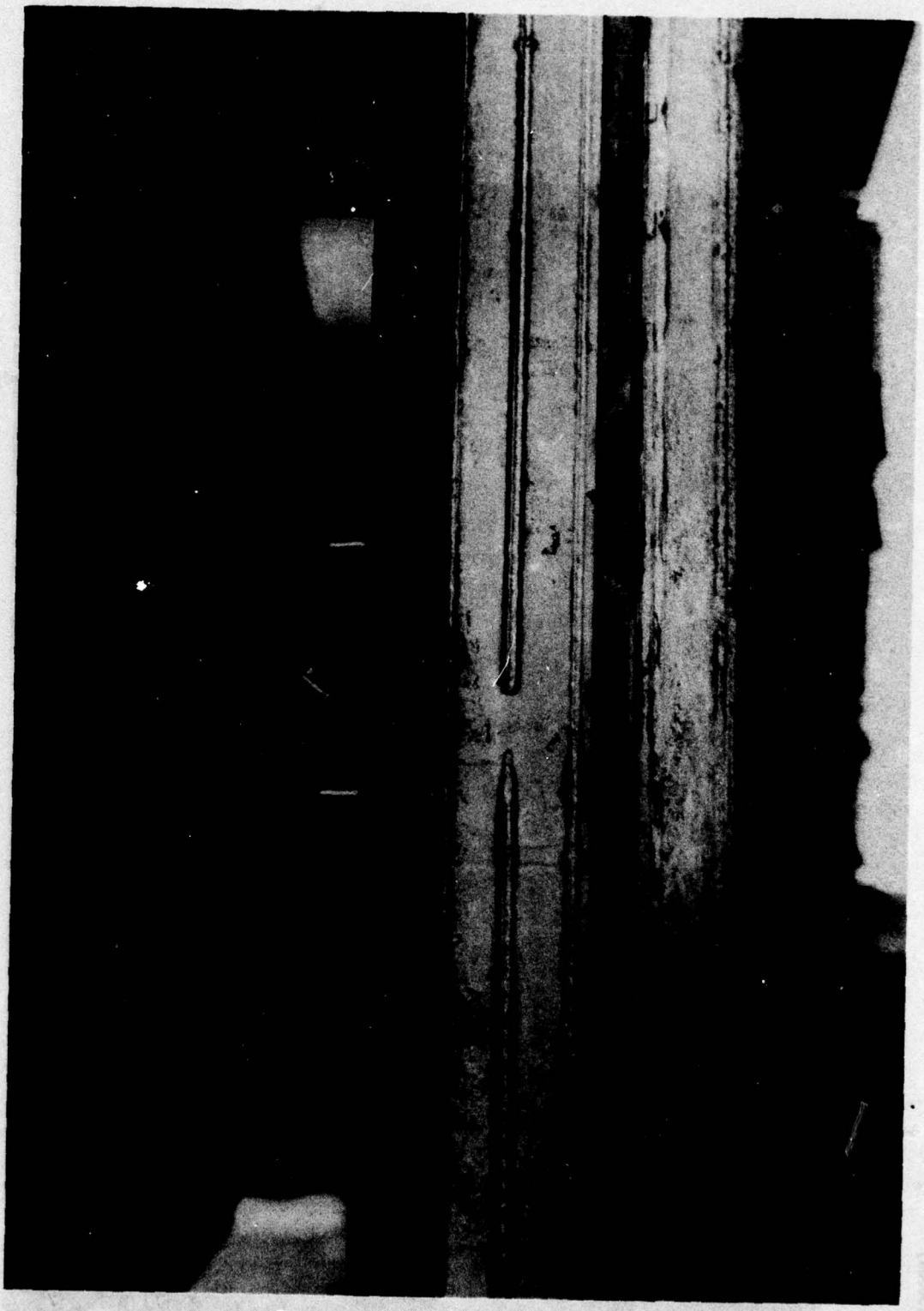

(29622)

Figure 5.1-5 Exhaust Survey Probes After Testing

5.3 DATA ACQUISITION AND PROCESSING

Two different frequency response ranges of data were required. High response (1000 Hz) inlet distortion data were recorded using an FM multiplex system and processed by Boeing. Lower response data, largely less than 10 Hz, were recorded using a NASA PCM system. These data were processed both by NASA and the contractors.

5.3.1 Data Acquisition

The majority of the data were recorded using the PCM system. Only the compressor face pressures and the outputs of the distortion computer were recorded using the FM system. Table 5.3-1 shows the FM channel assignments. Both PCM and FM data were recorded on a single AR700 tape recorder with the PCM data recorded on tracks 5 and 7 and time code on track 3. All of the data recorded on FM were also recorded on PCM to provide quicker turnaround of information not requiring high frequency response. Figure 5.3-1 illustrates the data flow.

The DPCU data were recorded on the PCM. Because the DPCU data are 16 bit words and the PCM system is 10 bit, each DPCU word was split into two PCM words with the other two bits serving as sync bits. The interface between the DPCU and the PCM system was provided by a NASA interface box built specifically for this purpose. This interface is described in Reference 6. A few problems developed during the initial checkout of the PCM interface (Reference 5), but no major changes to the system hardware were required. The analog channels were used primarily for on-line stripouts to evaluate system operation. During the ground runs the analog channels were available directly through the use of the TSU GSE Monitor Panel.

On all the flights and in general during the ground runs, the PCM data were recorded on a second ground based tape recorder in addition to the on-board recorder to serve as a backup in the event of on-board recording problems.

5.3.2 On-Site PCM Processing

The PCM data served two purposes on-site. During a flight the data were telemetered to the ground, converted from digital to analog signals and displayed on stripchart recorders and lights for on-line monitoring of the flight. After the flight the data were decommutated and processed to produce printed data and tapes for off-site processing. Figure 5.3-2 illustrates this procedure.

The on-line display of data consisted of 14-8 channel stripchart recorders, 4 in the control room and 10 in an adjoining room. This provided good visibility of the operation of the engine and controller. Because the DPCU data were recorded as two 8 bit words per DPCU work, only the most significant or least significant 8 bits could be displayed on a single channel. In addition to the stripchart display, lights were used to display discrete data. A panel was used to display the CMU lights and a series of lights showed the position of the various solenoids, sensor failure indicators, and the IPCS loop indicator, XLOOP.

The processing of digital data required a series of separate steps to be completed in sequence. The on-line stripouts from the flight were used for data editing.

The data request included the times of interest and desired sample rates. The data tape, recorded during the flight, was processed by the same decommutation equipment that is used during the flight for the stripouts. This processing produced a tape containing data for the specified time intervals in a format that was compatible with the CDC CYBER computer. This step at times created some delay due to interference between the need for the equipment for flight support and data processing.

The formatted data tape was run through a calibration program using a combination of pre-selected calibration curves and data from the pre- and post-flight calibration of NASA transducers. This program produced two engineering unit tapes - a 9 track tape for use at DFRC and a 7 track tape for processing at Boeing.

The last step in the process was to run the program to generate the printed data. Initially an existing NASA program was used to print the data. After flight 14, the Boeing transient data processing program (para 5.3.3) was rewritten to be compatible with the NASA system. This program reduced the number pages of printout by more than 40% and provided an output format more compatible with the desired use of the data.

Table 5.3-1 FM CHANNEL ASSIGNMENTS

Tape Recorder:
Type Ampex AR700
14 Data tracks
15 inch-per second
1.5 hr recording time

PCM System
Serial Output to tape on tracks 5 and 7
Time Code Track 3
80 Channels per frame
10 bit per word
160 K bit rate

PARAMETER	VCO CENTER FREQ.	BAND EDGE	AR700 Tape CH
PCF011	32 kc	28/36kc	1
PCF021	48	44/52kc	
PCF031	64	60/68kc	
PCF041	80	76/84kc	
PCF051	96	92/100kc	
PCF061	32 kc		14
PCF081	48		
PCF081	64		
PCF012	80		
PCF022	96		
PCF032	32 kc		12
PCF042	48		
PCF052	64		
PCF062	80		
PCF072	96		
PCF082	32 kc		10
PCF013	48		
PCF023	64		
PCF033	80		
PCF043	96		
PCF053	32 kc		8
PCF063	48		
PCF073	64		
PCF083	80		
PCF014	96		
PCF024	32 kc		6
PCF034	48		
PCF044	64		
PCF054	80		
PCF064	96		
PCF074	32 kc		4
PCF084	48		
PCF015	64		
PCF025	80		
PCF035	96		
PCF045	32 kc		2
PCF055	48		
PCF065	64		
PCF075	80		
PCF085	96		
KD	32 kc		9
KD-a	48		
KD-b	64		
KD-c	80		
KD-d	96		
KD-e	112		
Peak Detector	32	28/36kc	11
Reference Pressure (0 to 36 psia)	48	44/52kc	

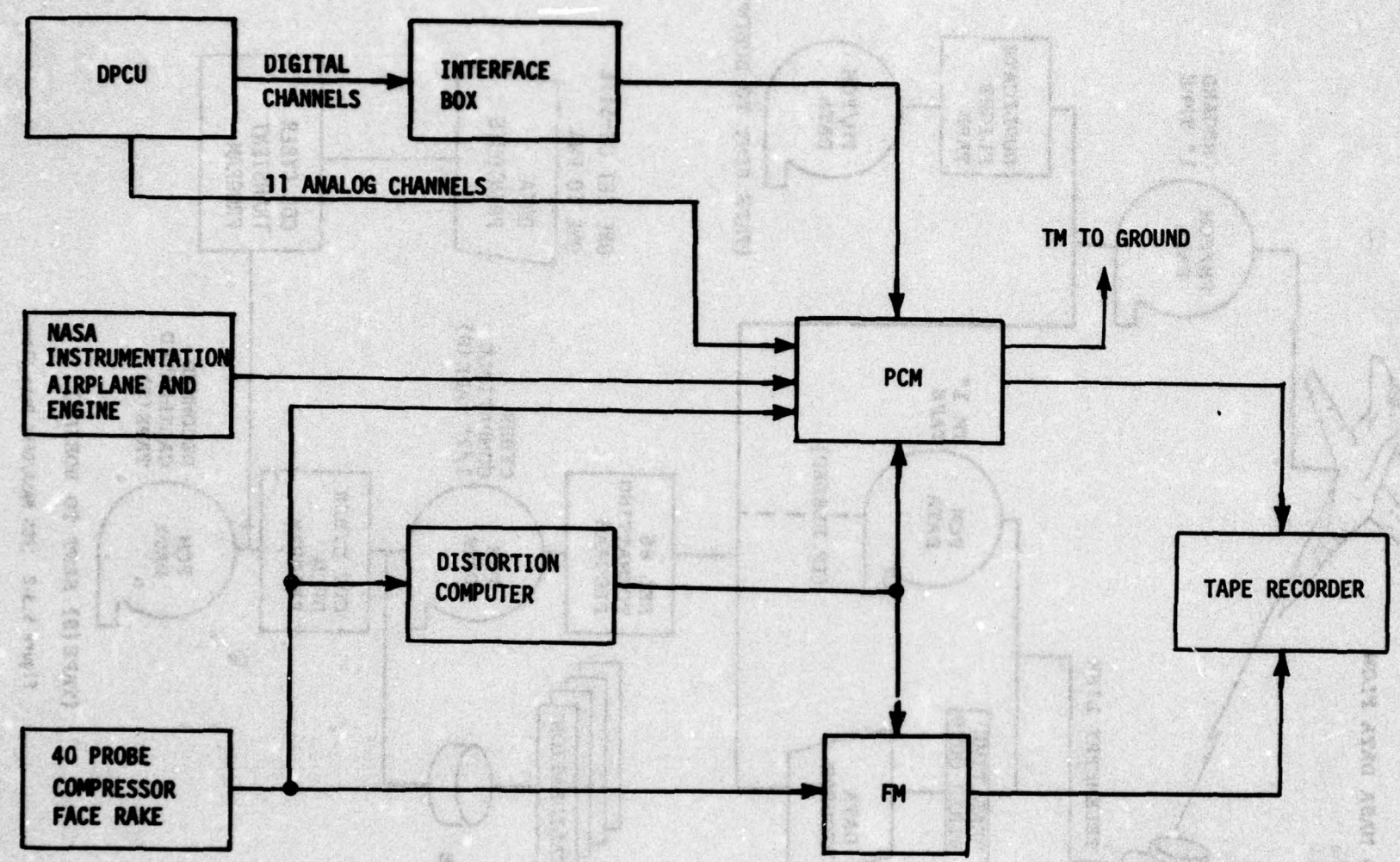

Figure 5.3-1 Data Recording Flow

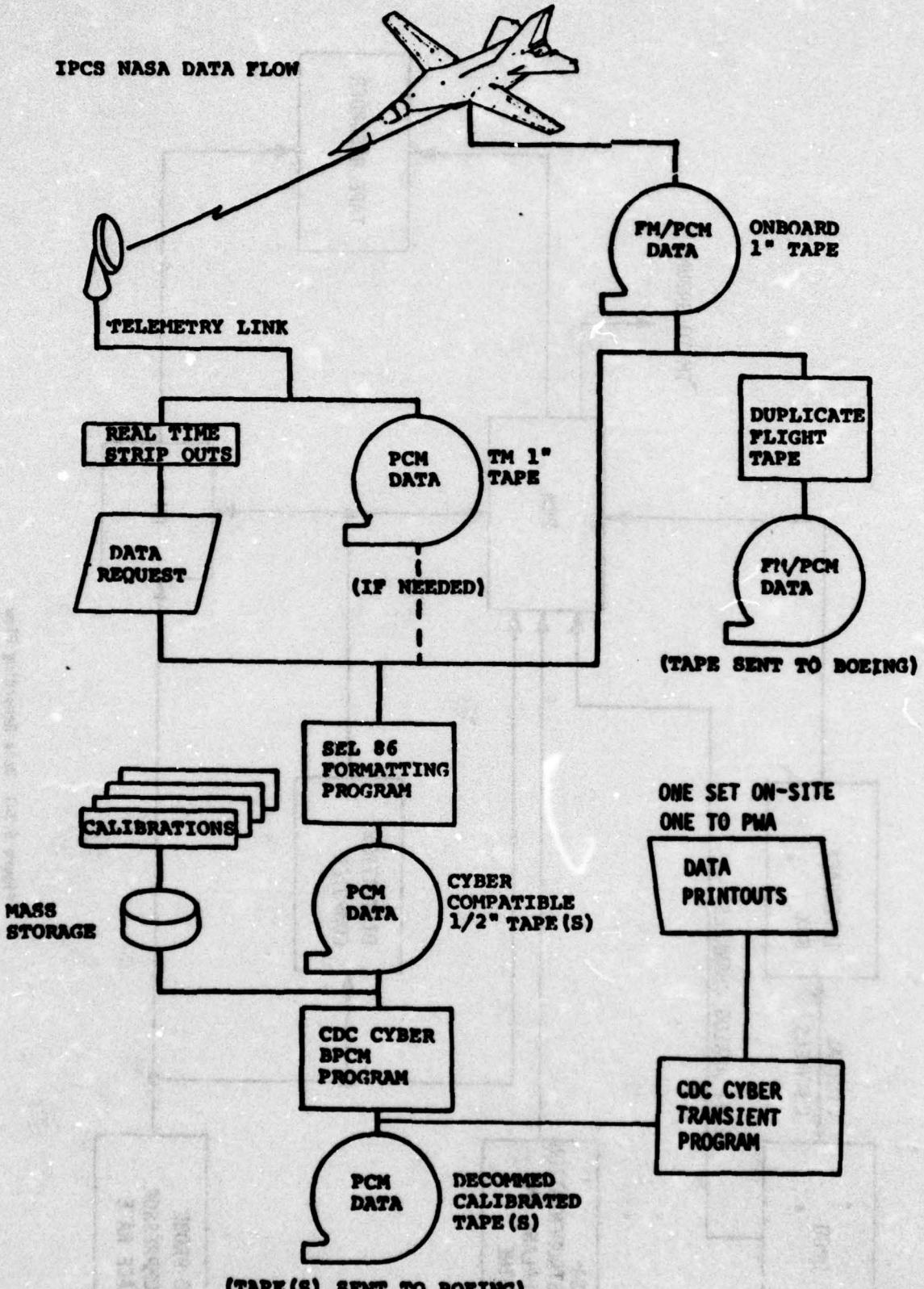

Figure 5.3-2 IPCS NASA/DFRC Data Flow

5.3.3 Contractor Processing of PCM Data

Off-line processing of the PCM data was performed at Boeing and P&WA (Figure 5.3-3). The data tape from NASA was first processed by the transient program. This program reformats the data to be read by the CDC 6600, computes a number of parameters and outputs the recorded and computed data. Reference 7 describes the program in detail. Microfilm is generated for long term data storage and transmittal to the government. The program printout is recorded on magnetic tape for use in a PDP11 for plotting, as input data to the steady-state program, and as a data source for P&WA. Magnetic tape was selected for the data transmittal to P&WA to simplify the use of plot programs and to reduce the volume required for paper printouts. The use of microfilm would have delayed data transmittal to P&WA.

At P&WA the tape data was read onto microfilm and then plotted using standard plot programs. Many of the plots presented in Section 6.0 were generated using the P&WA plot program.

5.3.4 High Response Data Processing

The FM data were demultiplexed and digitized at Boeing. Figure 5.3-4 shows the data flow for the processing of the analog tapes. The typical data sample was a 200 millisecond interval centered about an event such as a period of high inlet distortion or compressor surge. The analog signals were low-pass filtered (3 dB at 160 Hz) to retain only the frequency range of significance to the engine. The data were digitized at a rate of 1000 samples per second and recorded on tape in a format compatible with processing on the 6600.

The 6600 program applies the calibrations from pre and post flight data, corrects for zero shifts based on the flight data for rake zero, computes distortion, and generates a plot tape and data printout. Figure 5.3-5 shows a typical high response time history.

5.3.5 Data Processing Evaluation

On the whole the data processing scheme described in the preceeding paragraphs worked reasonably well, particularly from the standpoint of producing data for post-test analysis and report writing. However, data turnaround times were sufficiently long that most of the data were unavailable for control analysis in time to affect the course of the testing. Figure 5.3-6 presents average time to various stages in the data processing. The data for this figure were taken from the middle of the test period (1 November -15 January) avoiding both the initial processing system trouble-shooting phase and the later portion of the test when data output changes required program modifications.

During that same time period, the average time between one flight or engine run and the next was 2.6 days. Thus it can be seen that even the printed data were generally not available soon enough to be used in the development of the software configuration for the next run. The capability did exist for relatively rapid turnaround of small time segments (less than 1 minute) of data to trouble-shoot problems that might ground the airplane. This procedure tended to disrupt normal data processing so it was used infrequently.

It should be noted that at no time did the lack of data result in a flight cancellation or in any way risk flight safety. The data turnaround during the flight test was generally better than at previous tests, particularly with respect to the DPCU data needed for control evaluation.

The problem that became apparent during the course of the test was that the ability to refine and improve the controller had far out stripped the ability to process the data needed to identify the potential improvements. As a result changes to the control that might have greatly enhanced the usefulness of the test were not recognized until too late for orderly incorporation. Working within the constraints of interfacing the DPCU data with existing data processing systems at any test facility is likely to have this result. Data turnaround will always be dependent on availability of equipment shared by a number of programs. The facility data processing system cannot be dedicated to a single program.

The solution is to provide independent recording of the DPCU data and a small dedicated data processing capability for this data. In a program like IPCS or the development of a new engine and controller, substantial time and money can be saved by developing the hardware interface and software needed for data processing once rather than starting over at each test facility.

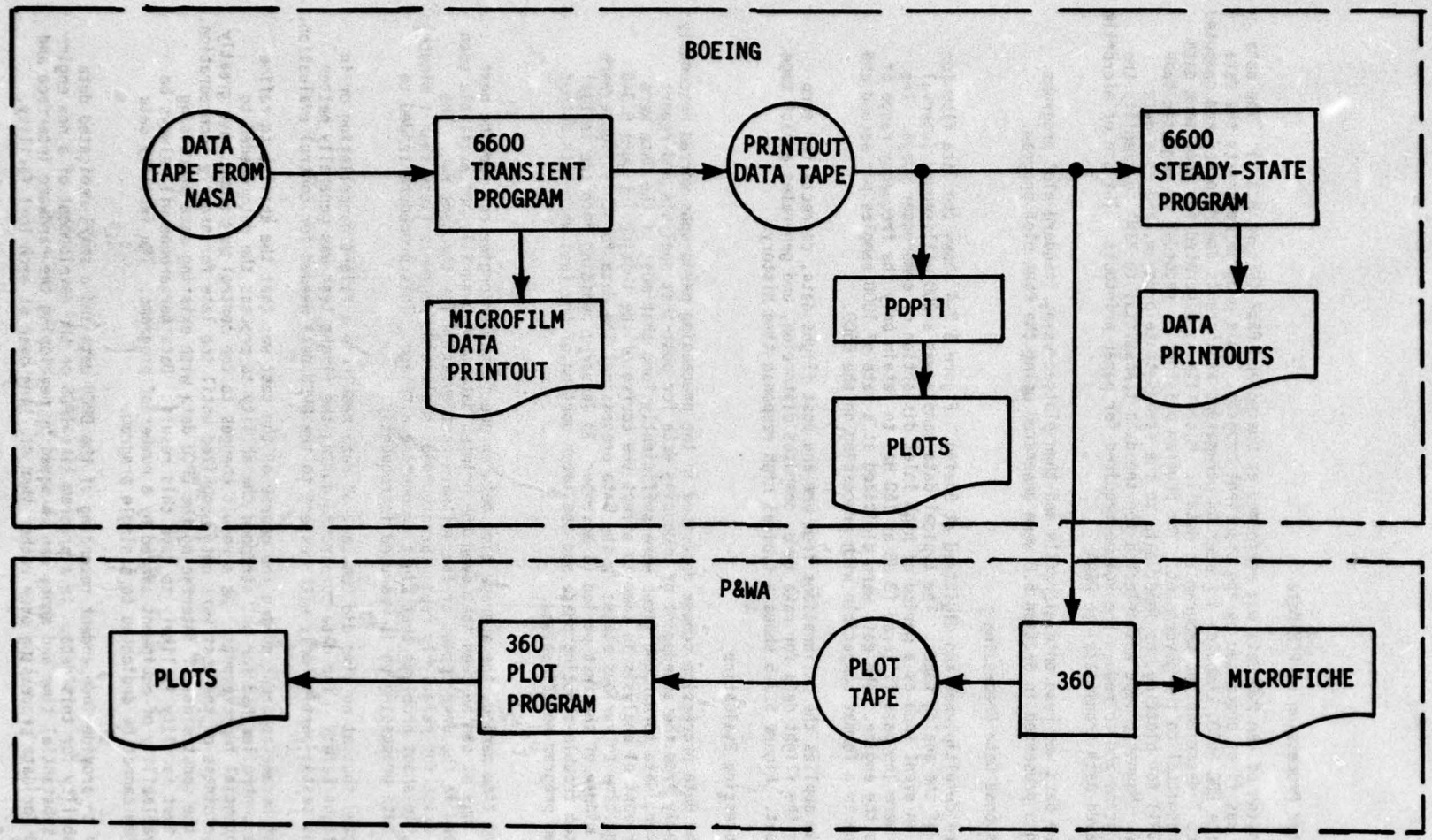

Figure 5.3-3 Off Site PCM Processing

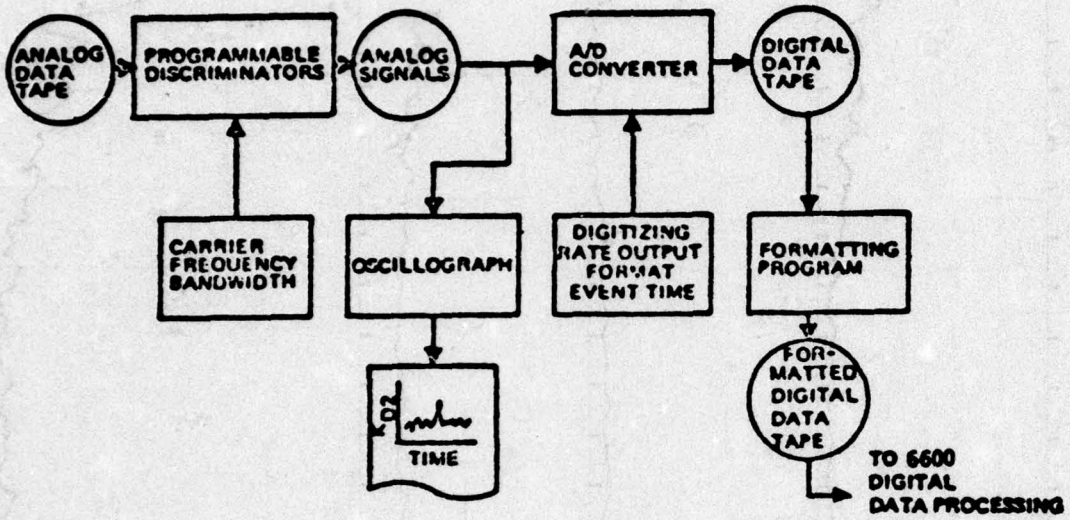

Figure 5.3-4 FM Analog Data Flow

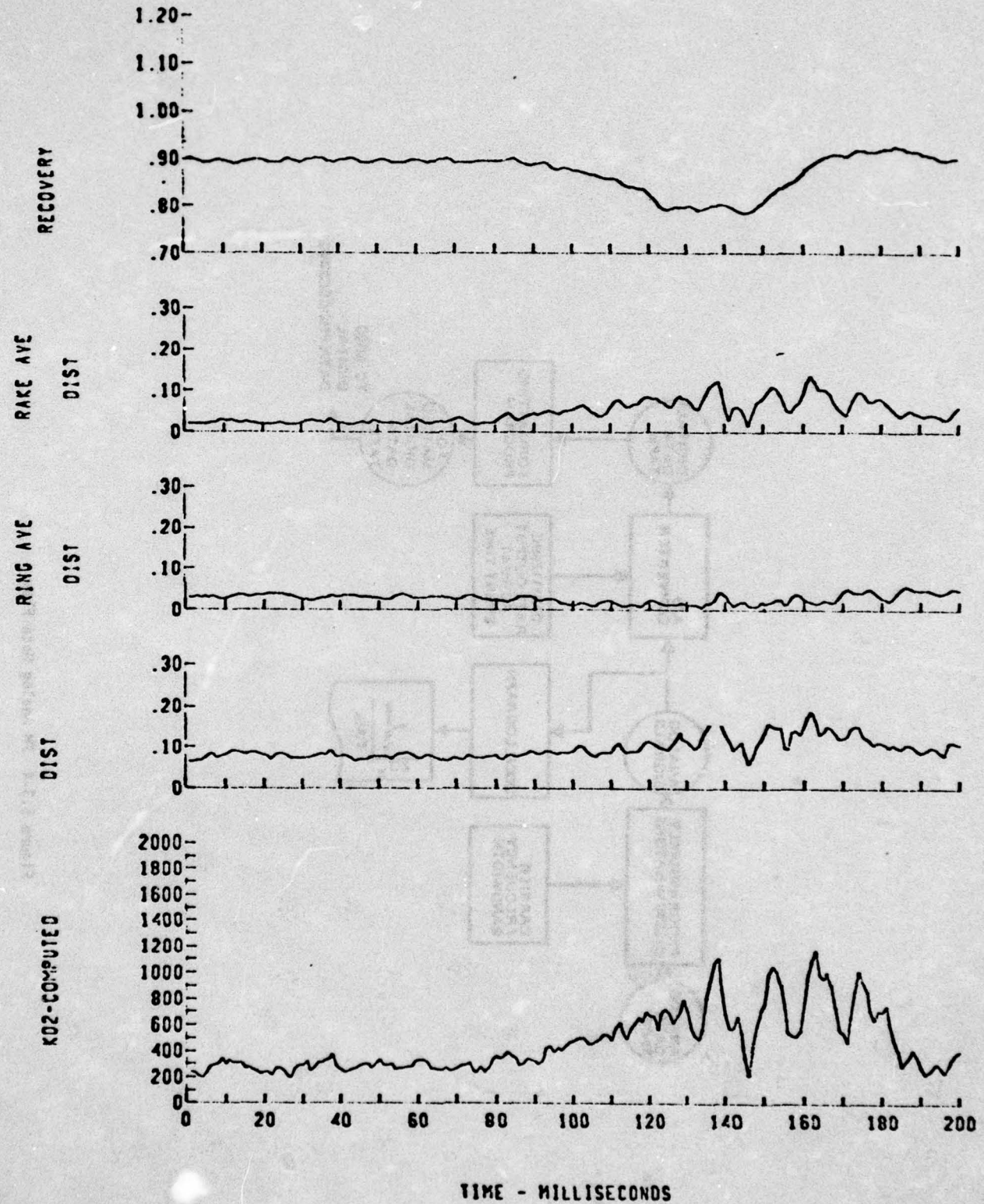

Figure 5.3-5 Typical Distortion Time Histories

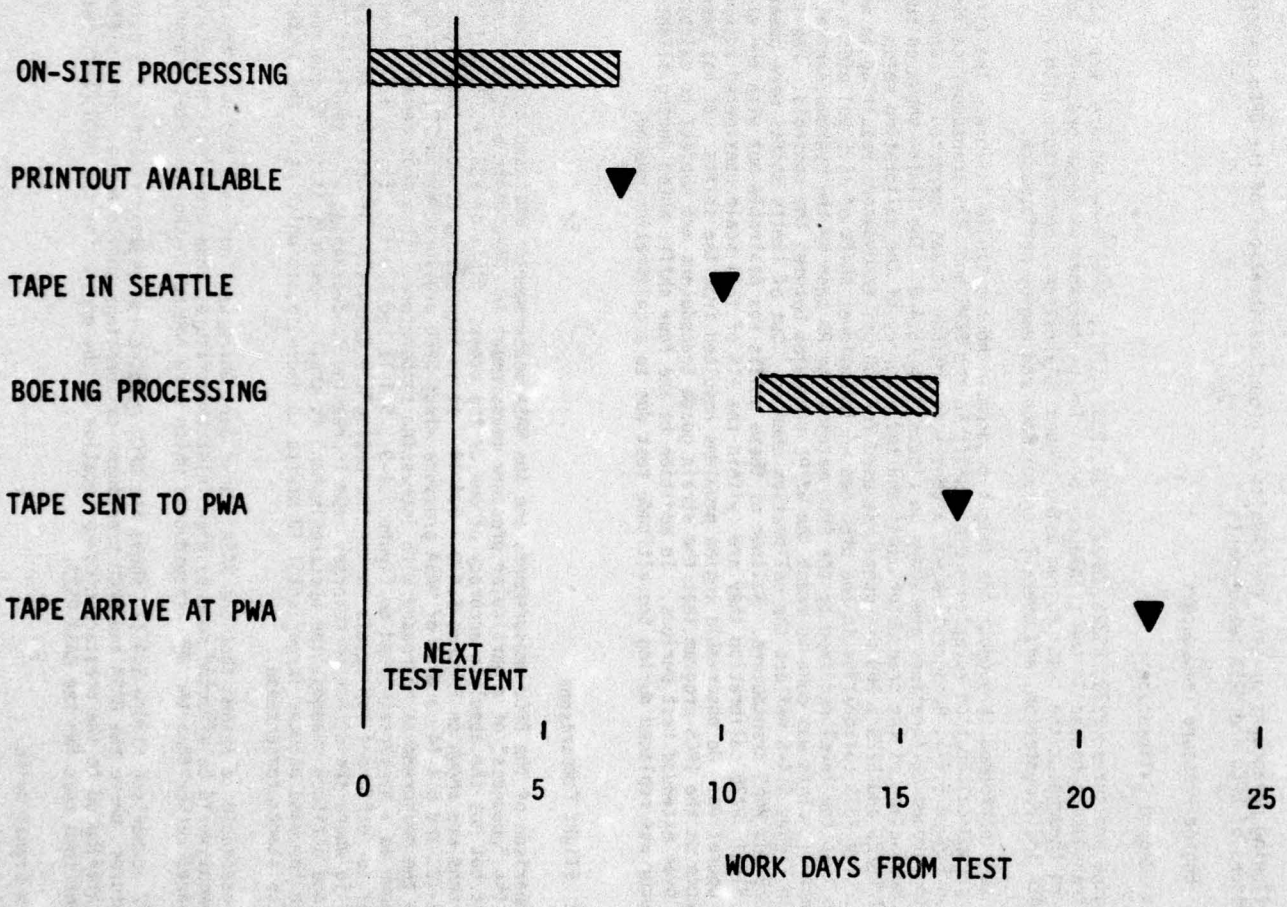

Figure 5.3-6 PCM Processing Times

A scheme has been devised using a small computer, such as a PDP11, to reduce the data. With magnetic tape, printer, and plotter capability the entire data processing could be done on-site at each test facility. Since the equipment would be dedicated, very rapid turnaround could be achieved. This scheme is described in paragraph 7.4 of Volume IV. This type of data processing is essential if the full use is to be made of the flexibility of digital control.

5.4 MEASUREMENT COMPARISONS

The following paragraphs present the results of ground calibrations of the DPCU sensors and comparisons of DPCU and NASA measurements.

5.4.1 Engine Pressure Transducers

5.4.1.1 Ground Calibration

The engine pressures (P22S, PS22S, ΔP22S, P3S, PS3S, ΔP3S, P6MS) were measured with strain guage transducers housed in the transducer box. The performance of these pressure signals was monitored throughout the test program using ground calibrations, comparisons with like signals from NASA instrumentation, and overall control mode and engine performance.

The sensors performed throughout the flight program without a single failure. The first pre-flight ground calibration revealed a minor shift in the P6MS and P3S transducer calibration as noted on Figure 5.4-1. Because this was a consistent offset it was corrected in software. The remaining ground calibrations are shown on Figures 5.4-2 5.4-8. The limits shown on the figures are a combination of the transducer limit and the accuracy of the calibration setup. In the case of PS22S and P22S a 300 psi guage was used for 100 psi transducers resulting in wider limits. The PS3S calibration in the DPCU had an intentional shift of +1.5 psi offset and +1% gain so that the level recorded by the DPCU matched the Pb seen by the hydromechanical main fuel control. This was done to match the Wf/Pb schedules between the controls. The limits shown in Figure 5.4-5 reflect the calibration changes. Out of limits shifts were observed on the P22S and P6MS transducers. Neither of these shifts was desirable but with the exception of the final P22S calibration they are within the +1% of full scale considered acceptable for engine operation. No observable engine problems resulted from the shifts. It has been the experience on the IPCS program that the strain guage transducers are subject to calibration shifts over extended test periods. In addition to the four shifts noted during flight test one transducer was replaced during the altitude test due to a calibration change.

5.4.1.2 Flight Comparisons

The comparison of the DPCU measurements and the NASA measurements was used as a guideline to assess the "goodness" of a particular pressure measurement in conjunction with performance analysis but not the absolute accuracy of one or the other. Plots of PS3, PS22, and P6M comparisons are shown on Figures 5.4-9 - 5.4-14. It is interesting to note from Figures 5.4-10, 5.4-12, and 5.4-14, a plot of NASA pressure minus DPCU pressure versus T2, that the difference between the measurements increased with increasing temperature. This measurement difference is also shown as a hysteresis band on Figure 5.4-9 , 5.4-11 and 5.4-13. Figure 5.4-13 shows the T2 level for different P6M levels in the increasing and decreasing direction. At the P6M level of 35 psia where the direction reverses from increasing to decreasing as a result of the Mach number and altitude changes, the hysteresis band is small. However, as the T2 continues to increase the band becomes larger until T2 starts to decrease, at which point the hysteresis band also starts to decrease.

It is reasonable to assume that the NASA transducers, which were not shielded from the nacelle environment, would be affected more by high inlet temperature, thus creating the measurement difference, rather than the DPCU transducers which were housed in the insulated transducer box.

The PS22 comparison Figure 5.4-11, shows the DPCU reading low by approximately 2.5 psia at low temperatures where the NASA and DPCU transducer calibrations should agree. This difference can be attributed to the pressure pick-up location on the engine for the DPCU PS22S being different than that for the NASA PS22.

Pressure Signal Noise

The only significant pressure signal noise which was experienced during the flight test program was that exhibited by the ΔP3S pressure measurement. As discussed in paragraph 5.4.4 the noise level of the absolute pressure measurements, P3S and PS3S is insignificant; however, the ΔP3S

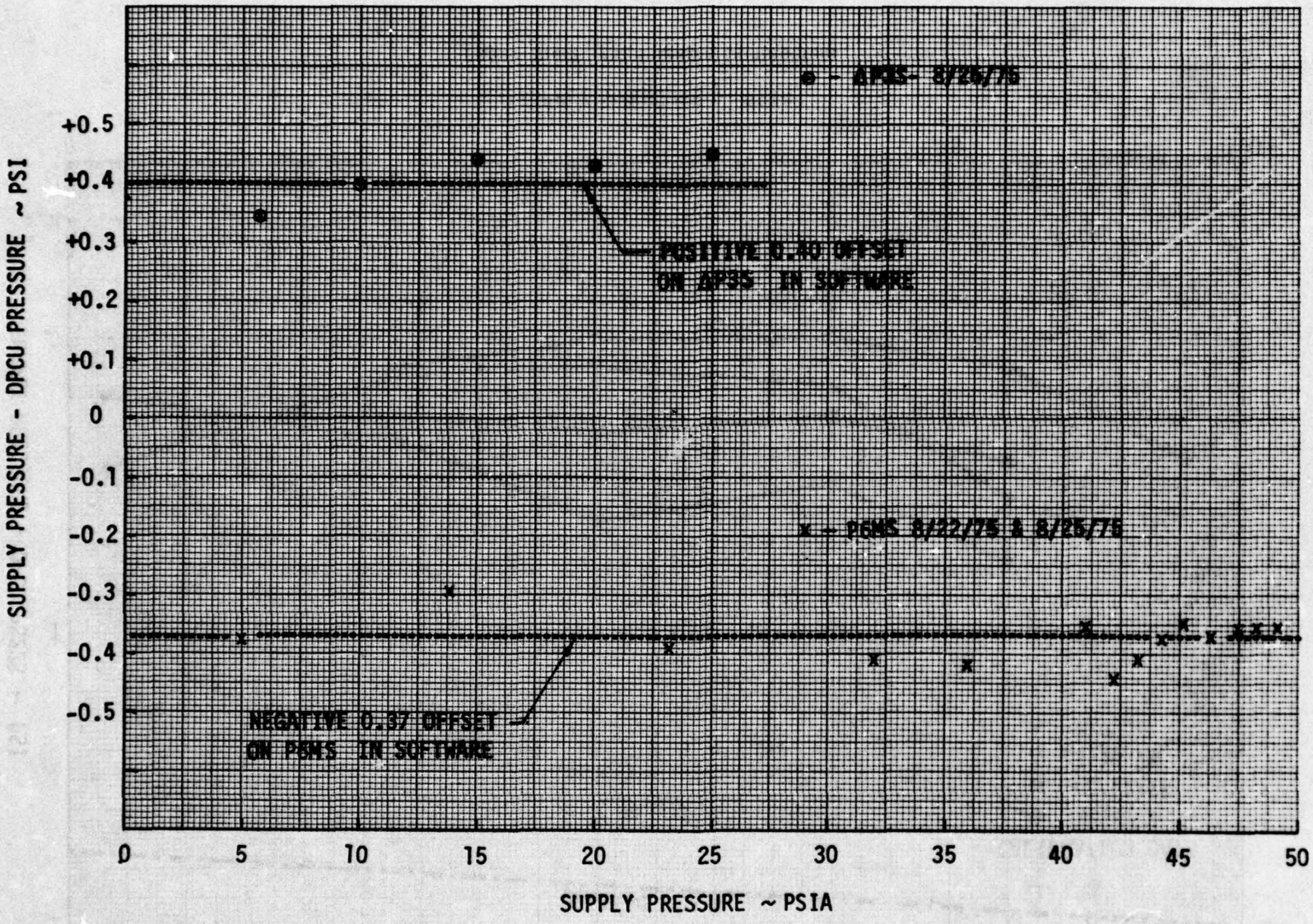

Figure 5.4-1 P6MS and ΔP3S Preflight Transducer Calibrations

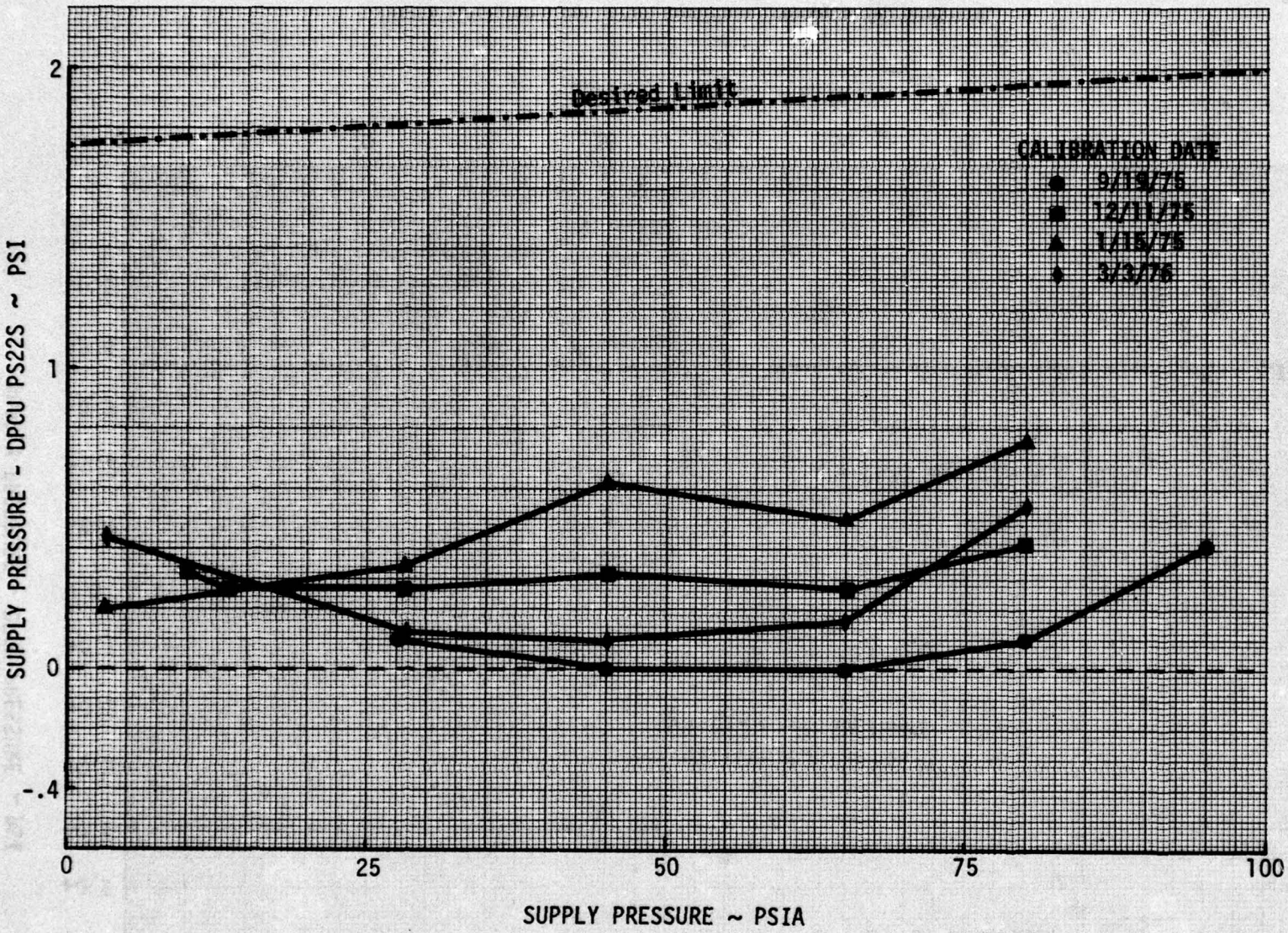

Figure 5.4-2 PS22S Ground Calibrations

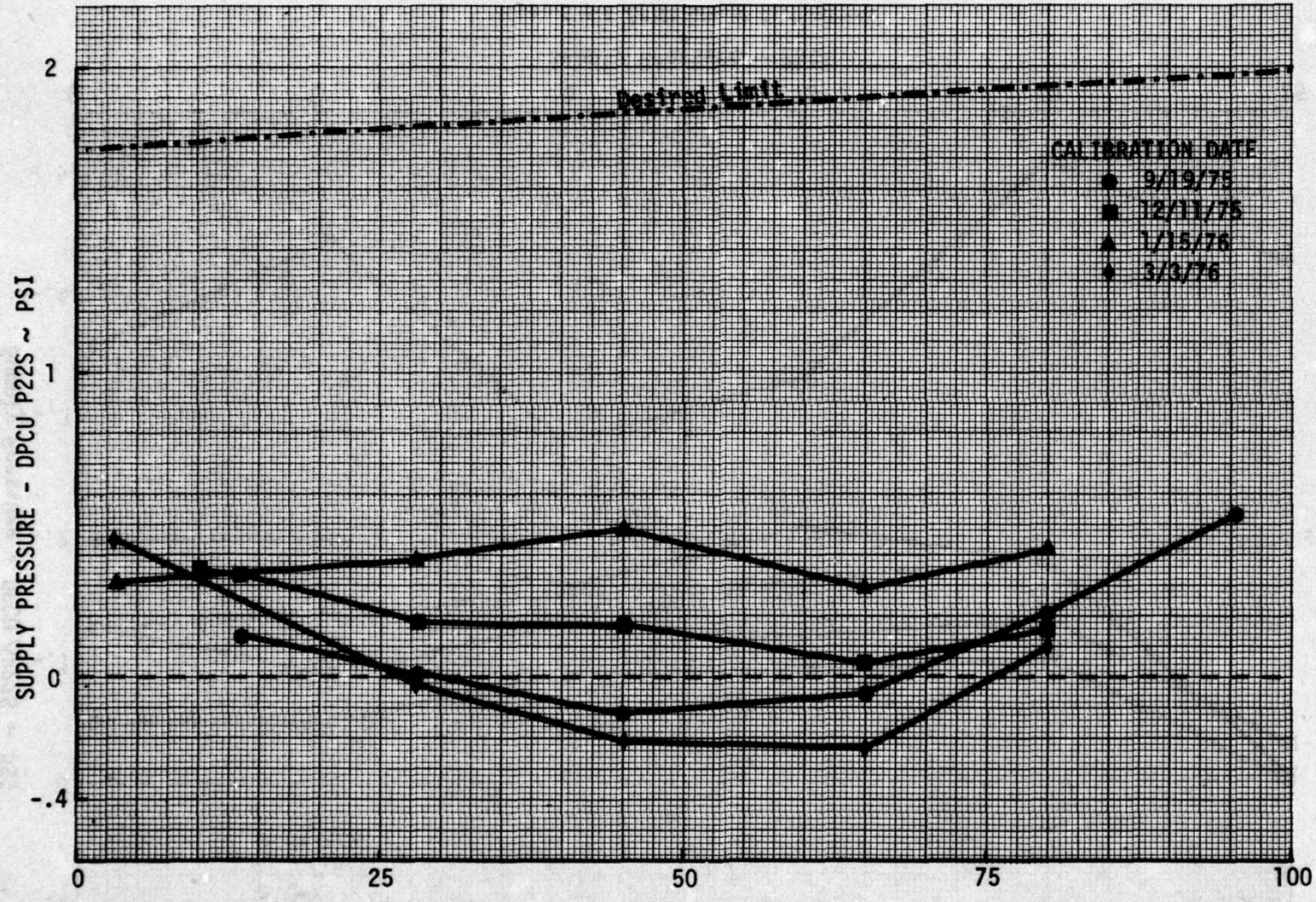

Figure 5.4-3 P22S Ground Calibrations

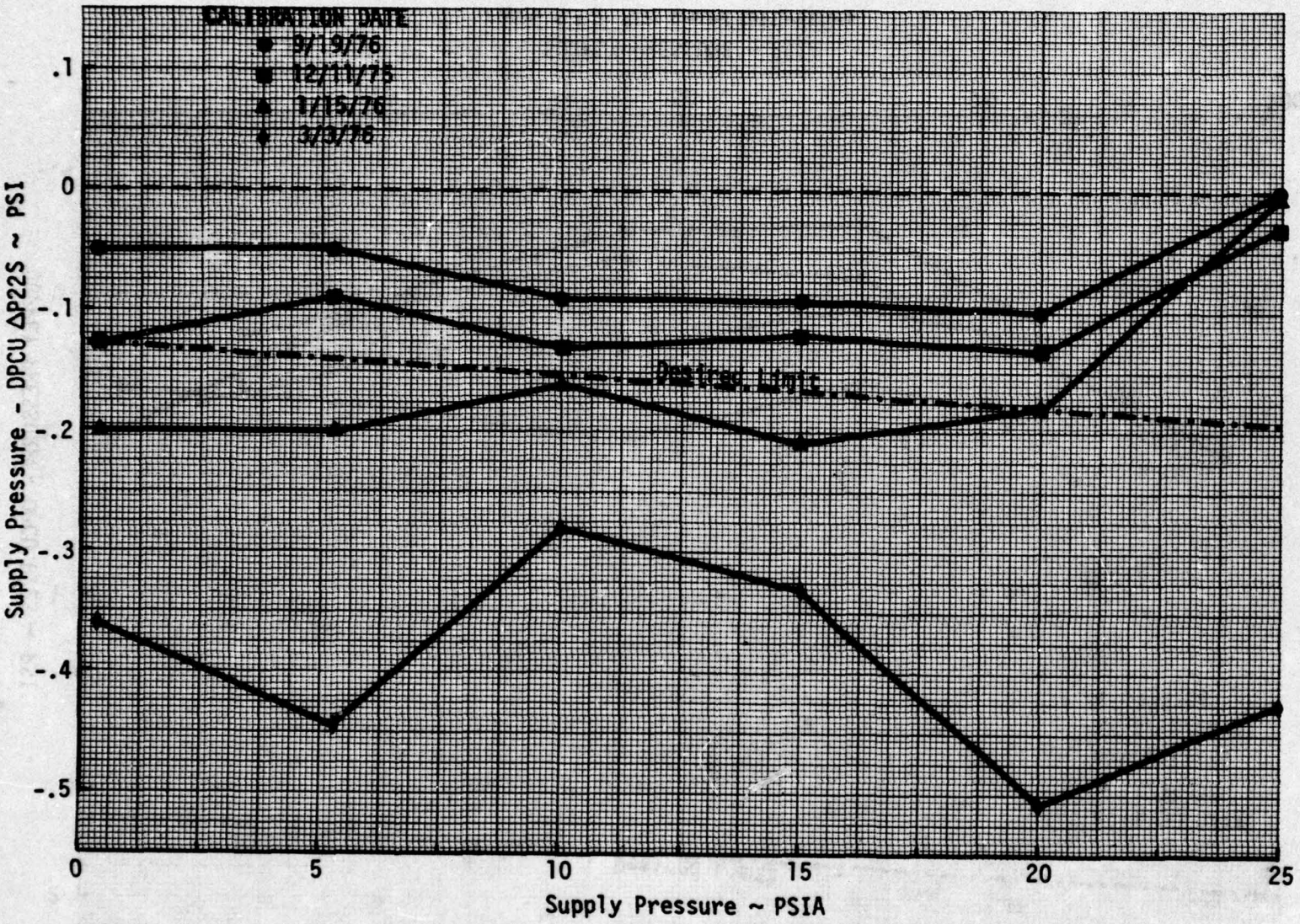

Figure 5.4-4 ΔP22S Ground Calibrations

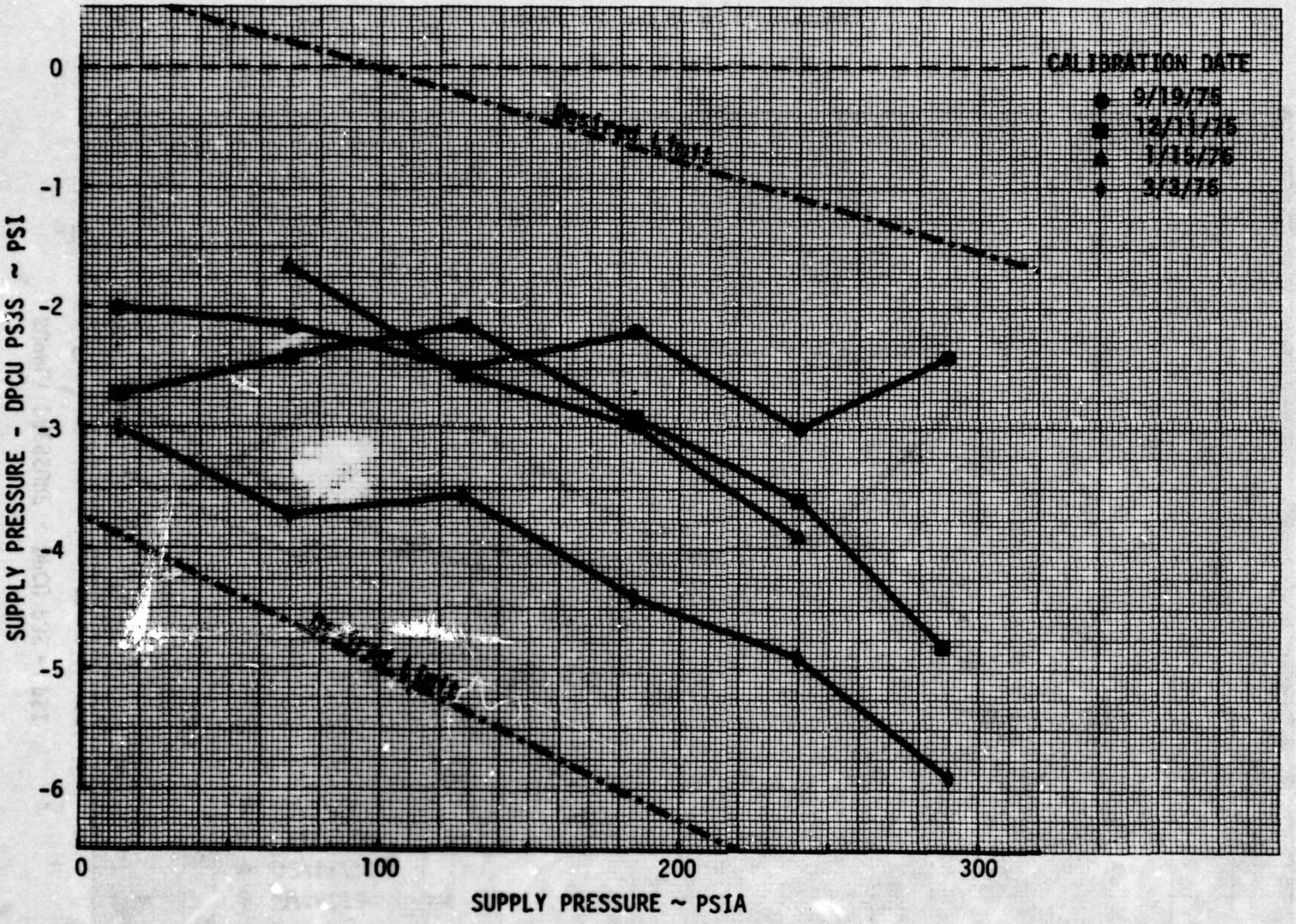

Figure 5.4-5 PS3S Ground Calibrations

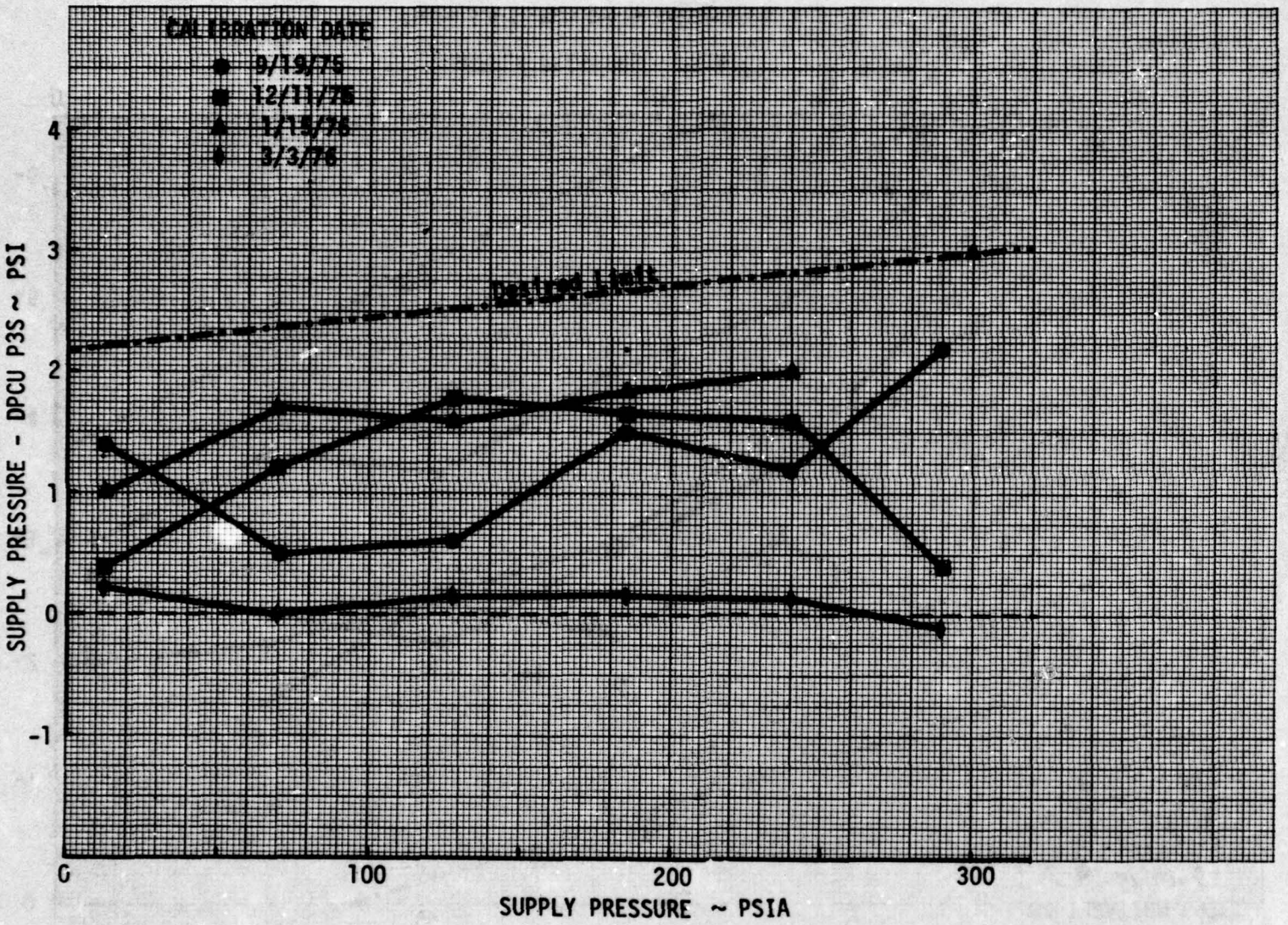

Figure 5.4-6 P3S Ground Calibrations

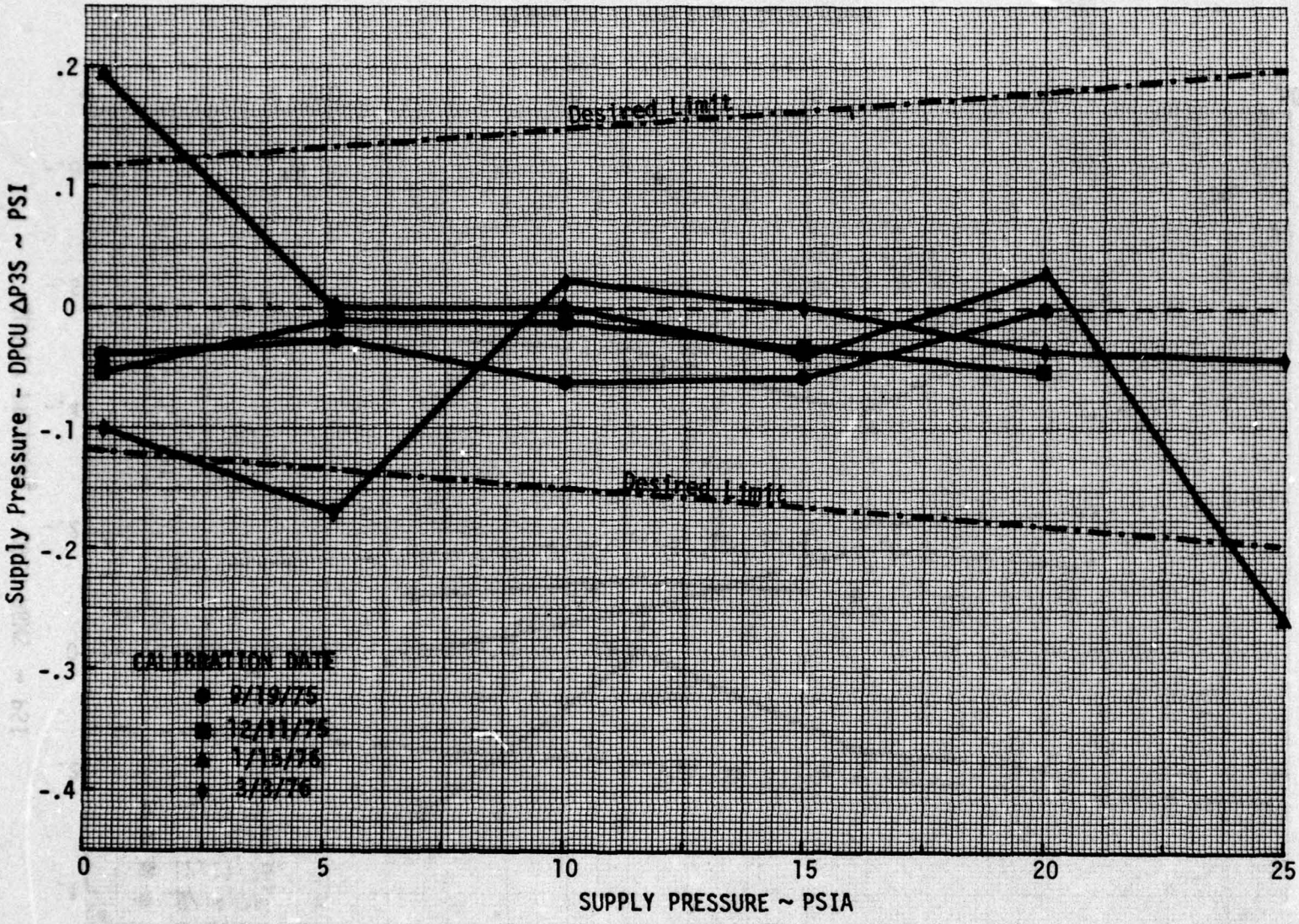

Figure 5.4-7 ΔP3S Ground Calibrations

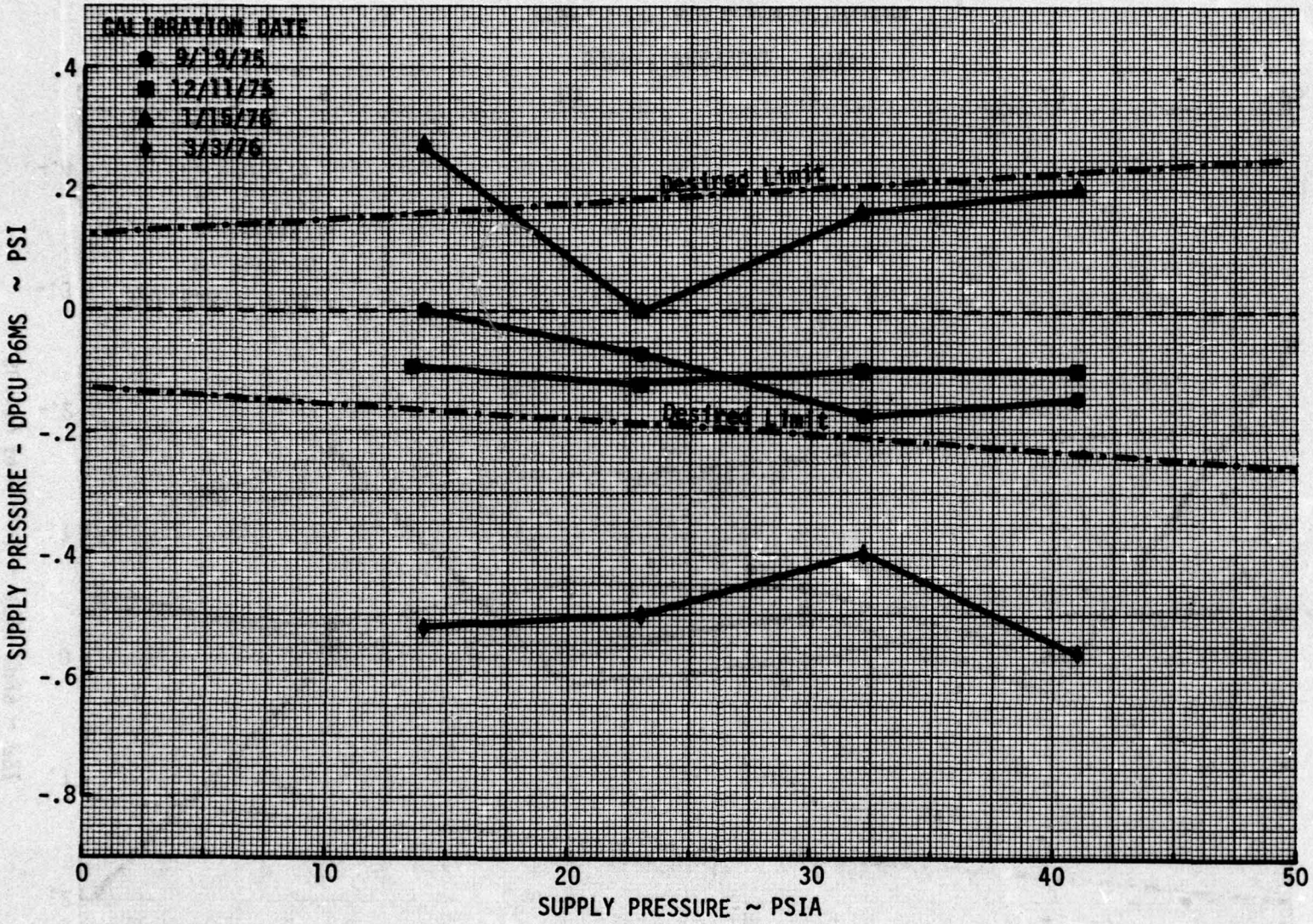

Figure 5.4-8 P6MS Ground Calibrations

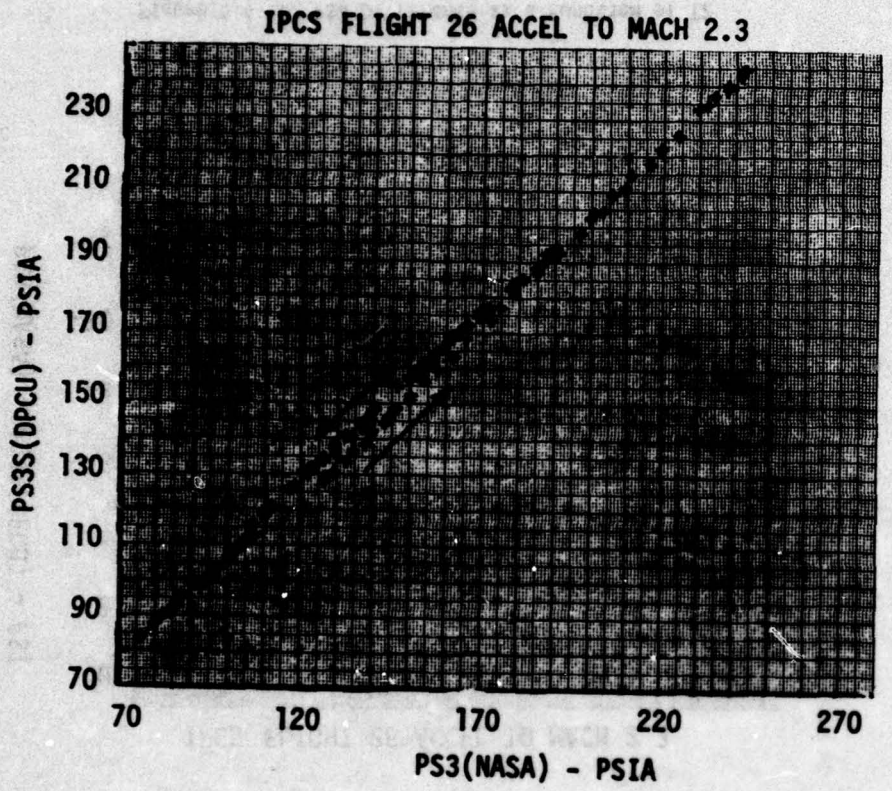

Figure 5.4-9 Comparison of NASA and DPCU PS3

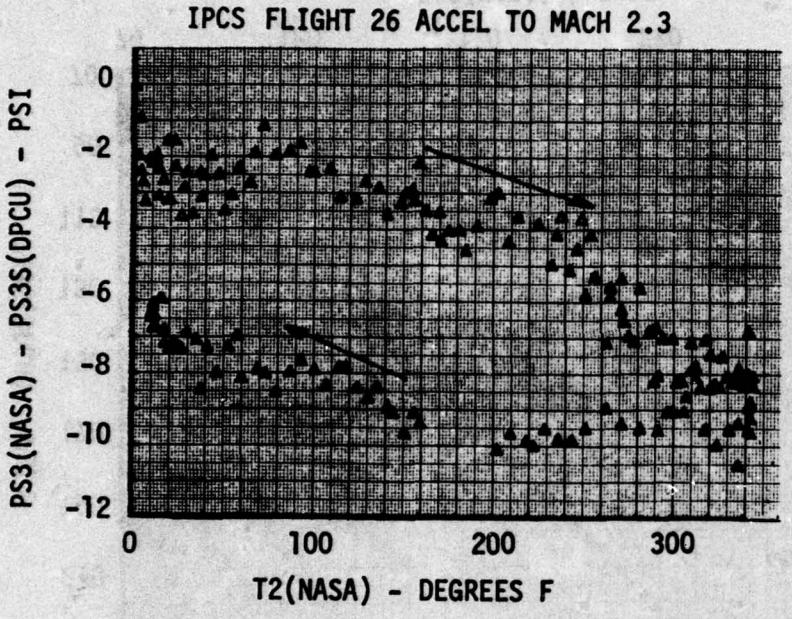

Figure 5.4-10 PS3 Difference as a Function of T2

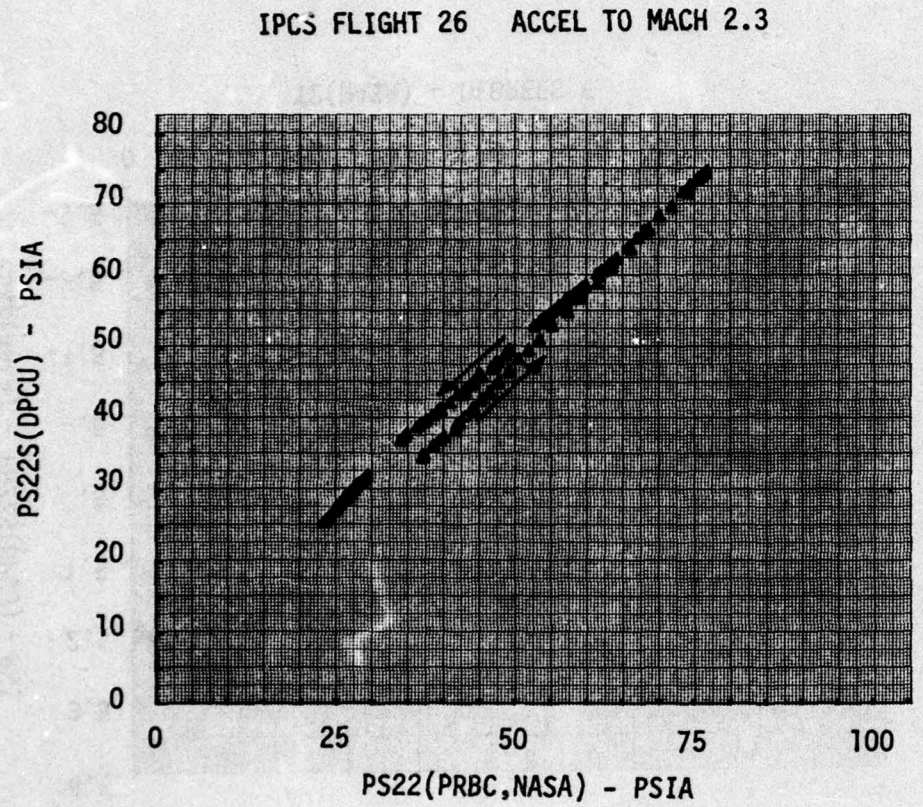

Figure 5.4-11 Comparison of NASA and DPCU PS22

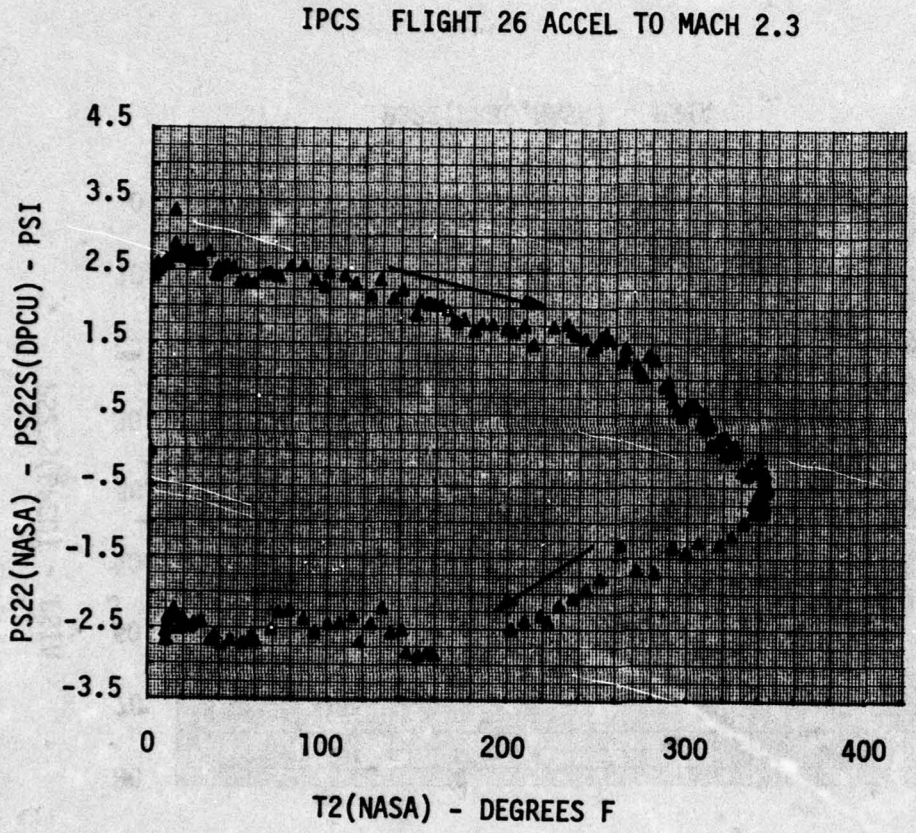

Figure 5.4-12 PS22 Difference as a Function of T2

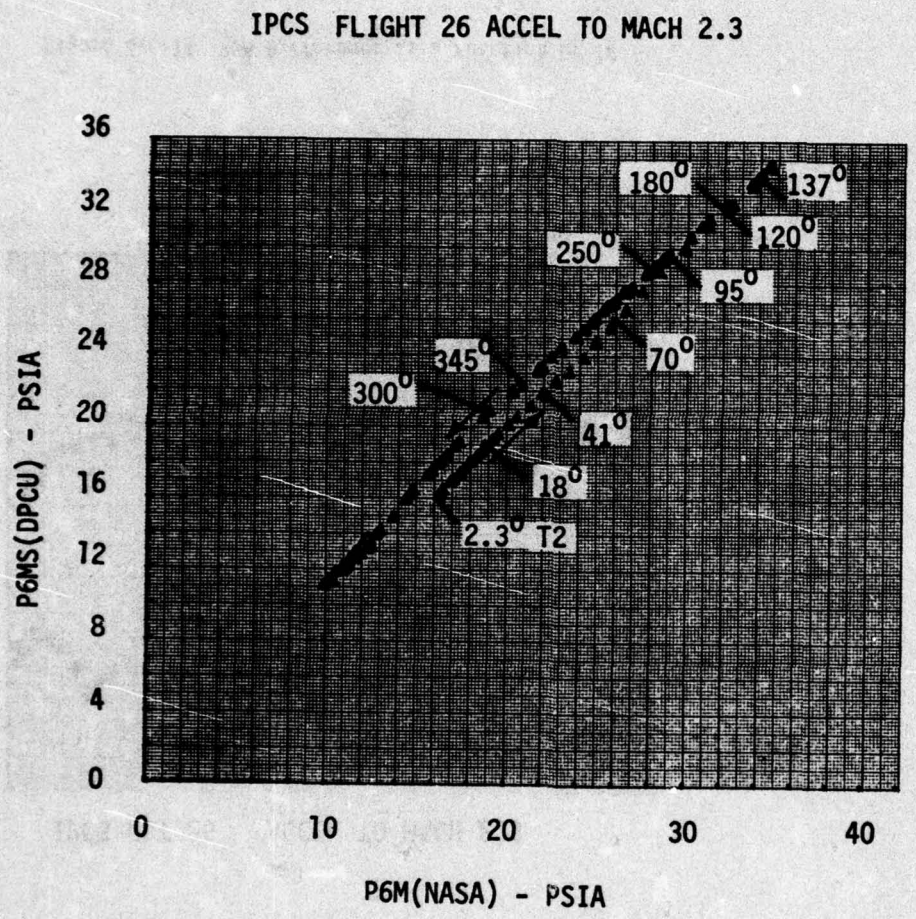

Figure 5.4-13 Comparison of NASA and DPCU P6M

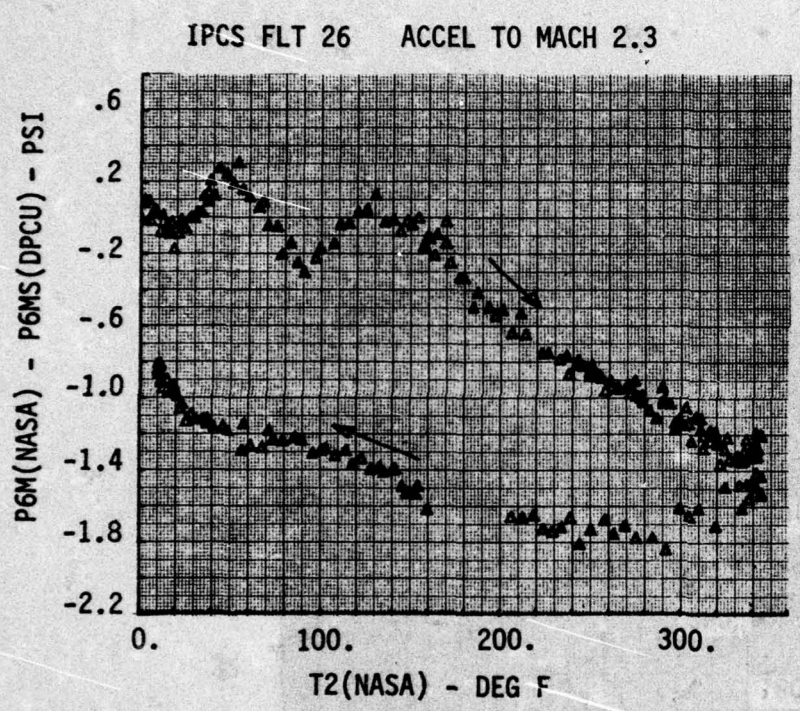

Figure 5.4-14 P6M Difference as a Function of T2

signal exhibits a level of 3.43% of point. This ΔP3S signal noise level was the major contributor to the T4SYN signal noise and also the MN3 signal noise. In both cases this is an undesirable characteristic which should be recognized and assessed early in the design process.

5.4.2 Thermocouples

Considerable difficulties were experienced in measuring temperatures on the engine. Most of the emphasis was on the T2 measurement because of its impact on the control.

5.4.2.1 T2S Performance History

Steady State Comparison

The existing TF30 bill of material T2 probes were selected for measurement of the T2S signal for the IPCS program because they met the control requirements and reduced the cost and risk of incorporating new probes. These probes are part of the T4 bill of material harness system which calculates the T4 temperature used for cockpit display and instrumentation purposes. These probes had never been used before as an individual T2S measurement for a control signal so there were no previous data available to compare with the T2S results from IPCS testing.

To assess the accuracy of the T2S measurement used for IPCS it was, therefore, compared to instrumentation T2 taken off the same probes. This comparison, through all phases of IPCS engine testing, indicated signal noise (until filtered) and a difference between the measurements. The cause of the difference never was fully defined.

From the results of the altitude testing at NASA/LeRC, it was concluded that a possible cause for the difference between the T2 measured by the DPCU and T2 measured from the bill of material T4 engine harness was a temperature gradient across the transducer box and heat conduction from the exposed connectors of the cold reference junction probes. To correct these deficiencies, a revised configuration was established which relocated the reference junction probes in the transducer box and the connectors on the reference junction probes were wrapped with insulating material to present heat conduction through the connector. Figure 5.4-15 shows a diagram of original configuration and revised configuration.

The revised configuration was not installed for the first flight, allowing for a baseline test of the original configuration. Figure 5.4-16 shows the T2 offset during an accel from 0.9 Mn to 1.9 Mn. The offset is 20° with the DPCU T2 reading higher than T2 from the T4 harness during the accel. Prior to takeoff the difference was only 5°.

The results of the revised configuration obtained from data during Flight 16 and spotted on Figure 5.4-16 indicate that the 20° offset is still present but with this configuration the DPCU is now reading lower than the T2 from the T4 harness.

The initial attempt at Flight 18 was aborted due to an out of range T3S signal because of a break in the extended portion of the T3S leg of the temperature harness. As a result of this and the T2 difference noted on previous flights, the IPCS temperature harness was eliminated and a new harness using solid state cold reference junctions (Con-Ohmic) was installed. The results of using this system are shown on Figure 5.4-16 and 5.4-17. It can be noted that the difference is still present at high T2 but had shifted from a fixed offset of 20° to a percentage difference. Data taken from different flights indicate that this difference was repeatable in direction and level.

For flight 26, the DPCU T2S signal was switched into the NASA measurement system, and the NASA T2 signal went into the DPCU system in an effort to isolate the cause of the difference. The outputs of the Con-Ohmic reference junctions were switched. With this configuration the difference was still present during Flight 26 (Figure 5.4-18) but had reversed such that the DPCU T2S was now reading lower than the T2 harness at high temperatures. This is just the opposite of previous results, indicating that the error was not a function of either the NASA or DPCU (IFU) measurement system, but rather a function of the system from the Con-Ohmic reference junction back to the engine harness.

To further investigate the problem, a test was performed in the hangar where the T2 probe was heated to 300°F, and a heat gun was applied to the different connectors in the system. This was to determine if a thermocouple effect might be present in the connectors, because of different pin material. The results of the test indicated that the NASA T2 and DPCU T2S were affected equally when heat was applied to the connectors, indicating that this was not the cause of the difference.

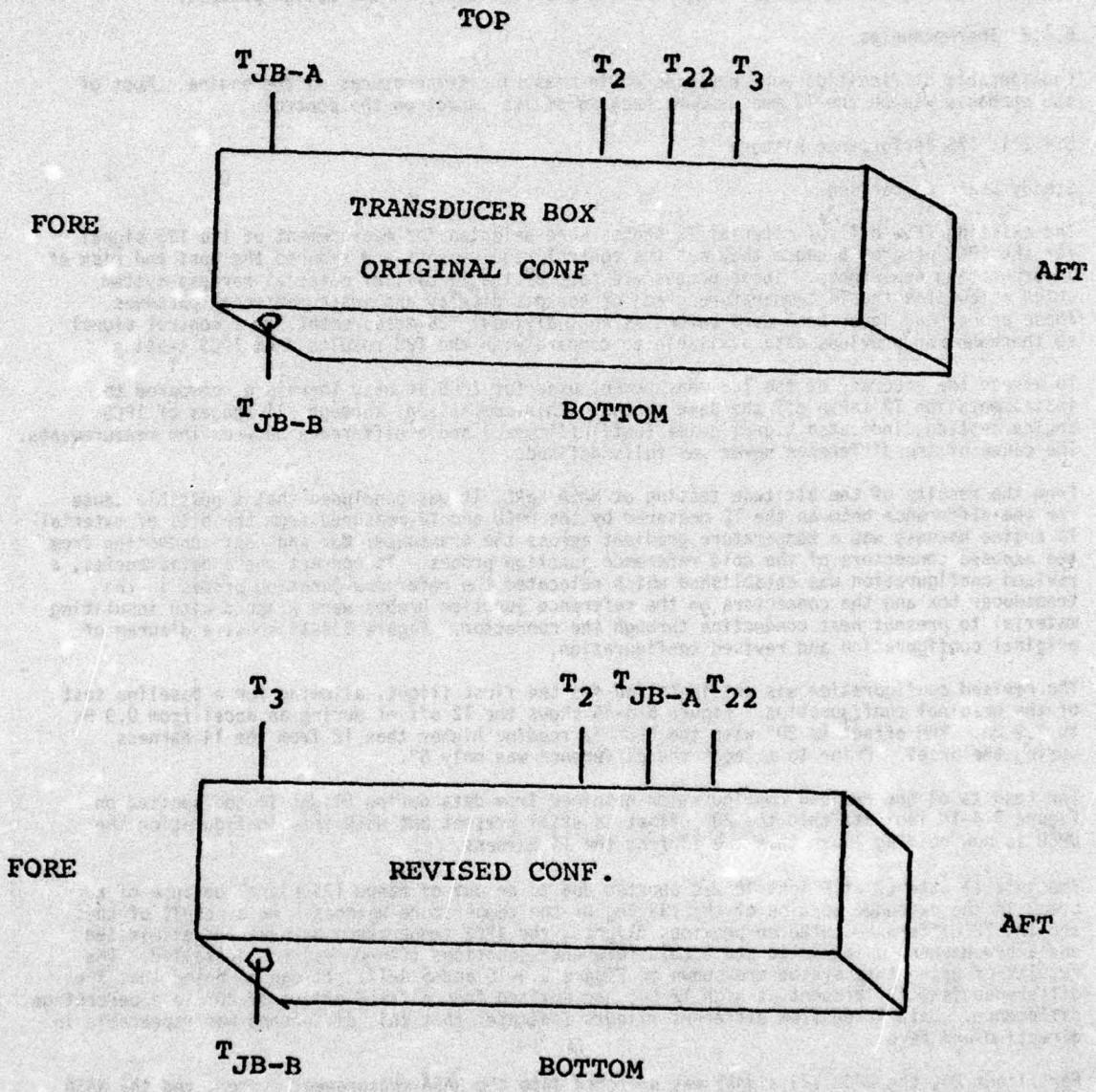

Figure 5.4-15 Transducer Box Configuration

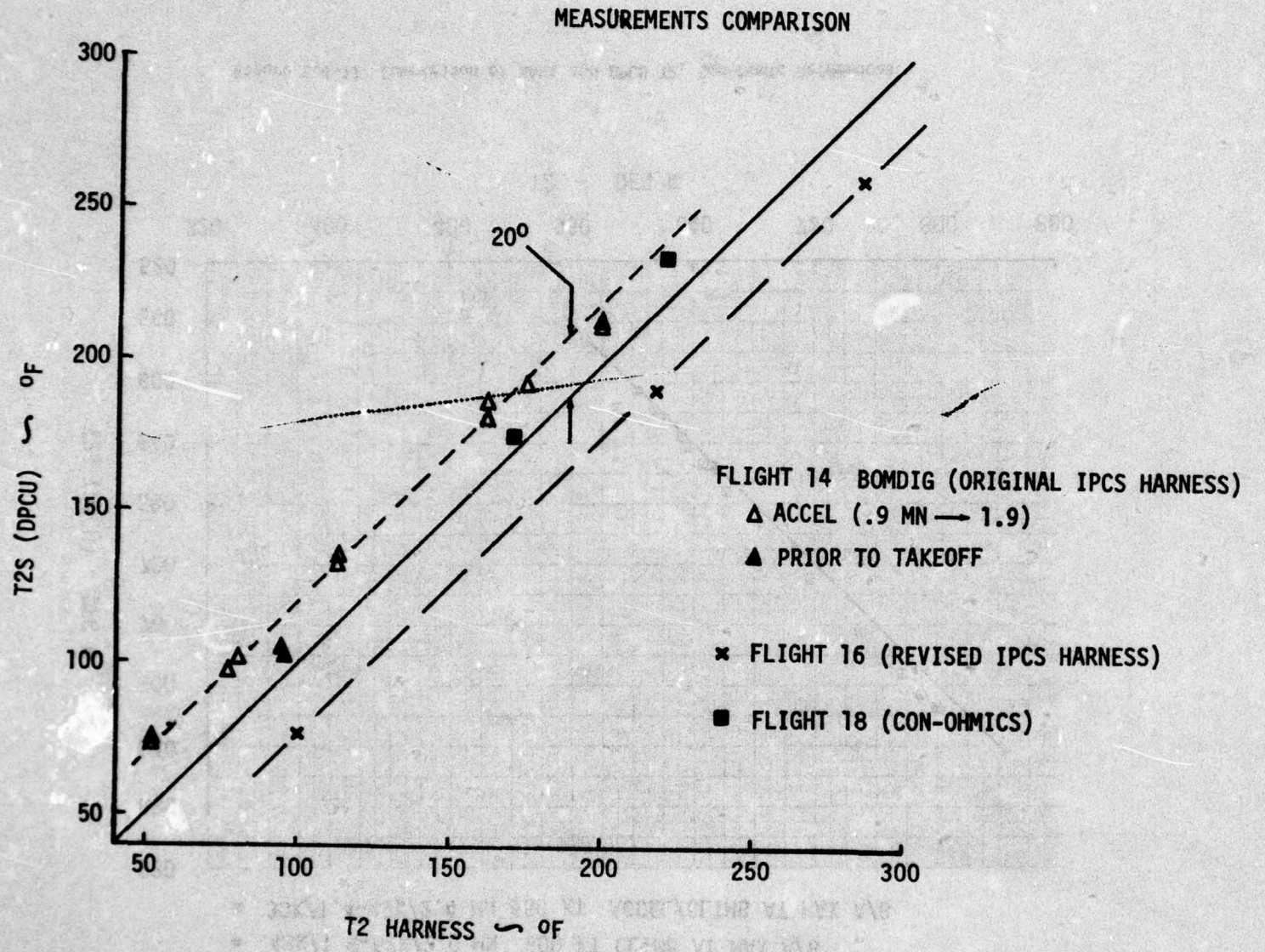

Figure 5.4-16 Comparison of NASA and DPCU T2, IPCS Harness

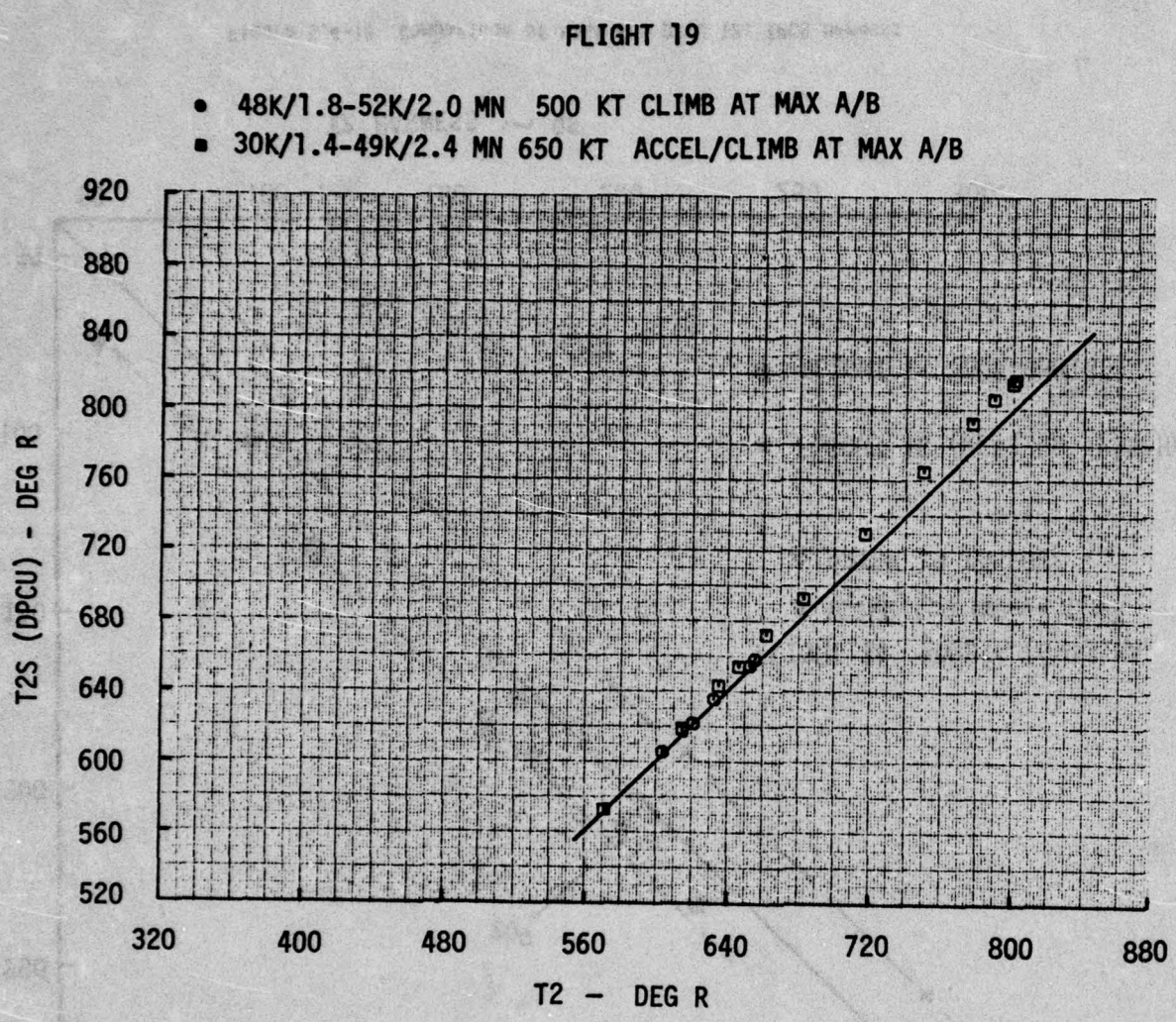

Figure 5.4-17 Comparison of NASA and DPCU T2, Con-Onmic References

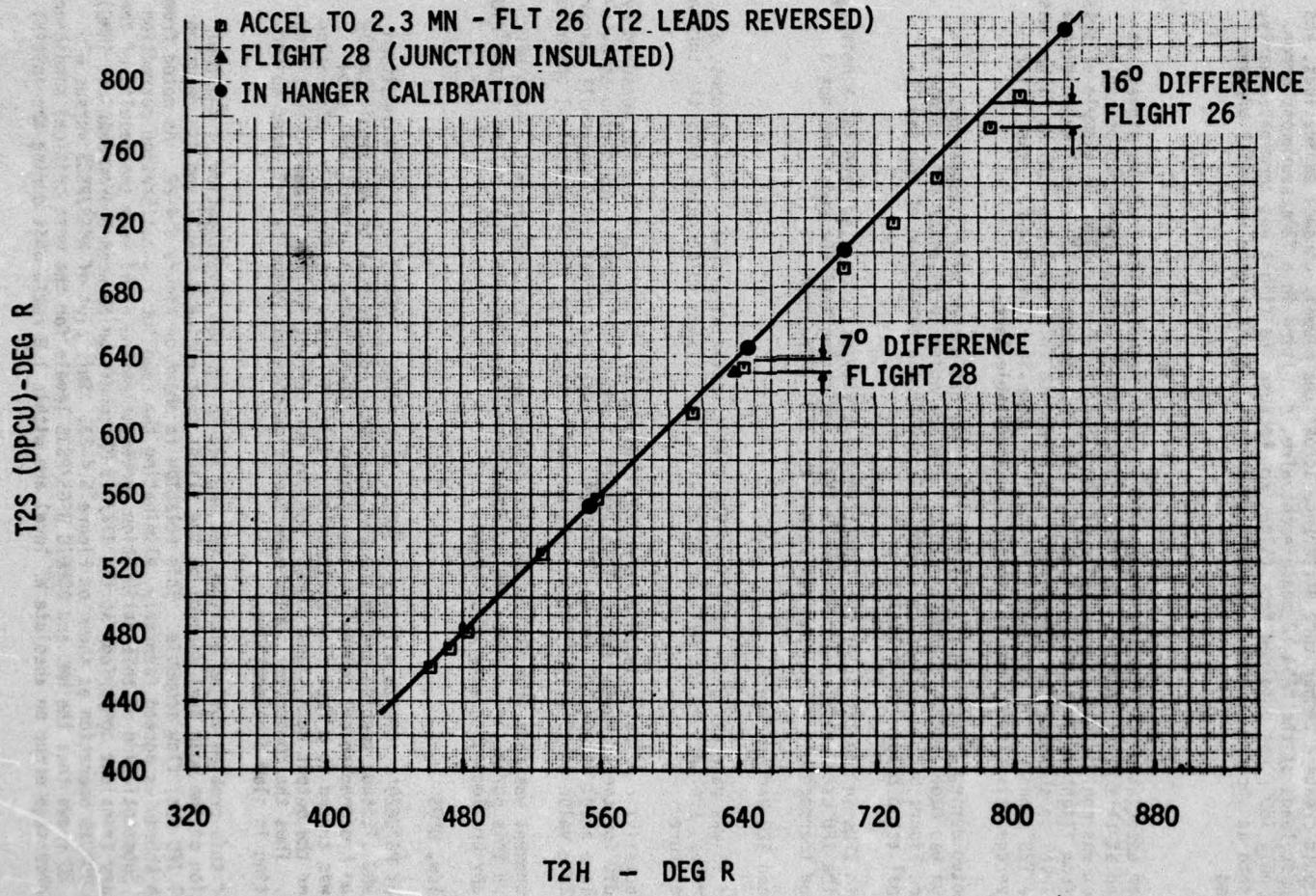

Figure 5.4-18 Comparison of NASA and DPCU T2, Hanger and flights 26 and 28

An in-hangar static calibration was performed by applying heat to the T2 probe from 90°F to 360°F and measuring the output of the NASA T2 and T2S. The results of this calibration, as noted on Figure 5.4-18 show that the two measuring systems are in complete agreement, implying that the T2 offset is a flight-oriented problem.

The final effort to solve the problem for the last flight, 28, was to insulate the front terminal block on the engine where the common T2 measurement originates. It was felt that a possible thermocouple effect could exist at the terminal block because of airflow around the block. This could create a temperature difference across the alumel/ chromel engine lugs, and the copper/copper leads of the NASA T2 measurement wire, resulting in a T2 measurement error. T2 data up to only 180°F was obtained from flight 28 because the flight was terminated early, however, the data as shown on Figure 5.4-18 indicates that the difference was still present and unexplained.

T2S Noise

Another problem associated with the measurement of T2S was the noise level of the signal. It should be noted at this point that the T2S noise did not affect control operation or engine performance but was confusing in the analysis of the T2S difference problem. An example of this noise, taken from flight 16 is shown on Figure 5.4-19. The comparable T2H signal exhibiting a ±1.25° noise level is shown on the same Figure. To eliminate this problem a 1.25 Hz filter was applied to the T2S signal. The filtered T2S signal is shown in Figure 5.4-20. The filter reduced the average noise level from ±5° to ±1°, an acceptable level.

It was also noted during ground run 23 that the T2S noise had essentially disappeared. This ground run was made after a change in IFU's. The T2S noise level after this change is also plotted on Figure 5.4-20. These data were obtained from a conversion of the raw T2S millivolt signal taken before the filter.

Testing of both IFUs in the lab after the flight test activity was completed revealed a noisy T2 signal on the IFU used prior to ground run 23 (V1), indicating that the noise was not a function of the thermocouple or harness but rather the IFU. (Paragraph 7.1.3).

5.4.2.2 T3S and T22 Performance

Measurement of T3 was made using the existing TF30 bill of material probes. These probes, as were the T2 probes, are part of the bill of material harness system which calculates the turbine inlet T4 temperature.

The same characteristic offset existed between T3S measured by the DPCU and the T3H measured by NASA/DFRC as did for the T2 measurement. This offset is shown in Figure 5.4-21 during an auto-throttle airplane accel at max A/B during flight 24. Because the offset (20°) was small compared with the absolute value of T3 (1400°) it was not deemed critical for engine or control operation.

The T22S measurement was made from the combination probe, new to the IPCS program. NASA DFRC did not measure this parameter so there was no comparison. The data obtained during flight did not indicate any problems with this measurement.

5.4.3 Fuel Flow, WFGS

A comparison of P676629's idle to military accelerations times at 45000 ft/ 0.9 MN condition during NASA/LeRC altitude testing showed the BOMDIG controlled acceleration was significantly slower than the hydromechanical controlled acceleration. The primary source of this slow acceleration was traced to a fuel flow calibration problem in which the fuel flow calibration was correct for the output data signal, WFGS, but was not correct for the commanded fuel flow to the engine. Thus the controller sensed more fuel flow than was actually delivered to the engine, resulting in slow accelerations.

Recognition of this problem during altitude testing led to further investigation of the fuel flow calibration of the main fuel control on the flight test engine P-676627 and its relation to the nominal IFU fuel flow schedule. This relation is shown on Figure 5.4-22. As noted from the curve both schedules agreed favorably, eliminating the need for any calibration correction in software. Substantiation of this calibration agreement can be noted from the results of the idle to military transient comparison at the 47K/0.9 MN condition between hydromechanical (HMC) operation and BOMDIG operation as shown on Figure 5.4-23. This plot of WFGS/PS3S versus N2S during flight 20 shows that the HMC and BOMDIG WFGS/PS3S levels for the most critical condition in terms of percentage error on absolute WF level are within 1.0 ratio unit during the initial

FLIGHT 16

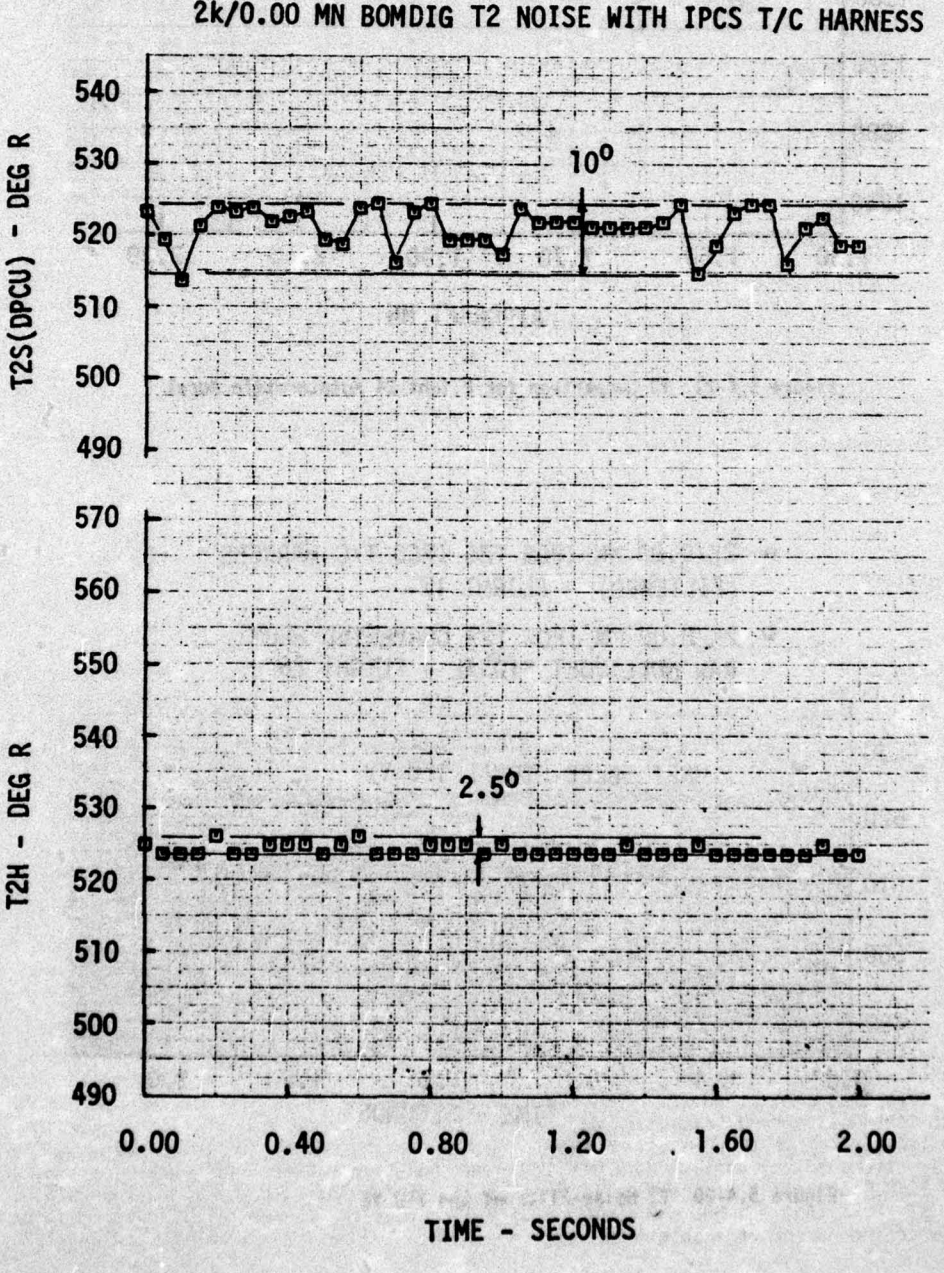

Figure 5.4-19 Unfiltered T2 Noise

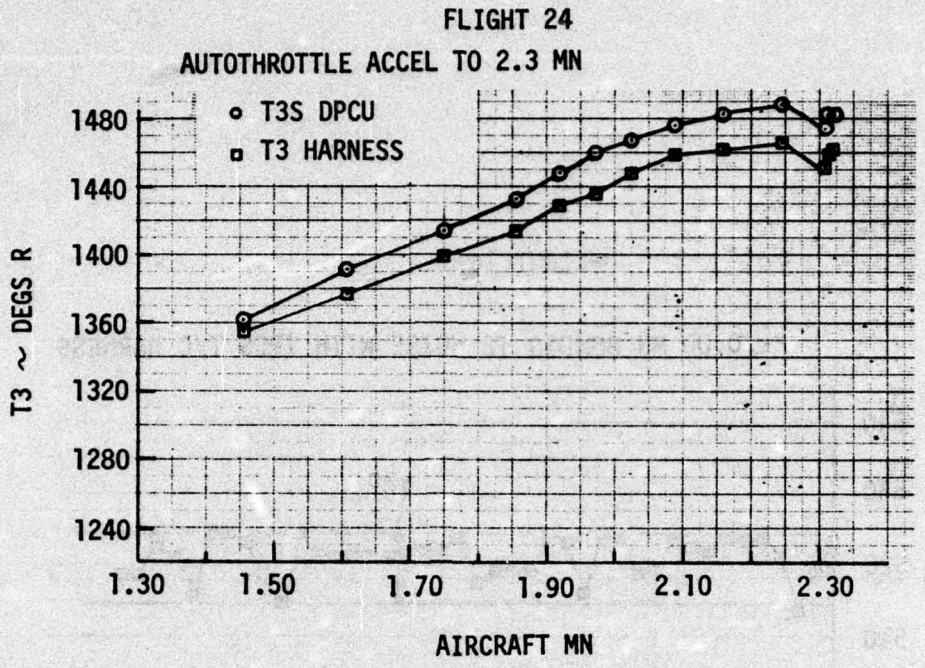

Figure 5.4-21 T3 Comparison for Flight 24 Autothrottle Accel

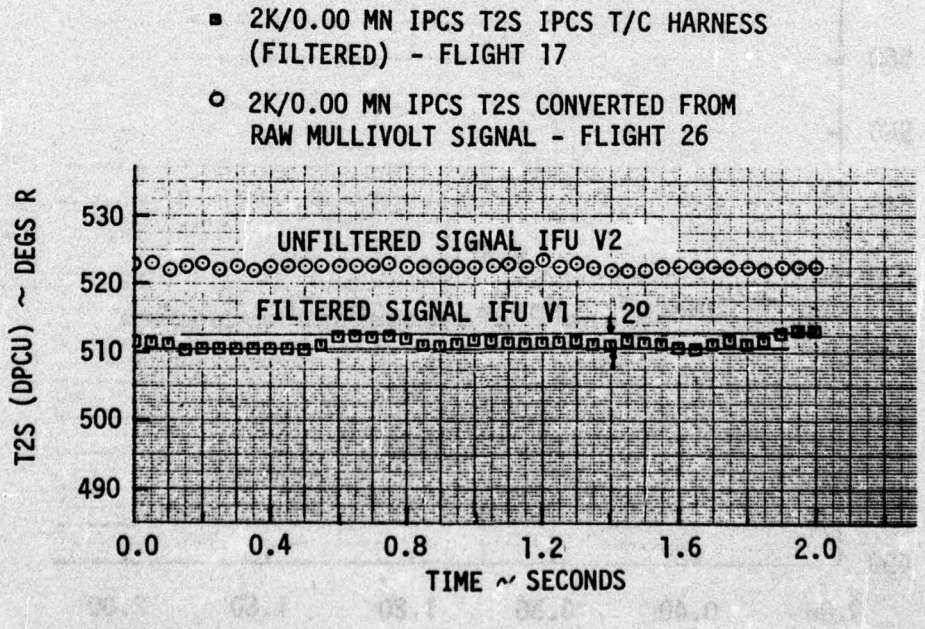

Figure 5.4-20 T2 Noise-Filtered and IFU V2

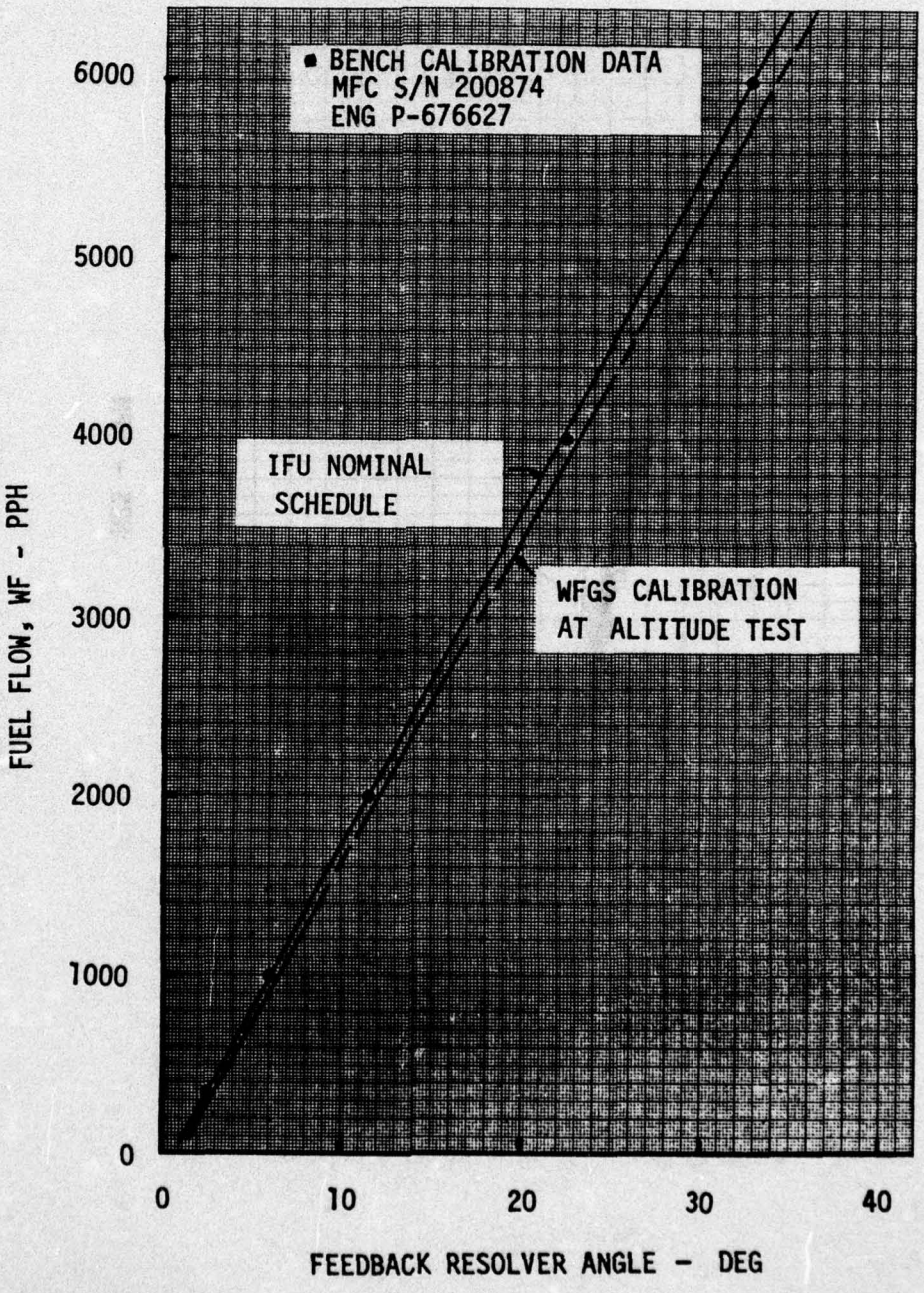

Figure 5.4-22 Gas Generator Fuel Flow Calibration

FLIGHT 20

47K/0.90 MN BOM IDLE - MIL SNAP ACCEL

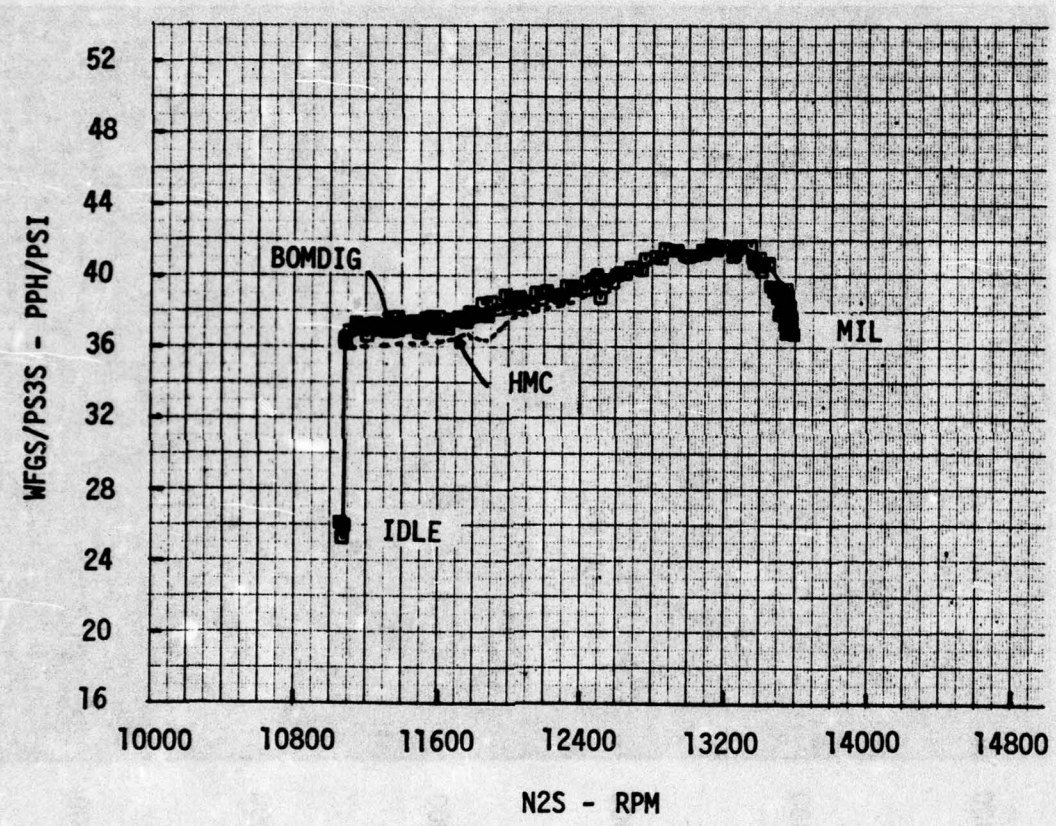

Figure 5.4-23 Idle-Mil Wf/Pb Plot, BOMDIG, HMC

part of the acceleration and line on line at the higher level. The acceleration times from idle to 95% N2 of 11.0 sec for HMC and 10.0 for BOMDIG indicate that the fuel flow delivered to the engine is approximately equal for both modes. As shown in Figure 6.2-44 the HMC and BOMDIG idle to mil accel times are comparable for a number of flight conditions.

5.4.4 Synthesized Turbine Inlet Temperature

The IPCS mode utilizes the turbine inlet gas temperature measurement as one of the limiting control loops. The flight test engine, P-676627, did not have the T4 probe installed. Therefore, for the flight test program the source of the measurement was a synthesized signal, T4SYN, calculated as follows:

$$T4SYN = T3SC + .95\ (\ -9.38 \times T3SC + 78.750) \times \frac{WFGS}{WAENG} + TSNB$$

$$WAENG = WRTPA3 \times PS3 \times \sqrt{T3SC} \times 3600$$

$$WRTPA3 = TF41 \left(\frac{P3S - \Delta P3S}{P3S} \right)$$

where:

T3SC - Compensated HPC discharge temperature, deg R ; $\frac{WFGS}{WAENG}$ - fuel/Air Ratio ;

TSNB - Bias factor ; WAENG - Core airflow ; $WRTPA3 - \left[\frac{W\sqrt{T}}{P} \right]_{\text{HPC exit}}$

5.4.4.1 Steady-State Comparison

The T4SYN signal was calibrated using the T4H measured by the bill of material harness as the baseline. The correlation of the T4SYN signal with harness T4H taken from ground run 16 indicates an error of approximately 50° at the high temperatures (figure 5.4-24). In an effort to reduce this error, the T4SYN bias (TSNB) was changed from +31° to -29°. Data from ground run 19 taken after this change are also shown on Figure 5.4-24 and indicate excellent agreement between the two signals.

The results of a steady state max A/B temperature comparison made during an airplane acceleration from 1.25 MN to 2.30 MN during flight 24 are shown in Figure 5.4-25. The correlation shows an average error of approximately 40° throughout the accel. In assessing the T4 synthesized equation it can be noted that the signal is dependent upon valid measurement of T3S, P3S, P3 and WFGS. For the same airplane acceleration there is a 20° error in T3 (figure 5.4-21). This will have approximately a 1:1 effect on T4SYN. Eliminating this error would reduce the T4SYN error from 40° to 20°. The shift in T4SYN at high Mach number results from opening the 7th stage bleed at Mach 2.29 as indicated.

The noise associated with the measurement of the T4SYN signal is documented in figure 5.4-26, obtained from a military power 20K/1.4 MN flight 18 condition. The noise level ±15°, for the 30K/1.4 MN condition is slightly higher than the 2.0K/0.0 ,M condition, ±10°, however a total review of all the data indicates that the noise level variation is approximately ±5° to ±15°, not dependent on flight condition. In addition to the T4SYN signal noise, the figures also show the noise levels of the signals that are used in the calculation of the T4SYN signal. It can be noted that all the signals contribute to the T4SYN noise with ΔP3 having the highest percentage noise level of 3.43% of point.

The noise level of the T4SYN signal did not have any detrimental effect on the use of this signal as a limiting control loop because the forward path integrator in the control filters the noise sufficiently when the T4 loop is in steady state control at high Mach numbers (Section 4.2).

AD-A034 172 BOEING AEROSPACE CO SEATTLE WASH F/G 21/5
INTEGRATED PROPULSION CONTROL SYSTEM (IPCS) VOLUME III. FLIGHT --ETC(U)
AUG 76 W J HASTINGS, C M CARLIN F33615-73-C-2035
UNCLASSIFIED AFAPL-TR-76-61-VOL-3 NL

2 OF 4
AD
A034172

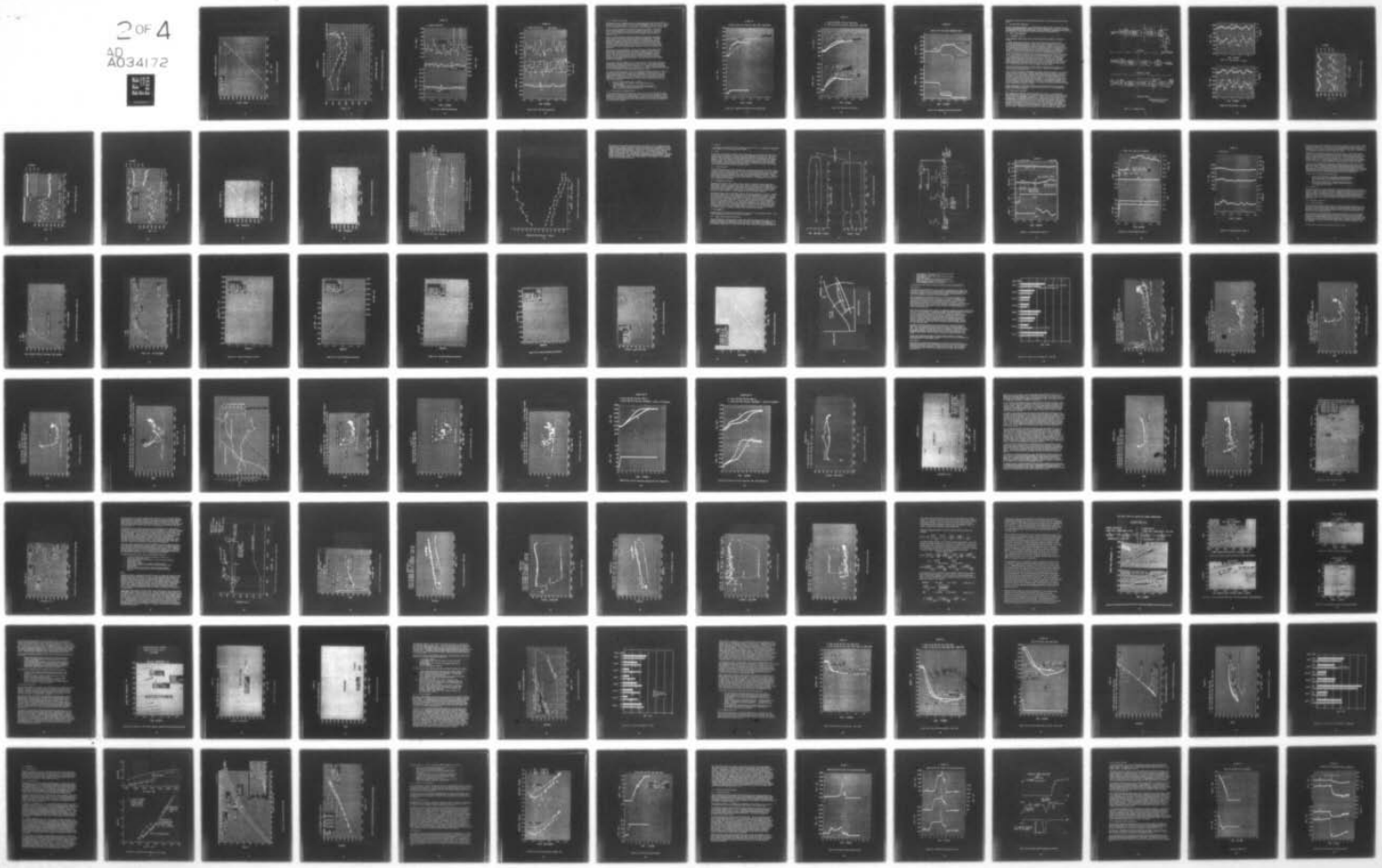

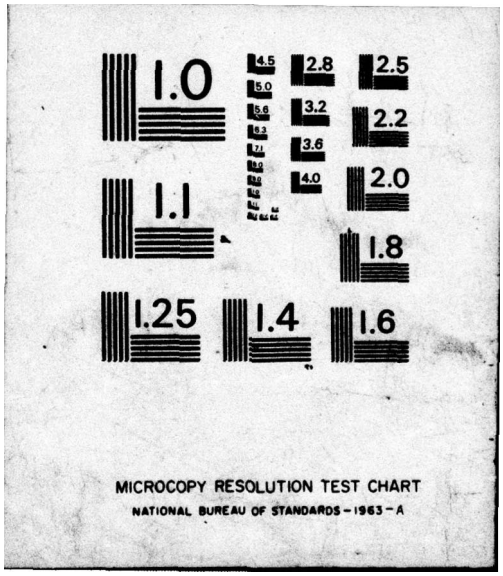
1.0
1.1
1.25
1.4
1.6
1.8
2.0
2.2
2.5
2.8
3.2
3.6
4.0
4.5
5.0
5.6
MICROCOPY RESOLUTION TEST CHART
NATIONAL BUREAU OF STANDARDS - 1963 - A

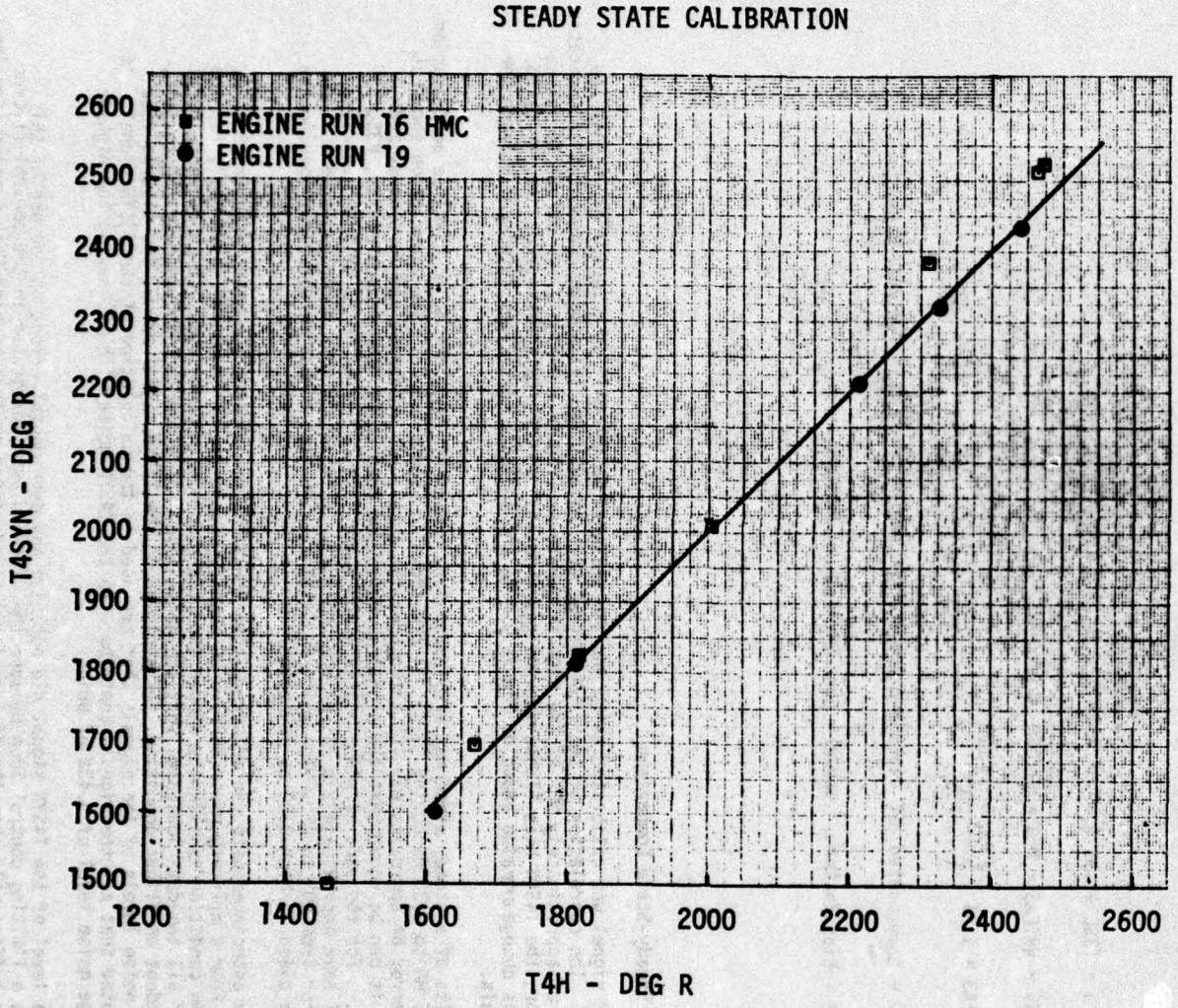

Figure 5.4-24 T4SYN Calibration

FLIGHT 24

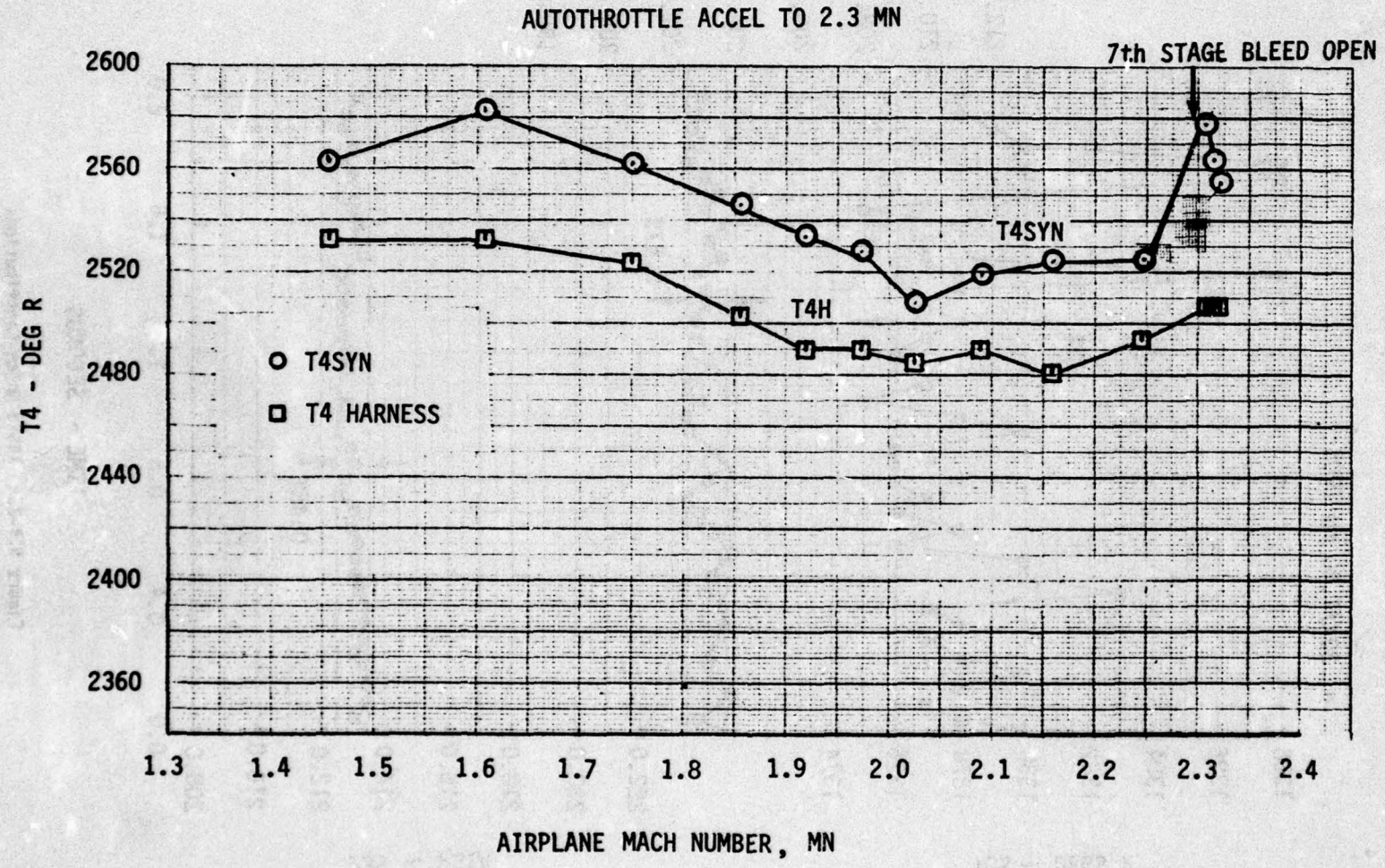

Figure 5.4-25 T4 Comparison for Flight 24 Autothrottle Accel

FLIGHT 18

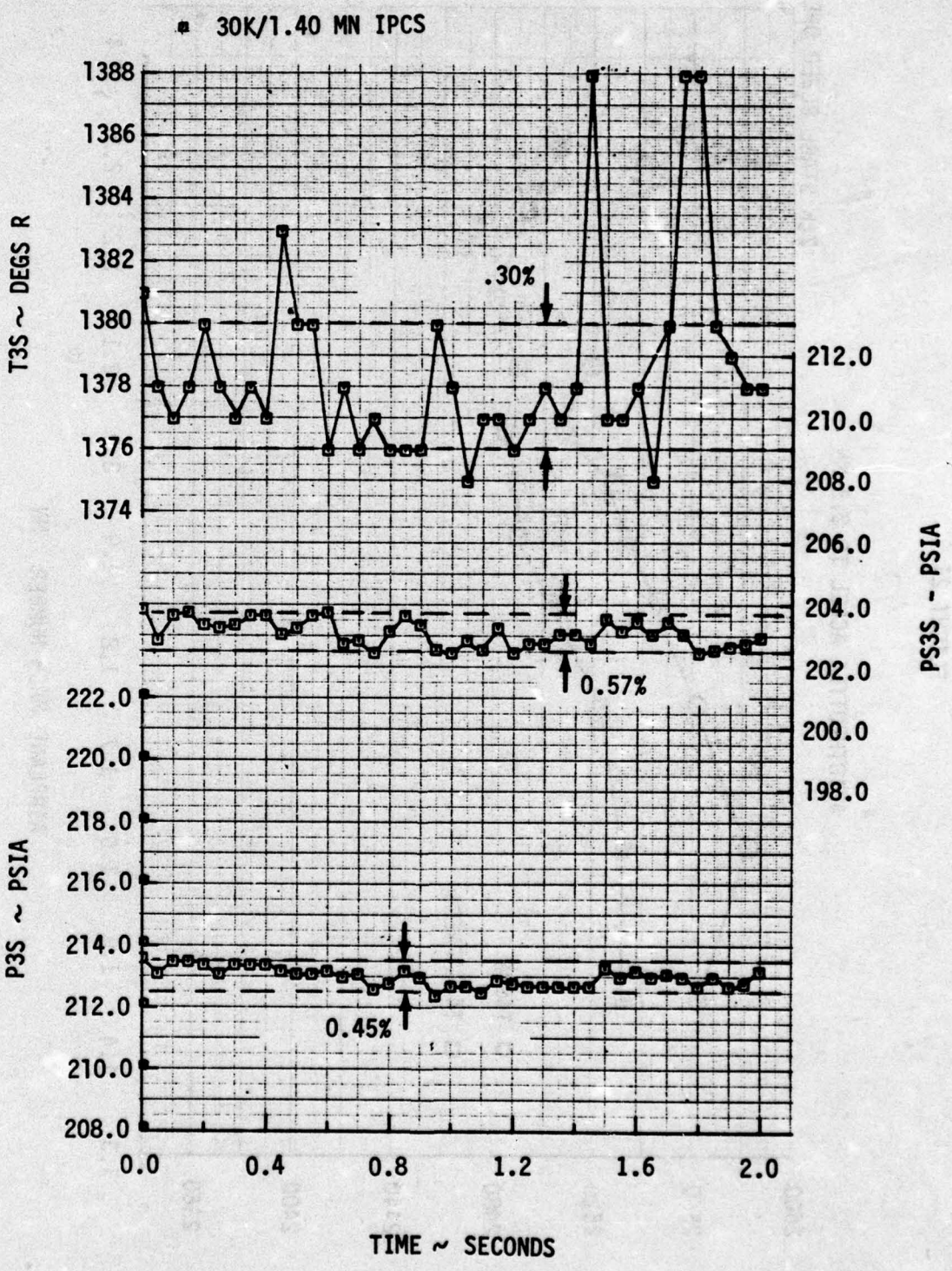

Figure 5.4-26a T4SYN Noise Contributions

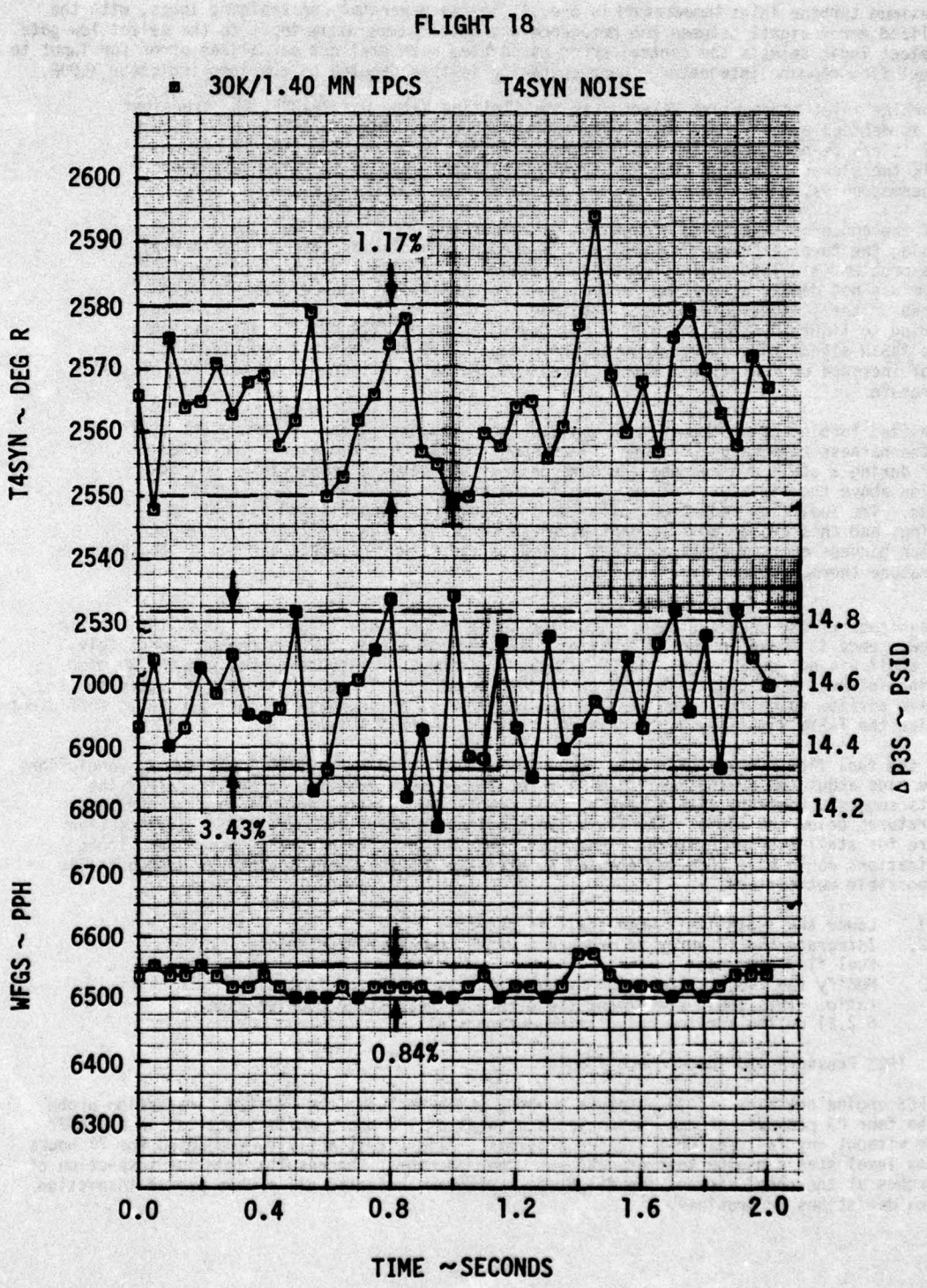

Figure 5.4-26b T4SYN Noise Contributions

5.4.4.2 T4SYN Transient Response

The maximum turbine inlet temperature is one of the gas generator constraining loops, with the normalized error signal between the reference and actual temperature input to the select low gate. The select logic selects the control error associated with smallest normalized error for input to the fuel flow command integrator. Loop operation is then denoted by the loop indicator XLOOP.

The turbine inlet temperature selected as the limiting value was 2640°F, the transient limit as defined by the TF30 T.O. 2J-TF30-36 and shown on Figure 5.4-27. From figure 5.4-27 it can be noted that the T4SYN signal response is faster than the T4H harness signal; the slow response of the T4H signal being attributed to the slow response of the thermocouples.

One of the concerns related to increasing gas generator accel times was the thermal stress on the turbine created by the rapid increase in gas temperature. The thermal stress problem is a life cycle problem and because of the short duration of the IPCS program was not deemed a limiting factor, however, an illustration of how the high response of the T4SYN signal reduced the thermal stress on the turbine can be noted. Referring to figure 5.4-28, an idle to mil transient at 41K/1.4 MN, the high response of the T4SYN signal causes operation on this loop. This results in a reduction in the rate of increase of fuel flow and therefore, reduced rate of increase in turbine inlet temperature.

Synthesized turbine inlet temperature was also more responsive during compressor stall than the harness temperature. Figure 5.4-29 shows the synthesized signal increased faster during a stall and reached the same peak as the harness temperature, but its duration above the limit was 0.2 sec., while the harness overtemperature lasted 1.9 seconds. The fuel flow reduction following the stall was accomplished with Wf/Pb limiting, and this caused an attendant decrease in T4SYN below the limit. The longer duration harness overtemperature is attributed to the slower response turbine discharge temperature thermocouple.

The magnitude of the peak synthesized turbine inlet temperature largely reflects the drop in airflow, hence increase in fuel/air ratio, following the stall. Flow stoppage immediately after stall was not detected by the DPCU because of the low response probes and the 30 msec. sampling interval (see Section 6.2.2 for further details). Instead, the DPCU detected small positive airflow rates following stall which resulted in an increase in fuel-air ratio sufficient to raise the T4SYN signal by 350 degrees above the pre-stall level.

Since the fuel flow cutback after the stall was accomplished with Wf/Pb limiting, no conclusions can be made about the synthesized turbine inlet temperature limiting during a stall. The results suggest, however, that a smaller fuel cutback would also have produced synthesized temperatures below the limit. The T4SYN logic was not originally conceived as a protective measure for stall overtemperatures. Had this been an objective of the IPCS program, logic modifications could have been implemented to directly control overtemperatures during stall. Some possible methods are:

1. Lower the T4SYN limit when stall is detected.
2. Integrate the T4 error to produce a Wf/Pb command rather than a fuel flow command.
3. Modify the T4SYN calculation by substituting Wf/PB for fuel air ratio. This would circumvent the effect of rear stage choking (see 6.2.2) on the airflow calculation during stall.

5.4.5 IPCS Pressure and Temperature Probes

The IPCS engine pressure and temperature probes, which include the P22-T22 combination probe, and the four P3 pressure probes, accumulated a total of 105 hours while installed in P-676627 engine without any failures or indicated problems. Flight test activity accounted for 77 hours and sea level static engine test at P&WA the other 28 hours. The results from the inspection of the probes at the conclusion of the flight test program indicated all probes passed inspection with no deviations or problems.

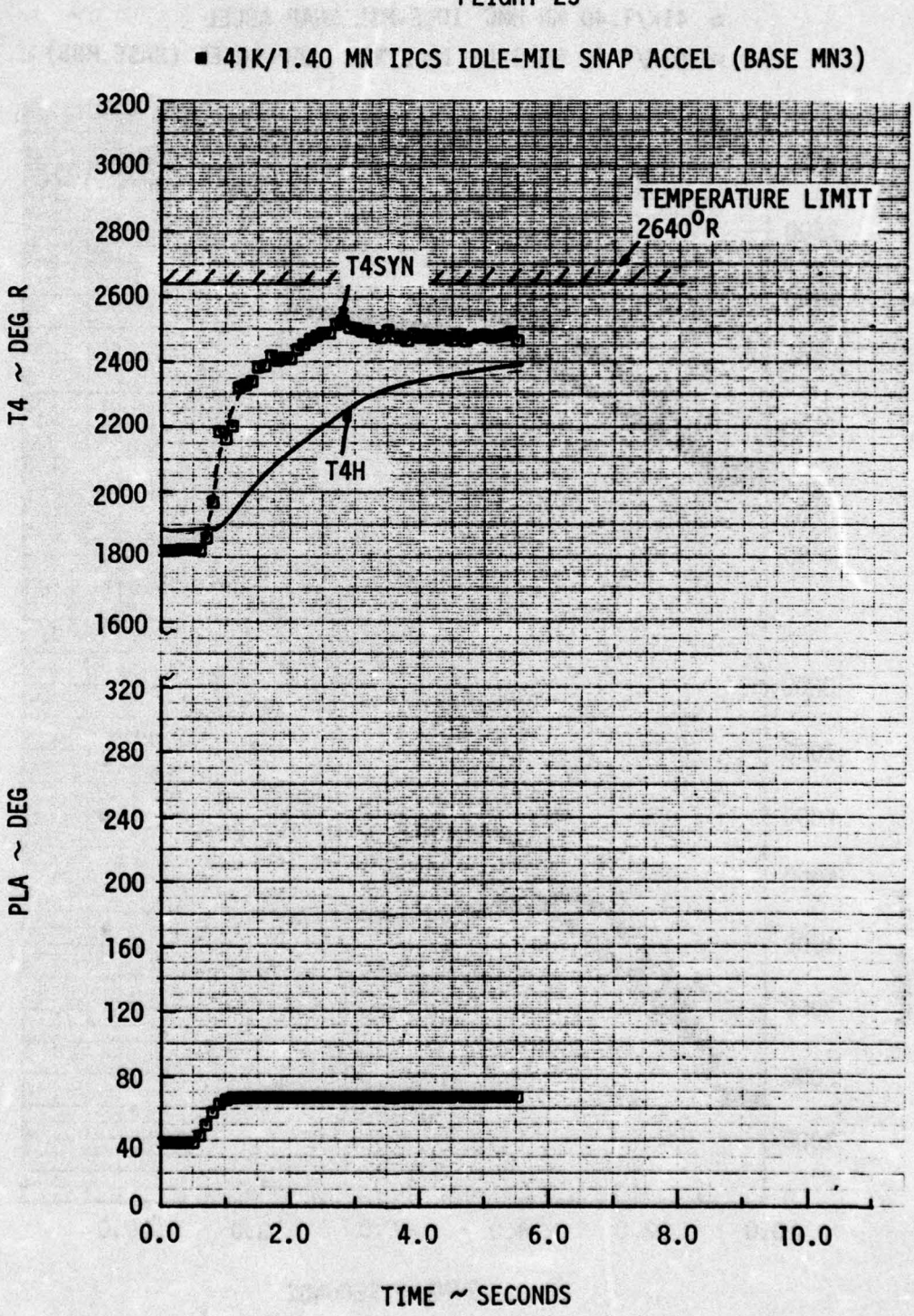

Figure 5.4-27 Comparison of T4SYN and T4H for Idle-Mil Snap

FLIGHT 25

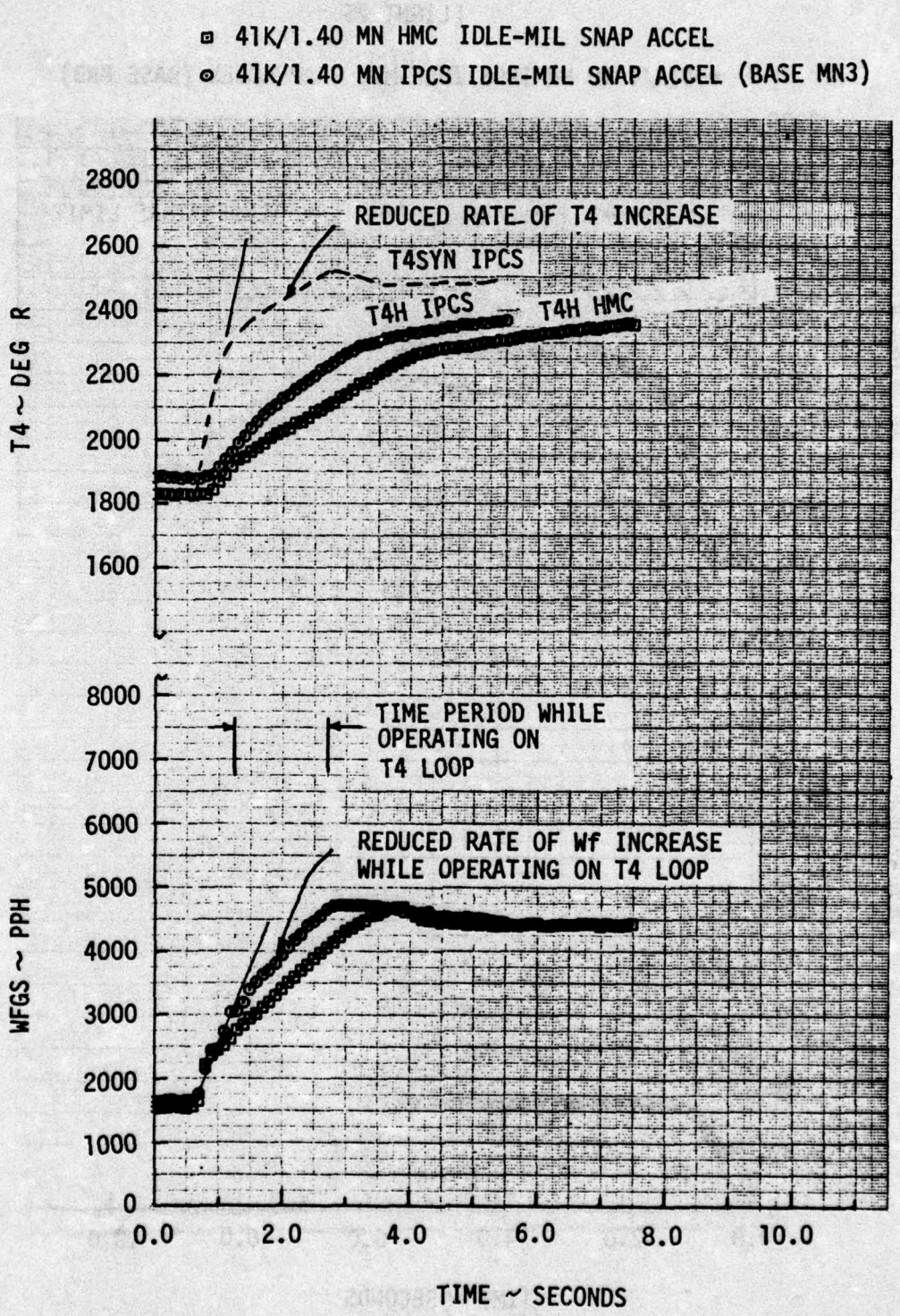

Figure 5.4-28 Operation of the T4 Loop

FLIGHT 25

41K/1.4 MN IPCS CONE EXPANSION STALL

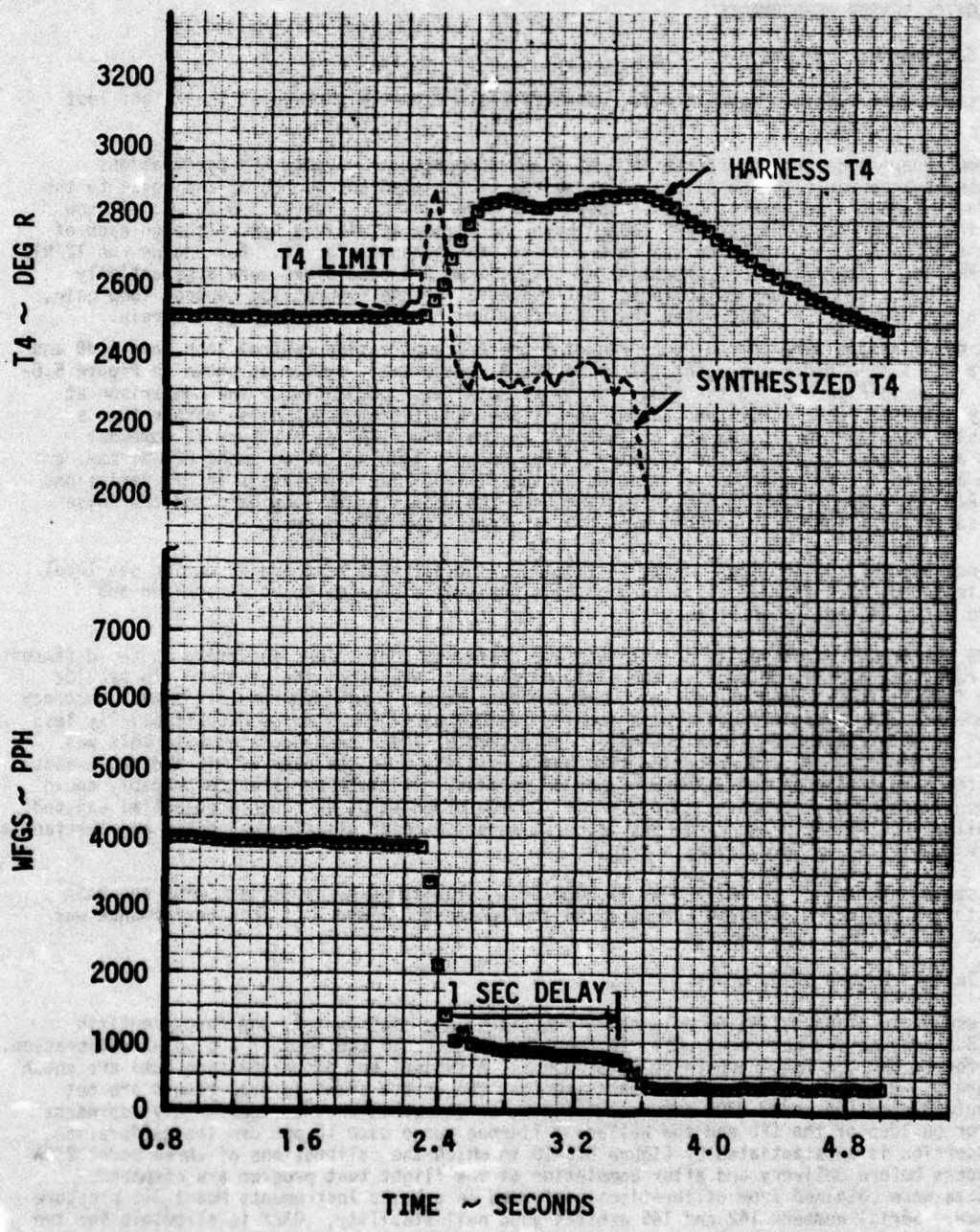

Figure 5.4-29 Temperature Time History During Stall

No problems occurred with the engine modifications required for the PS3S static pressure measurements.

5.5 HIGH LEVEL ANALOG TRANSDUCERS

The high level analog transducers, inlet surface position measuring LVDTs, and CMU, Manual Inlet Control, and CADC potentiometers, operated satisfactorily throughout the test program. No evidence of calibration shifts was noted during the test. The only calibrations required were offset and minor gain adjustments required to adapt to the airframe installation during ground test.

5.6 DIGITAL SENSOR PERFORMANCE

5.6.1 Tachometers - N1, N2

The N2 tachometer system, Figure 5.6-1a, operated satisfactorily throughout the Flight Test Program.

It became apparent during engine run 10 that a noise source was causing EPR oscillations which were unacceptable to the pilots. Engine run 11 isolated the source of the noise to the N1 signal, at that time generated as is shown in Figure 5.6-1b. Figures 5.6-2, -3, -4 show EPR variations for T2S, T3S, and P2S locked with the engine at minimum A/B. Although each of these variables has some contribution to EPR noise none accounts for it. For engine run 12 N1S was locked at military and EPR variations at the minimum A/B conditions were substantially reduced. In addition it was established that reduction of the suppression control loop gain, see para 6.3.1.2, further alleviated the EPR variations by increasing loop gain margin.

The EPR oscillations were corrected by reducing the A/B suppression control loop gain 6 dB and adding a six sample block averaging filter to the N1 measurement system as shown in Figure 5.6-1c. As shown in Figure 5.6-5 the reduction in N1 noise was substantial. The comparison at military demonstrates clearly that the N1 variations result from input noise rather than a suppression loop instability as was conjectured at one time. EPR at military is somewhat quieter after the addition of the N1 noise filter because loop switching among N2, N1 max. and maximum airflow due to noise was eliminated by the filter. The improvement in EPR variations during A/B operation, Figure 5.6-6, resulting from the reduction in loop gain and the noise filter satisfied flight crew concern over A/B roughness from this source.

Experience with N1 during flight test, T4 (TIGT) during altitude test and N2 during sea level static test indicates that aliasing in digital signals is a problem to be recognized and assessed early in the design process.

The IPCS system was developed to accommodate two different controllers operating at two different sample rates not clearly defined in the early development stages of the program. To provide maximum flexibility in development, hardware sample size was minimized consistent with accuracy requirements. As a result digital data samples in the baseline system used substantially less than 50% of data available within the major cycle sample. The risk associated with this was accepted to minimize program execution time and complexity. In the case of N1, and N2, events forced the acquisition of the maximum number of samples. T4 probe performance probably could have been improved by increasing sample rate. On the other hand, although a potential existed for similar problems with the Paros transducers, no evidence of aliasing was noted and substantial software complexity was avoided as a result.

Steady state accuracy of the N1 and N2 tachometers, established by comparison with the NASA flight test tachometers, was ±50 RPM as shown in Figures 5.6-7 and -8. This performance was adequate for all IPCS requirements.

5.6.2 Inlet Pressure Transducers

After resolution of installation related malfunctions, see section 7.4, the Paroscientific model 230A transducers performed well. A functional check, in the form of a 6 point calibration, was performed per the requirements of Reference 1. A typical set of calibration data are shown in Figure 5.6-9. It is important to emphasize that the errors shown in this figure are not representative of the model 230A accuracy, rather, as indicated on the figure, they represent the error buildup of the IFU and the Wallace & Tiernan guage used to perform the calibration. This assertion is substantiated by Figure 5.6-10 in which the calibrations of three model 230A transducers before delivery and after completion of the flight test program are compared. These data were obtained from calibrations performed on a Texas Instruments Model 145 pressure reference. Serial numbers 142 and 145 exhibit good null stability, .032% is allowable for two years of service. The apparent span (gain) shift is not within specification. However, the

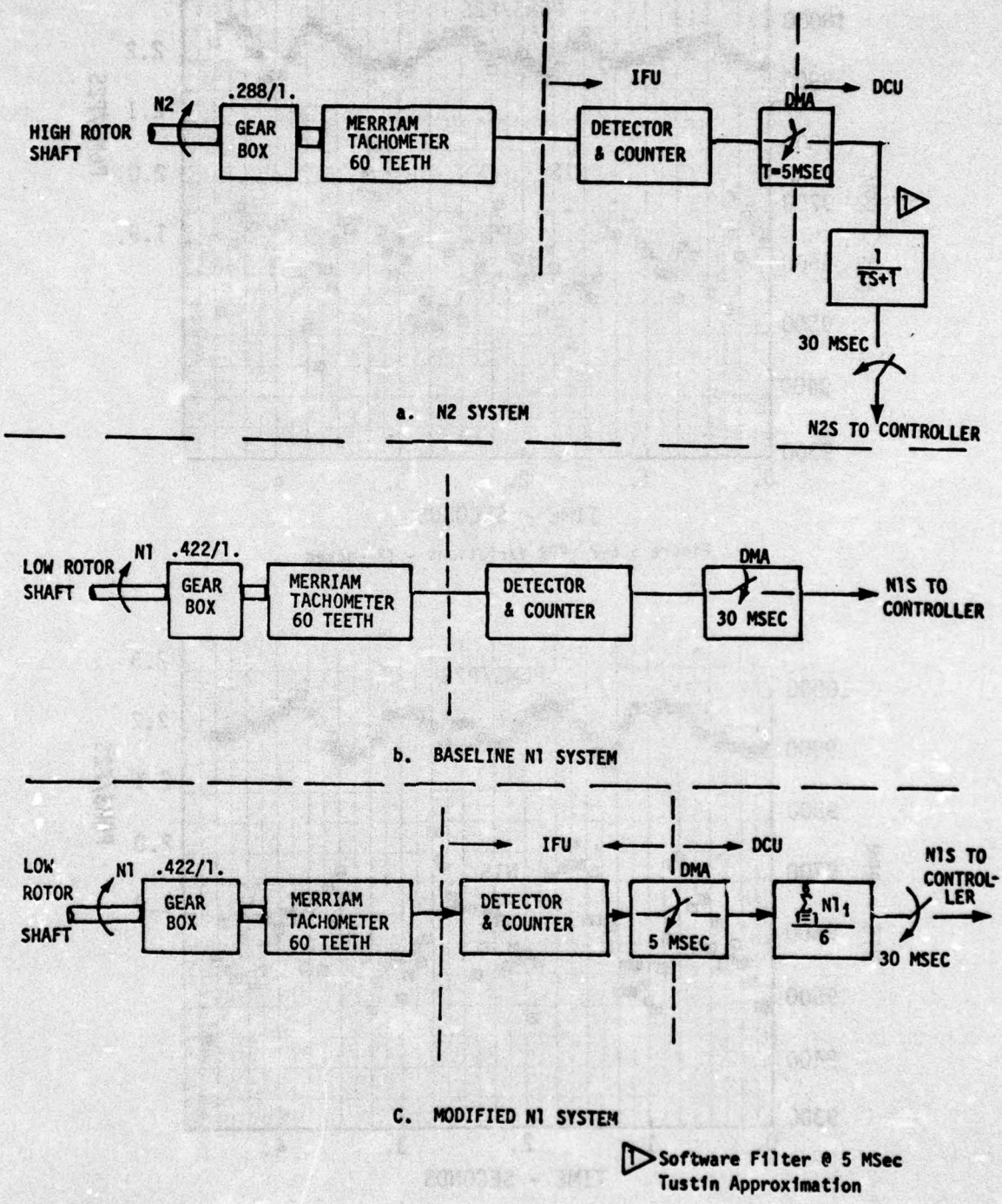

Figure 5.6-1 Tachometer Systems

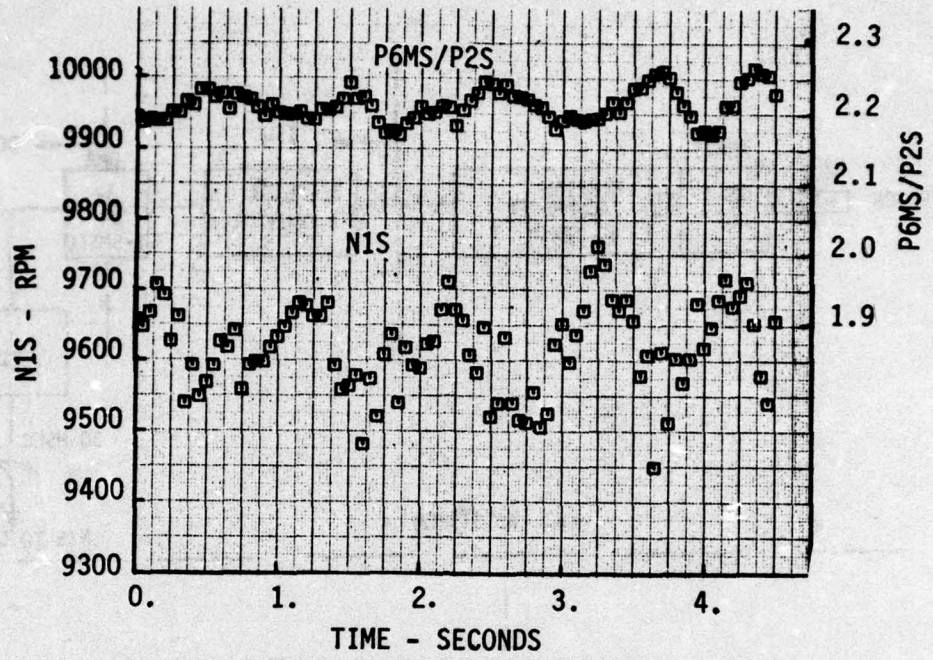

Figure 5.6-2 EPR Variations - T2 Locked

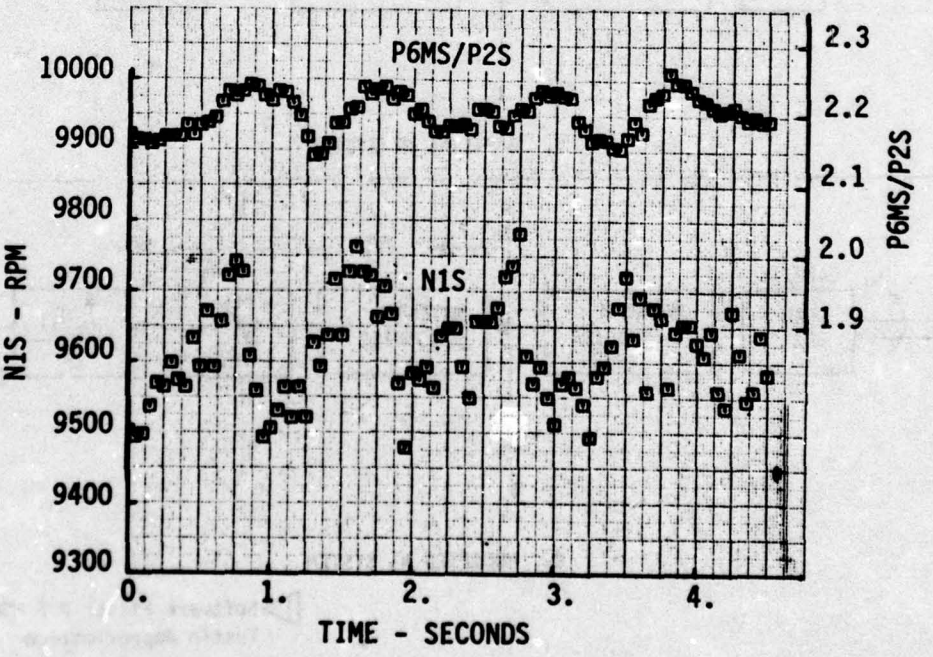

Figure 5.6-3 EPR Variations - T3 Locked

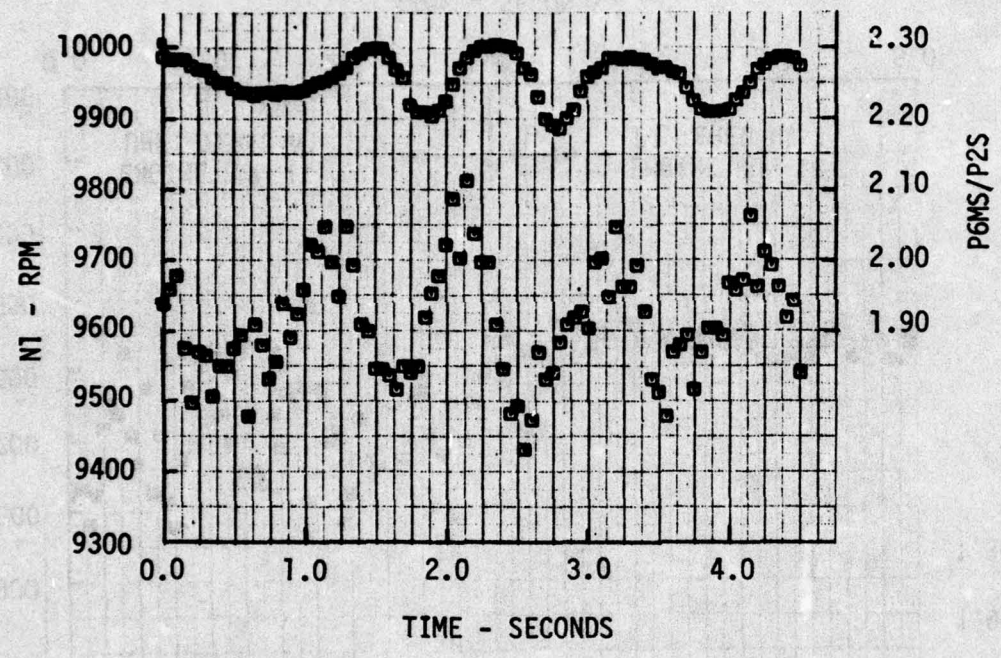

Figure 5.6-4 EPR Variations - P2 Locked

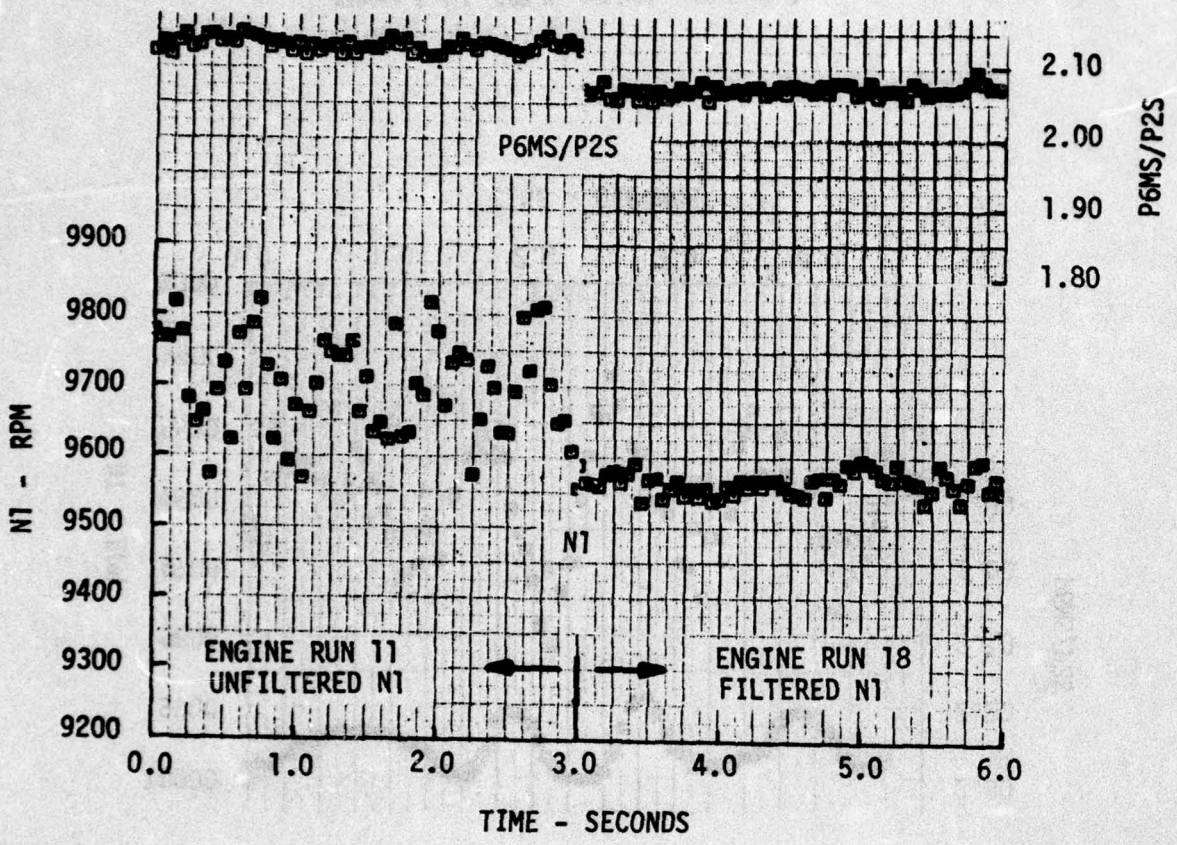

Figure 5.6-5 N1 Noise Comparison at MIL

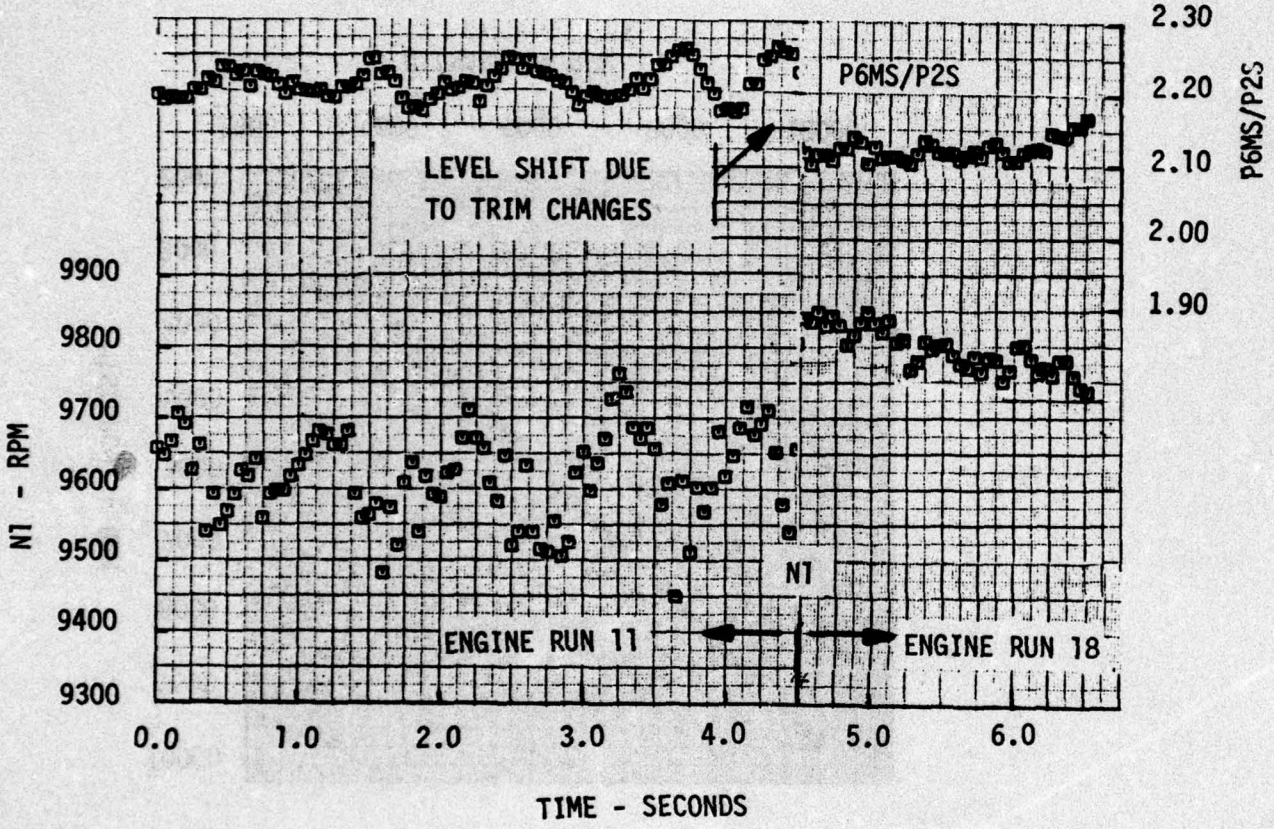

Figure 5.6-6 N1 Noise Comparison in A/B

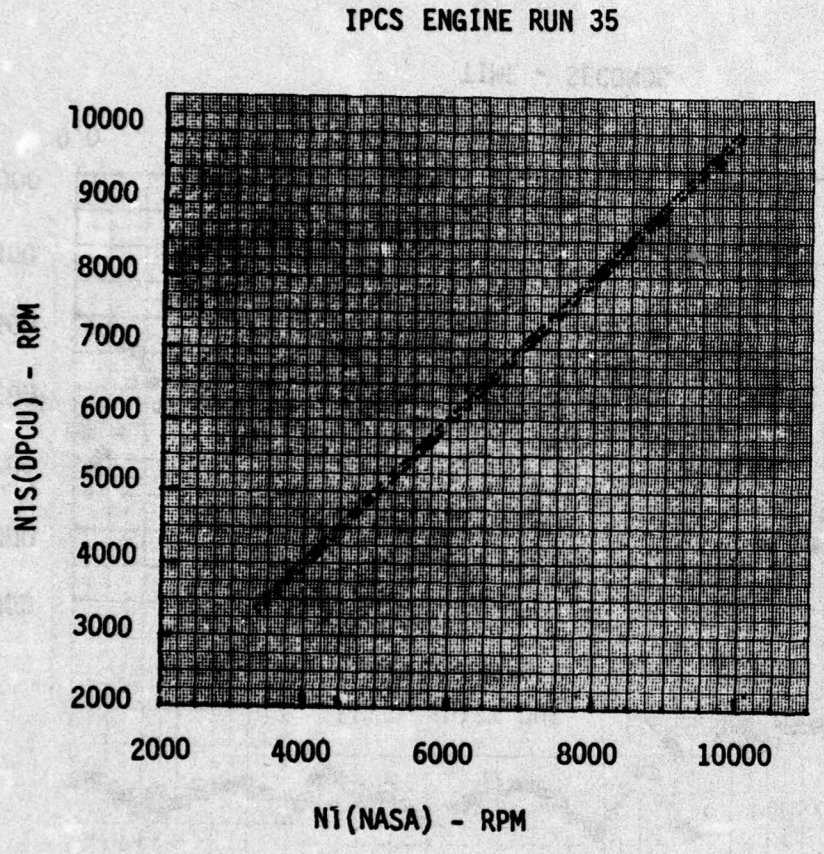

Figure 5.6-7 N1 Tachometer Steady-state State Performance

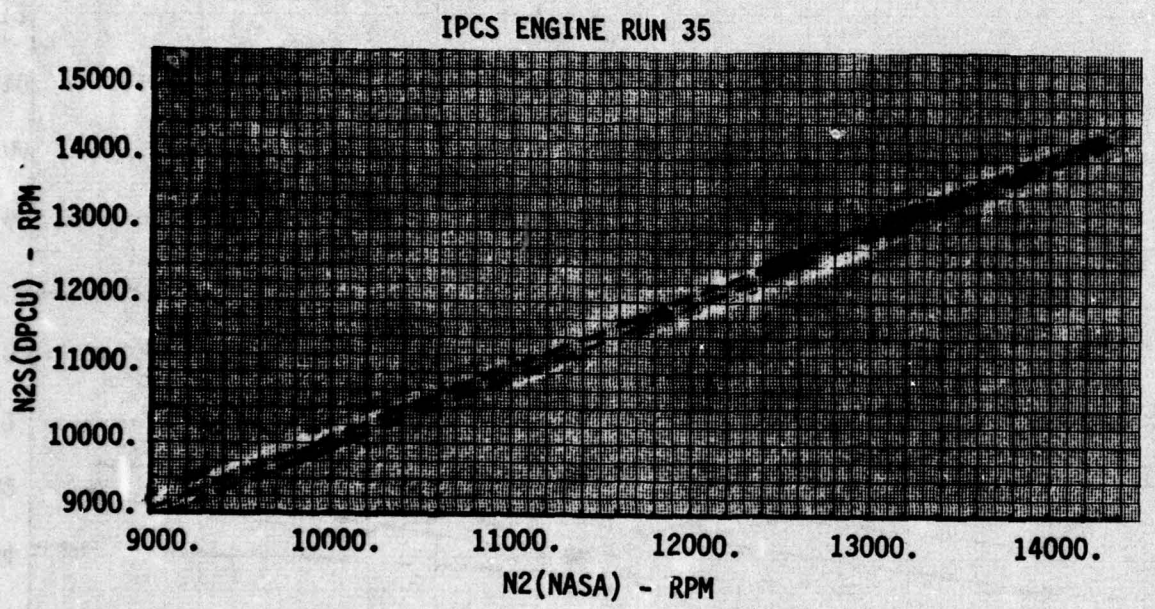

Figure 5.6-8 N2 Tachometer Steady-State Performance

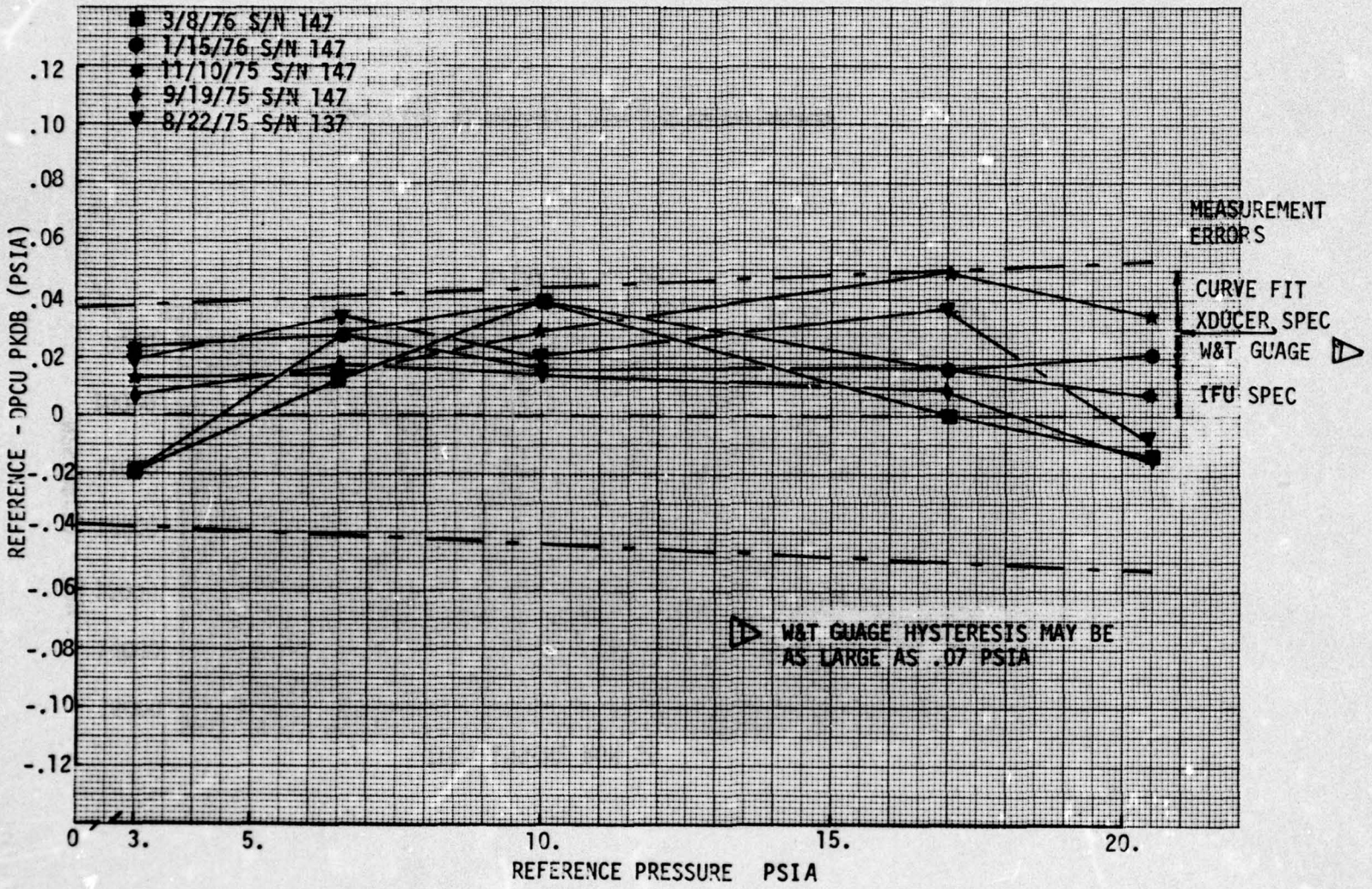

Figure 5.6-9 Paroscientific Transducer Calibrations

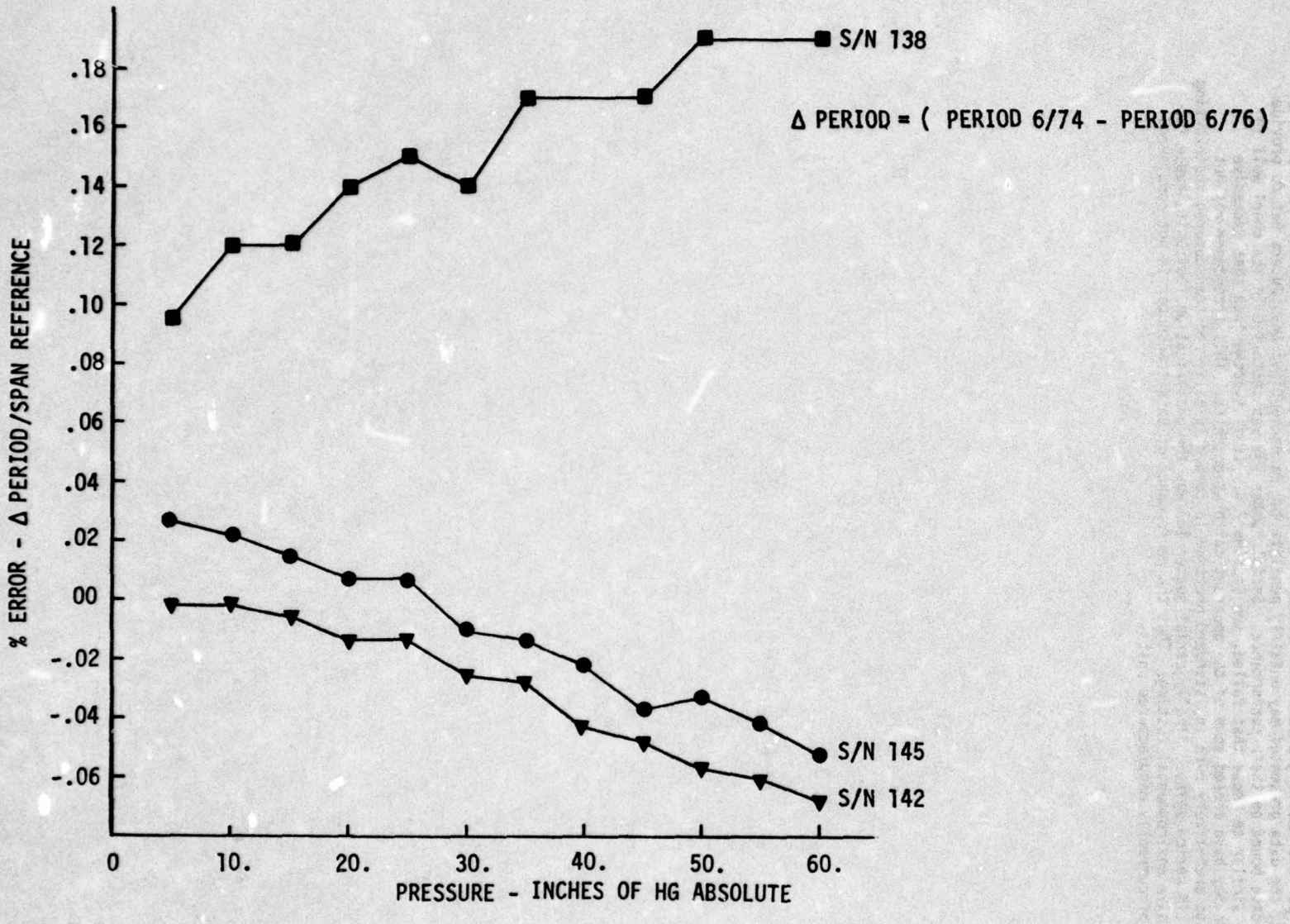

601

Figure 5.6-10 Paroscientific Transducer Long Term Stability

parallelism of the two curves leads one to question the stability of the TI reference over the two year period. Lacking a June 1974 calibration of the Paroscientific transducers on a primary standard, the data presented may unfairly penalize the Paroscientific transducers but do provide a worst case bound on their performance. Serial number 138 was installed in the wheel well in a manner similar to those that failed, see Section 7.4. It is hypothesized that excessive vibration may have caused some of the apparent calibration shift. This transducer was not subject to predelivery burn in, standard practice in currently delivered transducers, contributing perhaps .1% period shift. Finally serial number 138 was the qualification test unit, subjected to extensive environmental testing. Thus the performance of this transducer is not considered typical of currently manufactured units.

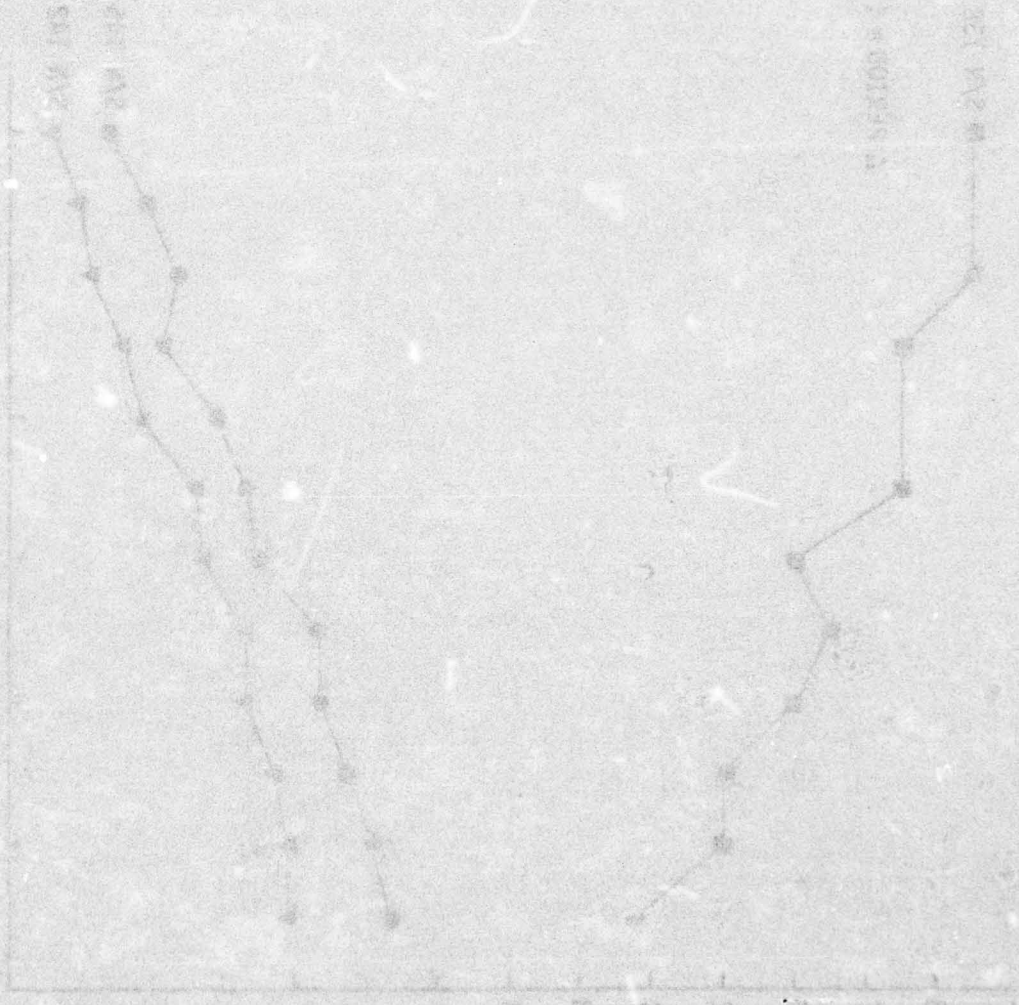

6.0 RESULTS

This section presents the test results organized by control function. As appropriate comparisons of HMC, BOMDIG, and IPCS are made in each paragraph.

6.1 INLET

As described in Reference 2 (Honeywell ICD) the hydromechanical inlet control and sensors were replaced with IPCS components. The resulting system is depicted in Figure 4.2-1. The bill of materials (BOM) inlet control consisted of open loop positioning of the spike and cone as a function of the local Mach pressure ratio (PRLM) and the duct exit Mach pressure ratio (PRDEM). BOMDIG duplicates this control. The IPCS inlet control includes the BOM control plus three additional modes - A/B anticipation, AFBIAS, and distortion adjustment to inlet positioning. Of these modes only A/B anticipation was active during the flight test program. Both the BOM control modes and A/B anticipation functioned correctly.

6.1.1 BOM Inlet Control

The BOM Inlet Control was verified in hanger tests by pressurizing the local and duct exit Mach probes to simulate various flight conditions and verifying correct position of the inlet surfaces in response to the simulated conditions. In order to reduce system noise sensitivity in steep gradient portions of the schedules, servo loop gain was reduced during Ground Test. Flight Test system performance demonstrated that this adjustment was acceptable. Figure 6.1-1 displays inlet surface positioning error at various flight conditions. As indicated it is within the bill of materials error allowance.

6.1.2 Afterburner Anticipation

Afterburner anticipation logic, Figure 6.1-2 was provided to demonstrate the feasibility of moving inlet surfaces in response to A/B control signals eventually reflecting themselves in shock motion. The A/B anticipation logic pulses the duct exit pressure ratio, PRDEM, coincident with the A/B light to temporarily reduce inlet area to match the reduction in engine airflow during the lighting transient. For simplicity in implementation the system is not inhibited coming out of A/B, although in a mixed compression inlet this might be necessary.

In-flight performance of the anticipation logic is depicted in Figures 6.1-3 and 6.1-4. The A/B manifold fill time at MN 1.4, 50K flight condition is long, approximately 1.3 seconds, so that the A/B anticipation logic actually completes its activity before the A/B lightoff. Although this mistiming is undesirable it does permit verification of the logic operation in isolation. In application to a mixed compression inlet the .5 second time delay would be replaced by a manifold fill time delay using a fill time calculation as used for the IPCS A/B sequencing logic, see Section 4.2, to achieve closer coordination between the inlet surface motion and the lightoff. Amplitude of the anticipatory surface motion might also be scheduled on the inlet pressure ratios. At the MN 1.6, 45K flight condition, Figure 6.1-4, the .5 second time delay corresponds fairly well to the A/B lightoff delay and the effect of the anticipation logic is to slightly reshape, as intended, the normal cone transient during lightoff.

6.2 GAS GENERATOR

A major portion of the flight test was devoted to evaluation of the gas generator control. The following paragraphs present the result of that evaluation.

6.2.1 Steady State Gas Generator Governing

The bill-of-material controller governs steady state operation with high rotor speed. It is a proportional control, and schedules are biased with engine inlet temperature and pressure. The schedules are shaped to provide proper thrust levels and to limit turbine inlet temperature, rotor speeds, burner pressure, and engine corrected inlet airflow at the appropriate conditions.

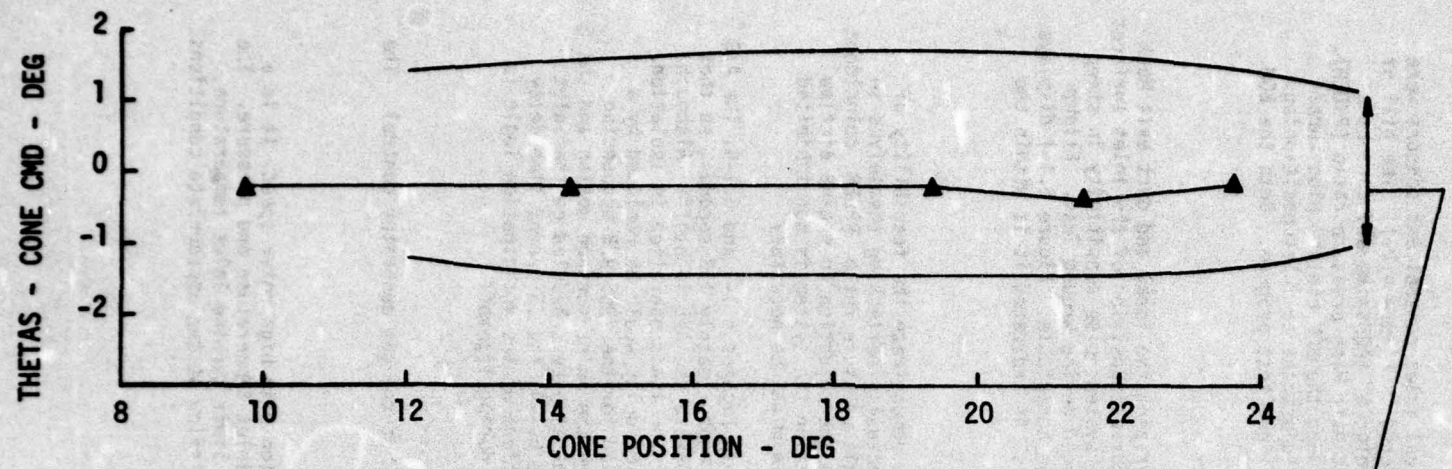

ALLOWABLE ERROR

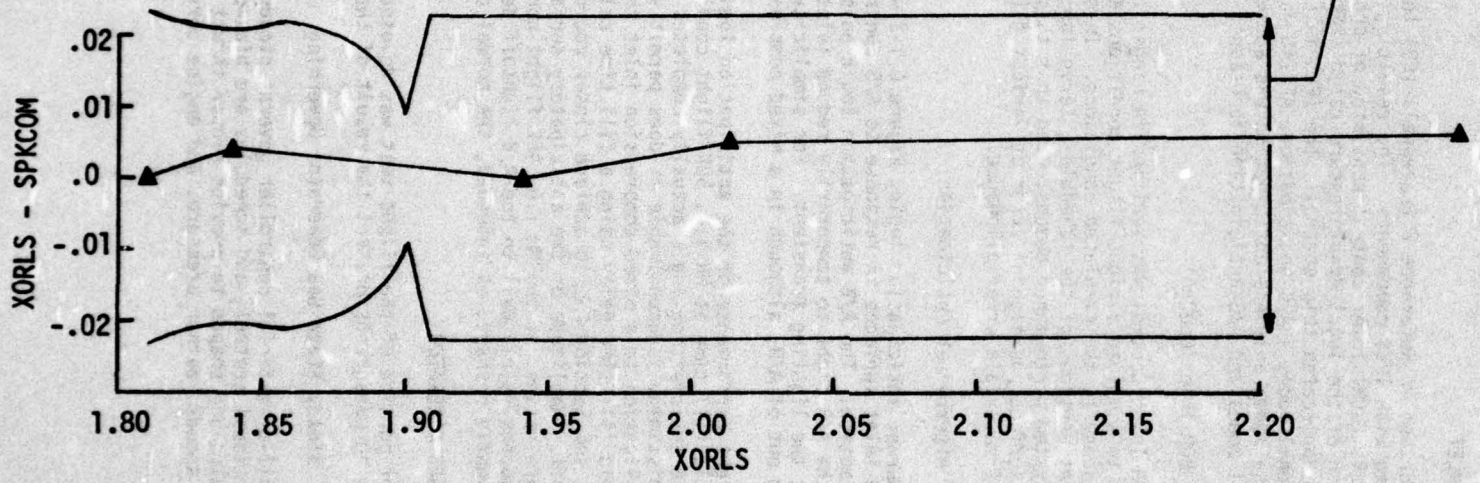

Figure 6.1-1 Inlet System Positioning Error

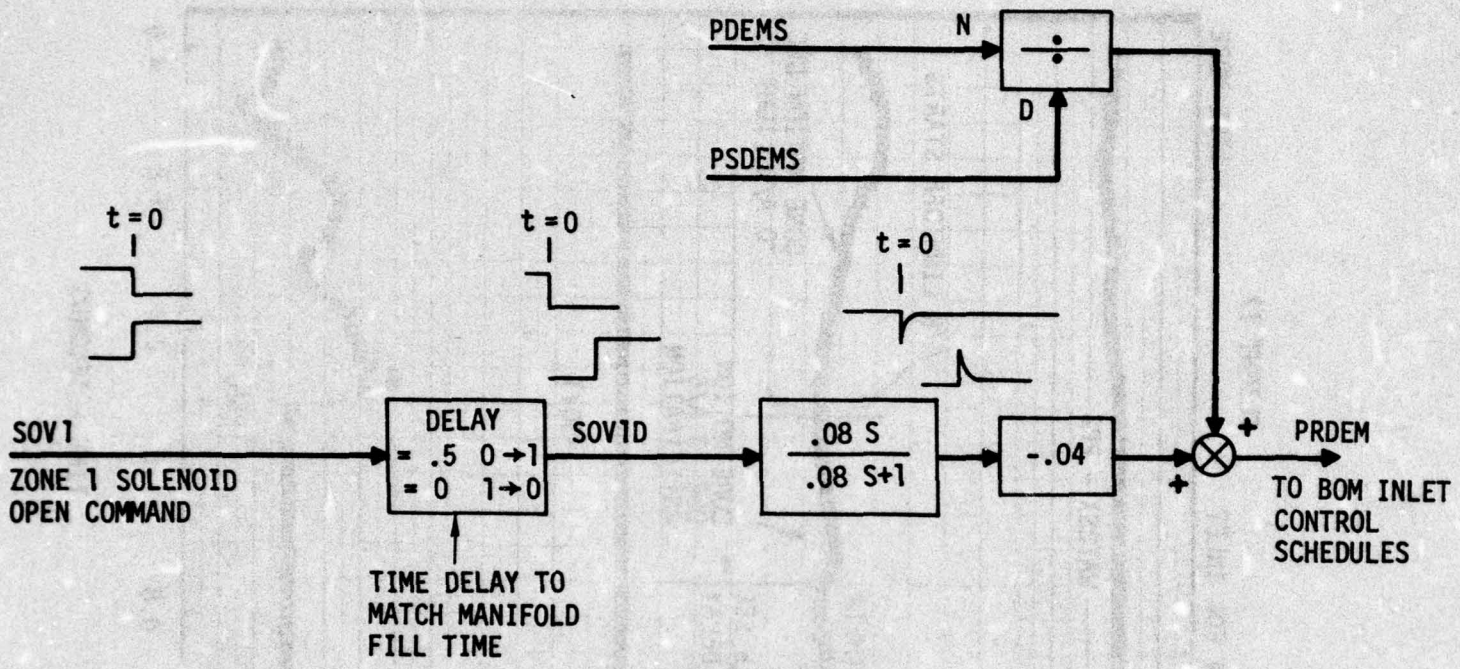

Figure 6.1-2 A/B Anticipation Logic

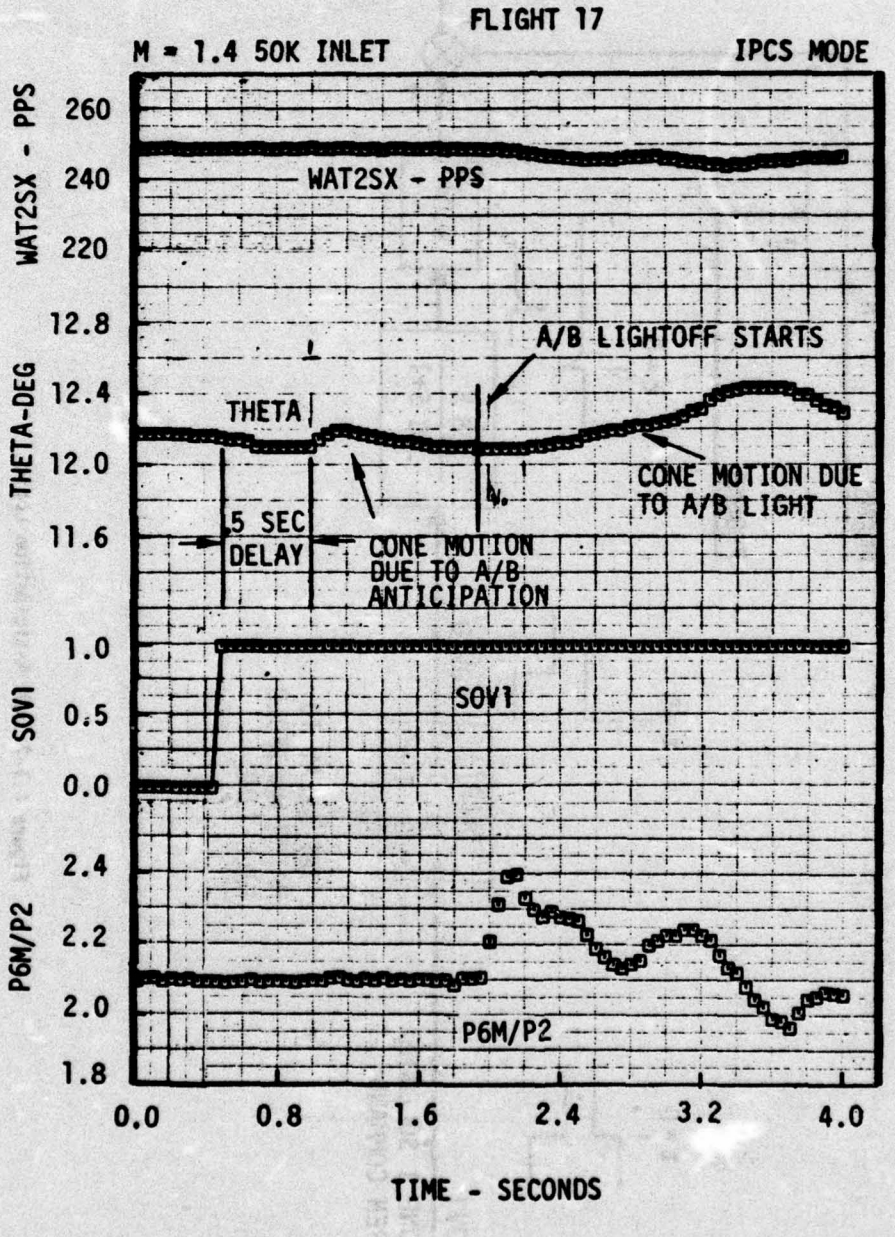

Figure 6.1-3 A/B Anticipation at Mach 1.4

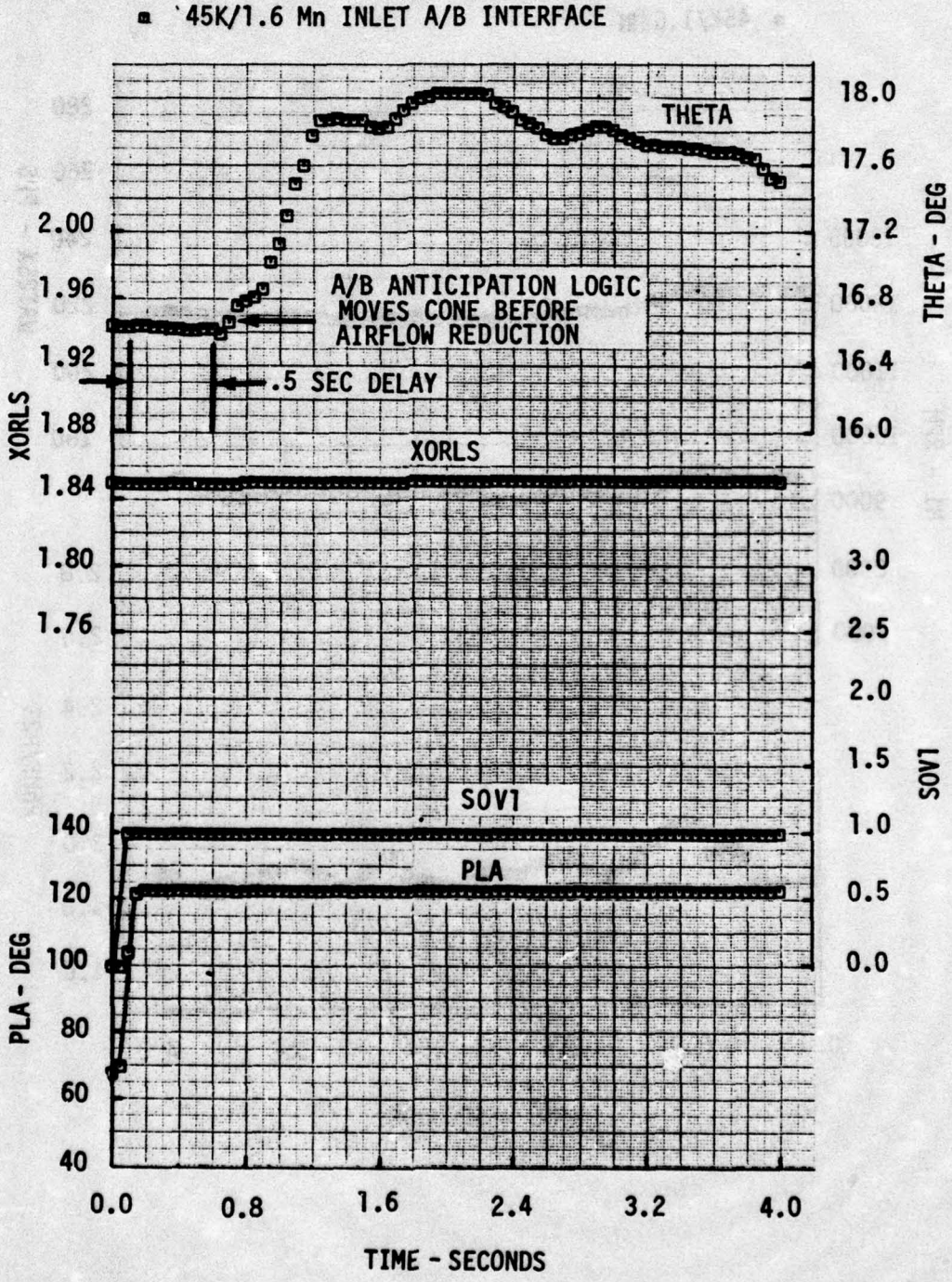

Figure 6.1-4a A/B Anticipation at Mach 1.6

FLIGHT 17

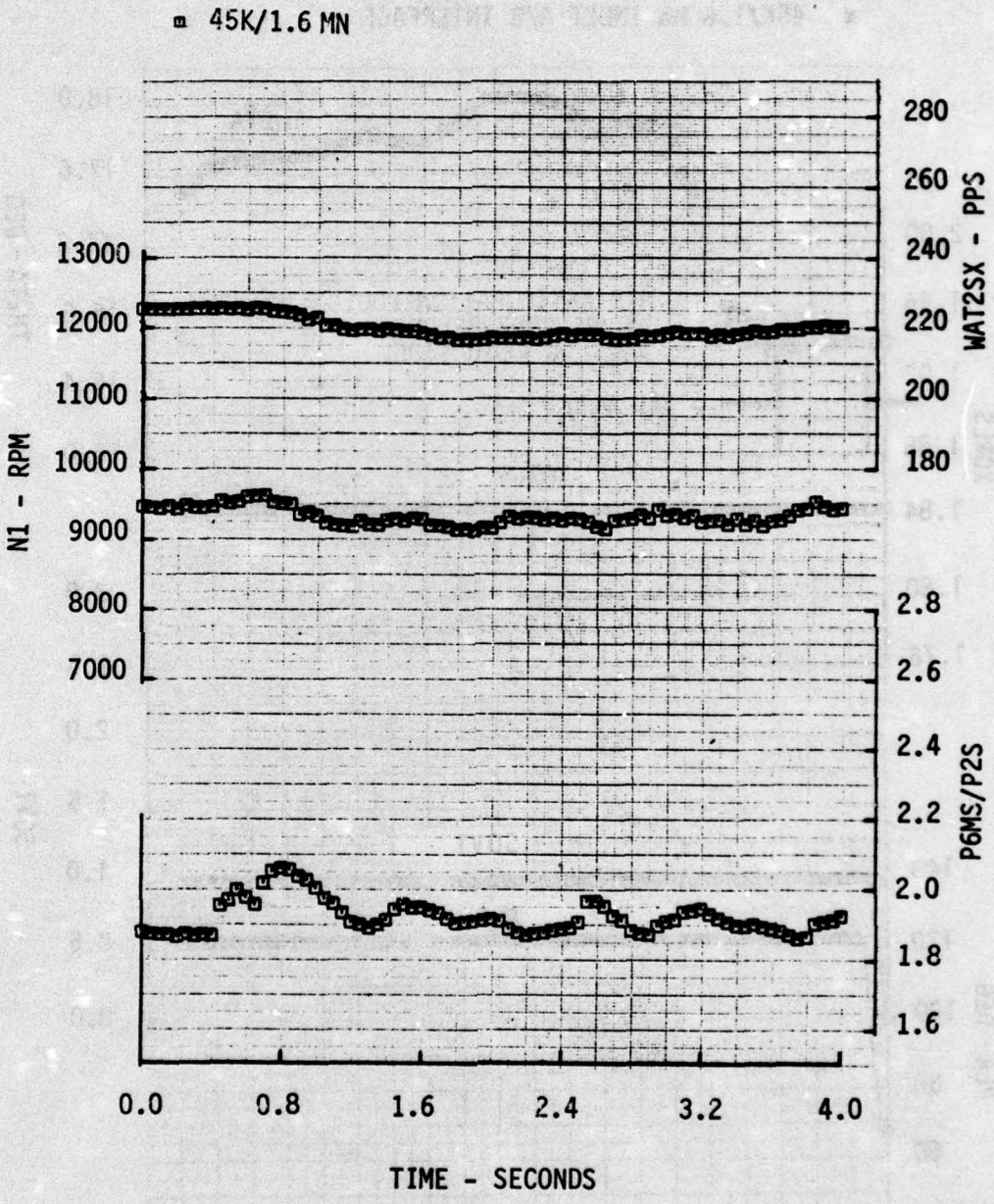

Figure 6.1-4b A/B Anticipation at Mach 1.6

The IPCS controller provides integral control of high rotor speed and ten other critical engine variables, see Section 4.2. The integral control provides droop-free engine operation in spite of changes in power extraction bleed status, and engine deterioration. Thus, an isochronous control results in less thrust loss with bleed or deterioration at the expense of higher turbine inlet temperatures required to maintain constant rotor speed.

In addition to controlling power settings with high rotor speed, the IPCS control provides direct limiting of turbine inlet temperature, rotor speeds, burner pressure, and engine inlet airflow. The most noticeable limiting occurred during idle operation where minimum levels of engine inlet airflow were maintained to avoid inlet buzz. This direct control of airflow provided a lower idle thrust than the bill-material control which operated above the schedule as seen in Figure 6.2-1. Pilots responded favorably to this feature because it enabled faster aircraft decelerations at high Mach numbers and less speed brake activity at lower speeds.

A comparison of the HMC and IPCS military power settings is shown in Figure 6.2-2 in terms of the three scheduling parameters: normalized high rotor speed; engine inlet temperature; and engine inlet pressure. The dashed lines represent schedule adjustments made to account for engine trim. At the high inlet temperatures, the IPCS operation was limited by maximum turbine inlet temperature, and thus actual rotor speeds were less than the scheduled values. Differences between the HMC and IPCS mil power settings are attributed to the HMC cam tolerances and to recovery characteristics of the HMC sensed engine inlet pressure and temperature.

A review of the IPCS steady state operation showed:

1. Minimum airflow limiting at idle provided a larger power range for the IPCS control, and it enabled faster airplane decelerations from high Mach numbers while providing protection from inlet buzz.
2. The IPCS control maintained its scheduled high rotor speed for military power settings except at high Mach numbers where turbine inlet temperatures were limited.

6.2.2 Engine Health

The TF30-P-9 test engine, P-676627, accumulated 77 hours and experienced 31 stalls during the flight test program. Two stalls occurred during Flight 16 which resulted in turbine temperatures slightly in excess of an overhaul action limit. Performance and visual checks at that time revealed no evidence of engine deterioration, and authority was granted to proceed with testing without an overhaul. The performance history of P-676627 during the flight test program is documented in Figure 6.2-3. It shows no change in performance from the initial ground test (Engine Run 1) to the post Flight 16 performance check (Engine Run 16) to the final ground test (Engine Run 35).

6.2.3 Gas Generator Transients

6.2.3.1 IPCS Accelerations

High compressor discharge Mach number was used to control gas generator accelerations in the IPCS mode. Compressor discharge Mach number is a measure of compressor excursion toward surge (Figure 6.2-4) and its use as a control parameter is intended to permit faster accelerations than a Wf/Pb controller while maintaining compressor stall protection and simplifying control schedules for variable geometry engines.

The high compressor discharge Mach number (MN3) was computed from four wall static pressure taps and four total pressure probes spaced approximately equidistant in the circumferential direction within hardware spacing constraints. Both the total and static pressure signals were manifolded to separate transducers and the difference was also sensed by a ΔP transducer. The transducers were sampled and the Mach number computed every .03 seconds. Discharge Mach number was scheduled as a function of high rotor corrected speed, and engine inlet Reynolds Index ($RNI = \delta/\theta^{1.24}$).

The IPCS flight test results were evaluated using four criteria:

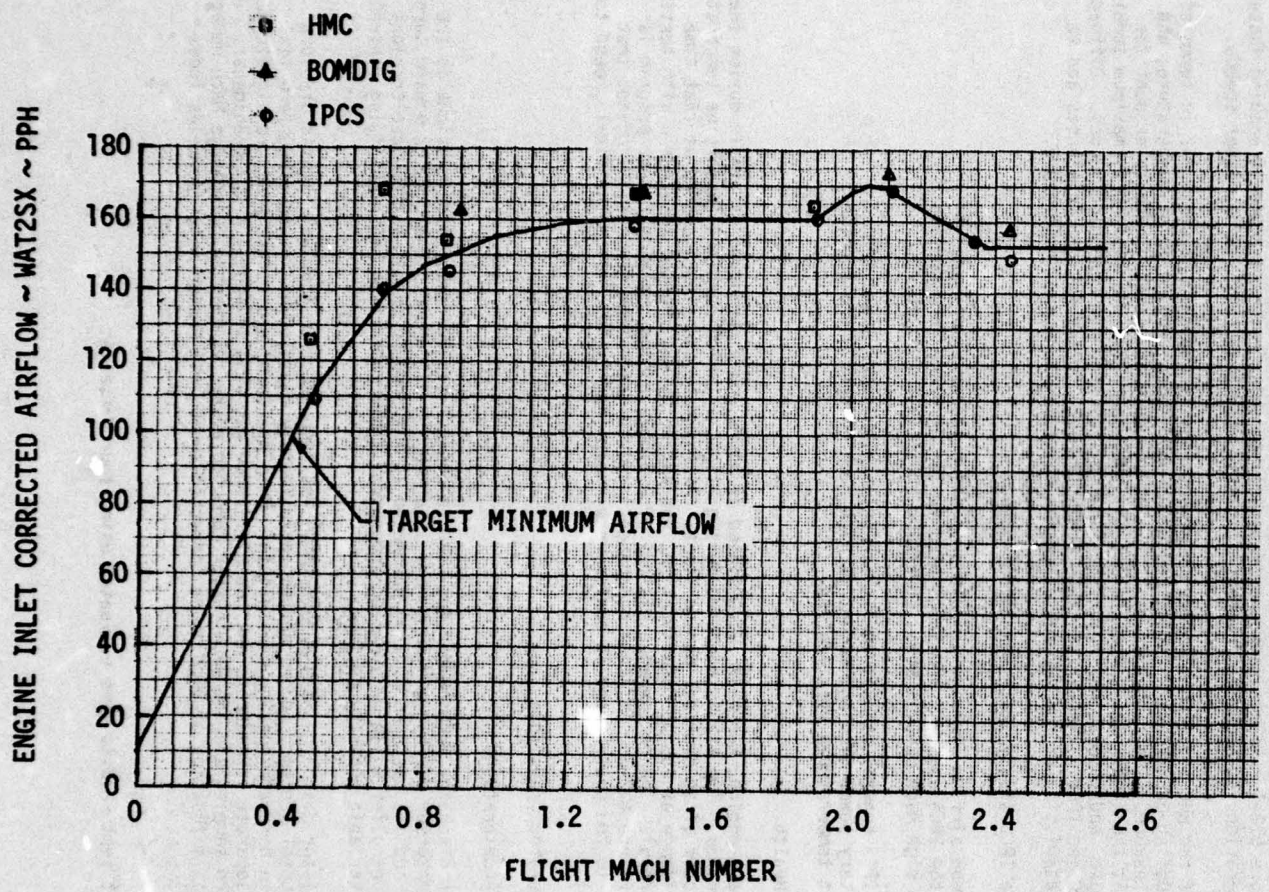

Figure 6.2-1 Idle Power Setting Comparison - HMC, BOMDIG, IPCS

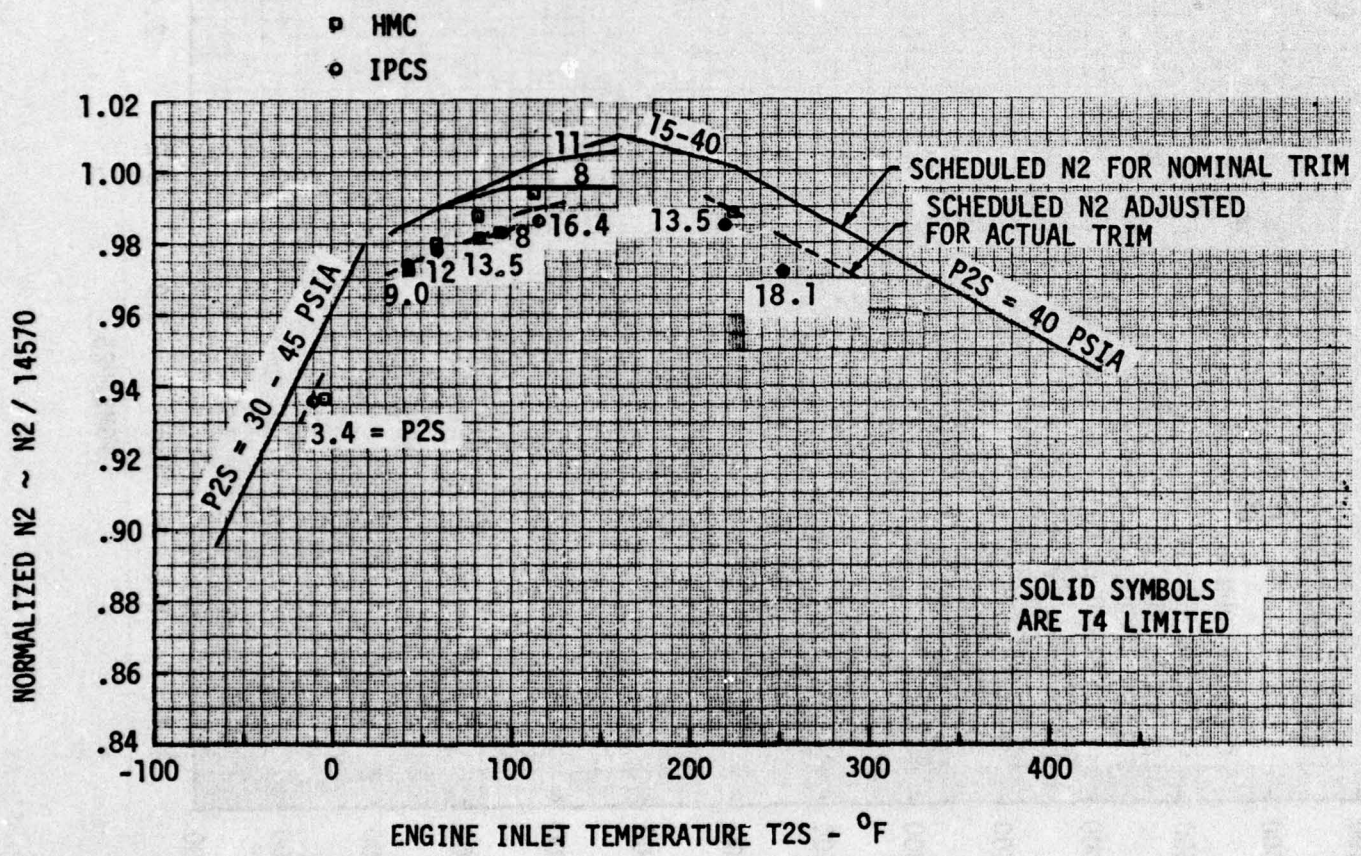

Figure 6.2-2 Military Power Setting Comparison - HMC, IPCS

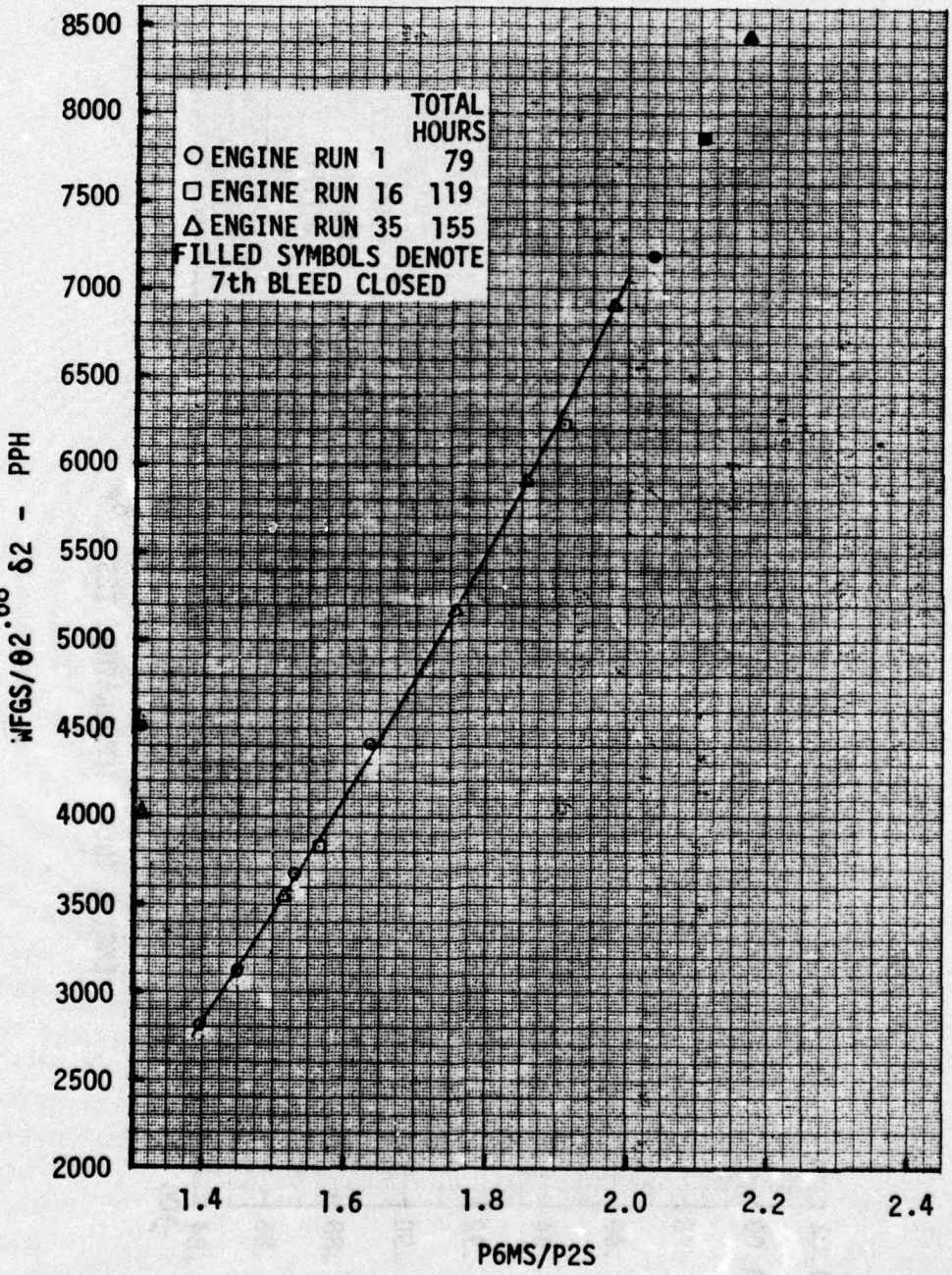

Figure 6.2-3a Installed Performance Calibrations

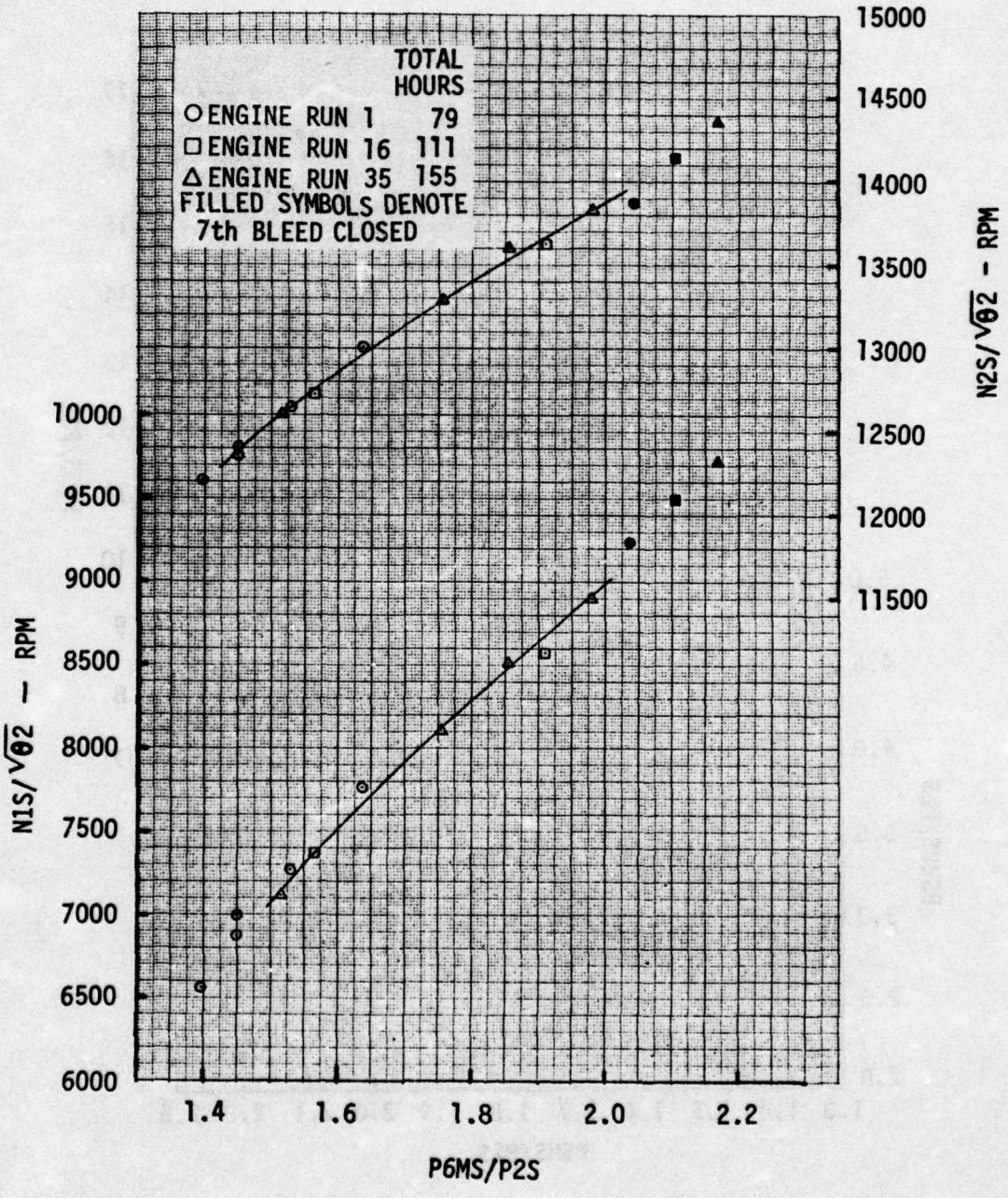

Figure 6.2-3b Installed Performance Calibrations

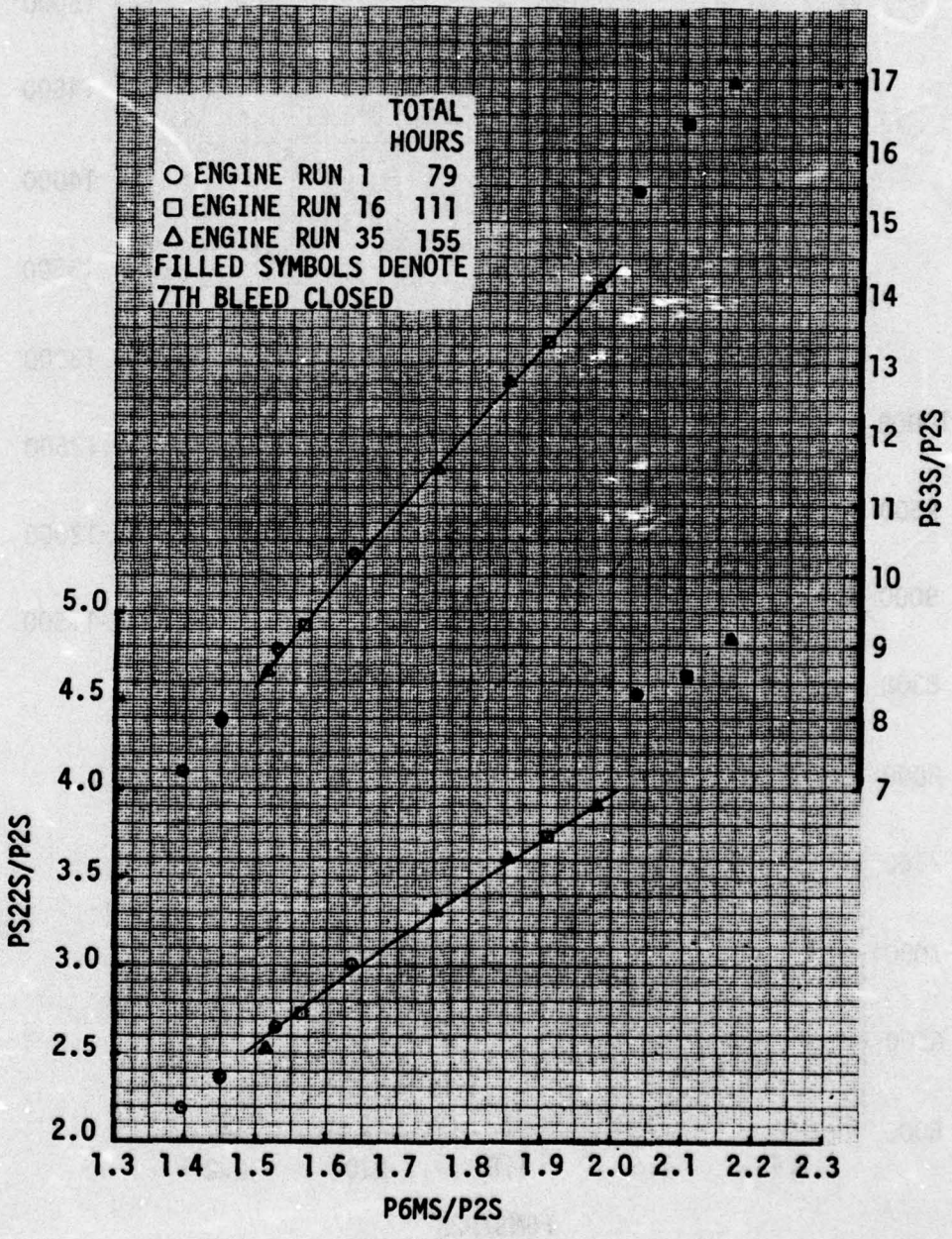

Figure 6.2-3c Installed Performance Calibrations

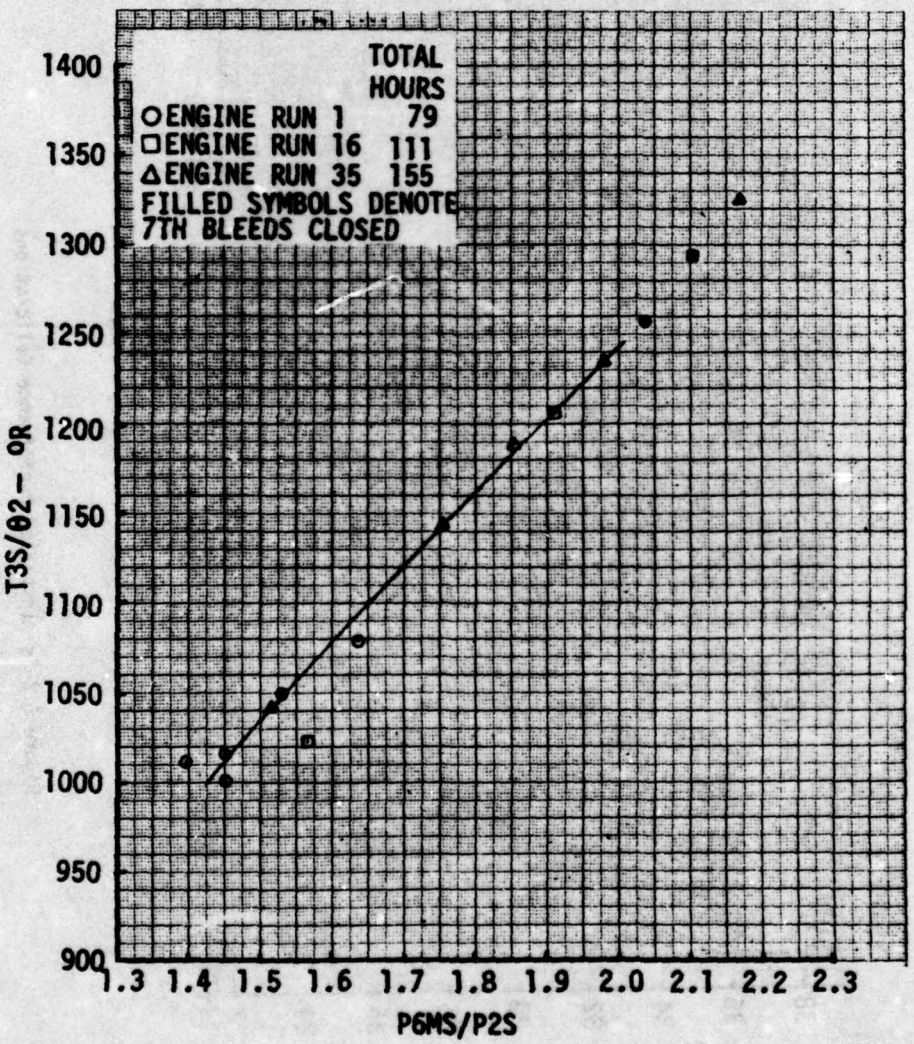

Figure 6.2-3d Installed Performance Calibrations

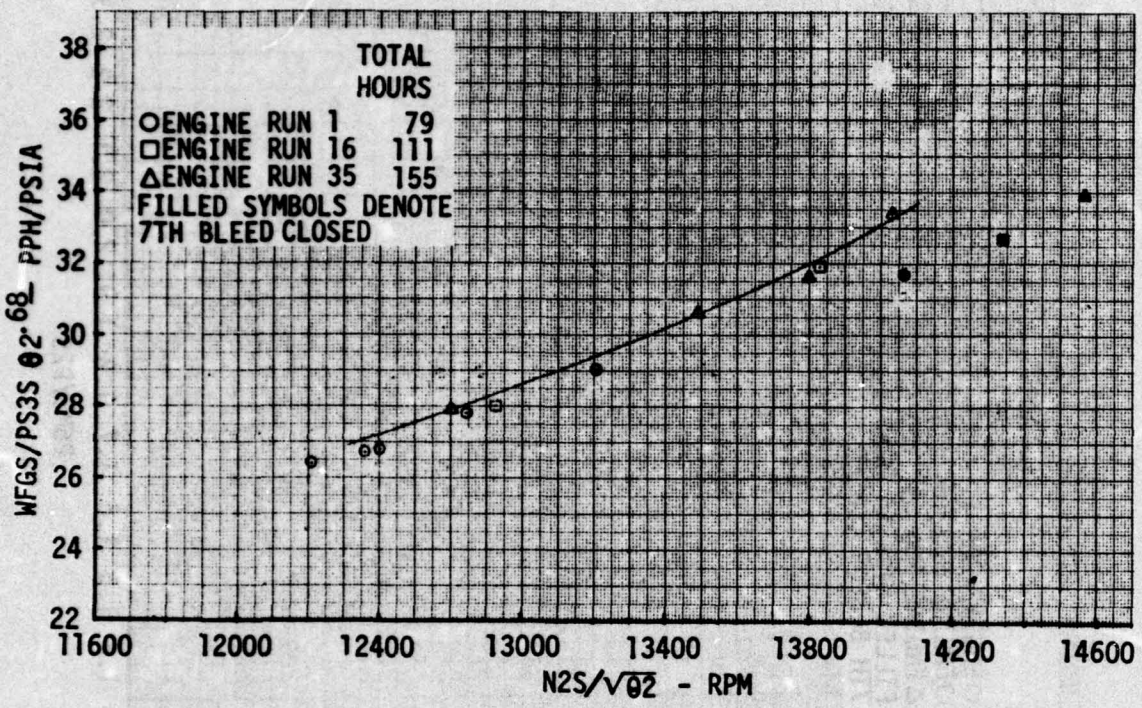

Figure 6.2-3e Installed Performance Calibrations

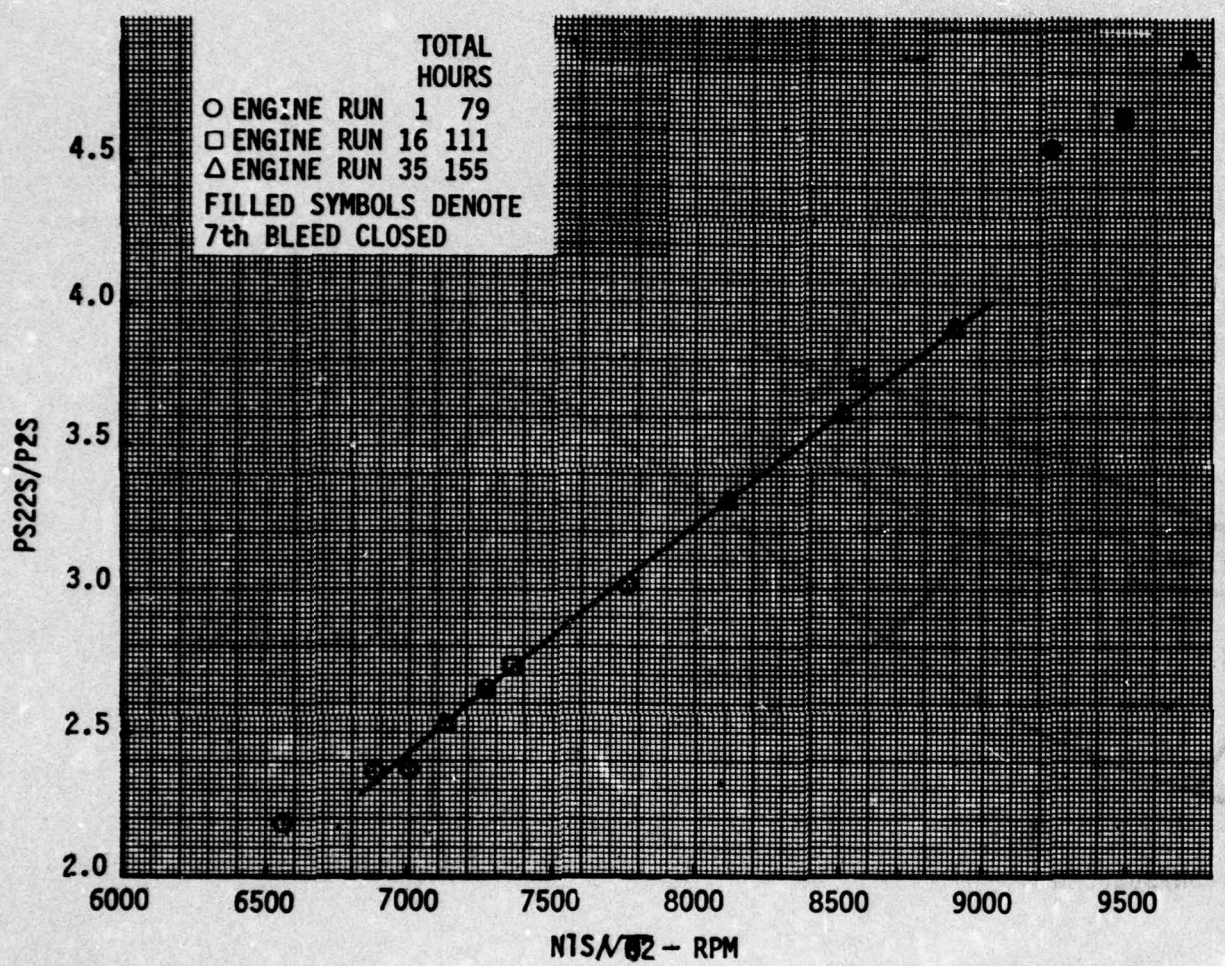

Figure 6.2-3f Installed Performance Calibrations

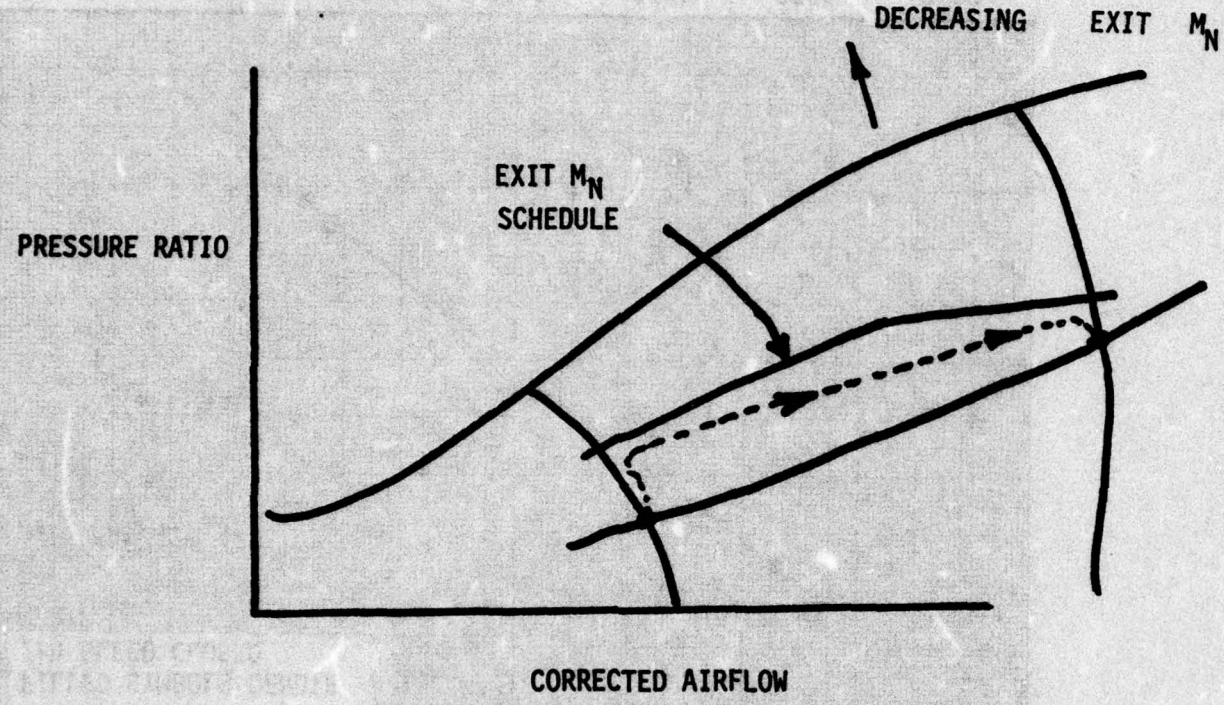

Figure 6.2-4 Compressor Exit Mach Number Control

1. Thrust Response - Is MN3 control a viable alternative to Wf/Pb control in terms of acceleration time?
2. Controllability - How well did the IPCS controller hold MN3 to its scheduled values?
3. Bodies - Did the MN3 controlled bodies result in compressor excursions no higher than the cold accelerations?
4. Fuel Derichment during Stall - Does a MN3 acceleration control result in automatic fuel decrease after stall?

A discussion of the IPCS flight test results with respect to these four criteria follows.

Thrust Response

Engine thrust response depends upon the level of overfueling scheduled during an acceleration. As overfueling increases, the risks of overtemperature and compressor stall also increase. One objective of the IPCS program was to demonstrate improved thrust response with the MN3 control by increasing the amount of overfueling while maintaining compressor surge protection. The turbine inlet temperature loop was used to limit overtemperature.

Engine response times during accelerations from idle to military power are compared for the IPCS and hydromechanical (HMC) controls in Figure 6.2-5. The comparison is based on time to reach 95% of the high rotor speed change from a common idle setting. The accelerations were made back-to-back in the same flight, so that ambient conditions were the same. The IPCS accelerations were predominantly controlled by MN3 during the initial portion of the accel where compressor stall protection is most critical. As shown in the figure, the IPCS accelerations were faster than the HMC at every condition except 45000 ft/1.9 Mn where the limited range between idle and military power resulted in an IPCS acceleration controlled primarily by the turbine inlet temperature loop.

Each of the IPCS accelerations shown in Figure 6.2-5, except one, was made with a backup Wf/Pb limit that was 4 ratio units above nominal. In some cases, the Wf/Pb limit controlled portions of the acceleration. The amount of each acceleration controlled by MN3 and Wf/Pb is indicated in Figures 6.2-6 - 6.2-13. When neither MN3 or Wf/Pb controlled the accel, the turbine inlet temperature (T4) or high rotor speed (N2) controlled the fuel flow increases. Conditions where the idle setting was below the secondary manifold filling region (approximately 1000 pph fuel flow) usually resulted in initial limiting by Wf/Pb because some of the fuel scheduled by the control was used to fill the manifold. Once the manifold was filled, all of the fuel scheduled by the control was delivered to the engine, and the MN3 loop controlled the acceleration. The 30000 ft/0.8 Mn acceleration, shown in Figure 6.2-10, illustrates the effect of secondary manifold filling on controlling loop.

One ground run acceleration was made with the backup Wf/Pb limit increased to 8 ratio units above nominal. This occurred during the last ground test (engine run 35), and as shown in Figure 6.2-5, the acceleration was accomplished in 70% of the time it took for the HMC acceleration. The rotor speeds, fuel flows, and turbine inlet temperatures for these two accelerations are compared in Figure 6.2-14 and the Wf/Pb vs N2 traces are compared in Figure 6.2-15. The MN3 controlled acceleration resulted in Wf/Pb levels up to 6 ratio units higher than the HMC without any Wf/Pb limiting. The MN3 excursion in relation to its schedule is shown in Figure 6.2-16.

The test results presented above demonstrated higher overfueling schedules and compressor discharge Mach number limiting resulted in accelerations as fast or faster than the hydromechanical Wf/Pb controlled accels without compressor stall.

Controllability

One measure used to evaluate MN3 control modifications during flight tests was the ability to closely track a schedule with minimal undershoots or oscillations. Four different MN3 controller configurations were tested on the ground, and three were tested inflight. They included the integral MN3 control with a nominal gain; an integral control with higher gains (not flown); a non-linear integral control with major cycle sampling; and a non-linear control with minor cycle sampling.

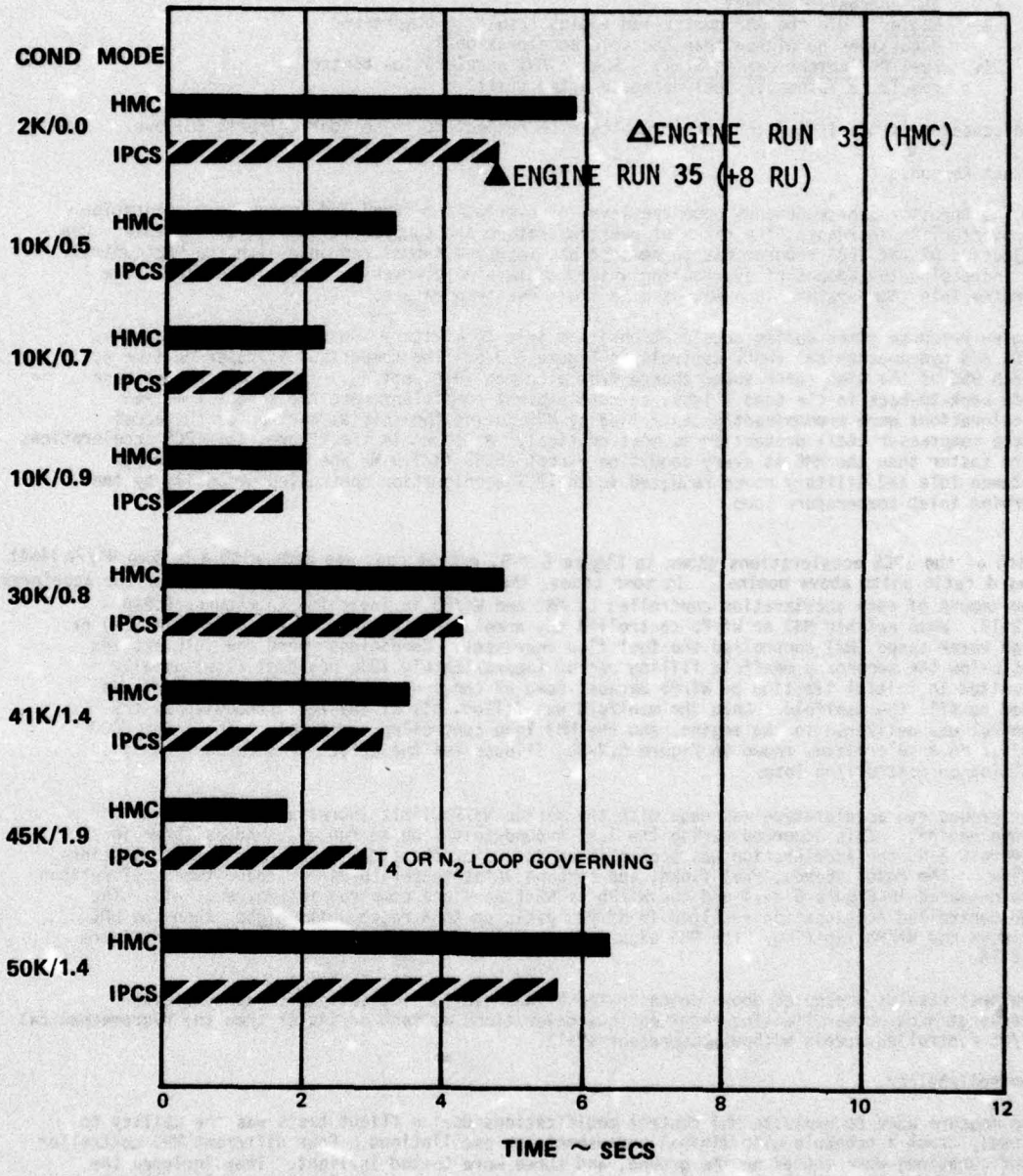

Figure 6.2-5 Idle-Mil Accel Time Comparison - IPCS, HMC

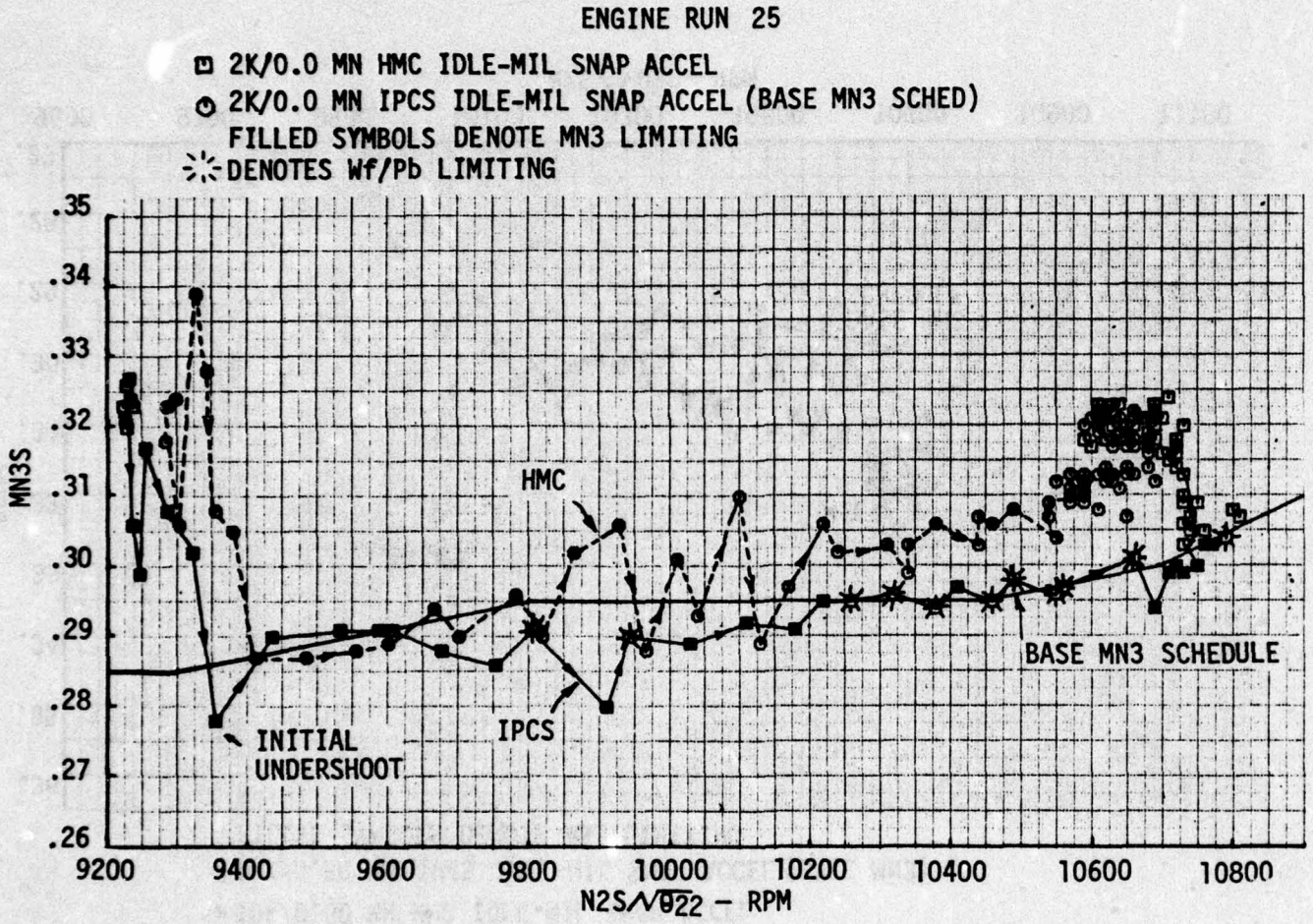

Figure 6.2-6 Accel Comparison - 2K, 0 MN

FLIGHT 25

- 10K/0.50 MN HMC IDLE-MIL SNAP ACCEL
- 10K/0.50 MN IPCS IDLE-MIL SNAP ACCEL (BASE MN3)
  FILLED SYMBOLS DENOTE MN3 LIMITING

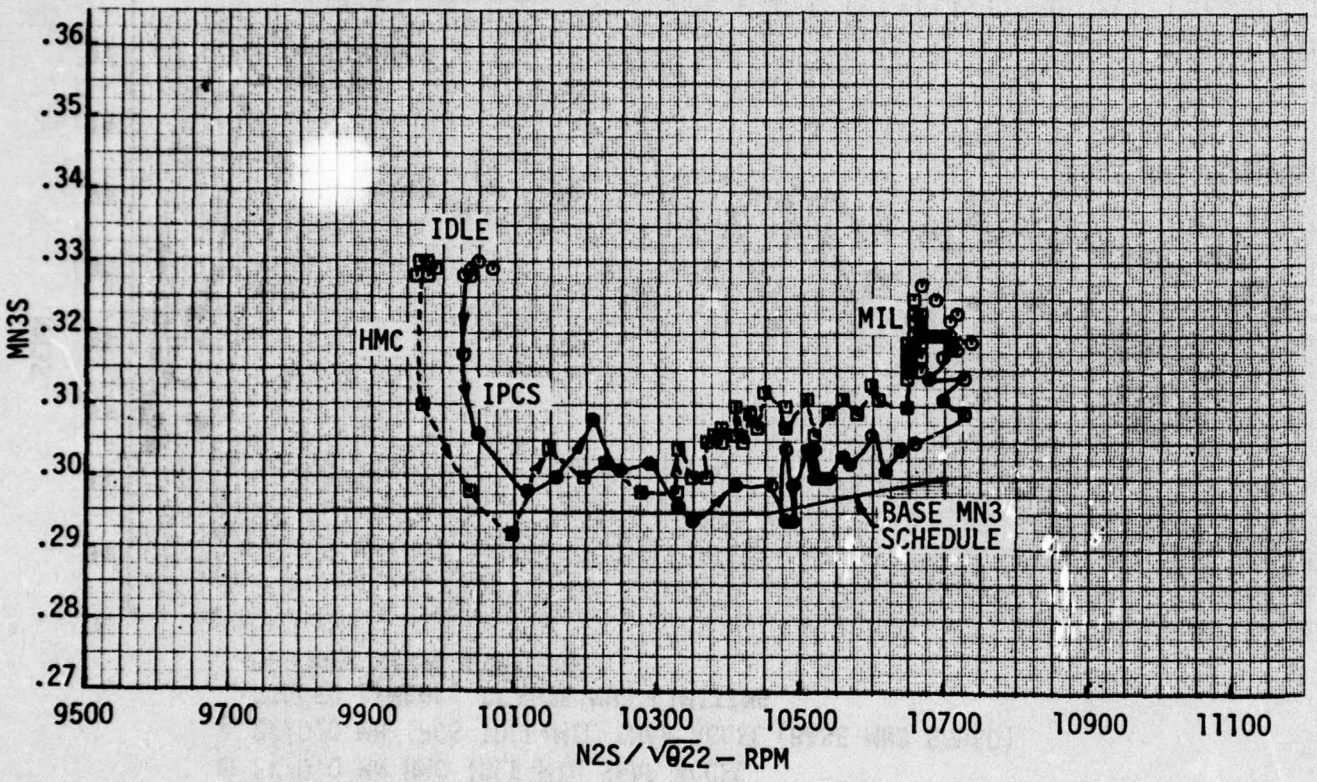

Figure 6.2-7 Accel Comparison - 10K, .5 MN

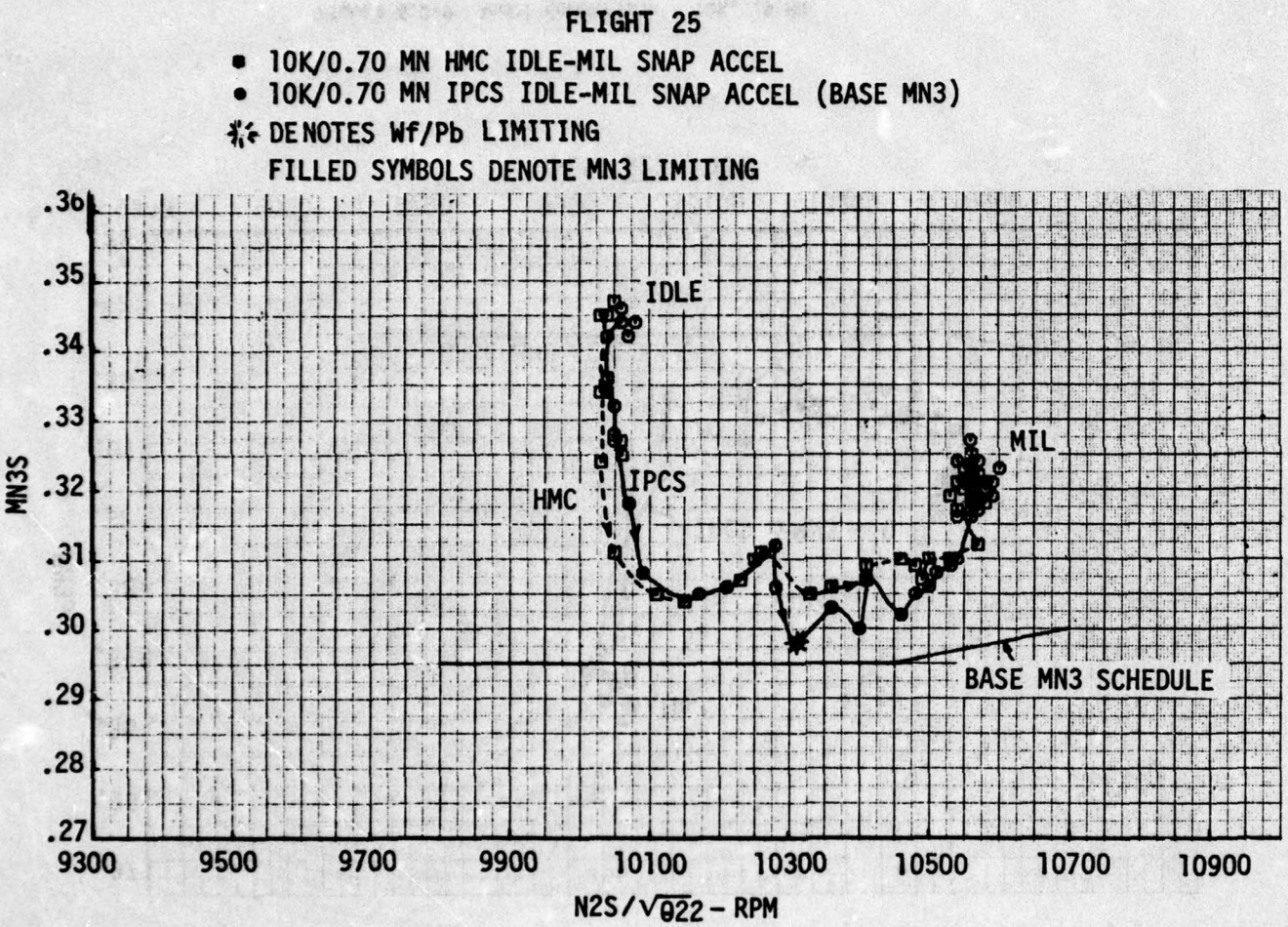

Figure 6.2-8 Accel Comparison - 10K, .7 MN

FLIGHT 25

- 10K/0.90 MN HMC IDLE-MIL SNAP ACCEL
- 10K/0.90 MN IPCS IDLE-MIL SNAP ACCEL (BASE MN3)
  FILLED SYMBOLS DENOTE MN3 LIMITING

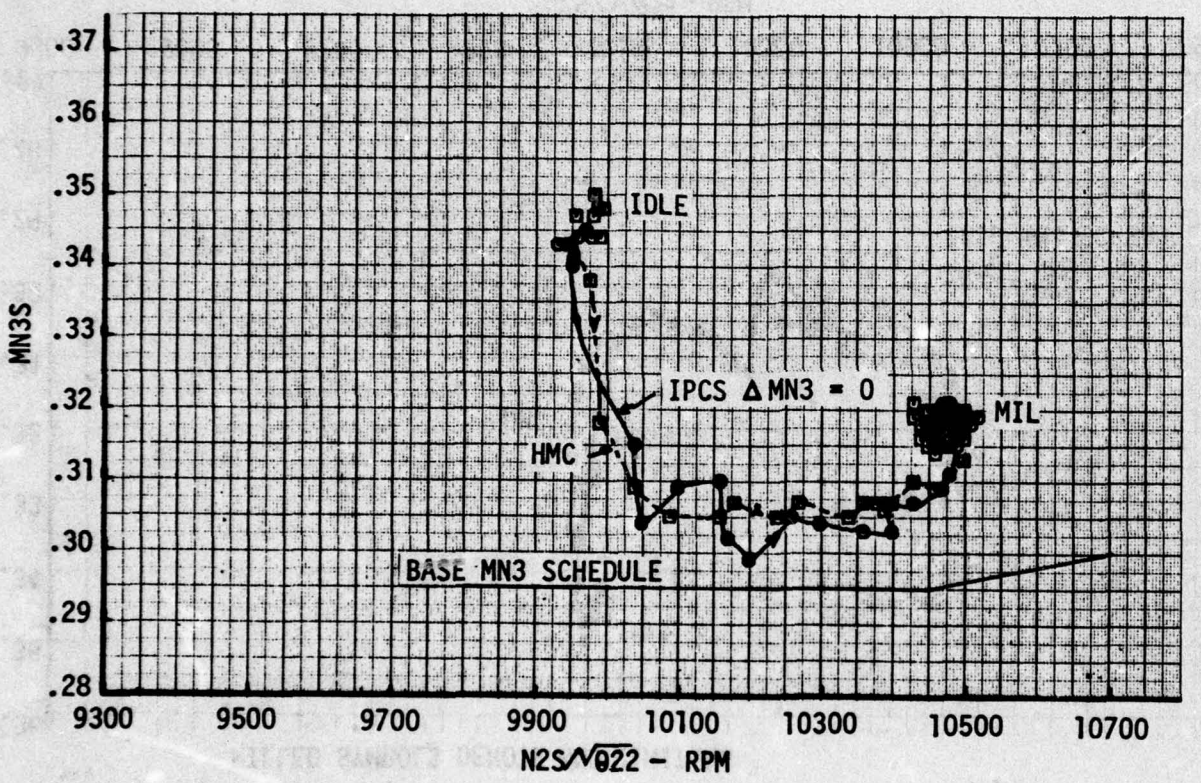

Figure 6.2-9 Accel Comparison - 10K, .9 MN

FLIGHT 24

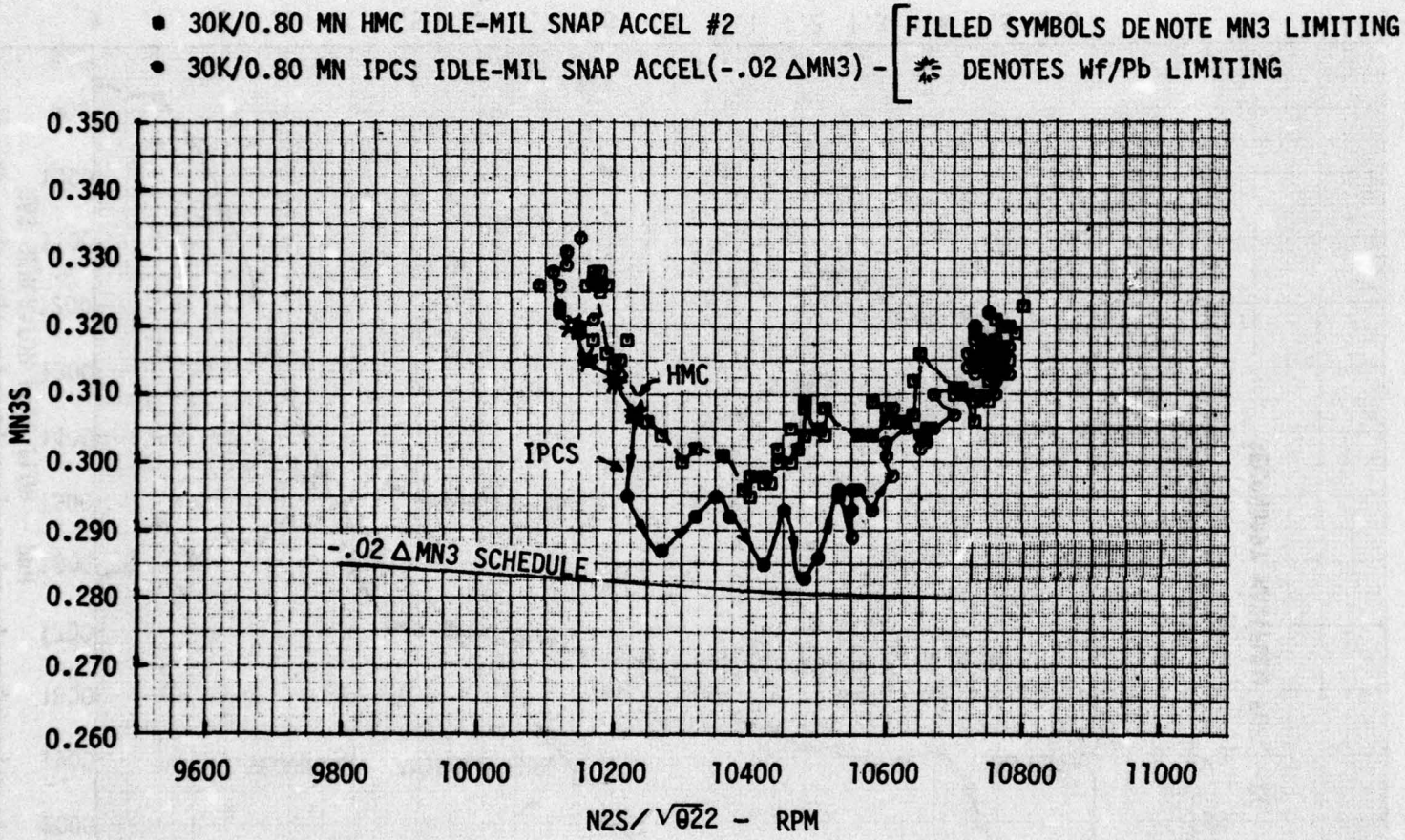

Figure 6.2-10a Accel Comparison - 30K, .8 MN

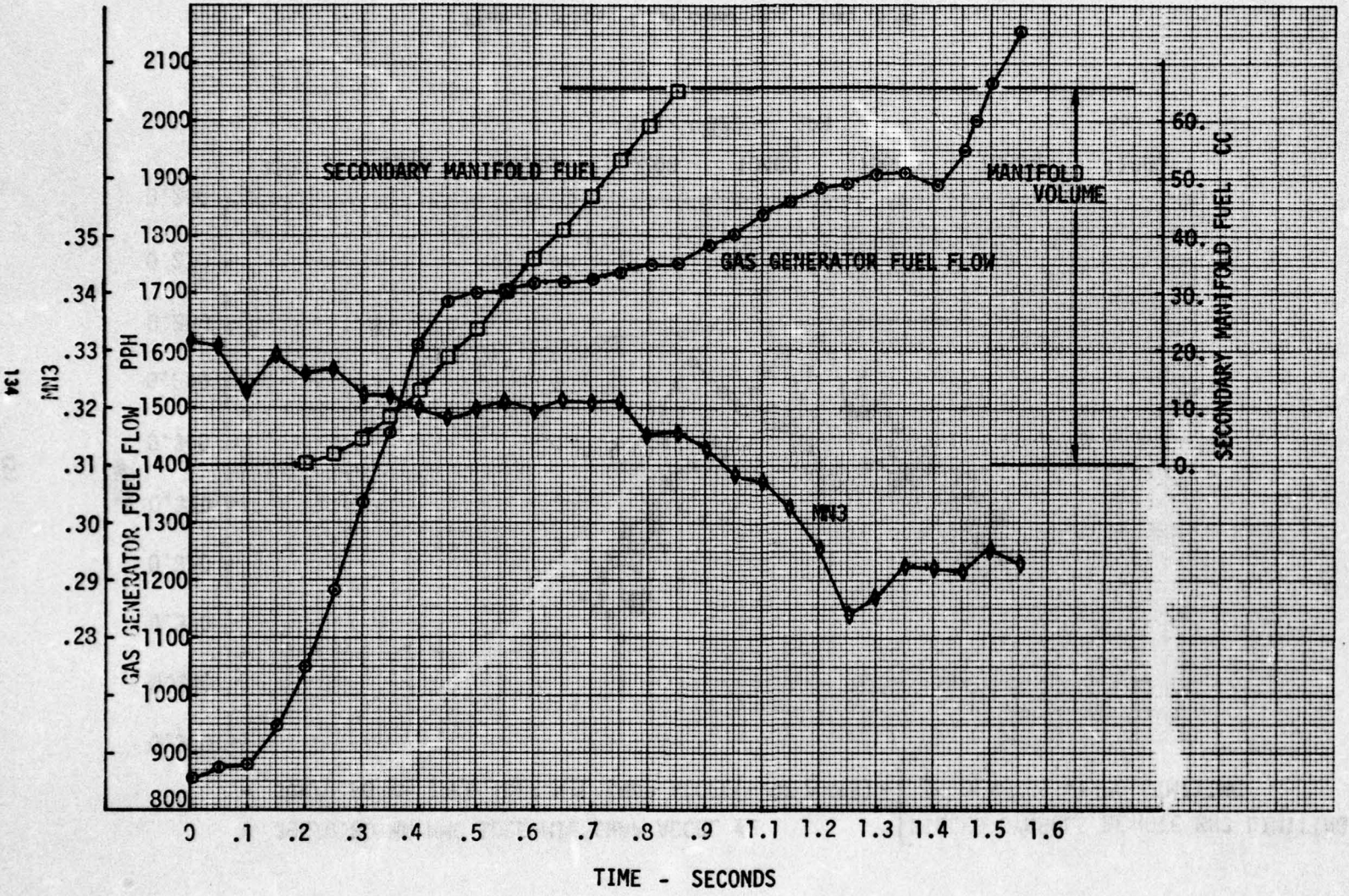

Figure 6.2-10b Accel Comparison - 30K,.8Mn

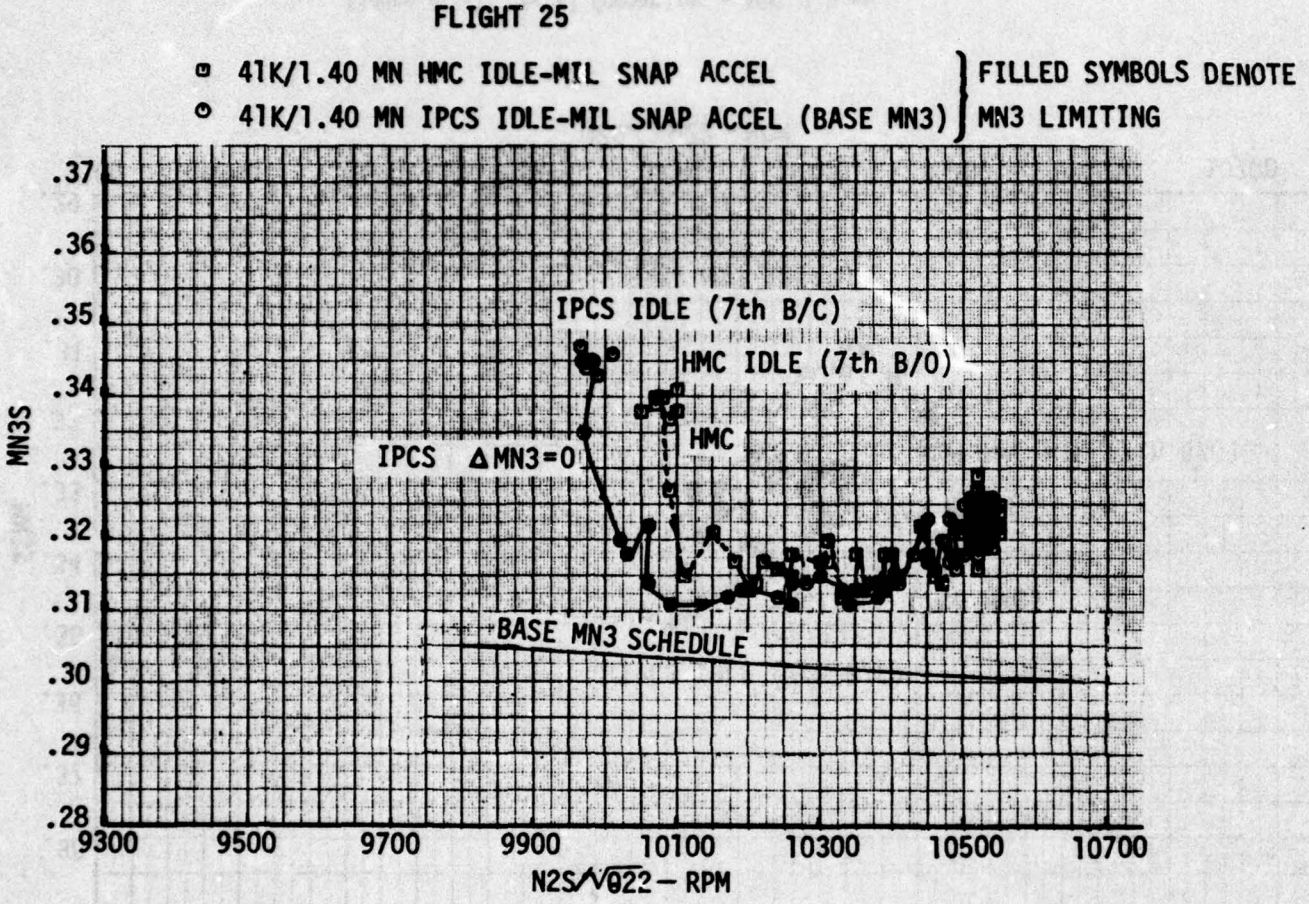

Figure 6.2-11 Accel Comparison - 41K, 1.4 MN

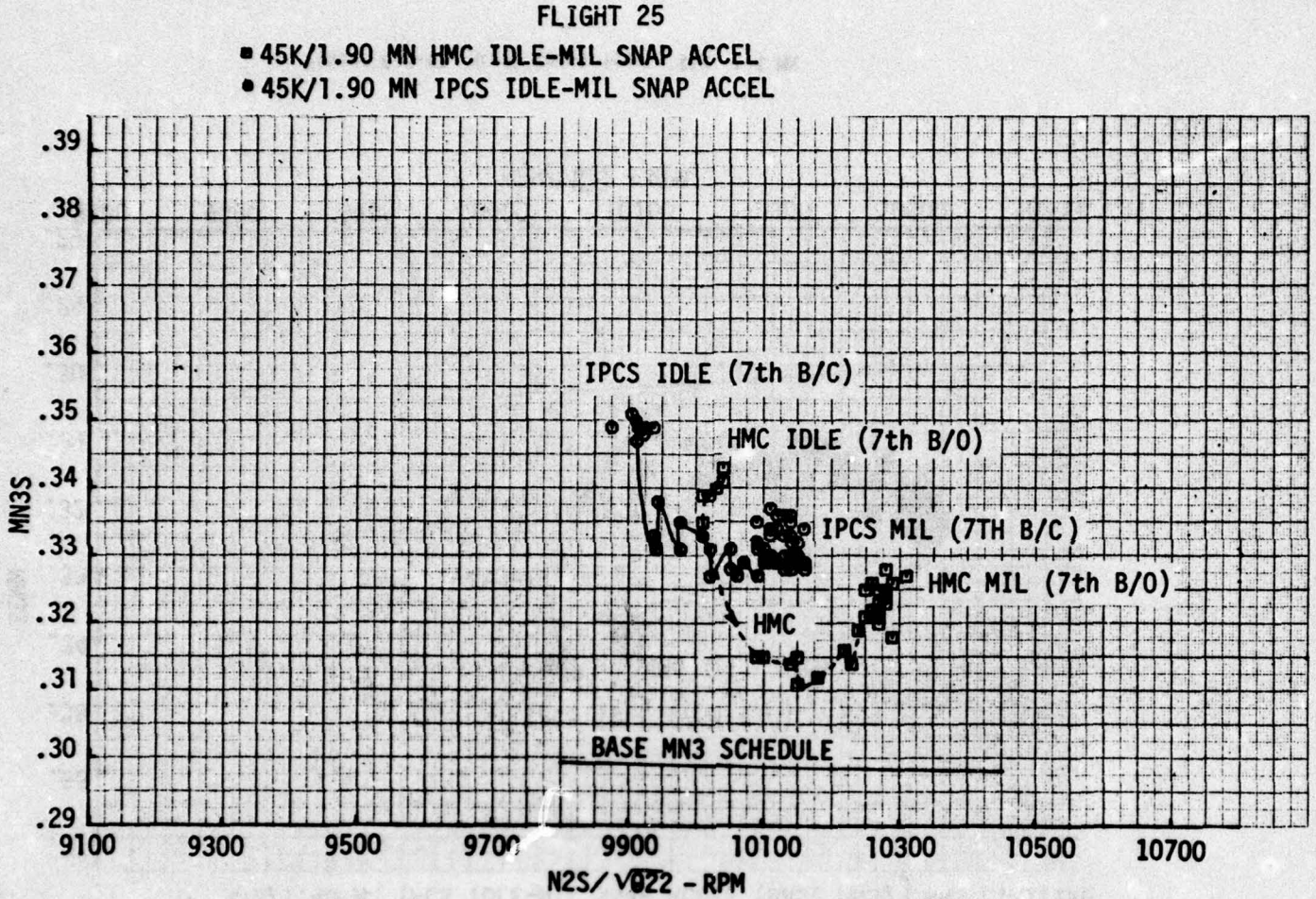

Figure 6.2-12 Accel Comparison - 45K, 1.9 MN

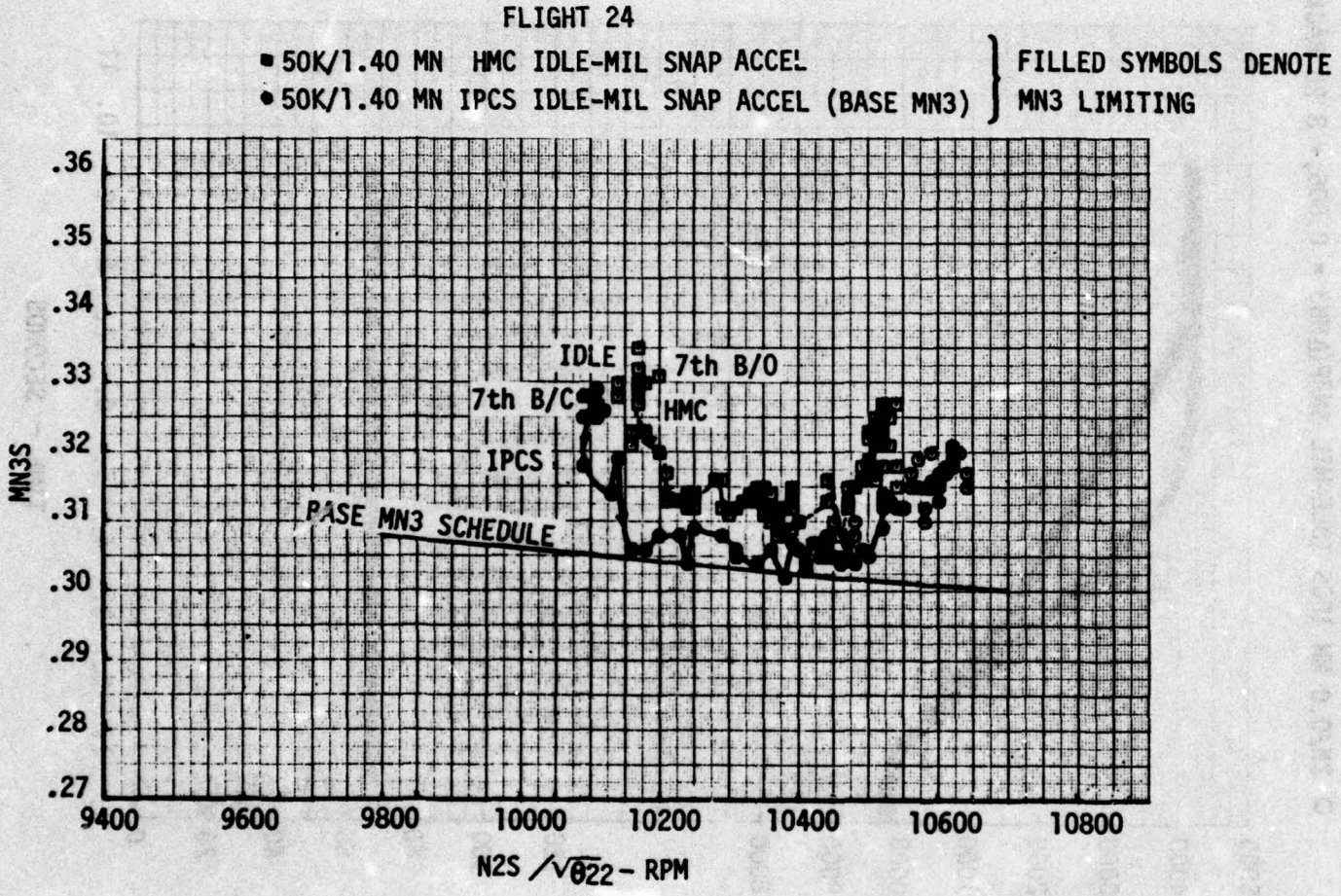

Figure 6.2-13 Accel Comparison - 50K, 1.4 MN

ENGINE RUN 35

□ 2K/0.0 MN HMC IDLE-MIL SNAP #1

○ 2K/0.0 MN IPCS IDLE-MIL SNAP(ΔMN3 = 0.006,+ 8 RU BACKUP)

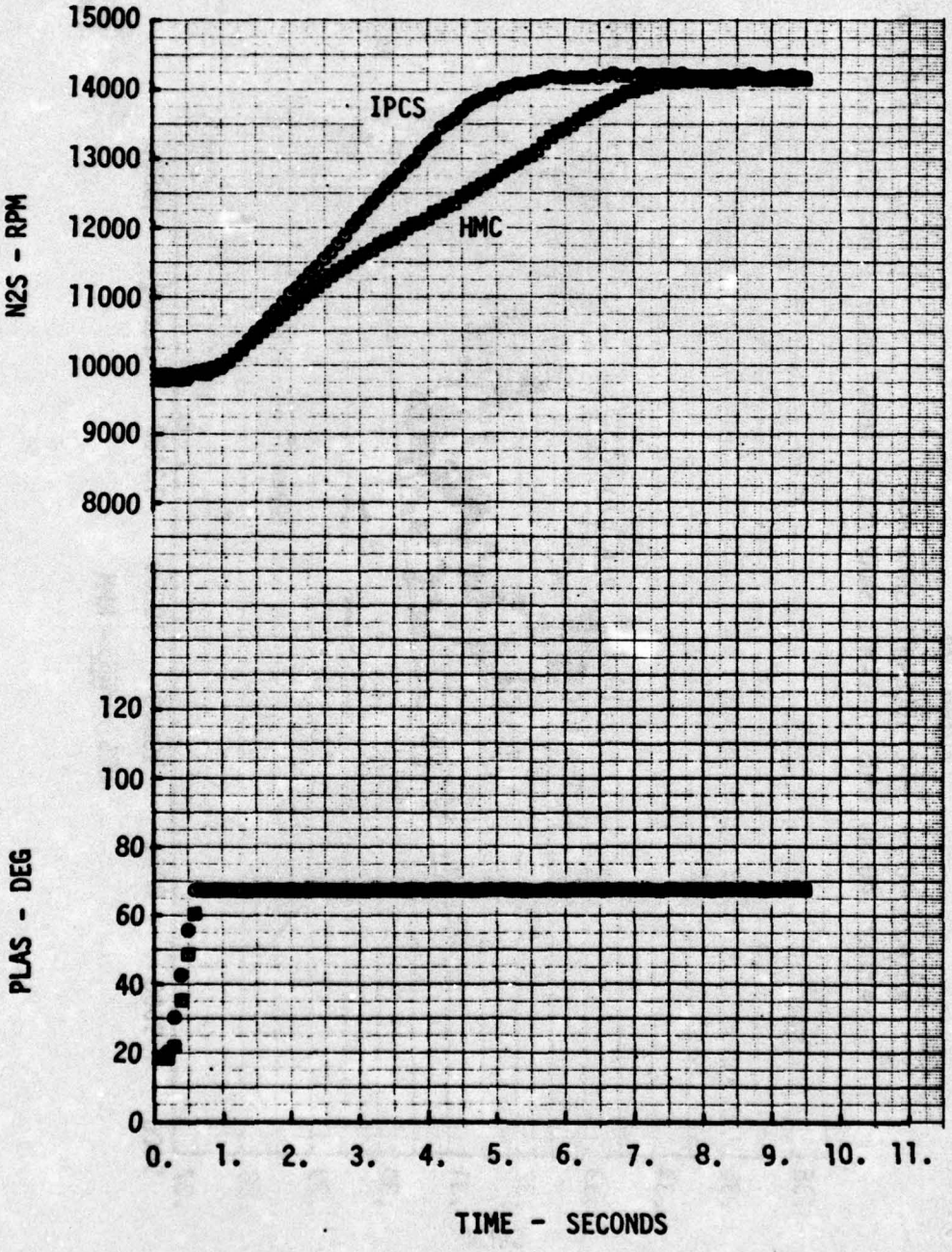

Figure 6.2-14a Idle-Mil Time History Comparison HMC, IPCS, Engine Run 35

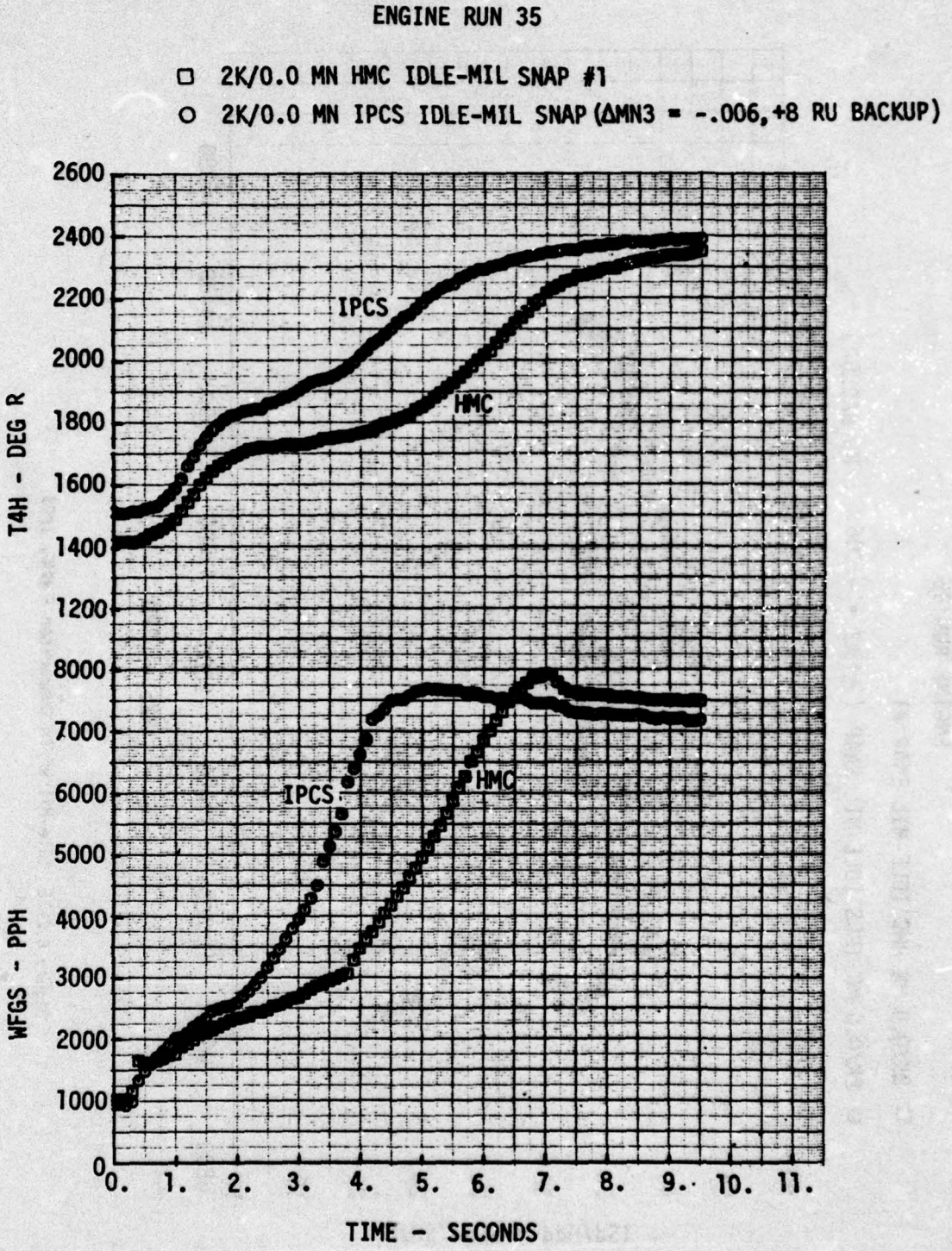

Figure 6.2-14b Idle-Mil Time History Comparison - HMC, IPCS, Engine Run 35

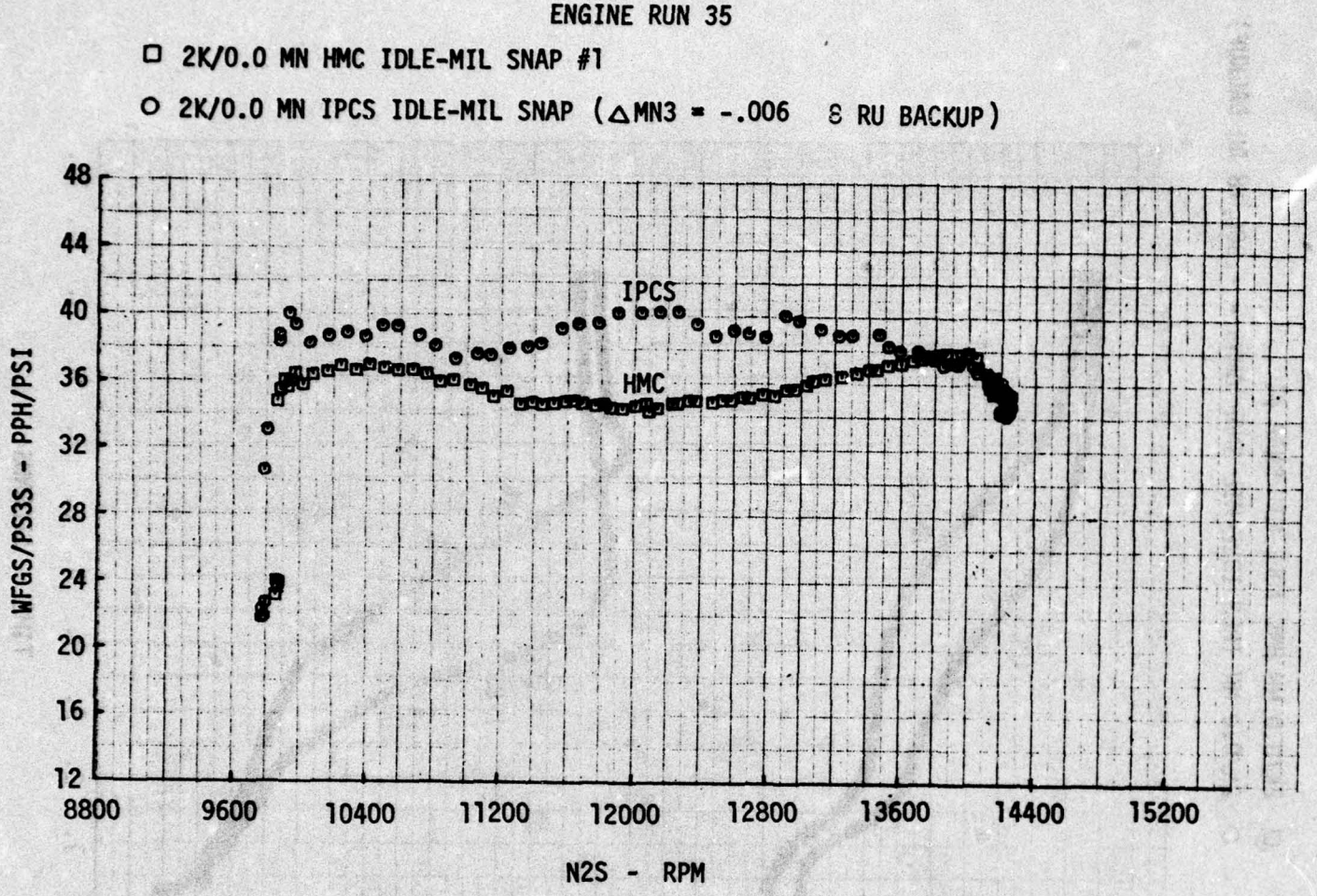

Figure 6.2-15 Idle-Mil Wf/Pb Comparison - HMC, IPCS

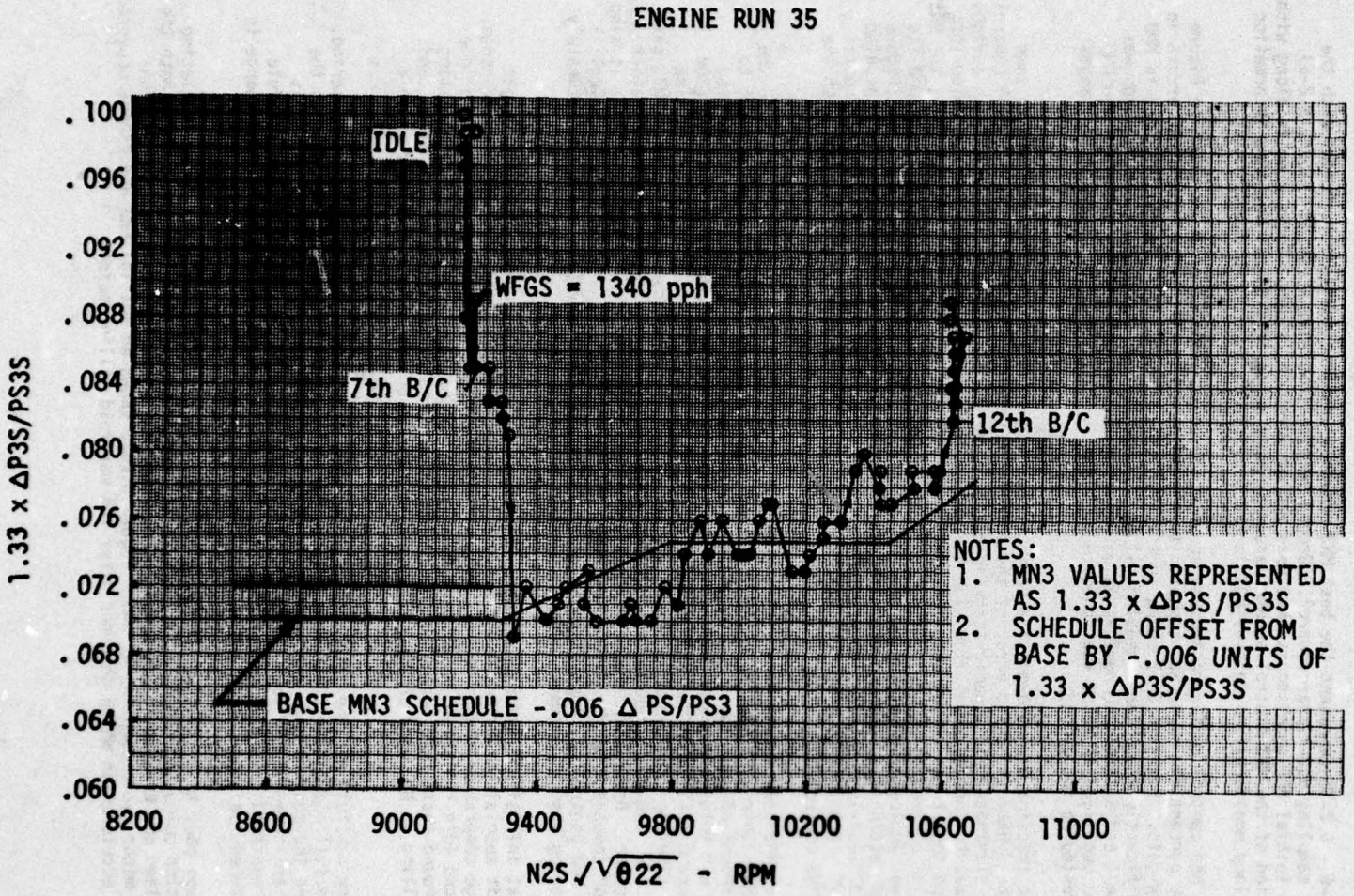

Figure 6.2-16 Idle-Mil MN3 IPCS

Figures 6.2-6 - 6.2-13 represent the best MN3 schedule tracking achieved in flight with the major cycle sampling non-linear control. Ground testing from engine run 25 (Figure 6.2-6) showed some initial MN3 undershoots that were not observed in flight. These results along with the evaluation of the MN3 control schemes are discussed below. Additional detailed information on the MN3 loop modifications is provided in Section 8.1.2.

The initial MN3 control configuration was an integral control on MN3 error as shown in Figure 8.1-5a. The percent MN3 error was compared to the percent N2, T4, N1 max, and Wf/Pb errors in a select low gate. Figure 6.2-17 shows that the initial integral MN3 control resulted in MN3 levels significantly above the scheduled values. Subsequently, the gain of the MN3 loop was increased to 4 and 8 times the nominal value. This resulted in operation closer to the MN3 schedule and oscillations about the schedule as shown in Figure 6.2-18. These gain changes were only tested on the ground.

The schedule tracking errors demonstrated with the integral MN3 control were caused to some extent by the dynamic tracking error of the integrator which is inherent to an integral control. In order to eliminate this dynamic tracking error, a non-linear MN3 limiting scheme was devised. The intent was to increase fuel flow with the integral N2 or T4 loops until MN3 was below its schedule, and then to hold fuel constant until MN3 increased above the schedule. Thus, the MN3 loop operation became more of a limiting function by taking action only when MN3 exceeded its limit. It was implemented by placing the MN3 logic downstream of the select low gate (Figure 8.1-5b) and setting the input to the integrator to zero when MN3 was less than its scheduled value. A 2:1 lead-lag compensation was applied to the signal to help avoid MN3 undershoots. Figures 6.2-6 - 6.2-13 illustrate the MN3 loop operation around the flight envelope with the non-linear MN3 control.

Since initial MN3 undershoots were observed during the ground tests (Figure 6.2-6) with the non-linear MN3 control, minor cycle (5m sec.) MN3 sampling was later used in an attempt to reduce the amount of undershoot and to smooth the MN3 oscillations. Minor cycle sampling represented a 6 fold increase in MN3 error computation rate over major cycle sampling (30m sec.). Figure 6.2-19 shows the MN3 in terms of $\Delta P/PS$ undershoot. In order to minimize computation time the variable $1.33\ \Delta P3/P3$ was computed every minor cycle rather than MN3, see Paragraph 8.1.2, and the reference schedule was tabulated in terms of pressure ratio rather than Mach number. Oscillations were virtually unaffected by the higher sampling rate. It also shows the ΔP component of the $\Delta P/PS$ signal was noisier than the PS signal. The next logical step in the MN3 control development would be to filter the ΔP or $\Delta P/PS$ signal. Unfortunately signal filtering was not attempted due to termination of testing.

The fact that initial MN3 undershoots were noticeably larger on the ground than in flight suggests that special conditions exist for ground operation and contribute to the undershoots. The 7th stage compressor bleeds and the exhaust nozzle area were open during all ground idle operation, and idle fuel flow levels were usually just below the secondary manifold filling region. Ground tests were conducted to isolate the effects of nozzle area, 7th bleed, and manifold filling on MN3 undershoots. The dynamic simulation was also used to aid in this analysis.

The secondary manifold has the potential to create MN3 undershoots during its filling period. Fuel used to fill the manifold has been metered by the control, but is not available to the engine. When the control does not sense an appropriate change in MN3 for the fuel it is commanding, it increases the fuel command in an effort to drive MN3 closer to its schedule. Then as the manifold is filled, more fuel is suddenly available to the engine, so the change in MN3 with metered fuel increases, and an undershoot may result.

An attempt was made to isolate the manifold filling effect during engine run 34 by initiating an acceleration below the manifold filling region (approximately 1000-1300 pph), while both the 7th stage bleed and exhaust nozzle were closed. The MN3 controller configuration was non-linear with minor cycle sampling of MN3. Figure 6.2-20 shows an initial MN3 undershoot occurred during this acceleration which occurred after the manifold filling point.

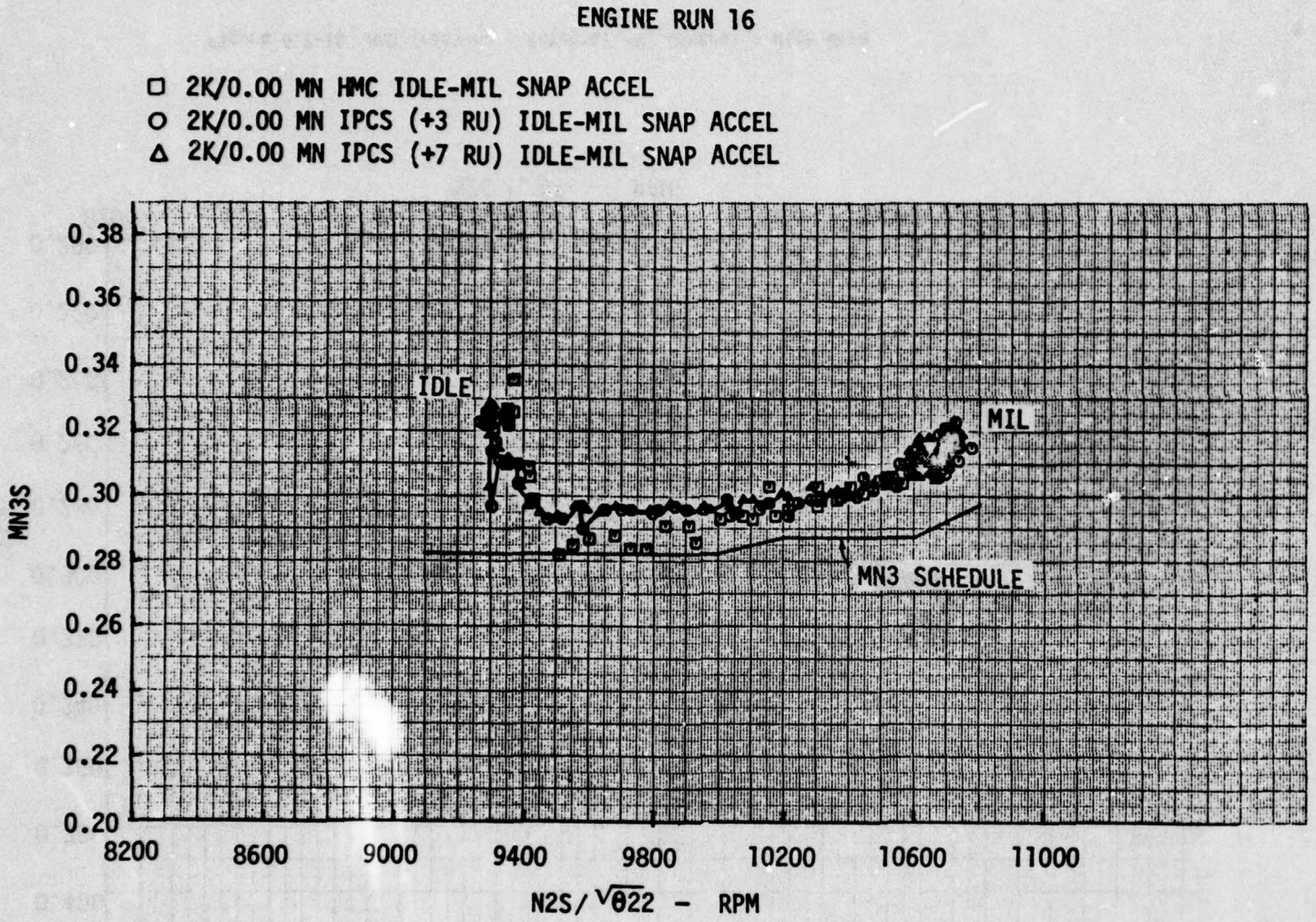

Figure 6.2-17 MN3 Tracking - Integral MN3 Control, Nominal Gain

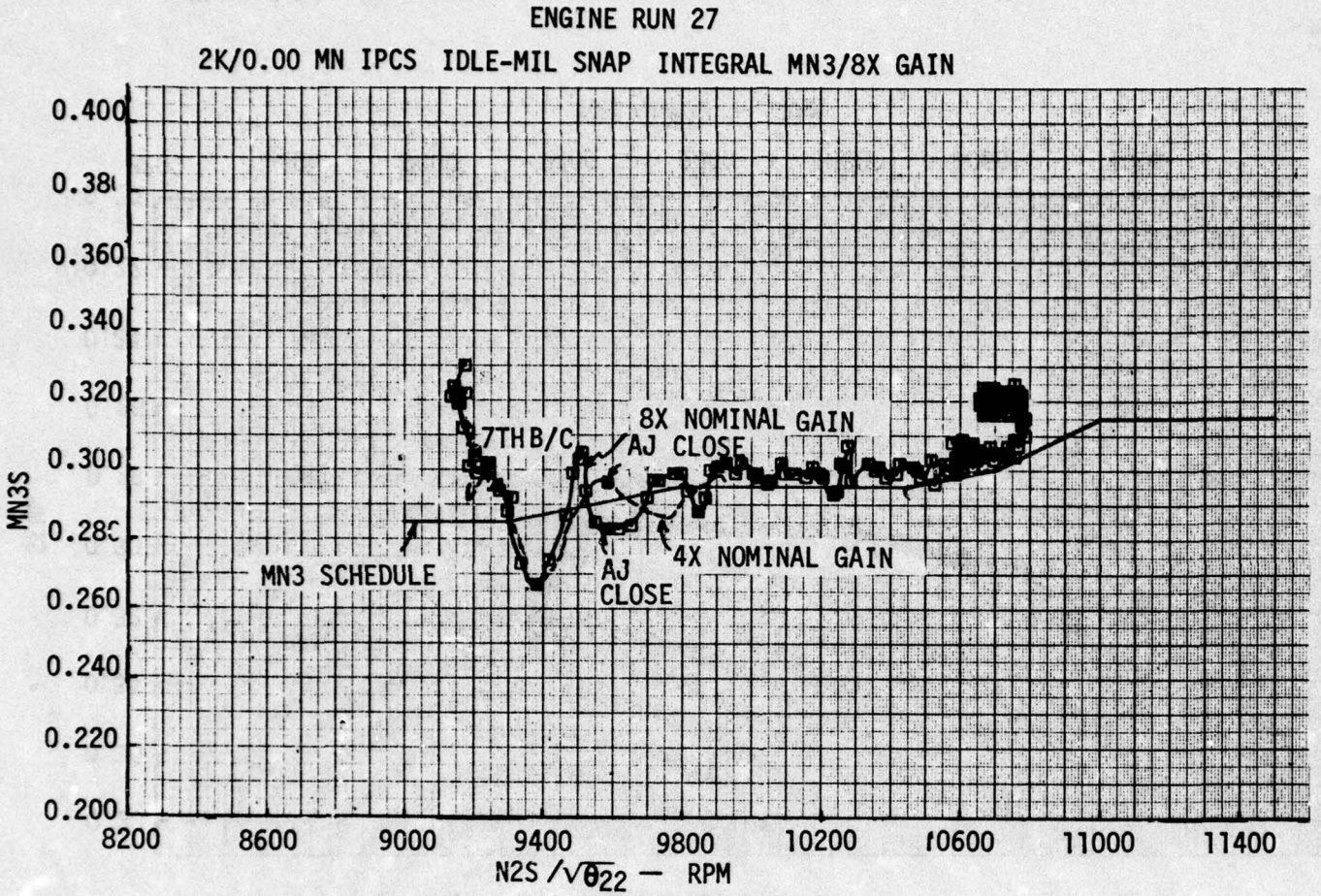

Figure 6.2-18 MN3 Tracking - Integral MN3 Control - High Gain

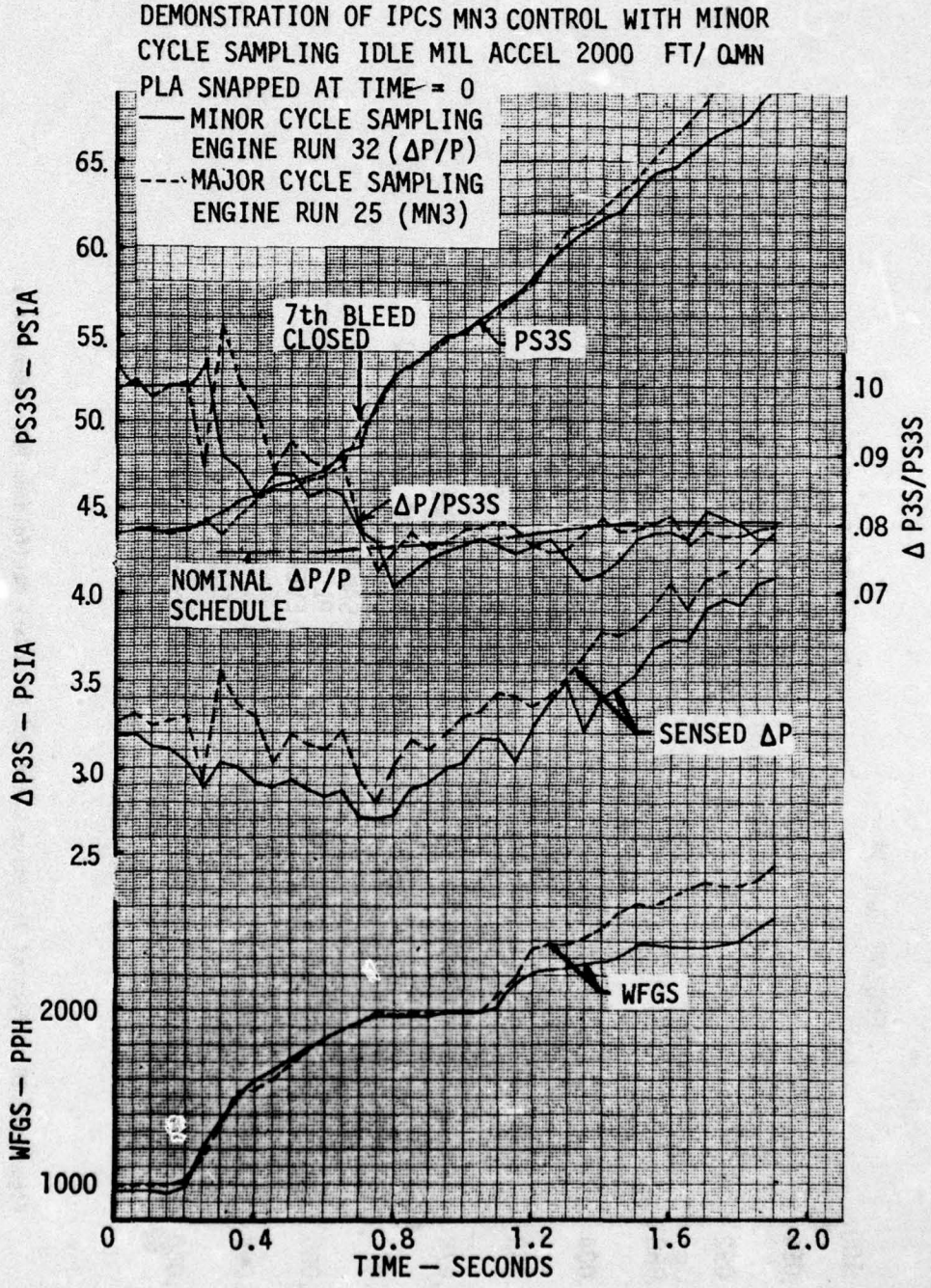

Figure 6.2-19 Minor Cycle Sample MN3 Accel

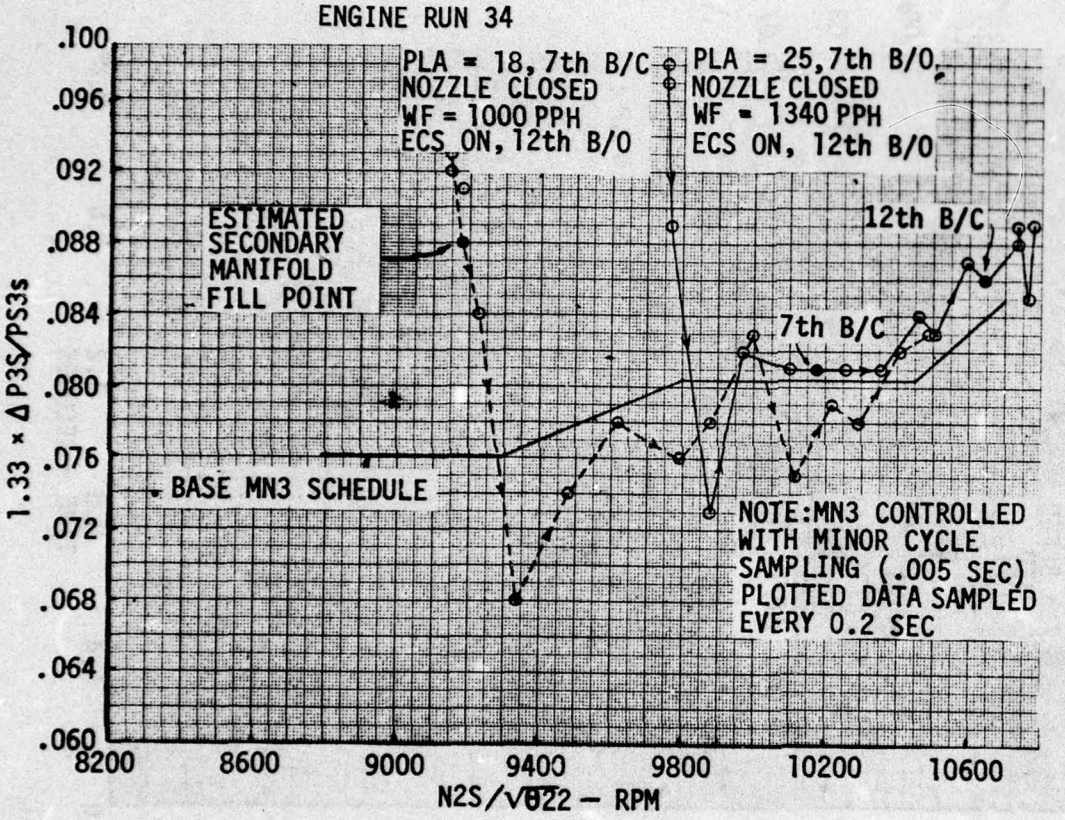

Figure 6.2-20 Effect of 7th Stage Bleed and Secondary Manifold on MN3 Undershoots

Even though these results suggest the manifold was responsible for the initial MN3 undershoot during ground tests, it cannot be identified as the sole factor because the initial undershoots were not observed in flight when accelerations were started from below the manifold filling region with the 7th bleed and nozzle area closed (Figures 6.2-10 and 6.2-13). The initial Wf/Pb limiting that occurred at the 30000 ft/0.8 Mn condition (Figure 6.2-10) may have prevented the initial undershoot, but Wf/Pb limiting was not observed during the 50000 ft/1.4 Mn accel (Figure 6.2-13).

Accelerations were also initiated from above the estimated manifold filling region during engine run 34 to isolate the 7th stage bleed effects on MN3 undershoots. Figure 6.2-20 indicates the undershoot occurred when the 7th bleed was open and the exhaust nozzle was closed. Since the 7th bleed closed after the undershoots, the dynamic effect of the closing bleed did not cause the undershoot. Figure 6.2-21 compares engine operating point in terms of 1.33 ΔP3S/PS3S, effectively MN3, and N2 corrected at Station 22 for various idle operating conditions. Data point separation for each condition reflects signal noise. An open 7th bleed increased the initial MN3 and may have contributed to the undershoot problem since it delays switching to the MN3 loop during the transient. An acceleration was not performed from the same power setting with the 7th bleeds closed to further isolate their effect on MN3 undershoots, so a conclusive cause and effect relationship was not established.

The dynamic simulation predicted an initial MN3 undershoot only when the exhaust nozzle was open at the initial steady state point (Figure 6.2-22). The cause of the predicted undershoot is the increased initial MN3 error associated with an open nozzle. This change in MN3 with exhaust nozzle position is not verified by test data, as seen in Figure 6.2-21. Furthermore, the nozzle closed accelerations in Figure 6.2-20 indicate the undershoot was not eliminated when the nozzle was closed prior to the accelerations. Since the simulation predictions were not substantiated by test data, it was not used to evaluate the undershoot.

In summary, the major conclusions concerning MN3 schedule tracking are:

1. A low gain integral control resulted in less MN3 oscillation, but did not track the schedule closely.
2. Higher gains resulted in closer schedule tracking but larger oscillations during ground testing.
3. The MN3 signal is noisy.
4. Smaller sampling intervals did not improve schedule tracking.
5. Exhaust nozzle position did not affect initial MN3 undershoots during ground testing.
6. Sufficient data were not available to identify secondary manifold filling and 7th stage bleed status as the sole sources of MN3 undershoots.

Bodies

The bodie transient is a rapid deceleration from high power to a lower power setting followed immediately by a rapid acceleration. In effect, it is an acceleration that is subject to heat transfer characteristics of a hot engine. Since the metal temperatures are higher during a bodie than during a cold accel, heat is transferred from the metal to the gas. In the high compressor, this additional heat takes the form of a higher operating line during the accel portion of the bodie. The bodie then becomes the critical event for establishing acceleration schedule levels unless the compressor excursion can be controlled directly. Direct control provides stall protection during bodies without compromising engine response during cold accels. Since compressor discharge Mach number is a measure of compressor excursion, its ability to maintain the same compressor path during a bodie and a cold accel was assessed and is discussd below.

A comparison of high compressor excursions during a ground test cold accel and a bodie with the BOMDIG (Wf/Pb) control is shown in Figure 6.2-23. The lower rpm bodie turnaround resulted in a 1.6% higher excursion, while the higher rpm bodie turnaround resulted in a 1.9% higher excursion than the cold accel. As shown in Figure 6.2-24, both of these transients were governed to the same Wf/Pb level. Ground test results with the IPCS MN3 control also showed a higher compressor excursion for the bodie than for the cold accel (Figure 6.2-25), and a comparison of the Wf/Pb traces showed essentially the same levels for both the bodie and the cold accel (Figure 6.2-26). A constant corrected inlet high compressor airflow data point is identified on the cold accel and bodie Wf/Pb traces for reference. A comparison of the MN3 traces for these two transients, Figure 6.2-27, shows the bodie MN3 at the constant corrected airflow condition was slightly higher than the cold accel MN3 which is an apparent contradiction with the compressor map trace of Figure 6.2-25.

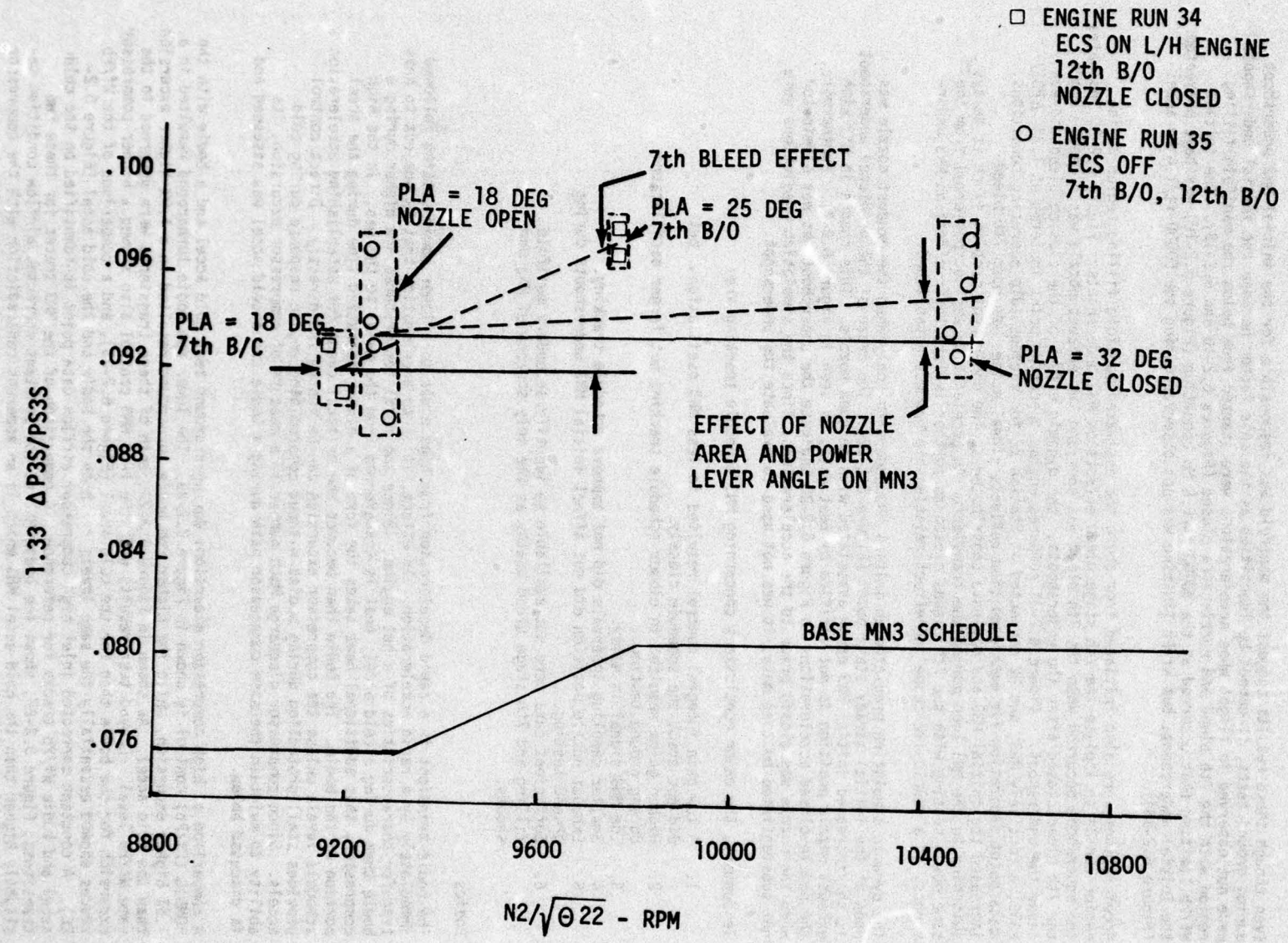

Figure 6.2-21 Effect of Nozzle, Bleeds and ECS on Idle (Δ P/PS)3 Value

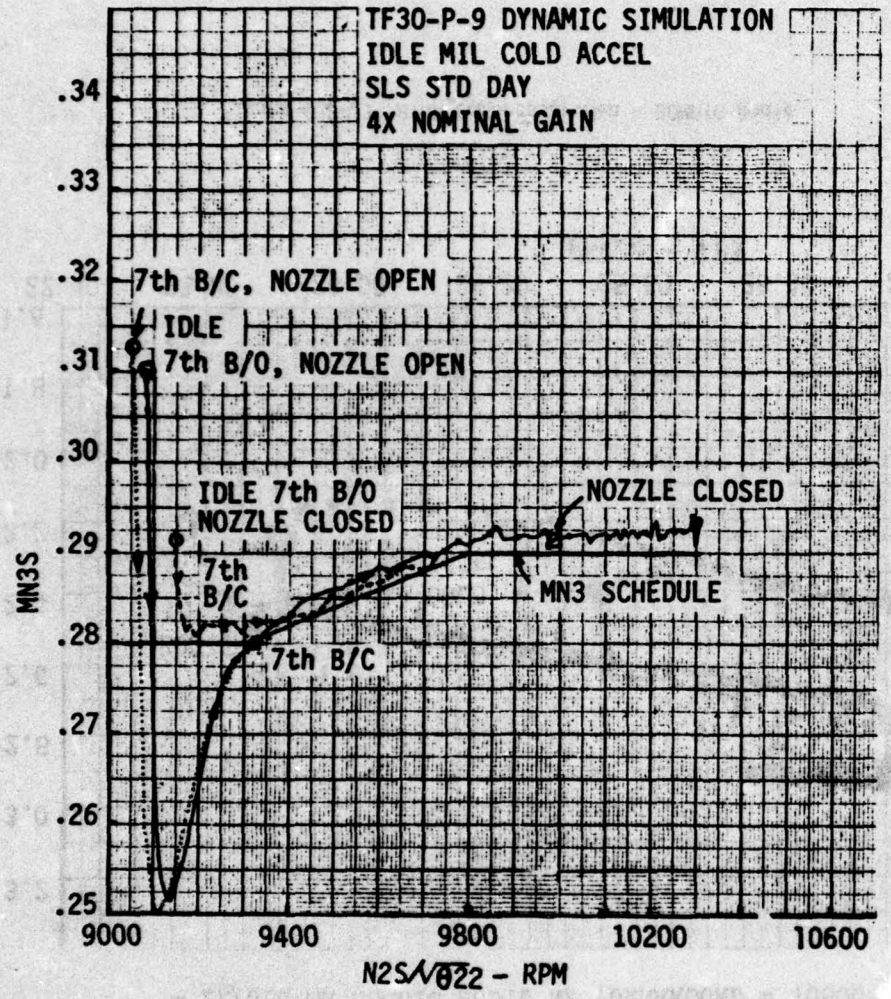

Figure 6.2-22 Dynamic Simulation Results Idle - Mil Accel

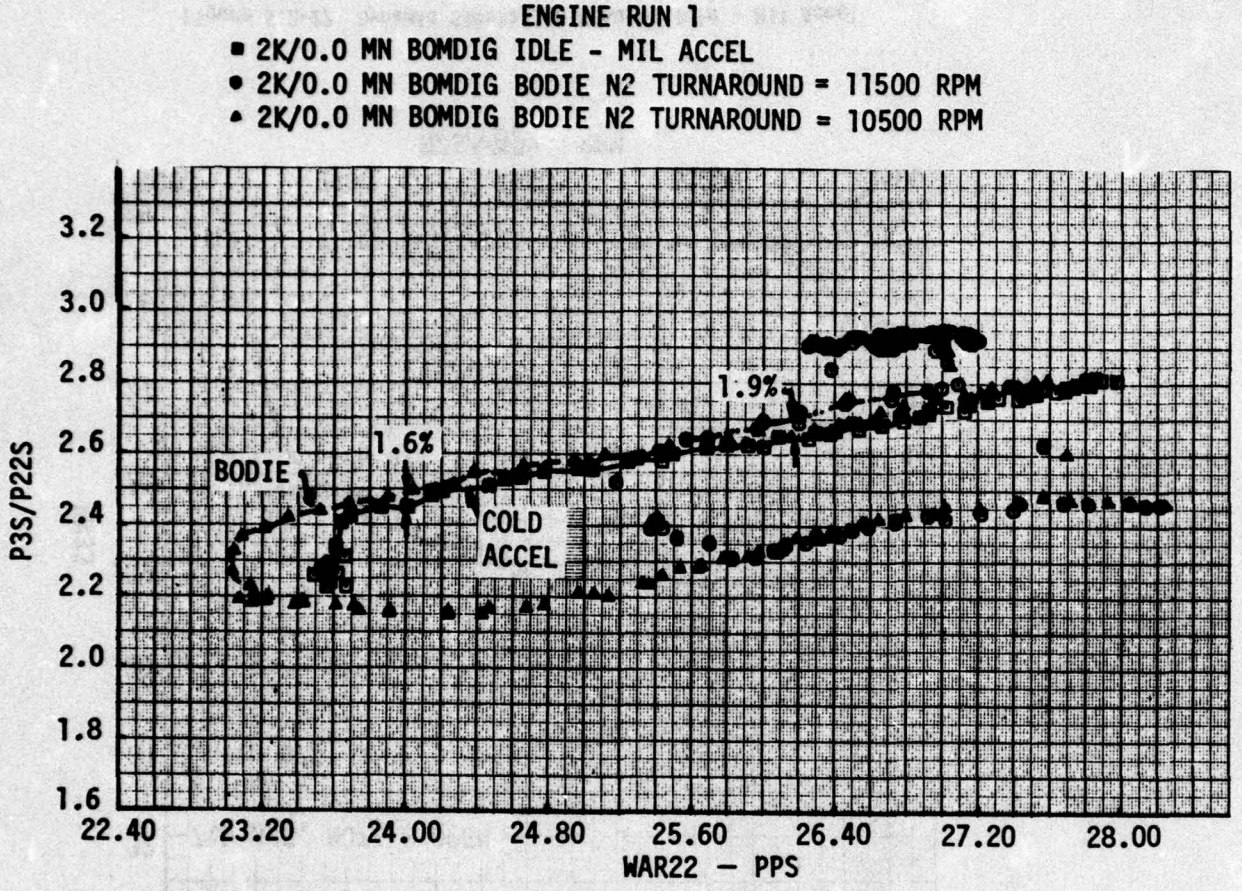

Figure 6.2-23 High Compressor Map - BOMDIG Bodie

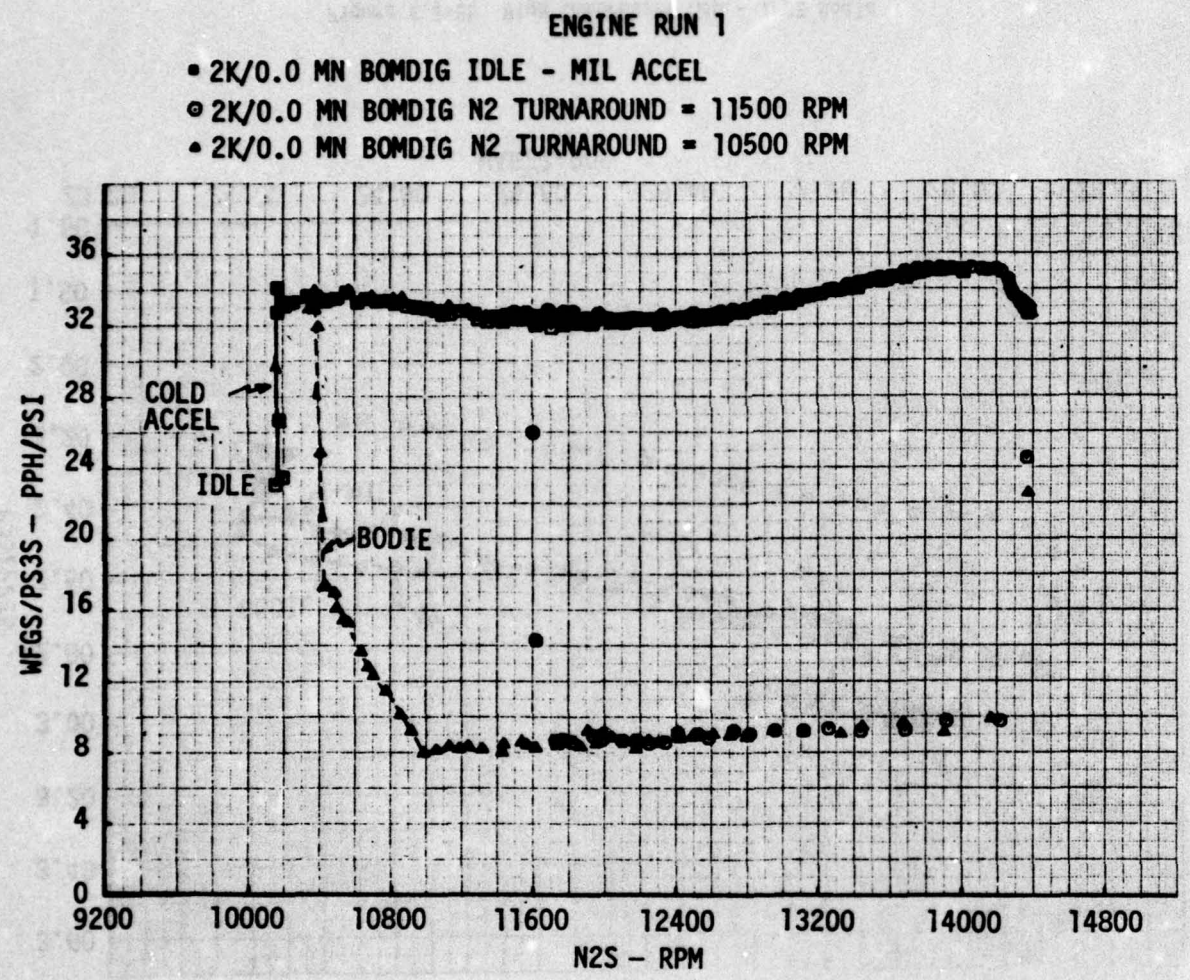

Figure 6.2-24 Wf/Pb Plot - BOMDIG Bodie

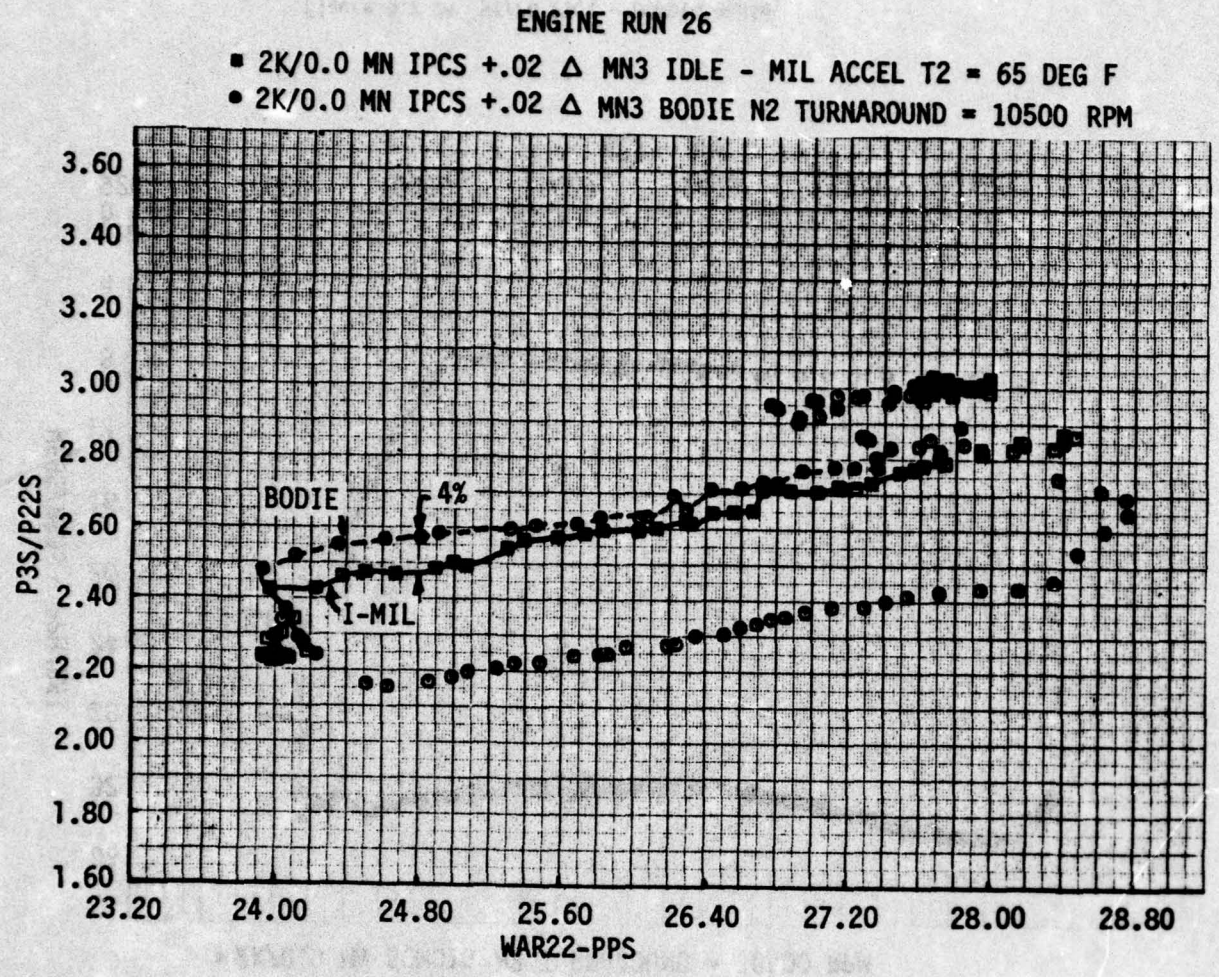

Figure 6.2-25 High Compressor Map - IPCS Bodie

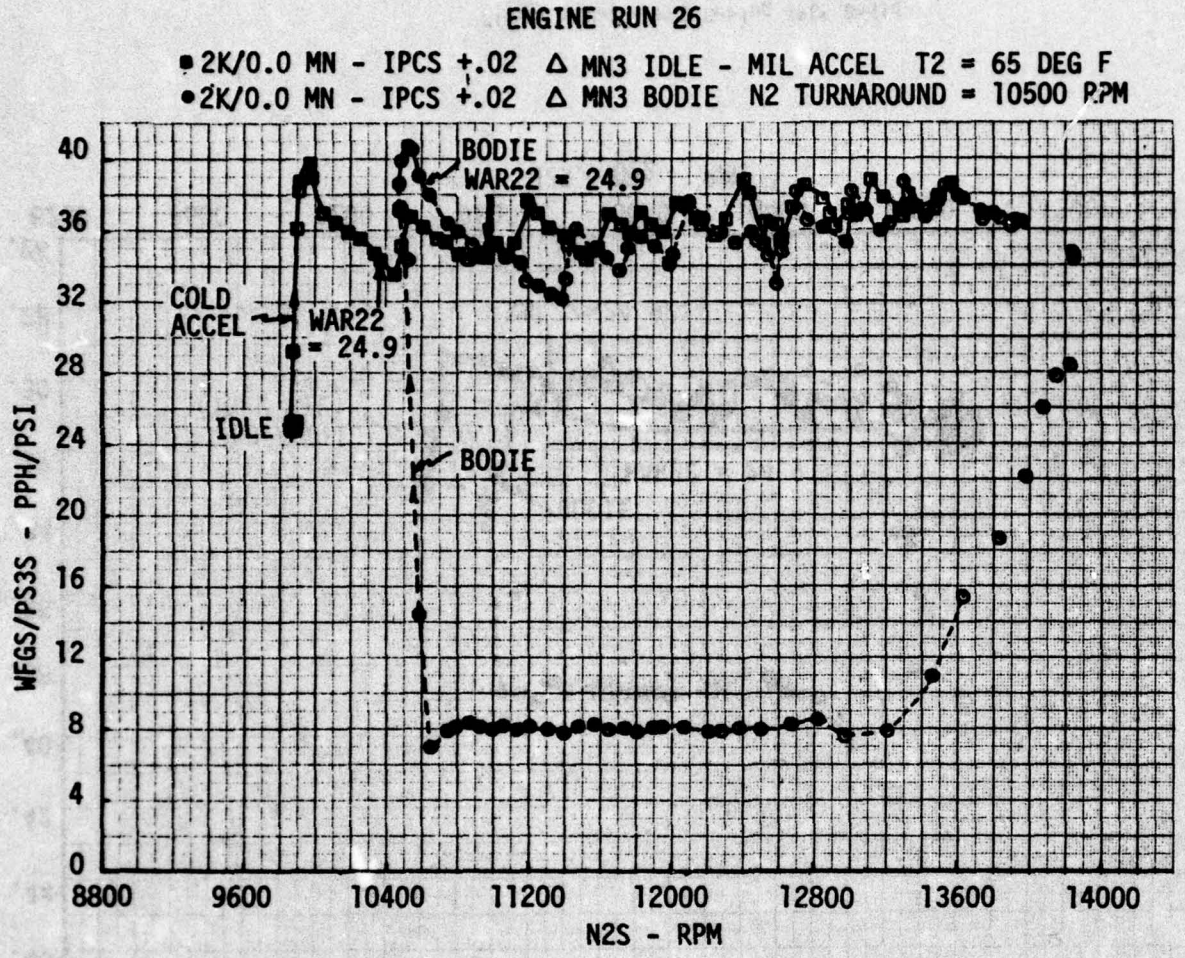

Figure 6.2-26 Wf/Pb Plot - IPCS Bodie

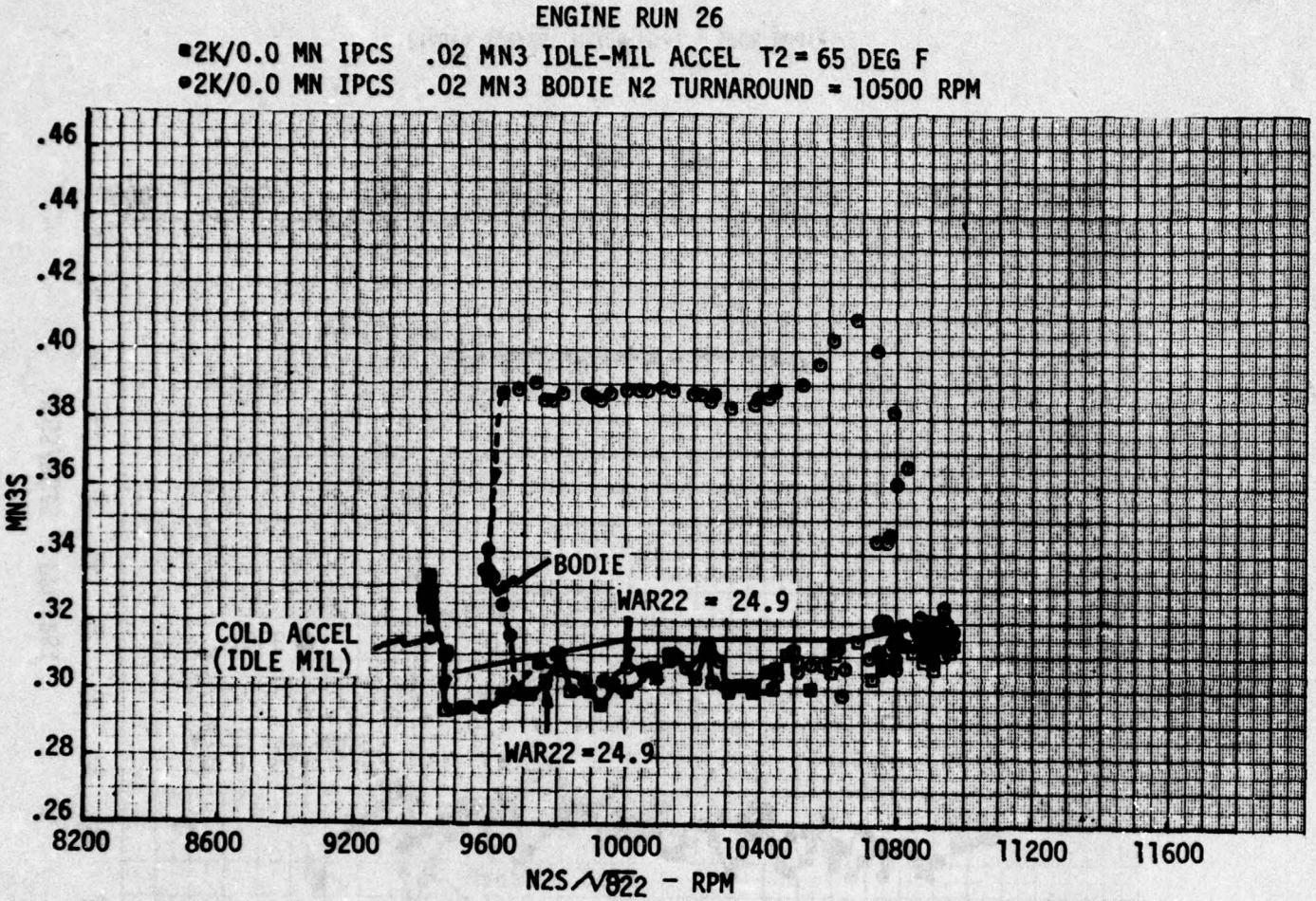

Figure 6.2-27 MN3 During IPCS Bodie

These results indicate the IPCS MN3 control produced results comparable to the Wf/Pb control; i.e., identical Wf/Pb levels for the cold accel and bodie and higher compressor excursions for the bodie. Since this conflicted with results observed during the altitude chamber testing at NASA/LeRC, further analysis was performed to explain the control of a bodie with high compressor discharge Mach number.

Compressor discharge Mach number is related to compressor operating point by the following:

$$(6.2.3\text{-}1)\quad MN3 \sim \left.\frac{W\sqrt{T}}{A\,P}\right]_{exit} = \left.\frac{W\sqrt{T}}{P}\right]_{in} \times \frac{1}{\frac{P\ EXIT}{P\ IN}} \times \sqrt{\frac{T\ EXIT}{T\ IN}} \times \frac{1}{A\ EXIT}$$

This equation assumes the entry airflow is equal to the discharge airflow. This is not precisely true during transients, but the magnitude of the difference is considered small. Assuming further that the compressor discharge area is constant, a bodie and cold accel will be governed to the same MN3 and the resultant compressor excursion will be evaluated at constant corrected inlet airflow, the following equations are developed:

MN3 bodie = MN3 cold accel

$$(6.2.3\text{-}2)\quad \left(\left.\frac{W\sqrt{T}}{P}\right]_{IN} \times \frac{1}{\frac{P\ EXIT}{P\ IN}} \times \sqrt{\frac{T\ EXIT}{T\ IN}}\right)_{\substack{COLD\\ACCEL}} = \left(\left.\frac{W\sqrt{T}}{P}\right]_{IN} \times \frac{1}{\frac{P\ EXIT}{P\ IN}} \times \sqrt{\frac{T\ EXIT}{T\ IN}}\right)_{BODIE}$$

$$\text{FOR}\quad \left.\frac{W\sqrt{T}}{P}\right]_{IN\ COLD\ ACCEL} = \left.\frac{W\sqrt{T}}{P}\right]_{IN\ BODIE}$$

$$(6.2.3\text{-}3)\quad \left(\frac{P\ EXIT}{P\ IN}\right)_{BODIE} \Big/ \left(\frac{P\ EXIT}{P\ IN}\right)_{\substack{COLD\\ACCEL}} = \left(\sqrt{\frac{T\ EXIT}{T\ IN}}\right)_{BODIE} \Big/ \left(\sqrt{\frac{T\ EXIT}{T\ IN}}\right)_{\substack{COLD\\ACCEL}}$$

The last equation directly relates the relative compressor excursion during a bodie to the relative compressor temperature ratio when governing to constant discharge Mach number. A check of the compressor operating temperatures during the bodie and the cold accel shown in Figure 6.2-27 indicated:

COLD ACCEL T IN = 610°R T EXIT = 791°R ; T OUT/T IN = 1.3

$\left.\frac{W\sqrt{\theta}}{\delta}\right]_{22}$ = 24.9 pps HIGH PRESSURE COMPRESSOR

BODIE T IN = 650°R T EXIT = 973°R ; T OUT/T IN = 1.5

or $\left(\frac{P\ EXIT}{P\ IN}\right)_{BODIE} \Big/ \left(\frac{P\ EXIT}{P\ IN}\right)_{\substack{COLD\\ACCEL}} = \sqrt{\frac{1.5}{1.3}} = 1.074$

Though the 7.4% higher excursion predicted by this equation was larger than the 4% indicated from the compressor map of Figure 6.2-25, the effect of the bodie on compressor match at constant exit Mach number and constant inlet corrected airflow was substantiated by the test data. In effect, the heat addition to the compressor during a bodie (hot accel) results in a higher discharge Mach number for the same compressor operating point, or a higher compressor pressure ratio for the same discharge Mach number and inlet corrected airflow.

Since this effect was not obvious from initial studies of the MN3 control loop or from earlier testing in the IPCS program, a review of these data was made to determine reasons for the apparent inconsistency. A cold accel and bodie were generated with the dynamic simulation and the resultant compressor temperatures near idle are compared to Engine Run 26 data in Figure 6.2-28. Although the predicted temperature response is faster than the test data indicate, the predicted temperature ratio for the bodie is 1.412, and for the cold accel it is 1.342 at constant corrected inlet airflow. These values indicate the compressor excursion should be 2.5% higher for the bodie, according to equation 6.2.3-3 for constant discharge Mach number and constant inlet corrected airflow. Figure 6.2-29 shows the cold accel and bodie have the same MN3 at a constant inlet corrected airflow of 24.9, and Figure 6.2-30 shows the bodie excursion is 2% higher than the cold accel at that airflow. The dynamic simulation thus verifies the higher bodie compressor excursion at constant MN3.

Altitude chamber test results at NASA/LeRC showed the compressor excursion was lower for a bodie at a simulated 10000 ft/0.9 MN condition when controlled with MN3 (Figure 6.2-31). Although high compressor temperature data for the bodie and cold accel were not available to explain this apparent discrepancy with the above results, inspection of Figure 6.2-31 provides a possible explanation. The "idle" setting for the cold accel was set artifically high for operational reasons by advancing the throttle to some point above normal idle. When the bodie was executed, the throttle was retarded to its normal idle setting and then returned to mil after a short period. The resultant bodie turnaround thus occurred below the cold accel "idle". This can be expected to produce lower compressor temperature ratios than a bodie turnaround at higher speeds, and consequently lower compressor excursions. A higher turnaround bodie is also shown in Figure 6.2-31, and its slightly higher excursion at the indicated constant corrected airflow is further proof that the bodie turnaround speed affects the magnitude of the compressor excursion.

Additional altitude chamber test results at the 41000 ft./1.4 Mn conditon did show lower Wf/Pb levels during the MN3 controlled bodie than during a cold accel. Although turnaround speeds were above the idle setting, deceleration rates were slower at this condition because of the minimum airflow loop operation. Slow decels would tend to minimize the bodie temperature effect. The MN3 excursion and the compressor pressure ratio as a function of corrected inlet airflow during the cold accel and the bodie are shown in Figure 6.2-32. Although the initial MN3 excursion was

SEA LEVEL STATIC ALL VALUES ARE SENSED TEMPERATURES

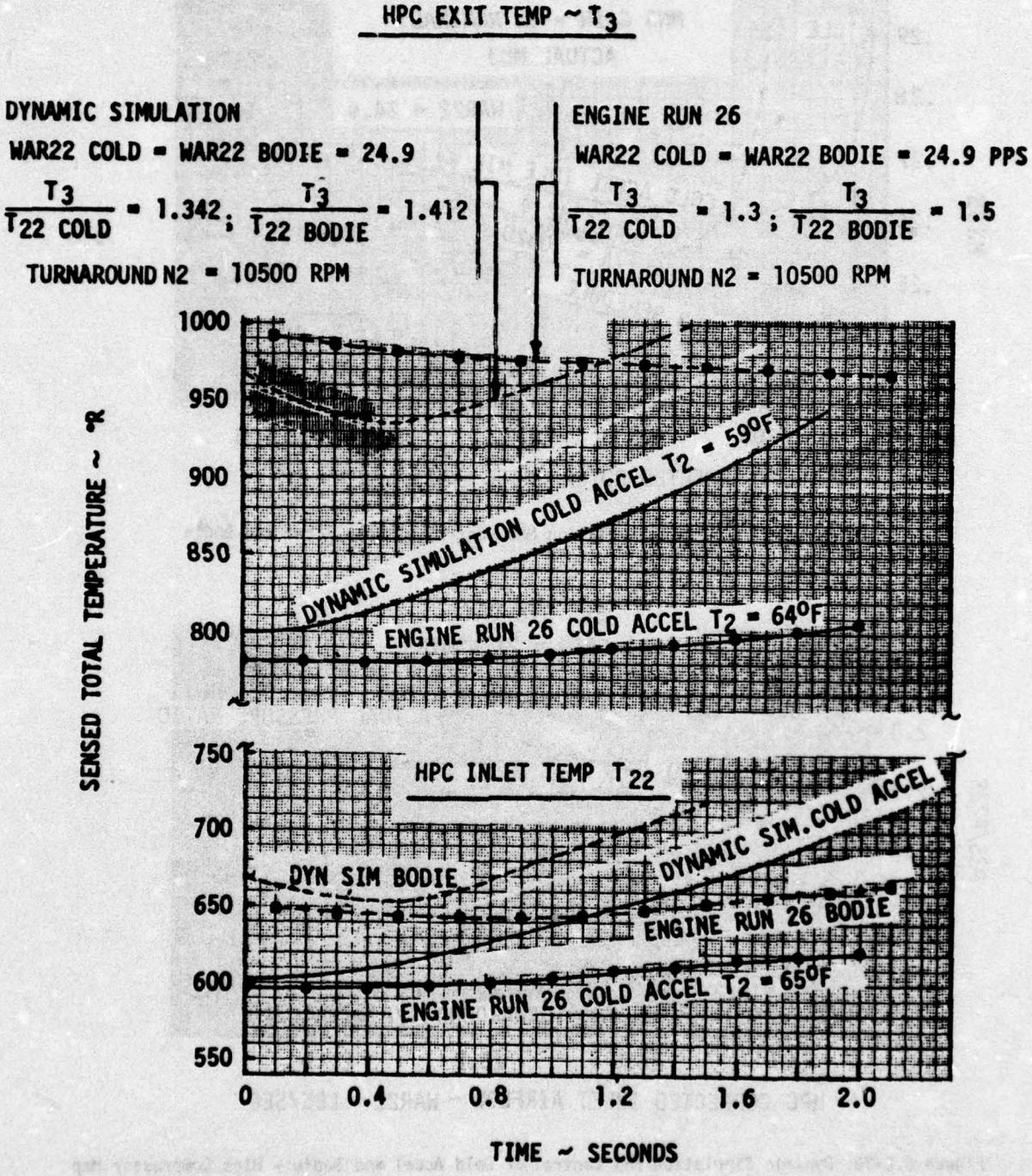

Figure 6.2-28 Predicted and Measured HPC Inlet and Discharge Temperature During Cold Accel and Bodie

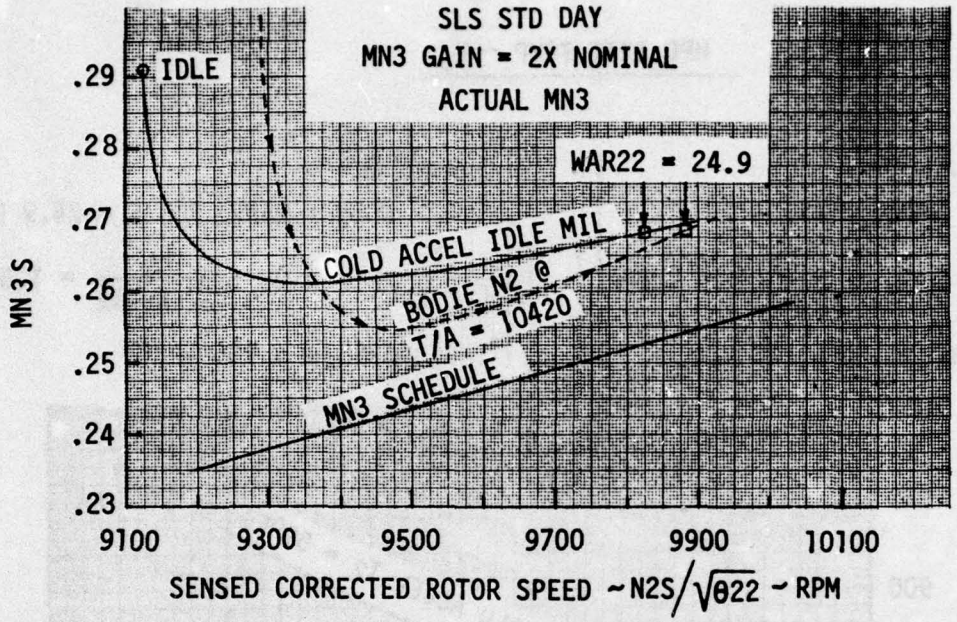

Figure 6.2-29 Dynamic Simulation MN3 Control of Cold Accel and Bodie

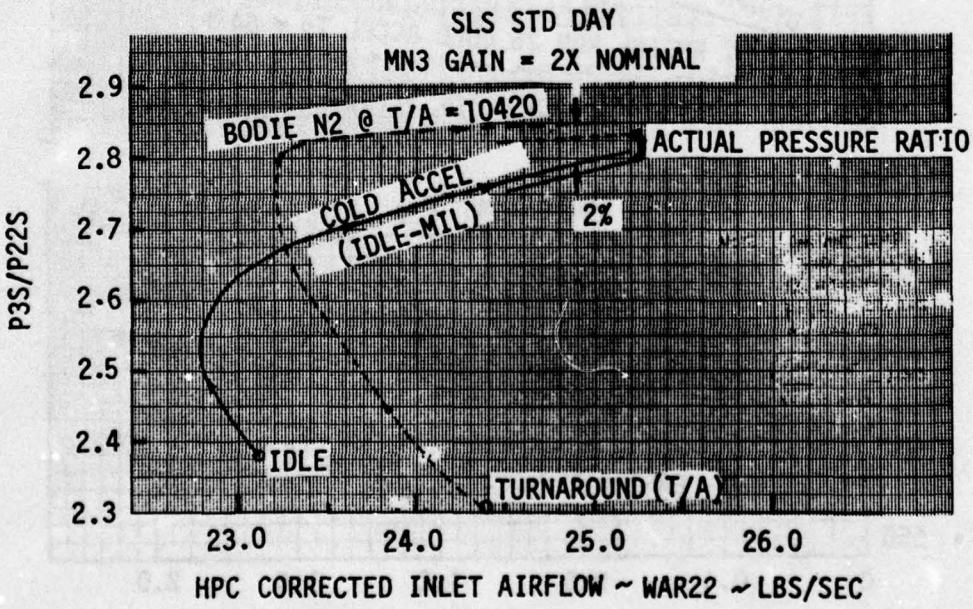

Figure 6.2-30 Dynamic Simulation MN3 Control of Cold Accel and Bodie - High Compressor Map

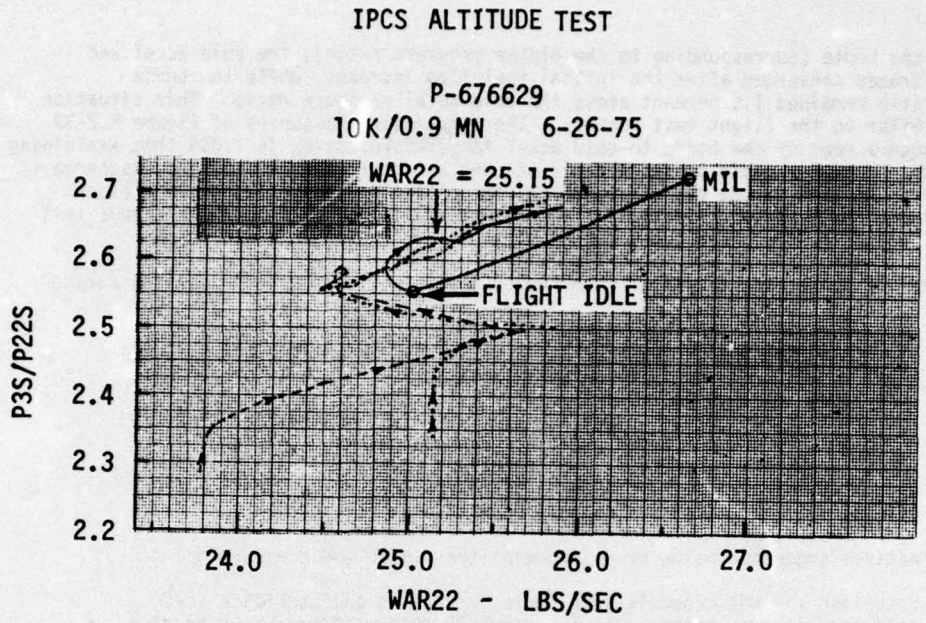

Figure 6.2-31 Altitude Test Bodie High Compressor Map

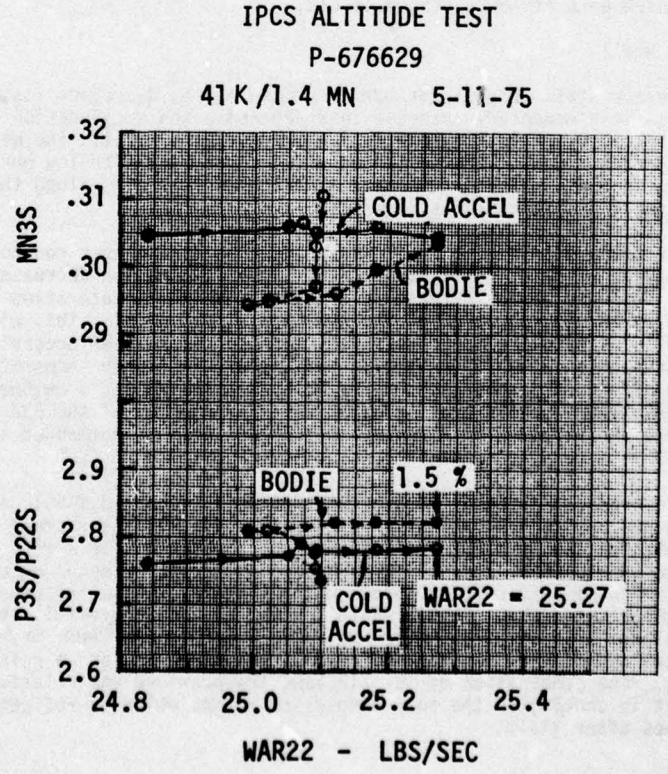

Figure 6.2-32 High Compressor Excursion During Bodie and Cold Accel

lower for the bodie (corresponding to the higher pressure ratio), the cold accel and bodie MN3 traces converged after the initial fuel flow increase, while the bodie pressure ratio remained 1.5 percent above the cold accel pressure ratio. This situation is then similar to the flight test results. The temperature histories of Figure 6.2-33 show the square root of the bodie to cold accel temperature ratios is 1.015 thus explaining the 1.5 percent higher bodie pressure ratio at constant corrected airflow and discharge Mach number. As seen by the discussion above, the effect of the bodie on the pressure ratio-discharge Mach number relationship was not readily apparent from the altitude test results. Further analysis confirmed the results observed during the flight test.

The conclusions concerning discharge Mach number control of compressor excursion during a bodie are:

1. Discharge Mach number control is equivalent to a Wf/Pb control during a bodie. It produced approximately the same Wf/Pb levels for both a cold accel and a bodie.
2. The relationship between compressor discharge Mach number and pressure ratio at constant corrected inlet airflow changes with the temperature ratio across the compressor. The temperature effect is significant enough during a bodie to prevent a discharge Mach number control from maintaining a bodie excursion no higher than a cold accel.

Some alternatives suggested below can circumvent the higher bodie excursion:

1. Establish the MN3 schedule with bodie excursions and sacrifice some cold accel thrust response as is currently done with the Wf/Pb accel schedules.
2. Use some "PLA history" critiera in a digital controller to sense a bodie and shift MN3 schedules accordingly.
3. Control accelerations to compressor operating line P3/P22 vs MN22 directly, thus ensuring equal excursions for the cold accel and the bodie. Control to pressure ratio establishes stringent transducer accuracy requirements at low pressure levels.

Fuel Derichment During Stall

When a prolonged compressor stall occurs, the burner pressure, Pb, decreases faster than fuel flow. This results in a momentary increase in Wf/Pb above the acceleration schedule as indicated by the spike in Figure 6.2-34. Shortly after stall, the Wf/Pb controller responds to reduce fuel to the scheduled Wf/Pb level, and with low burner pressures, this results in fuel derichment. The engine then decelerates along the acceleration schedule until the throttle is retarded.

Fuel scheduling after a stall with a high compressor discharge Mach number control is dependent upon the behavior of MN3. Test data indicate a short duration decrease in MN3 occurs after stall followed by an increase to a level above the acceleration schedule where it remains for the duration of the stall (Figure 6.2-35). This will result in a MN3 controller scheduling more fuel after stall until another control loop takes command. Consequently, a MN3 controller may result in higher temperatures after stall and a more difficult recovery than a Wf/Pb controller unless a method is devised to decrease fuel flow. Stalls that occurred during operation of the MN3 loop did not result in increases in fuel flow because a backup Wf/Pb limit commanded a decrease in fuel.

The increase in high compressor discharge Mach number during a prolonged stall can be explained by reviewing the physical events after stall. Immediately after stall the compressor "blows down" to a low pressure level, and airflow reverses for a very short period (several milliseconds). A negative discharge Mach number would occur during flow reversal, but it would be difficult to detect without high response instrumentation and very short data sample intervals. Following this momentary flow reversal, the flow resumes its normal direction but at a very low level. Energy continues to be imparted to the gas from the turning rotor in the form of a small pressure rise and a relatively large temperature rise. The combination of low airflow, low pressure and relatively high temperature result in choking of the rear compressor stages which is reflected by the larger MN3 values after stall.

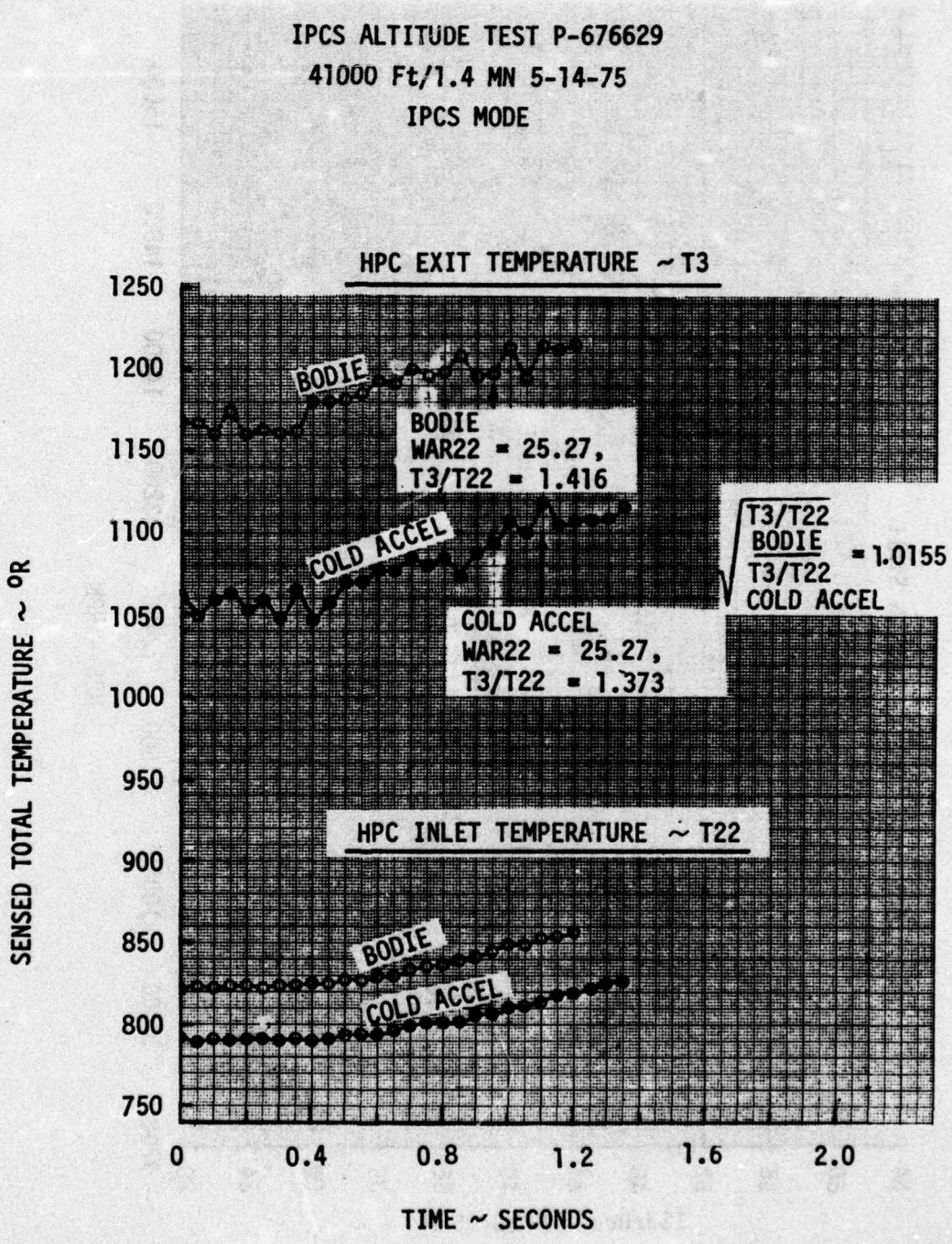

Figure 6.2-33 Comparison of High Pressure Compressor Temperatures During Bodie and Cold Accel

FLIGHT 25

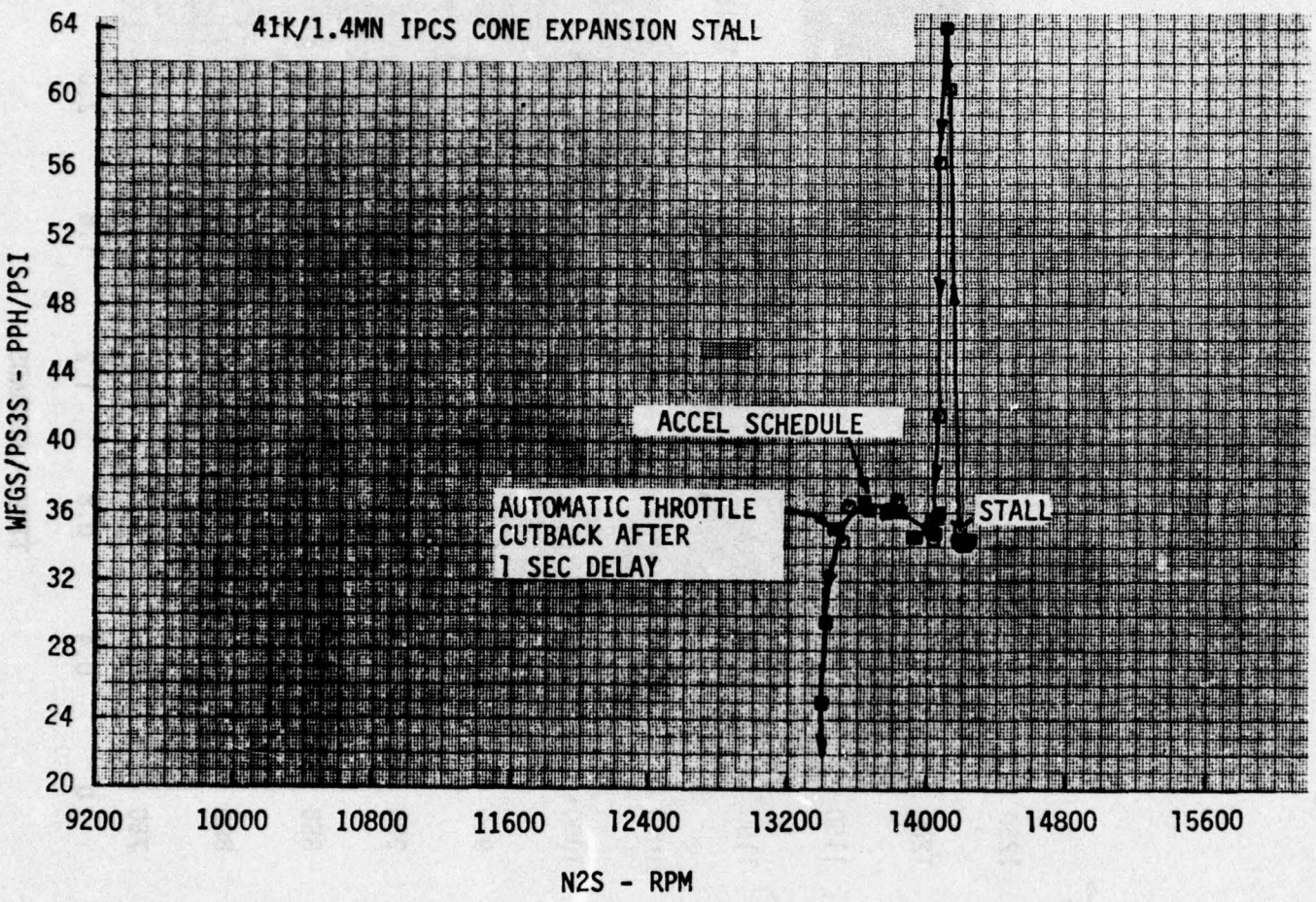

Figure 6.2-34 Wf/Pb Plot for Stall

FLIGHT 25

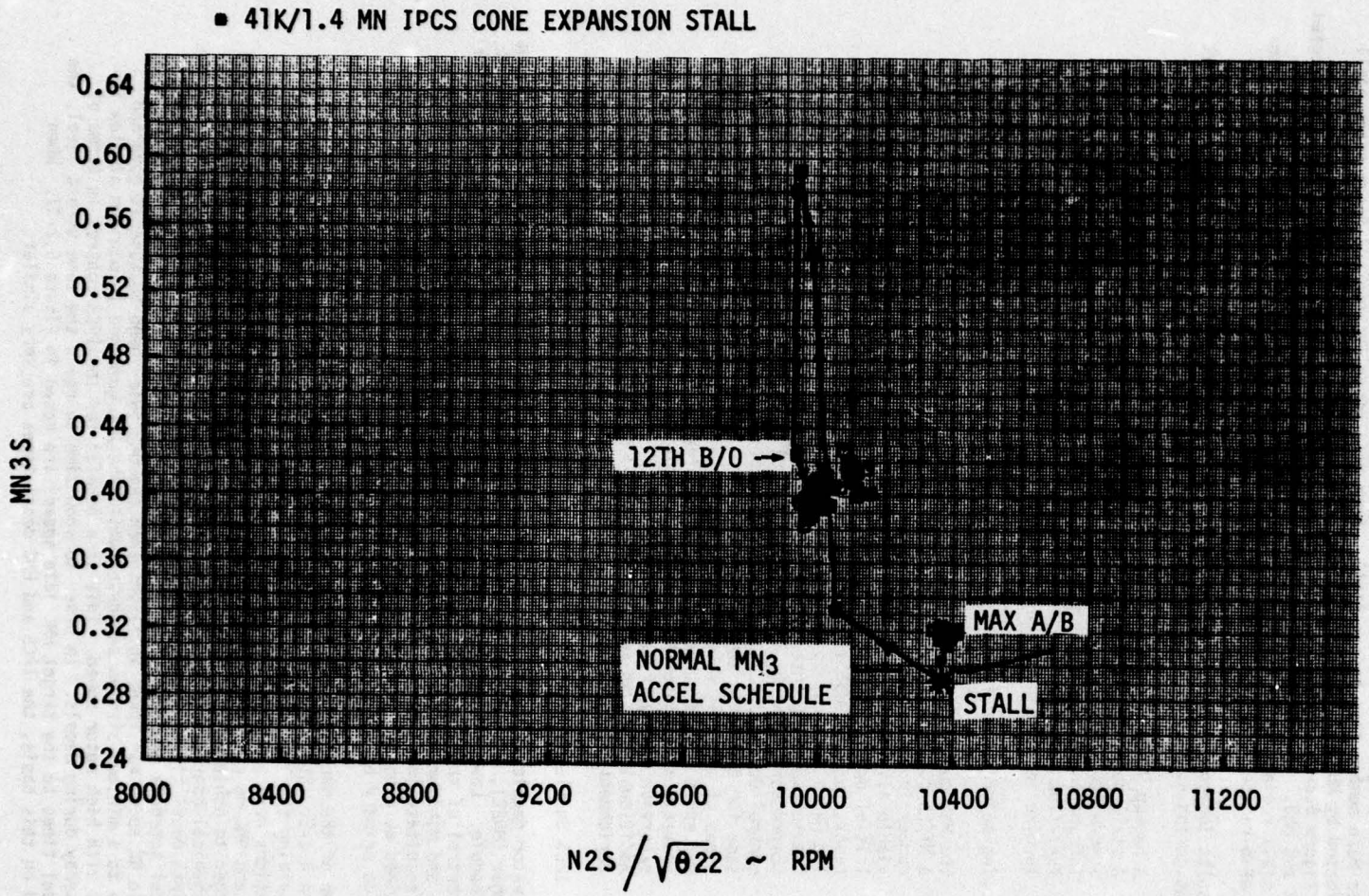

Figure 6.2-35 MN3 History after Stall

The choked rear stage(s) in turn throttle the airflow delivered to the compressor and force the front stages to remain stalled. The stalled front stages are thus operating at a lower Mach number than before stall. Both rear stage choking and front stage stall were reflected by MN3 and MN22 respectively after a stall during Flight 25. This is shown in Figure 6.2-36 which is a high compressor map showing post stall traces constructed from MN22 and MN3. The higher excursion is based on MN22 and indicates operation in or near the stall region, while the lower excursion is based on MN3 and indicates operation in the choked region.

These results indicate a MN3 acceleration control must include additional logic for fuel derichment during stall. Some possible schemes are:

1. A backup Wf/Pb schedule
2. A stall detector such as Pb that activates a large positive MN3 schedule offset.
3. Integrating MN3 error to produce a Wf/Pb command rather than a fuel flow command.
4. Turbine inlet temperature limiting.

The following major conclusions were made from the IPCS MN3 controller test restuls:

1. The MN3 control demonstrated acceleration times as good or better than a Wf/Pb controlled acceleration while governing to discharge Mach number in the initial phase of the acceleration. It is therefore a viable alternative to a Wf/Pb controller.
2. Initial undershoots below the MN3 schedule were observed during ground tests, but were not significant during flight testing.
3. The MN3 signal was noisy.
4. Smaller sampling intervals did not improve schedule tracking.
5. Compressor discharge Mach number control is equivalent to the Wf/Pb control during a bodie. The Wf/Pb excursion was approximately the same for the bodie and cold accel.
6. Lines of constant compressor discharge Mach number on a compressor map shift toward surge during hot accelerations, or bodies. This prevents a discharge Mach number control from maintaining a bodie excursion no higher than a cold accel.
7. Additional logic is required with a MN3 control to provide fuel derichment during a stall.

6.2.3.2 IPCS Decelerations

Gas generator decelerations in the IPCS mode were controlled by low compressor discharge Mach number (MN22), minimum engine inlet airflow (WAT2SX), or by a backup 10 ratio unit Wf/Pb schedule. Low compressor discharge Mach number governing was intended to provide direct control of the low compressor excursion during a deceleration for stall protection, and minimum airflow limiting was intended to avoid airflow undershoots that could precipitate inlet buzz. The bill of material 10-ratio-unit Wf/Pb decel schedule was retained as a backup to avoid excessive turbine thermal stress during decels and to provide primary burner blowout protection.

Selection of the decel governing loop was determined by a select high gate as seen in Figure 4.2-2. Since decels are governed by negative fuel flow rate commands, the loop providing the least negative error was always selected. Most of the inflight decelerations were predominantly governed by the minimum airflow loop. A comparison of IPCS and HMC decel times is provided in Figure 6.2-37, and it shows the IPCS control took longer to achieve 95 percent of its mil to idle high rotor speed change than the hydromechanical control everywhere except on the ground. There are two reasons for the longer IPCS decel times. First, the loop selection criteria with the backup 10 ratio unit decel schedule prevented fuel derichment rates greater than the HMC. Second, the IPCS idle N2 speed was lower in flight than the HMC idle speed because it governed directly to a minimum airflow schedule, while the HMC governed to minimum airflow indirectly with high rotor speed. This is a benefit for the IPCS control in terms of thrust decay during decels. In order to show time to reach the same thrust level, the IPCS decel times to the target HMC idle speeds are noted in Figure 6.2-37. When compared on this basis, the IPCS and HMC decel times are very similar.

FLIGHT 25

41000 Ft/1.4 MN CONE EXPANSION STALL

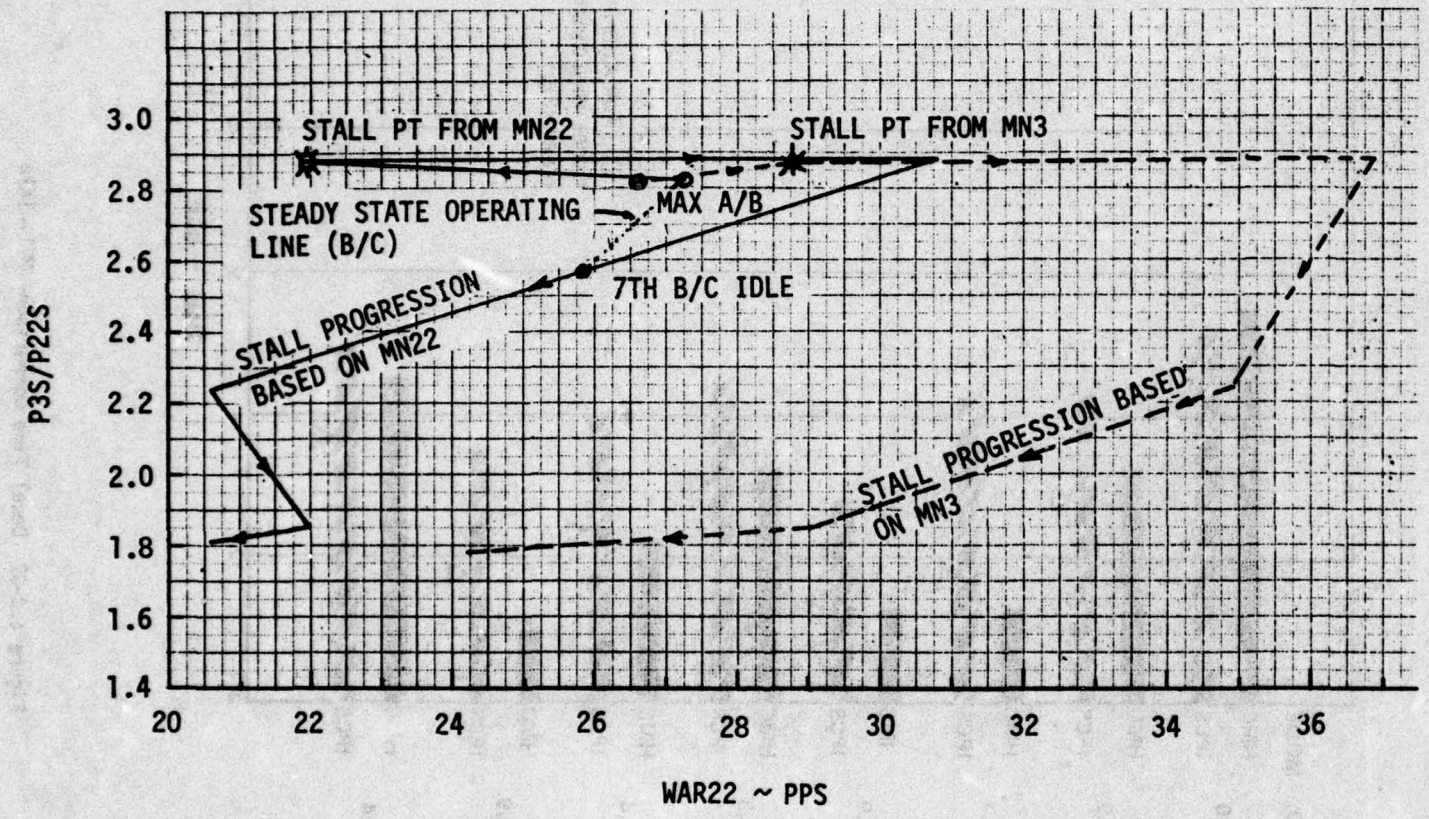

Figure 6.2-36 High Compressor Map After Stall

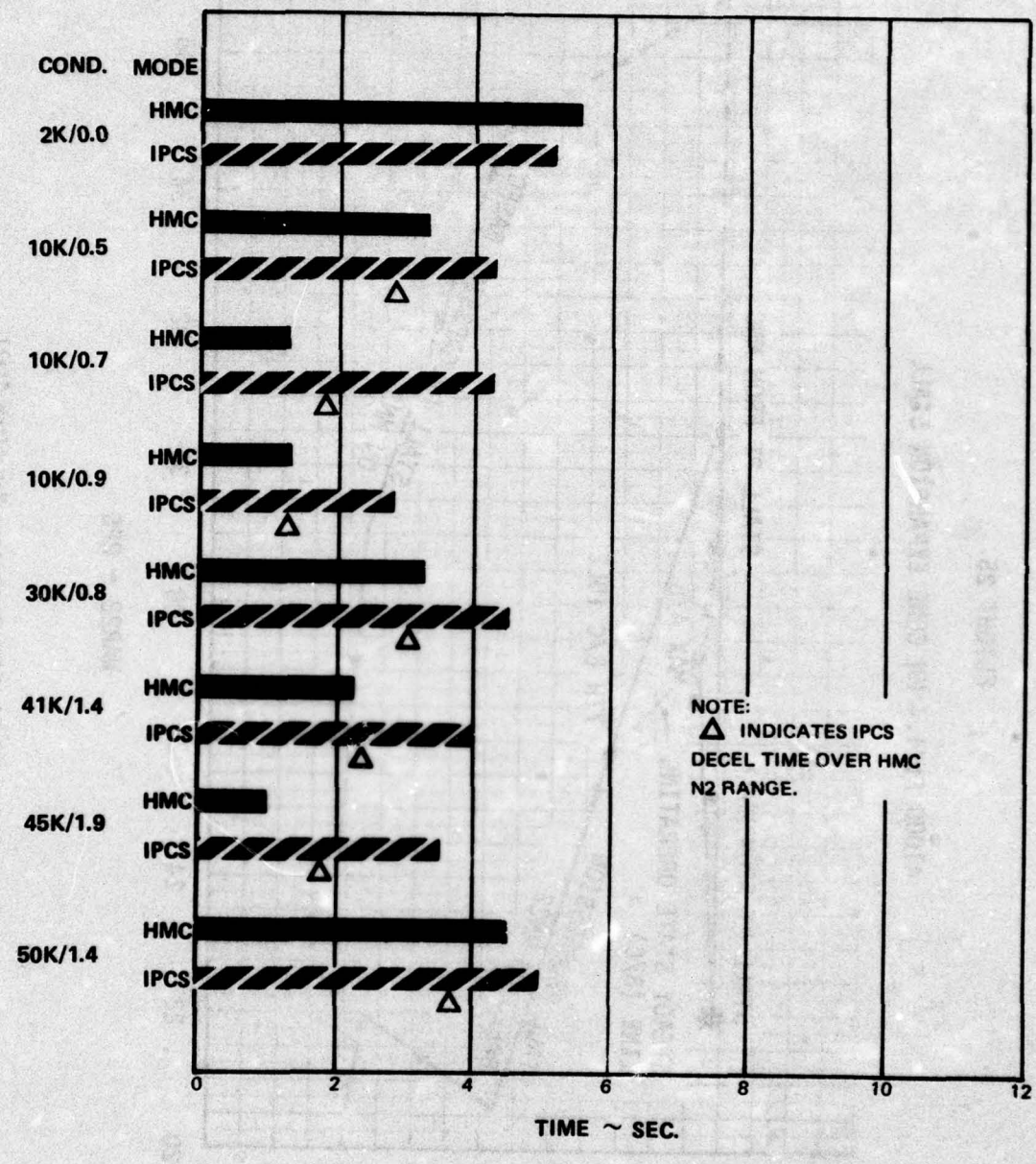

Figure 6.2-37 Decel Time Comparison Mil-Idle

Most of the IPCS decelerations to idle were made without lead/lag compensation on the airflow signal. The compensation evolved from an initial 10:1 lead/lag during altitude chamber testing to 2:1 lead/lag during the first IPCS flight.17. Compensation was then removed in an effort to decrease decel times at the added risk of incurring inlet buzz due to airflow undershoots. Figure 6.2-38 shows the uncompensated airflow did not result in airflow undershoots at 45000 ft/1.9 MN. This was also typical at higher Mach numbers where inlet buzz was most likely to occur. Airflow undershoots were observed without compensation at lower Mach numbers, as seen in Figure 6.2-39 for 50000 ft/ 1.4 MN, but inlet buzz did not occur at these conditions. The presence of airflow undershoots at the lower Mach numbers (1.6 and below) is attributed to the larger operating range between military and idle which results in larger changes in fuel flow during the decel. Figure 6.2-39 shows the 2:1 lead/lag compensation prevented an airflow undershoot and its removal shortened the decel time by 0.8 seconds (Figure 6.2-40). If necessary for future propulsion system controls, the airflow compensation could be varied with flight Mach number to optimize the trade between airflow undershoots and decel time.

Low compressor discharge Mach number (MN22) limiting during a deceleration provided more low compressor surge protection than the hydromechanical control. This was accomplished even though the 7th stage bleed was open for the HMC decel and closed for the IPCS decel at 50000 ft/1.4 MN. The low compressor excursions during these decels are shown in Figure 6.2-41 along with the operative IPCS control loops. The 12th stage bleeds were opened during both decelerations as Wf/Pb approached the 10 ratio unit deceleration schedule. This was a feature of the HMC that was retained for the IPCS control. For a new propulsion system, this decel proximity bleed could be eliminated by directly controlling the low compressor excursion during a decel.

Midway through the low compressor decel excursion, the controlling loop switched from MN22 to minimum Wf/Pb, as seen in Figure 6.2-41. This resulted in a slight increase in low compressor excursion relative to the HMC. The cause of the loop switch is shown in Figure 6.2-42. Soon after rotor speed begins to decrease, the 12th bleeds open and the MN22 schedule is increased accordingly. As the decel progresses through 8000 rpm corrected low rotor speed, the schedule turns downward which increases the magnitude of the MN22 error (MN22 ref-MN22 sensed). The MN22 error thus becomes more negative than the Wf/Pb min error, and Wf/Pb min becomes the controlling loop. This loop switch occurs once more when the Wf/Pb min error becomes more negative than the minimum airflow error, and minimum airflow becomes the controlling loop. Refinements to the MN22 schedule would prevent loop switching from the MN22 loop to the minimum Wf/Pb loop.

The following conclusions were made regarding the IPCS decelerations:

1. IPCS idle speeds were lower than the HMC because of direct control to minimum airflow, and this enabled more thrust decay during decelerations at rates comparable to the HMC. Fuel derichment rates were limited to the HMC levels to avoid increased turbine thermal stress and primary burner blowout.
2. The minimum airflow control demonstrated decelerations without airflow undershoots. A compensated airflow signal is required at intermediate Mach numbers (1.6 and below) to prevent undershoots at the expense of a longer deceleration time.
3. The low compressor discharge Mach number control demonstrated deceleration low compressor stall protection with the 7th bleed closed equal to or better than the HMC with the 7th bleed open.

6.2.3.3 BOMDIG Accelerations

Accel times from idle to mil for the HMC and BOMDIG controls are compared in Figure 6.2-43. Times were measured from the power lever snap to 95% of the high rotor speed (N2) change. The accel times for both controls were essentially the same, thus reflecting proper implementation of the bill of material mode in the digital control and a correct fuel flow calibration (Section 5.4.3).

FLIGHT 25

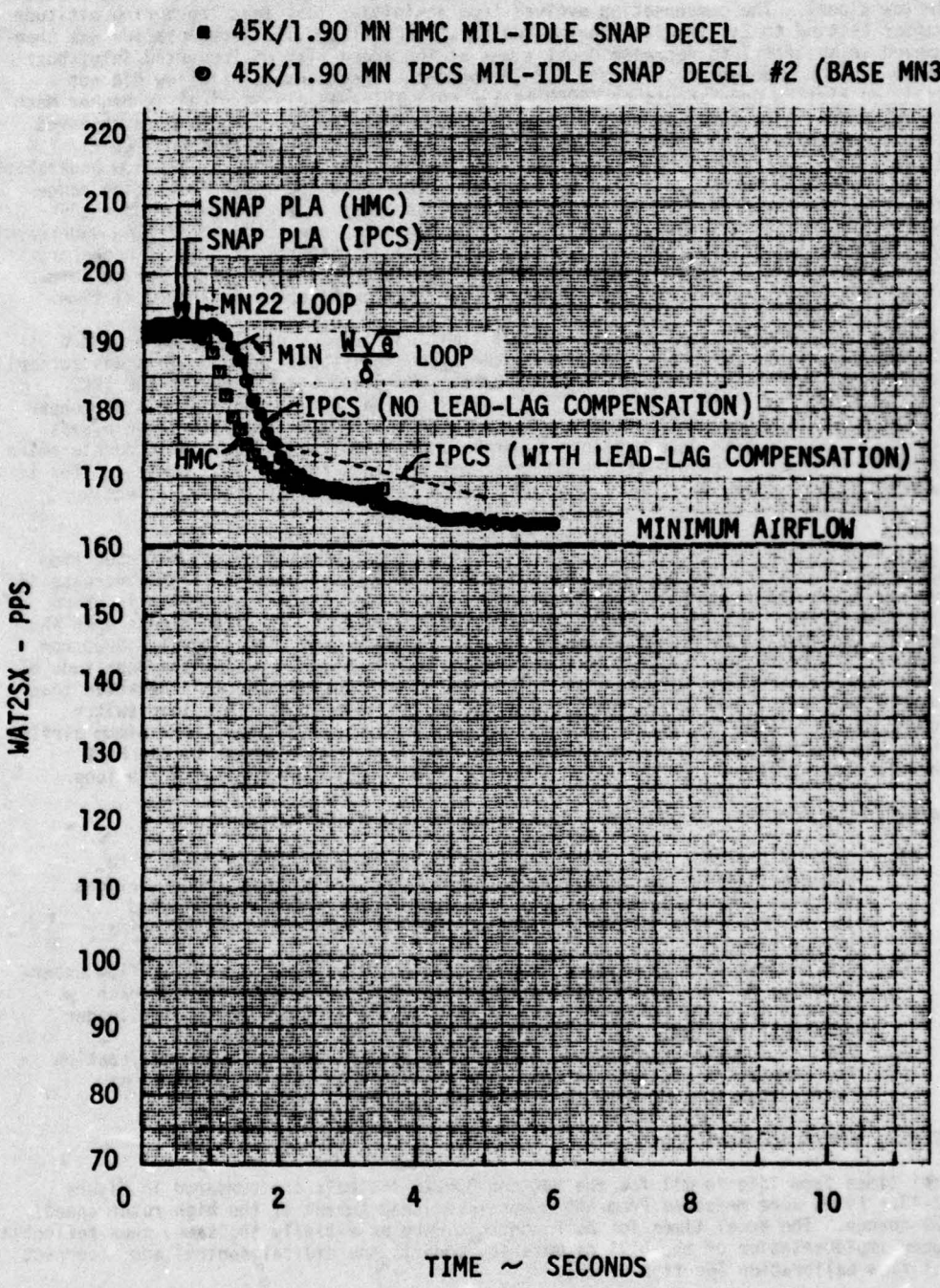

Figure 6.2-38 Decel Airflow Time History - 45K, 1.9 MN

FLIGHT 24

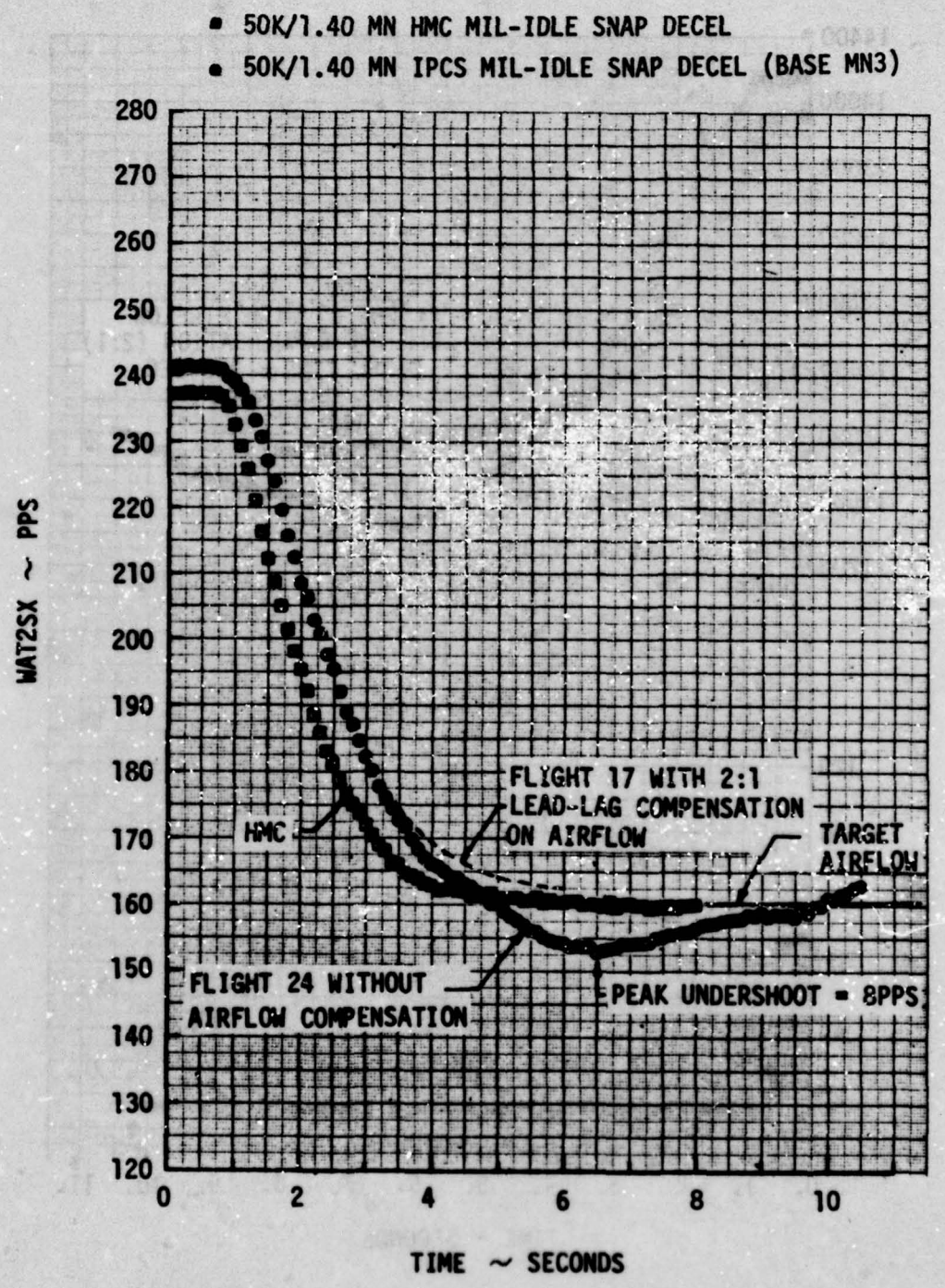

Figure 6.2-39 Decel Airflow Time History - 50K, 1.4 MN

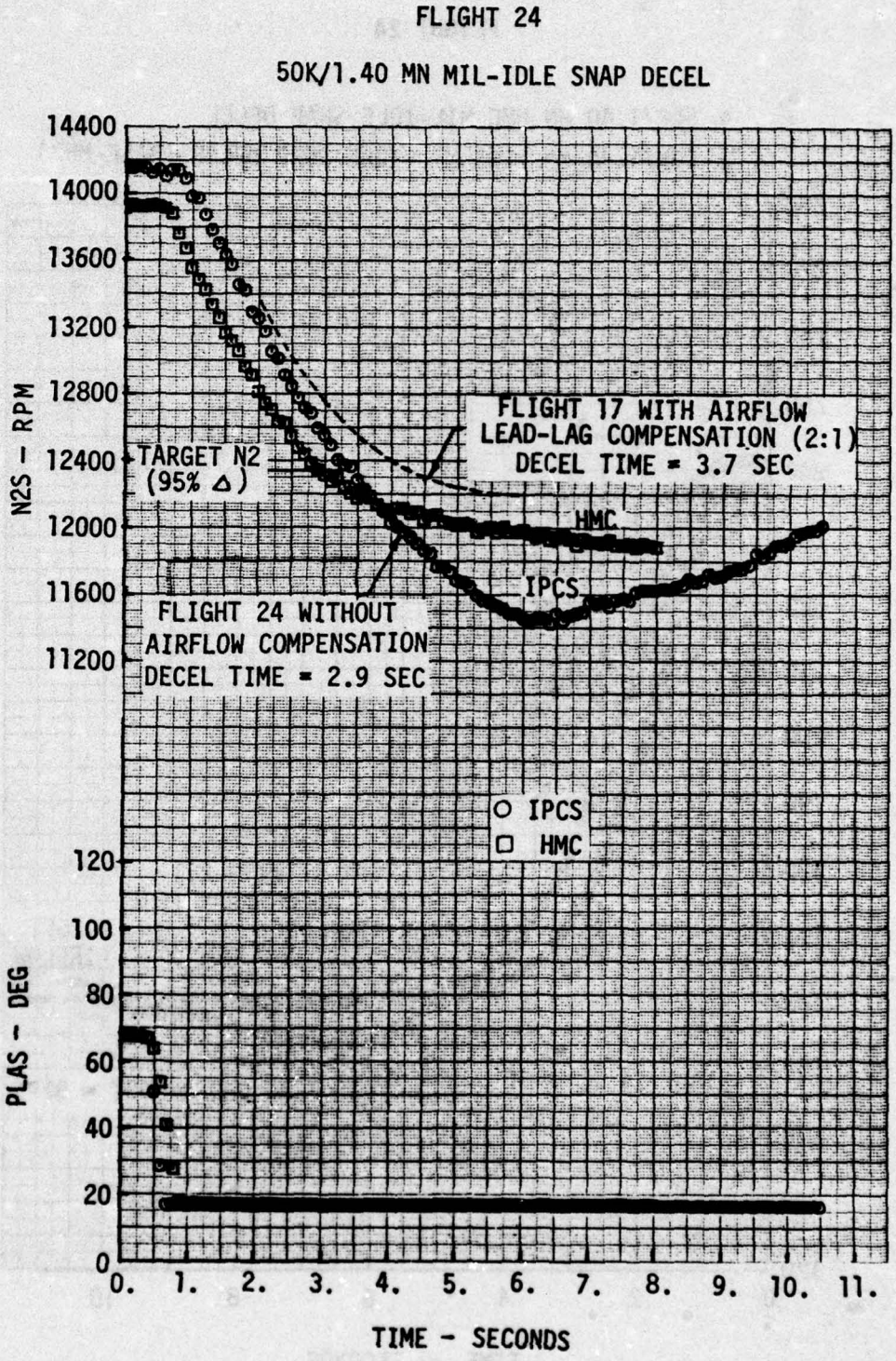

Figure 6.2-40 Decel High Rotor Speed Time History - 50K, 1.4 MN

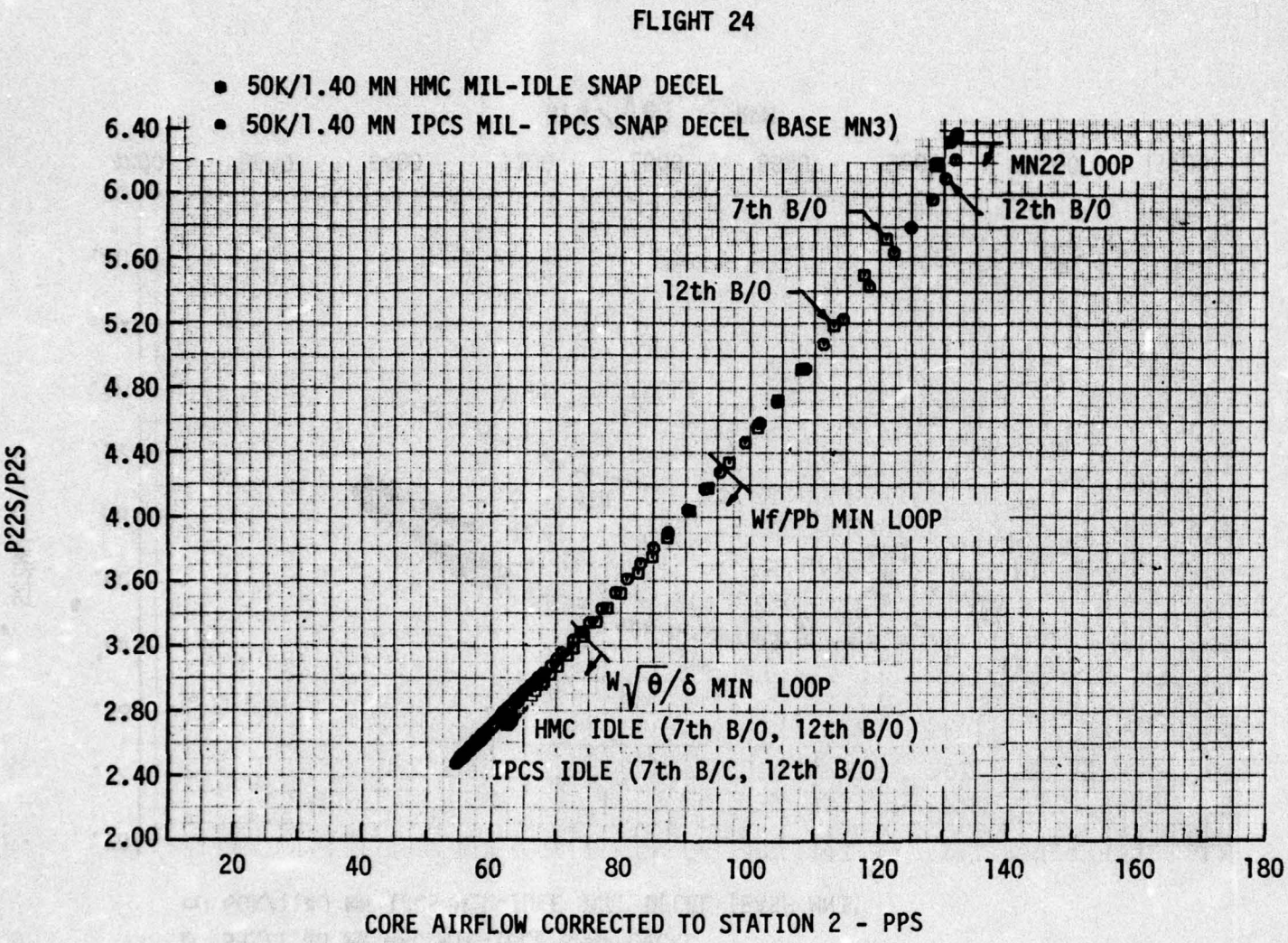

Figure 6.2-41 Low Compressor Map During Mil-Idle Decel

FLIGHT 24

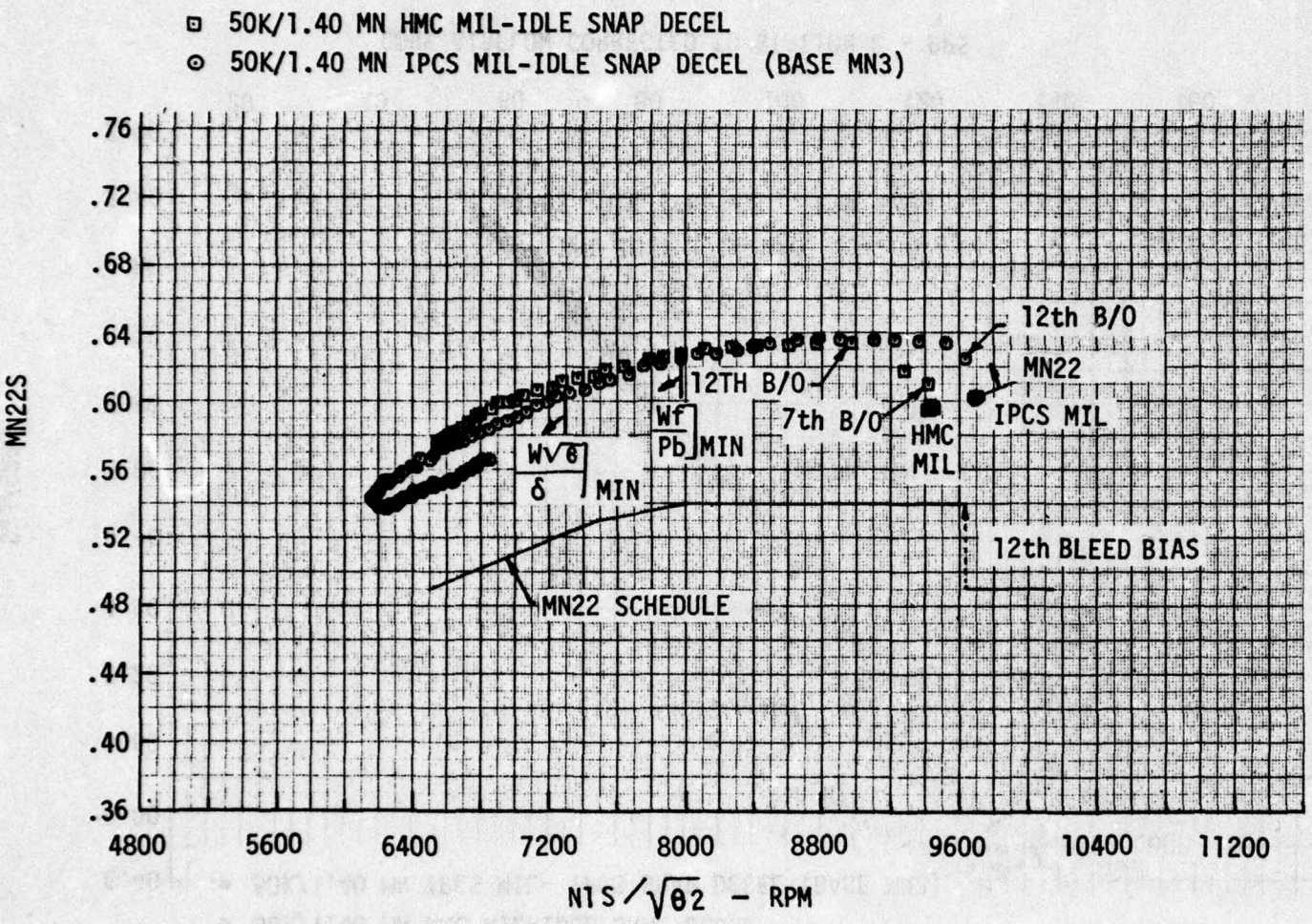

Figure 6.2-42 MN22 During Mil - Idle Decel

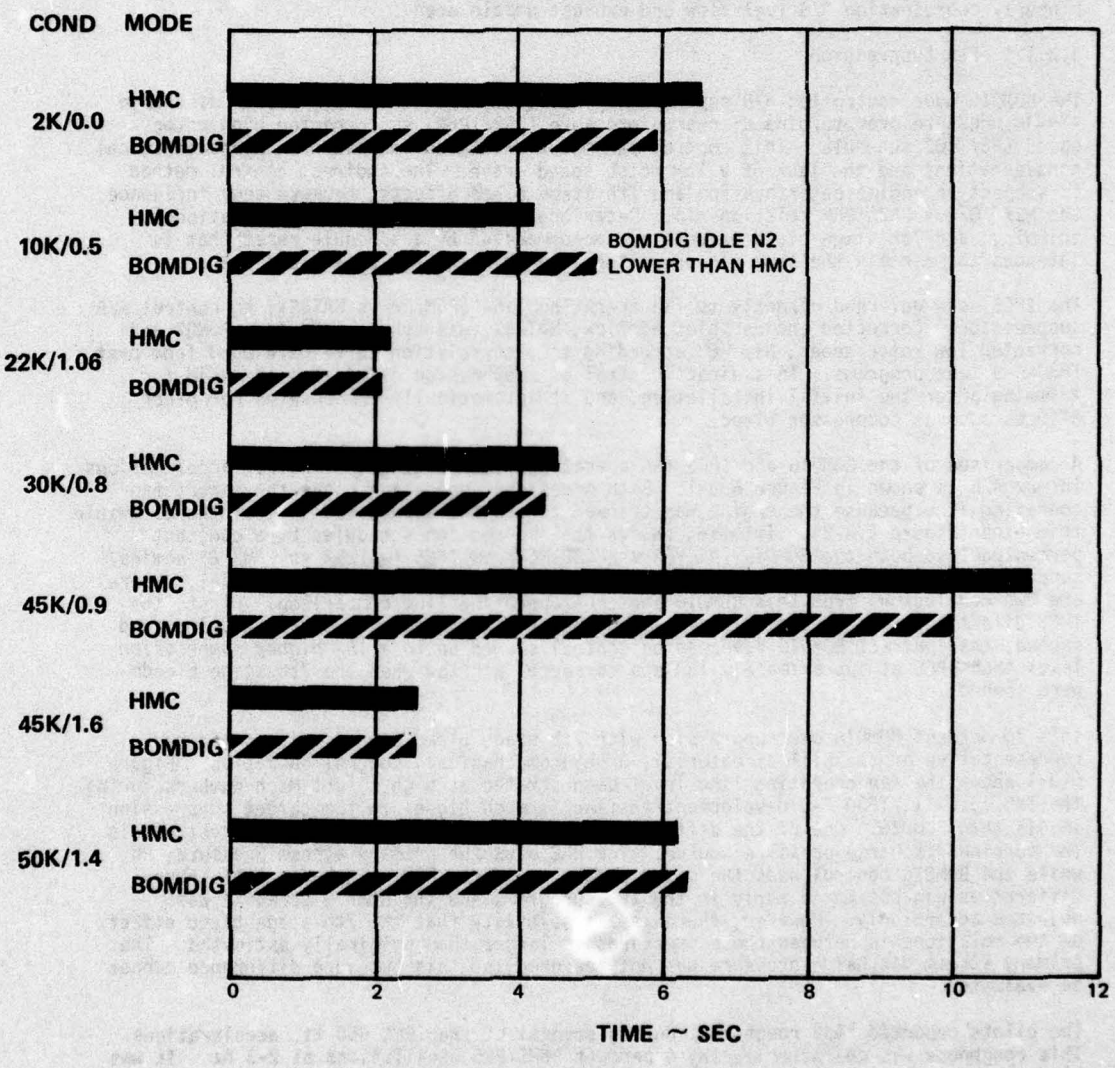

Figure 6.2-43 Idle - Mil Accel Time Comparison - BOMDIG, HMC

6.3 AFTERBURNING

6.3.1 Steady State A/B

Steady state afterburning operation is influenced by afterburner fuel scheduling and exhaust nozzle position as well as turbine inlet temperature. Exhaust nozzle area together with A/B fuel flow determine fan suppression, or level of fan pressure ratio for a given inlet corrected airflow. The primary function of the fuel control during A/B operation is to maintain a target suppression level, or fan operating line, by properly coordinating A/B fuel flow and exhaust nozzle area.

6.3.1.1 Fan Suppression

The BOMDIG mode controlled A/B suppression indirectly with a low compressor discharge static pressure over turbine discharge pressure (PS22/P6M) vs corrected high rotor speed ($N2/\sqrt{\theta 2}$ schedule. This control parameter selection was based on hydromechanical considerations and the lack of a low rotor speed drive. The indirect control method is subject to engine deterioration and 7th stage bleed effects, because they influence the $N2/\sqrt{\theta 2}$ vs PS22/P6M relationship. Deterioration is accommodated by occasional trimming, and 7th stage bleed effects are accommodated by a schedule reset that is intended to maintain the same fan operating line when the 7th bleeds are open.

The IPCS mode governed directly to fan operating line (P6M/P2 vs WAT2SX) to control A/B suppression. Corrected engine inlet airflow, WAT2SX, was synthesized from P6MQ2 and corrected low rotor speed, $N1/\sqrt{\theta 2}$, according to a correlation curve developed from past TF30-P-9 test programs. This direct control of suppression eliminates the need for trimming after the initial installation, and it automatically compensates for other effects such as compressor bleed.

A comparison of the BOMDIG and IPCS fan operating lines during the 650 kt. accelerations in max A/B is shown in Figure 6.3-1. Both modes show operation above the target fan operating line because the engine was trimmed toward the suppressed side of the allowable trim band (Figure 6.3-2). Trimming shifts the suppression schedules by a constant percentage, so both the BOMDIG ($N2/\sqrt{\theta 2}$ vs PS22/P6M) and IPCS (WAT2SX vs P6M/P2) nominal suppression schedules are offset from the data points as shown in Figure 6.3-1. There are two conclusions from this BOMDIG and IPCS operating line comparison. First, the IPCS direct suppression control maintained the trimmed target fan operating line, and second, the indirect BOMDIG suppression control showed up to a 10% higher suppression level than IPCS at approximately 180 pps corrected airflow when the 7th stage bleeds were opened.

This 10 percent BOMDIG oversuppression with 7th stage bleed open is not considered representative of the bill of material, or hydromechanical, control operation. Figure 6.3-1 shows the fan operating line level demonstrated at high flight Mach numbers during the TAC 16 F-111/TF30-P-9 development testing is much closer to the target suppression levels than BOMDIG. One of the differences between the HMC and BOMDIG A/B controls is the turbine discharge pressure source. The HMC uses the primary stream pressure, P6, while the BOMDIG control uses the mixed stream pressure, P6M. The effect of these differences was estimated early in the IPCS program, and the BOMDIG schedule was adjusted accordingly. However, there is a possibility that the 7th stage bleed effect on the relationship between these pressures is larger than originally estimated. The primary stream discharge pressure was not measured, so this pressure difference cannot be evaluated.

The pilots reported "A/B roughness" during several of the IPCS 650 kt. accelerations. This roughness was characterized by 4 percent P6MS/P2S oscillations at 2-3 hz. It was also observed during the TAC 16 development testing (Figure 6.3-1) and was caused by a marginal unsuppression. In an effort to eliminate this reported roughness during the IPCS flights, the target fan operating line was increased in the region where the oscillations were observed as seen in Figure 6.3-3. The first revision eliminated the roughness, as indicated by the table summary in Figure 6.3-3, but since A/B stalls were also encountered during this flight, a second revision was made. The second revision resulted in a reoccurrence of the roughness, so a third and final change was made which resulted in neither pilot reporting roughness or A/B stalls.

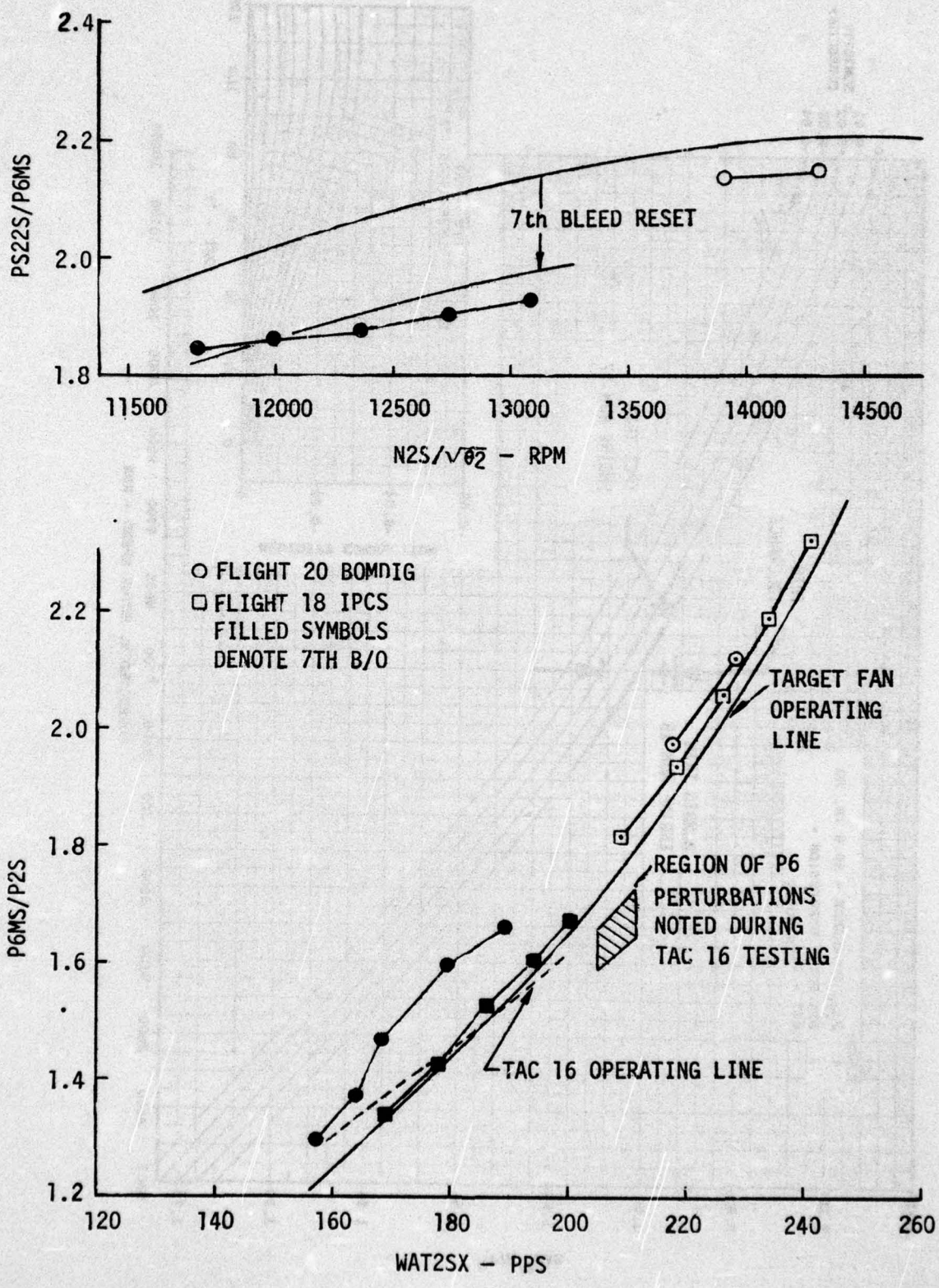

Figure 6.3-1 Suppression Control Comparison IPCS Vs BOMDIG

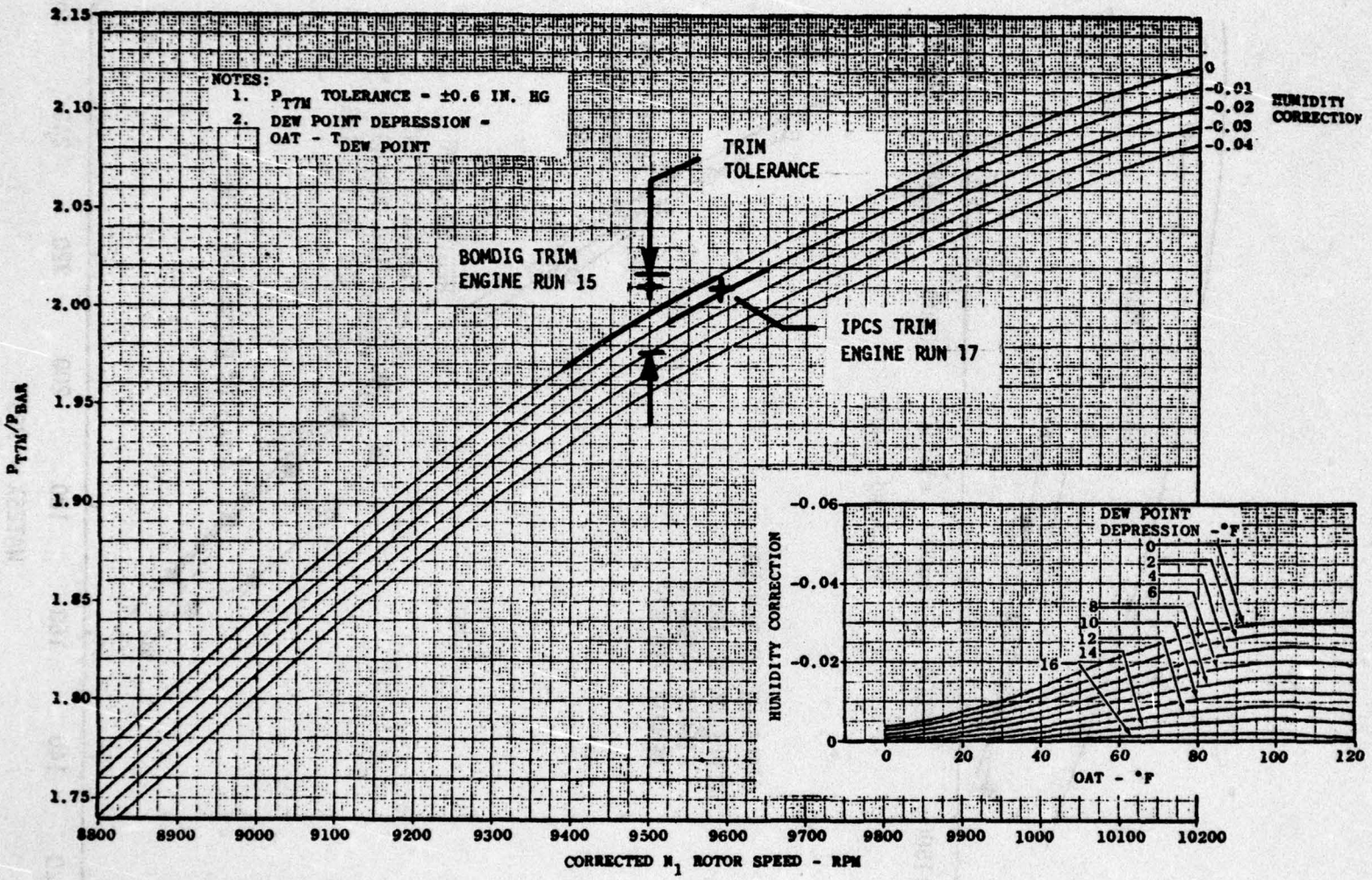

Figure 6.3-2 Exhaust Nozzle Control Trim Curve

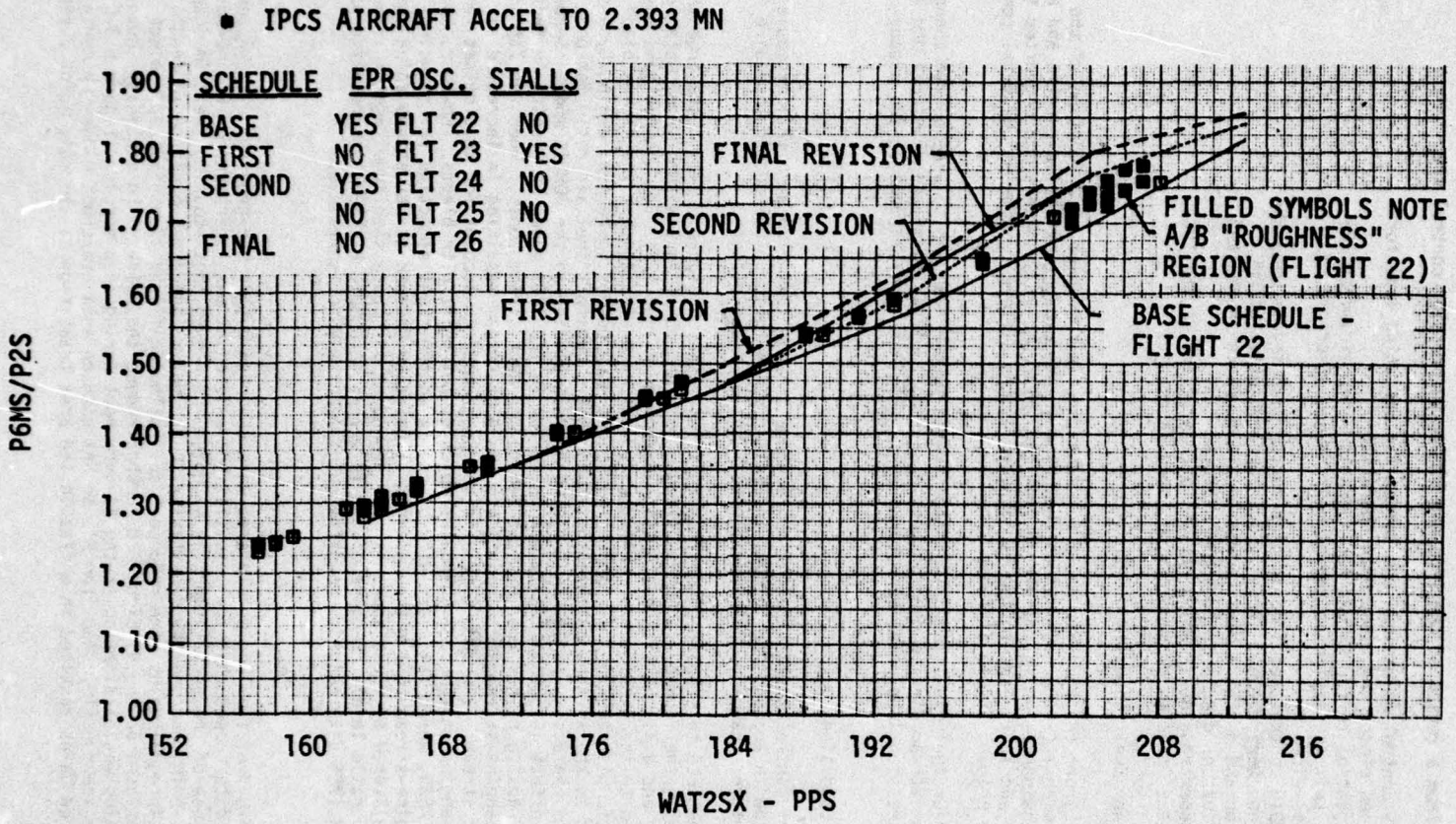

Figure 6.3-3 A/B Suppression Schedule Changes to Eliminate A/B "Roughness"

Conclusions made from a review of the IPCS and BOMDIG suppression control are:

1. The IPCS control maintained the target fan operating line for both bleed closed and bleed open operation.
2. Direct control to the target fan operating line minimizes the need to trim the engine as engine performance deteriorates during service.
3. The BOMDIG control resulted in high suppression levels when the 7th bleeds were opened. This is not representative of HMC operation and may have been caused by a difference in HMC and BOMDIG turbine discharge pressure sources.
4. Afterburner roughness during 650 kt. accelerations in the IPCS mode was eliminated by suppression schedule changes.

6.3.1.2 Afterburner Fuel Scheduling

In the IPCS afterburner the fuel-air ratio for each zone is scheduled as a function of the rate limited throttle signal (PLAP). Commanded fuel flow is the product of fuel-air ratio and airflow. Primary stream flow parameter is calculated from the ΔP3S and PS3S signals and converted to airflow using P3S and T2S. Fan airflow is computed as the difference between the total compressor face flow and the primary stream airflow.

The IPCS afterburner fuel flow scheduling demonstrated better reaction to unscheduled changes in engine and duct stream airflow due to bleed operation. Filtering of the N1 signal and a reduction in suppression loop gains were required to eliminate oscillations during steady-state A/B operation.

Effect of Flight Conditions

The BOMDIG mode of control has a "Theta bias" (change in zone fuel flow with T2.) schedule that modulates zone flow to account for changes in engine bypass ratio. IPCS does not require any biasing to account for changing duct stream conditions or bleed effects.

The ability of the IPCS to schedule fuel flow is illustrated on Figure 6.3-4. Data from three flights are shown in the figure - a BOMDIG flight (20), an IPCS flight with bill of material bleed logic (19), and a flight with distortion control of bleeds (22). Two observations may be made in comparison to the BOMDIG data. First, IPCS has demonstrated that the "Theta bias" effect is automatic with the fuel-air mode. As flight Mach number increases, engine bypass ratio is inherent in the airflow calculations such that a constant fuel air ratio for peak zone two and zone three operations result in a rising Wf/PS3S similar to the BOMDIG mode. Secondly, the entire bleed effect is automatically accounted for in the IPCS mode, by a shift in duct stream air flow, causing higher fuel distributed to the duct stream zones. When the 7th stage bleeds are open, engine-stream air is ported to the duct-stream resulting in increased air flows in the duct stream. The BOMDIG mode is not programmed to account for this offset, as evidenced by the engine stream zone schedules which do not shift with bleeds. However, main burner pressure, PS3S, which falls off with bleed, is in the right direction for reducing BOMDIG fuel. Engine-stream zone ratios are not illustrated because at Max afterburning the amount of fuel delivered by these zones is more dependent on suppression requirements than on a specific fuel-air ratio level. Because of the T2 effect on BOMDIG Wf/PS3S, the relative positions of the BOMDIG and IPCS data recorded on different flights may not correlate.

A/B Oscillations

Oscillations in A/B fuel flow and nozzle area were observed during the ground tests. A review of altitude test data showed that fuel oscillations existed at max afterburning. Engine running identified the cause of the oscillations as N1 noise and showed that reducing the trim loop gains was effective in reducing the sensitivity to the noise (paragraph 5.6). As a result the proportional and integral gains were reduced 6 dB. Following flight 17 a six sample block average filter was used on the N1 signal to further reduce the noise. The secondary advantage of the reduced gains was elimination of the Aj overshoot during snap accels. Figure 6.3-5 shows an early engine run (10) snap from MIL to MAX with an area overshoot midway up during the accel. The reduced gains resulted in a flat in the area transition at the same point during a later run.

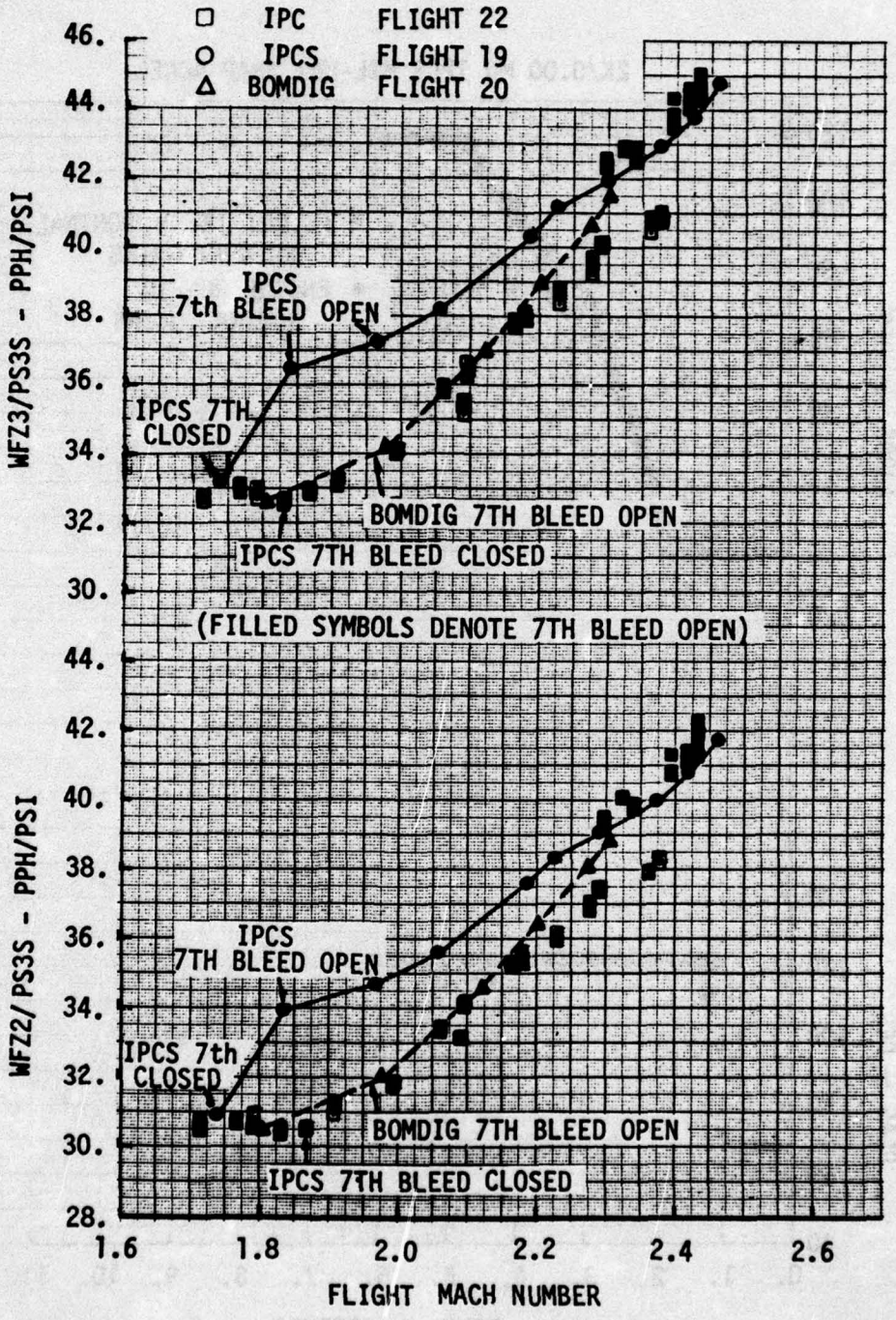

Figure 6.3-4 A/B Fuel Flow Scheduling - BOMDIG, IPCS

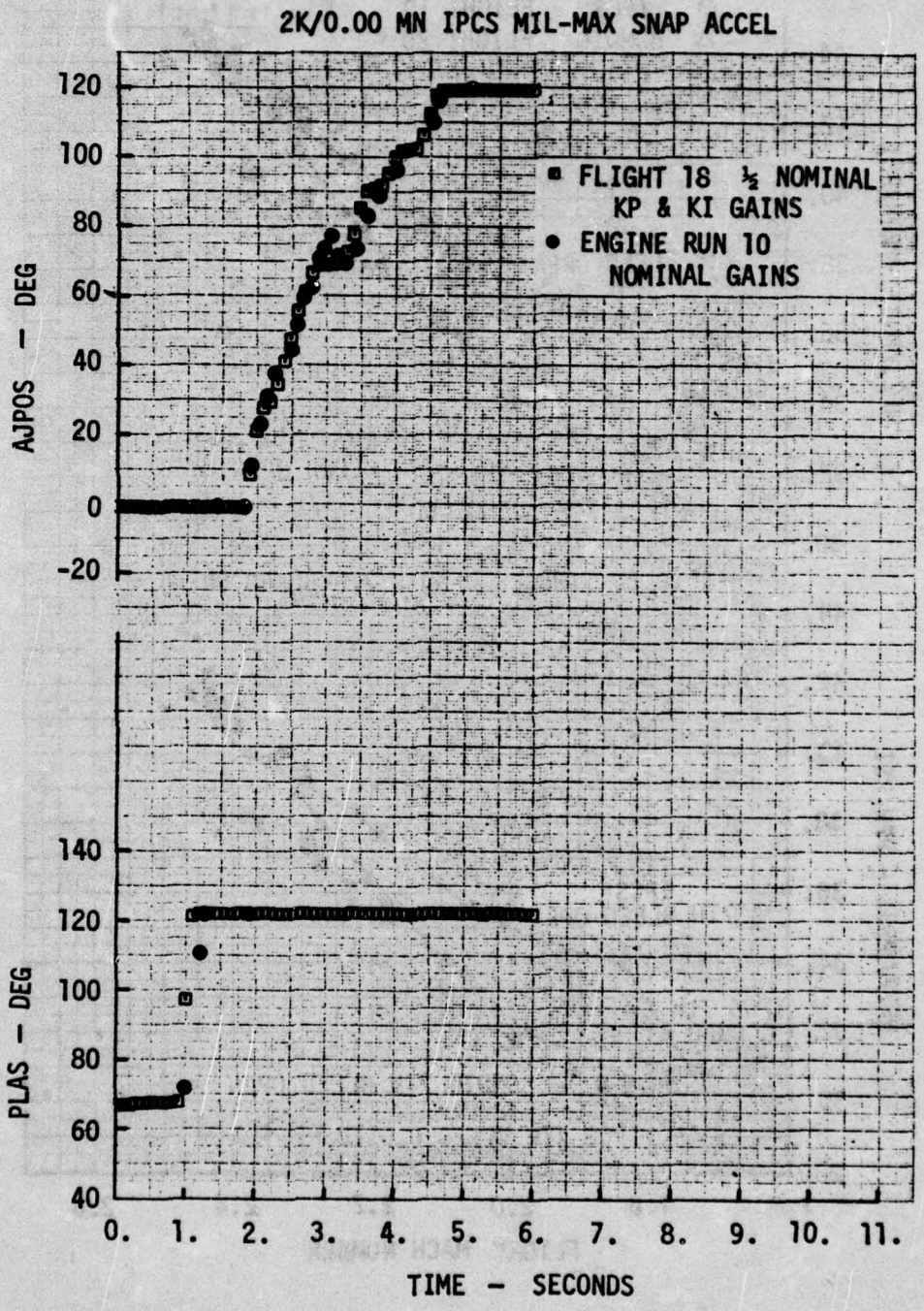

Figure 6.3-5 IPCS M11-Max Nozzle Overshoot

The IPCS mode has consistently reacted to a stall event by activating the blowout sequence. Thus, when a stall occurs, the IPCS mode deriches the gas generator, opens the bleeds, and shuts off the afterburner. Afterburner shutdown is implemented by slewing PLAP to the shutoff position. The fuel shutoff sequence for the five zones of afterburning has exhibited an interesting characteristic that appears related to the fuel-air mode of scheduling afterburner fuel. Figures 6.3-6 and 6.3-7 illustrate the effect of stall on scheduled fuel. The stall was on an Idle-Max snap accel at 49000 ft, Mach 2.4. The figures show zones one and five shutting down in an orderly manner, however, zones two, three, and four exhibit a rise in scheduled fuel in response to the stall. The BOMDIG mode, being scheduled with Wf/Pb, exhibited fuel reduction in all zones in response to the Pb decay caused by the stall event. The IPCS fuel increase in the three duct zones is apparently caused by the relative rate of airflow collapse in the engine stream relative to the duct stream during the stall. When the engine stream airflow collapses faster than the total engine airflow, the duct stream airflow exhibits a momentary increase. This causes the duct stream fuel flow to momentarily increase. This is not a potential shortcoming of scheduling fuel-air ratio, in that fuel flow will follow the airflows of each stream to maintain the desired fuel-air ratio.

6.3.2 Afterburning Transient Operation

6.3.2.1 Light Off Detection

The IPCS afterburner light-off detection used during the Flight Test Program has remained the same as that tested during the Altitude Test, with the exception of a low Reynolds Index schedule change. The schedule adjustment was an unsuccessful attempt at assuring 100% afterburner light reliability at the 45000 ft., Mach 0.9 flight condition. Post test analysis has indicated that the afterburner lighting problem is probably associated with the afterburner lighting characteristics rather than with the mode of detection.

The IPCS mode is unique in its implementation of afterburner light detection, since it measures the time derivative of the actual fan operating point relative to its reference value.

The derivative calculation involves taking the difference between the current and past value of % airflow error (reference airflow - actual airflow)/reference airflow and dividing by the control computer sampling period (.03 sec). Originally an average derivative was calculated over four sample periods, however, appropriate measurement filtering permitted use of the derivative calculated during the most recent sample period. The derivative threshold was determined during Altitude testing.

The IPCS afterburner light off detection was very successful. This was demonstrated at all of the flight test conditions during Mil to Max, and Idle to Max transients, except the 45,000 feet., 0.9 Mach number test condition. This condition should not be considered as a failure to detect lighting, but a failure of the afterburner to light. This flight condition has exhibited lighting problems for both control modes during the altitude test, and is not considered to be an unusual problem. The development engines have also exhibited these characteristics due to the proximity of the A/B relight envelope imposed by the low duct pressures of the high altitude condition. IPCS does not permit false afterburner release, since the logic requires the tailpipe area to be open at least 5 degrees as measured by the area feedback resolver. The tailpipe area will open only if an oversuppression signal exists, as would be caused by combustion in the afterburner. If an EPR spike, due to the igniter squirt occurs, without substaining a level of oversuppression, then the tailpipe will not open and the afterburner will not be released, as was the case at 45000 feet, 0.9 Mach number.

Figure 6.3-8 shows an IPCS accel idle to Max, with two unsuccessful light attempts, followed by one successful light and afterburner release to Max power. The EPR spike due to the igniter squirt is shown on the first two light attempts as a short duration rise in EPR. The successful light on the third attempt not only exhibits the EPR spike rise, but the higher EPR level is maintained by the afterburner combustion causing the tailpipe area to open and release the afterburner to Max power.

FLIGHT 19

49K/2.40 MN IPCS STALL ON IDLE-MAX SNAP ACCEL

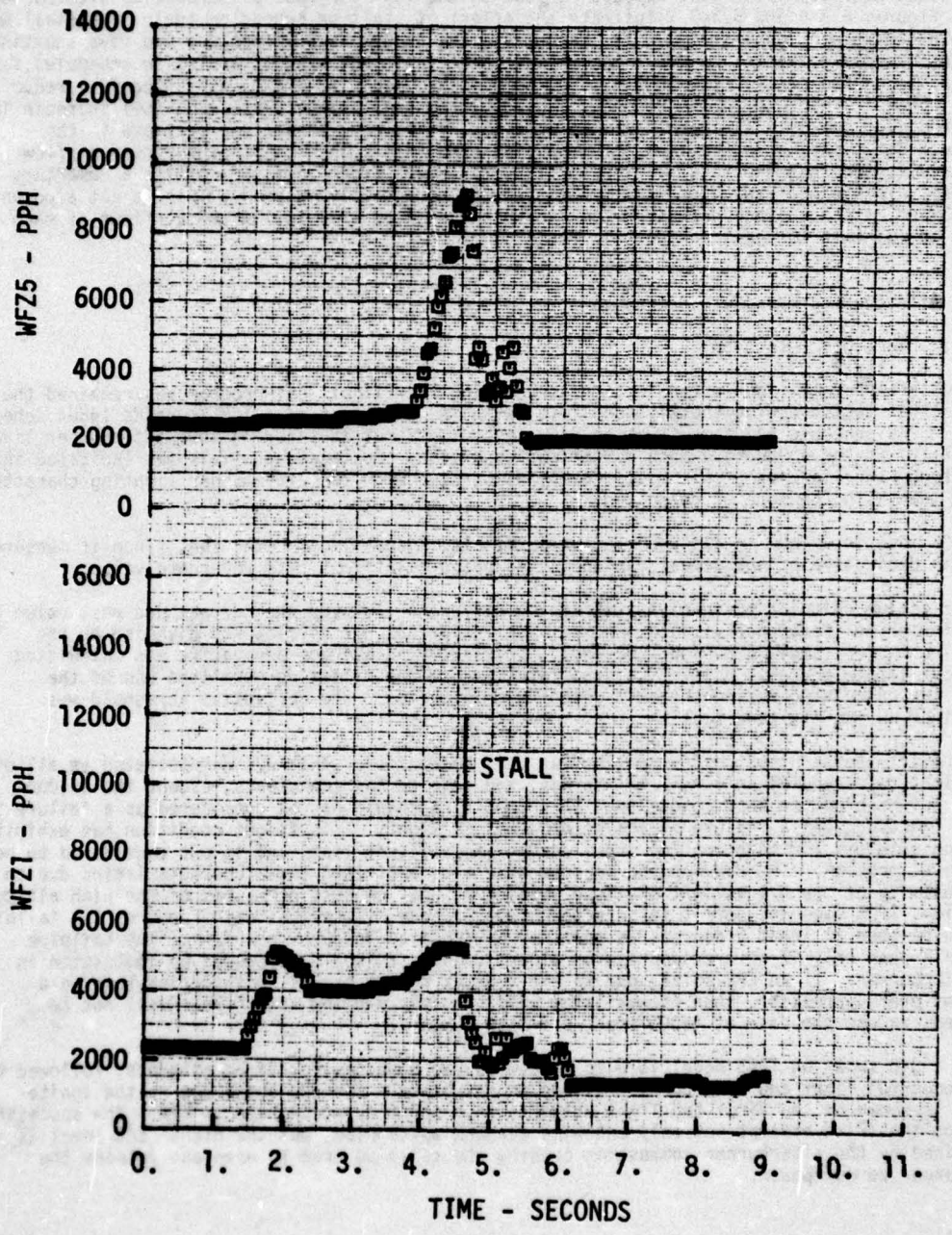

Figure 6.3-6 Response of Core A/B Zones to Stall

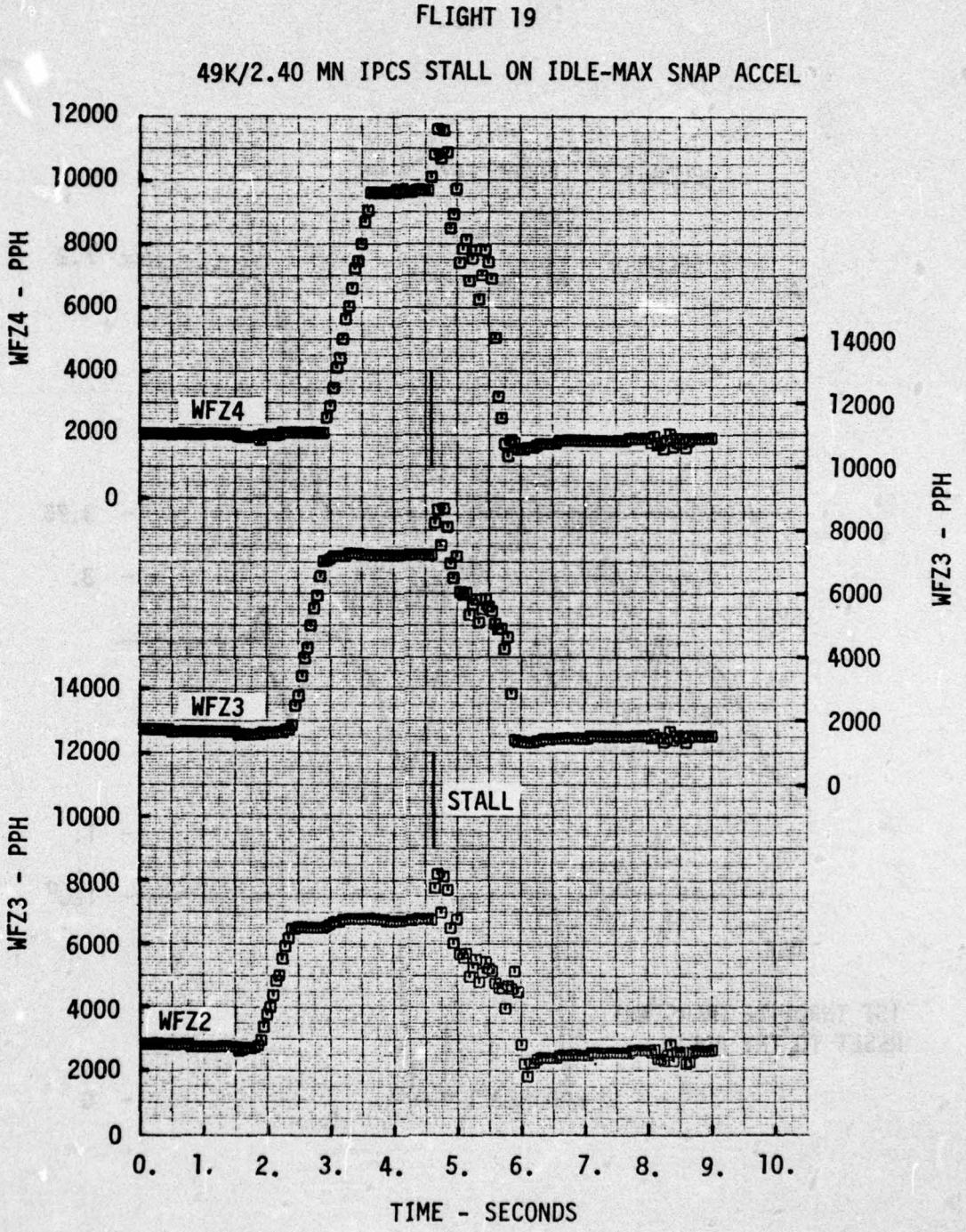

Figure 6.3-7 Response of Duct A/B Zones to Stall

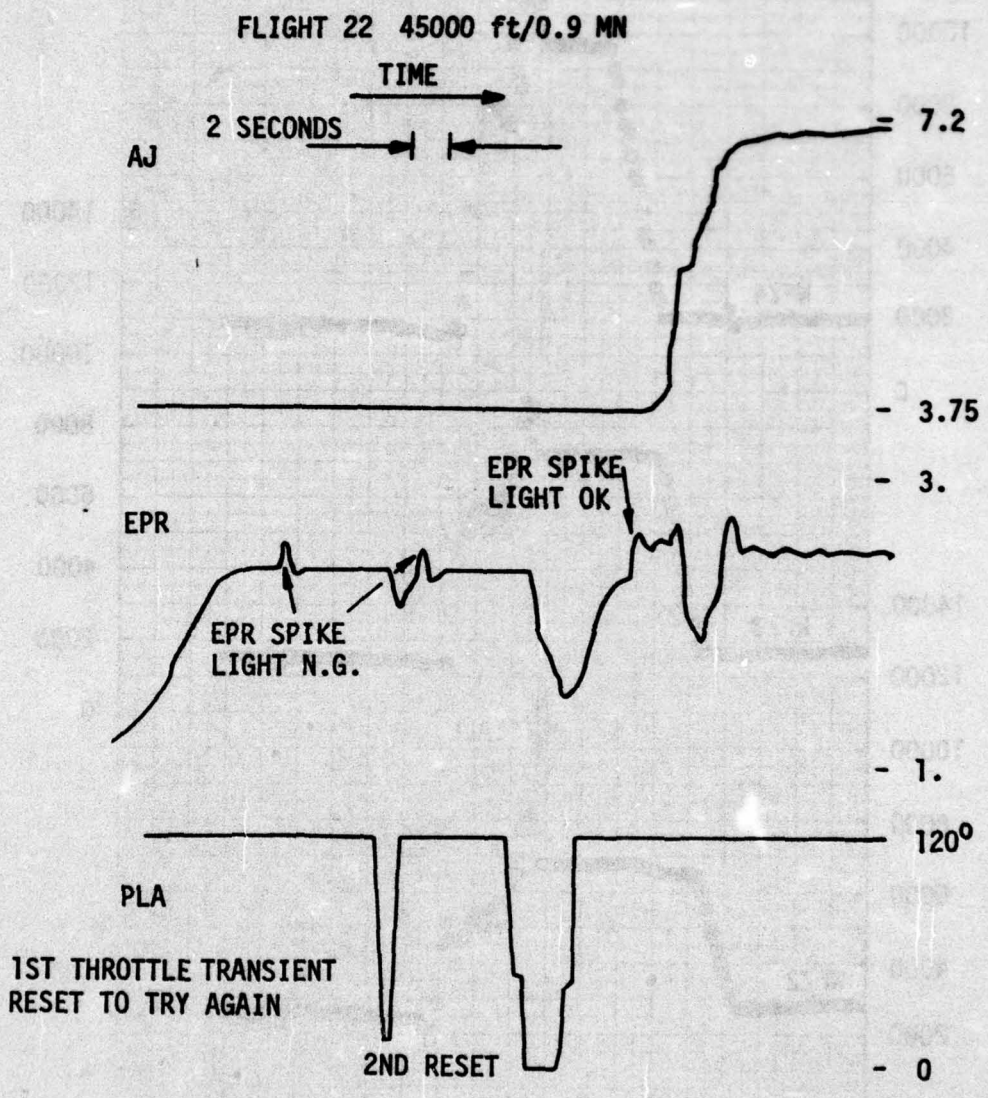

Figure 6.3-8 Afterburner Lightoff Attempts at 0.9 MN, 45K

6.3.2.2 Blowout Detection

The IPCS test engines have not experienced afterburner blowouts, except when coupled with another incident such as engine stall. Blowout detection always reacted according to the design criteria. An interesting fact was the IPCS mode always reacted to stall as if it was a blowout, however, some BOMDIG stalls did not.

IPCS blowout detection is identical to the light-off detection, discussed in paragraph 6.3.2.1, using the rate of fan operating point motion relative to the reference value as a measure of blowout indication. The major difference is the direction of operating point movement. For blowouts, the percent airflow error decreases. The negative derivative threshold determined during the design phase was used successfully throughout the program. Upon receipt of a blowout signal, the IPCS control turns off the afterburner in one second, while it deriches the gas generator and opens the 7th and 12th stage bleeds. The BOMDIG mode operates on a suppression error signal and performs the same functions, except it does not open the 7th stage bleed.

The afterburner did not blow out except as induced by engine stall. In each event, the blowout detection mode for IPCS operated successfully. The afterburner was shut down and the gas generator was deriched to prevent overspeed. BOMDIG performed in a like manner except the afterburner blowout signal was not activated by stall in all cases. Figure 6.3-9 shows a BOMDIG snap decel from Max to Mil with stall occurring without an afterburner blowout reaction. A normal reaction to a blowout signal would be a rapid rate closure of tailpipe area, AJPOS, and cut off of zone fuel flow.

One of the more interesting blowout events in IPCS is shown on Figure 6.3-10 which was a 50,000 ft/2.36 Mach "Seal Saver Turn" (SST) through an angle of attack of nearly twelve degrees while at max afterburning. The first signal indicating a problem was the buzz detector (the buzz loop was not operative for this test, but the signal was available), followed by the afterburner shutdown and gas generator derichment. At first, this event was appraised as a stall, however, the Wf/Pb signal, the T4 signals and the fuel valve signals indicate the gas generator was being deriched. This was followed by an afterburner shutdown. This event was different from other stall/blowout events, in that the gas generator was deriched prior to the decay in main burner pressure, therefore, it was concluded that a blowout signal was detected. However, review of tailpipe pressure P6MS, indicates that the afterburner did not blowout since the derichment occurs prior to pressure decay.

It is speculated, based upon the data, that the unusual event was tripped by a short duration "pop-stall" in concert with inlet buzz. The pop-stall resulted in the blowout trigger setting up the decel. A problem occurs when the decel drives airflow below the minimum acceptable value of 153 pounds per second causing inlet buzz to self sustain. This was due to an airflow schedule reset to permit blowout "temporary decels" without airflow constraint. This was corrected by retaining the minimum airflow schedule during blowout for subsequent tests. The feature of IPCS reacting to each stall as a blowout may not necessarily be considered an advantage for the case where a momentary "pop-stall" occurs without an afterburner blowout. Detecting a blowout would interrupt power since the afterburner is shutdown.

6.3.2.3 Afterburner Accel Time Comparisons

The IPCS control consistently demonstrated faster Mil to Max accel times than BOMDIG during both altitude and flight test. This was due to the IPCS prefill feature which minimizes manifold filling effects. The accel time is calculated as the time between the start of the throttle snap and the point in time when the tailpipe area achieves its final value.

The IPCS mode is programmed to achieve Max afterburning power about 3 1/2 seconds after the snap from Mil. The variation in flight test accel times, as shown on Figure 6.3-11 deviates from this amount by the time it takes to fill the manifold for Zone 1.

The average savings in accel time was about two seconds with the least improvement being 0.7 seconds at 10K/0.9 Mn, and the greatest gain of 3 sec occurring at 45K/0.9 Mn and 41K/1.4 Mn, both of which have relatively large manifold filling effects. These savings in accel times were achieved without greatly impacting the control of fan suppression as discussed in paragraph 6.3.2.5.

FLIGHT 20

45K/2.10 MN BOM STALL ON MAX-MIL

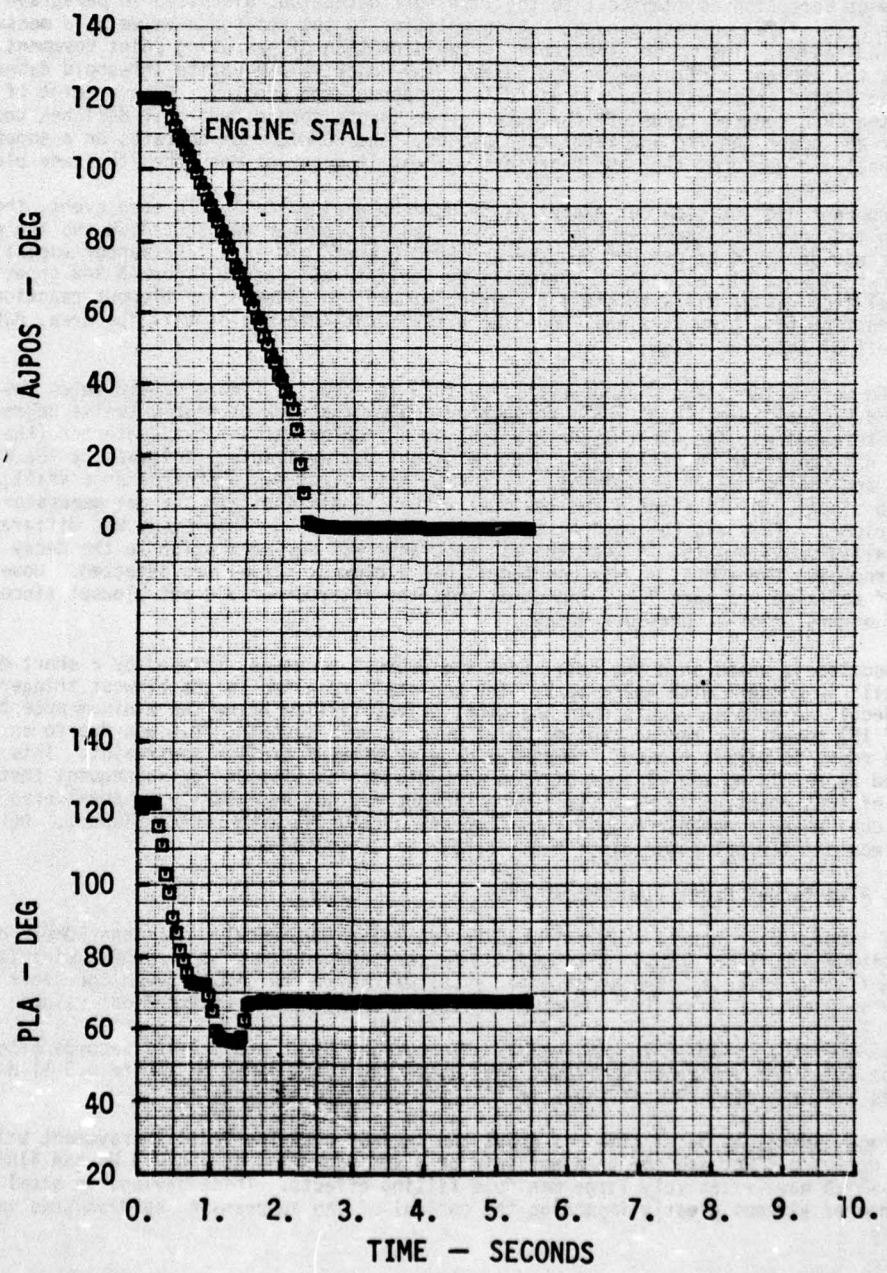

Figure 6.3-9 BOMDIG Stall

FLIGHT 18

50K/2.36 MN IPCS ENGINE STALL DURING SST

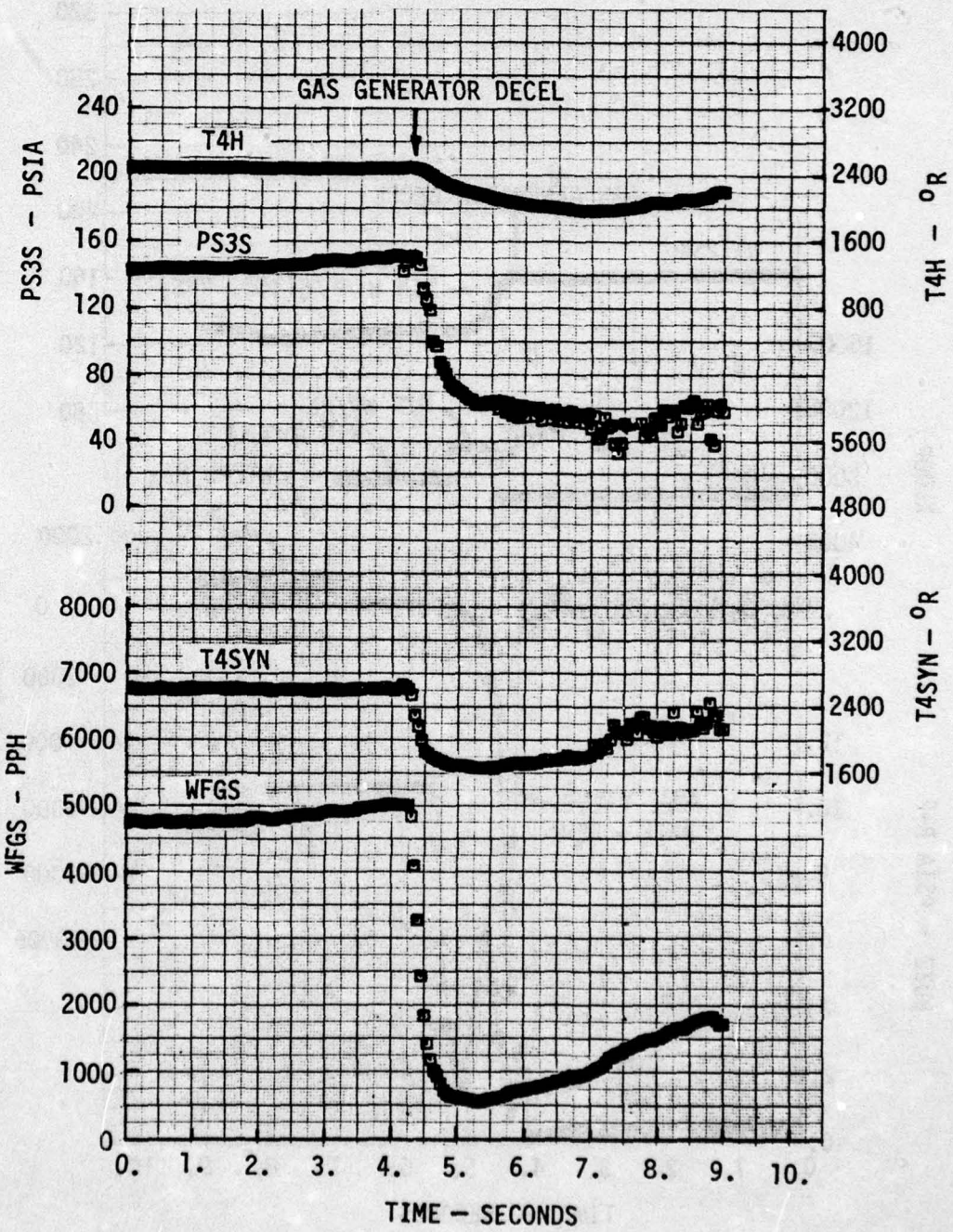

Figure 6.3-10a IPCS SST Stall and Blowout Detection

AD-A034 172 BOEING AEROSPACE CO SEATTLE WASH F/G 21/5
INTEGRATED PROPULSION CONTROL SYSTEM (IPCS) VOLUME III. FLIGHT --ETC(U)
AUG 76 W J HASTINGS, C M CARLIN F33615-73-C-2035
UNCLASSIFIED AFAPL-TR-76-61-VOL-3 NL

3 OF 4
AD A034172

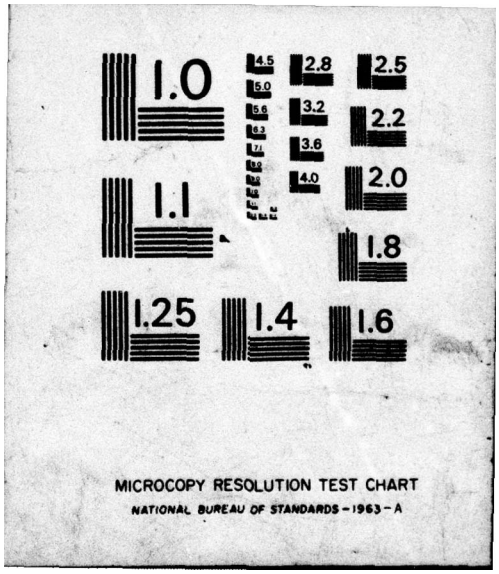
1.0
1.1
1.25
1.4
1.6
1.8
2.0
2.2
2.5
2.8
3.2
3.6
4.0
4.5
5.0
5.6
6.3
7.1
8.0
9.0
MICROCOPY RESOLUTION TEST CHART
NATIONAL BUREAU OF STANDARDS - 1963 - A

FLIGHT 18

50K/2.36 MN IPCS ENGINE STALL DURING SST

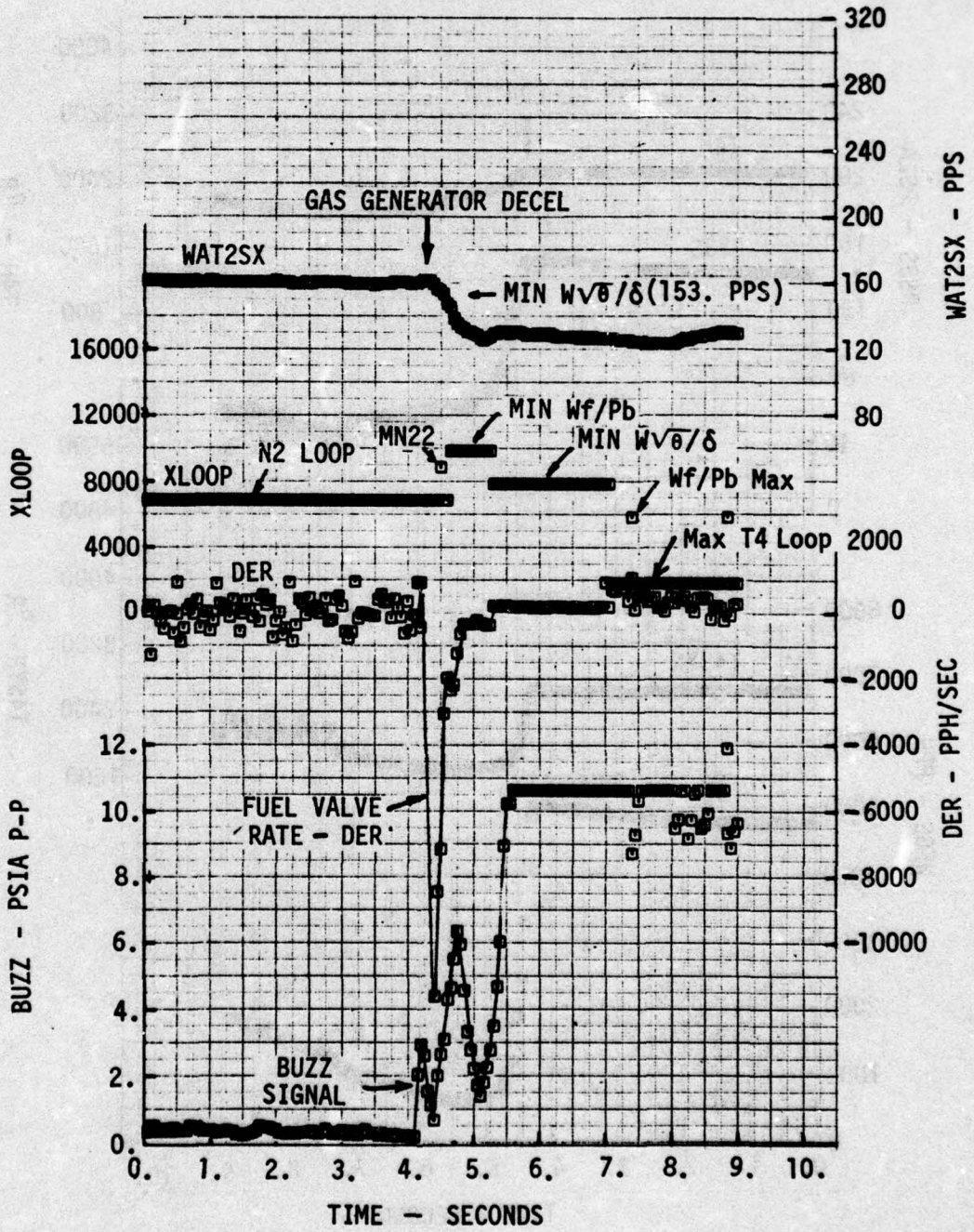

Figure 6.3-10 b IPCS SST Stall and Blowout Detection

FLIGHT 18

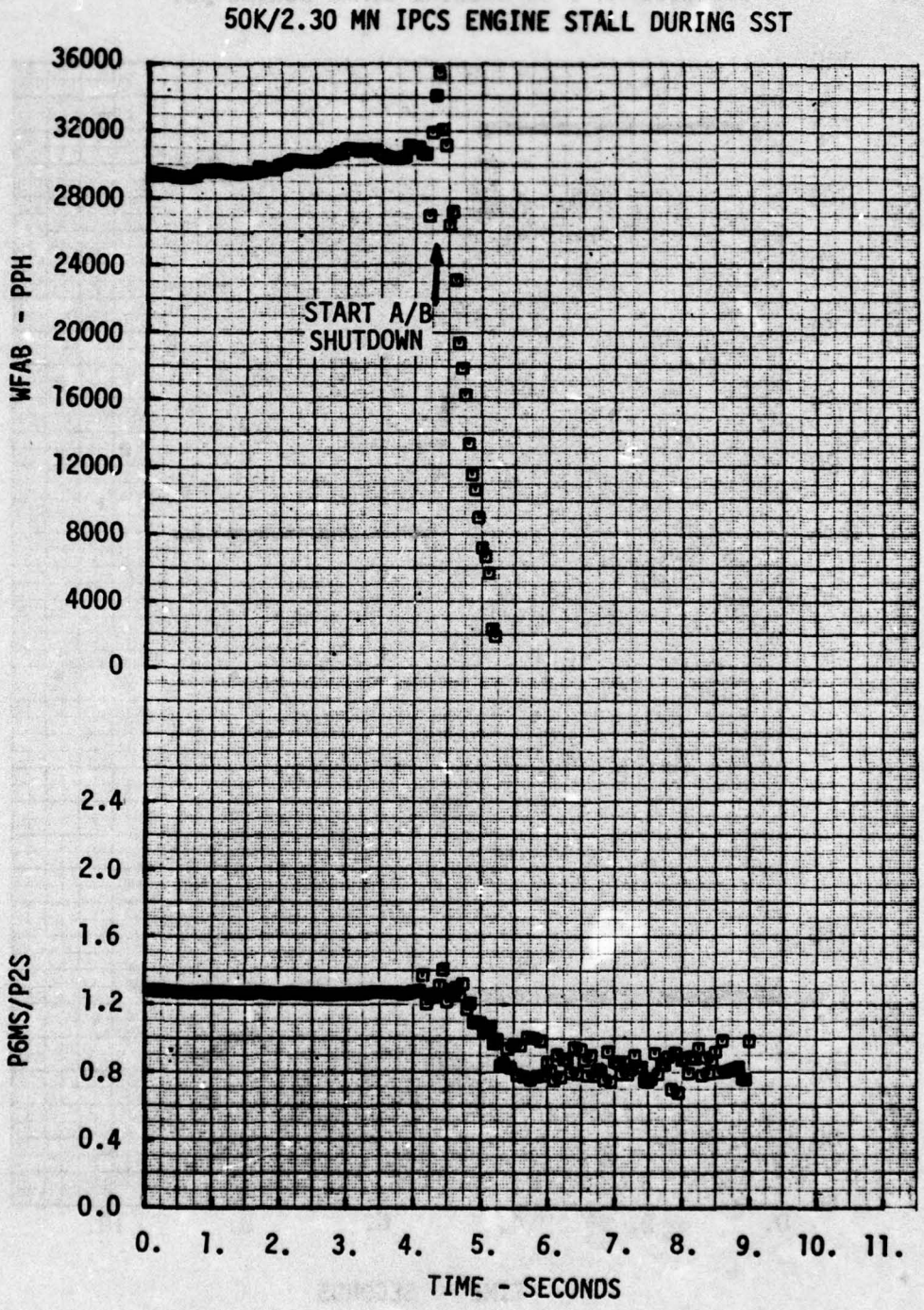

Figure 6.3-10c IPCS SST Stall and Blowout Detection

FLIGHT 18

50K/2.30 MN IPCS ENGEINE STALL DURING SST

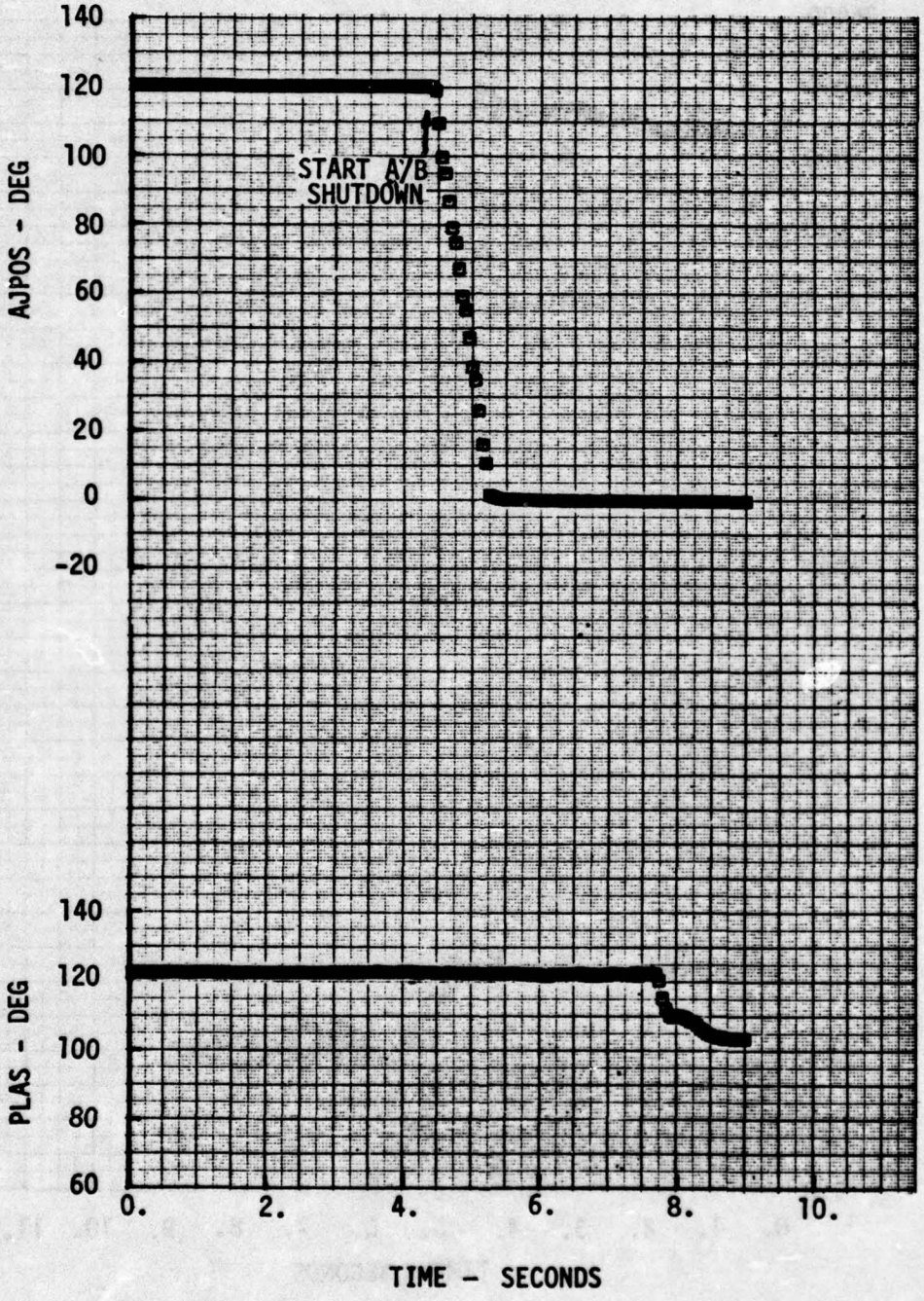

Figure 6.3-10d IPCS SST Stall and Blowout Detection

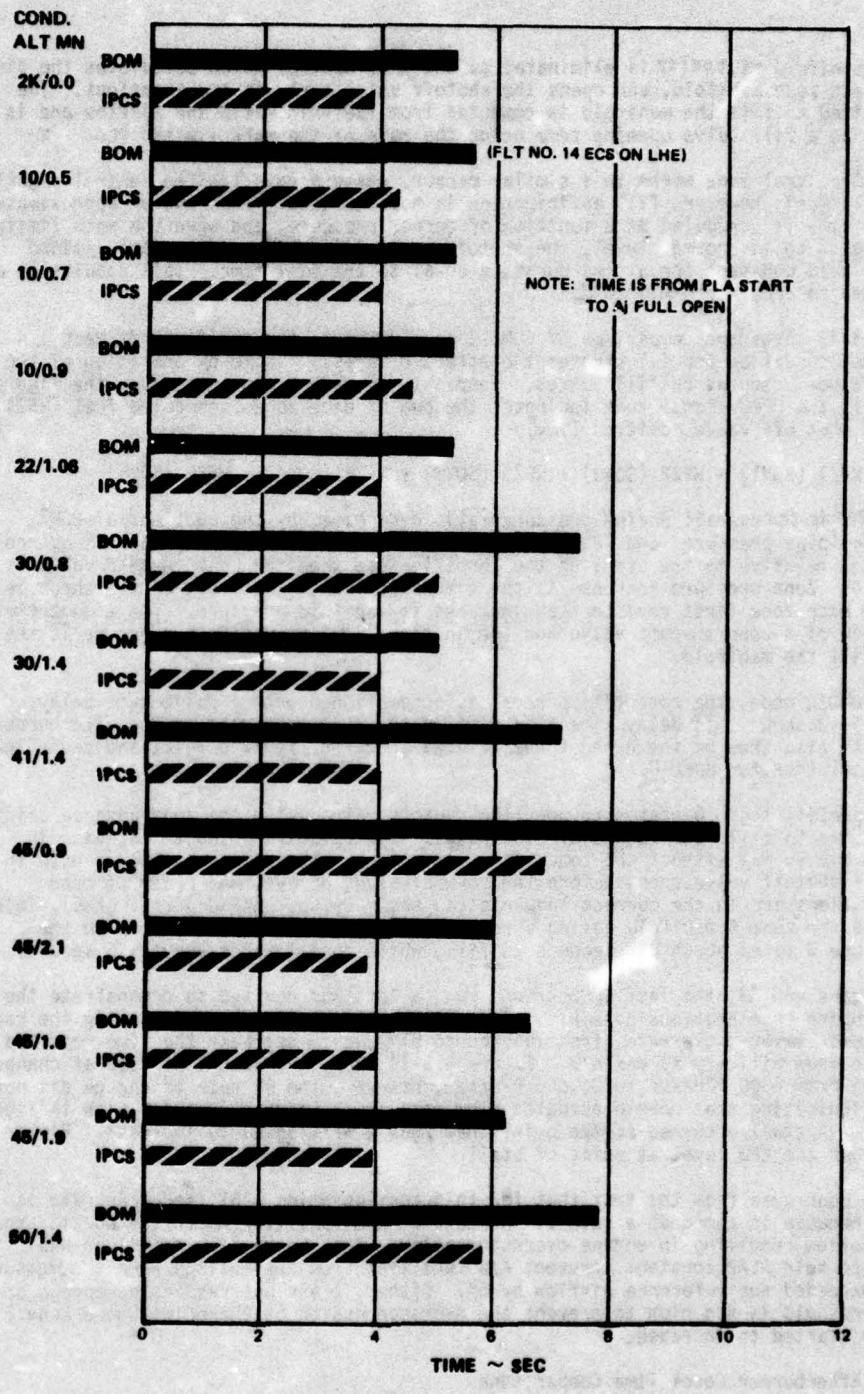

Figure 6.3-11 Accel Time Comparisons Mil- Max

The fuel manifold fill delay is eliminated by the IPCS control which calculates the time to fill each zone manifold, and opens the shutoff valve early in the transient. The time required to fill the manifold is computed from fuel-air ratio and airflow and is converted to a fill valve opening time using the rate of the rate limited PLA.

The BOMDIG control mode works in a similar manner, using a rate limited control signal to schedule fuel, however, fill anticipation is not included. Instead, an approximate zone fill time is scheduled as a function of burner pressure, and when the rate limited schedule gets to its normal level, the shutoff valve is opened and the rate limited signal is held constant for a time duration equal to the fill time. This results in a larger time to accel from Mil to Max.

Figure 6.3-13 shows the comparison of BOMDIG and IPCS data for the 41000 ft/Mach 1.4 flight test condition and illustrates the effect of prefill logic on operation of the shutoff valves, used as prefill valves. Four sets of data are presented on the figure: 1) WFAB is the DPCU signal that indicates the sum of each zones scheduled fuel (WFZ) times its shut off valve position (SOV):

$$WFAB = WFZ1\ (SOV1) + WFZ2\ (SOV2) + WFZ3\ (SOV3) + WFZ4\ (SOV4) + WFZ5\ (SOV5)$$

2) P6MS/P22S is the overall engine pressure ratio determined by the quotient of P6MS average tailpipe pressure, and P2S, engine inlet pressure. 3) Shutoff valve sequence is the time relative to the start of the throttle snap when the zone shutoff valve is opened. 4) Zone pressure increase is the time relative to the start of the throttle snap when each zone first registers an increase in manifold pressure. The time between the opening of a zone shutoff valve and the increase in zone manifold pressure is the time to fill the manifold.

For the BOMDIG mode, the zone fill process is accomplished with a deliberate delay. Figure 6.3-13 shows this delay time as a flat in the fuel scheduled to the afterburner. These flats also show on the exhaust nozzle area trace on Figure 6.3-12, and cause the longer accel time for BOMDIG.

The IPCS prefill logic operates to open the shutoff valve using the zone advance calculated from the time to fill each manifold. The result is a relatively smooth increase in fuel from Mil to Max without the zone fill delay times. It is interesting to note that the zone 4 shutoff valve opens before the zone 3 valve, however the order of zone pressurizations are in the correct sequence (as shown by the unshaded triangles). This was due to the zone 4 manifold having a relatively long fill time. As seen on the figure, zone 3 takes about 0.7 seconds to fill, while zone 4 takes about 1.6 seconds.

During engine run 35, the last IPCS ground run, a test was devised to demonstrate the fastest engine accelerations possible. Part of the plan called for increasing the rate limited power lever angle rate, from 15° sec to 51°/sec to decrease the time required to advance from military to max A/B. Figure 6.3-14 shows the zone 1 Wf rate of change increasing from 8000 PPH/sec to 26,600 PPH/sec, however, the Aj rate of change did not increase indicating that nozzle actuator slew rate limit had been reached with 15°/sec PLAP rate. A stall occurred at the point that Zone 2 Wf started to increase. Figure 6.3-15 shows the EPR level at point of stall

It can be concluded from the test that for this configuration a 51°/sec PLAP rate is too fast because it commands a rate of increase of A/B fuel flow which the nozzle area can not follow resulting in engine oversuppression. The suppression trim loop was intended to hold PLAP constant (prevent A/B fuel flow from increasing) when the measured airflow exceeded the reference airflow by 5%. Either it was not responsive enough or the 5% threshold is too high to prevent the oversuppression at the point where Zone 2 fuel flow started to increase.

6.3.2.4 Afterburner Decel Time Comparisons

The IPCS decel time demonstrated during Altitude Test was improved upon during the flight test program by scheduling the rate of PLAP reduction to turn off A/B fuel at a point in time equal to BOMDIG. This resulted in IPCS decel times about 1/2 second slower than BOMDIG, when measuring decel times to Aj closure.

FLIGHT 16

41K/1.40 MN BOM MIL-MAX SNAP ACCEL

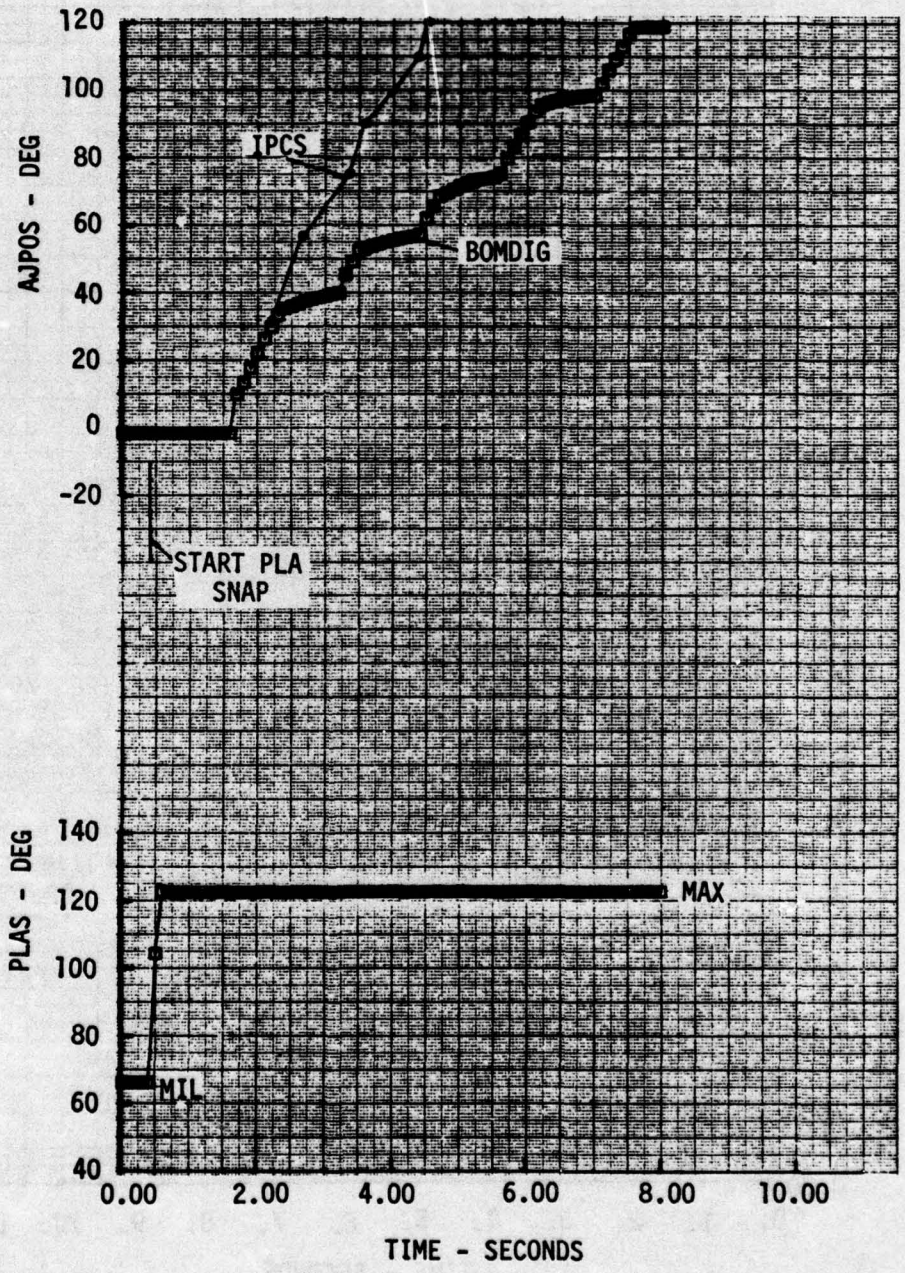

Figure 6.3-12 BOMDIG, ICPS A/B Acceleration

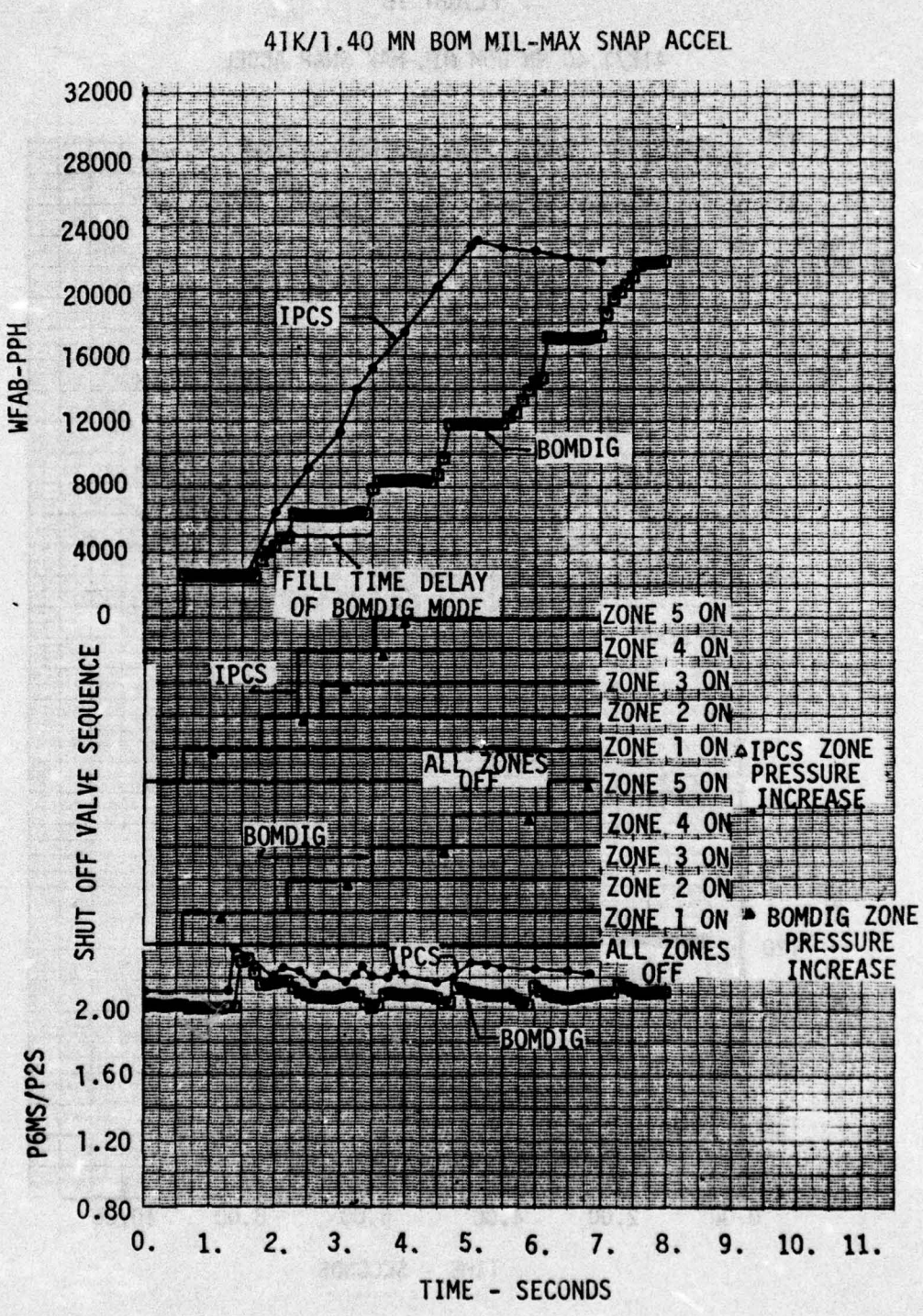

Figure 6.3-13 Manifold Fill Comparison, BOMDIG , IPCS

ENGINE RUN 35

2K/0.0 MN IPCS STALL ON MIL-Z3 SNAP, 51 DEG/SEC PLAP RATE

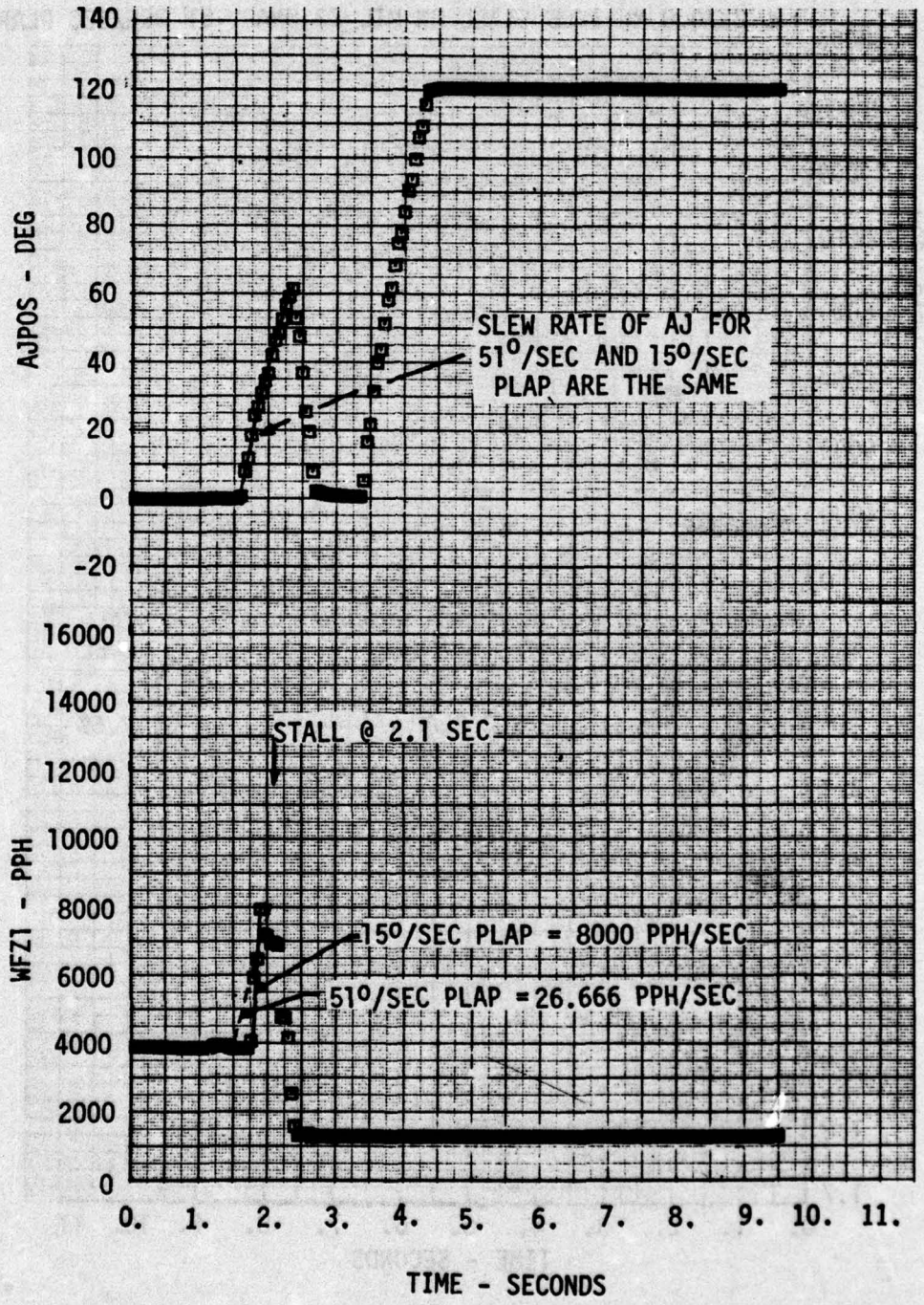

Figure 6.3-14 Fuel Flow and Nozzle Area Transient wtih 51°/Second PLAP Rate

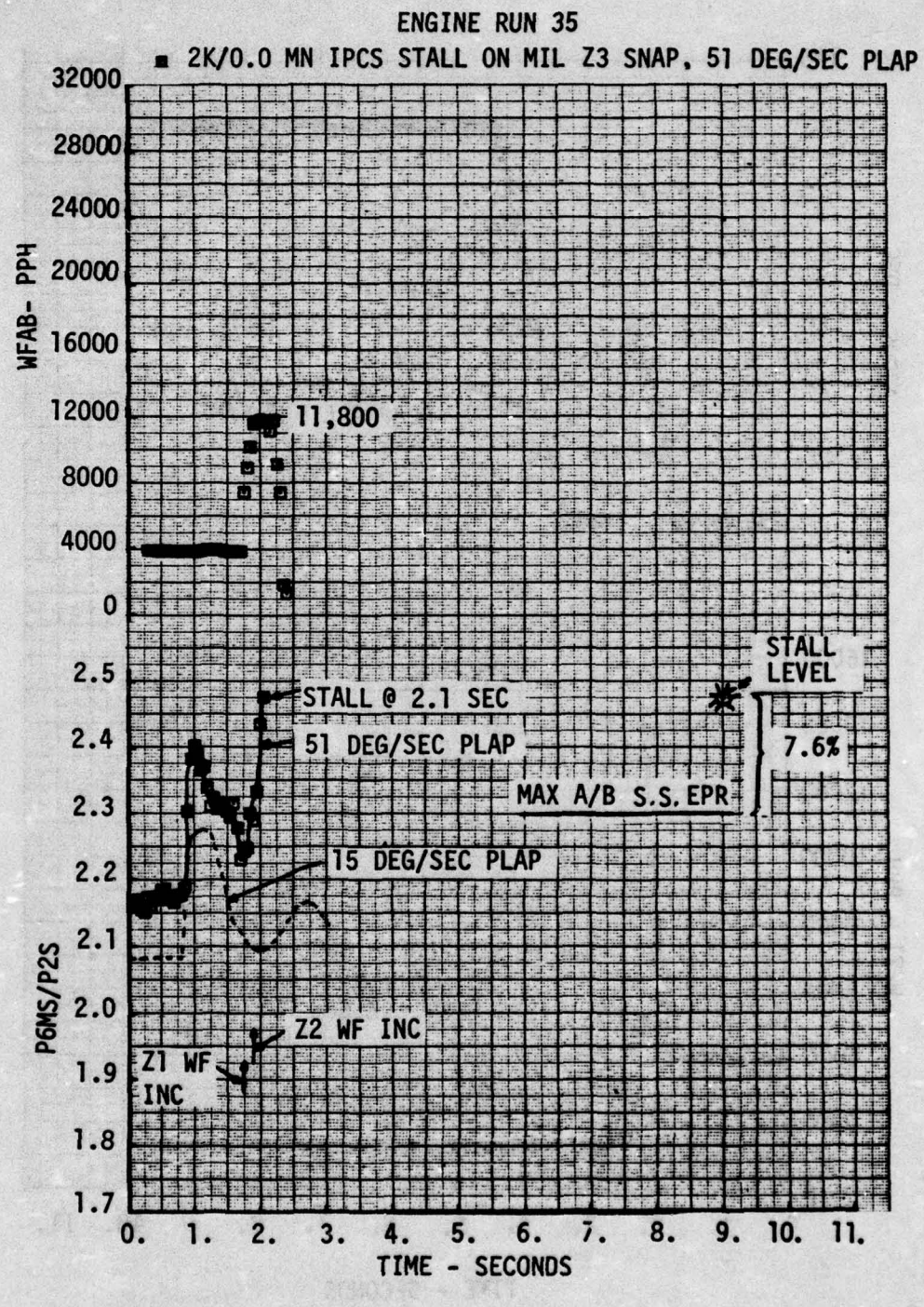

Figure 6.3-15 EPR Transient with 51°/Second PLAP Rate

The IPCS was originally programmed to result in a Max to Mil decel time of 3 1/2 seconds, the same time as programmed for accels. However since the BOMDIG mode was decelerating in about 2 1/2 seconds, the IPCS mode was changed. This was accomplished by changing the rate of PLAP for decels, from -15 degrees per second to -21 degrees per second. In essence, this change results in turning off IPCS A/B fuel in about 2 1/2 seconds (51° PLAP at 21°/sec = 2.42 seconds.) With tailpipe area lagging on decels to provide unsuppression during transients, the actual decel times averaged about three seconds as shown on Figure 6.3-16.

The effect of the decel time improvement change is illustrated on Figure 6.3-17 and 6.3-18 which shows the nozzle area and the fan suppression respectively. While increasing the rate of PLAP closure improves decel time, the effect on the fan map was to use more excursion room. This trade was considered very satisfactory since the IPCS fan map excursion does not exceed the BOMDIG excursion.

6.3.2.5 *Suppression Control During Afterburner Transients*

IPCS demonstrated fan surge margin control equal to or better than the BOMDIG mode during afterburner accels and decels. During accels, where manifold prefill was used to obtain accel time improvements, the envelope of fan suppression is about equal to the BOMDIG mode. For afterburner decels, the IPCS fan surge margin is decidely superior to that demonstrated by BOMDIG. BOMDIG was not able to provide sufficient surge margin to decelerate without stalls at the 45000 ft., 0.9 Mach flight test condition.

IPCS afterburner control of suppression during transients operates the same as during steady state. The BOMDIG afterburner also controls transient suppression similarly to steady state except during snap decels, where the nozzle area is shut down at a fixed rate.

Both modes have a reference suppression schedule. The IPCS mode schedules the fan operating line airflow $W\sqrt{\theta 2}/\delta 2$ as a function of overall engine pressure ratio (EPR) and the loop is closed with a measurement of engine airflow obtained from EPR and corrected speed ($N1/\sqrt{\theta 2}$), The BOMDIG mode schedules the fan operating line indirectly, providing a reference engine pressure ratio (PS22/P6M) as a function of high rotor corrected speed ($N2/\sqrt{\theta 2}$) and provides loop closure with a direct measure of PS22/P6M. The errors formed by the loop closure drive the integrator which trims nozzle area to maintain the desired suppression. During the transient from Mil to Max, the trim integrator operates in both IPCS and BOMDIG to control suppression. During the transient from Max to Mil, the IPCS time integrator is operative on nozzle area. For BOMDIG, the trim integrator operates on A/B fuel. In addition, the nominal IPCS schedules of afterburner fuel and tailpipe area as a function of the rate limited power lever signal (PLAP) are set to provide area lead on accels, and area lag on decels (BOMDIG provides area lead on accels and decels). Figure 6.3-19 is illustrative of this principle, which always biases the fan match in the lower suppression direction since more tailpipe area at a given fuel matches the fan away from surge. This deliberate mismatch is eliminated by the trim integrator during steady state operation.

The results from the altitude test showed the IPCS decels from Max to Mil to be approximately one second slower than BOMDIG. The goal during the flight test phase was to improve IPCS decel times to be approximately equal to BOMDIG, and if possible to be even faster. This was accomplished by increasing the PLAP shut down rate from -15 degrees/second to -21 degrees/second. The faster shutdown resulted in the fan operating more unsuppressed which was considered an acceptable trade for improved decel time. The change in decel time was about one-half second as discussed in paragraph 6.3.2.4, and was not pursued further.

The approach taken to compare suppression effects was to select those DPCU parameters which are common to each control mode. This resulted in using EPR and $N1/\sqrt{\theta 2}$ as an indication of fan suppression. Since these data are common in each mode, and comparisons were made for flights with consistent measurement calibration, a good relative suppression effect was obtained. To avoid the confusion associated with illustrating numerous data points, or transients paths overlapping in many different directions, the fan suppressions are presented as envelopes. The fan suppression envelope is the locus of extreme points during an afterburner transient and provides an immediate assessment of which mode is operating with higher or lower suppression at some time during the transient.

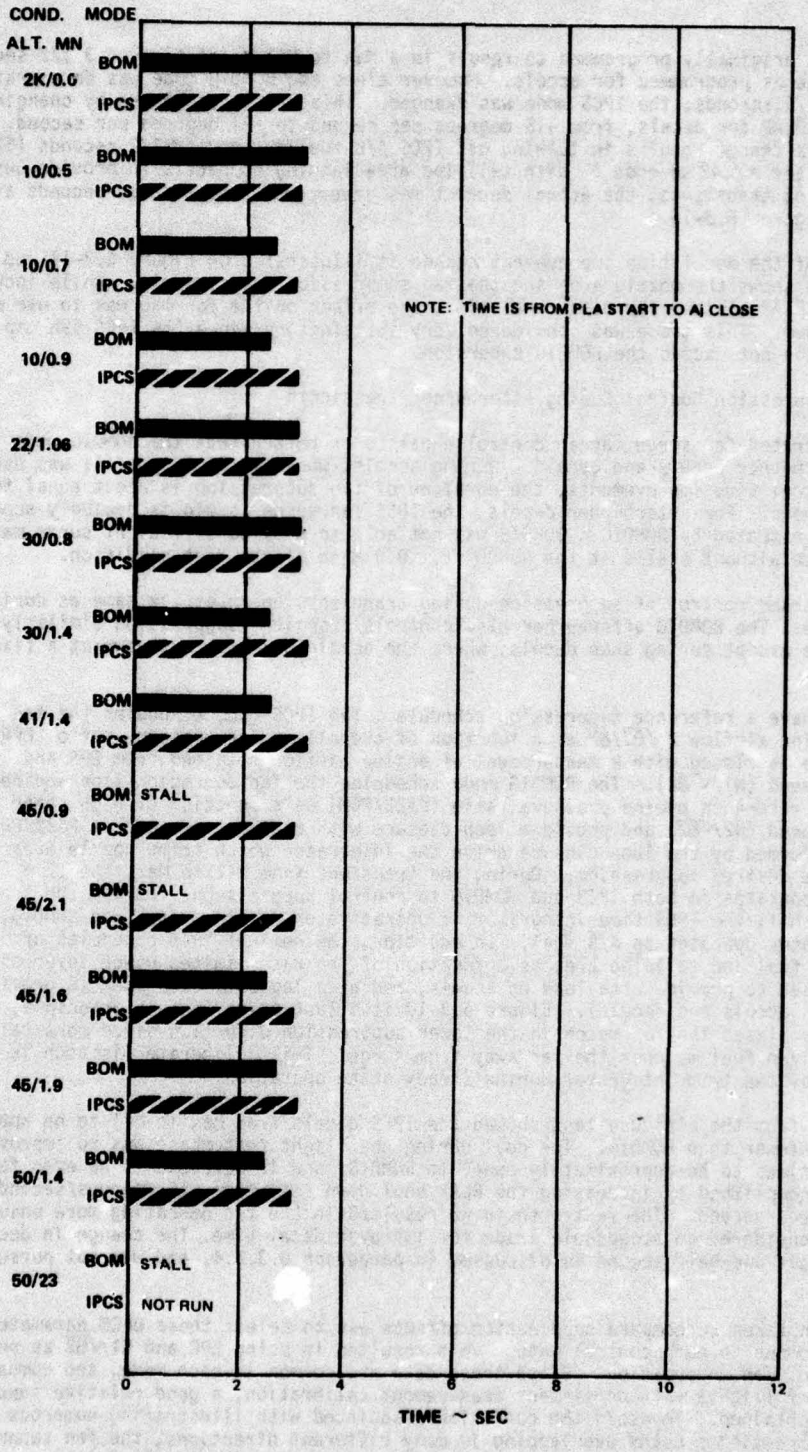

Figure 6.3-16 Decel Time Comparisons Max - Mil

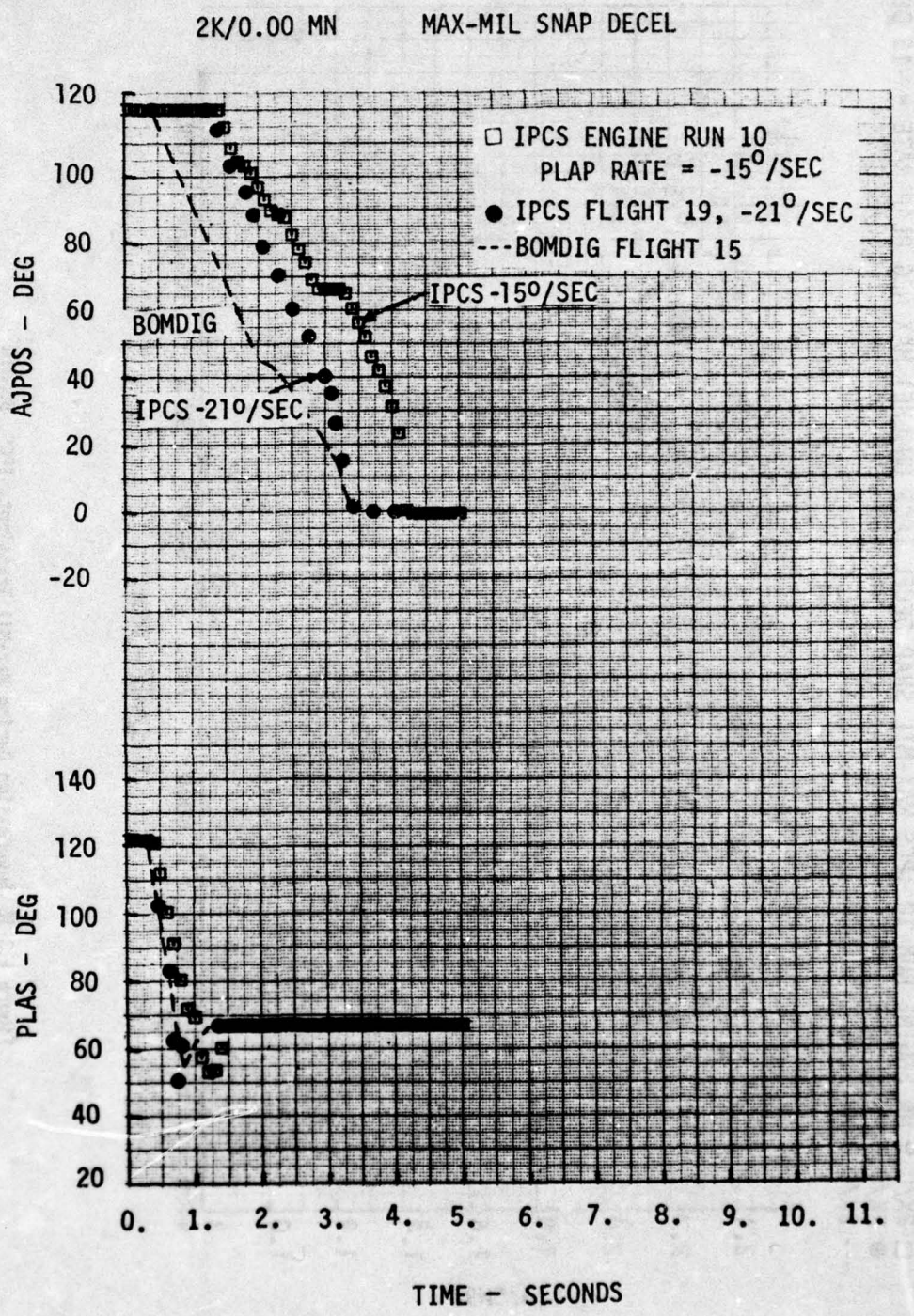

Figure 6.3-17 Nozzle Area Transient for Max-Mil Transient, IPCS, BOMDIG

□ 2K/0.0 MN ENGINE RUN 10 IPCS MAX-MIL SNAP DECEL (ECS ON LHE) MAX NEG PLAP RATE = -15 DEG/SEC
● 2K/0.0 MN FLIGHT 19 IPCS MAX-MIL SNAP DECEL MAX NEG PLAP RATE = -21 DEG/SEC
--- 2K/0.0 MN FLIGHT 15 BOMDIG MAX-MIL SNAP DECEL

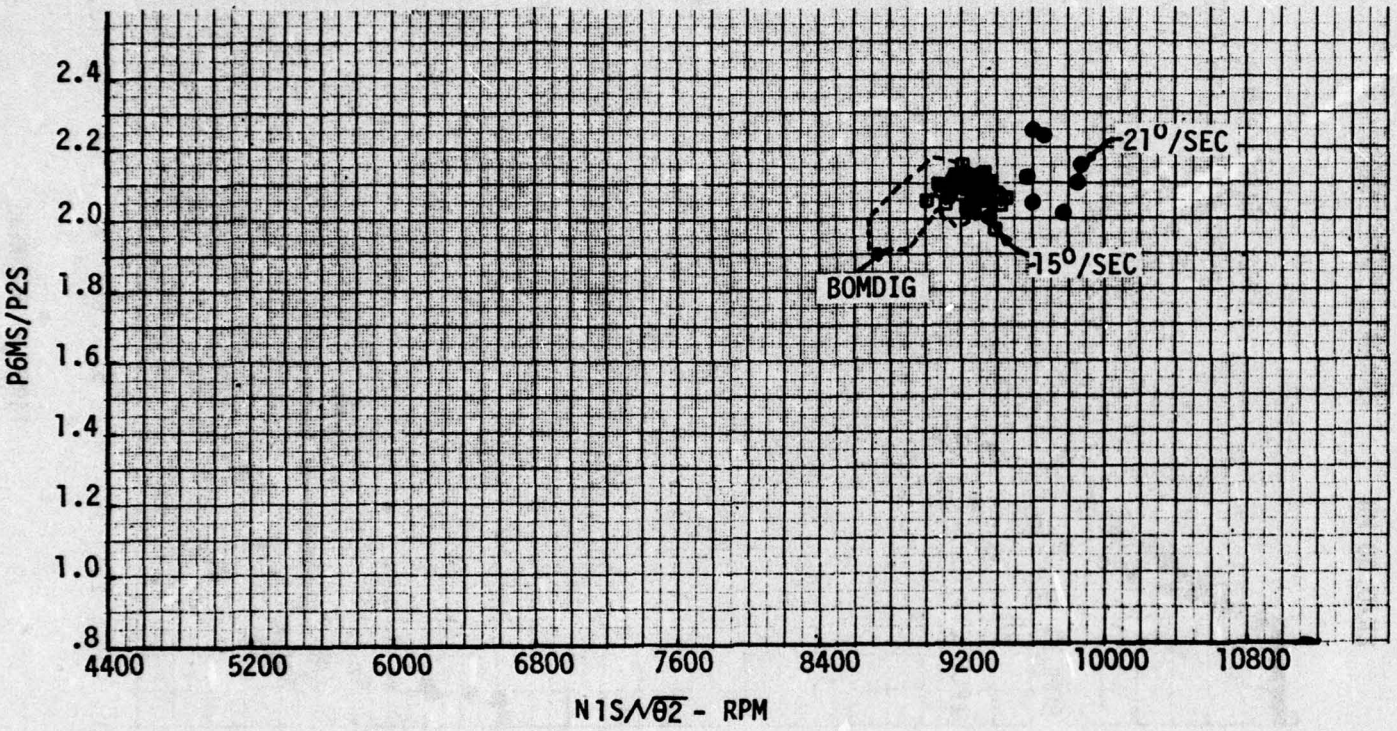

Figure 6.3-18 Suppression During Max-Mil Transient, IPCS, BOMDIG

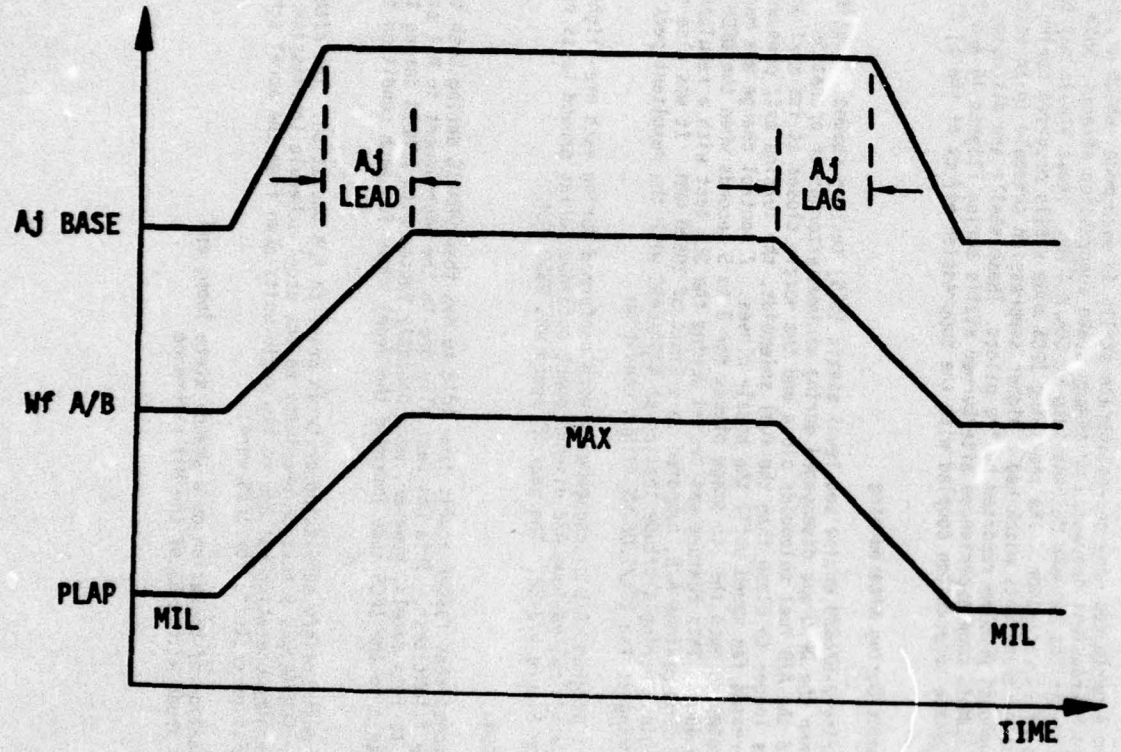

Figure 6.3-19 IPCS Base Area Schedule

The IPCS and BOMDIG modes have consistently demonstrated similar suppression control. This can be observed by comparing the fan operating path envelope during Mil to Max and Max to Mil afterburner transients. Figure 6.3-20 shows the locus of the extreme points on Mil to Max transient operating paths. Test events from the corners of the flight envelope are shown. The lighting spike is determined by light off fuel flow which was the same regardless of mode, thus, the suppression differences are related to the different steady state operating lines as discussed in Section 6.3.1, and the transient paths during the accel. The key IPCS feature was the demonstration of suppression control nearly identical to that exhibited by BOMDIG as measured by the shape and area of the envelopes shown on Figure 6.3-20, even with the manifold prefill providing faster accel times. Figure 6.3-21 shows the locus of the extreme points on Max to Mil transient operating paths. The IPCS mode works with nozzle area lagging behind the fuel flow to unsuppress the fan during decels. This is evident by the suppression envelopes. The BOMDIG mode resulted in engine stalls at 45K, .9 MN and 45K, 2.1 MN.

The flight test program experienced many non-deliberate stalls in each mode, which may be attributed to afterburner transient operation or steady state suppression effects. Both control modes stalled during transitions between Max and Idle at 50K/2.4 MN. These stalls may be attributed to excess airflow variation. The remaining IPCS mode stalls occurred during Flights 23 and 24 with afterburner transients which had a higher suppression schedule in an attempt to understand the A/B roughness problem reported by the pilots. These stalls are discussed in paragraph 6.3.1. The BOMDIG mode experienced afterburner stalls during Flights 16 and 20 which are related to steady state suppression coupled with the suppression effect of the Aj closure rate.

6.3.3 DPCU Disengagement During Afterburning

Test data acquired during P-676629 engine sea level static (SLS) testing showed a potential for low rotor overspeed when the DPCU was disengaged during maximum afterburner operation. When the DPCU is disengaged the A/B fuel solenoids close and the nozzle closes at its maximum rate. Since the nozzle takes longer to close than the fuel solenoids, the turbine exit pressure, P6M is reduced. This increases fan speed until the nozzle closes. A control change was made to add a relay to the system to open the 7th stage bleeds for 3 to 5 seconds when the DPCU is disengaged or powered down. This feature was tested during the SLS test with a resultant peak speed of 10370 RPM N1 from maximum A/B, compared to a limit of 10500 RPM. It was also tested at each of the test points during altitude testing at NASA/LeRC with the resultant peak speed of 10250 RPM N1 occurring at the 22K/1.06 MN flight condition.

During the flight test program, A/B disengagements were performed during each pre-flight ground run. The results of a typical maximum A/B disengagement obtained during ground tests prior to Flight 15 are shown on Figure 6.3-22. The peak N1 speed was 9950 PRM.

6.4 IDLE/MAX OPERATION

IPCS consistently demonstrated faster accels from Idle to Max than BOMDIG during both the altitude test and the flight test. This was basically due to the improvement in Mil to Max accel time. The Max to Idle decels, however, were decidely faster with BOMDIG during the altitude test. A change to the IPCS mode improved the decel times for each condition tested by 2 to 3 seconds.

Both IPCS and BOMDIG must satisfy permission criteria prior to A/B operation. The afterburner permission signal for BOMDIG was a test on proximity to the accel schedule (permission was granted when Mil governing operation was one to two ratio units down from the accel schedule). The afterburner permission criteria for IPCS were:

1. XLOOP indication of operation on a steady state loop, and
2. High rotor speed within 5% of the Mil reference

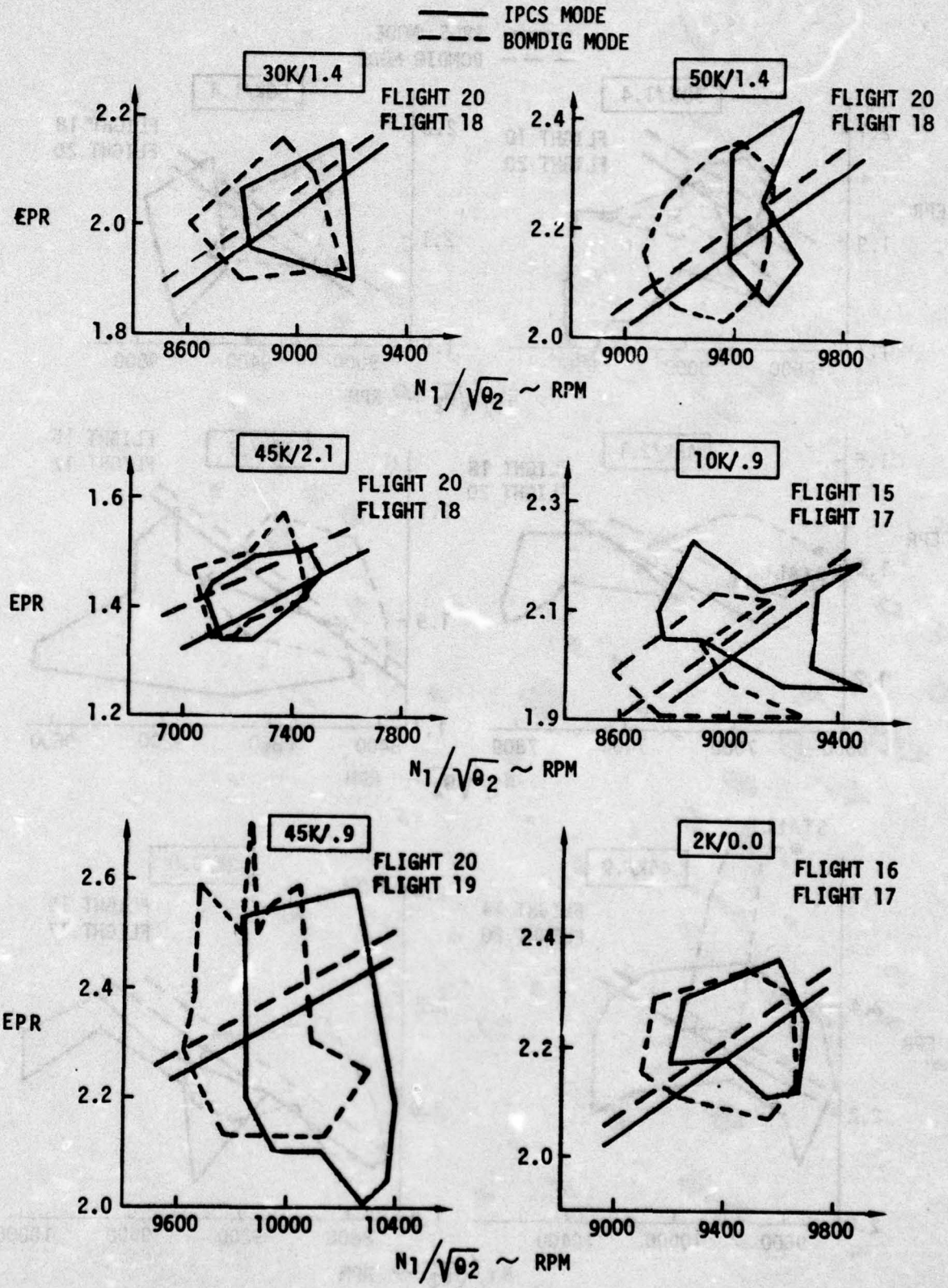

Figure 6.3-20 Fan Suppression Comparison During Mil to Max

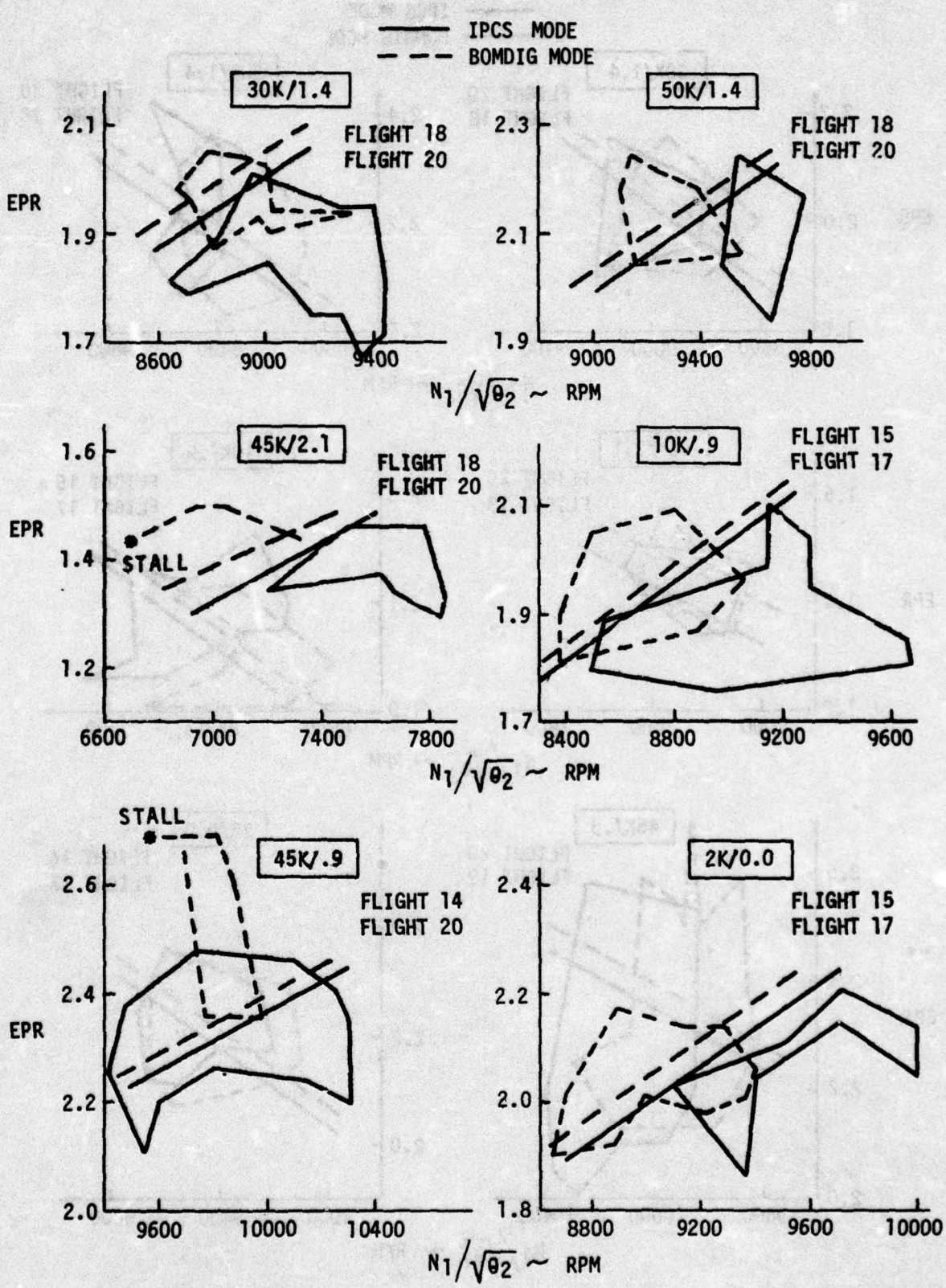

Figure 6.3-21 Fan Suppression Comparison During Max to M11

FLIGHT 15

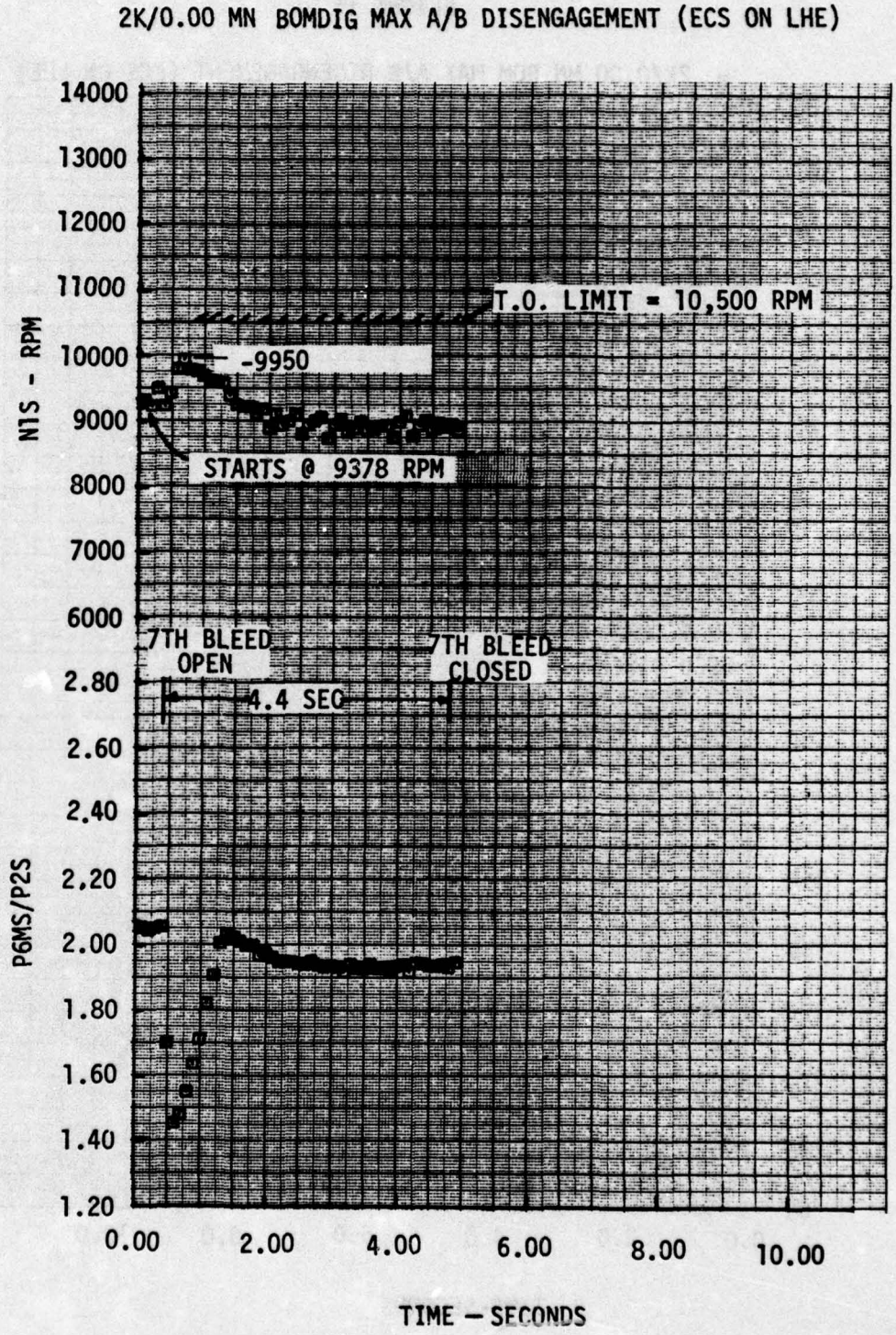

FIGURE 6.3-22a Max A/B Disengage

FLIGHT 15

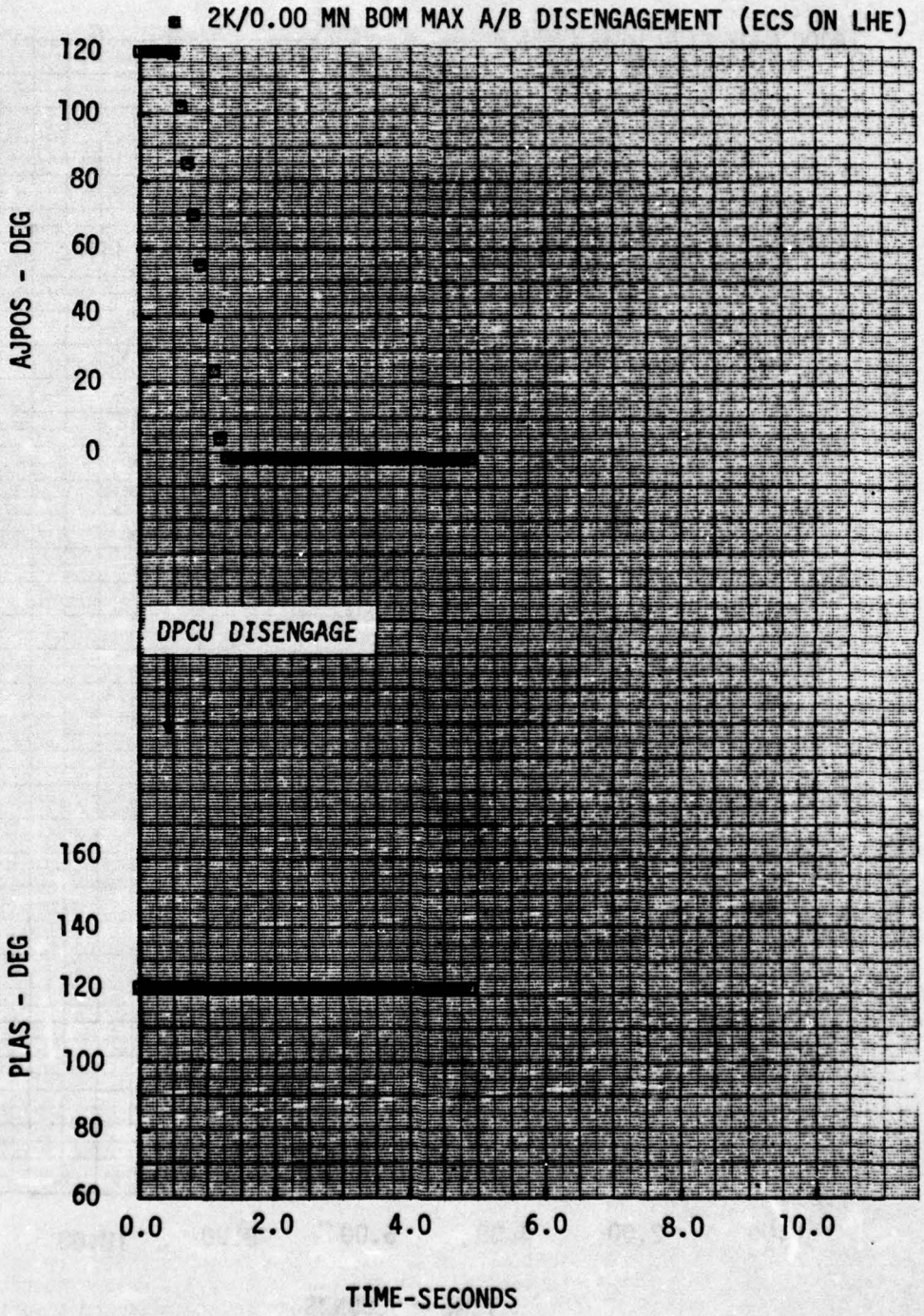

6.3-22b Max A/B Disengage

Another difference between the two modes was the light-off indicator which, for IPCS used the rate of change of air flow error as discussed in paragraph 6.3.2.1. The BOMDIG mode worked using a suppression error level indicator. Both modes worked well, providing appropriate gas generator lockout and positive indications of afterburner lights.

In IPCS the Max to Idle transient was originally designed to provide the best control of fan surge margin, by first decelerating the afterburner, followed by the gas generator decel after the afterburner shutoff was indicated by closure of the Zone 1 shutoff valve.

The serial decel provided better IPCS control of fan suppression during Max to Idle transients than BOMDIG, as evidenced by altitude test data, at the expense of decel time. To improve on transient decel time, the IPCS mode was changed from serial decels to parallel decels, in a manner similar to BOMDIG.

The effect of this change is illustrated on Figures 6.4-1 and 6.4-2 which show the high rotor decel rates and fan suppression effects respectively. Engine run 10 shows the serial decel for the original IPCS configuration where the afterburner shuts off prior to the gas generator decel. The data shown for the Flight 19 preflight series illustrates the parallel decel mode showing high rotor speed decelerating at a rate similar to BOMDIG. The fan suppression data shows that while the serial decel is along a path of more unsuppression, the parallel decel results in a transient path with suppression similar to BOMDIG. The transient path for the IPCS decel is either along the fan steady state part power operating line, or below it, indicating surge margin control equal to or better than during steady operation. The BOMDIG decel, however, results in a slight over-suppression at the high power end due to the transient suppression mode of control. The IPCS mode provides Aj lag on afterburner shutdowns as discussed in paragraph 6.4.2.4, to improve transient fan suppression.

Idle to Max and Max to Idle throttle transients were part of the normal test series at each flight test condition to illustrate the gross transient accel and decel time differences between the two modes of control. Figure 6.4-3 summarizes the accel times for the various flight conditions tested. The accel times were calculated as the time between the start of the throttle snap and the point in time when nozzle area achieves its final value. As shown on the figure, IPCS consistently demonstrated faster accel times than BOMDIG. The average improvement in accel time was approximately 2.5 seconds.

Figure 6.4-4 summarizes the decel times for the various flight test conditions. The decel times were calculated as the time between the start of the throttle snap and the point in time when the nozzle area closes or the point where 95% of the change in the high rotor speed occurs, whichever is longer. Since most Max to Idle decels take longer for the high rotor speed to change than for nozzle area to close, the decel times are closely related to the Mil to Idle decels, with deviations occurring due to ambient effects or secondary effects of decelerating the gas generator and afterburner simultaneously.

6.5 IPCS SPECIAL LOOPS

Five IPCS control loops were enabled for a portion of the flight test to evaluate special features: Buzz, distortion control of bleeds, airflow trim, stall and recovery detection, and autothrottle. These features are discussed in the following paragraphs.

6.5.1 Buzz Loop Performance

In flight, the buzz loop performed essentially as predicted by the approximate simulation incorporated in the digital engine simulation. Comparison and analysis were somewhat complicated by the inclination of the engine to stall when exposed to buzz and a software error which occasionally caused engine accels when the inlet was not buzzing.

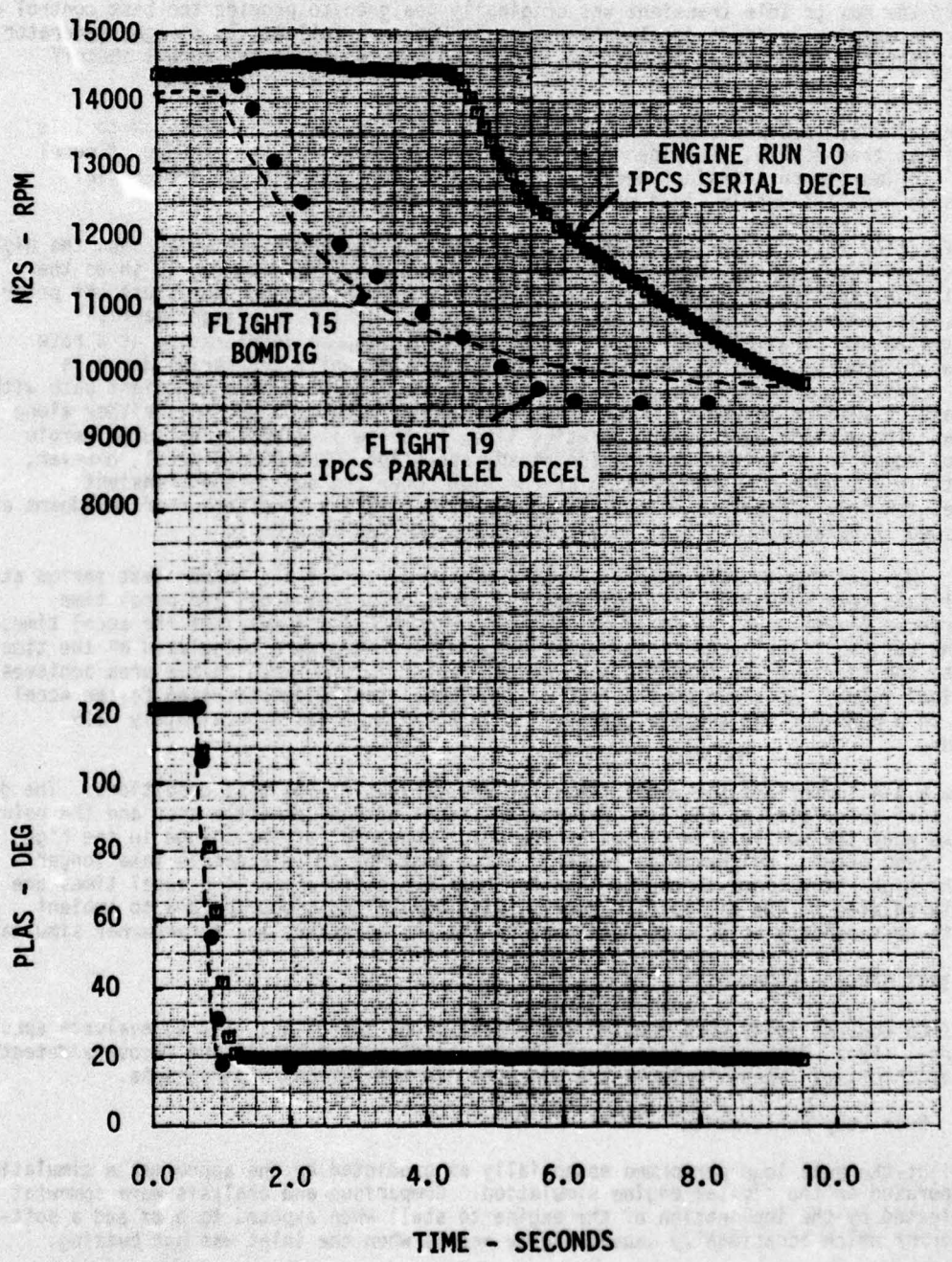

Figure 6.4-1 Speed Comparison for Serial and Parallel Max-Idle Decel

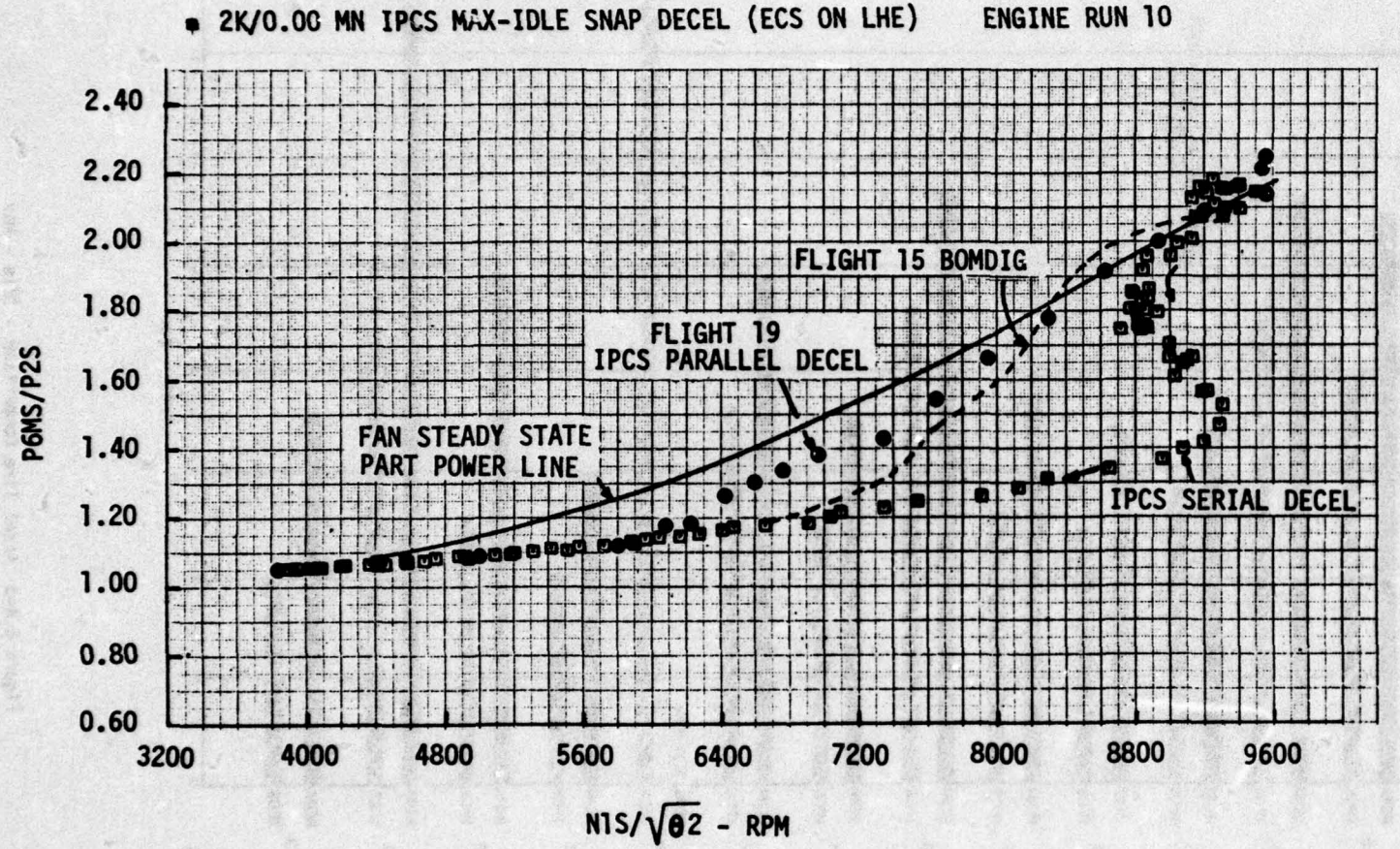

Figure 6.4-2 Suppression Comparison for Serial and Parallel Max-Idle Decel

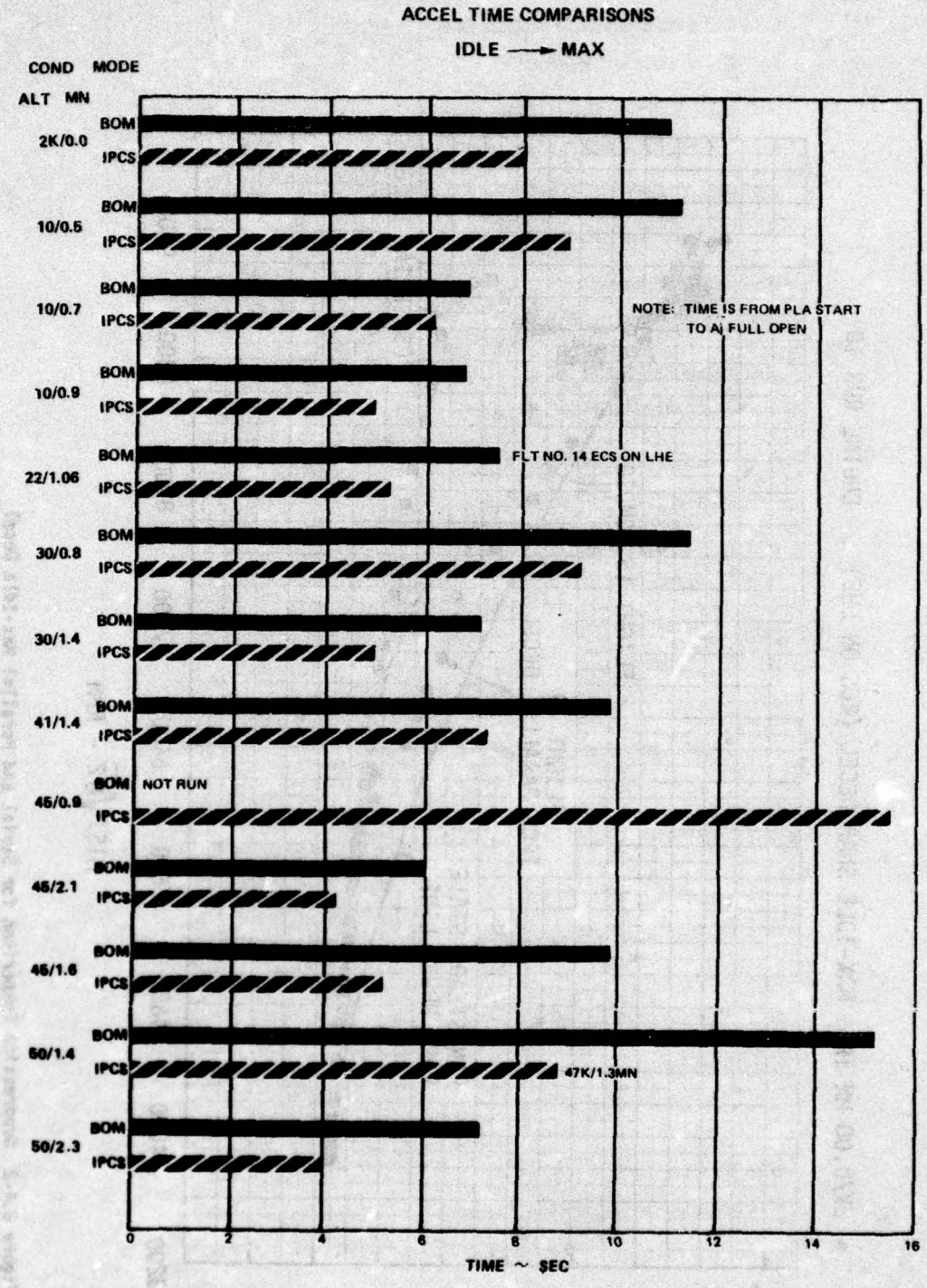

Figure 6.4-3 Accel Time Comparison - Idle - Max

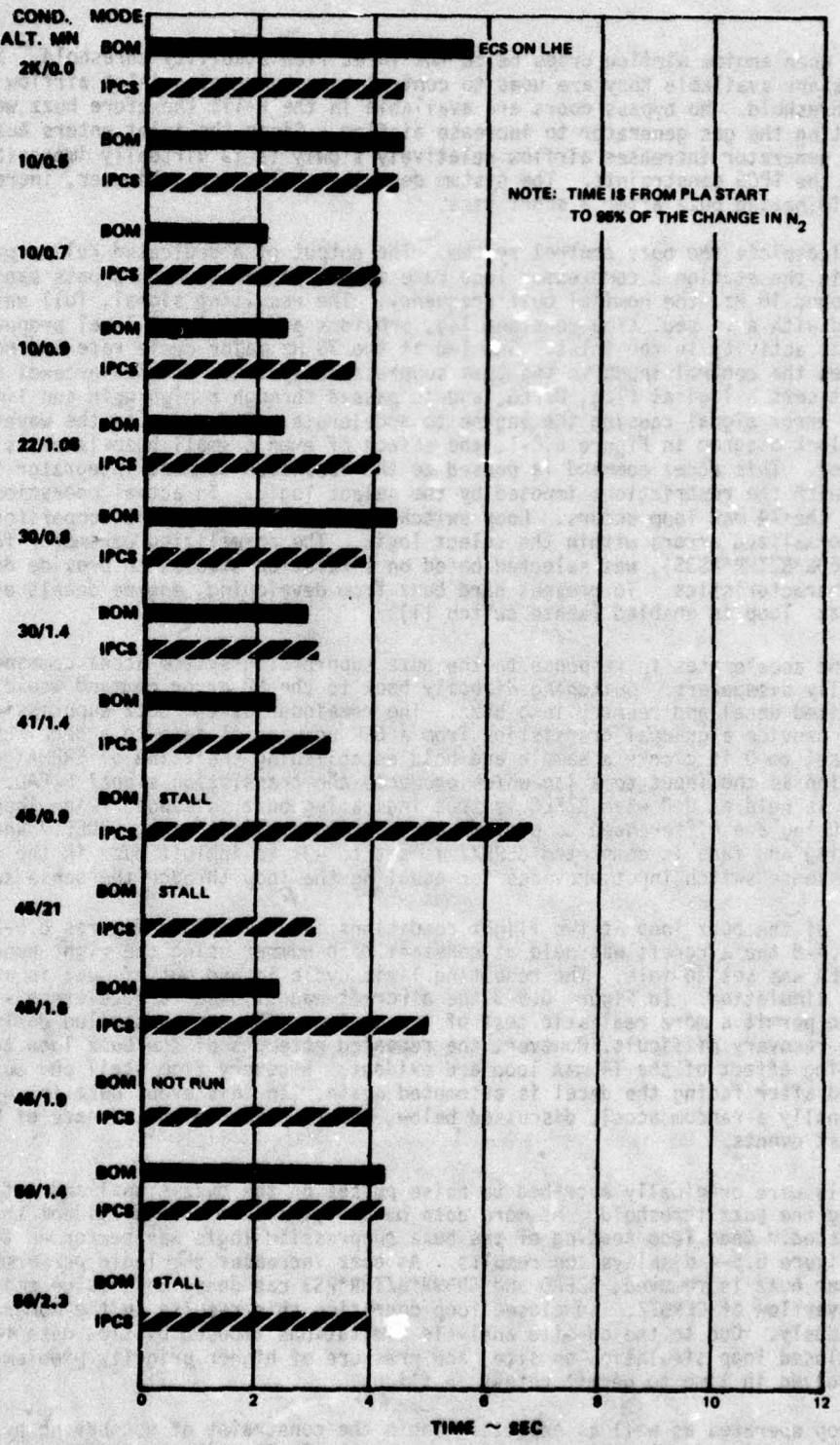

Figure 6.4-4 Decel Time Comparison Max - Idle

Buzz occurs when engine airflow drops below the inlet flow stability threshold. If inlet bypass doors are available they are used to control buzz by raising inlet airflow above the stability threshold. No bypass doors are available in the F-111 therefore buzz was controlled by accelerating the gas generator to increase airflow. Since the inlet enters buzz precipitously and the gas generator increases airflow relatively slowly it is virtually impossible to prevent buzz within the IPCS constraints. The system described below does, however, increase engine airflow, eliminating buzz after a short time.

Figure 6.5-1 depicts the buzz control system. The output of a dedicated Kulite pressure transducer in the station 2 compressor face rake system passes through a pass band filter centered around 10 Hz, the nominal buzz frequency. The resulting signal, full wave rectified and smoothed with a .1 sec. time constant lag, provides a d.c. signal level proportional to the level of buzz activity in the inlet. Sampled at the 33 Hz major cycle rate and normalized by P2 it becomes the control input to the buzz suppression system. As BZZS exceeds a noise suppression threshold it sets a logical flag, BZFLG, and is passed through a high gain and limited to generate an error signal causing the engine to accelerate. Referring to the waveforms sketched below the block diagram in Figure 6.5-1, the effect of even a small buzz level is to command a maximum accel. This accel command is passed to the fuel flow command integrator if it is consistent with the restrictions imposed by the select logic. In actual operation an immediate transfer to the T4 max loop occurs. Loop switching is dictated by the comparison of CERBZZ to the other normalized errors within the select logic. The normalizing parameter for CERBZZ, (BZFAD + CN69G*BZTHR*PS3S), was selected based on simulation studies to provide desired loop switching characteristics. To prevent hard buzz from developing, engine decels are rate limited when the buzz loop is enabled (sense switch 11).

As the engine accelerates in response to the buzz suppression system accel command, buzz decays and eventually disappears. Switching directly back to the N2 error command would result again in rate limited decel and reentry into buzz. The remainder of the buzz suppression logic is intended to provide a gradual transistion from a DER command of zero to a decel command. When BZFLG is reset to 0 it clocks a sample and hold establishing the value of ERRMAX at the moment of transistion as the input to a lag which produces the transistion signal BZFAD. The output of this lag is held at 0.0 when BZFLG is true indicating buzz is sensed. The input and output of the BZFAD lag are differenced to provide a fade complete indicator, BZDET. When the inlet is not buzzing and fade is completed CERBZZ is set to -31 to inhibit buzz in the select logic. The sense switch input provides for enabling the loop through the sense switches.

Performance of the buzz loop at two flight conditions is depicted in Figures 6.5-2 and 6.5-3. In Figure 6.5-2 the aircraft was held at constant Mach number using the right hand engine while left hand PLA was set to idle. The resulting limit cycle in and out of buzz is as predicted by the digital simulation. In Figure 6.5-3 the aircraft was allowed to decelerate - both throttles to idle - to permit a more realistic test of the system. The engine stalled early in the decel making buzz recovery difficult. However, the repeated attempts of the buzz loop to recover and the overriding effect of the T4 max loop are evident. Recovery from stall and buzz is eventually achieved and after fading the decel is attempted again. In this event buzz is suppressed as desired. Finally a random accel, discussed below, occurs prior to the advance of PLA leading to the next test events.

Random accels were originally ascribed to noise pulses on the buzz signal and a fix was attempted by expanding the buzz threshold. As more data became available it was evident that a software anomaly existed. Open loop testing of the buzz suppression logic was performed to isolate the problem. Figure 6.5-4 displays the results. As buzz increases the logic performs as discussed above. After buzz is removed, BZFAD and CN69G*BZTHR*PS3 can decay to a value small enough to create an overflow of CERBZZ. In closed loop operation this results in the momentary accel noted previously. Due to the on-site analysis limitations imposed by slow data turn around, lack of a closed loop simulation on site, and pressure of higher priority problems this problem was not resolved in time to permit retest in flight.

The buzz loop operated as well as expected within the constraint of not having bypass doors. Engine airflow during deceleration was reduced roughly 30 PPS below the IPCS minimum airflow schedule as indicated in the figures. Buzz, when encountered, was suppressed -although slowly.

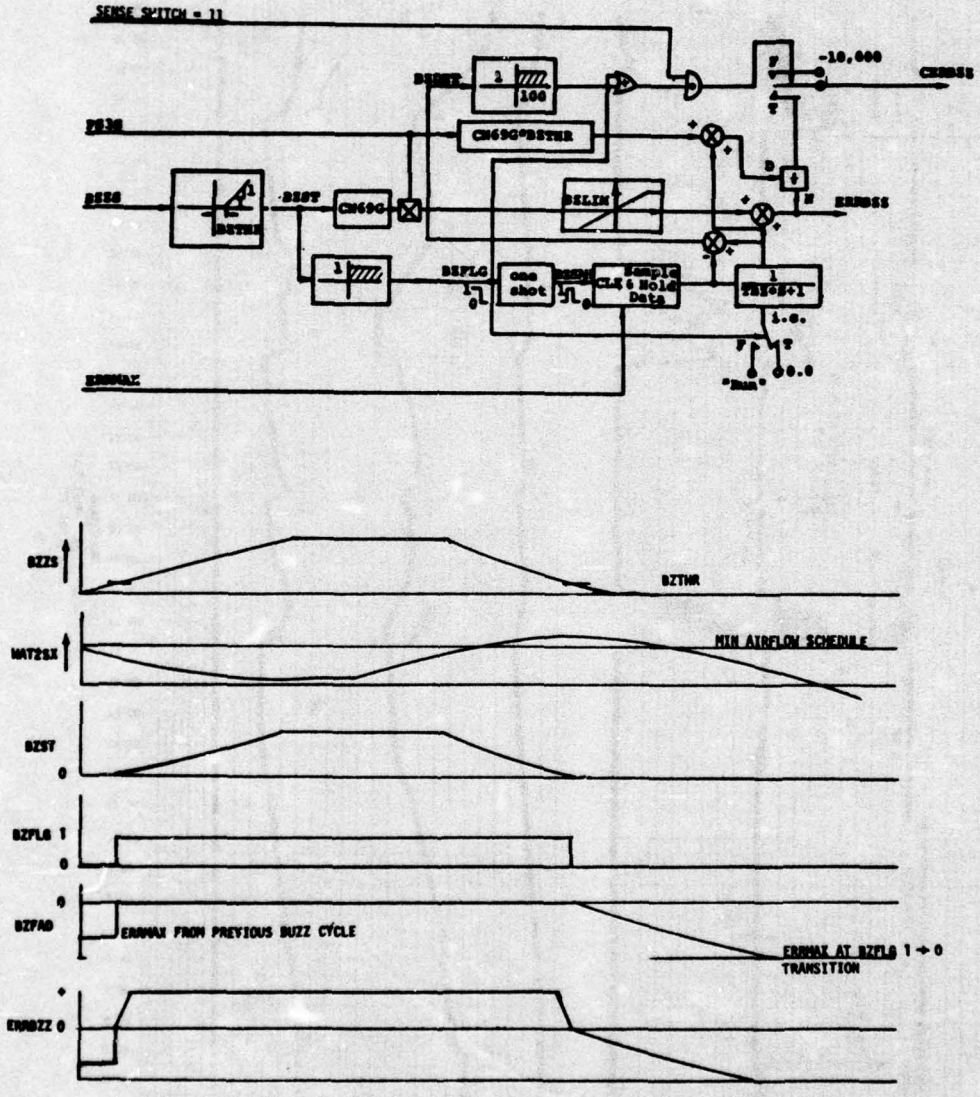

Figure 6.5-1 Buzz Loop Block Diagram

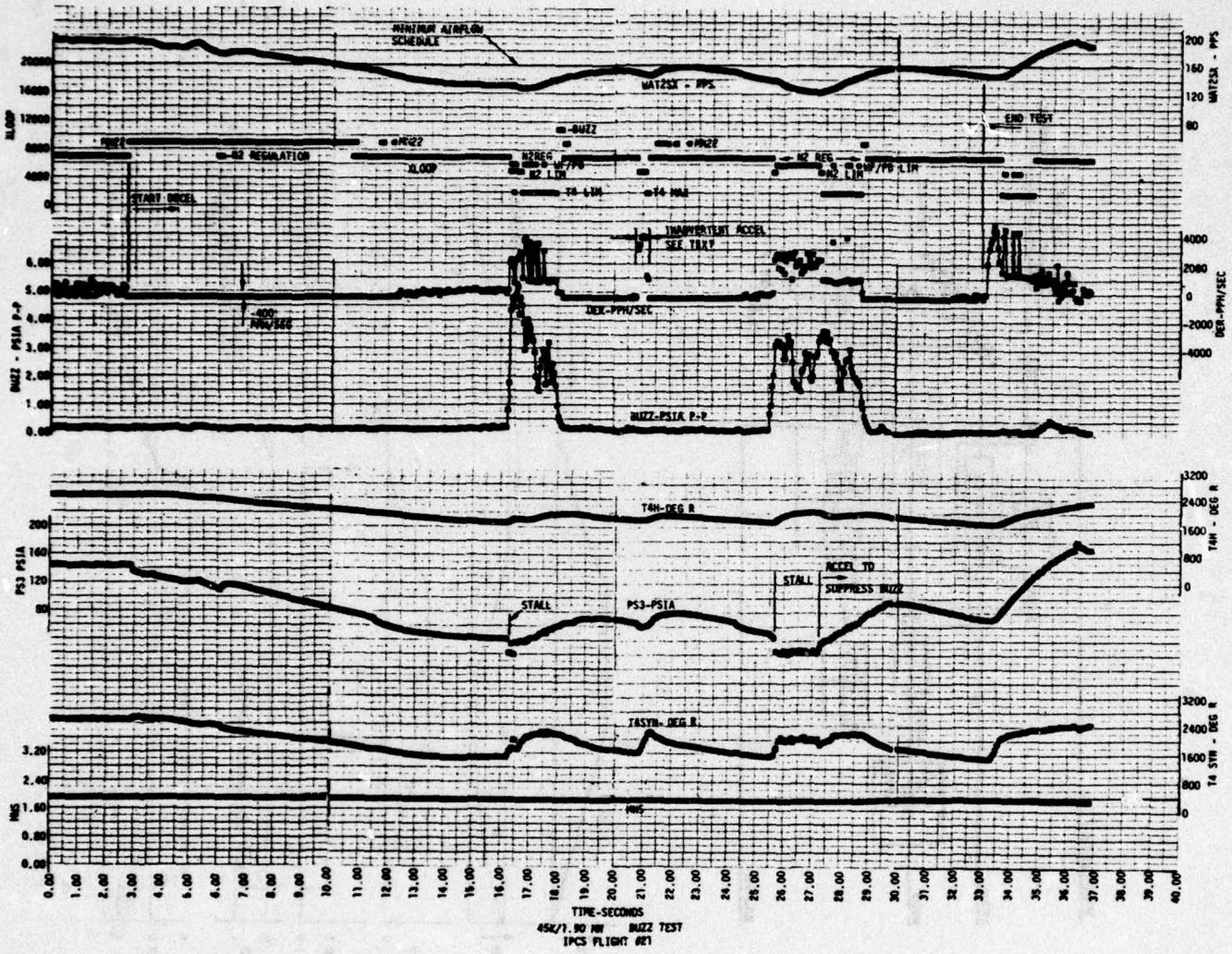

Figure 6.5-2 Mach 1.9 Buzz Loop Evaluation

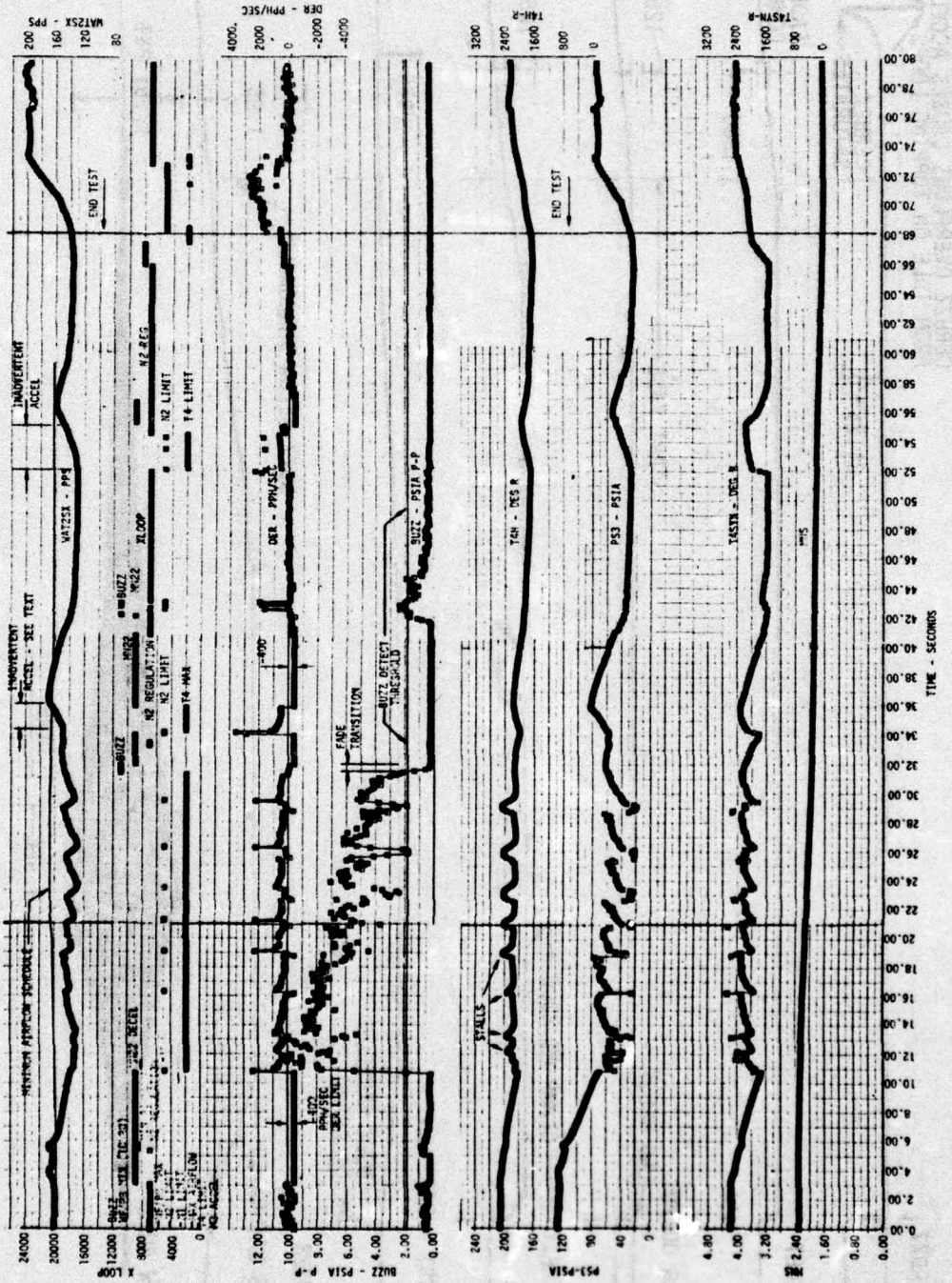

Figure 6.5-3 Mach 2.3 Buzz Loop Evaluation

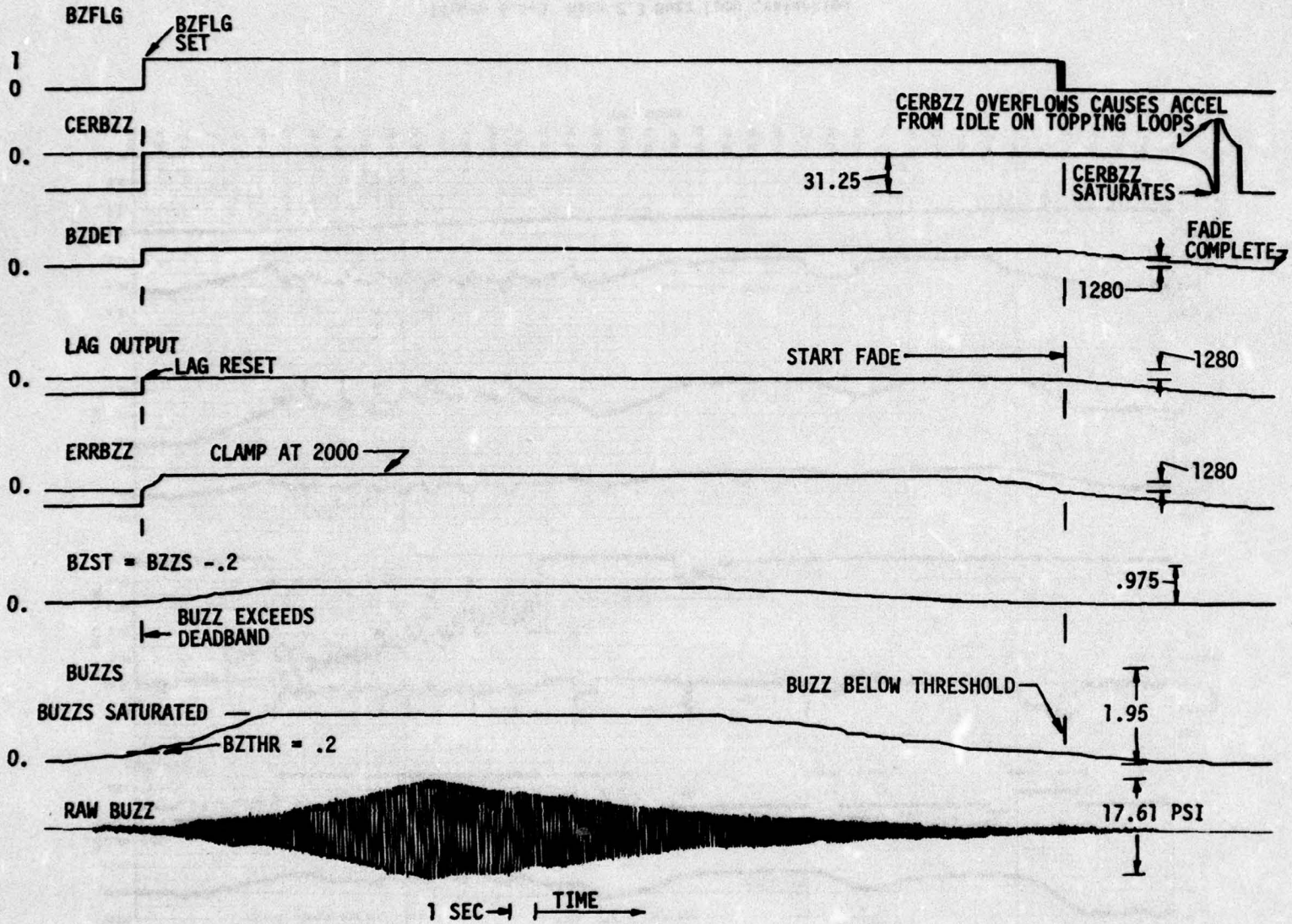

Figure 6.5-4 Buzz Loop Laboratory Test

6.5.2 Distortion Control of Bleeds

Distortion control of bleeds was successfully demonstrated during the flight test program. The loop worked by maintaining a continuous comparison between measured distortion and the distortion tolerance of the engine. Airplane accelerations from subsonic to supersonic conditions showed that distortion control could keep the 7th bleed closed to Mach 2.25 compared to Mach 1.75 for the bill of materials bleeds control.

The measured distortion signal was generated from four steady-state compressor face pressure measurements and a single compressor face turbulence measurement. The four probes were added to the compressor face rake (para 5.1.2) prior to the flight tests. The turbulence signal is from one of the compressor face Kulites. The output is filtered and processed by the IFU to produce a signal proportional to the turbulent activity in the 15-150 Hz range (Reference 8). Distortion is calculated from a curve as a function of (Pmax-Pmin)/Pmin from the four steady-state probes plus a constant times the turbulence normalized by Pmin. The correlation was generated from Baseline Flight Test data.

The engine tolerance to distortion is computed as a function of corrected low rotor speed, N1S/$\sqrt{\theta 2}$, engine pressure ratio, P6MS/P2S, and bleed configuration (see Figure 6.5-5). The tolerance is biased by the effect of Reynolds number. Figure 6.5-6 shows the bleed control. If the sensed distortion, ZKDS, is within 200 KD of the bleeds closed tolerance the 7th bleed opens. If ZKDS is within 200 KD of the tolerance for 7th bleed open the 12th bleed opens. Both bleed commands have hysteresis to prevent bleed cycling. If the 12th bleed is open the 7th bleed is opened when ZKDS is within 100 KD of the tolerance for 12th bleed open. This was necessary as the 12th bleed can be opened by the non-distortion portion of the bleed control. An increase in the 12th stage bleed hysteresis prevented premature closure of the bleed during operation on the deceleration loops (MN2 and Wf/Pb mjn). A test on large negative fuel flow rate of change (DER) also provides decel stall protection by opening the 12th stage bleed. Both blowout and stall open 7th and 12th bleeds.

A portion of the bill of material bleed functions were retained. The hydromechanical PRBC control was active regardless of control configuration. Since there is no bleed position measurement, the PRBC logic is included to predict the 12th bleed opening. The BOM feature to open 7th bleed on the ground for PLA < 61° was also retained.

Figure 6.5-7 shows a comparison of the bill of material and distortion bleed controls, both operating as part of the IPCS control. The steps in the distortion tolerance curve indicate 7th bleed opening and closing. As shown the distortion control keeps the bleeds closed through most of the transonic acceleration providing more thrust. The bleed cycling above Mach 2.3 was due to changes in the distortion level. For this flight the hysteresis was 75 KD. It was increased to 300 KD to prevent bleed cycling. Figure 6.5-8 shows an accel with 300 KD hysteresis.

Performance improvements associated with closing the 7th stage bleeds during a climb to maximum altitude and during transonic accelerations from 1.7 to 2.3 MN are shown in Figures 6.5-9 and 6.5-10. When the left hand (IPCS) engine 7th stage bleed was closed during an accelerating climb, a substantial increase in excess thrust resulted as evidenced by the greater rate of climb and higher longitudinal acceleration. Figure 6.5-10 shows that the distortion control reduced the time to accelerate from Mach 1.7 to 2.3 on flight 22 by 8% and saved 10% on the fuel. Performance is also influenced by the variations in engine inlet temperature for each flight (Figure 6.5-11). On Flight 26, the acceleration took 22% longer due to the higher inlet temperature, but the improved operating efficiency of the engine with closed bleeds is demonstrated by a reduction of 2.7% in fuel used in spite of the longer time.

Maneuver performance improvements for the F-111E airplane can be inferred from the changes which occurred at the point where bleeds closed in Figure 6.5-9. An important performance parameter for a combat airplane such as the F-111 is Specific Excess Power, Ps, computed by the following formula:

$$Ps = \frac{\text{Excess Thrust}}{\text{Airplane Weight}} \times \text{Airplane Velocity}$$

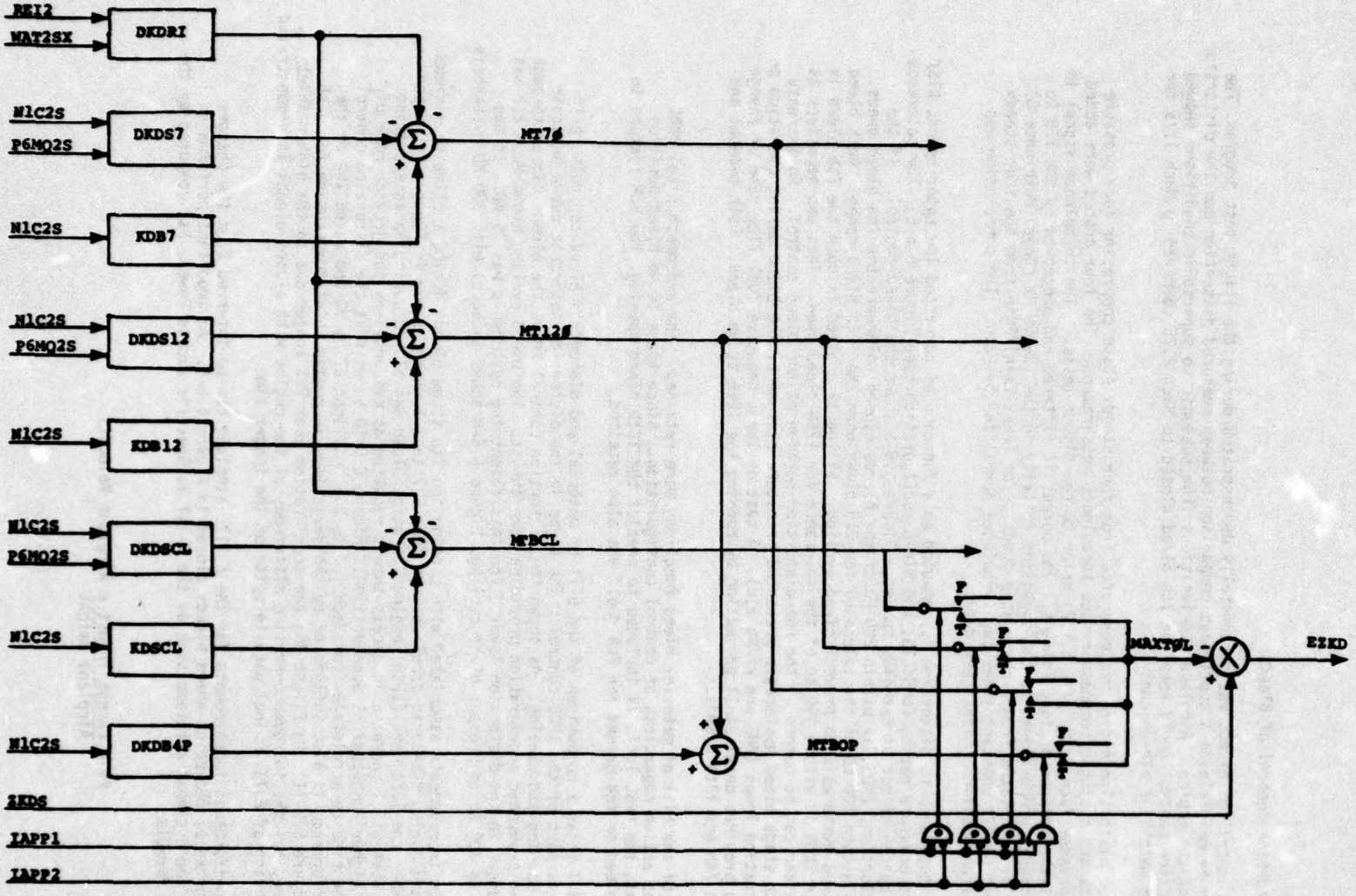

Figure 6.5-5 Engine Distortion Tolerance Computation

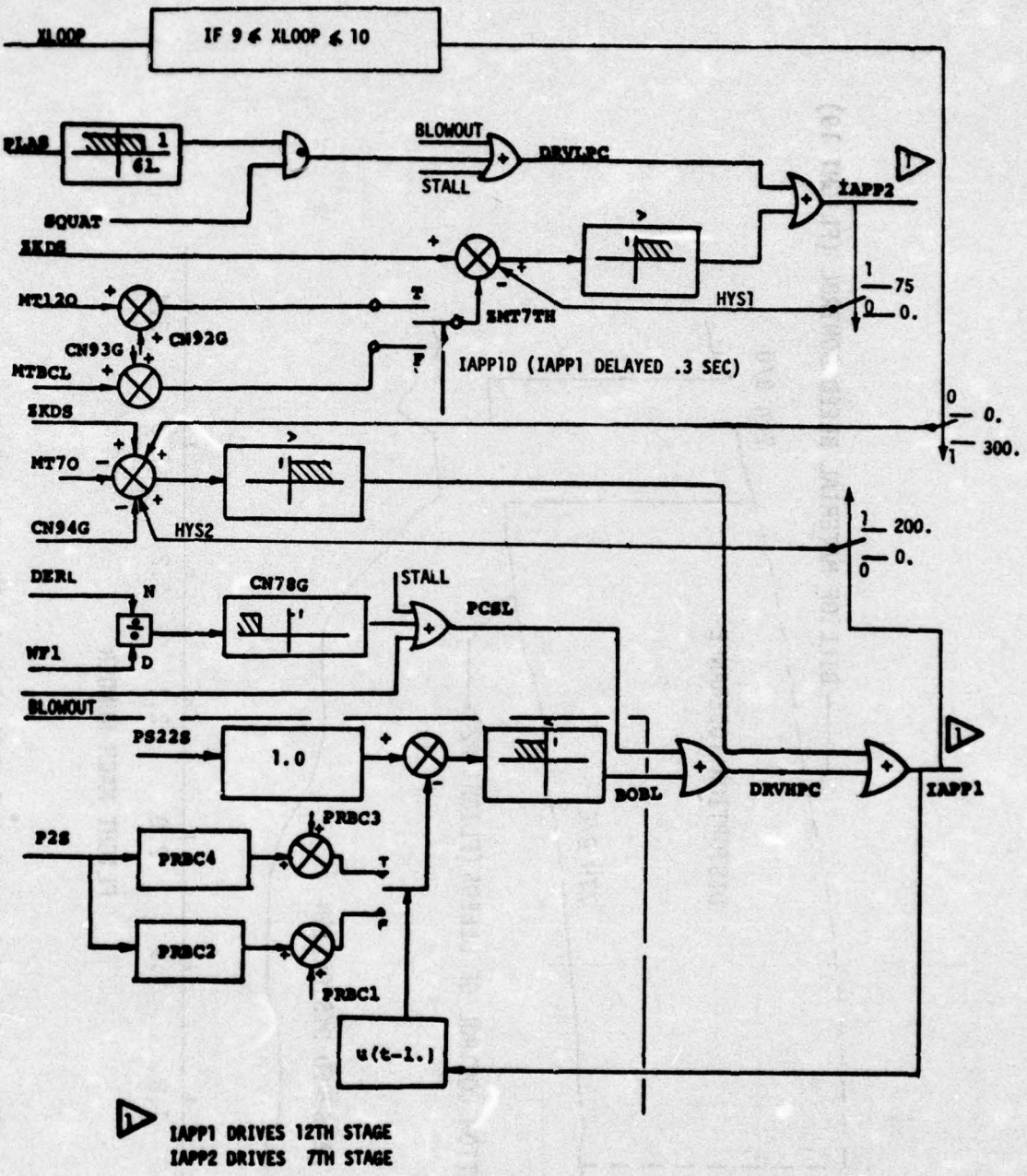

Figure 6.5-6 Bleed Logic

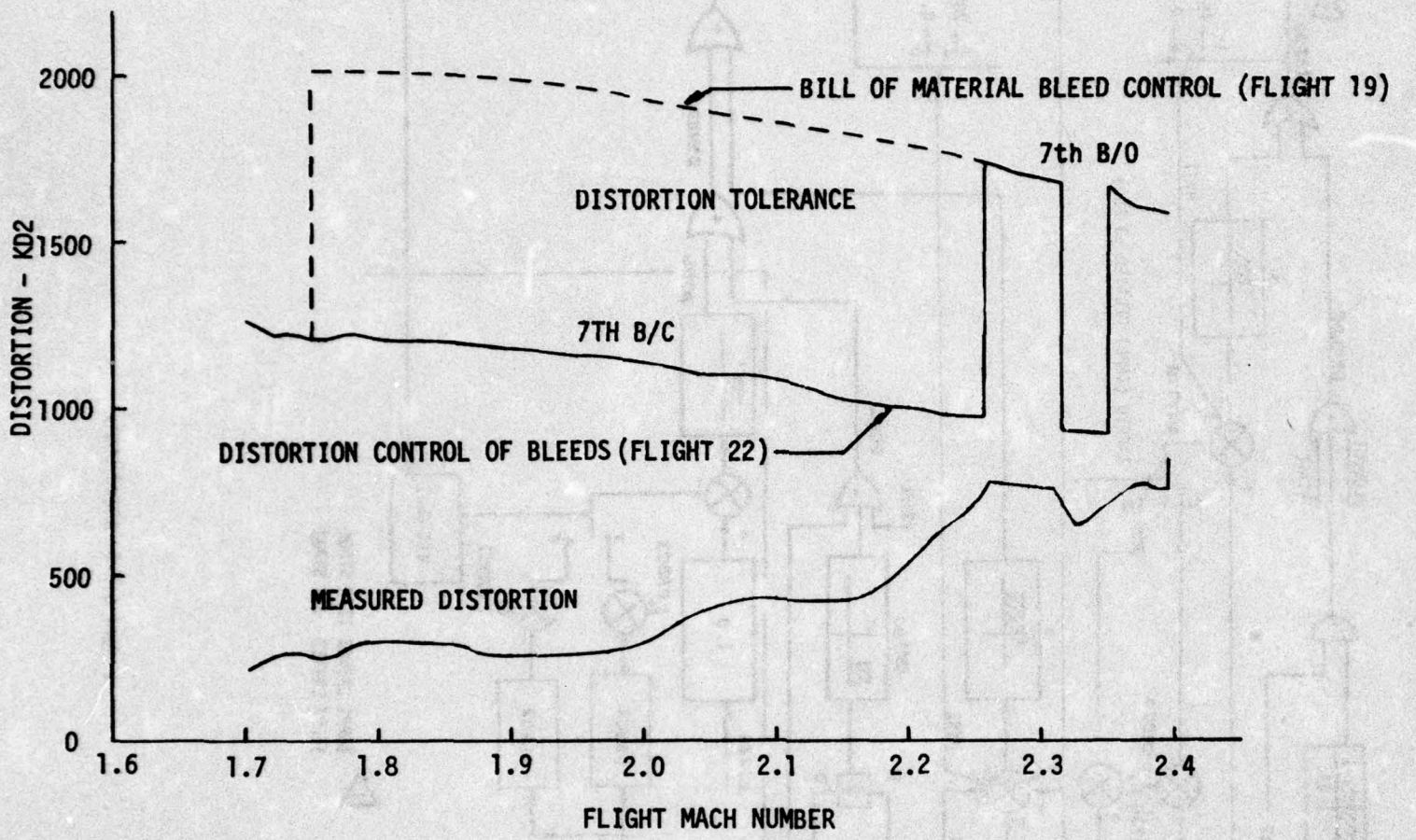

Figure 6.5-7 Distortion Control of Bleeds During 650 KT Acceleration

FLIGHT 26

ACCEL TO MN = 2.3 DISTORTION CONTROL OF BLEEDS

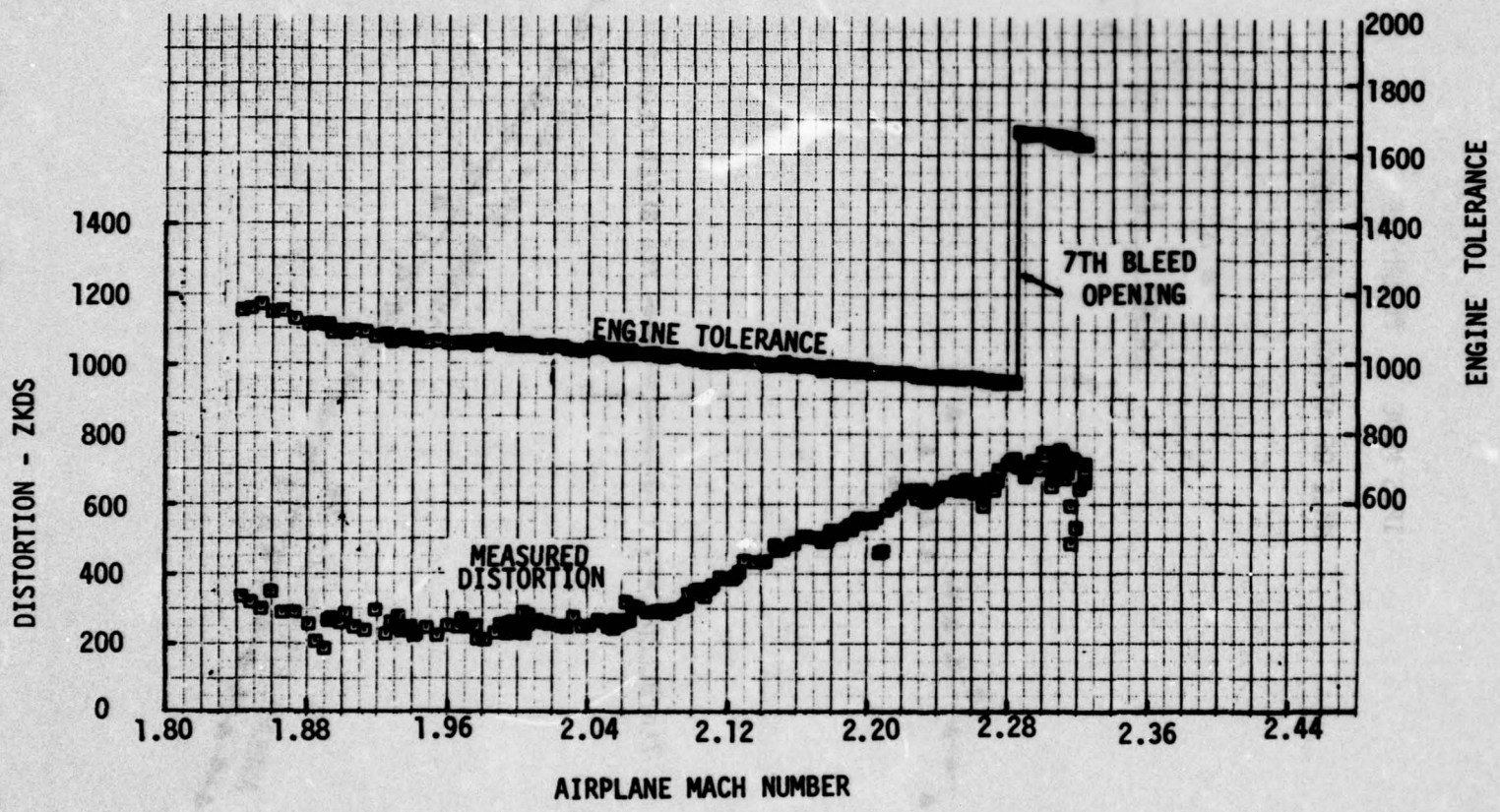

Figure 6.5-8 Distortion Control of Bleeds with 300 KD Hysteresis

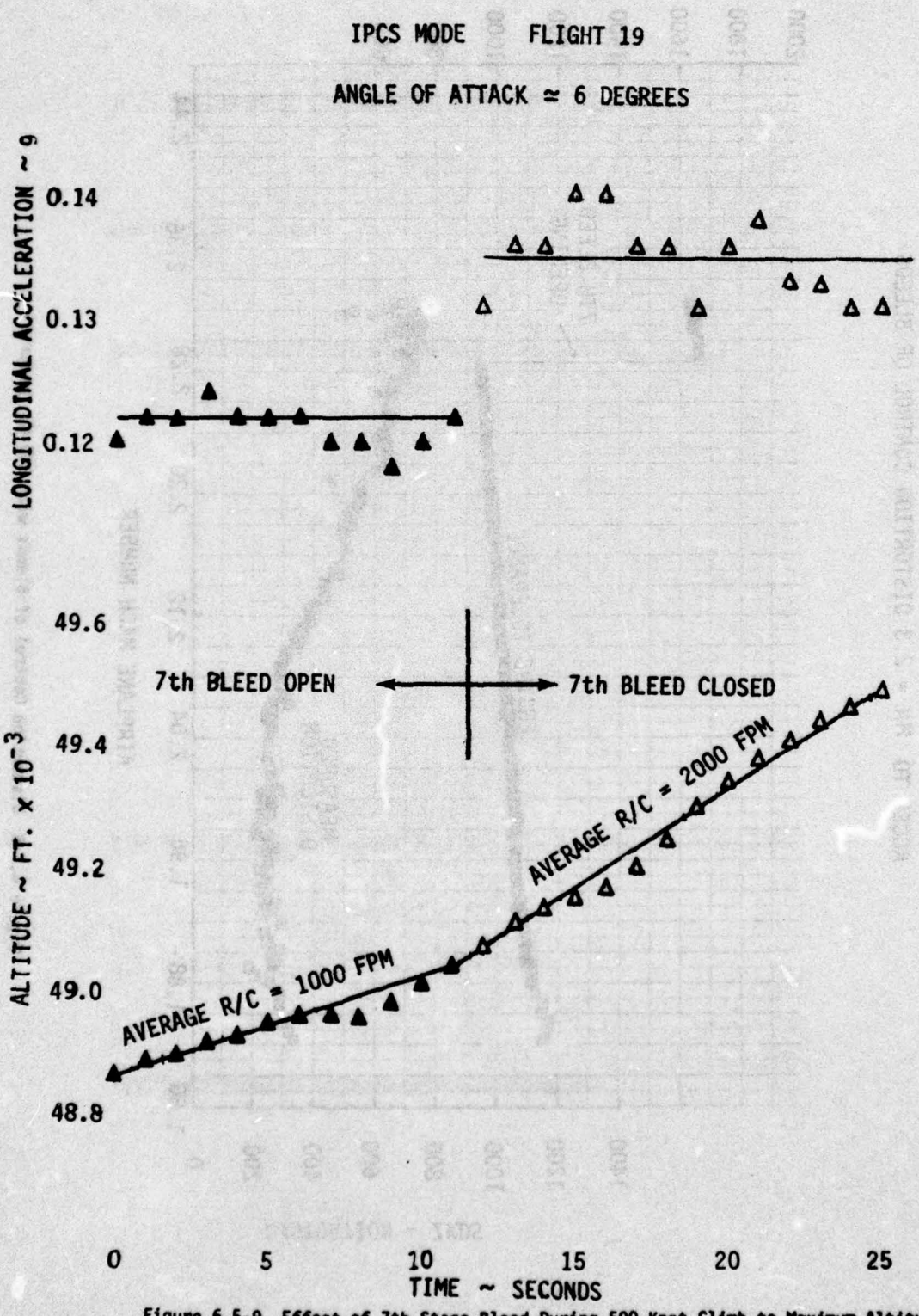

Figure 6.5-9 Effect of 7th Stage Bleed During 500 Knot Climb to Maximum Altitude

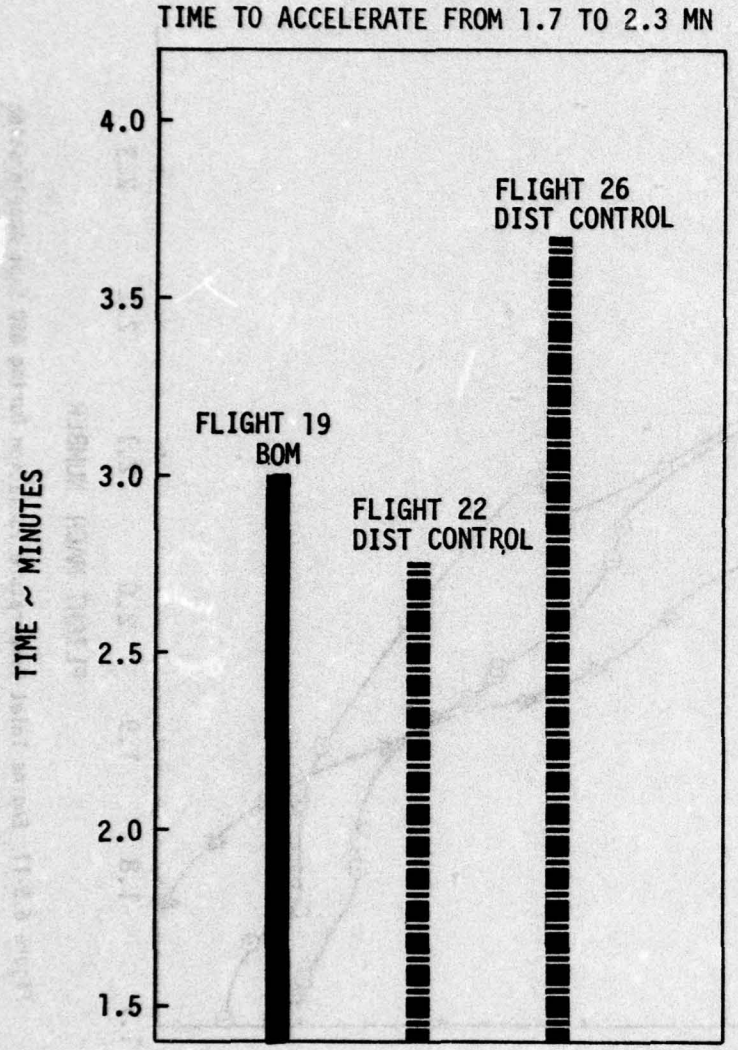

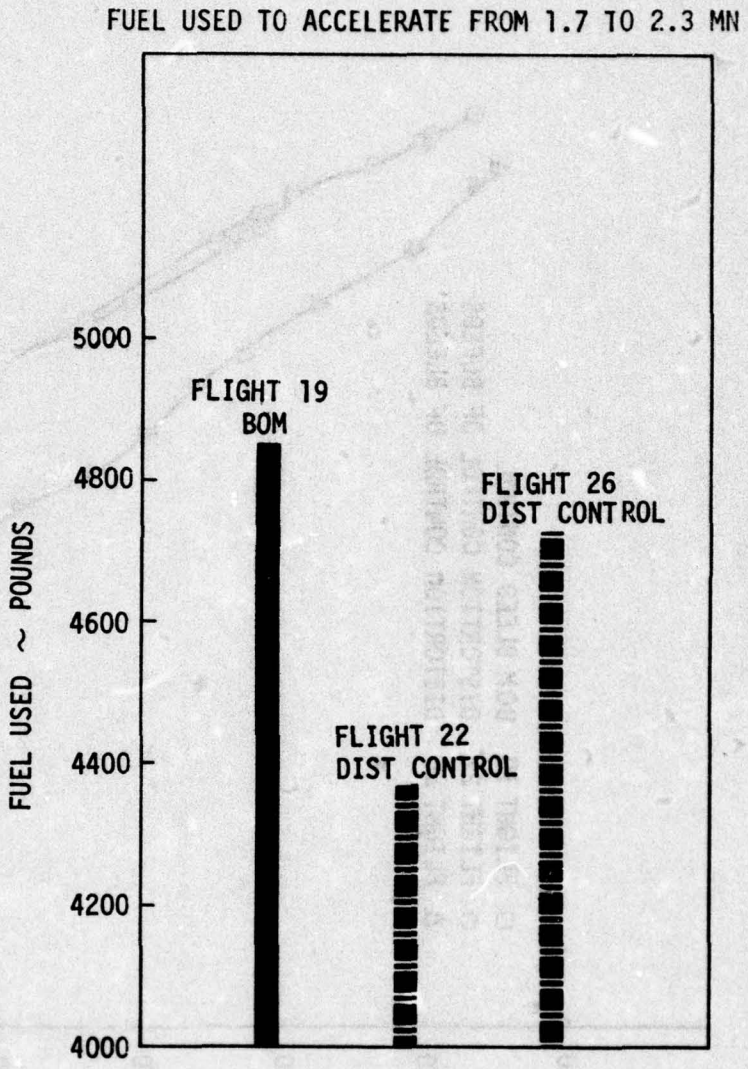

Figure 6.5-10 650 Knot Acceleration Comparison

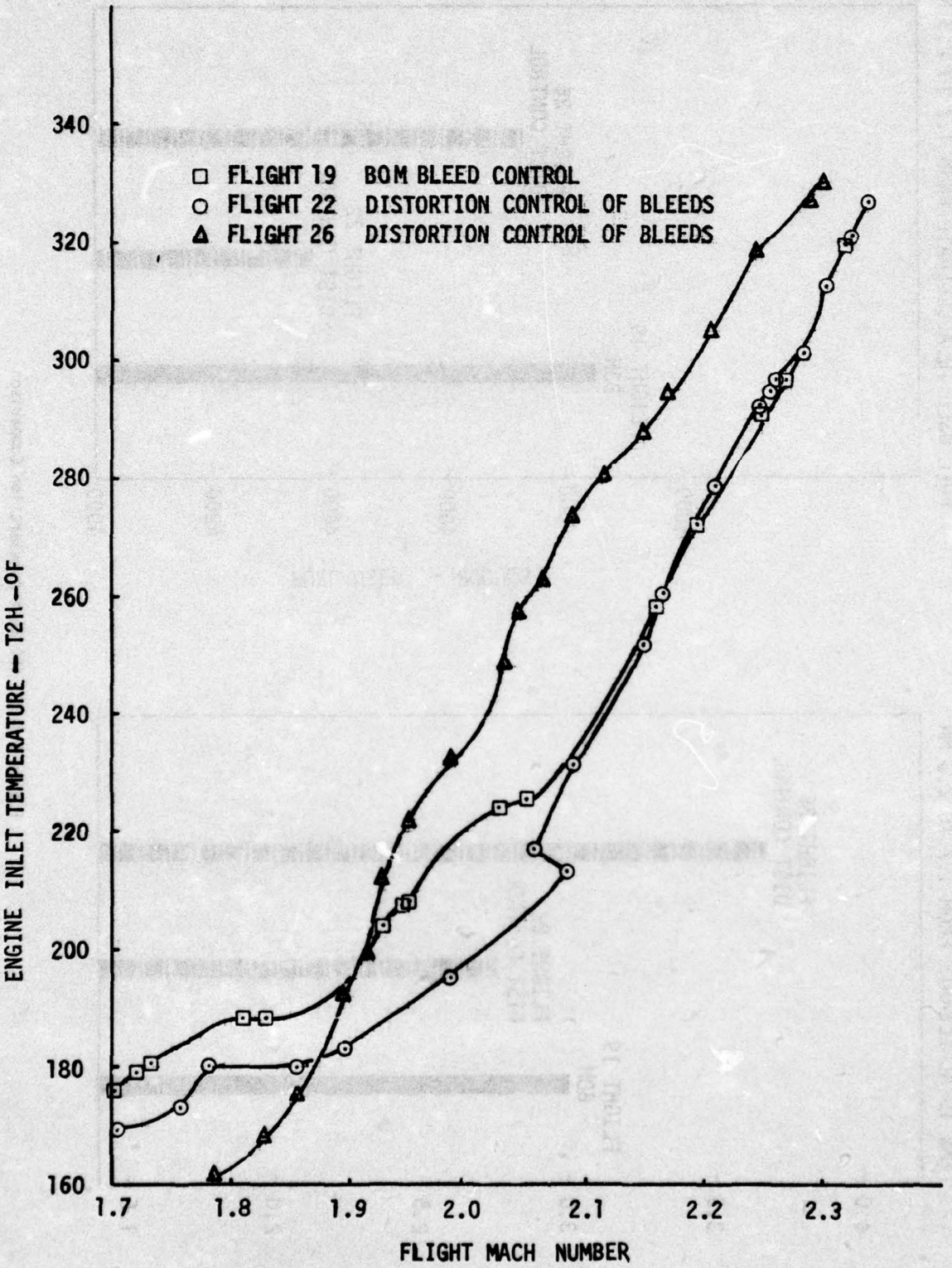

Figure 6.5-11 Engine Inlet Temperature Variation During 650 Knot Acceleration

where: $\frac{\text{Excess Thrust}}{\text{Weight}} = \frac{\text{long acc}}{g} + \frac{\text{Rate of Climb}}{\text{Velocity}}$

and, from the flight data:

	Bleed Open	Bleed Closed
Average Airplane Weight, lb	60,000	60,000
Average Airplane Velocity ft/sec	1750	1750
Average Acceleration/g	.122	.135
Average Rate of Climb ft/sec	16.7	33.3
Therefore,		
Specific Excess Power, Ps	230	270

Since a similar thrust increase would result on the right hand engine if it too were controlled by the IPCS, the Ps would increase further to 310, representing a very significant 35% improvement. This increase in thrust also corresponds to an increase in service ceiling at this condition of about 3000 ft.

Manual inlet operation provided another source of distortion induced stalls. Figure 6.5-12 is a distortion time history for a cone angle transient. As the distortion increases first the 7th and then the 12th bleeds open. Once the 12th bleed opens a problem is apparent. Figure 6.5-13 illustrates the situation. As the distortion increased the 12th bleed opened. When the distortion decreased the sum of hysteresis and offset for 7th and 12th bleeds resulted in both bleeds closing at the same time. This eventually resulted in a stall because the bleeds were not open. An increase in either the offset or hysteresis would probably eliminate this problem. There was not sufficient test time after the increase in hysteresis to 300 to retest this flight condition.

During rapid manual cone induced stalls the distortion bleed control did not always succeed in opening bleeds prior to stall. This was due to a sudden spike in the high response distortion that was represented as a slower increase by the distortion signal. As shown in Figure 6.5-14, the slower increasing distortion signal was sufficient to command the 7th bleeds to open before the spike, but bleed actuation time (approximately 0.1 sec) delayed the bleed protection sufficiently to result in compressor stall. The distortion signal, ZKDS, was not designed to follow such rapid transients in distortion. It is not considered practical to actuate the bleeds in response to such a distortion spike.

The manual cone stalls are a somewhat artificial case. However, in another airplane attitude changes may present a similar problem. It is likely that some form of distortion signal compensation as a function of attitude or rate of change of attitude will be required.

FLIGHT 21

IPCS MODE

FLT 21 CONE EXPANSION DISTORTION CONTROL OF BLEEDS

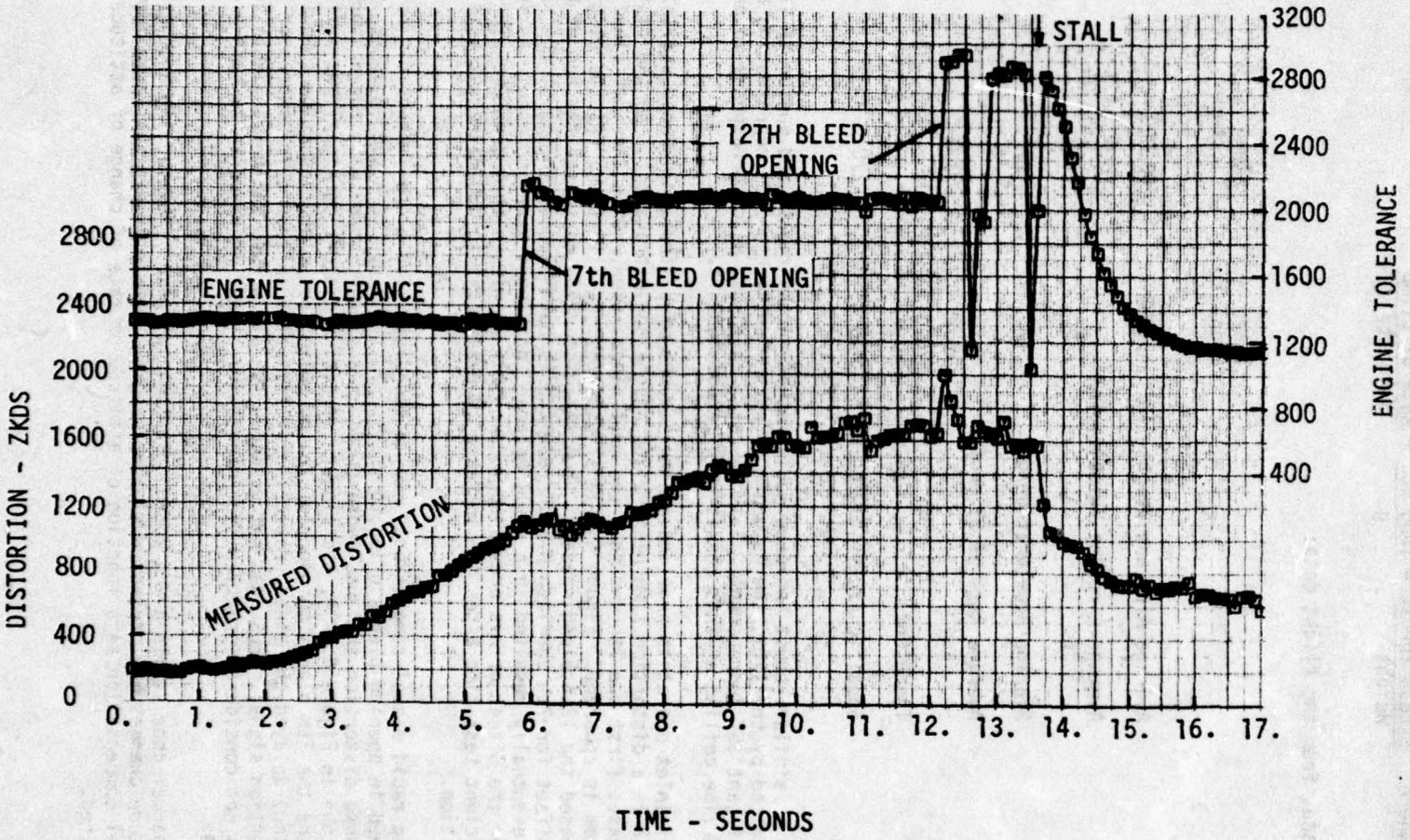

Figure 6.5-12 Manual Cone Induced Distortion

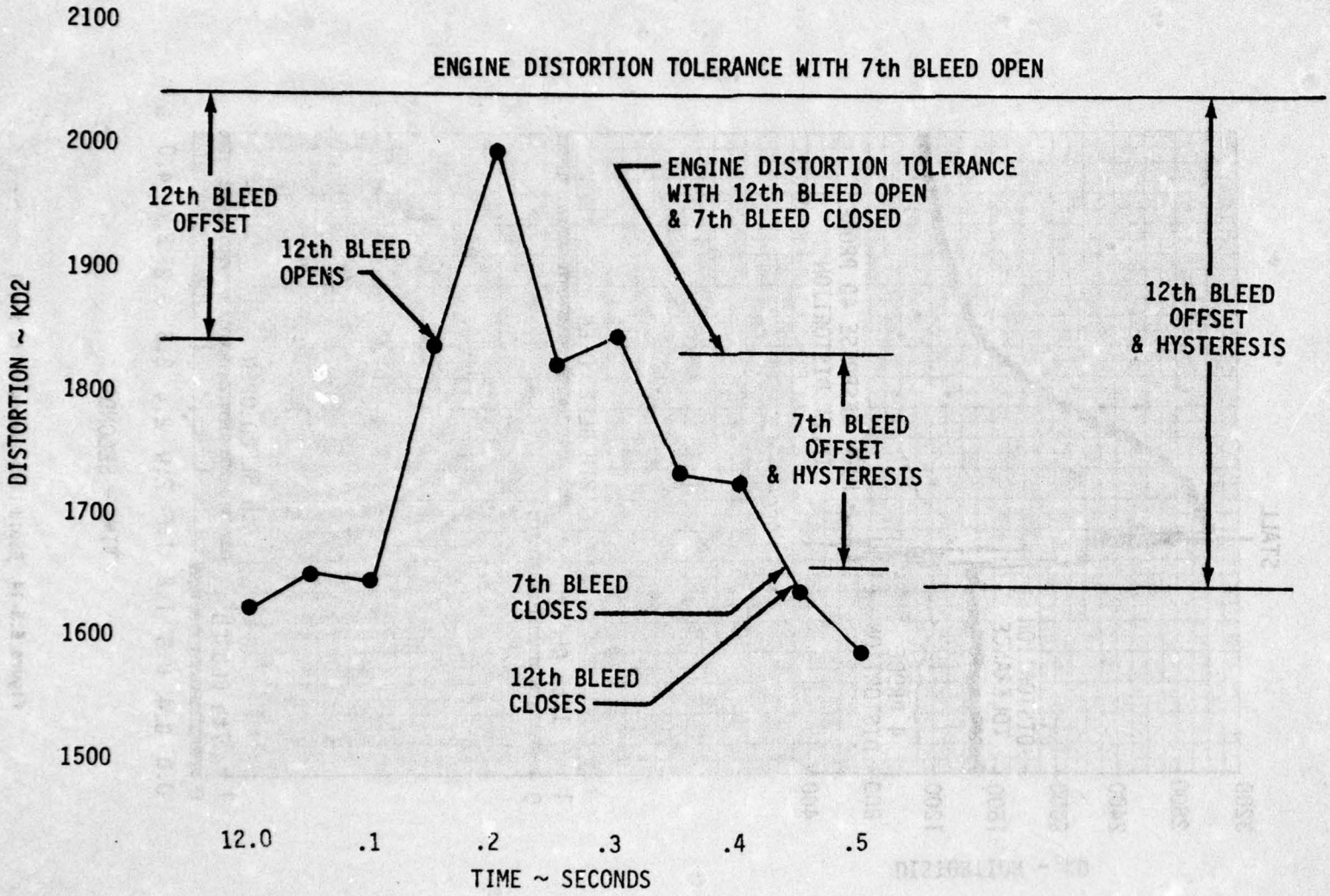

Figure 6.5-13 Bleed Cycling in Response to Distortion

FLIGHT 25

41K/1.4 MN IPCS CONE EXPANSION STALL

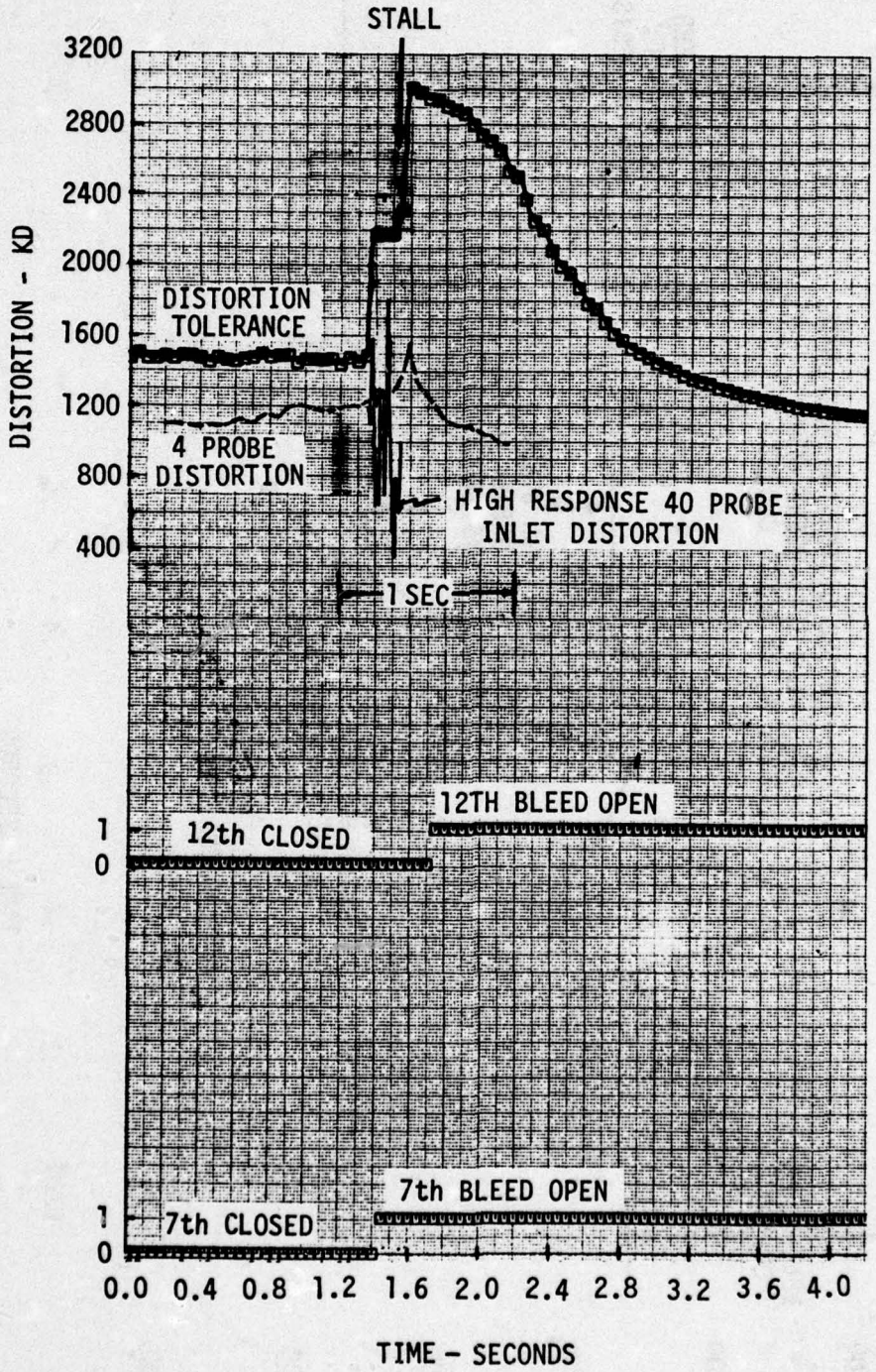

Figure 6.5-14 Rapid Cone Expansion to Stall

The IPCS distortion control was developed for an existing system. The inlet distortion pattern was known and repeatable. Engine tolerance was well documented, and an accepted distortion index existed. In a new airplane program the distortion control would have to be developed in parallel with the definition of the engine tolerance and the inlet patterns. This will certainly complicate the task, but the flexibility of a digital control will permit adjustment to the schedules during the test program. The testing on IPCS has shown significant potential engine thrust benefits to the use of distortion bleed control.

6.5.3 Airflow Bias, AFBIAS

The Airflow Bias Control demonstrated the ability to modulate the gas generator to match engine airflow to a reference airflow computed from inlet throat Mach number. Figure 6.5-15 depicts the relevant portion of the controller. A reference A*/A is computed based on Local Mach pressure ratio and compared to actual A*/A computed from engine corrected airflow and inlet geometry. The resulting error is passed through a deadband to reduce noise sensitivity, clamped to assure limited authority and finally inhibited for subsonic operation. It is then applied as a delta to the N2 command signal, thus only affecting engine operation when the engine control is in the N2 regulating mode.

In Section 6.1 provision is also shown for AFBIAS modulation of the inlet. Review of baseline test data showed no benefit to using this mode for the F-111E inlet. Hence, since the gas generator mode tests discussed below demonstrate the AFBIAS concept, the inlet mode was not exercised.

Performance of the gas generator AFBIAS loop was satisfactory. Typical responses of the loop to deliberately off design inlet configurations are shown in Figures 6.5-16 and 6.5-17. The cone is deflected by means of the manual inlet control to create an A*/A error. When the loop is enabled using the CMU sense switches, the engine responds by decelerating to reduce A*/A error. In the Mach 1.4, 45K case, response is well damped but steady-state error is relatively large. In addition to the evident steady-state error, half the AFBIAS deadband must be incorporated in the total error. At Mach 1.9 plant gain has increased reducing both stability and steady-state error. Scheduling compensation on XPOLE is not promising since burner pressure is essentially identical in the two cases. Scheduling compensation on EPR may provide useful results. Certainly in a system where an AFBIAS signal is used on more than a demonstration basis some form of compensation will be required. Performance may also be improved by reducing or eliminating the deadband.

6.5.4 Stall and Recovery Detection Loop

Control logic that automatically detects compressor stall and stall recovery was successfully demonstrated. This feature provided "hands-off" compressor stall recovery capability by sensing the stall; retarding the power lever and opening the bleeds; sensing the stall recovery; and advancing the throttle and closing the bleeds. Stall detection was accomplished with a burner pressure decay rate threshold (Figure 6.5-18), and stall recovery was detected with a burner pressure boundary which varied with engine inlet pressure (Figure 6.5-19).

The stall loop was tested at the 41000 feet/1.4 MN condition where the inlet cone was expanded until compressor stall occurred (Figure 6.5-14). The stall generated a burner pressure decay rate of 480 psi/sec (Figures 6.5-18 and 6.5-20) which was above the stall threshold thus indicating the presence of a stall. Burner pressure also dropped below the recovery threshold, and one second later, the control power lever was commanded to idle and both compressor bleeds were opened (Figures 6.5-19 and 6.5-21). The one second delay was incorporated to allow for the possibility of a quick self-recovery. If burner pressure had returned above the threshold within the first second, no corrective action would have been taken. This one second delay was an arbitrary selection and may be different for another propulsion system. By opening bleeds and reducing fuel flow, the control provided conditions favorable for recovery, but it did not directly control stall recovery.

The one second delay before reducing power lever angle after stall can increase the risk of overtemperature if recovery is not accomplished in that first second. Figure 6.5-21 compares turbine inlet temperature during stalls at the same condition with and without a one second delay before power lever retard. Fuel flow initially dropped even without power lever retard because of the rapid drop in Pb (Wf = Wf/Pb x Pb). The one second delay before retarding the power lever resulted in a 0.6 second longer overtemperature.

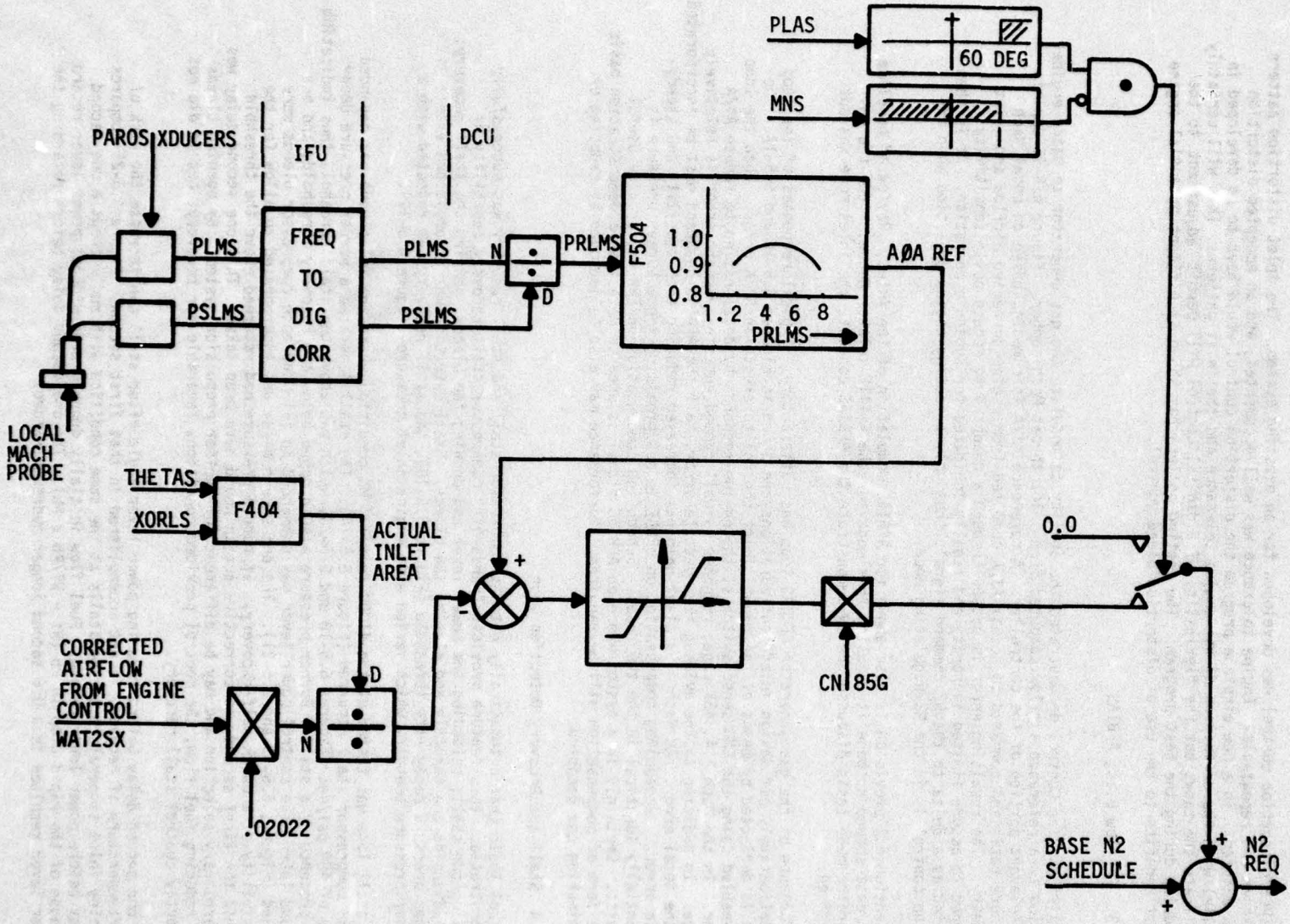

Figure 6.5-15 AFBIAS Control Loop

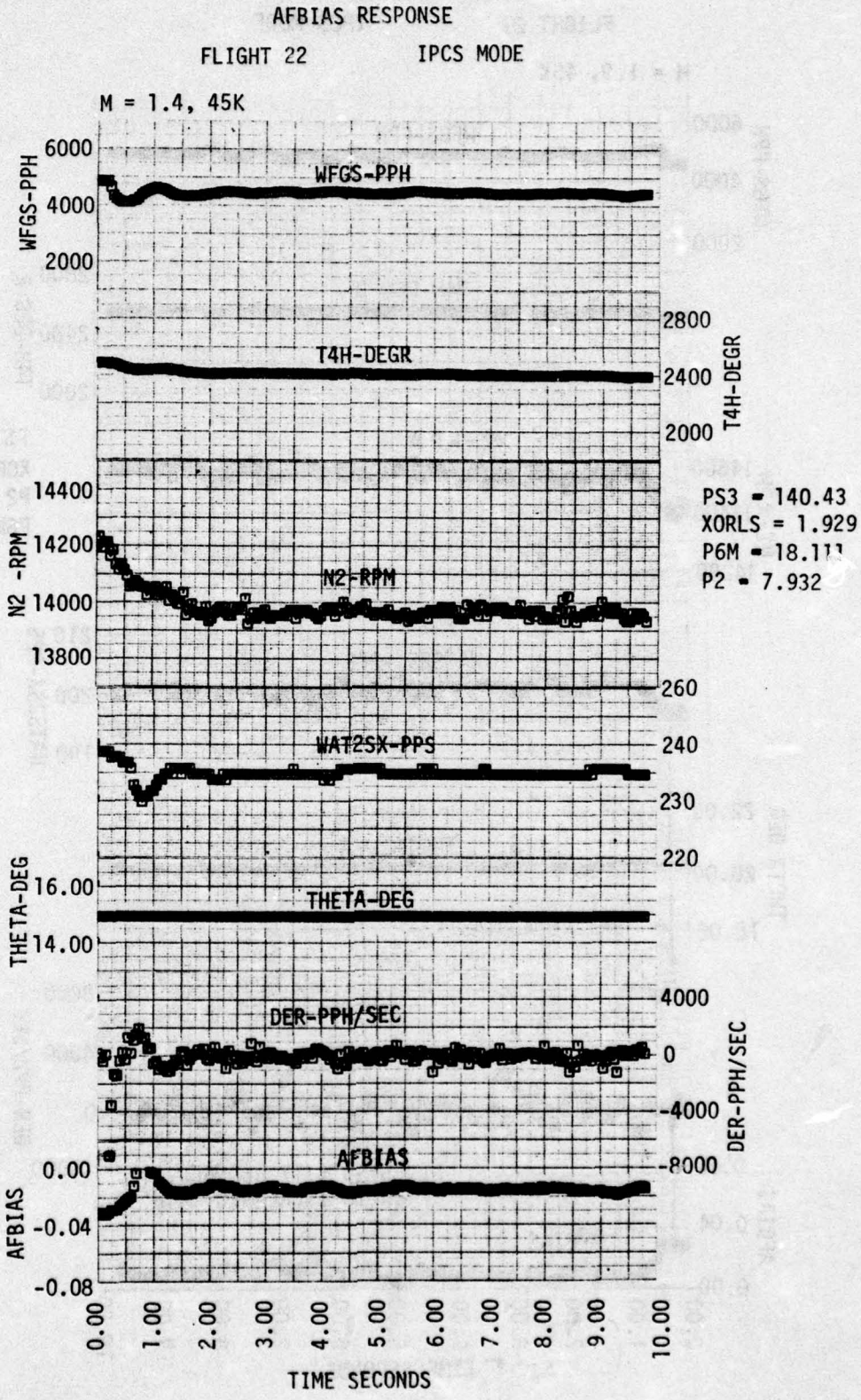

Figure 6.5-16 AFBIAS Response at Mach 1.4

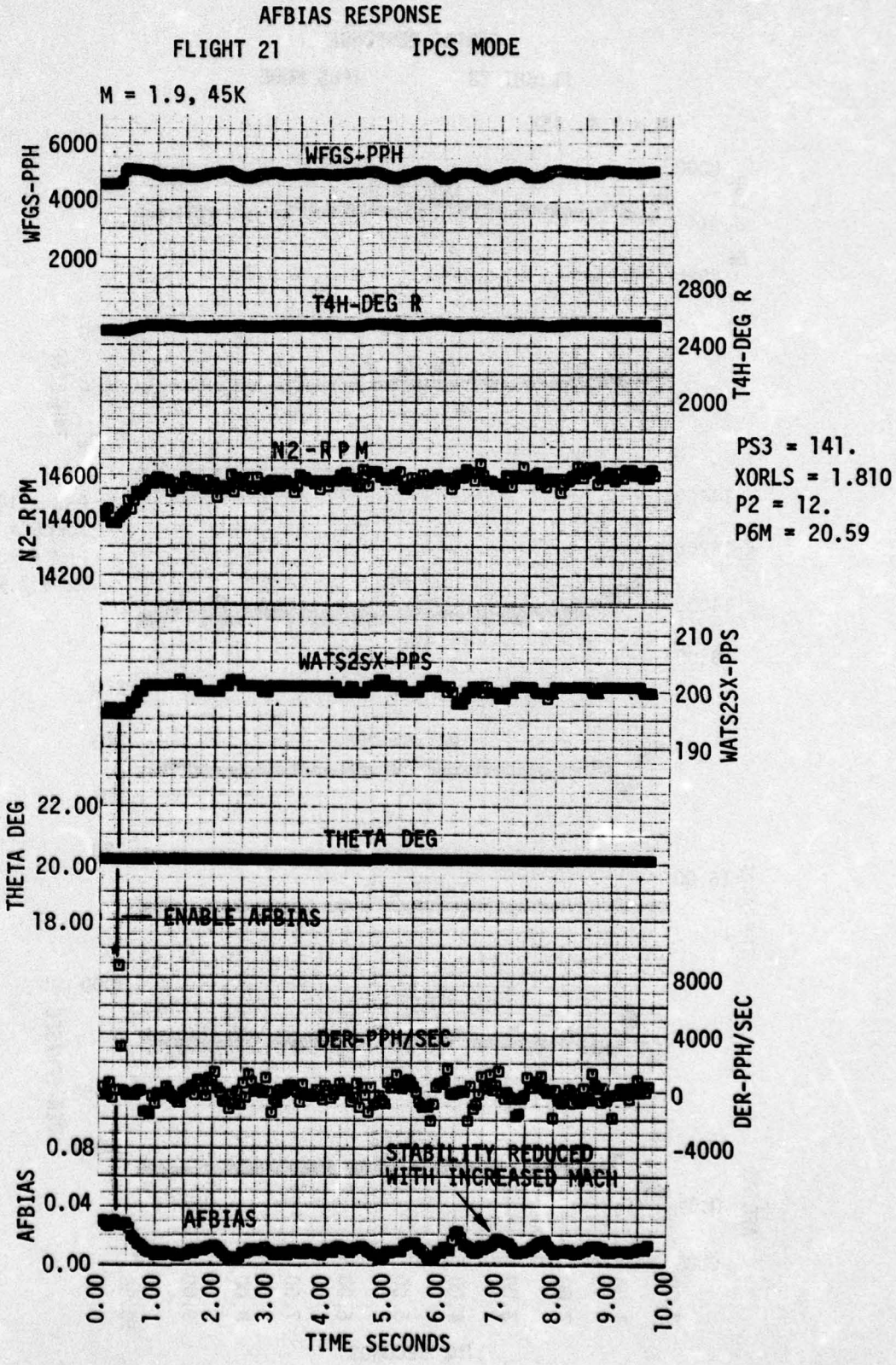

Figure 6.5-17 AFBIAS Response at Mach 1.9

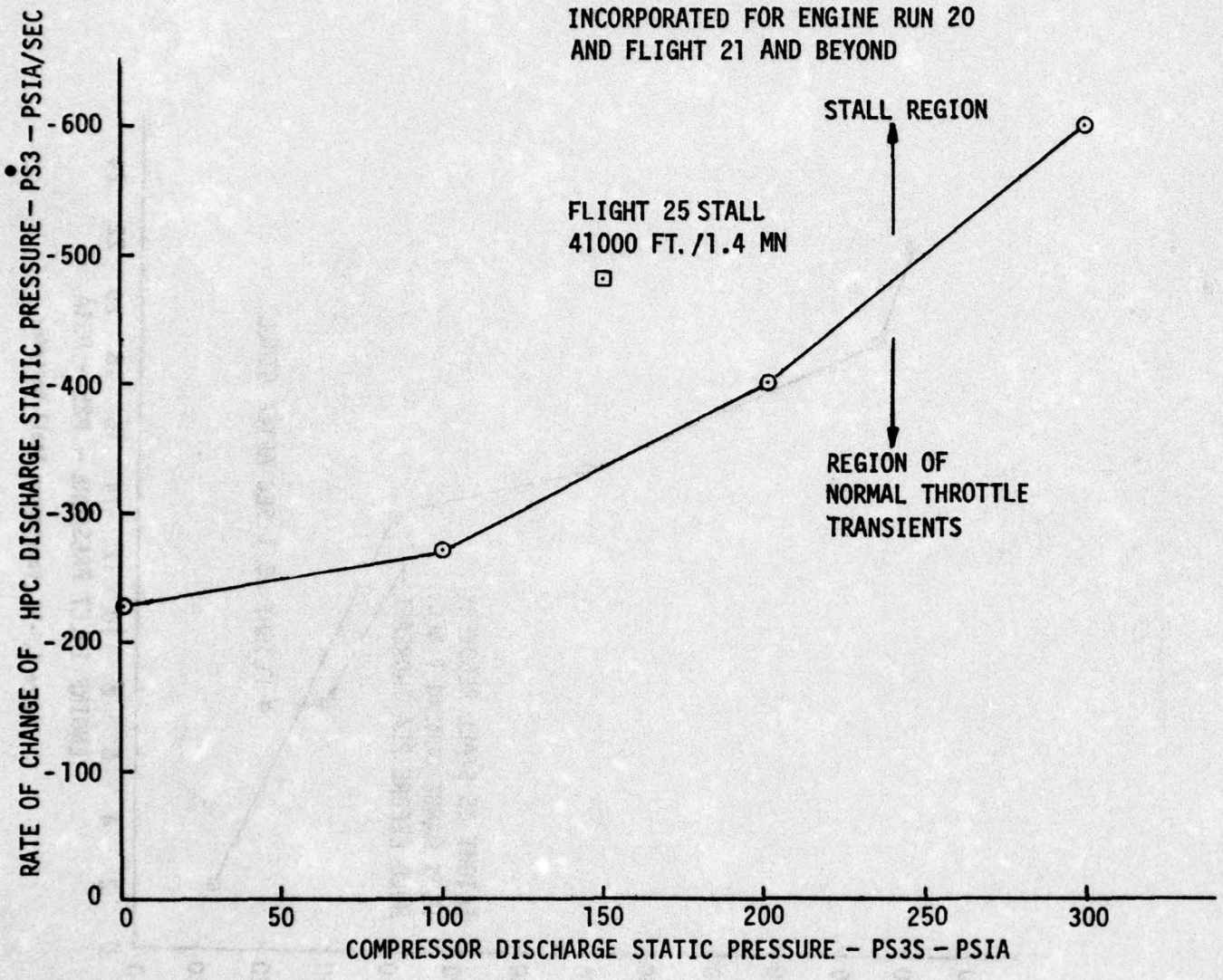

Figure 6.5-18 Compressor Stall Detection Threshold

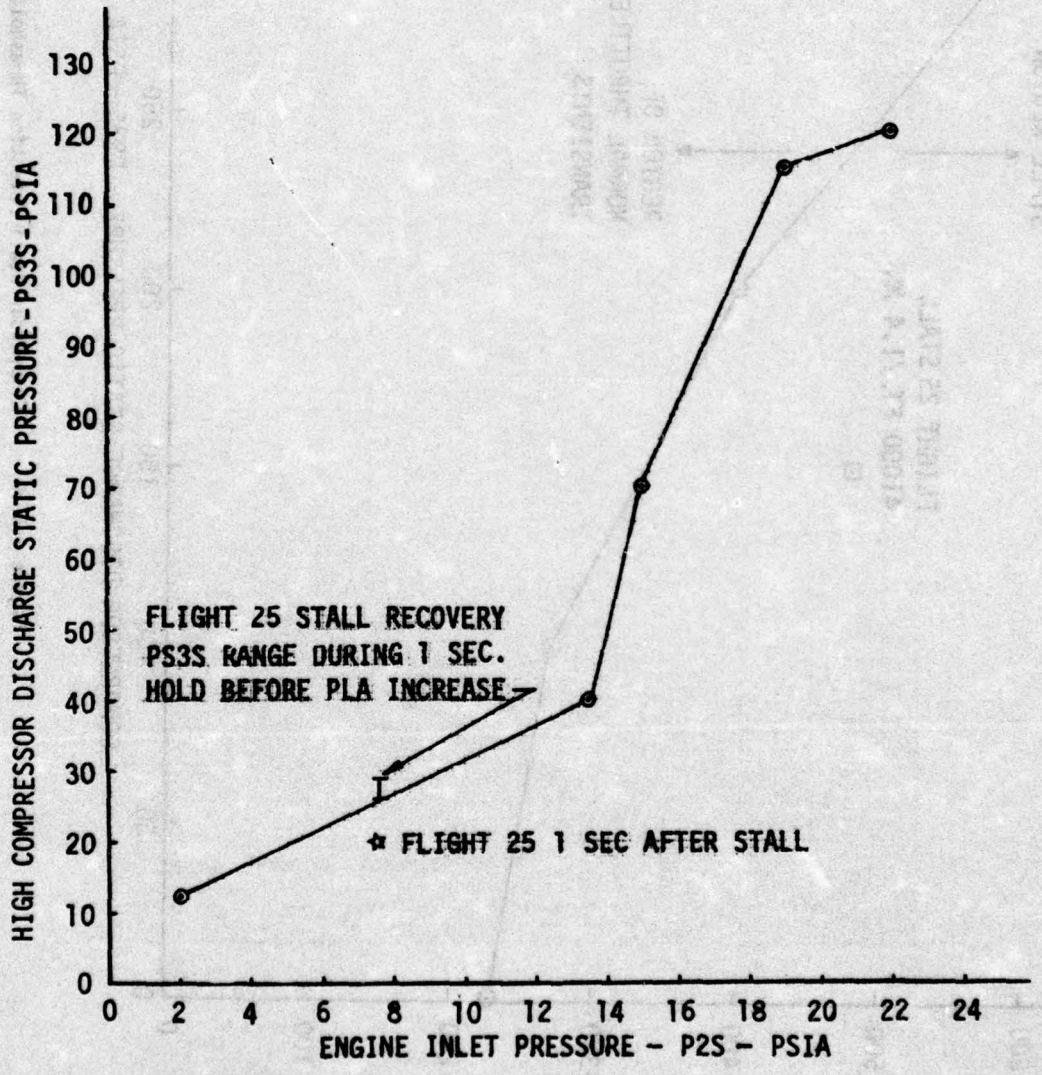

Figure 6.5-19 Compressor Stall Recovery

FLIGHT 25

41K/1.4 MN IPCS CONE EXPANSION STALL

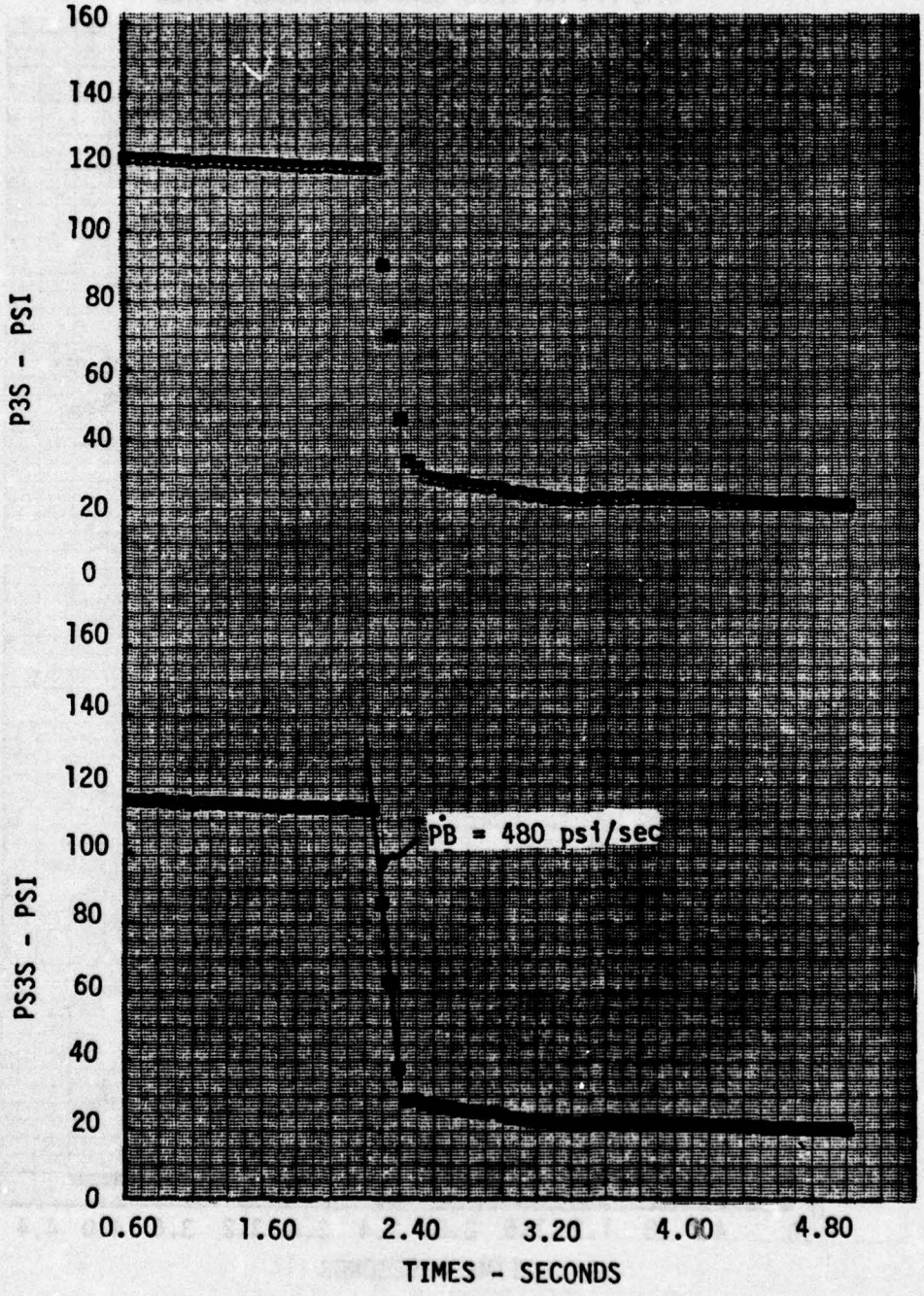

Figure 6.5-20 PS3S Decay Rate Following Stall

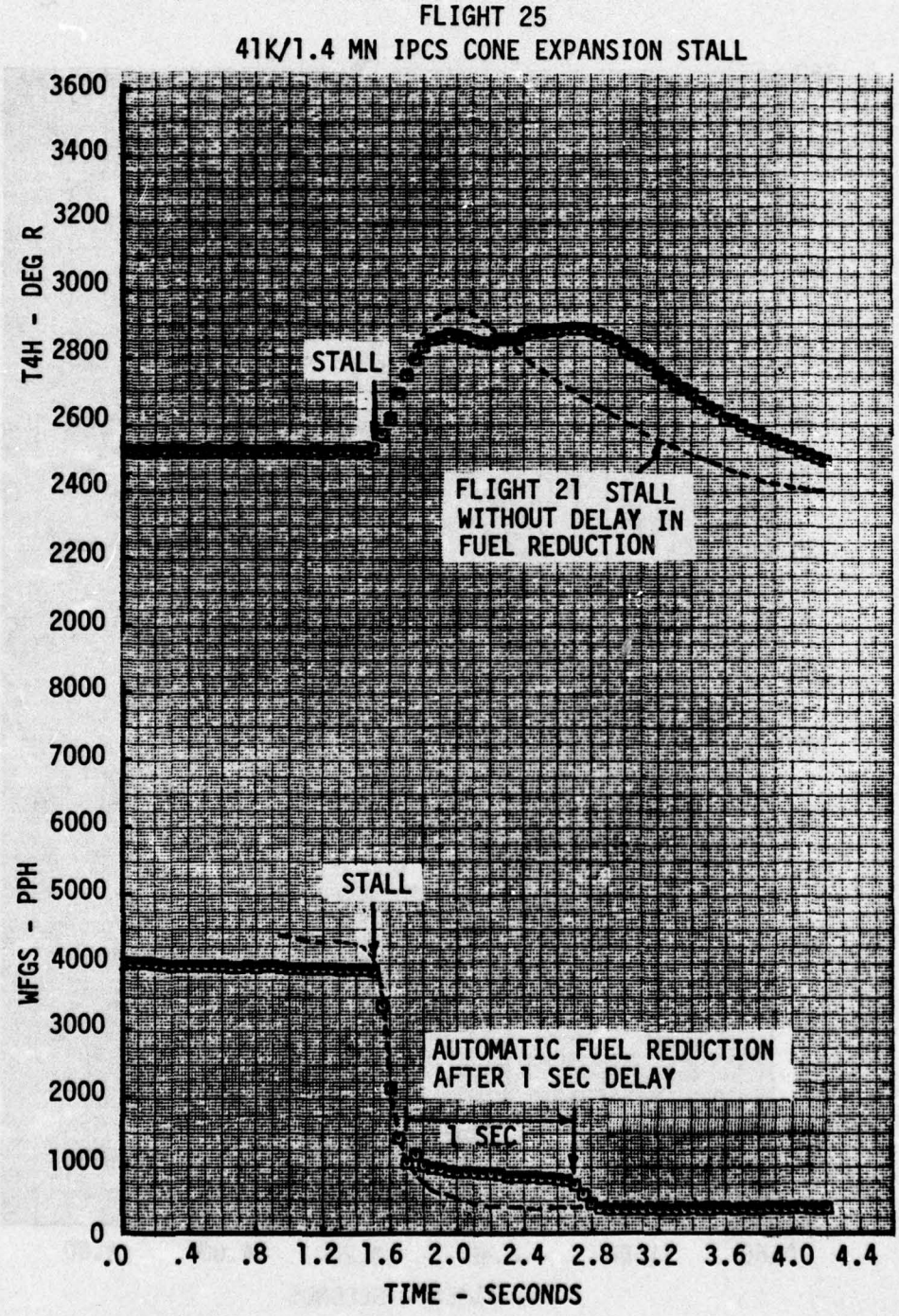

Figure 6.5-21 Stall Detection

The 50° higher peak temperature for flight 21 without the delay was probably caused by a higher initial fuel flow. Peak temperatures during stall can be expected to vary with fuel flow level before stall and fuel scheduling after stall.

Stall recovery occurred approximately 35 seconds after stall. Recovery was detected when burner pressure returned above the recovery boundary (Figure 6.5-22). Again, a one second delay was used to ensure the recovery process was stable before advancing the control power lever to its pre-stall position. An active afterburner blowout sensor prevented closure of bleeds and return to A/B power during this event. The logic was corrected later to clear the blowout sensor after stall recovery. As seen by the constant pilot throttle position during this event, the control automatically performed functions normally performed by the pilot to clear compressor stall.

6.5.5 Autothrottle

The autothrottle is discussed in Section 8.1.5.3 incorporating a block diagram of it, Figure 8.1-12. Initial flights were made with limited authority and low gains since no simulation capability was available to support development. Performance of the final system configuration is depicted in Figure 6.5-23. Given the demonstration nature of the loop and the total lack of analytic tools, loop performance is excellent. Response is nicely damped and response times are limited primarily by airplane acceleration capability which suffers by the IPCS ability to control the left hand engine only. Operation subsonic and supersonic is similar, apparently indicating the "XPOLE" compensation used in the autothrottle forward loop is beneficial. Unfortunately the opportunity to test with and without this compensation was not available.

Opportunities exist for improving the loop performance. The slight steady state offset in Figure 6.5-23 results from offsets in the lead-lag and integrator implemented in the software. These are reduceable by using double precision arithmetic. Since no absolute performance requirement existed for the system this was not pursued. Limit cycles around engine non linearities, primarily A/B zone turn on, were anticipated. With the exception of zone 1, where valve chatter due to noise as the PLA command passed through 69° was evident, no such problems arose. Such difficulties are readily resolved if the autothrottle has access, as it did in IPCS, to all engine control variables. The IPCS autothrottle with its purely electronic loop closure eliminated limit cycles resulting from mechanical linkage non-linearities frequently found in autothrottles mechanically coupled to the PLA linkage.

6.6 NOISE TESTING

6.6.1 Background

Duct burning and mixed burning engine configurations produce substantially different jet velocity profiles. In the mixed burning engine, like the TF30, the afterburner is downstream of the turbine and afterburning takes place across both the fan and core streams (Figure 6.6-1). At maximum afterburning this produces a relatively uniform profile. The duct burning engine with afterburning only in the fan stream and separate nozzles has a high velocity outer layer around a low velocity core. Figure 6.6-2 illustrates the profile differences.

Model testing simulating these profile differences have shown significant noise reduction for the duct burning profile. Noise reduction is a prime consideration in any supersonic transport development program. Since the duct burning configuration appears suitable for a supersonic transport there was considerable interest in substantiating the model test results. Both ground test and flight test data were needed to eliminate the concern that airplane velocity effects might reduce or eliminate noise benefits demonstrated in ground tests. By mid January the IPCS control was mature enough to consider significant control changes to achieve additional program objectives. Two months of flight test experience had established both the IPCS control mode and the software change control and test procedures.

In the TF30 engine there are five afterburner zones, three in the fan flow and two in the core flow. The outer core zone is turned on first, followed by the three fan zones. Thus at maximum zone 4 afterburning most of the burning is done in the fan stream yielding a profile somewhat similar to the duct burning engine. Obviously the TF30 could not achieve the high velocity ratio possible with no core burning and high fan nozzle pressure ratio of a duct burning engine. However, the test offered an opportunity for an inexpensive flight evaluation of the concept.

FLIGHT 25

41K/1.4 MN IPCS CONE EXPANSION STALL RECOVERY

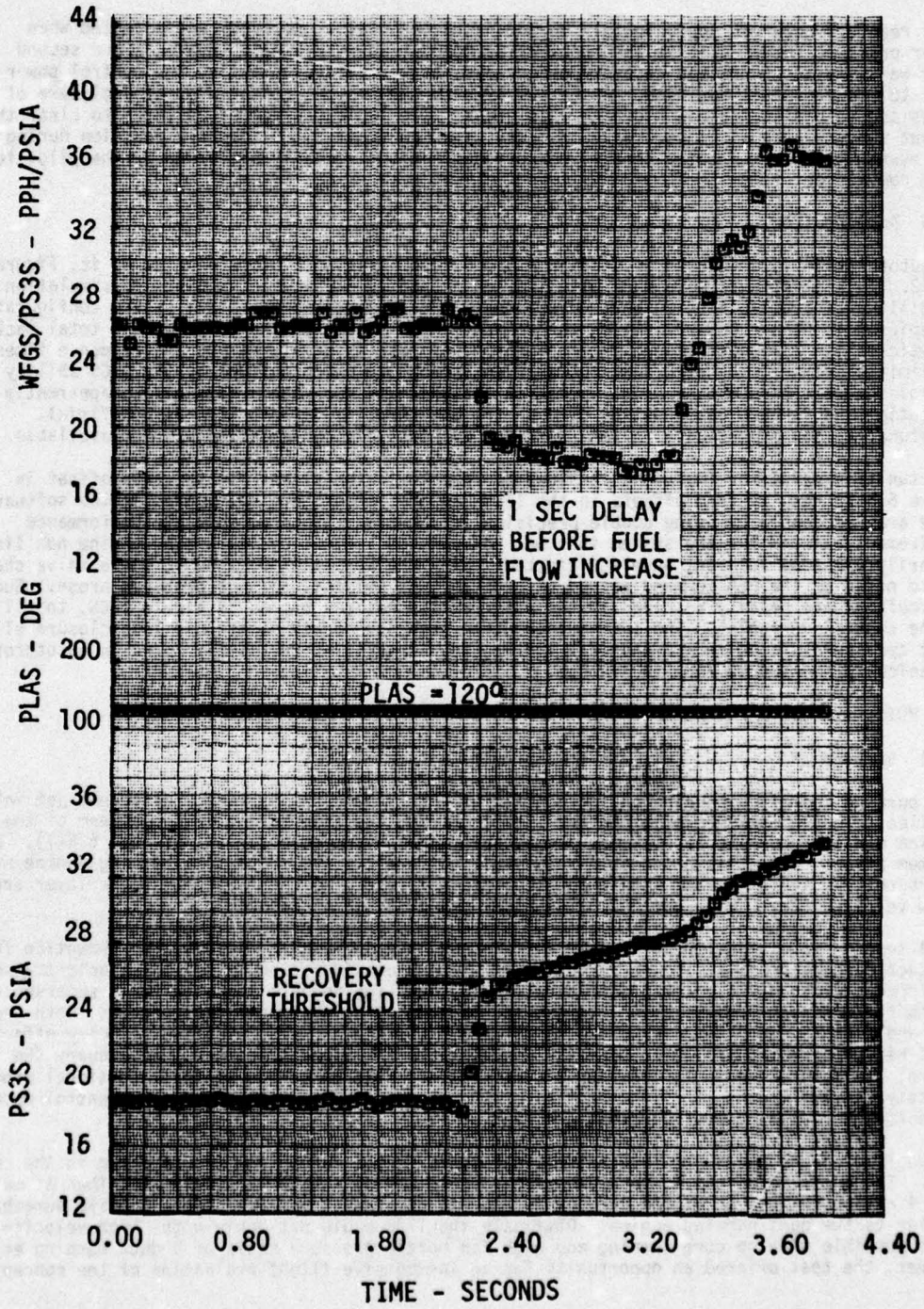

Figure 6.5-22 Stall Recovery Detection

FLIGHT 28

▫ 30K/0.8 MN AUTOTHROTTLE

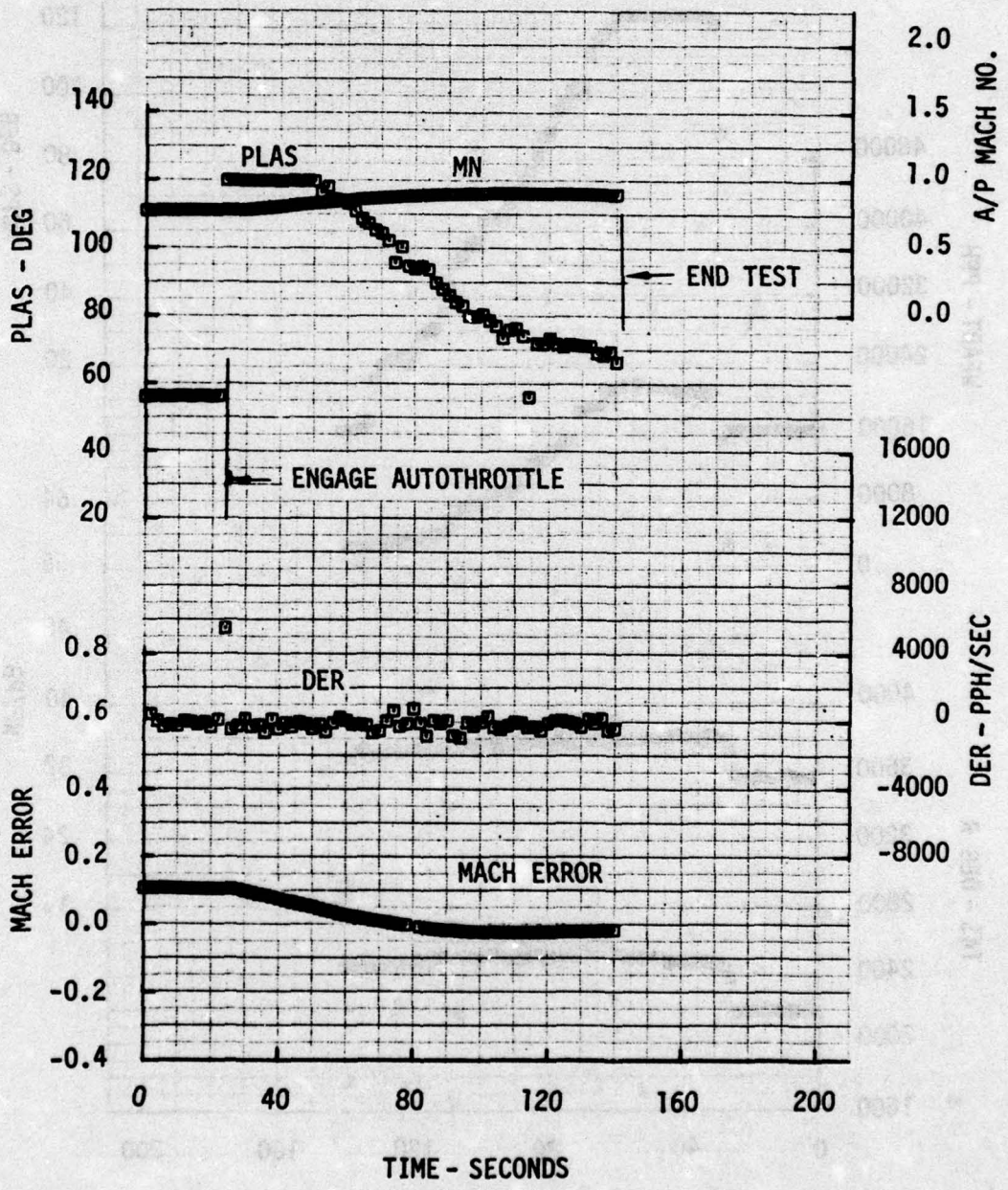

Figure 6.5-23a Autothrottle Performance

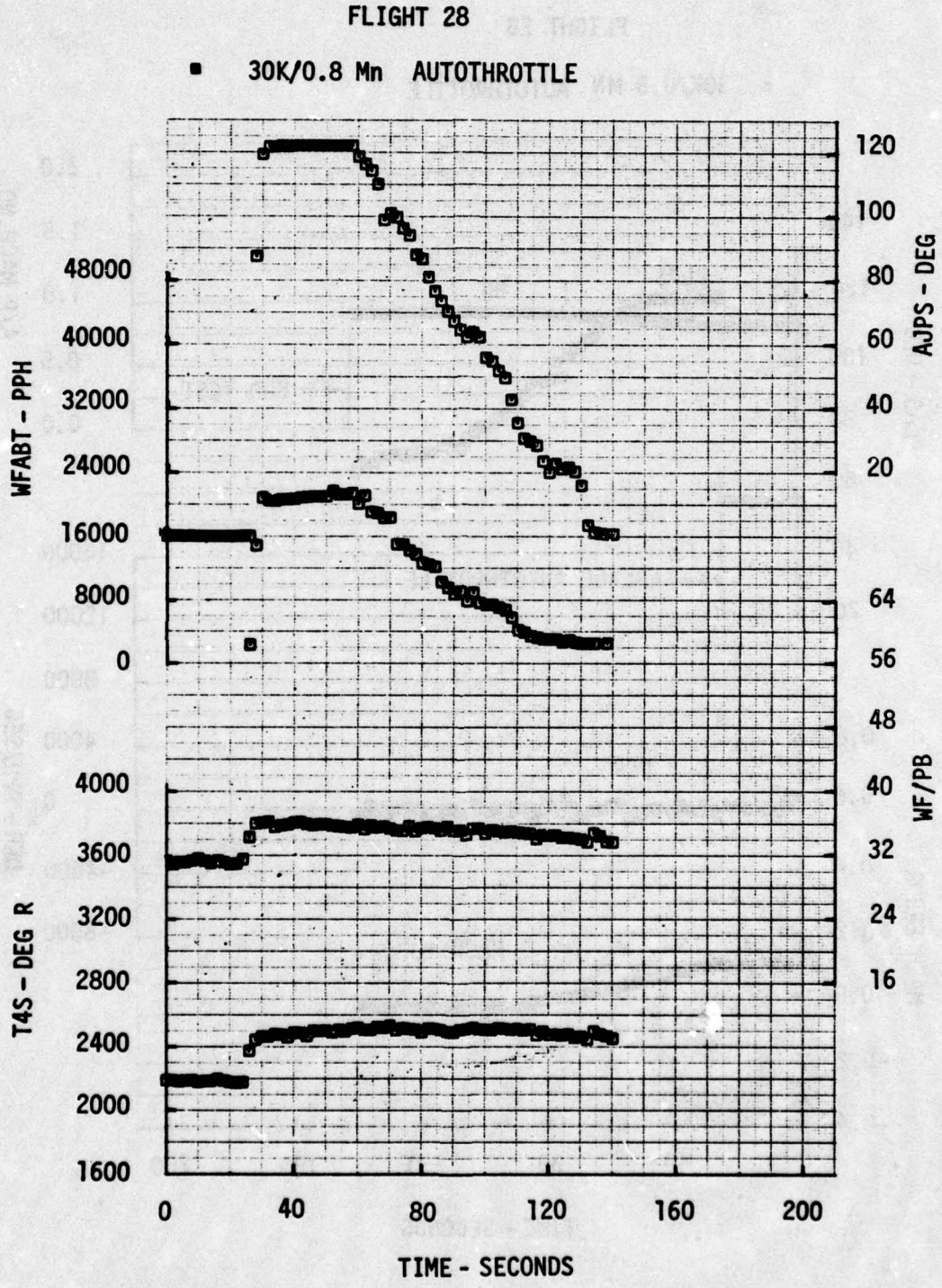

Figure 6.5-23b Autothrottle Performance

MIXED BURNING ENGINE

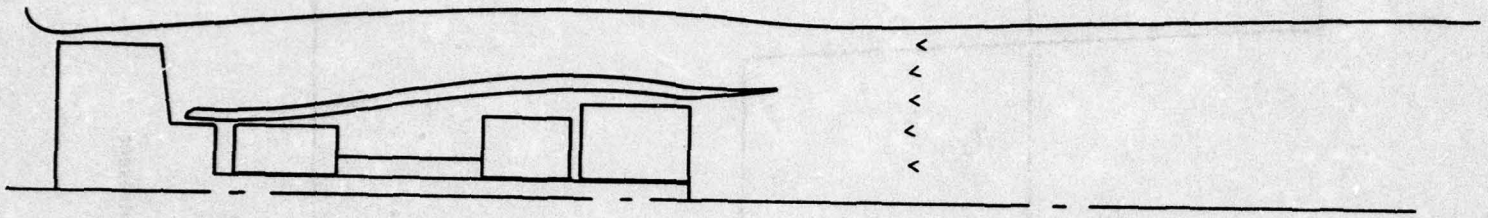

DUCT BURNING ENGINE

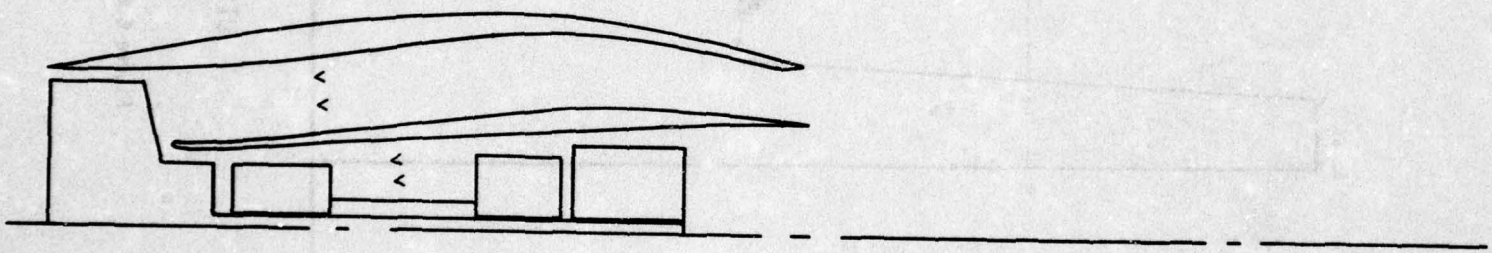

Figure 6.6-1 Afterburner Configurations

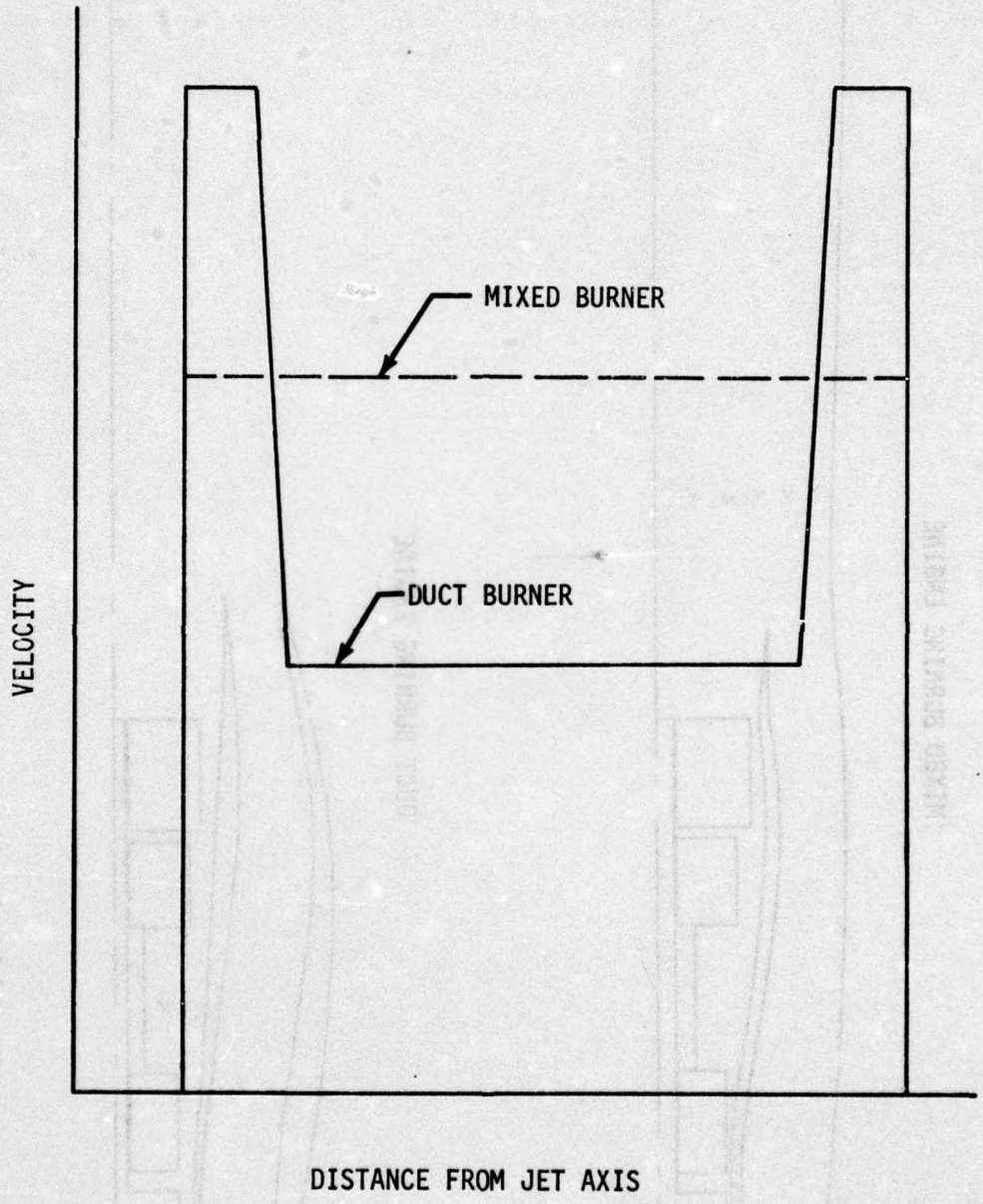

Figure 6.6-2 Velocity Profile Comparisons

6.6.2 Configuration and Procedures

Consideration was given to two modifications to the normal afterburner configuration to increase the velocity ratio, reduction or elimination of the zone 1 fuel flow and increase in the zone 4 (outer fan zone) fuel flow. As either modification represented significant deviation from the established afterburner configuration careful consideration had to be given to the possibility of afterburner damage. After reviewing available experience on non-production TF30 afterburner operation at P&WA, NASA, and the Air Force the following conclusions were reached:

1. increasing the zone 4 fuel flow would incur too great a risk of burning the afterburner liner,
2. decreasing or turning off the zone 1 fuel flow appeared unlikely to result in serious problems,
3. the IPCS rumble detector should be active for all non-production A/B operation to shut down the A/B in the event of rumble,
4. vibration sensors should be monitored during the initial ground running to see if the non-production configuration increased vibration levels.

The IPCS control software was modified to provide the necessary capability to reduce and shut off zone 1 and to reduce all 5 zones to provide the same thrust level as zone 4 (para 8.1.5.1). An additional capability was included to adjust the N2 setpoint during A/B operation. This varied the total airflow and as a result the nozzle pressure ratio. This capability was needed to achieve the same nozzle pressure ratio in flight as in the ground testing. The software and procedures evolved over a series of engine runs. Table 6.6-1 presents the procedures used in the majority of the noise testing. For crew convenience the trim pots were labeled as follows (Figure 4.1-3):

IDLE TRIM	Z1
MIL TRIM	EPR
A/B TRIM	AJ

Table 6.6-1 Noise Test Procedures

I. MAX Zone 4 (Non-Uniform Profile)
   A. Normal Max Zone 4
      1. PLA to Mil
      2. Sense switch 10
      3. Verify all trim pots full clockwise
      4. PLA to Max
      5. Record data
      6. PLA to Mil

   B. MAX Zone 4 with Zone 1 Downtrimmed
      Repeat 1 - 4
      5. Turn zone 1 pot full counter clockwise
      6. Record data
      7. PLA to Mil
      8. Zone 1 pot full clockwise
      9. Sense switch 0

   C. MAX Zone 4 with N2 Downtrim
      Repeat 1 - 4
      5. If Zone 1 downtrim required turn zone 1 pot full counterclockwise
      6. Turn the EPR pot to the specified EPR
      7. Record cockpit AJ
      8. Record data
      9. Throttle to MIL
      10. EPR pot full clockwise
      11. Zone 1 full clockwise
      12. Sense Switch 0

II. MAX A/B (Uniform Profile)
   A. MAX A/B Downtrimmed to MAX Zone 4
      1. PLA to Mil
      2. Sense Switch 0
      3. Verify all pots full clockwise
      4. PLA to Max (A/B stable)
      5. Sense switch 17
      6. Turn AJ pot to specified cockpit AJ (Match area from IA or IB)
      7. Record data
      8. Throttle to Mil
      9. Aj pot full clockwise
      10. Sense switch 0

   B. MAX A/B Downtrimmed with N2 Downtrim
      Repeat 1 - 5
      6. Turn EPR Pot counterclockwise to specified PER
      7. Turn Aj pot to specified cockpit AJ (Match AJ from IC)
      8. Record data
      9. Throttle to Mil
      10. EPR pot full clockwise
      11. Aj pot full clockwise
      12. Sense switch 0

6.6.3 Testing

Four different kinds of tests were required - ground noise measurement, thrust measurement, exhaust jet profile measurement, and flight noise measurement. The initial testing was devoted to thrust and noise measurement on the ground. Engine runs 26 and 28 were conducted on the Edwards thrust stand. It was necessary to measure thrust since noise reduction at the same thrust is the relevant comparison parameter. The intent of the early testing was to determine whether or not measurable noise reduction could be achieved within the configuration constraints and halt the noise testing if not. These initial runs did indicate sufficient noise reduction to warrant continued testing. The thrust data also demonstrated that nozzle area is a good indicator of relative thrust. Thus regardless of afterburner configuration matching nozzle area resulted in matched thrust. This formed the basis for the procedures used in most of the noise testing in which direct thrust measurements were not available. The vibration sensors showed no increase in vibration due to the non-production configurations.

Noise measurements were made at 35 and 105 foot sideline distances from the jet centerline over a flat, concrete surface. Engine run 33 provides most of the noise data. This is the run with the same control configuration as the noise flight and velocity profile run. Table 6.6-2 lists the configurations for which noise data were taken. These data will be supplemented with data from engine runs 26 and 28. Rumble was a problem on two configurations. Rumble always occurred on an attempt to shut off zone 1 so this configuration was dropped. The Max A/B downtrimmed to match the area from max zone 4 with zone 1 downtrimmed was marginal on rumble, but ground data were obtained for this configuration.

Flight 27 was a noise flight. Passes were made over the microphones at 250 KTS and 400 feet. For most A/B configurations the airplane accelerated even with the right hand engine at idle. Therefore, the speed brake was used to reduce the acceleration. Table 6.6-3 lists the configurations tested. Rumble was detected during one test point at max A/B with the fuel flow downtrimmed to a cockpit nozzle area readout of 7.8, attempting to match max zone 4 with zone 1 downtrimmed. One additional rumble occurred going into max A/B. A repeat of the transient did not cause rumble.

Jet profile measurements were made with the rake described in paragraph 5.1.4. This testing produced total pressure and temperature profiles for the following configurations: Idle 76%, 82%, 88%, 92%, Mil, Zone 1, Zone 2, Zone 3, Zone 4, and Max A/B with a normal afterburner configuration, Max Zone 4 with Zone 1 downtrimmed and Max A/B downtrimmed to match the Max zone 4 nozzle area. The only difficulties encountered during this run involved the survival of the probes on the rake as described in paragraph 5.1.4.

Table 6.6-2 A/B Configurations

For Engine Run 33 Noise Data

1. Mil
2. Max Zone 4
3. Max Zone 4 with Zone 1 downtrimmed
4. Max Zone 4 with Zone 1 downtrimmed and EPR downtrimmed to 2.0
5. Max A/B
6. Max A/B downtrimmed to match the Max zone 4 area
7. Max A/B downtrimmed to match the area for configuration 3
8. Configuration 6 downtrimmed to EPR = 2.0
9. Configuration 7 downtrimmed to EPR = 2.0

Table 6.6-3 A/B Configurations

For Noise Flight

1. Mil
2. Max. Zone 5
3. Max Zone 4
4. Max. A/B downtrimmed to MAX Zone 4 Aj
5. Max. Zone 4 with Zone 1 downtrimmed
6. Gas Generator EPR = 1.74
7. Max Zone 5, N2 downtrimmed to EPR = 1.84
8. Max Zone 4, N2 downtrimmed to EPR = 1.84
9. Max Zone 5, N2 downtrimmed to EPR = 1.84, downtrimmed to match the Aj from configuration 8
10. Max Zone 4, Zone 1 downtrimmed with N2 downtrimmed. EPR = 1.84
11. Max Zone 5, N2 downtrimmed to EPR = 1.84 downtrimmed to match the Aj of configuration 10

6-10 were repeated

6.6.4 Results

Analysis of the data from the noise testing is being conducted separately from the IPCS program. This analysis is still underway at the writing of this report. Preliminary analysis indicates the desired profiles were approximated and that some noise reduction was achieved. Figure 6.6-3 presents preliminary velocity profile data.

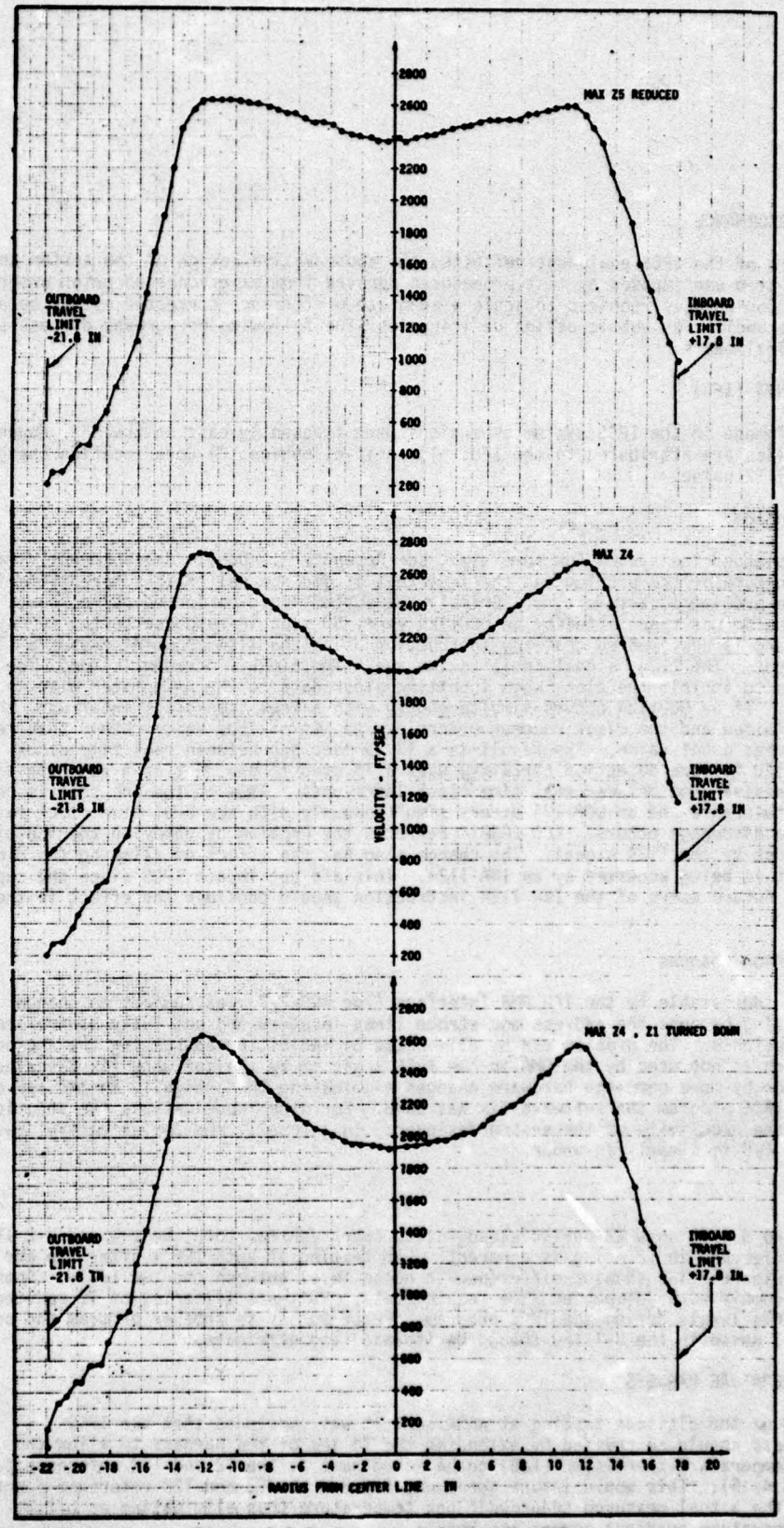

Figure 6.6-3 Exhaust Velocity Profiles

7.0 HARDWARE PERFORMANCE

Reliable operation of the IPCS equipment reflected the conservative design of the system and precautions in system use imposed by test procedures derived from experience on prior programs. System configuration changes required to achieve adequate performance corrected either mechanical damage due to mishandling or subtle design deficiencies. The following paragraphs discuss such changes on a topical basis.

7.1 INTERFACE UNIT (IFU)

As the central element in the IPCS system aspersions were frequently cast on the IFU. However, only three anomalies are attributed to the IFU: 1) Auto-disengage; 2) Core location changes in Section 0, 3) T2 noise.

7.1.1 Auto-disengage

Auto disengages plagued the system for some time, see Appendix A. Due to the apparently random warm up related nature of the problem and the fact that it did not halt flight operations final resolution of the problem took some time. Briefly the system logic performed as follows: A PCM frame synch pulse was transmitted by an OCP1124 every 50 msec in response to the PCM system. The DIO decode card is designed so that any instruction using the 1124 argument causes a 1124 signal to be output. The 1124 signal inhibits the real time clock (increment) line. The intent of this is to inhibit the clock when inputting clock data to the A Register with an INA 1124 instruction. If an OCP1124 occurs simultaneously with a real time clock interrupt, the interrupt is inhibited and the clock counter underflows to its maximum value rather than resetting to the preset 5 msec count value. The result is a 13.19 msec gap between real time clock interrupts. The IFU failure detection circuitry uses a 15 msec ±3 one shot as a watchdog timer to check for excessive gaps between real time clock interrupts. Thus if the one shot is on the low side of its tolerance and an OCP1124 occurs simultaneously with the real time clock failure is detected and a disengage occurs. ECO-EG3314 corrects the problem by removing the inhibit of the real time clock by the 1124 signal. The change also has the effect of allowing the clock to increment when it is being accessed by an INA 1124. This did not impact IPCS since the capability was never used. Future users of the INA 1124 instruction should consider the effect in their system design.

7.1.2 Core Location Changes

The area of core addressable by the IFU DMA Interface (loc 400-777) was subject to change during power cycling because the address and strobe lines involved are not fully controlled during power transients. The problem can be eliminated by inhibiting addressing the region from 600-777 which is not used by the DMA in the IPCS logic or by the software fix described in Section 8.1.4.3 or by more complete hardware changes eliminating the ambiguity in the I/F data lines. For the IPCS program the software fix was used. For other applications the solution must be left to the proclivity of the system designer. In a totally new design careful review of this critical I/F is clearly in order.

7.1.3 T2 Noise

Figures 5.4-19 and 5.4-20 show T2 during steady-state operation for both the V-1 and V-2 IFU's. A significant difference in T2 noise is apparent. Lab testing of both IFU's after the end of flight testing, Figure 7.1-1 shows a difference in noise level between the two IFU's. Both units, however, comply with ATP performance requirements. Software filtering of T2 reduced the noise to negligible levels during the IPCS program. Prior to use in another program the source of this low level noise in the V-1 IFU should be isolated and eliminated.

7.2 ENGINE TEMPERATURE HARNESS

From the results of the altitude testing at NASA/LeRC it was concluded that the IPCS temperature harness should be revised by extending the T3 leg of the harness to allow the transducer box temperature thermistor (TJB) to be moved next to the T2 and T22 reference junction probe (Figure 5.4-15). This would insure agreement between the T2 and T22 reference junction temperature and the actual measured transducer box temperature thus eliminating an offset created by a temperature gradient across the box.

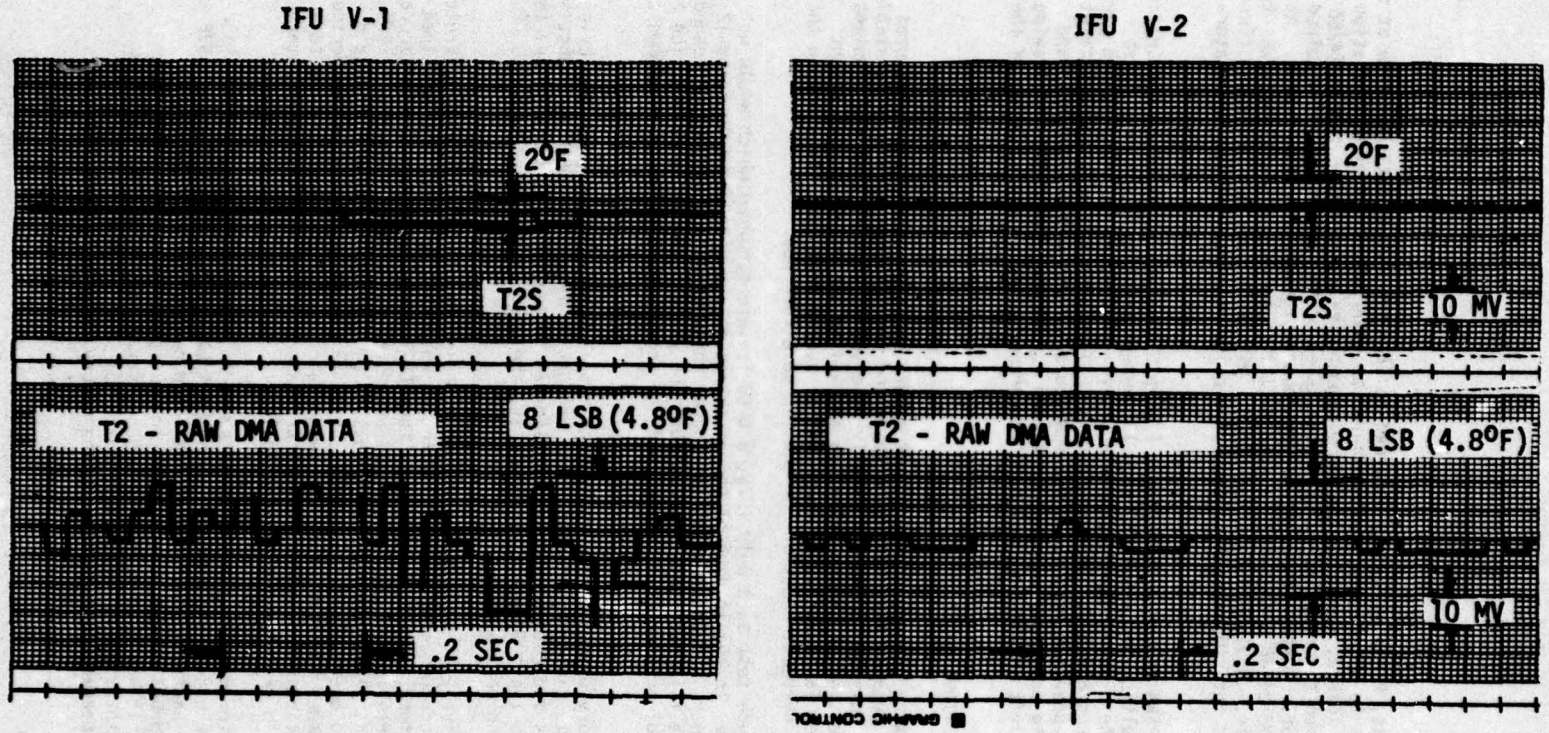

NOTE: T2 INPUT ON TSU SET TO 3.56 MV IN BOTH CASES. TRACES OFFSET TO PERMIT DISPLAY OF NOISE. DATA ARE OUTPUT VIA SPARE D/A CHANNELS.VOLTAGE GAIN FROM LOW LEVEL A/D THROUGH D/A IS 340.

Figure 7.1-1 IFU Noise Comparison

The old temperature harness, P/N 751170, was returned to P&WA from NASA/LeRC, modified at the vendor by adding 18 inches to the T3 leg, and delivered to NASA/DFRC. During installation of this revised harness, P/N 761515, a problem was encountered with a connector, P/N MS 24266 R12T 12P. The problem was traced to broken wires on the backside of the connector and required the purchase of a new connector. Installation of the new connector corrected the problem. At the same time connector, P/N MS 24266 R 10T5S (T22) also exhibited an open circuit which was traced to a broken wire on the pin. Replacement of the pin and wire resolved this problem. (Installation of the revised harness did not significantly reduce the noise or offset of the temperature signals).

A failure of the revised P&WA temperature harness, P/N 761515, occurred prior to the initial attempt of flight 18, resulting in an out of range T3 temperature signal and, therefore, abortion of flight 18. The problem was traced to a broken copper wire in the extended portion of the T3 leg of the revised harness. Because of this failure plus the existing T2 offset problem identified during previous flights, the temperature harness was disconnected and replaced with a solid state temperature reference system (Con-Ohmic) per NASA/DFRC drawing FS-C-0289. The harness was left in place to maintain the proper clipping and clamping of the other harnesses.

7.3 DCU V2 MEMORY MALFUNCTIONS

As recounted in the following paragraphs the DCU V2 memory suffered intermittent failures during the test program. Because the unit was a spare and the failures were non-repeatable, a minimum of time was spent pursuing them. As finally resolved it appears that the problems probably were the result either of excess vibration applied to the DCU V2 during Flight Assurance Testing (FAT) see Table 7.3-1, or "burn in" of hybrid circuits. Thus beyond the repair described below no corrective action is required on either DCU.

Near the end of the altitude test on 2 July 1975, a DPCU failure occurred which would not permit tapes to be loaded. In the loading of the bootstrap it was noted that location-12, bit-12 would not load as a "one". Subsequent testing showed that bit-12's could not be loaded. The unit "self healed" the following day. The malfunction was ascribed to a malfunction of the Computer Control Unit (CCU) because prior experience had shown some difficulty in communications between the CCU and DCU.

After a week of satisfactory operation the failure of Bit-12 loading reoccurred. Believing the CCU to be the most probable cause, a second CCU was brought in from NASA/ DFRC and substituted, the failure remained, thus indicating that the problem was in the DCU. As the altitude test was completed, further DCU tests were not performed and the DPCU was returned with its DCU V2 to Honeywell for repair and refurbishment.

The system was run extensively at Honeywell throughout the month of August 1975 in a fruitless attempt to cause the reoccurrence of the Bit-12 problem which had apparently disappeared during shipment. Therefore, the DPCU including the DCU V2, was installed in the laboratory at DFRC and an ATP was performed successfully on 11 September 1975. On 16 September 1975. two "power-downs" occurred. These were due to a loss of Bit -12 in location -73. Again the DPCU "self healed" and operated satisfactorily until 23 September 1975. In the period between 23 September and 30 September the DCU failed and recovered a number of times leading to a decision to pursue DCU troubleshooting rather than software development. The DCU A-3 card (memory interface), was replaced in order to isolate the failure.

On 6 October 1975 the system failed with the replacement A-3 card installed. This indicated that the failure was in the memory. Subsequent memory tests on 9 October 1975 by EM&M at the factory in Hawthorne, California indicated no problem with the memory. On 13 November 1975, the problem re-occurred, with the exception that bits other than bit-12 were failing now. It was ascertained through conversations with EM&M that the prior memory test on 9 October was an incomplete test. It was then ascertained that the data guard circuit appeared to be failing in the memory. It was recommended that

Table 7.3-1 DCU V2 Vibration Test Anomalies

Date	Description of Failure	Test Being Run	Fault Isolation Procedures	Action Taken
12/11/73	Program stopped during 5g vibration at 650 Hz, 300 Hz, 142 Hz, and 7 Hz.	Vibration portion of acceptance test.	Visual Insp. revealed that the computer was not mounted securely.	Bussing and bracket added to restrain lateral axis stress. Print changed.
			Internal examination revealed loose hardware from the core memory and missing (not installed) groundwire on the A11 board.	Memory hardware re-fastened and wire installed.
1/8/74	DCU power shut down DCU power fuze blown.	Vibration portion of acceptance test	Internal examination revealed coil D34018228 shorted to ground through upper rail cover screw.	Screw replaced with shorter one. Print changed to reflect shorter screw.
			Power supply module A22, found to fail when printed circuit board flexed. Problem due to insufficient spacer length allowing board to flex.	Print changed to provide spacers to eliminate board flexure. A22 module S/N P1 replaced with S/N P2. (Components in area of maximum flexure replaced on S/N P1).
1/24/74	I/O Test would not run	Confidence Test	Several wires from external connectors to board A1 connector found to be damaged or open due to vibration.	Wires repaired and secured per Workmanship Standard.
1/24/74	Locations changed between power cycles	Confidence Test	Memory installed in DPCU S/N P2 chassis. External (bench) power supplies were varied to observe power status signal. Power status signal was not being generated for all required conditions.	Core memory returned to vendor who replaced one hybrid. Upon return it was found to exhibit same failure. Memory again sent to vendor. This time it was determined that a core memory design change had not been taken into account at computer level). (In grounding "data guard" in the DCU power status signal was also grounded). Print changed to reflect proper grounding of "data guard".
2/5/74	Could not turn DCU on.	Confidence Test (Post vibration)	Visual examination of power supplies revealed 2 fractured resistor leads.	Board given heavy coat of conformal coating following replacement of broken parts. Coil L2 reinforced with spares (like L1). Print changed to reflect addition of spacer.
2/9/74	DCU fails punch test	Punch test portion of acceptance test	Power supplies found to exhibit excessive 400 Hz RIPPLE under loading.	Module A22 S/N P2 replaced with Module S/N P1. A23 module capacitor value increased to provide adequate filtering. Print changed to reflect change.
2/16/74	Failed ATP paragraph 3.7.3.4 (not an electrical failure).	Acceptance test, post-vibration inspection	Visual examination of the A22 module revealed coil L1 bond broken.	Coil recemented to board

the memory be returned to EM&M and tested in order to verify the failure. On 17 November, the unit was tested by EM&M where the data guard hybrid chip Z1 was found to trip outside its sense limits. Subsequent replacement, conformal coating, ATP testing of the memory, and re-installation in the DPCU seemingly resolved the so called bit-12 intermittent problem.

On 19 January 1976, after approximately six weeks of satisfactory operation, the bit-12 failure reoccurred while DCU V2 was mounted in the aircraft. On 26 January, the failure reoccurred and it was ascertained that the memory was not capable of writing "ones" into bit-12. Subsequently the intermittent nature of the failure was confirmed as it momentarily healed itself while under test.

The memory was returned to EM&M's plant in Chatsworth, California for the replacement of the bit-12 sense amplifier and inhibit line driver hybrid. The intermittent hybrid was delidded and examined. No failure was evident leading to the conclusion that the problem resulted from a flawed bond somewhere in the hybrid. The memory passed an acceptance test and was returned to NASA/DFRC for reinstallation on 20 January 1976.

The DCU was used extensively in the lab until the end of flight testing on 5 March and performed satisfactorily in this period.

7.4 PAROSCIENTIFIC TRANSDUCERS

Early in the flight test program a number of failures either of the Paros transducers or associated hardware occurred. After correction of these early failures the Paros transducers performed flawlessly. As discussed below the failures are all attributable to correctable design, installation, or assembly errors. The various failures encountered are as follows:

1) S/N 139 and S/N 136 were failed when first checked during ground test, 14 July.
2) A P2 failure was noted during taxi test but could not be reproduced in the hanger, 28 August.
3) The Paros mating connector for the PKDC transducer failed during engine run up for first flight, 14 September
4) PKDB, S/N 137, failed after first flight during post flight testing in the hanger, 9 September
5) Vinyl tubing used to provide flexible coupling between Paros transducers and airframe plumbing failed at a high temperature flight condition, 6 November

All failures occurred in the wheel well Paros installation - PKDA, PKDB, PKDC, PKDD, PDEM - pictured in Figure 7.4-1. The original installation provided for hard mounting the five transducers to a bracket assembly clamped to the brake accumulators. During lab calibration and test of the transducer, the crystal in one unit was broken by a sharp contact of the transducer case with a hard surface. As a result a shock and vibration isolation case was developed to protect the units from damage.

Use of this case necessitated redesign of the wheel well bracket assembly to accommodate the added bulk of the case. A gear swing was performed on 30 June to check mechanical clearance of the Paros installation with respect to landing gear linkages. In fact there was an interference and the Paros installation bracket was bent during the test. The problem was corrected by moving one transducer and sawing and grinding the offending bracket to provide clearance. These mechanical activities were performed with the remaining transducers installed thus exposing them to some unknown level of high frequency vibration.

When the system was first turned on, 14 July, both PDKAS, and PKDDS were observed to be failed. Subsequent testing showed the S/N 136 had a broken crystal while S/N 139 had an electronics failure causing the output to degenerate under load. S/N 137 experienced a similar electronics failure after the first flight. The crystal failure is clearly a handling problem, probably associated with the gear swing, although perhaps a result of rough handling during shipping.

(29613)

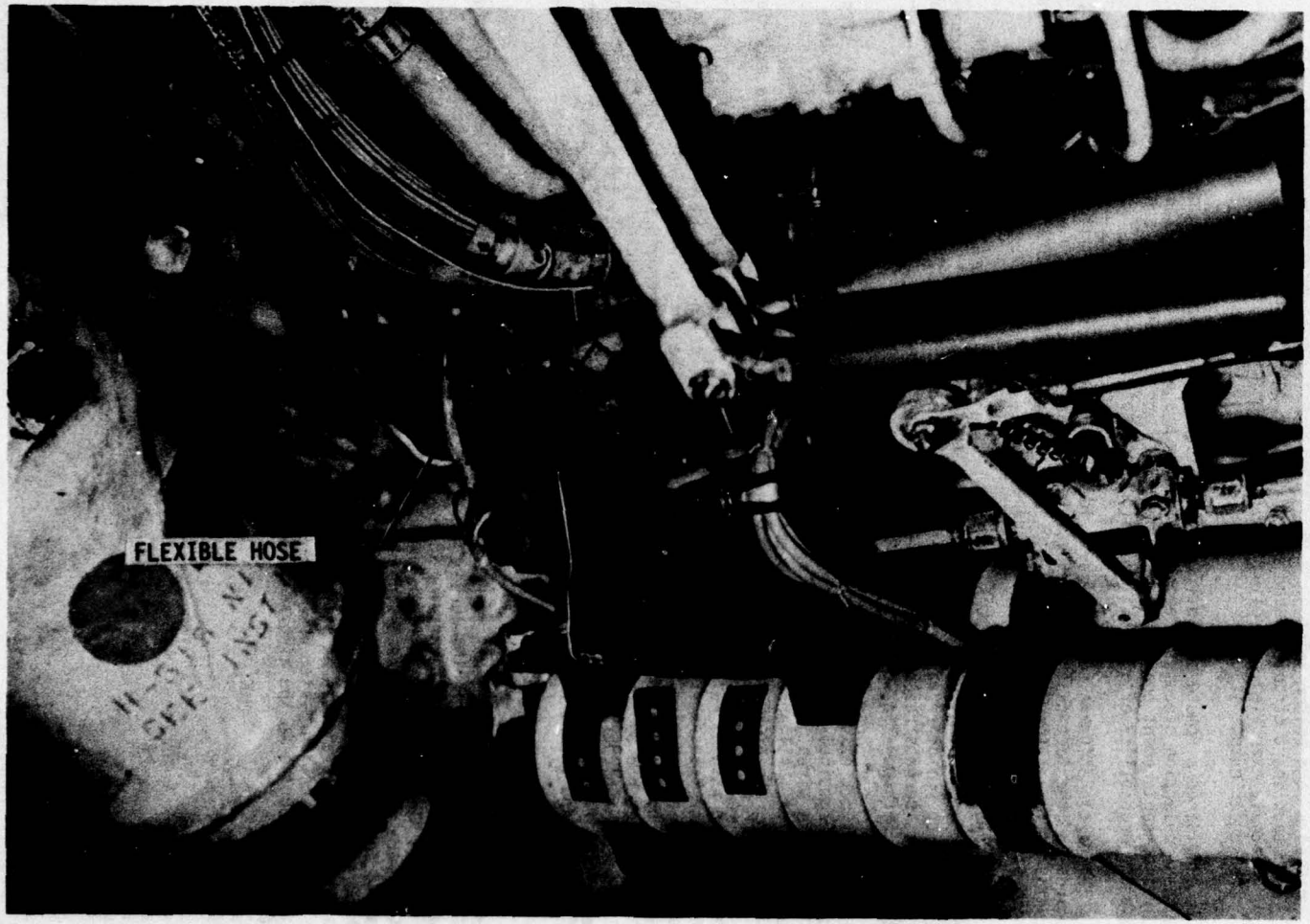

Figure 7.4-1 Paroscientific Transducer Installation

The electronics failures are less clearcut. The Paros transducer electronics consist of an RCA CD4007 AD FET used as a crystal driver and a complimentary pair output driver capactively coupled through .1 μf to the output connector. Tuning of the crystal oscillator is achieved by selection of a fixed resistor during transducer assembly. Units used for the IPCS program were built early in the company's history and may as a result have been subject to improper assembly practices. Thus three possible explanations are presented for electronics failures:

1) An electronic component was broken by mechanical vibration,
2) Assembly procedures overheated an electronic component or caused a cold solder joint,
3) An output short circuit loaded or an airplane power transient repeatedly exercised by cycling DPCU power overstressed the transducer output stage.

Item 3) is considered a remote possibility because the failure would only occur under worst case component selection circumstances combined with a short circuit in the airplane wiring harness. Since replacement transducers did not fail, and the cable was continuity checked before use the probability of a short is considered remote.

Item 2) - this explanation is supported by evidence of rework and excessive resin on one of the failed boards and the fact that the trim resistor selected when S/N 139 was repaired was significantly different than that originally selected. Mechanical vibration and aging combined with a cold solder joint could create this phenomenon.

Item 1) is also probable since the exposure to vibration is documented. However, since the units are potted and the failure is load sensitive it is difficult to envision a clear mechanical failure. Based on two other failures relating to i.c. chips in the IPCS program see Paragraphs 7.3 and 7.6 it is perhaps reasonable to assume some form of partial failure - a fatigued connecting wire perhaps - in CD4007 chips.

The connector failure of 4 September was eventually determined to result from mechanical stress on the connector combined with use of chlorine based solder flux resulting in corrosion and failure of harness wires. Paroscientific revised their process specifications to eliminate chlorine based flux. All accessible connectors were inspected visually for signs of excess flux or corrosion. No problems were found on inspection and no further failures were experienced.

In response to the rash of Paros failures in the wheel well installation the hard stainless line connecting the transducers to the probes was replaced, as shown in Figure 7.4-1, with a copper stub, with a grounding wire attached, connected to the original stainless line through a flex hose. This both improved vibration isolation and electrical ground return. The flex hose originally selected had an inadequate temperature range and failed during its first flight. It was replaced with a higher temperature nose which performed satisfactorily throughout the remainder of the flight test. No further transducer failures were experienced after the installation of the flex hose and ground wires.

7.5 N1 TACHOMETER

As indicated in Section 5.6.1, N1S tachometer noise induced excessive perturbations in A/B fuel flow. In an effort to isolate the cause of the problem the N1S tach was removed while the engine was removed from the aircraft for other reasons and run on a drill motor as was the instrumentation N1 tachometer. Neither anomalies in output wave forms nor crosstalk between tachometers were observed in this testing. In the course of this testing it was observed that the breakout torque on the DPCU system N1S tachometer was substantially higher than normal. Although no substantive evidence was available that this was affecting system operation, a spare tachometer was available on site so the questionable unit was replaced. The interchange of units had no effect on system operation. Since access to the N1S tachometer was relatively awkward with the engine in the airplane, the spare unit remained installed for the remainder of the test.

7.6 FLIGHT 28 TEMPERATURE MEASUREMENT FAILURE

Flight 28 was aborted during the supersonic accel due to what appeared to be a failure of T2S and a cockpit indication of excessive T4 on the left hand engine. Post flight trouble-shooting revealed that a failure in the NASA PCM System low level input section caused 12 volts to appear on the T2S input of the DPCU. As shown in Figure 7.6-1, this 12 volt signal traveled through the entire floated, low impedance, engine thermocouple harness saturating DPCU T3S and T2S and the cockpit T4 indicator. In addition other DPCU low level signals were disturbed by crosstalk effects in the over-driven IFU input mux. Upon removal of the offending 12 volt signal all DPCU variables returned to normal as did the cockpit T4 indicator. No damage to the IFU was expected because the 12 volts was less than the spec maximum of 15 volts. This was verified by running an end point check calibration of the low level mux prior to the next engine run and a full calibration of the low level signals at the end of the test program.

The source of the 12 volt signal was a foreign object (loose wire) inside the dual in-line chip containing the FET switch used in the T2 input to the PCM system. The existence of the wire was verified by opening the flat pack. After opening the wire had apparently moved from its failure inducing position, connecting the T2 input line to the 12 volt supply.

It is a classic demonstration of Murphy's law that such a failure occurred in the only area where instrumentation and engine control systems were interconnected. This interconnection was recognized during design reviews and was accepted for a number of reasons:

1) Potential failures - loss of engine temperature measurement - were non catastrophic,
2) Instrumentation connections to BOM thermocouple harness had been used throughout F-111 flight test program,
3) Total isolation of DPCU and instrumentation system was impractical without addition of probes,
4) PCM system input is high impedance thus probability of PCM failure impacting DPCU was remote.

The first three items were true and vindicate the design approach. However, it was an error to assume that a high impedance input assures isolation in case of a component failure. Therefore FMEA's should be reviewed carefully on future programs with regard to potential failure modes of high impedance circuits. Careful review may reveal potential failures, either open ground returns or, as in this case, poor quality control by the chip vendor, resulting in relatively high voltages emanating from supposedly passive high impendance inputs.

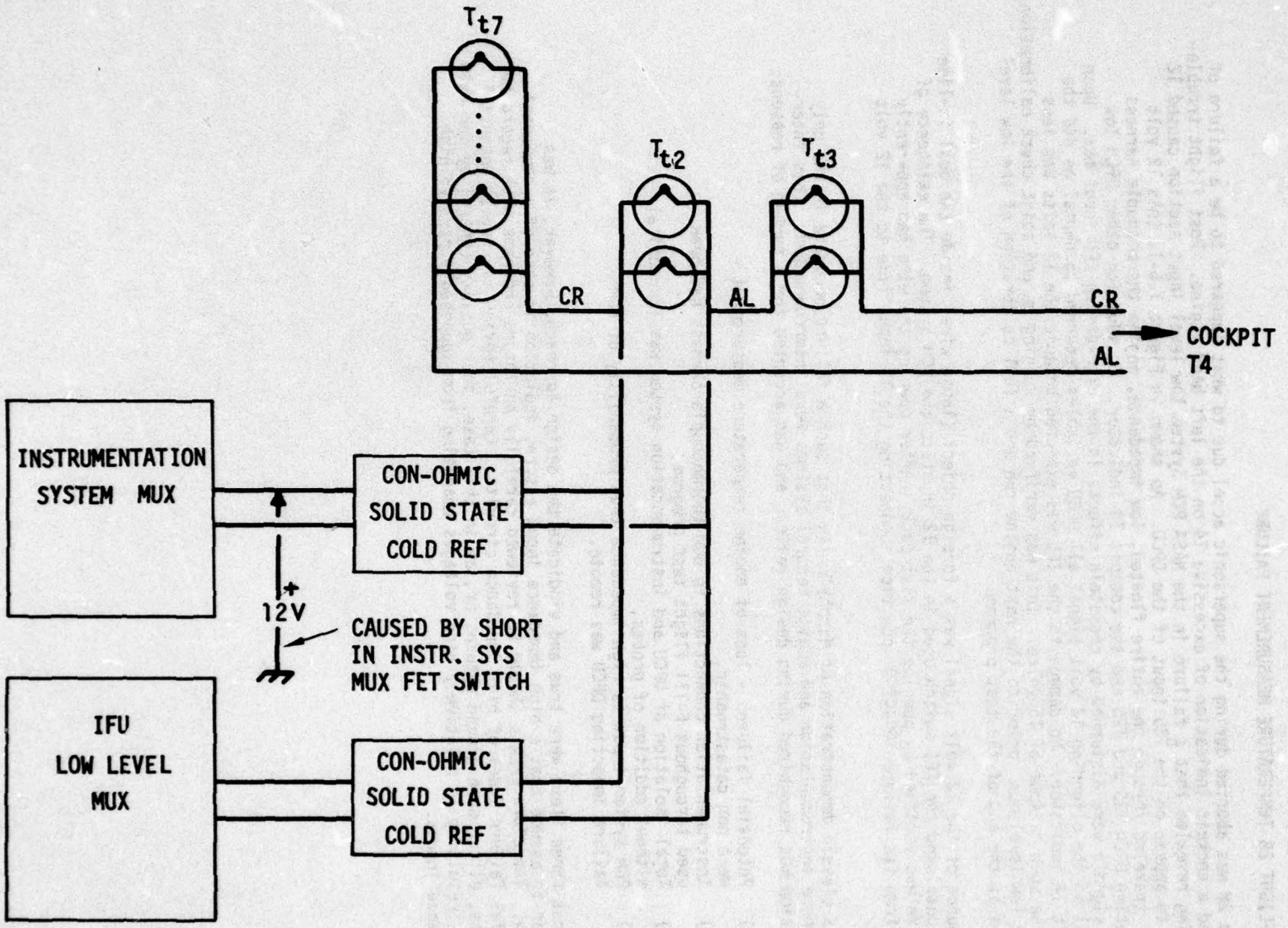

Figure 7.6-1 Thermocouple Harness Interfaces

8.0 SOFTWARE

Revisions C of both BOMDIG and IPCS CPCEI's (Computer Program Contract End Item) were used throughout the flight test to implement BOMDIG and IPCS engine control. Field modifications were made to both CPCEI's using the procedure documented in Section 3.3 in order to meet the requirements of the flight test. Checkout of both CPCEI's was conducted at the end of altitude test and resulted in numerous SFCO's to make the system operable. Further SFCO's were generated in adapting the DPCU system to the aircraft during Ground Test. Those SFCO's generated prior to flight test are discussed in the Altitude and Ground Test Reports, References 9, and 5 respectively. For the convenience of the reader all SFCO's to the Revision C CPCEI's are tabulated in the following write up although the reader is referred to the appropriate references for a detailed discussion of SFCO's generated prior to the start of flight test.

In Section 8.1, Configuration History, all SFCO's associated with Revision C software are tabulated to permit rapid determination of changes in effect for a given engine run or flight. SFCO's modifying controller function are discussed in detail as are those which correct DPCU hardware problems. In addition a history of controller coefficient changes is presented. Section 8.2 discusses the reasons for software changes and comments on their implications. Section 8.3 presents an overview of the IPCS program execution sequence and timing describing the framework within which the changes were made.

8.1 CONFIGURATION HISTORY

Figure 8.1-1 is a summary of all SFCO's used with Revision C of the BOMDIG program. Figure 8.1-2 is a similar diagram for IPCS. The intent of these diagrams is to permit the reader to determine the software configuration used for any engine run or flight during the flight test period. These data were compiled by reference to the SFCO's and the Patch Tape Records. As an example consider the differences between flight 22 and engine run 21.

The software for flight 22 consisted of IPCS C + Tapes 7508111, 7509171, 7501241, 7511251, 7512121, and 7512221. Tape 7512221 was incorporated into a new tape, 7601081, which also included the basic autothrottle code and a revision to the suppression schedule, WAXM. Tape 7601082 was generated to incorporate modifications to the autothrottle code. Thus the configuration for engine run 21 was IPCS C + MEDIC + TAPES 7508111, 7509171, 7510241, 7511251, 7512121, 7601081, and 7601082.

The following paragraphs discuss the significant changes made to the CPCEI's during the flight test program. Minor changes are not discussed.

8.1.1 Stall Detection

The stall detection system defined in paragraph 3.2.4.6 of Reference 2 was modified during altitude testing to the configuration shown in Figure 8.1-3. This system, which retards the gas generator to N2 min for 2 seconds after stall is detected and then returns PLA to its setpoint, operated satisfactorily in the altitude cell. During flight test stall recovery took substantially longer than 2 seconds and was unpredictable. As a result SFCO's 96, 96A converted the stall detector to the system shown in Figure 8.1-4. Stall is detected by comparing rate of change of burner pressure against a schedule as a function of burner pressure as in the original scheme. After a one second delay stall is verified by comparing PS3S to minimum PS3S (7th and 12th bleed open operating line) scheduled as a function of P2S. If a stall is determined to exist the stall flag is set and stays set until 1 second after recovery occurs, as determined by PS3S level compared to scheduled PS3S level. Performance of the revised system is discussed in Section 6.5.4.

8.1.2 Acceleration Loop Control Modifications

The baseline IPCS control limited fuel flow during acceleration through the action of linear MN3 and Wf/Pb error signals acting through the select logic - see Section 4.2 and Figure 8.1-5A. In order to establish the source of tracking errors in these loops a series of controller changes were made:

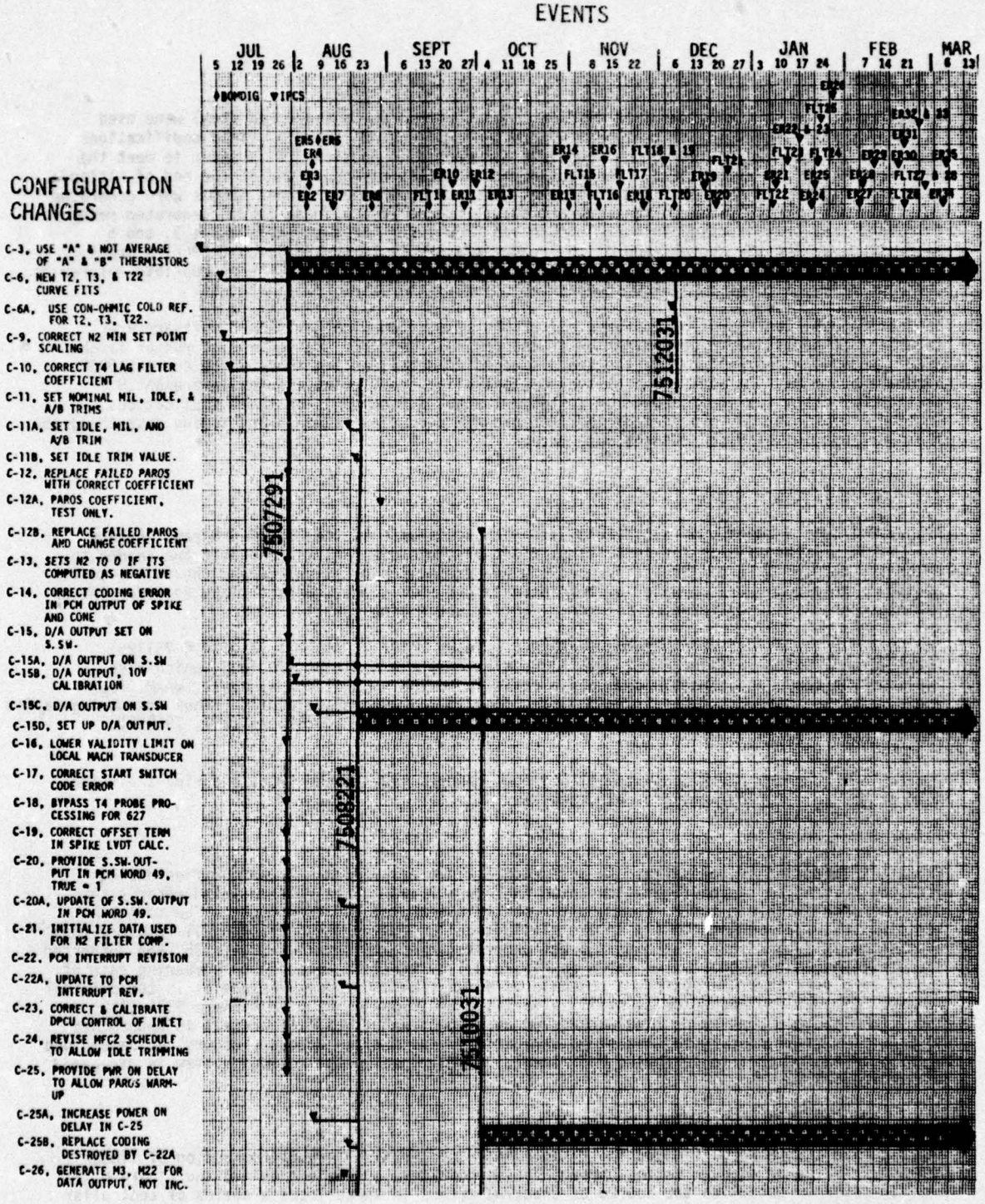

Figure 8.1-1 BOMDIG SFCO Summary

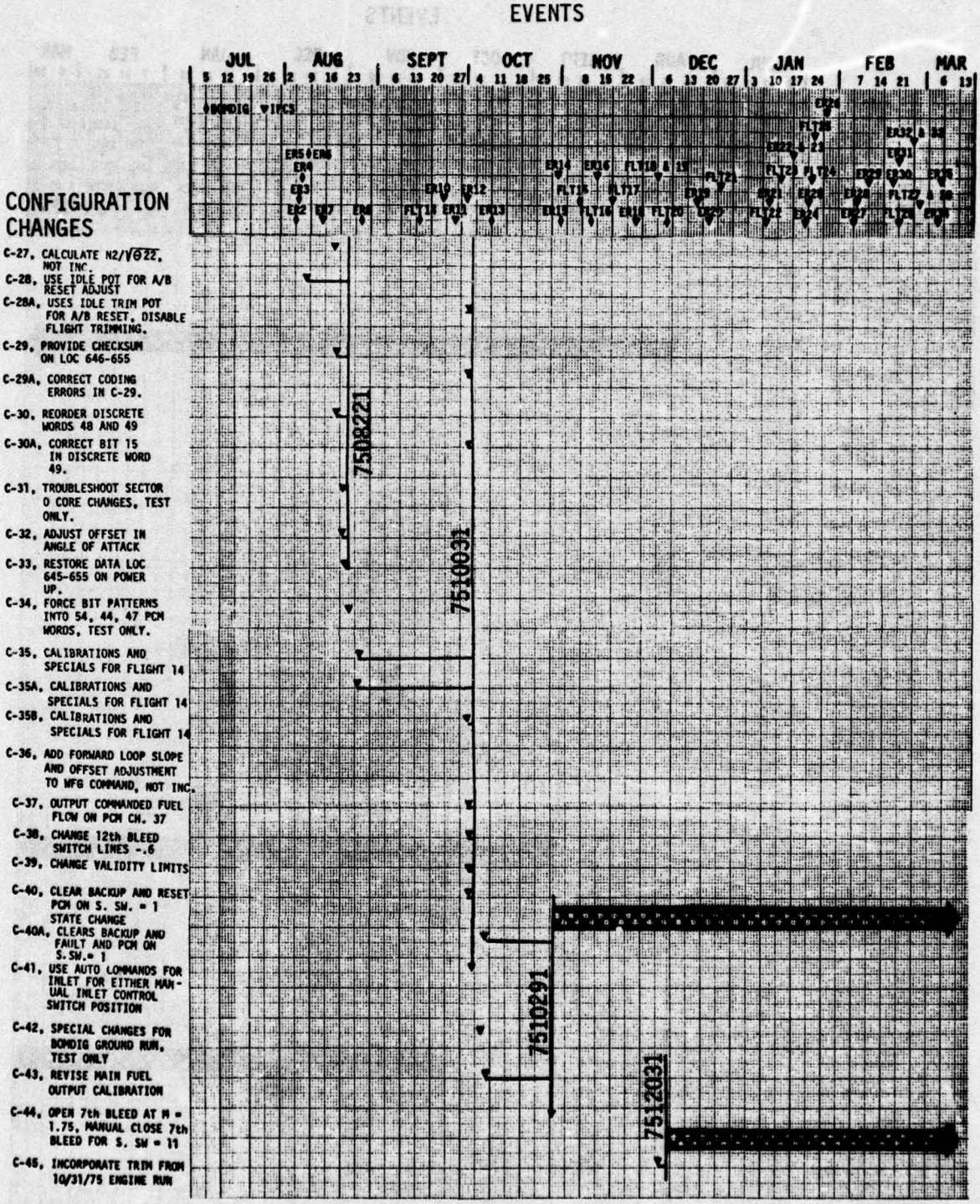

Figure 8.1-1 BOMDIG SFCO Summary (Cont.)

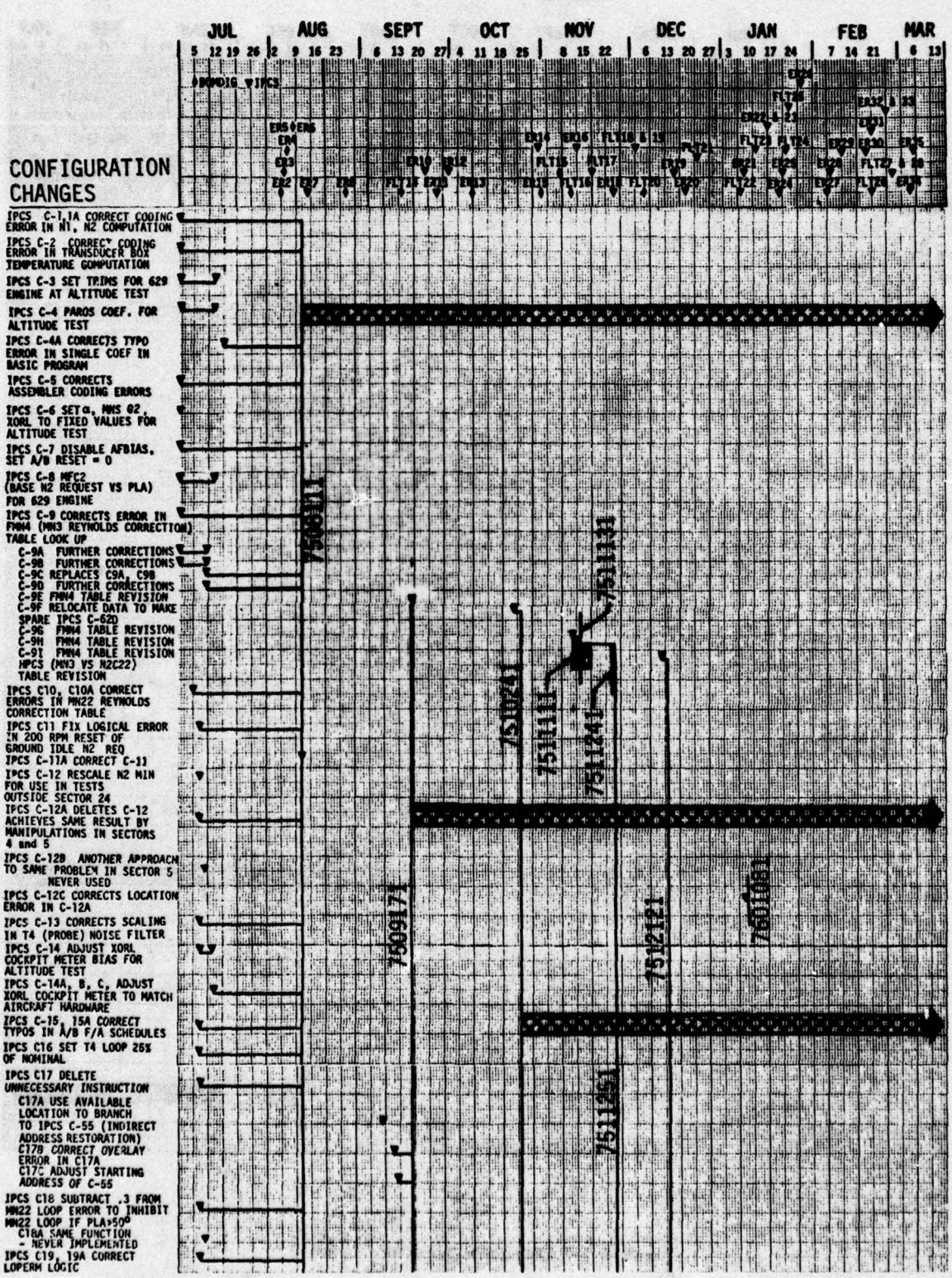

Figure 8.1-2 IPCS SFCO Summary

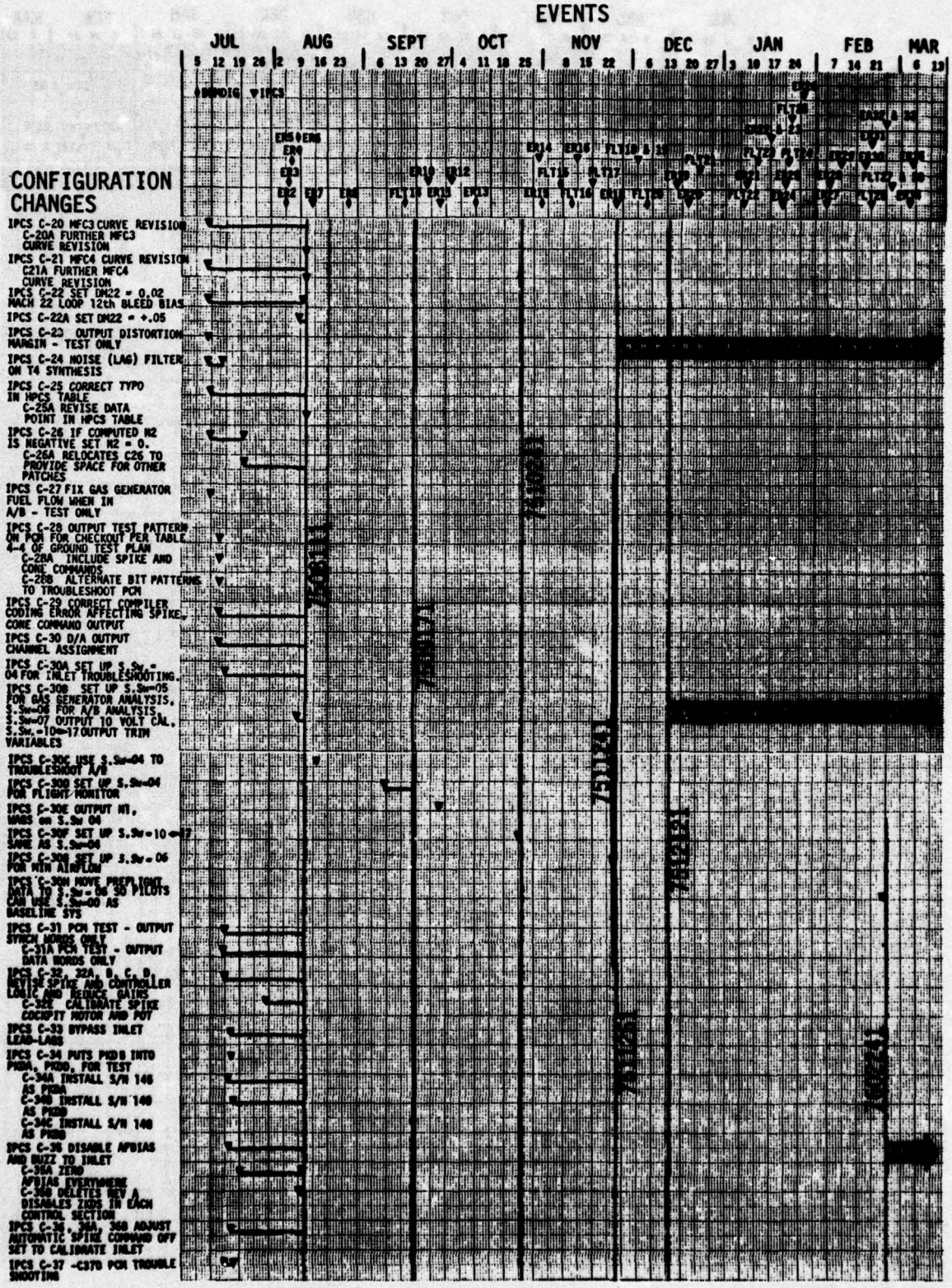

Figure 8.1-2 IPCS SFCO Summary (Cont.)

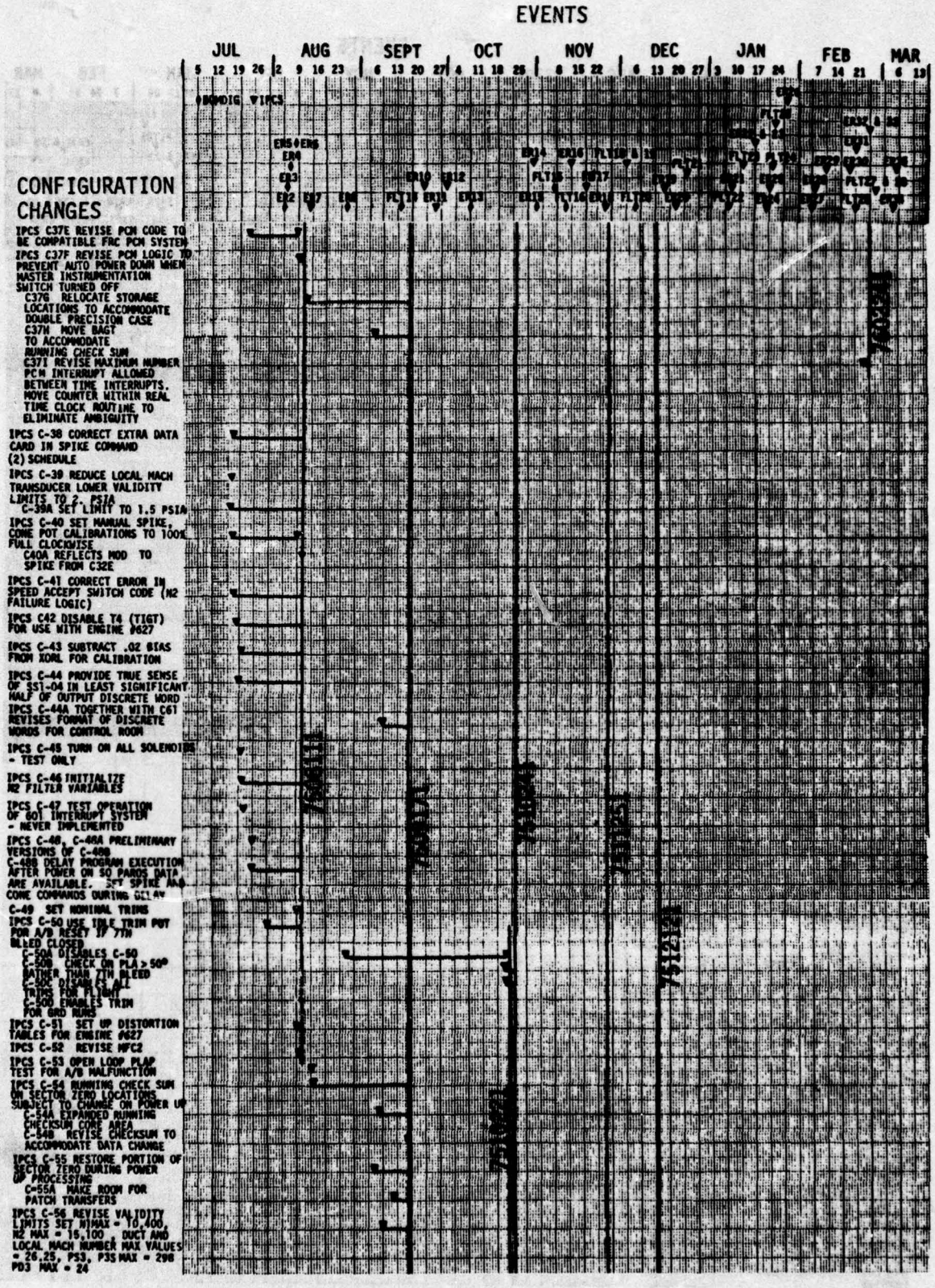

Figure 8.1-2 IPCS SFCO Summary (Cont.)

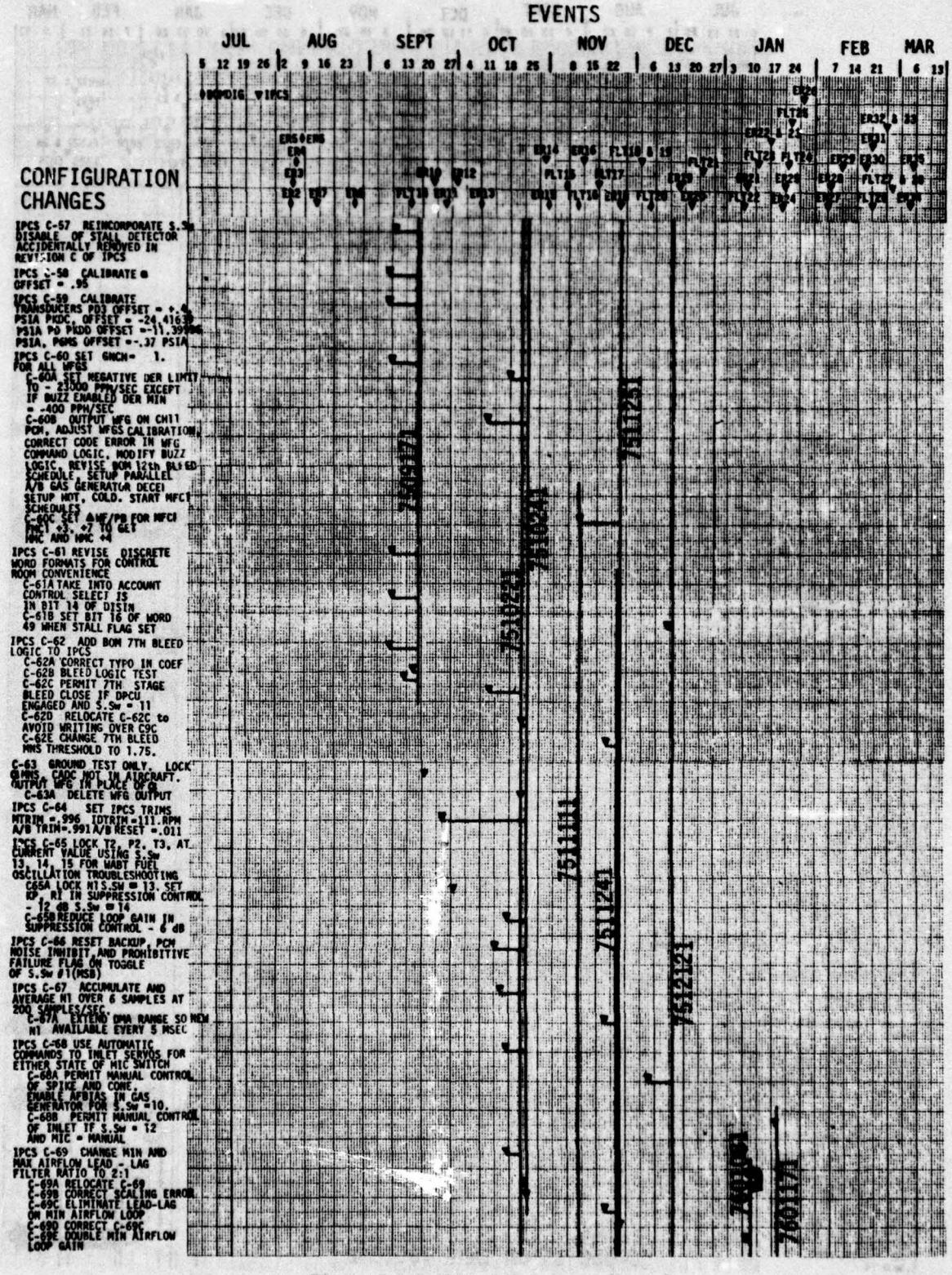

Figure 8.1-2 IPCS SFCO Summary (Cont.)

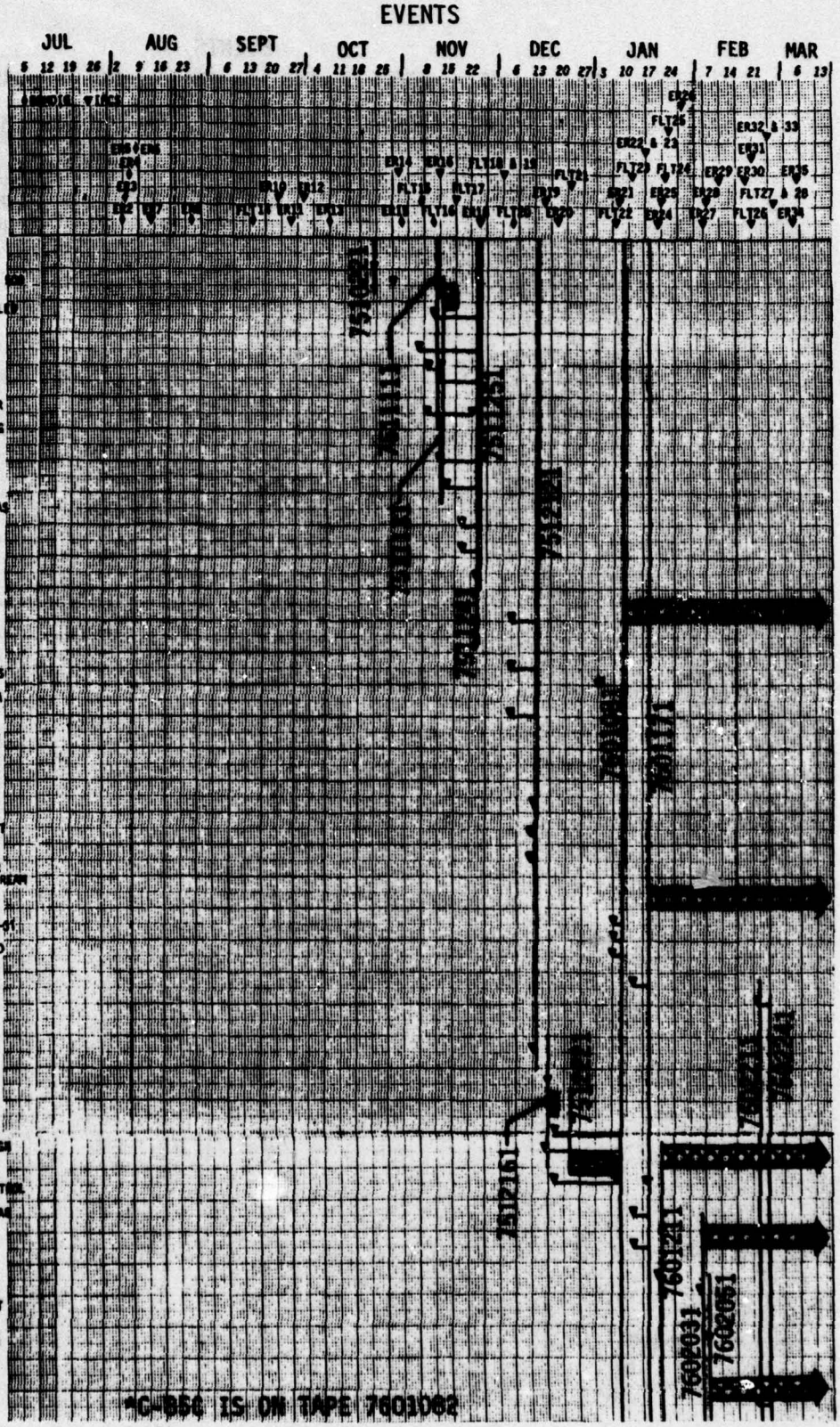

Figure 8.1-2 IPCS SFCO Summary (Cont.)

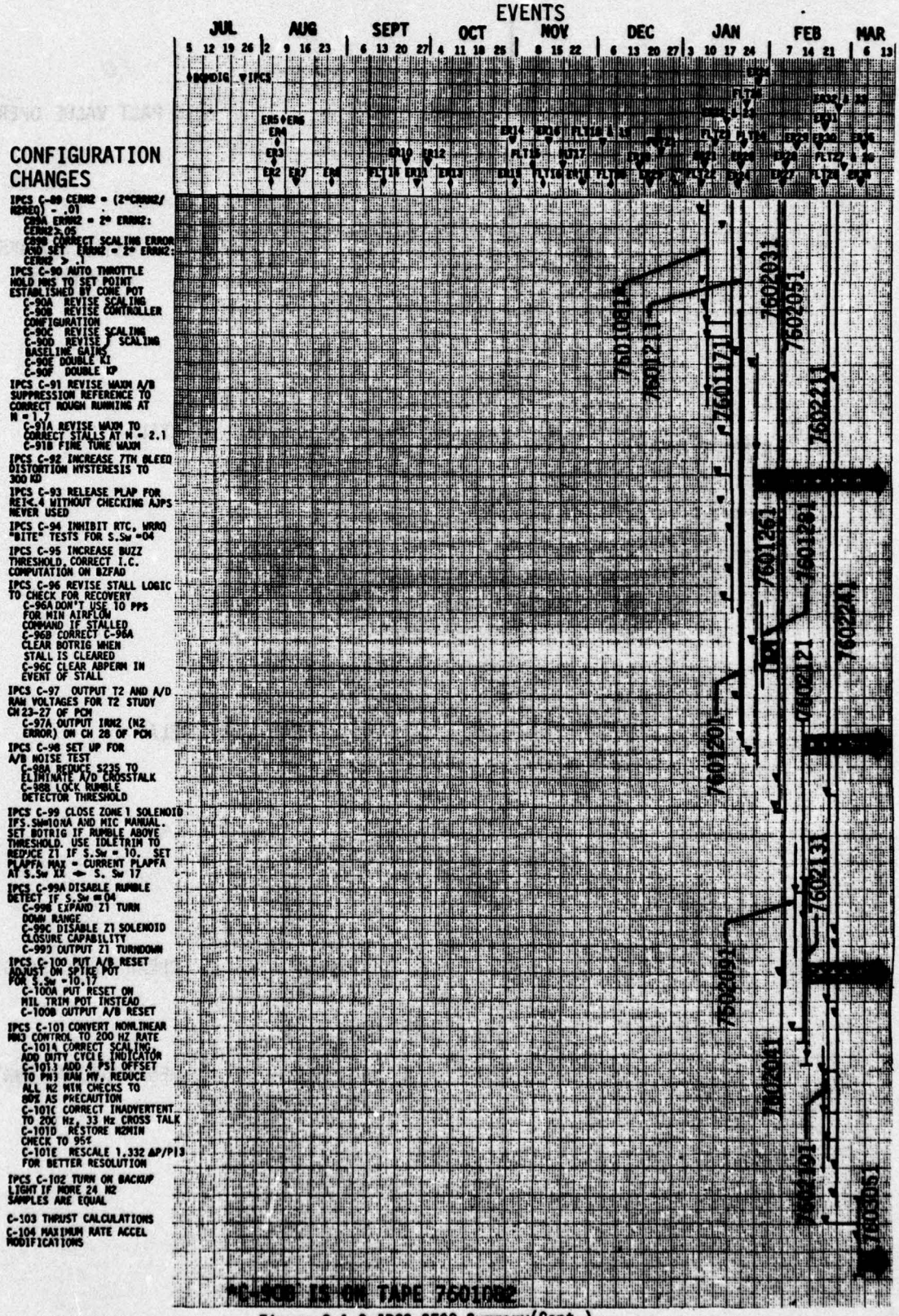

Figure 8.1-2 IPCS SFCO Summary(Cont.)

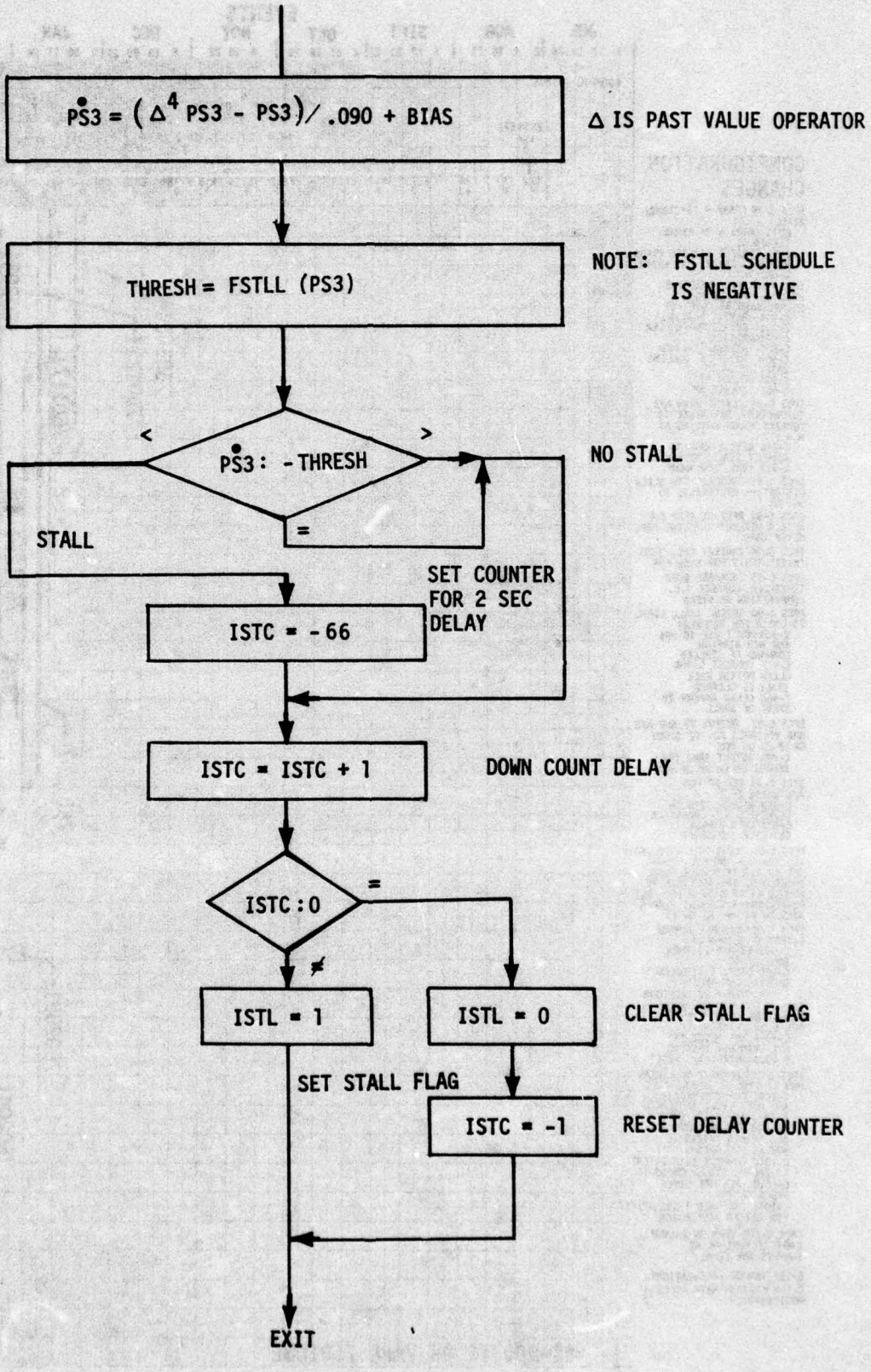

Figure 8.1-3 ICD (IPCS C) Stall Detector

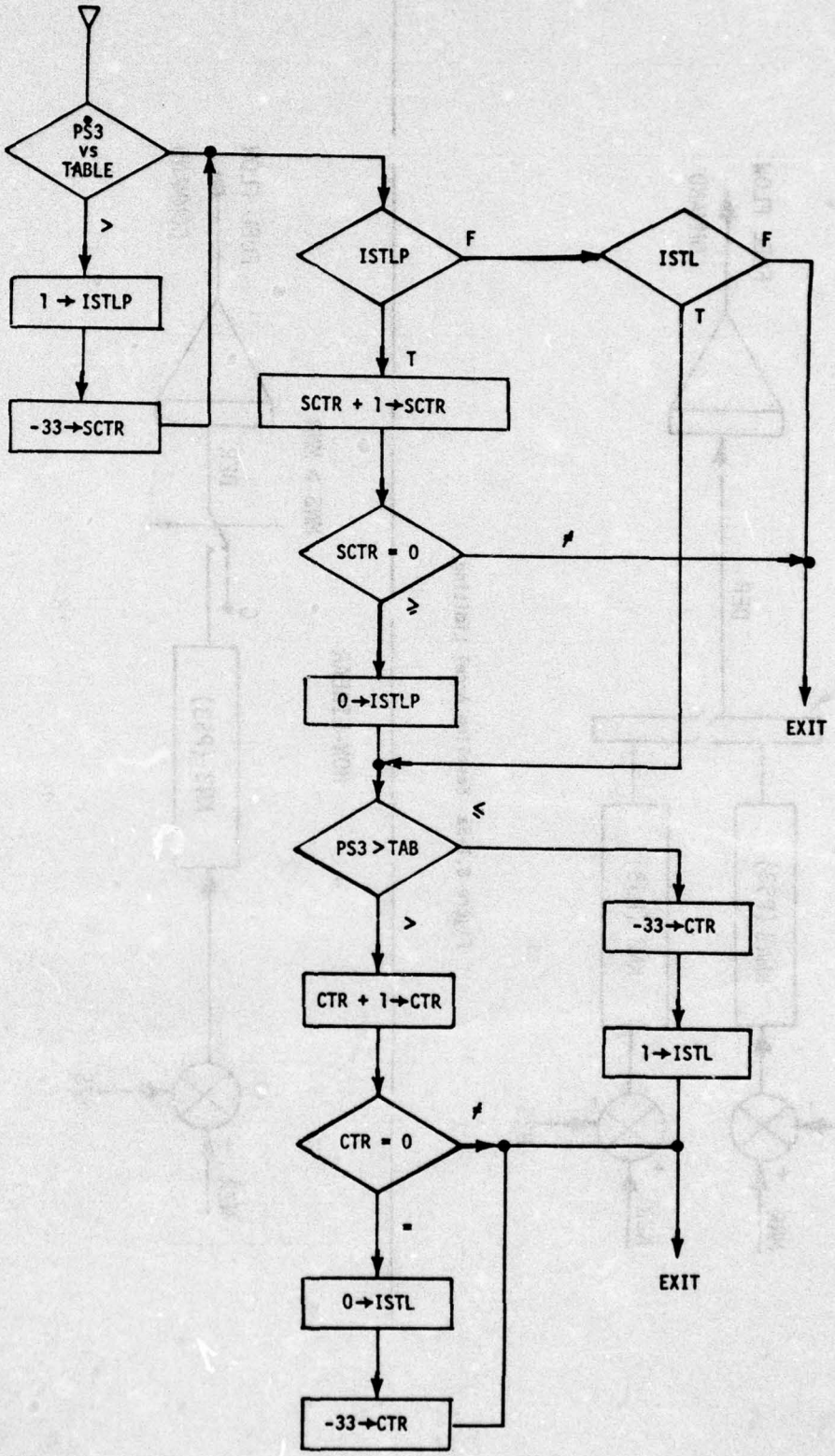

Figure 8.1-4 Revised Stall Detector

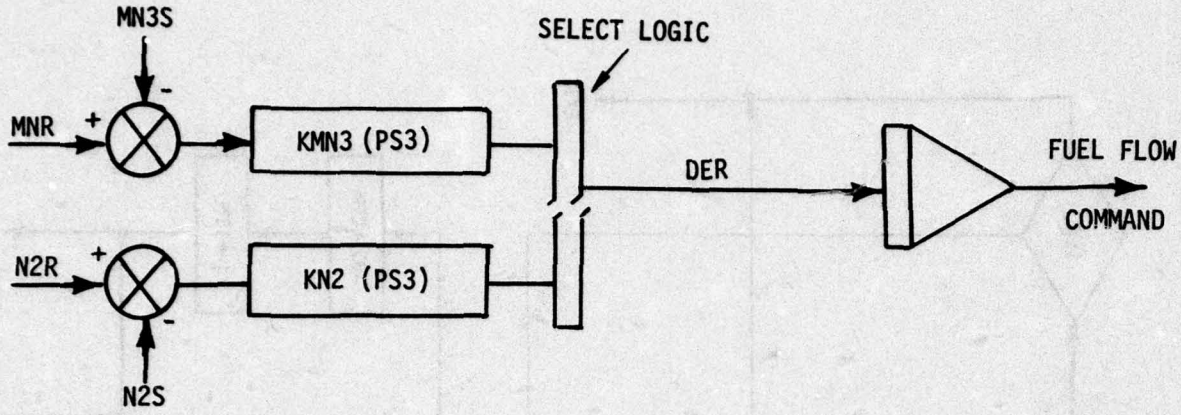

Figure 8.1-5a Baseline Accel Limiting

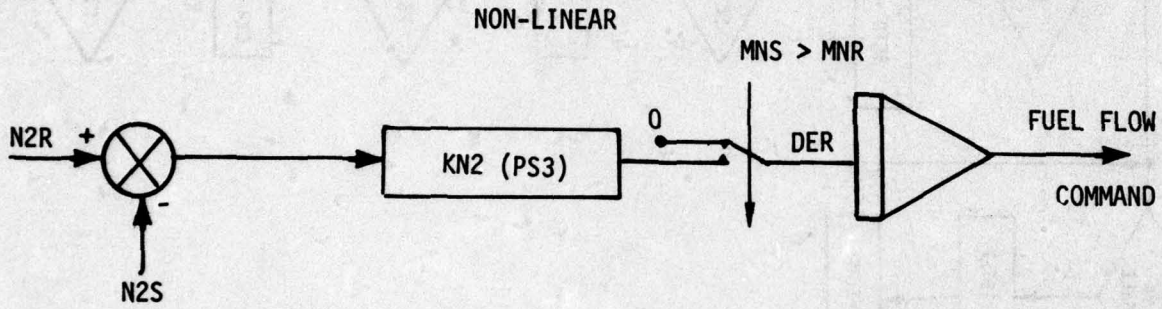

Figure 8.1-5b Non-Linear MN3 Control

1) Wf/Pb was removed from the select logic and instead used to directly limit the output of the fuel command integrator, Figure 8.1-6.
2) MN3 control was removed from the select logic and replaced by a non-linear control operating on the integrator input, Figure 8.1-5B.
3) The non-linear MN3 control was further modified by lead/lag compensation of the MN3S signal in an effort to introduce damping on the initial transient.
4) The original MN3 control was restored and its loop gain varied from 1→8 times nominal.
5) The non-linear MN3 control was implemented at a high sample rate, Figure 8.1-7.

The first four of these modifications are straight forward in that data sampling rates are unchanged from the baseline system and they are functionally described by block diagrams.

High rate sampling of the MN3 loop combined with non-linear MN3 control and high sample rate fuel command outputs requires further comment and discussion. Figure 8.1-7 describing this system shows that the control is both dual rate and asymetric. MN3 command reference is generated at a 33 Hz rate based on N2S and T22S. This is justified by the relatively slow change of MN3 reference during the accel. Likewise, N2 error, which defines the magnitude of DER input to the integrator, changes slowly and was, therefore, computed at the 33 Hz rate. Sensed MN3, the rapidly changing variable, was sampled at a nominal 200 Hz rate. However, as shown in the timing diagram, uniform 5 msec intervals were not possible due to the structure of the CPCEI executive. In order to reduce computation time the normal sensor processing and failure detection logic for PD3S and PS3S were not used for the MN3 control although the computations were retained in the 33 Hz loop. For MN3 control the pressure ratio was computed directly as a ratio of raw counts from both sensors. An offset calibration for PD3S was incorporated to permit use of previously developed MN3 schedules which were converted to $\Delta P/P$ form to eliminate the MN3 table lookup at the 200 Hz rate. This introduces a minor problem in that the RNI correction cannot be translated directly from MN3 to $\Delta P/P$ since the appropriate $\Delta P/P$ is a function of operating point. The error introduced is small relative to system noise and is not considered significant. The results produced by these modifications are discussed in Section 6.2.

8.1.3 Schedule Changes and Minor Revisions

As controller testing proceeded changes were required to various parameters. Figure 8.1-8 provides a summary of these changes relating them to calendar date, and engine run/flight number. When necessary successive schedule data are tabulated in Figure 8.1-8a,b etc.

8.1.4 Hardware Adaptions

It was convenient or in some cases necessary to modify software to adapt the system to hardware peculiarities. These changes are discussed in the following paragraphs.

8.1.4.1 Noise Filters

A 1.25 Hz Tustin first order lag at 33 Hz sample rate was used to filter T2S noise in IPCS. The filter was a duplicate of Tustin lags used elsewhere.

An N1S filter was required to minimize fuel flow variations during steady-state A/B operations caused by the effect of N1S on corrected airflow and thus the A/B suppression control. N1S sample rate was increased to 200 Hz - a relatively simple change since fuel flow and N2S were already sampled at 200 Hz - and the resulting six samples per major cycle were averaged with equal weighting to produce N1 at the 33 Hz major cycle sample rate.

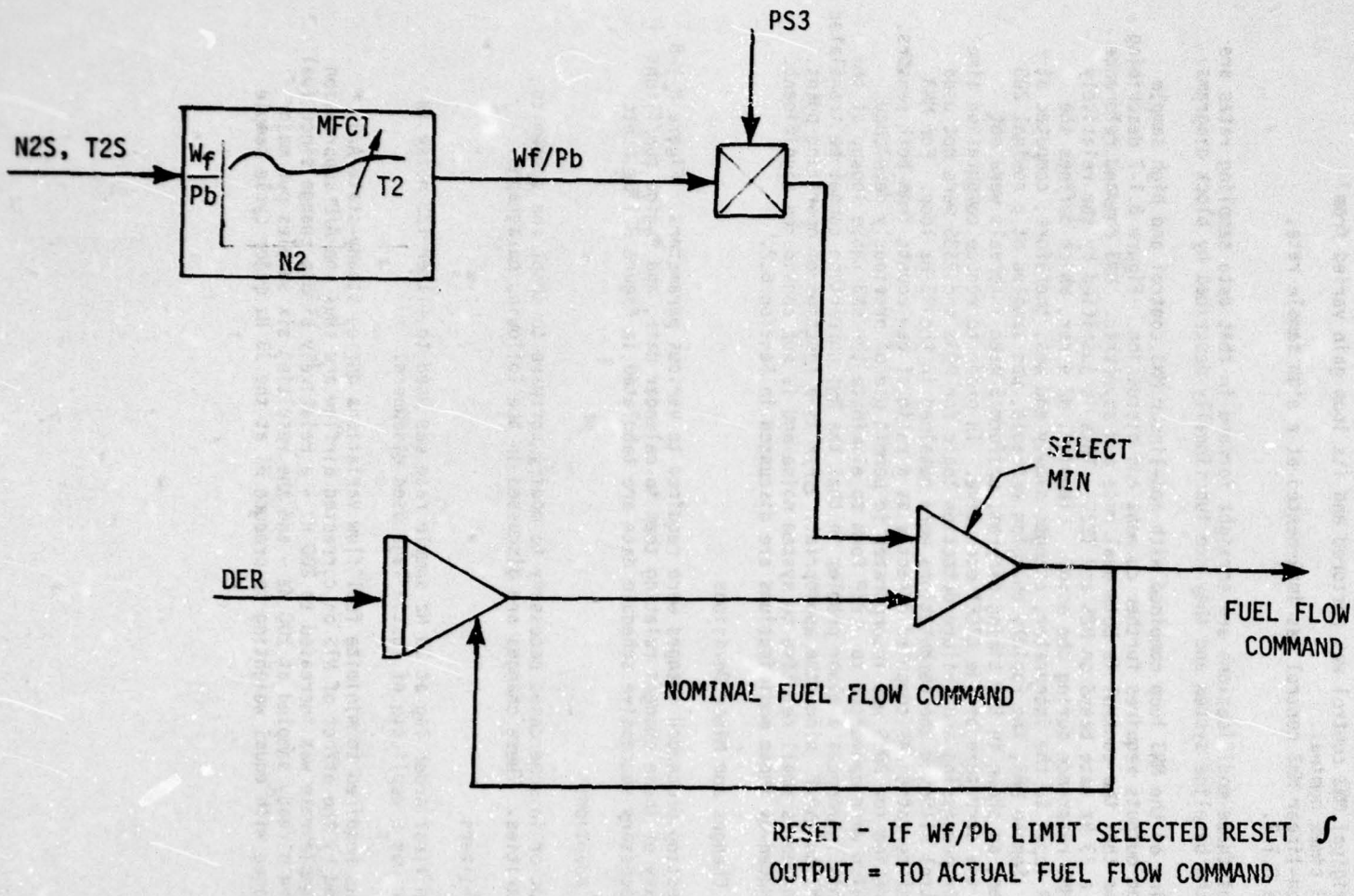

Figure 8.1-6 Downstream Wf/Pb Limiting

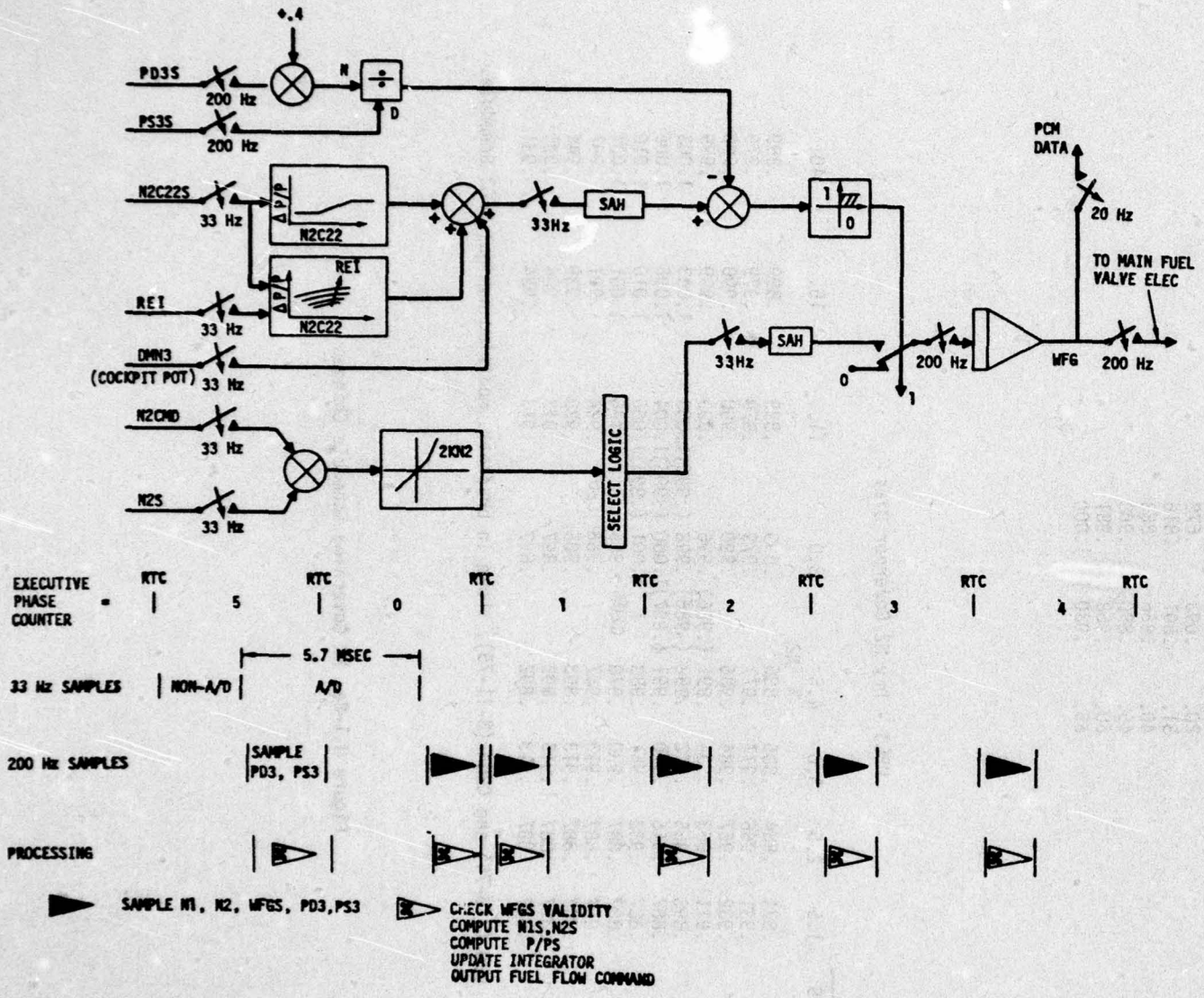

Figure 8.1-7 High Rate Sampling Non-Linear MN3 Control

MFC2 - Base N2 Request

PLA	REV C % N2	C52 (8/11/75) % N2
0	.671	.625
18.	.671	.625
20.	.693	.678
31.	.801	.816
40.	.866	.883
45.	.890	.908
60.	.958	.981
65.	.980	1.000

MFC3 - Dry N2 Governor Bias

T2S/P2S → ↓	1.5	2.5	3.0	4.5	8.0	11.	15.	40.
				% N2				
-65	.874	.884	.896	.896	.899	.899	.899	.899
+15	.931	.966	.977	.977	.979	.979	.979	.979
+60	.932	.967	.984	.986	.990	.990	.990	.990
+100	.911	.963	.984	.991 (.986)	.996	.999	.999	.999
+120	.898	.955	.972	.992 (.986)	.998 (.996)	1.003	1.003	1.003
+135	.887	.946	.970	.991 (.987)	1.000 (.996)	1.004	1.006	1.006
+160	.887	.932	.961	.988 ↑	1.001 (.996)	1.006	1.010	1.010
+225	.887	.887	.930	.970 C20A	.985 ↑	.995	1.001	1.001
+260	.887	.887	.913	.957	.966 C20	.984	.991	.991
+430	.887	.887	.913	.895	.905	.928	.939	.944
+485	.887	.887	.913	.892	.897	.913	.924	.931
+600	.887	.887	.913	.892	.897	.913	.924	.931

NOTE: C20 (7-9-75) and C20A (8-11-75), shown in brackets, modified nominal MFC3 Schedule.

Figure 8.1-8a N2 Governing Schedule Changes

MFC4 - Augmented N2 Governor Bias

T2S/P2S	1.500	2.500	3.000	4.000	5.000	8.000
			% N2			
-65.0	.830	.850	.860	.868	.868	.873
15.0	.898	.931	.945 C21A	.953 C21A	.953 C21A	.960
40.0	.896	.940	.953	.960	.963	.967 C21
78.0	.877	.936	.953 (.947)	.962 (.953)	.965 (.956)	.972 (.970)
115.0	.837	.920	.942	.960 (.951)	.964 (.958)	.974 (.972)
153.0	.794	.900	.930	.950	.960	.974 (.972)
215.0	.794	.850	.888	.929	.948	.973 (.971)
265.0	.794	.799	.836	.902	.935	.971
332.0	.794	.730	.756	.850	.904	.964
415.0	.794	.730	.756	.750	.848	.948
540.0	.794	.730	.756	.750	.776	.873

T2S/P2S	11.000	15.000	20.000	40.000
		% N2		
-65.0	.873	.873	.876	.876
15.0	.960	.960	.964	.964
40.0	.970	.970	.974	.974
78.0	.976	.978	.981	.981
115.0	.980	.984	.986	.986
153.0	.981	.986	.988	.988
215.0	.980	.984	.988	.994
265.0	.980	.986	.990	.972
332.0	.976	.984	.990	.942
415.0	.968	.978	.986	.904
540.0	.968	.918	.926	.848

NOTE: C21 (7-9-75) and C21A (8-11-75), shown in brackets modify nominal MFC4 Schedule.

Figure 8.1-8a N2 Governing Schedule Changes

HPCS Base MN3 Loop Schedule

	Rev C	C9I (12-10-75)	C88 12-18-75		C88A (1-16-75)		C101 (2-11-76)
N2C22	MN3	MN3	N2C22	MN3	N2C22	MN3	1.3332 ΔP/P
9000.	.26	.255	9000	.29	9000	.285	.07674
9600.	.26	.255	9300	.29	9300	.285	.07674
9800.	.26	.255	9800	.301	9800	.295	.08161
10000.	.26	.255	10000	.306	10000	.295	.08161
10200.	.2649	.2585	10200	.311	10200	.295	.08161
10400.	.2649	.262	10400	.311	10450	.295	.08161
10600.	.27	.27	10600	.311	10700	.300	.0842
10800.	.275	.275	10800	.311	10850	.3075	.08964
11000.	.281	.281	11000	.311	11000	.315	.09446
12000.	.305	.305	12000	.311	12000	.315	.09446

FMN4 MN3 Reynolds Index Bias

	Rev C			C9E (9-17-75)		
REI/N2C22	9000	9600	10500	9000	9600	10000
	MN3				MN3	
0	.025	.025	.025	.025	.025	.025
.5	.025	.025	.025	.025	.025	.025
.8	.0275	.0275	.0275	.01	.01	.01
1.	.03	.035	.03	0.	0.	0.

	C9G (11-11-75)				C88A (1-16-76)		
	MN3				9800	10450	10750
0	.03	.03	.03	.3	.014	.0075	0.
.5	.03	.03	.03	.5	.010	.006	0.
.8	.024	.024	.024	.8	0.	0.	0.
1.	.02	.02	.02	1.	0.	0.	0.

REI/N2C22	9800	10450	10750
	1.3332 P/P		
.3	.008995	.004819	0.
.5	.006426	.003855	0.
.8	0.	0.	0.
1.0	0.	0.	0.

Figure 8.1-8b MN3 Loop Schedule Changes

MN3 Compensation

1. None 6-23-75 through 1-15-76 Rev C
2. ((.614 S + 1)/(.307 S + 1) 1-16-76 through 2-2-76 88A
3. None 2-3-76 through 2-5-76 88CP
4. ((05 S + 1)/(.02 S + 1) 2-6-75 only not retained 88E
5. None 2-7-76 through 3-5-76

MN3 Schedule Offset

1. DMN3 = 0. Rev C
2. After 1-15-76 Variable on Spike Pot C88A
3. After 2-24-76 DMN3=0 if SS≠14 C88F

MN3 Loop Gain

1. Nominal, except from 2-5-76 through 2-10-76
2. Gain was variable from 0-8 on cone pot

MN3 Loop Configuration

1. Nominal through 12-18-75 Rev C
2. Non Linear MN3 control ER 20, 12-19-75,only C88
3. Nominal through 1-15-76
4. Non Linear 1-16-76 through 2-4-76 C88, C88A
5. Nominal 2-5-76 through 2-17-76
6. Non Linear at high rate 2-18-76 through 3-5-76 C101
7. Offset PD3+.4 PSIA 2-19-76 through 3-5-76 C101B
8. Rescale ΔP/P ratio 2-25-76 through 3-5-76 C101E

Figure 8.1-8c MN3 Loop Configuration Changes

8.1.4.2 Pulse Code Modulation Data Output

In a philosophical sense this was perhaps the most radical revision made to the software in that the original design was abandoned and replaced by new code. Both IPCS and BOMDIG were revised in the same manner thus the following discussion applies to both.

Figure 8.1-9 depicts the PCM system. The aircraft system, or Recorder Monitor Panel, outputs two signals. The data request every .8333 msec requests a 16 bit output word from the DCU. The frame synch pulse occurs every 5 msec and requests an indication of end of frame from the DCU. Since the DCU frame is 60 words long - frame synch word plus 59 data words, the DCU PCM processing software must ignore 9 out of 10 frame synch pulses and respond by outputting a frame synch word after the last data word. The major problem with the original PCM processing scheme was that it unmasked PIL080 - the frame synch interrupt - after the 59th data word. The DCU interrupt structure however recognizes and stores interrupt events even when they are masked out. Thus when PIL080 was unmasked the software responded to the stored interrupt rather than waiting for the frame synch. This did not impact operation at ground facilities because the DCU PCM data was the only PCM data. However, on the airplane this phenomenon made synching impossible.

The solution, referring to the flow chart, was to honor all PIL080's and check the data word counter, ERWC, against 59 to decide whether or not a frame synch word output was required.

A second problem developed because the airplane PCM system power supply shutdown transient was too slow. The result was a burst of PCM interrupts as airplane PCM output voltage sagged, resulting in DPCU autopower down due to failure to complete a computational cycle within 30 msec. Again referring to the flow chart, the total number of PCM related interrupts between Real Time Clock interrupts is counted and compared to a maximum allowable number. If the number is exceeded both PCM interrupts are masked out and the backup light turned on. PCM is turned back on and the backup light cleared by toggling the left most CMU sense switch.

In order to meet an aircraft PCM system requirement for response to the frame synch pulse within 62.5 μseconds the reset of the PCM interrupt counter in the RTC interrupt routine was placed late in the routine. This resulted in an ambiguity in the maximum allowable number of counts. This was changed late in the flight test program when the PCM interrupt counter was used to check the Real Time Clock, see below. However, the change made frame synch timing marginal resulting in occasional data drop outs.

8.1.4.3 Memory Restoration

During ground test it was discovered that random core locations from location 400 to 777 were occasionally reset during power down/up cycles due to a design pecularity of the DMA interface. To correct the problem a memory restore system was added to the power on interrupt processing. In addition, a check sum of these locations was computed every major cycle. In combination these changes resolved the problem without requiring any hardware modifications.

8.1.4.4 Paroscientific Transducers

Three Paroscientific transducers were replaced due to hardware failures, see Section 7.4. The appropriate calibration coefficients were changed in the software to adapt to the replacement transducers.

8.1.4.5 Autodisengage

The autodisengage problem is disucssed elsewhere in Section 7.1. By masking out in software the DCUDWN1 bit in the discrete input word, the hardware Built In Test Equipment (BITE) test creating the "autodisengage" was absolutely inhibited. For demonstration test purposes the inhibit was incorporated at all times. For flight test and engine runs the inhibit was selected for sense switch 04.

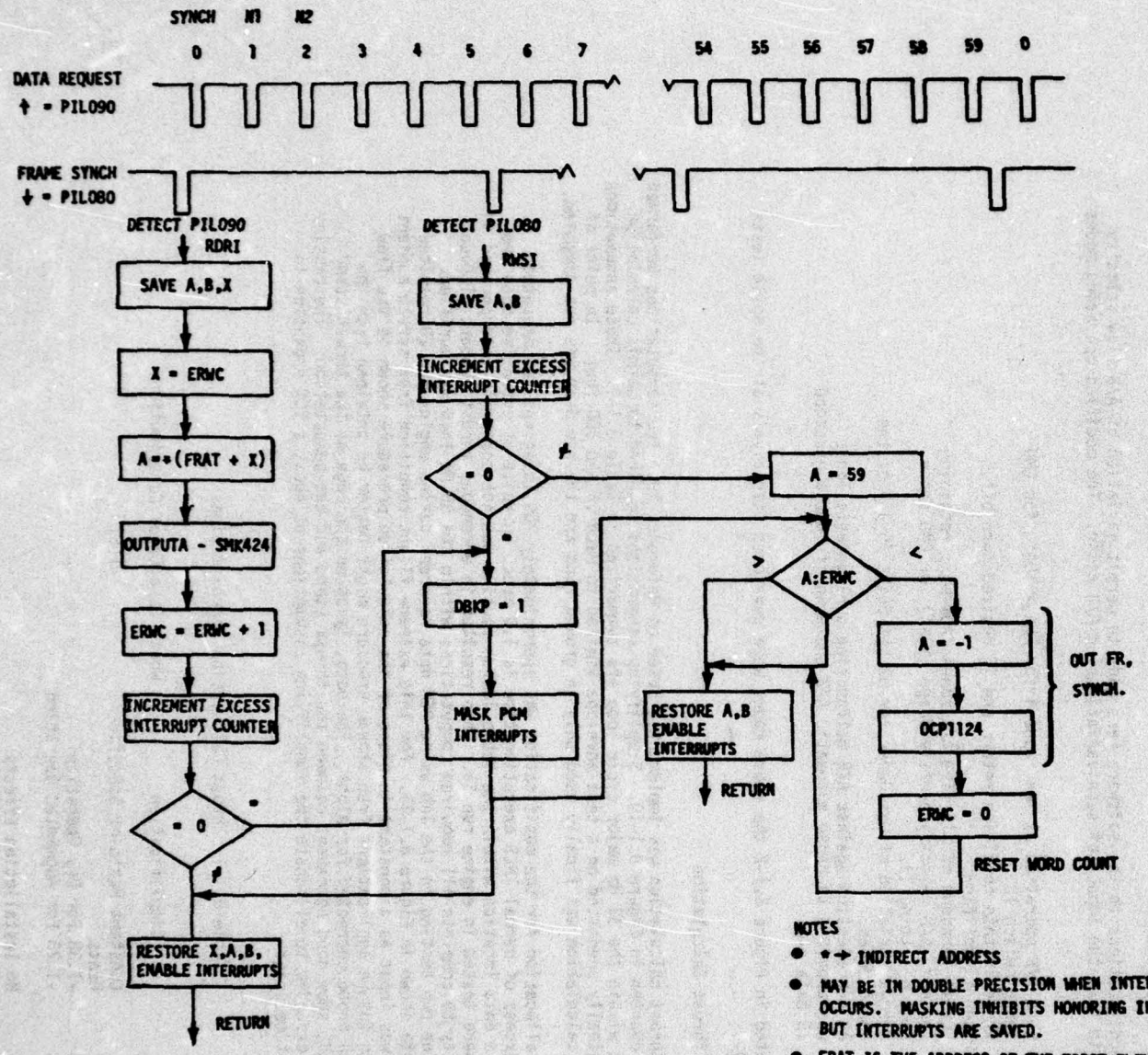

Figure 8.1-9 PCM Interrupt Processing Logic

8.1.5 Functional Additions to IPCS

As controller development proceeded it became apparent that many functions could be implemented in the software that would provide useful test data in areas not originally envisioned as part of the IPCS program. These included noise, thrust computation, and autothrottle functions.

8.1.5.1 Noise Reduction

Various modifications to the software were made to permit variation of A/B flow velocity profiles to test the impact of such variations on A/B noise. The modified operating modes included:

1) Lock A/B operation at max. zone 4 for PLA > 104°, for CMU sense switch 10.
2) While in this condition retard and if desired turn off Zone 1 fuel flow.
3) Permit turndown of all five A/B zones from max. retaining the max. A/B velocity profile shape (flat) for CMU sense switch setting 17.
4) Permit variation of Gas Generator N2 set point in any of the above modes.
5) As a protection against A/B malfunction during tests logic was provided to cause automatic A/B shutdown if rumble exceeded .5 psia p-p.

As indicated in Figure 8.1-2 the above modes were developed iteratively as the noise tests proceeded.

8.1.5.2 Thrust Calculation

A gross thrust calculation was implemented based on Reference 10. The computations performed are flow charted in Figure 8.1-10. Simplifying assumptions required to permit calculation of thrust within the 33 Hz major cycle loop are summarized in Table 8.1-1. These assumptions were originally predcated on a test envelope limited to Mach .5 and 500 feet. In point of fact the calculation was finally used only in ground runs and the ram drag was not computed.

The core allocation for the modification was approximately 700 locations and execution time in excess of normal IPCS execution time is 1.9 msec. In spite of extensive open loop checking a data location within the table lookup routine was not correctly incorporated in the software tested in engine run 35. This resulted in erroneous thrust numbers although the ability to complete all required computations within the 33 Hz loop was verified. Post engine run testing in the lab using PCM data recorded during engine run 28 resulted in the data shown in Figure 8.1-11. For this extreme flight condition free stream ambient pressure was input as a constant in place of the calculation procedure shown in the flow chart. In future applications free stream pressure might better be obtained from the local Mach probe corrected for alpha. The data, lying on the edge of the thrust stand error band, show good agreement between the thrust stand and the computation. The routine could be expanded to eliminate the simplifying assumptions at about a 50% expansion in core and time usage.

Table 8.1-1 Thrust Calculation Approximations

Simplification	*Worst Case Error Contribution*
Constant Ratio of Specific Heats -1.38 For Dry Operation -1.28 For Augmented Operation	-1.6%
No Installation Effects	
-Ejector Performance Correction	+10%/Mach; Mach < .5
-Secondary Airflow Correction	-5.%
-Kidney Bleed Flow Correction	+2.5%

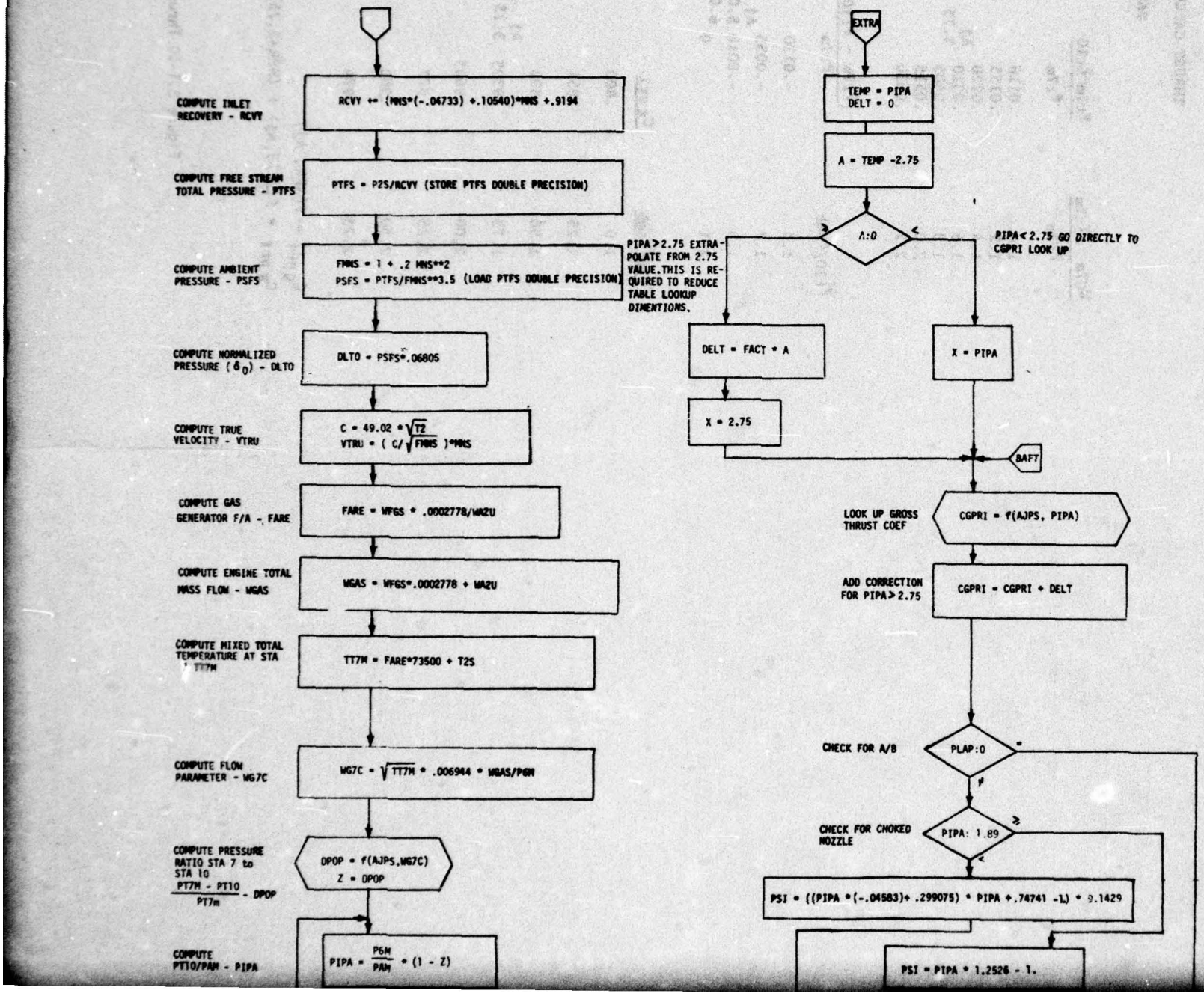
COMPUTE INLET RECOVERY - RCVY
RCVY ← (MNS*(-.04733) +.10540)*MNS +.9194
COMPUTE FREE STREAM TOTAL PRESSURE - PTFS
PTFS = P2S/RCVY (STORE PTFS DOUBLE PRECISION)
COMPUTE AMBIENT PRESSURE - PSFS
FMNS = 1 + .2 MNS**2
PSFS = PTFS/FMNS**3.5 (LOAD PTFS DOUBLE PRECISION)
COMPUTE NORMALIZED PRESSURE (δ0) - DLTO
DLTO = PSFS*.06805
COMPUTE TRUE VELOCITY - VTRU
C = 49.02 * √T2
VTRU = (C/√FMNS)*MNS
COMPUTE GAS GENERATOR F/A - FARE
FARE = WFGS * .0002778/WA2U
COMPUTE ENGINE TOTAL MASS FLOW - WGAS
WGAS = WFGS*.0002778 + WA2U
COMPUTE MIXED TOTAL TEMPERATURE AT STA 7 - TT7M
TT7M = FARE*73500 + T2S
COMPUTE FLOW PARAMETER - WG7C
WG7C = √TT7M * .006944 * WGAS/PGM
COMPUTE PRESSURE RATIO STA 7 to STA 10 (PT7M - PT10)/PT7m - DPOP
DPOP = f(AJPS,WG7C)
Z = DPOP
COMPUTE PT10/PAM - PIPA
PIPA = P6M/PAM * (1 - Z)
EXTRA
TEMP = PIPA
DELT = 0
A = TEMP -2.75
A:0
PIPA>2.75 EXTRAPOLATE FROM 2.75 VALUE.THIS IS REQUIRED TO REDUCE TABLE LOOKUP DIMENTIONS.
PIPA<2.75 GO DIRECTLY TO CGPRI LOOK UP
DELT = FACT * A
X = 2.75
X = PIPA
AAFT
LOOK UP GROSS THRUST COEF
CGPRI = f(AJPS, PIPA)
ADD CORRECTION FOR PIPA>2.75
CGPRI = CGPRI + DELT
CHECK FOR A/B
PLAP:0
CHECK FOR CHOKED NOZZLE
PIPA: 1.89
PSI = ((PIPA *(-.04583)+ .299075) * PIPA +.74741 -L) * 9.1429
PSI = PIPA * 1.2526 - 1.

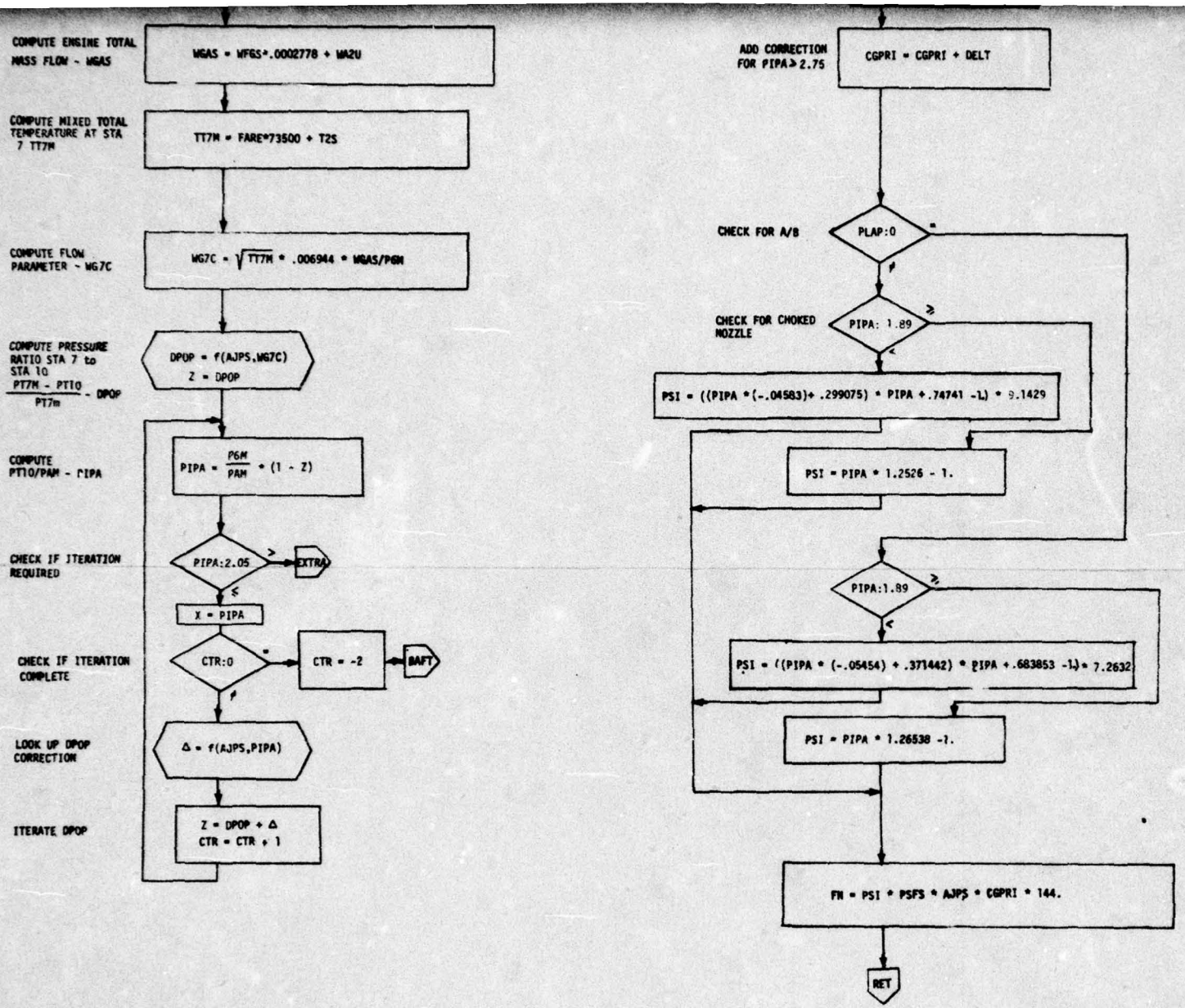

Figure 8.1-10. Thrust Calculation Block Diagram (cont.)

THRUST CALCULATION PROCEDURE

TABLE FITS

W_{G7m} T_{t7m} / P_{t7m}	$\frac{P_{t7m}-P_{t10}}{P_{t7m}}$							
1.0	.0110		.0680		.1285		.1865	
1.2	.0155		.0680		.1285		.1865	
1.4	.0220		.0680		.1285		.1865	
1.6	.0310	Aj 3.75	.0680	Aj 5.0	.1285	Aj 6.0	.1865	Aj 7.05
1.8	.0405		.0630		.1060		.1525	
2.0	.0515		.0660		.0960		.1260	
2.2	.0630		.0825		.1035		.1260	

P_{t10}/P_{amb}	$\frac{(P_{t7m}-P_{t10})}{P_{t7m}}$		
1.5	-.0130	-.0110	
1.7	-.0055	-.0032	Aj
1.9	-.0010 Aj 5.0,	0	7.05
2.1	0 6.0	0	

P_{t10}/P_{amb}	$C_{g\,pri}$							
1.0	.800		.780		.890		.968	
1.25	.851		.8425		.932		.985	
1.50	.893		.878		.966		1.0015	
1.75	.9305	Aj 3.75	.916	Aj 5.0	.981	Aj 6.0	1.0170	Aj 7.05
2.00	.9605		.945		.9865		1.025	
2.25	.977		.956		.9885		1.0255	
2.50	.982		.961		.989		1.026	
2.75	.984		.9615		.989		1.026	

$C_{g\,pri} = f(NPR, Aj)$ for $NPR \leq 2.75$

$C_{g\,pri} = f(2.75, Aj) + (NPR-2.75) * \frac{.002}{(11 - 2.75)}$ for $NPR > 2.75$

Figure 8.1-10 Thrust Calculation Block Diagram

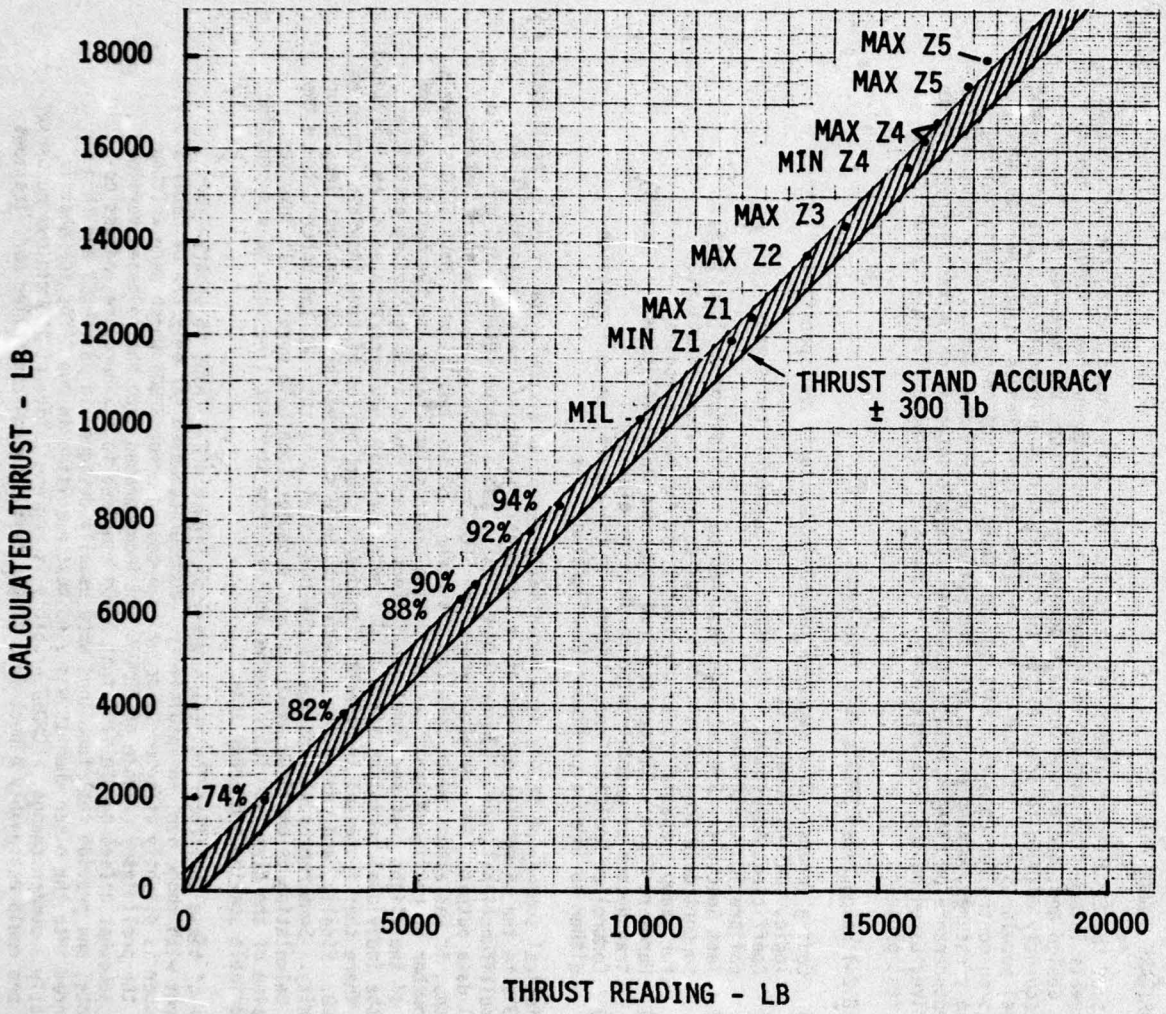

Figure 8.1-11 Thrust Data Correlation

8.1.5.3 Autothrottle

The block diagram of Figure 8.1-12 depicts the autothrottle developed on site at DFRC. It is a simplified version of an autothrottle originally developed for the C-5 and currently being developed for use on the YF-12. For use in this application the autothrottle was operated on the left hand engine and did not incorporate a pitch attitude correction. Stabilization was provided by a lead/lag scheduled on XPOLE (Volume II) and the zero resulting from the proportional plus integral control. The all electronic implementation of the system eliminated stability problems sometimes encountered in throttles using mechanical PLA linkages having hysteresis and stiction within the control loop. In this system Mach command was provided by appropriately scaling the cone command pot for use as a Mach command pot. Cockpit PLA was entirely disabled when the DPCU was engaged in the autothrottle mode.

8.2 SOFTWARE CHANGE ANALYSIS

Analysis of the SFCO's generated relative to the two CPCEI's used during the IPCS flight test reveals interesting commonalities and differences between them. BOMDIG, a mature control design and, due to the software development process, the more mature CPCEI was most frequently changed to adapt either to special test requirements or plant (engine and airframe) pecularities. IPCS had roughly 4 times as many changes as BOMDIG with more emphasis on controller changes. With the increased level of changes and accompanying schedule pressures, coding errors are more evident in IPCS than BOMDIG. For both CPCEI's the preponderance of changes relate to either aircraft integration or test support. It is imperative, based on the IPCS experience, to maintain software flexibility during the flight test program.

Figure 8.2-1 categorizes SFCO's into five types:

1) Coding Errors - Discrepancies between coded logic and specified logic, scaling errors, etc.
2) Coefficient Adjustments - Revisions to schedules and sensor calibration coefficients.
3) Test Specials - Special code required to troubleshoot malfunctions, support data acquisition, or to provide special test functions, for example special bleed configuration, for test purposes.
4) Hardware Fixes - Changes required to accommodate replacement of failed transducers or unanticipated hardware pecularities.
5) Controller Modifications - Changes to the controller configuration either to improve or expand its function.

A statistical summary of SFCO's is a potentially deceptive accumulation of data. Assignment of SFCO's to the categories defined above frequently is subjective because SFCO's are often multifunctional, one SFCO may change a gain, add a filter network, and provide for special data output. In some cases where the SFCO is apparently equally split between functions, it was allocated to both for the purpose of the tabulation. Many SFCO's have a large number of revisions sometimes reflecting progressive changes to the system over the course of the flight test and sometimes reflecting one day's troubleshooting activities. Where the individual revisions stand as discrete entities they were treated as an individual SFCO. Where they represent troubleshooting over a short period of time they are lumped as one SFCO. Finally, and perhaps most important, SFCO's are neither of constant length nor complexity. Some represent a change of one numerical constant. At the other extreme the thrust calculation is one SFCO which is over a sector long (512 words). It involves conversion of the bivariate table lookup routine from straight line code to a subroutine with variable scaling and array size.

In spite of these qualifications the summary of Figure 8.2-1 leads to observations consistent with those derived intuitively. BOMDIG accounted for only 27% of total SFCOs. This number is slightly affected by dropping 5 coding error SFCOs which were written against the preliminary release of BOMDIG and incorporated into the released version. This is somewhat offset by the fact that SFCOs required to fix hardware, adjust coefficients, and provide test functions were usually designed in one CPCEI and then transferred into the other when it was used next resulting in two SFCOs for what is essentially a common change. BOMDIG probably is representative of the minimum number of changes one could reasonably expect in a flight test program--controller modifications

AD-A034 172 BOEING AEROSPACE CO SEATTLE WASH F/G 21/5
INTEGRATED PROPULSION CONTROL SYSTEM (IPCS) VOLUME III. FLIGHT --ETC(U)
AUG 76 W J HASTINGS, C M CARLIN F33615-73-C-2035
UNCLASSIFIED AFAPL-TR-76-61-VOL-3 NL

4 OF 4
AD
AD34172

END

DATE
FILMED
2-77

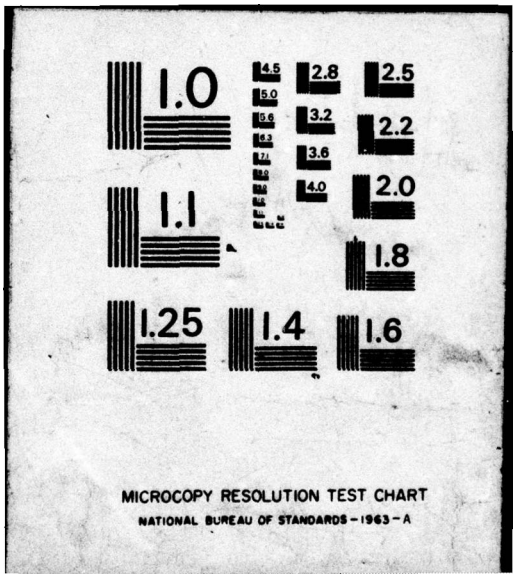
1.0
1.1
1.25
1.4
1.6
1.8
2.0
2.2
2.5
2.8
3.2
3.6
4.0
4.5
5.0
MICROCOPY RESOLUTION TEST CHART
NATIONAL BUREAU OF STANDARDS - 1963 - A

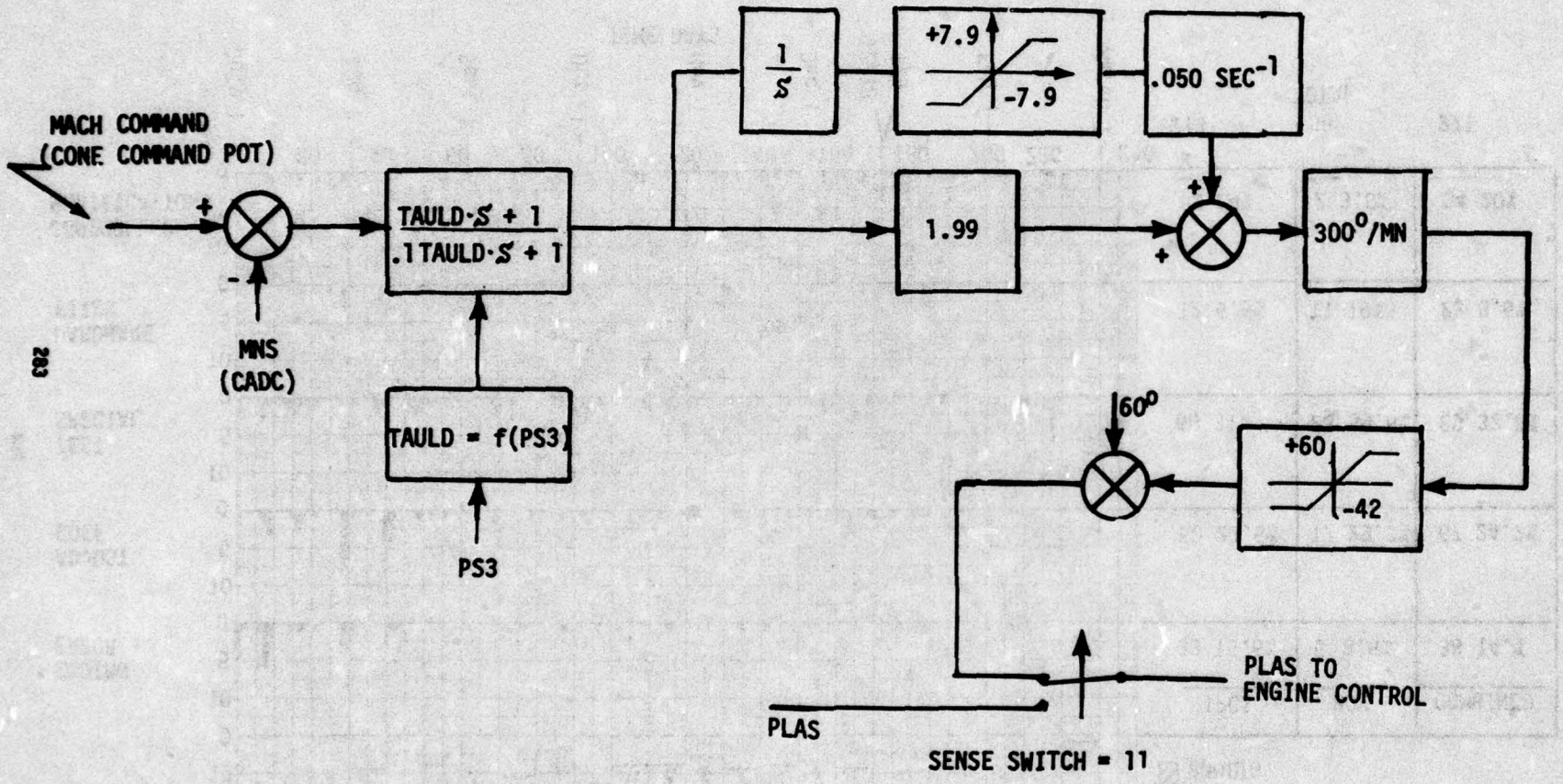

Figure 8.1-12 Autothrottle System

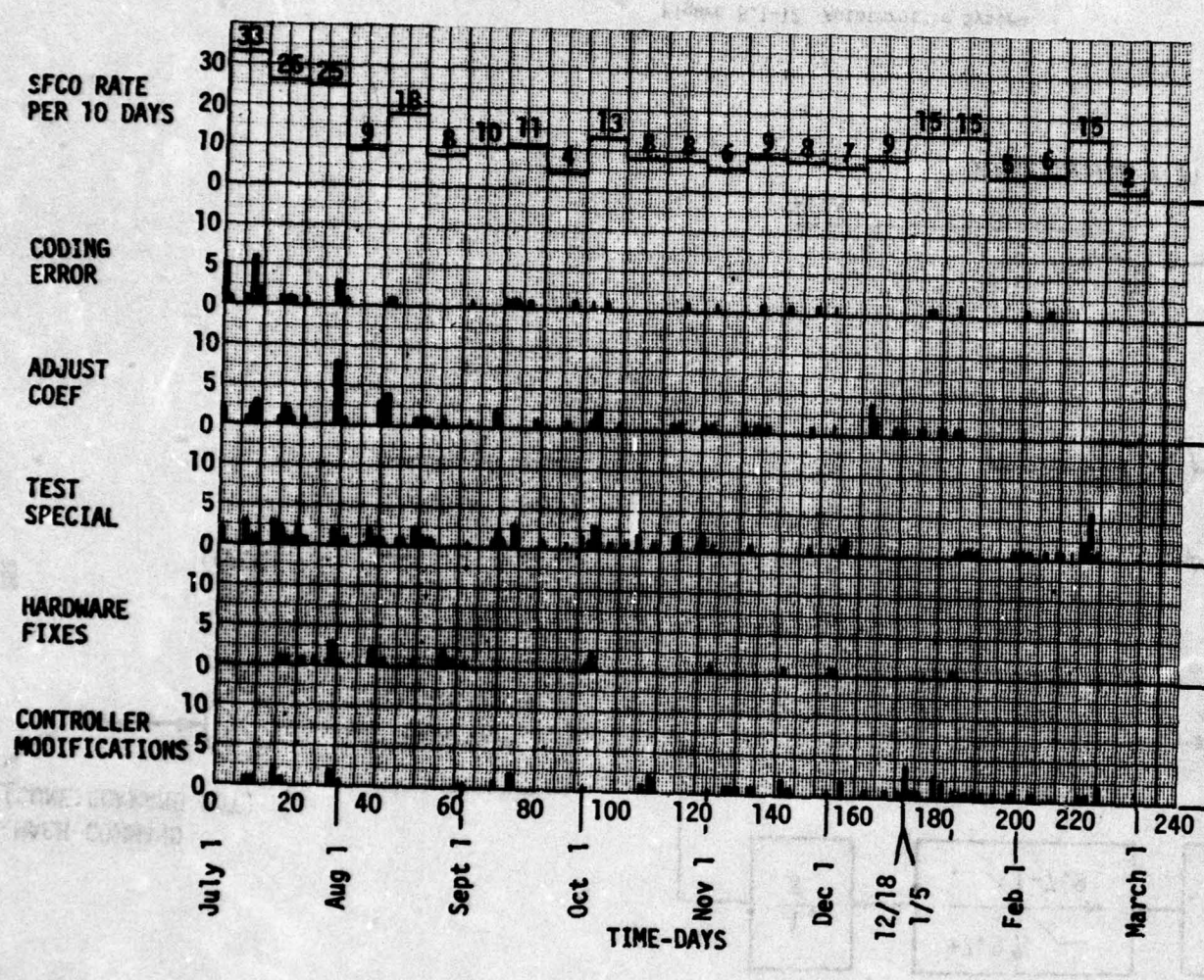

	IPCS	BOM	COMBINED
CODING ERROR	33 15.5%	5 8.6%	38 14.%
ADJUST COEF	50 23.5%	17 29.3%	67 24.7%
TEST SPECIAL	66 31%	23 39.6%	89 32.8%
HARDWARE FIXES	12 5.6%	11 19%	23 8.5%
CONTROLLER MODIFICATIONS	52 24%	2 3.5%	54 20%
TOTAL	213	58	271

Figure 8.2-1 SFCO Summary - Revision C CPCEIs

and coding errors account for less than 15% of the total BOMDIG changes. Although some reduction in the other categories is possible, more formal test planning would reduce the number of test special items, more complete integration testing might reduce the number of hardware fixes - the absolute minimum number of changes probably hovers around 50.

Conversely, IPCS probably approximates the maximum rate of software changes one might expect in a development flight test program. Coding errors tend to concentrate in the early part of the test cycle resulting mostly from the original compilation. Their correction tends to be distributed over a series of tests as each operating condition exercises a different portion of the software. Coding errors found after 1 August are primarily corrections to SFCOs. The number should be discounted since they frequently represent corrections generated either by review of code or open loop checkout and thus were never used in engine operation. Over the entire flight test period the need for a closed loop system simulation capability on site was apparent. It would not have reduced the number of SFCOs but would have significantly reduced the time and effort associated with finding coding errors and virtually eliminated the possibility of coding errors in the software configuration used for engine runs and flight tests.

Coefficient changes and test peculiar SFCOs comprise better than 50% of the SFCOs and are spread fairly evenly over the entire flight test program. Although software organization could be such as to accommodate most of the code involved in a fairly small segment of core, making it compatible with a ROM/RAM memory configuration, some of these changes satisfy requirements only discovered during flight test and thus not easily accommodated in a rigidly confined software configuration. For example the BOM 7th stage bleed was incorporated into IPCS software to provide bleed control while sufficient distortion data were obtained to permit activation of IPCS distortion control of the 7th bleed.

Hardware fix SFCOs are concentrated early in the program. This is consistent with their nature, most correct a design or interface deficiency rather than an outright failure. They are probably the most costly SFCOs in that the final SFCO usually reflects extensive troubleshooting and consulation with all parties involved in a particular interface. On the IPCS program an attempt was made to avoid problems with the PCM interface by using a PCM simulator and data readout device, the Recorder Monitor Panel, throughout the development program. As on prior programs the simulator did not adequately represent the airplane PCM system and a major troubleshooting exercise was required to sort things out. The only certain way to eliminate this problem is to integrate all such hardware prior to flight test.

The early IPCS controller modifications are primarily noise suppression filters. After baseline IPCS testing was complete numerous changes were made both to improve control modes and add functions not originally in the scope of the IPCS control.

The SFCO rate data tabulated in Figure 8.2-1 may be useful to the program planner in assessing support and recompilation requirements on future programs. In the IPCS situation, no program activity anticipated after flight test, a decision was made not to recompile during the flight test once the hurdle of ground test and first flight was successfully passed. For a continuing program a recompilation based on the program state in mid-August would have been appropriate to avoid allowing the field configuration to diverge too far from the library version of the program and to simplify the field software job. A further recompilation and a flight test verification of it, perhaps three flights, would have been required at the end of March to generate a production release of software had one been required.

8.3 PROGRAM SEQUENCE

Figure 8.3-1 depicts the execution sequence of the IPCS program as of completion of ground test. BOMDIG program execution is similar except that N1 processing is handled in the major rather than minor cycle and there are four rather than six major cycles. EMCC, the minor cycle counter, is incremented by each real time clock interrupt. The EMCC value indicated alongside the main program blocks provides some indication of the execution time of each function. Each increment in EMCC represents 5 msec, of which .75 msec is spent in the executive, processing minor cycle sampled data, or transferring data to the PCM system.

8.3.1 Executive Operation

The executive includes the following subcomponents: Mode Identification/Selection, Major Cycle Executive, Recorder Data and Frame Synch Interrupt Processing (Paragraph 8.4.1.2), Real Time Clock Interrupt Processing, Power Failure and Recovery Interrupt Processing, and the executive data base.

The major cycle executive controls execution of the program. When the DPCU is turned on a power interrupt is generated by hardware. In response the software initializes all integrator outputs and flags and the minor cycle counter EMCC and terminates in a wait loop. The first real time clock interrupt following entrance to the wait loop is processed by the executive using path "C", EMCC is incremented from four to five. This pass serves to transfer all non A/D data to memory via the DMA system and start A/D conversion and data transfer. Minor cycle data processing N1, N2, fuel flow and the fuel flow validity check are completed and the program returns to the wait loop. The next real time clock interrupt causes the program to execute path "B" of the executive, EMCC is incremented from five to six and reset to zero. Digital data is processed to engineering units and loop closure data processing for Zone 1 through Zone 4 stepper motors is completed. The program then waits for completion of the A/D data transfer, nearly complete at this time, before proceeding through minor cycle sampling and the fuel flow validity check to the main program.

The main program resets the Paros F/D converters, their data already having been transferred to memory, and outputs the digital data formatted earlier and analog outputs fromatted at the end of the last major cycle. Analog and inlet pressure data are converted to engineering units for use in succeeding computations.

One of the analog inputs processed is the LVDT measuring the position of the stepper motor controlled exhaust nozzle pilot valve. This information is used to compute the pilot valve stepper motor command which is immediately output along with the Zone 5 stepper command formatted in the same output word. Closing the exhuast nozzle loop early in the major cycle allows the stepper motor the remainder of the cycle to slew to its new position which is the key to stabilizing this servo loop. The remainder of the processing proceeds as indicated interrupted every 5 msec by the real time clock to do minor cycle processing and, for EMCC=2, to start the Paros F/D converters. PCM data and frame synch interrupts are processed as they occur inhibited only during the first section of the Real Time Clock Interrupt Routine. Once initiated by the Power Recovery Interrupt the process repeats every 30 msec, six minor cycles.

8.3.2 Failure Response

Failure detection and response are performed at various places in the program.

At the end of each major cycle the process complete flag is checked to verify that program execution time has not exceeded 30 msec. If it has the DPCU is immediately turned off. Gas generator fuel flow is checked against upper and lower limits every 5 msec. If the test is failed in two consecutive minor cycles the DPCU disengages immediately following the second failure.

As each input variable is converted to engineering units limit tests are performed and in case of failure an appropriate flag is set in the so called failure word. The word is decoded and appropriate system response is made in the designated block.

Finally a computer self test, in which each instruction in the repertoire is executed and the operation results are verified, is performed once each major cycle. If a given instruction test fails it is reexecuted. As soon as two failures are accumulated in the execution sequence, either the same instruction twice, or two instructions once, DPCU power is turned off.

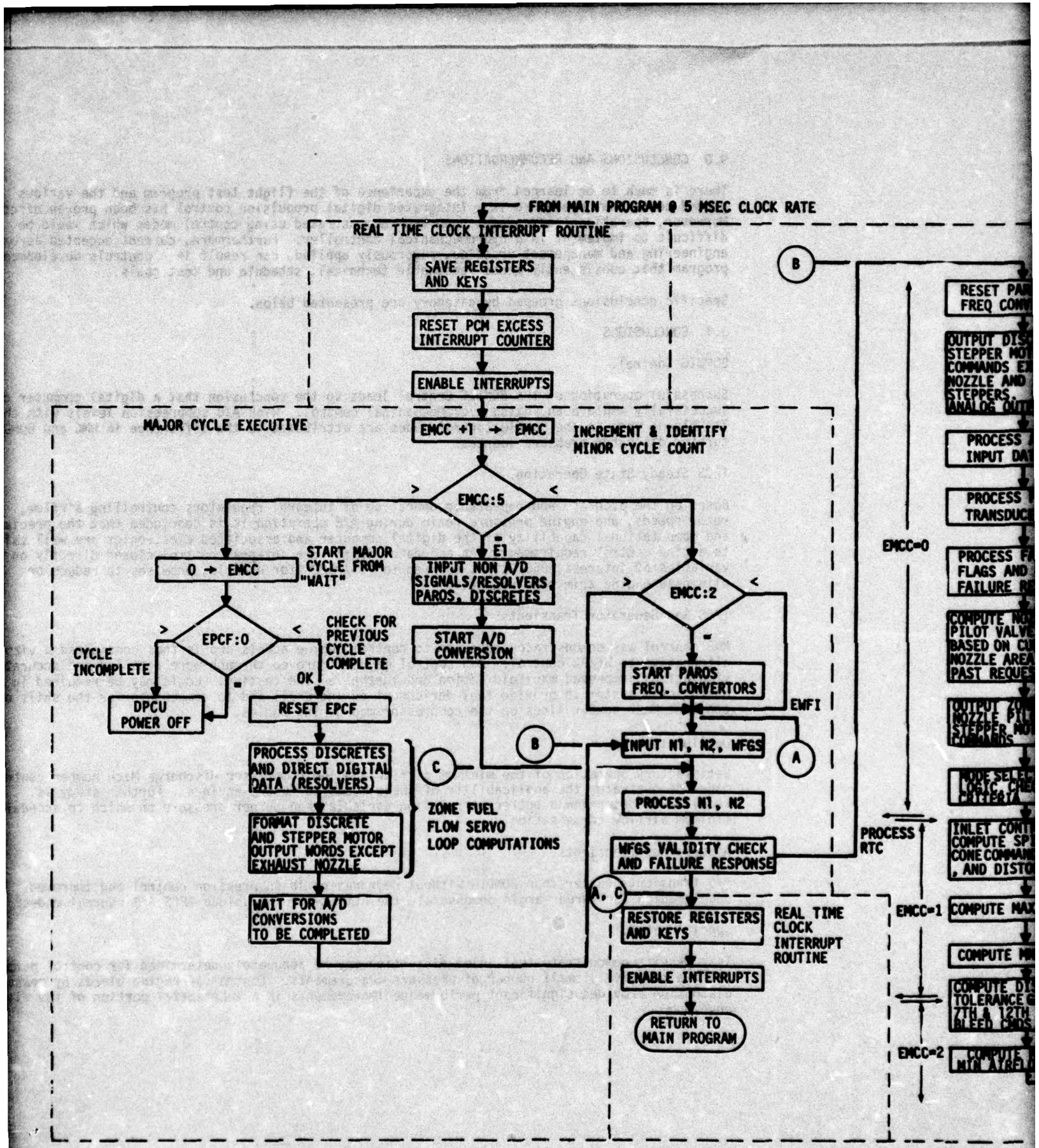
FROM MAIN PROGRAM @ 5 MSEC CLOCK RATE
REAL TIME CLOCK INTERRUPT ROUTINE
SAVE REGISTERS AND KEYS
RESET PCM EXCESS INTERRUPT COUNTER
ENABLE INTERRUPTS
MAJOR CYCLE EXECUTIVE
EMCC +1 → EMCC
INCREMENT & IDENTIFY MINOR CYCLE COUNT
EMCC:5
0 → EMCC
START MAJOR CYCLE FROM "WAIT"
EPCF:0
CHECK FOR PREVIOUS CYCLE COMPLETE
CYCLE INCOMPLETE
OK
DPCU POWER OFF
RESET EPCF
PROCESS DISCRETES AND DIRECT DIGITAL DATA (RESOLVERS)
FORMAT DISCRETE AND STEPPER MOTOR OUTPUT WORDS EXCEPT EXHAUST NOZZLE
WAIT FOR A/D CONVERSIONS TO BE COMPLETED
INPUT NON A/D SIGNALS/RESOLVERS, PAROS, DISCRETES
START A/D CONVERSION
ZONE FUEL FLOW SERVO LOOP COMPUTATIONS
EMCC:2
START PAROS FREQ. CONVERTORS
EWFI
INPUT N1, N2, WFGS
PROCESS N1, N2
WFGS VALIDITY CHECK AND FAILURE RESPONSE
RESTORE REGISTERS AND KEYS
ENABLE INTERRUPTS
RETURN TO MAIN PROGRAM
REAL TIME CLOCK INTERRUPT ROUTINE
A
B
C
A, C
EMCC=0
EMCC=1
EMCC=2
PROCESS RTC
RESET PAR FREQ CONV
OUTPUT DIS STEPPER MOT COMMANDS EX NOZZLE AND STEPPERS, ANALOG OUT
PROCESS INPUT DAT
PROCESS TRANSDUCE
PROCESS FA FLAGS AND FAILURE RE
COMPUTE NO PILOT VALVE BASED ON CU NOZZLE AREA PAST REQUES
OUTPUT ZO NOZZLE PIL STEPPER MOT COMMANDS
MODE SELEC LOGIC CHE CRITERIA
INLET CONT COMPUTE SP CONE COMMAN , AND DISTO
COMPUTE MAX
COMPUTE MI
COMPUTE DI TOLERANCE G 7TH & 12TH BLEED CMDS
COMPUTE MIN A/REL

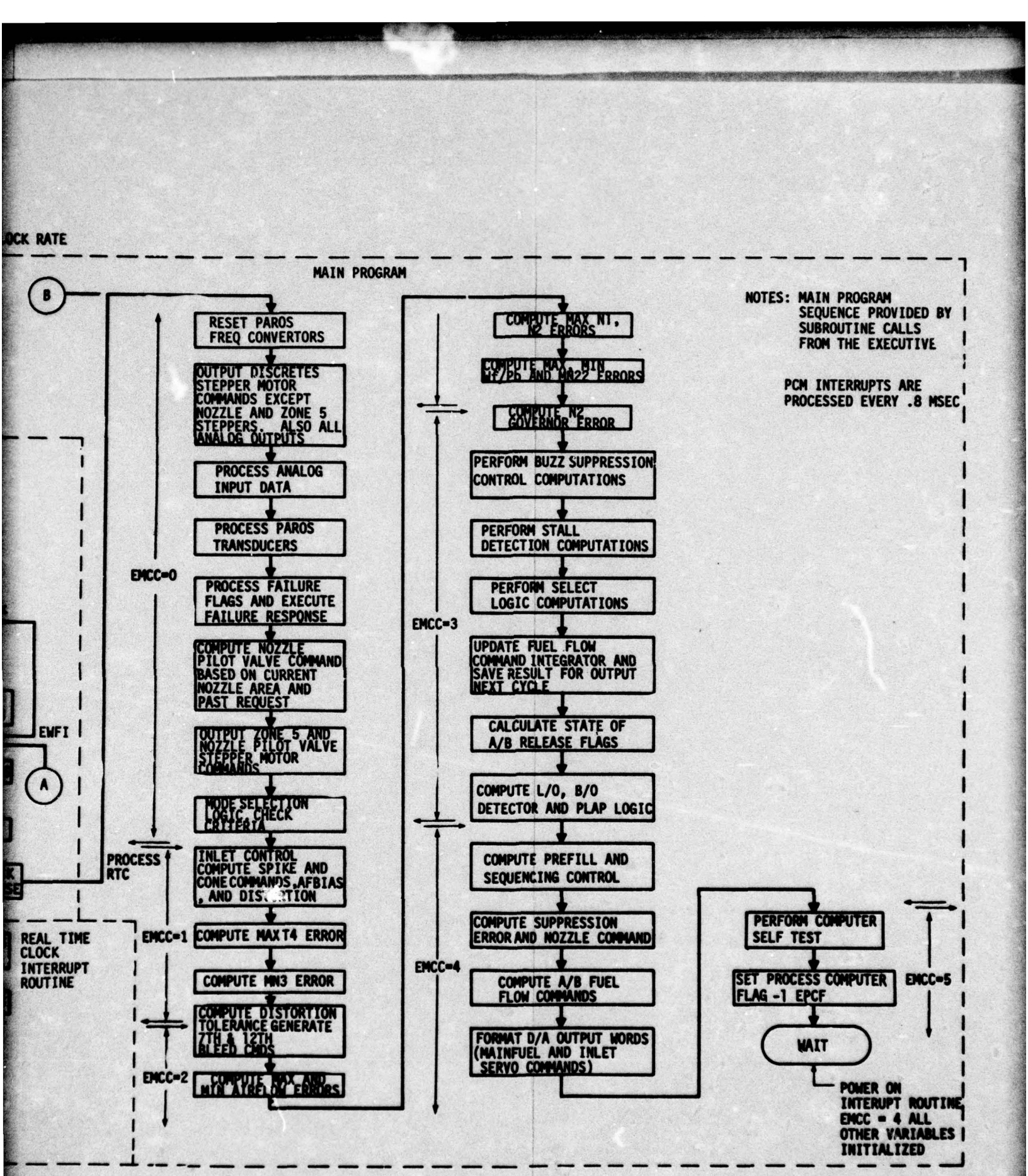

Figure 8.3-1 IPCS Program Execution Sequence

9.0 CONCLUSIONS AND RECOMMENDATIONS

There is much to be learned from the experience of the flight test program and the various ground tests that preceeded it. Integrated digital propulsion control has been proven effective. Moreover, operational advantages have been demonstrated using control modes which would be difficult to implement in a hydromechanical controller. Furthermore, current accepted aerospace engineering and management practice, rigorously applied, can result in a controls development program that consistently meets reasonable technical, schedule and cost goals.

Specific conclusions grouped by category are presented below.

9.1 CONCLUSIONS

BOMDIG Control.

Successful operation of the BOMDIG Control leads to the conclusion that a digital computer can successfully emulate an analog hydromechanical control. High A/B suppression levels with the 7th bleeds open in the BOMDIG control modes are attributed to the difference in HMC and BOMDIG turbine discharge pressure sources.

IPCS Steady State Operation.

Based on the accurate and repeatable operation of integral regulators controlling airflow, rotor speeds, and engine pressure ratio during A/B operation it is concluded that the precision and computational capability of the digital computer and associated electronics are well suited to engine control requirements. An accurate, drift free integral control closed directly on the variables of interest, P6S/P2S as opposed to P6S/PS22S for example, promises to reduce or eliminate engine trim requirements.

IPCS Gas Generator Transients.

MN3 control was demonstrated adequate to control engine accels and is thus considered a viable alternative to Wf/Pb control. MN3 control may be improved through more detailed and accurate simulations, improved manifold design and further engine testing. Logic may be required in an operational system to provide fuel derichment during stall and to compensate for the shift of constant Mach number lines on the compressor map during Bodies.

Decelerations.

Satisfactory operation of the minimum airflow and low compressor discharge Mach number control modes demonstrates the applicability of these modes to future engines. Further study is required to determine a better correlation variable than burner pressure on which to schedule minimum airflow compensation.

Afterburner Transients.

A/B transients faster than BOMDIG without degradation in suppression control and improved deceleration fan surge margin demonstrate the utility of the unique IPCS A/B control modes.

Special Loops.

Test results demonstrate that inlet distortion may be adequately determined for control purposes using a relatively small number of pressure measurements. Control of engine bleeds by measured distortion provides significant performance improvements in a substantial portion of the flight envelope.

Compressor stall and stall recovery can be reliably detected by comparing burner pressure and rate-of-change of burner pressure to suitable schedules. Incorporation of this feature in future engine controls will reduce pilot workload and engine stress in an operational environment.

Buzz loop testing demonstrated successful operation of the buzz sensing concept and a substantial reduction in idle airflow relative to BOMDIG. An operational buzz control mode would require the incorporation of high response inlet bypass doors to fully realize the potential of this control mode.

Satisfactory operation of the airflow trim and A/B anticipation modes provides confidence that these may be incorporated into future controls with strong assurance of successful application.

Successful operation of the autothrottle leads to the conclusion that direct access to engine variables for autothrottle compensation and fully electronic autothrottle loop closure are beneficial to control design and implementation since they simplify compensation and eliminate objectionable nonlinearities.

Hardware.

Trouble free operation of the IPCS hardware clearly demonstrates the practicality of the full authority digital electronic engine control. Calibration shifts in strain gage transducers indicate that future sensor selection activities should emphasize sensor stability to assure achieving the full potential of electronic controls in reducing and simplifying maintenance which is limited by sensor stability and interchangeability.

Sensor system noise was a significant problem solved primarily on an empirical basis. Future programs may benefit from an early emphasis on noise tolerant control modes and more detailed analysis of noise effects on system operation.

Quartz crystal pressure transducers, when properly vibration isolated, are an accurate, drift-free device for propulsion system control variable sensing.

Data Processing.

1) Turnaround of printed and plotted data in 16 hours or less is essential to the orderly development of a digital control.
2) Interfacing the DPCU with a facility data system at a number of different facilities is costly and time consuming.

Software.

1) IPCS software, both IPCS and BOMDIG CPCEI's, was successful and relatively trouble free due to good basic design and thorough documentation of the original CPCEI release.
2) Thorough, well documented, module and closed loop simulator system testing is essential to provide reliable software for bench and engine testing.
3) Roughly 50% of software changes after release are either coefficient changes or test peculiar modifications. These changes are unlikely to be eliminated by any amount of pre-release testing. The flexibility of IPCS software was crucial to permitting these changes in a timely manner.

9.2 RECOMMENDATIONS

It is not practical to recommend specific control features for an unknown future program. The Methodology Volume (Volume IV) addresses the problem of organizing a control development program. However, as a result of the experience from the IPCS program, recommendations are being made in three specific areas; data processing, software control and modifications to the IFU:

Data Processing.

It is strongly recommended that 16 hour turnaround data reduction capability be provided for the DPCU data. The same scheme may not be satisfactory for all programs but the requirement for quick, dependable turnaround is always there. A portable, dedicated data processing capability for the DPCU data can provide the needed turnaround and eliminate the unnecessary data interface problems.

Software Control.

As with the data reduction capability, software flexibility at the test site is essential to successful control development. The specific procedures developed for IPCS may not apply to all programs, but it is recommended that procedures be developed consistent with program requirements that allow the control software to be modified on-site to respond to test results.

Reassembly and formal documentation of software changes should be performed in a timely manner. On IPCS a reassembly required at least a week. As a result, reassemblys were deferred to major program milestones and became relatively monumental tasks. A biweekly reassembly performed in the later half of the second week of the period would provide better software quality and simplify staffing requirements.

The IPCS program was fortunate in avoiding word length problems. Late in the program as software modifications were made, the thin design margins inherent in the 16 bit machine were noticeable. A thorough review of filter performance during module testing is strongly recommended to insure that quantization effects, particularly about null, are not overlooked.

IFU Hardware.

Future users of the existing IPCS IFU are advised to consider making three revisions to it prior to using it in a major program.

The current DMA design permits inadvertant changes to data in locations 400 to 777 of memory. Since locations 400 to 577 are currently used as the DMA buffer only the volatility of locations 600 to 777 is of concern. The problem may be resolved in software by restricting use of these locations to volatile storage or in hardware by disabling the appropriate address line. The hardware modification is described in Appendix C.

The existing automatic failure detection, BITE, system does not adequately identify in the data stream the cause of failure response, disengage, or power down. Minor modifications, Appendix C, are recommended to set flags in the discrete input word, DISIN1, identifying the specific failure.

The N1/N2 frequency to digital converters are cleared by the first input data pulse in the pulse train sample. Shorting the input data lines thus may prevent clearing and result in a plausible converter output when the input is failed. This situation should be corrected either by revising the hardware to clear the counter prior to every conversion, see Appendix C, or by using more sophisticated software validity checks, for example checking for sequentially identical speed samples.

10.0 REFERENCES

1. "IPCS Flight Test Plan", Boeing Aerospace Company Document D251-10033, 26 June 1975.

2. "Interface Control Document for the Digital Propulsion Control Unit", Boeing Aerospace Company Document D251-10006, 24 January 1974.

3. "IPCS/Airplane (F-111E) Interface Specification - Basic IPCS Hardware", Revision D, Boeing Aerospace Company Document D251-10018-1, 1 October 1974.

4. "Design and Flight Testing of a Nullable Compressor Face Rake", NASA TND-7162, January 1973.

5. "IPCS Ground Test Report", Boeing Aerospace Company Document D251-10039, 6 February 1976.

6. "IPCS/Airplane (F-111E) Interface Specification - Instrumentation, Data Acquisition, and Data Processing", Boeing Aerospace Company Document D251-10018-2, 24 May 1974.

7. "Data Reduction Requirements Integrated Propulsion Control System Program", Boeing Aerospace Company Document D251-10004, 15 May 1973.

8. "Source Material Data Document, IPCS, Vol I, Inlet and Engine Simualtion Data", Boeing Aerospace Company Document D251-10010-1, 23 August 1973.

9. "IPCS Altitude Test Report", Boeing Aerospace Company Document D251-10037, 29 October 1975.

10. "In Flight Performance Determination for TF30-P-7 and TF30-P-9 Engines",Pratt and Whitney Aircraft Document PWA 3994, 15 October 1970.

APPENDIX A - CONFIGURATION CHANGES AND TEST EVENTS

The following paragraphs discuss the changes in hardware and software configuration and the test events on a flight by flight basis. In general the ground runs are discussed in the paragraphs for the relevant flight. Table A-1 describes the engine runs and identifies the paragraph in which they are discussed.

The V1 DPCU system was installed in the airplane for flights 14-23. The following components were changed for flights 24-28:

CMU (V1 to V2)
PSU (V1 to V2)
IFU (V1 to V2)

The changes were made as part of the auto-disengage investigation and not due to failures in any component. The units were functionally interchangeable although it was observed that T2 signal noise was reduced with IFU V2 (see paragraph 7.1.3).

A.1 Preflight Engine Runs

A series of ground tests were conducted on each control mode prior to flight testing. These tests served to document the system static performance, identify and correct any problems, checkout the data systems, and demonstrate the flight worthiness of the IPCS installed in the F-111. The conduct of the tests has been discussed in some detail in the IPCS Ground Test Report, Reference 5. Table A-1 identifies the engine runs. Table A-2 defines the software configuration for each run.

Most of the preflight testing was routine, establishing the steady-state and transient performance as a baseline for the flight tests with problems confined to data system interfacing, control room display, etc. One item which did affect both control programs was the inadvertent reprogramming of some core locations in the 600-777 portion of sector 0 as a result of a direct memory access (DMA) problem (Reference 4-1). The problem was solved with restoration of the affected locations as part of the power up routine. The DMA problem resulted in afterburner stalls during engine run 7. The other significant problem was encountered in IPCS. Operating steady-state in A/B there was a significant oscillation in A/B fuel flow. As the result of engine runs 11 and 12 the problem was identified as response to N1 noise. The gain of the suppression loop was reduced by a factor of 2 for flight 17 to reduce sensitivity to N1 noise.

A.2 Flight 14 - September 4, 1975

A.2.1 Hardware Configuration

The IPCS hardware was in the basic configuration defined in Reference 4-2. One electrical harness on PKDC (Figure 5.1-1) was found to be open circuit and replaced.

A.2.2 Software Configuration - BOMDIG

The software for flight 14 was the baseline configuration developed through engine run 6. Engine runs 8 and 9 (taxi test) also used this software configuration.

A.2.3 Event Summary

The verification engine run (8) was conducted without difficulty. The taxi test was run with no major problems. Data display in the control room, etc., was revised as a result of the taxi test.

There were no control problems on Flight 14. The following test events were completed:

Mach 0.5, 10,000 ft.
HMC MIL-IDLE-MIL
BOMIDG MIL-MAX-MIL-IDLE-MIL, SST, YAW

Table A-1 Engine Run Summary

Engine Run No.	Date	Ref. Para	Control	Description
0	7/31/75	A.1	HMC	Trim, Engine Checkout
1	8/04/75	A.1	HMC	Steady-State and Transient Performance
2	8/04/75	A.1	BOMDIG	Gas Generator Trim and Steady-State Performance
3	8/05/75	A.1	BOMDIG	Gas Generator Transients
4	8/06/75	A.1	BOMDIG	Initial A/B Trim and A/B Transients
5	8/08/75	A.1	BOMDIG	A/B Trim A/B Steady-State Performance
6	8/08/75	A.1	BOMDIG	Control Room Checkout, Start, Recheck Gas Generator Transients
7	8/13/75	A.1	IPCS	Gas Generator Trim, Steady-State and Transient Performance, A/B Stalls Due to DMA Problem (Ref. 4-1)
8	8/26/75	A.2	BOMDIG	Software Verification for Flight 14
9	8/28/75	A.2	BOMDIG	Taxi Test
10	9/22/75	A.1	IPCS	A/B Transient Performance, Encounter A/B Fuel Flow Oscillation
11	9/26/75	A.1	IPCS	Diagnostic - A/B Oscillation Problem
12	9/30/75	A.1	IPCS	Diagnostic - A/B Oscillation Problem
13	10/08/75	A.3	BOMDIG	Performance Improvement Evaluation
14	10/29/75	A.1	IPCS	Performance Improvement Evaluation
15	10/31/75	A.3	BOMDIG	Software Verification for Flight 15
16	11/12/75	A.1	IPCS	Performance Improvement Evaluation
17	11/13/75	A.5	IPCS	Software Verification for Flight 17
18	11/25/75	A.6	IPCS	Software Verification for Flight 18
18a	11/26/75	A.6	IPCS	Calibration Check on Nozzle Area Rigging
19	12/15/75	A.9	IPCS	Software Verification for Flight 21
19a	12/17/75	A.9	IPCS	ECS and Stall Detection Level Test
20	12/19/75	A.10	IPCS	Checkout of the Non-Linear MN3 Loop
21	1/08/76	A.12	IPCS	Software Verification for Flight 23
22	1/16/76	A.13	IPCS	Diagnostic - Auto Disengage
23	1/16/76	A.13	IPCS	Diagnostic - Auto Disengage
24	1/20/76	A.14	IPCS	Evaluation of Non-Linear MN3 Loop & Non-Linear N2 Gain
25	1/21/76	A.14	IPCS	Software Verification for Flight 24
26	1/27/76	A.16	IPCS	Noise and Thrust Measurement
27	2-05/76	A.17	IPCS	Software Checkout for Noise Flight and Evaluation of Variable Gain on Integral MN3 Loop
28	2/06/76	A.18	IPCS	Noise and Thrust Measurement
29	2/10/76	A.19	IPCS	Software Checkout of Rumble Disable for SSO4, Check On Spike Switch
30	2/18/76	A.19	IPCS	Software Checkout of Minor Cycle Sample MN3 Loop
31	2/19/76	A.19	IPCS	Software Verification for Flight 26
32	2/25/76	A.20	IPCS	Software Verification for Flights 27 & 28
33	2/25/76	A.20	IPCS	Noise Measurement
34	3/04/76	A.21	IPCS	Velocity Profile Measurement
35	3/05/76	A.22	IPCS	Fast Accel and Thrust Measurement

Table A-1 Engine Run Summary

Engine Run No.	Date	Ref. Para	Control	Description
0	7/31/75	A.1	MMC	Trim, Engine Checkout
1	8/04/75	A.1	MMC	Steady-State and Transient Performance
2	8/04/75	A.1	BOMDIG	Gas Generator Trim and Steady-State Performance
3	8/05/75	A.1	BOMDIG	Gas Generator Transients
4	8/06/75	A.1	BOMDIG	Initial A/B Trim and A/B Transients
5	8/08/75	A.1	BOMDIG	A/B Trim A/B Steady-State Performance
6	8/08/75	A.1	BOMDIG	Control Room Checkout, Start, Recheck Gas Generator Transients
7	8/13/75	A.1	IPCS	Gas Generator Trim, Steady-State and Transient Performance, A/B Stalls Due to DMA Problem (Ref. 4-1)
8	8/26/75	A.2	BOMDIG	Software Verification for Flight 14
9	8/28/75	A.2	BOMDIG	Taxi Test
10	9/22/75	A.1	IPCS	A/B Transient Performance, Encounter A/B Fuel Flow Oscillation
11	9/26/75	A.1	IPCS	Diagnostic - A/B Oscillation Problem
12	9/30/75	A.1	IPCS	Diagnostic - A/B Oscillation Problem
13	10/08/75	A.3	BOMDIG	Performance Improvement Evaluation
14	10/29/75	A.1	IPCS	Performance Improvement Evaluation
15	10/31/75	A.3	BOMDIG	Software Verification for Flight 15
16	11/12/75	A.1	IPCS	Performance Improvement Evaluation
17	11/13/75	A.5	IPCS	Software Verification for Flight 17
18	11/25/75	A.6	IPCS	Software Verification for Flight 18
18a	11/26/75	A.6	IPCS	Calibration Check on Nozzle Area Rigging
19	12/15/75	A.9	IPCS	Software Verification for Flight 21
19a	12/17/75	A.9	IPCS	ECS and Stall Detection Level Test
20	12/19/75	A.10	IPCS	Checkout of the Non-Linear MN3 Loop
21	1/08/76	A.12	IPCS	Software Verification for Flight 23
22	1/16/76	A.13	IPCS	Diagnostic - Auto Disengage
23	1/16/76	A.13	IPCS	Diagnostic - Auto Disengage
24	1/20/76	A.14	IPCS	Evaluation of Non-Linear MN3 Loop & Non-Linear N2 Gain
25	1/21/76	A.14	IPCS	Software Verification for Flight 24
26	1/27/76	A.16	IPCS	Noise and Thrust Measurement
27	2-05/76	A.17	IPCS	Software Checkout for Noise Flight and Evaluation of Variable Gain on Integral MN3 Loop
28	2/06/76	A.18	IPCS	Noise and Thrust Measurement
29	2/10/76	A.19	IPCS	Software Checkout of Rumble Disable for SS04, Check On Spike Switch
30	2/18/76	A.19	IPCS	Software Checkout of Minor Cycle Sample MN3 Loop
31	2/19/76	A.19	IPCS	Software Verification for Flight 26
32	2/25/76	A.20	IPCS	Software Verification for Flights 27 & 28
33	2/25/76	A.20	IPCS	Noise Measurement
34	3/04/76	A.21	IPCS	Velocity Profile Measurement
35	3/05/76	A.22	IPCS	Fast Accel and Thrust Measurement

TABLE A-2 SOFTWARE CONFIGURATION
FOR PREFLIGHT ENGINE RUNS

DATE	ENGINE RUN	TAPES	HAND LOADS
7/31/75	0	BOMDIG-C, 7507291	BOMDIG C-15A
8/04/75	1	BOMDIG-C, 7507291	BOMDIG C-15A, C-15B, Trims - Idle = 00701_8 MIL = 37654_8 A/B = $.37650_8$
8/04/75	2	"	"
8/05/75	3	"	"
8/06/75	4	"	"
8/08/75	5	"	BOMDIG C-15A, -15B, -15C, C-28, C-25A, Trims-MIL = 37735_8 IDLE = 01440_8 A/B = 37336_8
8/08/75	6	"	"
8/13/75	7	IPCS-C, 7508111	IPCS C-37G
8/26/75	8	BOMDIG-C, 7507291, 7508221, 7508251	None
8/28/75	9 (Taxi Test)	"	"
9/22/75	10	IPCS-C, 7508111, 7509171	IPCS C-63
9/26/75	11	IPCS-C, 7508111, 7509171	IPCS C-50A, C-63, C-64, C-65
9/30/75	12	IPCS-C, 7508111, 7509171	IPCS C-12C, C-50A, C-63, C-64, C-65A
10/08/75	13	BOMDIG-C, 7507291, 7508221, 7510031, 7510071	BOMDIG-C-42
10/29/75	14	IPCS-C, 7508111, 7509171, 7510241	IPCS C-63A, C-50D, C-71
10/31/75	15	BOMDIG-C, 7507291, 7508221, 7510031, 7510291	BOMDIG-C-42A
11/12/75	16	IPCS-C, 7508111, 7509171, 7510241, 7511111	IPCS 50D
11/13/75	17	IPCS-C, 7508111, 7509171, 7510241, 7511111, 7511131	IPCS 50D

Mach 0.7, 10,000 ft.
HMC MIL-IDLE-MIL

Mach 0.8, 30,000 ft.
HMC MIL-IDLE-MIL

Mach 0.9, 10,000 ft.
HMC MIL-IDLE-MIL
BOMDIG MIL-MAX-MIL-IDLE-MIL, SST, YAW

Mach 1.06, 22,000 ft.
HMC MIL-IDLE-MIL
BOMDIG MIL-MAX-MIL-IDLE-MIL, MAX-IDLE-MAX, SST

Mach 1.6, 45,000 ft.
BOMDIG MIL-MAX-MIL-IDLE-MIL, SST, YAW

Mach 1.9, 45,000 ft.
BOMDIG MIL-MAX-MIL-IDLE-MIL, SST, YAW

An ECS problem required operation throughout the flight on L/H ECS which takes bleed air from the IPCS engine. Later flights were all flown with the ECS on the R/H engine.

A.3 Flight 15 - November 6, 1975

A.3.1 Hardware Configuration

Paroscientific transducer S/N 137 (PKDB) failed after flight 14. It was replaced with S/N 147. A flexible line segment was installed in each of the pressure lines for the wheel well mounted Paros transducers. The specific gravity adjustment on the HMC control was changed from JP-5 to JP-4 prior to engine run 10. After engine run 13 the engine was removed. The probes were inspected and the IPCS temperature harness replaced.

The effect of the harness change was to change the location of the cold references relative to the thermistor (Figure 5.4-15.) While the engine was removed the N1 tach. was replaced to see if this would reduce the N1 noise (paragraph 7.5).

A.3.2 Software Configuration- BOMDIG

The following software changes were made for engine run 13: incorporate the coefficients for transducer S/N 147, enable A/B reset changes for sense switch 17 and PLA > 50° rather than sense switch 17 and 7th bleed closed, output WFG, lower 12th bleed thresholds by .6 psi to the lower edge of the HMC tolerance band, revised upper validity limits, cleared backup and fault on a transition of sense switch #1., and provide automatic inlet commands for both positions of the manual control switch.

The following additional changes were made for engine run 15 and flight 15: revise the sensed main fuel flow (WFGS) calibration to match the IFU calibration and open the 7th bleed at Mach 1.75 rather than 1.8.

A.3.3 Events Summary

Engine run 13 was a checkout of the performance improvements approved at the 1 October 1975 meeting (Reference 5). No problems were encountered. Engine run 15 was the software verification run for flight 15. No software problems were encountered. However, there were two DPCU auto-disengages during the engine run. It was concluded that since the disengages occurred soon after turning the system on, it was acceptable to go ahead with the flight as planned.

An additional disengage occurred during the pre-taxi engine running. No auto-disengages occurred in flight. The following events were successfully completed:

Mach 0.5, 10,000 ft
HMC MIL-IDLE-MIL
BOMDIG MAX-IDLE-MAX

Mach 0.7, 10,000 ft.
HMC MIL-IDLE-MIL

Mach 0.8, 30,000 ft.
HMC MIL-IDLE-MIL
BOMDIG MIL-MAX-MIL-IDLE-MIL, MAX-IDLE-MAX, SST, Yaw

Mach 0.9, 10,000 ft.
HMC MIL-IDLE-MIL
BOMDIG MIL-MAX-MIL-IDLE-MIL, MAX-IDLE-MAX
Mach 0.9, 45,000 ft.
HMC MIL-IDLE-MIL

Mach 1.06, 22,000 ft.
HMC MIL-IDLE-MIL

Mach 1.4, 41,000 ft.
HMC MIL-IDLE-MIL

During the acceleration to supersonic conditions failures occurred in the flexible lines to the wheel well Paroscientific transducers at approximately Mach 2.2. The lines were unable to operate in the temperatures encountered at supersonic flight conditions. The DPCU system responded properly to the reduction in sensed compressor face pressure. It disengaged when two failures were detected and indicated failures of PDEMS and P2S for all subsequent flight conditions except when the wheel well pressure was within acceptable limits (2.8 - 26.25 psia). A compressor stall resulted from the disengage transient.

A.4 Flight 16 - November 10, 1975

A.4.1 Hardware Configuration

The flexible lines for the wheel well Paroscientific transducers were replaced with high temperature lines.

A.4.2 Software Configuration - BOMDIG

No software changes were made since flight 15.

A.4.3 Events Summary

The following events were completed during the flight. Four stalls occurred as indicated:

Mach 0.7, 10,000 ft.
BOMDIG MIL-MAX-MIL-IDLE-MIL, MAX-IDLE-MAX, SST, YAW
Mach 0.9, 45,000 ft.
HMC MIL-IDLE-MIL
BOMDIG MAX-MIL (STALL), MAX-MIL, MIL-MAX, MIL-MAX-MIL
(STALL)
Mach 1.4, 41,000 ft.
BOMDIG MIL-MAX-MIL-IDLE-MIL, MAX-IDLE-MIL, SST, YAW

Mach 2.47, 50,000 ft.
BOMDIG MAX-IDLE-MAX (STALL), YAW, SST (STALL)

650 KT Accel

500 KT Climb

One auto-disengage occurred during the pretaxi ground running.

The first supersonic stall occurred during a max-to-idle transient and the second occurred during an SST maneuver. These stalls were recovered without any significant engine over-temperature. Both subsonic stalls occurred during max to mil transients and were caused by operation at minimum zone fuel flows during the A/B shutdown. The minimum fuel flows limited fuel derichment as the nozzle area was closing down until engine stall occurred. Engine overtemperatures did result from the two subsonic stalls. An attempted relight following the second stall was hot, the engine was shutdown and the airplane returned to base on the right hand engine. A subsequent engine run (17) demonstrated that there was no performance loss and thus the engine was not damaged by the overtemperature.

A.5 Flight 17 - November 17, 1975

A.5.1 Hardware Configuration

No hardware changes were made following flight 16.

A.5.2 Software Configuration - IPCS

As this was the first IPCS Flight the software for both engine run 17 and flight 17 was the baseline IPCS configuration developed through engine run 16.

A.5.3 Events Summary

The following events were completed:

Mach 0.5, 10,000 ft.
IPCS MIL-MAX-MIL-IDLE-MIL, MAX-IDLE-MAX, SST, YAW

Mach 0.7, 10,000 ft.
HMC MIL-IDLE-MIL
IPCS MIL-MAX-MIL-IDLE-MIL, MAX-IDLE-MAX, SST, YAW
MIL-MAX-MIL, IDLE-MIL-IDLE(2)

Mach 0.8, 30,000 ft.
IPCS MIL-MAX-MIL-IDLE-MIL, MAX-IDLE-MAX, YAW, SST

Mach 0.9, 10,000 ft.
IPCS MIL-MAX-MIL-IDLE-MIL, MAX-IDLE-MAX, YAW, SST

Mach 1.06, 22,000 ft.
IPCS MIL-MAX-MIL-IDLE-MIL, MAX-IDLE-MAX, YAW, SST

Mach 1.4, 50,000 ft.
HMC MIL-IDLE-MIL
IPCS MIL-MAX-MIL-IDLE-MIL, MAX-IDLE-MAX, YAW, SST

Mach 1.6, 45,000 ft.
IPCS MIL-MAX-MIL-IDLE-MIL, MAX-MIL-MAX-IDLE-MAX, YAW
SST

Mach 1.9, 45,000 ft.
IPCS MAX-MIL-IDLE-MIL-MAX, MAX-IDLE-MAX, YAW, SST

Two relatively minor controller anomalies were observed during the flight. Operation in afterburner, particularly during the airplane acceleration to supersonic speeds, showed oscillations in fuel flow which produced thrust variations noticeable to the crew. The oscillations were due to noise on the low rotor speed signal (N1S), Early nozzle release occurred during idle to max transients at supersonic flight conditions. This appeared to result in an afterburner mis-light at Mach 1.9, 45,000 feet. The early release was caused by a nozzle unlock command from the airflow match loop (AFBIAS).

An auto-disengage occurred during the pre-taxi engine running.

A.6 Flight 18 - December 2, 1975

A.6.1 Hardware Configuration

A new temperature harness configuration was tested and appeared to work well. The old harness used for DPCU measurement of T2, T22, and T3 developed an open circuit in the T3 leg which resulted in cancellation of an attempt to fly flight 18 on November 17. The open circuit was traced to the failure of a splice incorporated by the vendor to lengthen the T3 leg for the transducer box configuration change (figure 5.4-1). The harness was replaced with a NASA harness and the cold junctions in the transducer box replaced with solid state references mounted in the wheel well to improve accuracy. The nozzle area feedback pully was adjusted +1.5° to correct the reading to the DPCU.

A.6.2 Software Configuration - IPCS

The software changes since flight 17 consisted of 1) incorporation of an N1 filter to reduce A/B fuel flow oscillations, 2) inhibit "airflow trim" nozzle unlock which resulted in premature nozzle opening during idle max transients, 3) modifications for the incorporation of solid state references for the T2, T22, T3 thermocouples, 4) open 7th stage bleed at 1.75 Mach rather than 1.8, and 5) elimination of the leadlag compensation on the minimum airflow loop.

A.6.3 Event Summary

The following events were completed on flight 18:

Mach 1.4, 30,000 ft.
HMC MIL-IDLE-MIL
IPCS MIL-MAX-MIL-IDLE-MIL, MAX-IDLE-MAX, YAW SST

Mach 1.4, 41,000 ft.
IPCS MIL-MAX-MIL-IDLE-MIL, MAX-IDLE-MAX, YAW SST

Mach 1.4, 50,000 ft.
HMC MIL-IDLE-MIL
IPCS MIL-MAX-MIL-IDLE-MIL

Mach 1.6, 45,000 ft.
HMC MIL-IDLE-MIL
IPCS MAX-IDLE-MAX (2 for different D/A output)

Mach 2.o, 45,000 ft.
IPCS MIL-MAX-MIL-IDLE-MIL, MAX-IDLE-MAX, YAW, SST

Mach 2.3, 50,000 ft.
IPCS MAX-IDLE-MAX, YAW, SST (STALL)

The two control anomalies identified during flight 17 (A/B fuel oscillations and premature nozzle opening) were corrected. No significant controller problems were identified. The pilot reported small EPR oscillations (±.02) at Mach 1.6 during the supersonic acceleration. One stall was encountered during an SST at Mach 2.3 with no overtemperature.

During afterburner operation suppression is maintained by controlling nozzle area as a function of suppression error. When the nozzle is at the maximum stop, zone 5 fuel flow is modulated to control suppression. At Mach 2.1 nozzle oscillation resulted from switching between the two suppression control modes.

A.7 Flight 19 - December 2, 1975

A.7.1 Hardware Configuration

There were no hardware changes for this flight.

A.7.2 Software Configuration - IPCS

There were no software changes for this flight.

A.7.3 Event Summary

The following events were completed in flight 19:

Mach 0.7, 21.000 ft.
HMC MIL-IDLE-MIL BODIE
IPCS MIL-IDLE-MIL BODIE

Mach 0.85, 21,000 ft.
HMC MIL-IDLE-MIL BODIE
IPCS MIL-IDLE-MIL BODIE(2)

Mach 0.9, 45,000 ft.
HMC MIL-IDLE-MIL, MIL-IDLE-MIL BODIE
IPCS MIL-MAX-MIL-IDLE-MIL, MIL-IDLE-MIL BODIE,
MIL-MAX-IDLE-MAX, YAW, SST

650 KT Accel
500 KT Climb
Mach 2.4, 54,000 ft.
IPCS MAX-IDLE-MAX (STALL)

The controller operated well over the Mach range from 0.7 to 2.4+. The MAX-IDLE transient at 0.9 Mach, 45,000 ft., which resulted in stalls BOMDIG, was successfully executed in IPCS control. One stall occurred at Mach 2.4+ during an IDLE-MAX transient without serious overtemperature. Recovery from the stall was difficult at this condition due to the strength of the inlet buzz induced by the stall. Another stall occurred in Max A/B at approximately Mach 1.8 and 40,000 ft. This stall recovered very rapidly with no overtemperature. At Mach 0.9, 45,000 ft. there were two apparent afterburner mislights.

The pilot again reported EPR oscillations (±.01) at high indicated air speed.

During the pretaxi ground running two auto disengages occurred at idle PLA.

A.8 Flight 20 December 5, 1975

A.8.1 Hardware Configuration

There were no hardware changes.

A.8.2 Software Configuration - BOMDIG

The only software change from the last BOMDIG flight (Flight 16) was to incorporate the solid state cold reference system for temperature measurements.

A.8.3 Event Summary

The following events were completed on Flight 20:

Mach 0.7, 21,000 ft.
HMC MIL-IDLE-MIL BODIE (2)
IPCS MIL-IDLE-MIL BODIE

Mach 0.85, 21,000 ft.
HMC MIL-IDLE-MIL BODIE
BOMDIG MIL-IDLE-MIL BODIE

Mach 0.9, 45,000 ft.
HMC MIL-IDLE-MIL
BOMDIG MIL-IDLE-MIL, MIL-MAX-MIL (STALL)

Mach 1.06, 22,000 ft.
HMC MIL-IDLE-MIL
BOMDIG MIL-MAX-MIL-IDLE-MIL

Mach 1.4, 30,000 ft.
BOMDIG MIL-MAX-MIL-IDLE-MIL, MAX-IDLE-MAX, YAW SST

Mach 1.4, 50,000 ft.
HMC MIL-IDLE-MIL
BOMDIG MIL-MAX-MIL-IDLE-MIL, MAX-IDLE-MAX

Mach 1.6, 45,000 ft.
HMC MIL-IDLE-MIL, MIL-IDLE-MIL 7th Bleed Closed
BOMDIG MIL-MAX-MIL-IDLE-MIL, MAX-IDLE-MAX, MIL-IDLE-MIL
7th Bleed Closed

Mach 2.1, 45,000 ft.
BOMDIG MIL-MAX-MIL-IDLE-MIL (STALL), MAX-IDLE-MAX(STALL),
YAW, SST, A/B Retard(STALL)

Mach 2.3, 50,000 ft.
BOMDIG A/B Retard(Stall), MAX-IDLE(STALL), YAW, SST,
A/B Retard(STALL)

At most flight conditions the controller operated quite successfully. Seven compressor stalls were encountered, six occurring at high Mach number (2.3 and 2.1) and one at 0.9, 45,000 ft. None of the stalls resulted in serious overtemperature. The supersonic stalls all occurred as the result of throttle retards from max A/B. The stall at 0.9, 45,000 ft., also during a max to mil transient, was consistent with the results of flight 15 and the performance of the hydromechanical controller. One auto disengage was experienced during the pretaxi engine running.

A.9 Flight 21 December 23, 1975

A.9.1 Hardware Configuration

An incorrect pin material was discovered in the Cr pin of the ConOhmic box connector in the DPCU T2 harness. The pin was replaced and the lead connecting the shields across the ConOhmic box was added.

The ring A card 2 of the distortion computer (not DPCU related) was replaced with a spare card due to excessive noise on the ring A output on the previous flights

A.9.2 Software Configuration IPCS

Flight 21 was the initial flight with the IPCS special loops enabled. Many of the software changes were to enable these loops. The following software changes for flight 21 were made since the last IPCS flight (.19):

1) Reduced light off detection schedule for REI < .4, 2) add hysterisis to the test for use of fuel flow rather than nozzle area for A/B trim, 3) re-enable manual inlet control, 4) enable distortion control of 7th and 12th stage bleeds, 5) enable airflow trim of gas generator on sense switch 10, 6) set up stall flag in discrete word 49 (bit 16), 7) incorporate revised MN3 schedule, 8) incorporate revised nozzle area calibration, 9) revise the T4 syn offset (+31° to-29°), 10) incorporate a Wf/Pb fuel flow limit on the downstream rather than the upstream side of the control integrator. A flag indicating when this limit is in use is included in word 49 (bit 8), 11) revised PS3 decay rate bias for stall detection (ΔPS3 = 150 psi/sec), 12) corrected sign error on the blowout bias to the MN22 schedule.

Engine run 19a (12-17-75) had the same configuration except the stall detection rate bias was ΔP_{S3} = 250. The ΔP_{S3} = 150 rate bias was validated in engine run 20 (para 4.11).

Engine run 19 had the flight 21 configuration except for the stall detection rate bias (ΔP_{S3} = 350) and it did not contain the sign correction on the blowout bias to the Mn22 schedule. It also included a ground patch to enable AFBIAS for test purposes.

A.9.3 Event Summary

Engine run 19 verified most of the software for flight 21. Two problems were identified during the run - inadvertant stall detection during a MIL-IDLE or MAX-IDLE snap and incorrect operation on the Mn22 loop following stall detection during the MAX-IDLE transient. A sign error on the blowout bias to the Mn22 loop caused the later problem (stall triggers blowout trigger in A/B).

The stall detection level bias was reduced to 250 for engine run 19a.

Engine run 19a was intended as a checkout of the airplane ECS system following repair, but it was also used to checkout the reduced stall detection rate. Since 250 still resulted in incorrect stall detection during transients a level of 150 for the bias was selected for flight 21. Engine run 20 (para. A.10) validated this number.

The following events were completed during flight 21:

Mach 0.5, 10,000 ft.
IPCS MIL-IDLE-MIL BODIE (2)
Attempted expand cone to stall (stall at low power setting)
Mach 1.4, 41,000 ft.
IPCS Expand cone to stall, AFBIAS-Steady-state and zone 3-IDLE-MIL
Mach 1.4, 50,000 ft.
IPCS MAX-IDLE-MIL-IDLE-MIL
Mach 1.6, 45,000 ft.
IPCS Expand cone to stall

Mach 1.9, 45,000 ft.
IPCS MAX-IDLE-MAX, SST, BUZZ(MAX-IDLE), AFBIAS-STEADY-STATE and IDLE-MAX

Accel to Mach 2.3 (Distortion Bleed Control)

This flight was the first evaluation of the IPCS special loops - distortion control of bleeds, stall detection, buzz, and airflow trim. In general, these loops performed quite well. The buzz loop was tested at Mach 1.9, 45,000 ft with the right hand engine used to hold the flight condition. The loop detected buzz and increased engine speed. This resulted in the anticipated limit cycle. The pilots did not find the limit cycle to be a problem. The airflow trim loop, also tested at Mach 1.9, 45,000 ft., worked as anticipated. The distortion control of bleeds worked well during the acceleration to Mach 2.3 opening the 7th bleed at approximately Mach 2.2 without a compressor stall. Stall detection was good, detecting all but very low power stalls and not inadvertently detecting stalls during throttle transients. Recovery from stall was quite slow in most cases and the stall loop did not seem to assist in recovery. No significant overtemperatures resulted from the stalls. The pilots reported oscillations in EPR during the acceleration to supersonic conditions.

One auto-disengage occurred during the pre-taxi engine running.

A.10 Engine Run 20 - December 19, 1975

The hardware configuration for engine run 20 was the same as for flight 21. The software was the same as flight 21 except for the MN3 loop. A nonlinear MN3 loop, described in paragraph 8.1.2, replaced the integral MN3 loop used previously. The run was conducted to provide an early evaluation of the non-linear MN3 loop which was flown on Flight 24. Several IDLE-MIL snap accelerations were conducted and the loop appeared to work satisfactorily.

A.11 Flight 22 - January 7, 1976

A.11.1 Hardware Configuration

There were no hardware changes since flight 21.

A.11.2 Software Configuration - IPCS

There were no software changes since flight 21.

A.11.3 Event Summary

The following events were completed during flight 22:

Mach 0.9, 10,000 ft.
HMC MIL-IDLE-MIL (ECS both and ECS R/H ENG)
IPCS IDLE-MIL-IDLE

Mach 0.9, 45,000 ft.
HMC MIL-IDLE-MIL(2)
IPCS MAX-IDLE-MIL-IDLE-MAX, MIL-MAX-MIL(2)

Mach 1.4, 41,000 ft.
IPCS AFBIAS

Mach 1.9, 45,000 ft.
IPCS Stall attempting to set up for AFBIAS test.
IPCS AFBIAS (Reduced cone increment)

Mach 2.1, 45,000 ft.
. IPCS BUZZ, SST

Mach 2.4+, 50,000 ft.
IPCS MAX-IDLE-MAX, YAW (SST (Stall)

650 KT Accel

This flight extended the flight range over which the special loops had been tested to Mach 2.4. The buzz, airflow trim, and distortion control loops were tested with good results. Changes to the lightoff detection were tested at Mach 0.9, 45,000 ft., with relatively limited success. Afterburner lights at this flight condition are marginal. Two high power stalls were encountered, one at Mach 2.4 during an SST and one at Mach 1.9 during airflow trim testing. The Mach 1.9 stall occurred as the result of high distortion induced by manual cone operation as part of the airflow trim test. The test was successfully repeated with a smaller increase in cone angle. The pilots again reported EPR oscillations at transonic speeds. The pilots reported for the first time an airplane disturbance in the 10-20 Hz frequency range at Mach 0.9, 10,000 ft., in IPCS engine idle and between Mach 1.05 and 1.3 at max A/B.

One auto disengage occurred during the first few minutes of DPCU operation.

A.12 Flight 23 - January 12, 1976

A.12.1 Hardware Configuration

There were no hardware changes since flight 22.

A.12.2 Software Configuration - IPCS

The following changes were made to the flight 22 software for flight 23 and engine run 21:

1) Inlet uses auto commands for either manual or auto control selection -used in Flights 15-20. 2) Increase the N2 loop selection gain to force the control to stay on the MN3 loop for more of the acceleration. 3) +4 ratio units on the downstream Wf/Pb limit for sense switch 14. 4) Double the minimum airflow loop gain. 5) Revised suppression schedule which increases EPR in the transonic Mach region to eliminate EPR oscillations. 6) Incorporate a Mach hold auto throttle. 7) Correct an error in the PD3 failure detection logic which resulted in a backup light during start.

A.12.3 Event Summary

The following events were completed on flight 23:

Mach 0.5, 10,000 ft.
HMC IDLE-MIL-IDLE-MIL
IPCS IDLE-MIL-IDLE-MAX

Mach 0.8, 30,000 ft.
HMC IDLE-MIL-IDLE-MIL
IPCS IDLE-MIL-IDLE-MAX, MIL-IDLE-MIL BODIE,
MIL-PT PWR-MIL, MIL-ZONE3-ZONE4-ZONE3,
ZONE3-MAX-ZONE3-MIL

Mach 0.9, 10,000 ft.
HMC IDLE-MIL-IDLE-MIL
IPCS IDLE-MIL-IDLE-MAX

Mach 1.4, 50,000 ft.
HMC IDLE-MIL-IDLE-MIL
IPCS IDLE-MIL-IDLE-MAX

Mach 1.9, 45,000 ft.
HMC IDLE-MIL-IDLE-MIL
IPCS IDLE-MIL-IDLE-MAX-MIL, PT PWR-MIL-ZONE3,
ZONE3-ZONE4-ZONE3-MAX-ZONE3-MIL-PT PWR(STALL)

Mach 2.1, 45,000 ft.
IPCS MAX-IDLE-MIL-IDLE-MAX(STALL), MAX-MIL-IDLE-MIL-
ZONE2

Autothrottle

It was a good flight achieving most of the objectives. The control operated properly throughout the flight. Autothrottle testing showed the system to work properly. Oscillations in fuel flow were encountered when the integral portion of the autothrottle control was saturated due to the very limited authority used in this initial test.

Two stalls occurred during the flight - one during a max to idle transient at Mach 2.1, 45,000 ft., and the other during a ZONE3 to mil transient at Mach 1.9, 45000 ft. Both stalls recovered in 5-6 seconds without overtemperature problems. The EPR oscillations in the transonic range were essentially eliminated with the higher suppression.

During the taxi back to the hanger the right hand engine was shutdown with the DPCU engaged. This resulted in a disengagement apparently due to the power transient associated with the shutdown of the R/H generator. A subsequent engine run (23) showed that generator transfers either on or off at high power settings did not result in disengagements. At low power settings turning on a generator did cause the DPCU to disengage about half the time, but turning off the generator did not cause disengagment. In this test right hand engine shutdown did not result in a disengagement.

A.13 Autodisengage Engine Runs

An attempt to fly flight 24 on January 12, 1976 was aborted due to several auto disengages during the preflight engine running.

As a result the CMU and IFU were replaced with the spare units (CMU V1 to V2 and IFU V1 to V2). Hanger testing was conducted in which the DPCU was engaged for several minutes to see if it would autodisengage. Disengages occurred with this configuration. An additional hanger test with the DCU and PSU replaced (V1 to V2 in both cases) also resulted in disengages, demonstrating that the problem was not due to a hardware failure.

Engine run 22 was conducted with the flight 23 software plus the non-linear MN3 loop tested in engine run 20 and a software inhibit of the IFU tests of the DMA and the real time clock for sense switch 04. In a 30 minute test with the inhibit on, there were no autodisengages. During testing without the inhibit, the DCU experienced a bit 12 failure which caused a program halt and DPCU disengage. The bit 12 failure was in no way related to the auto disengage problem. The bit 12 problem is discussed in paragraph 7.3.

The DCU was interchanged again (V2 to V1) and engine run 23 repeated the testing planned for engine run 22. No disengages occurred during a 20 minute test with the mask on. Testing in the lab identified the autodisengages as the result of a detected failure of the real time clock - either due to a real loss of the clock or a failure of the detection circuit. Lab testing also indicated that the use of a pull-up resistor on the 0624 instruction line, which commands reprogramming of the real time clock rate, eliminated the autodisengages. This testing was not regarded as conclusive and subsequent results showed that the pull-up was not effective.

A decision was made to incorporate the pull-up resistor in the flight IFU and use the software inhibit of the real time clock and DMA checks during takeoff. The pull up resistor was not put in until after engine run 26 to avoid schedule impact.

A.14 Flight 24 - January 22, 1976

A.14.1 Hardware Configuration

Since flight 23 the following components were changed:

1) CMU (V1 to V2)
2) PSU (V1 to V2)
3) IFU (V1 to V2)

A.14.2 Software Configuration -IPCS

The following software changes were made to the flight 23 software for flight 24 and engine run 25:

1) Changed the MN3 control loop to the non-linear control. (para 8.1.2) 2) Non-linear N2 gain - for N2 error greater than 5% the N2 gain is doubled. This is designed to work with the Mn3 control to improve the acceleration time. 3) Expanded authority of the integral portion of the autothrottle to 18°-120°. 4) Revised stall logic - the loop uses the stall detector validated in previous flights to begin action. One second after stall is detected the loop checks burner pressure for one second to see if the compressor is still stalled. If not no action is taken. If it is stalled the PLA command to the engine is reduced to idle and 7th and 12th bleeds are opened. After the burner pressure indicates stall has cleared the engine is returned to the pre-stall configuration (see para. 8.1.1). 5) Manual inlet control active or sense switch 12 and manual inlet control switch at manual. 6) Revised suppression schedule - stalls were encountered at Mach 1.9 and 2.1 on flight 23 so the suppression was reduced in that range (see para 6.3.1.1) 7) Increased the hysterisis on the distortion control of 7th bleed from 75 to 300. 8) Revised the fuel command logic to operate on the accel schedule during start. 9) Changed PCM data outputs to examine the D/A power supplies. 10) Inhibit the IFU checks on the real time clock and write request for sense switch 04. This prevents the inadvertent disengages experienced on previous flights. 11) Increased the threshold on buzz detection from .01 to .02.

The software for engine run 24 was the same as for flight 24 except for the range on the ΔMN3 schedule input with the spike pot ($\pm$01 for engine run 24 - $\pm$.02 for flight 24) and coding errors in the variable N2 gain which were corrected for engine run 25 and flight 24.

A.14.3 Event Summary

Engine run 24 had a successful IPCS start, but exhibited problems at idle. The idle problems were identified as being due to coding errors in the variable N2 gain. A number of accels were run to evaluate the non-linear MN3 loop. The errors were corrected and the range of the ΔMN3 schedule pot doubled for engine run 25. No DPCU related problem developed in engine run 25, but the inlet spike unlock indicator light was on again during the run.

The following events were completed on flight 24:

Mach .5-.9, 10,000 ft.
IPCS Authothrottle Accel

Mach 0.8, 30,000 ft.
HMC IDLE-MIL, IDLE-MIL-IDLE
IPCS IDLE-MIL-IDLE-(0 ΔMn3),
IDLE-MIL-IDLE (-.02 ΔMn3)
IDLE-MIL-IDLE (+.02 ΔMn3),
Autothrottle

Mach 1.-2.3, 650 KTS
Autothrottle Accel

Mach 1.4, 50,000 ft.
HMC IDLE-MIL-IDLE
IPCS IDLE-MIL-IDLE (0 ΔMn3)
IDLE-MIL-IDLE (-.02 ΔMn3)

Mach 1.9, 45,000 ft.
IPCS Expand Cone to Stall, ZONE3-MIL

Mach 2.3, 50,000 ft.
BUZZ

Flight 24 was a good flight and no control system anomalies were observed. The autothrottle was tested at subsonic and supersonic speeds with good results. The buzz loop was evaluated at Mach 2.3. The loop is functioning properly; however, the buzz resulted in several off idle stalls. Three stalls occurred at Mach 1.9, 45,000 ft., in afterburning with the inlet expanded beyond the normal position. None of the stalls resulted in an overtemperature. The ZONE 3 to mil throttle transient at 1.9, 45,000 ft., did not result in a stall with the reduced suppression schedule, but the pilots reported that the EPR oscillation was back. Engine acceleration comparisons were made between HMC and IPCS at Mach 1.4, 50,000 ft., and Mach 0.8, 30,000 ft. In these tests the cone pot on the manual inlet control was used to input a bias to the MN3 schedule to run different acceleration rates and force the controller to operate more or less of the time on the Mach control.

A.15 Flight 25 - January 23, 1976

A.15.1 Hardware Configuration

There were no hardware changes between flight 24 and 25.

A.15.2 Software Configuration - IPCS

There were no software changes since flight 24.

A.15.3 Event Summary

The following events were completed:

	Mach	Alt
HMC IDLE-MIL-IDLE IPCS IDLE-MIL-IDLE (0 ΔMn3)	.5	10,000
IDLE-MIL-IDLE (+.02 ΔMN3)	.7	10,000
IDLE-MIL-IDLE-MAX (-.02 ΔMn3)	.9	10,000
	1.4	41,000
	1.9	45,000

Mach .85, 21,000 ft.
HMC MIL-IDLE-MIL BODIE (2)
IPCS MIL-IDLE-MIL BODIE

Mach 1.4, 41,000 ft.
Stall Loop (Expand Cone to Stall)

Flight 25 was routine, providing data on the nonlinear MN3 loop at a number of flight conditions. The revised stall loop was tested at Mach 1.4, 41,000 ft., by manually expanding the cone to stall. The stall loop worked exactly as intended, detecting stall, throttling the engine back to idle, and returning the engine to the prestall configuration after the stall cleared. The overtemperature was of short duration.

The DPCU disengaged during the taxi back to the hanger possibly as the result of shutting down the right engine.

A.16 Engine Run 26 - January 27, 1976

Three engine runs were conducted to measure noise - engine run 26 (1-27-76), engine run 28 (2-06-76), and engine run 33 (2-25-76). The results of this testing are discussed in section 6.6.

The following software changes from flight 25 were made for engine run 26: 1) Disable AFBIAS, 2) limit the control PLA to 104° (max ZONE4) for sense switch 10, 3) downtrim all zones of A/B with the A/B trim pot (changes SGA), 4) enable rumble for SGA <1. Rumble will add .1 to SGA with a limit of 1.0 for SGA. Rumble threshold varied with the MIL trim pot. 5) Revise the stall loop to clear blowout trigger when the stall flag is set, 6) revise the suppression schedule, and 7) double the integral gain on the autothrottle.

Thrust measurements were made by attaching the airplane to the Edwards thrust stand. Noise data were recorded twice, once at 35 feet from the airplane and again at 105 feet in a separate run series. The second series was necessary because there was not sufficient space with the airplane on the thrust stand and the thrust measurements were required for one series.

After the run a problem was discovered in the turned down max A/B case. At max A/B the nozzle is on the stop and suppression is controlled by cutting back on ZONE 5 fuel flow relative to the other zones. Thus rather than uniformally cutting back all zones, ZONE 5 was cut back much less than the other zones.

A.17 Engine Run 27 - February 5, 1976

A.17.1 Hardware Configuration

The pull up resistor to reduce noise on the command to reprogram the real time clock was added. The change was made to the real time clock card from IFU V1 and this card interchanged with the real time clock card in V2 which was in the airplane. IFU V2 was reinstalled in the airplane.

A.17.2 Software Configuration - IPCS

The following changes were made since engine run 26: 1) Revised the STALL loop to reset ABPERM along with resetting blowout trigger when the stall flag is set and to use min airflow. 2) Corrected the problem with the max A/B downtrim (See A.16). 3) Included a downtrim of the A/B reset on N2 for either Sense switch 10 or 17 using the spike pot. 4) Went back to the integral MN3 loop using the schedules flown on flights 24 and 25 with the loop gain a variable controlled with the cone pot. 5) Shut off ZONE1 solenoid for Sense Switch 10 and Manual Inlet Control On.

A.17.3 Event Summary

Since the weather was not suitable for noise measurement, this run was devoted to evaluation of the performance of the integral MN3 loop with various gains and schedule offsets. This testing involved a number of IDLE-MIL throttle snaps. As a part of the run the software for the next noise run was checked out. A problem was discovered with the pot setup. Both the MN3 offset and the A/B reset of N2 were controlled by the spike pot and the settings are not compatible.

A.18 Engine Run 28 - February 6, 1976

The software of engine run 27 was modified to read the pot for ΔMN3 for sense switch position 14. The weather permitted only limited testing. Thrust was measured along with noise at 35 feet from the airplane.

A.19 Flight 26 - February 20, 1976

A.19.1 Hardware Configuration

The following hardware changes were made between flight 25 and flight 26: 1) Pullup resistor on the real time clock card (para A.17.1). 2). Separate T2 inputs from the engine to the NASA data system and the DPCU were reversed to provide data on the source of the T2 difference (para 5.4.2).

A.19.2 Software Configuration - IPCS

The following software changes were made between flight 25 and flight 26: 1) Modify the non-linear MN3 loop to operate at the minor cycle rate. 2) Modified stall loop - use minimum airflow and relight A/B if stall occurred in A/B (clear blowout trigger and ABPERM). 3) Revised suppression schedule. 4) Double autothrottle integral gain. 5) Disable AFBIAS so sense switch 10 is available for noise. 6) Limit PLA to 104° (max ZONE4) for sense switch 10. 7) Turn down ZONE1 fuel flow with the idle trim pot for sense switch 10. 8) Turn off ZONE1 fuel flow for sense switch 10 and manual inlet control on. 9) Limit PLAPFA (PLA input to the A/B fuel air curves) to the current value and reduce the fuel flow to all A/B zones with the A/B trim pot for sense switch 17. 10) Reduce the gas generator N2 set point (A/B reset) using the spike pot for sense switch positions 10 and 17. 11) Set the blowout trigger if rumble is detected except for sense switch 04. This has the effect of forcing the control out of A/B and opening the 7th and 12th stage bleeds. The rumble threshold is set with the mil trim pot using sense switch 17.

The software for engine run 31 was the same as flight 26. The only changes between engine runs 30 and 31 were the correction of a coding error and the addition of +.4 psi to ΔP3 in the minor cycle sample MN3 loop. The two changes between engine runs 29 and 30 were the incorporation of the minor cycle MN3 loop and an increase in the authority of the ZONE1 downtrim pot.

A.19.3 Event Summary

Engine run 29 was a short, non-data run to check out the hardware changes, checkout the spike light fix and checkout the software change to disable rumble for sense switch 04.

Engine run 30 evaluated the minor cycle sample MN3 loop. Two required changes were identified. An error caused oscillations in the idle fuel flow and the failure to include a .4 psi correction to the ΔP3 resulted in a MN3 computation error. These were corrected and no problems were encountered in engine run 31.

The following events were completed during flight 26:

Mach 0.7, 10,000 ft.
HMC IDLE-MIL-IDLE
IPCS IDLE-MIL (ΔMn3 = .004), IDLE-MIL (ΔMn3 =-.004)

Mach 0.8, 29,000 ft.
IPCS Autothrottle

Mach 0.8, 30,000 ft.
HMC IDLE-MIL
IPCS IDLE-MIL (ΔMN3 = .004), IDLE-MIL (ΔMn3 = -.004)
IDLE-MIL-IDLE-MAX (ΔMn3 = .0024)

Mach 0.9, 10,000 ft.
HMC IDLE-MIL-IDLE
IPCS IDLE-MIL (ΔMn3 = 0, +.004, +.008, +.012)
IDLE-MIL-IDLE MAX (Δ Mn3 =-.004)

Accel to Mach 2.3

Evaluation of Noise Procedures

Three problems were encountered during this flight. In spite of these difficulties a great deal of needed data were acquired. The acceleration to Mach 2.3 provided T2 data which identified the temperature harness rather than the recording devices (PCM or IFU) as the source of the difference between NASA and DPCU T2 measurement. The autothrottle was evaluated with higher integral gain. The minor cycle sampling Mn3 loop worked successfully at several subsonic flight conditions for various schedule offsets. Toward the end of the flight data were recorded on the A/B operation in some of the configurations intended for the noise flight test.

The desired level of rumble threshold was not set during the preflight procedure. Therefore during the early portion of the flight the threshold was zero causing the control to continuously indicate rumble. This in turn kept the blowout trigger set except for sense switch 04. The problem was not discovered during the ground runs since sense switch 04 was used for all running prior to takeoff. The effect of the low threshold was twofold - it held open the bleeds and prevented afterburner operation. A scheduled test of the DPCU disengagement when the burner pressure exceeds the limit failed because the bleeds kept the pressure down. It was decided to continue with the acceleration to Mach 2.3 for T2 data using sense switch 04.

After the supersonic portion of the flight a test was conducted to identify the sense switch positions which result in the open bleeds. During this test the problem was identified and the planned testing proceeded with the autothrottle test and Mn3 acceleration tests at subsonic speeds.

The final portion of the planned test was a trial run of the intended noise flight test procedures. The initial test of the max ZONE 4 condition worked satisfactorily. The attempt to test the downtrimmed max A/B resulted in some problems.

Sense switch 17 was set prior to going A/B. This had the effect of limiting the afterburner fuel flows to the minimum for each zone. On one light the sense switch was changed from 17 to 14 while in A/B. This caused a large increase in A/B fuel flow and a compressor stall. No serious overtemperature resulted from the stall.

As a result of the sense switch transition through 14 a cold acceleration bias was set into the Mn3 loop. This caused slow accelerations and prevented A/B operation. At this point the pilots elected to disengage the IPCS and return to base.

One additional difficulty occurred in the later portion of the flight during operation on sense switch positions other than 04. Autodisengages occurred at a rate that made testing difficult.

A.20 Flight 27 - February 27, 1976

A.20.1 Hardware Configuration

Lab testing identified the cause of the autodisengage problem (para 7.1). As a result the INA 1124 instruction line was disabled on the real time clock card previously modified with the pull up resistor. The T2 thermocouple sense lines were insulated at the engine J box in order to further isolate the source of the T2 measurement discrepancy.

A.20.2 Software Configuration - IPCS

A number of software changes were made in response to the difficulties encountered during flight 26. In general these changes were designed to simplify DPCU operation and reduce the problems which result from switching through the various sense switch positions. These changes included: 1) Moving the N2 reset for A/B operation from the spike pot to the MIL trim pot. 2) Elimination of the variable rumble threshold (previously on the MIL trim pot) and set the threshold at 0.5. 3) Elimination of the capability to shut off ZONE 1 afterburning. This capability had been included for noise and was tested in ground runs. Since it resulted in A/B blowout it was no longer required. 4) Return the MN3 offset to 0, (equivalent to spike pot = 500) for all sense switch positions other than 14.

Two changes were made to check on possible autodisengages. The tolerance on the PCM interrupt was reduced to detect failures of the real time clock. A check of the N2 raw data was added to test the DMA. Twenty-four successive samples that are equal is regarded as a DMA failure. Either failure will set the backup light with the PCM test also halting PCM data output.

Three changes were made for IPCS test purposes: 1) The proportional gain on the autothrottle was doubled. 2) The MN3 loop scaling was revised to improve resolution. 3) The outputs of the ZONE 1 downtrim and the A/B N2 reset pots were added to the PCM data for the noise flight.

The software for engine runs 32 and 33 was the same as for flight 27.

A.20.3 Event Summary

Engine run 32 was the software verification run for flight 27. All the noise procedures were evaluated without any problems. Engine run 33 was for noise measurement. No thrust measurements were made. Noise data were recorded at both 35 ft. and 105 ft. for all of the afterburner configurations planned for flight 27. On flight 27 noise measurements were made for the following engine configurations:

1) MIL
2) Max Zone 5
3) Max Zone 4
4) Max A/B downtrimmed to Max Zone 4 Aj
5) Max Zone 4 with Zone 1 turndown to Min fuel flow
6) Gas generator EPR = 1.74
7) Max Zone 5, N2 downtrimmed to EPR = 1.84
8) Max Zone 4, N2 downtrimmed to EPR = 1.84
9) Max Zone 5, N2 downtrimmed to EPR = 1.84, downtrimmed to match the Aj from 8.
10) Max Zone 4, Zone 1 downtrim with N2 downtrimmed to EPR = 1.84
11) Max Zone 5, N2 downtrimmed to EPR = 1.84 downtrimmed to match the Aj of 10

6-10 were repeated.

Rumble was detected during one test point at max A/B with the fuel flow downtrimmed to a cockpit nozzle area reading of 7.8. One additional rumble occurred going into max A/B. A repeat of the transient did not cause rumble so it caused no major problem.

A.21 Flight 28 - Febraury 27, 1976

A.21.1 Hardware Configuration

There were no hardware changes since flight 27.

A.21.2 Software Configuration

There were no software changes since flight 27

A.21.3 Event Summary

The following events were completed on flight 28:

Mach 0.5, 10,000 ft
HMC IDLE-MIL-IDLE
IPCS IDLE-MIL-IDLE (ΔMn3 = .002)
IDLE-MIL-IDLE-MAX-IDLE (Δ Mn3 = -.002)
IDLE-MIL-IDLE (Δ Mn3 = -.006)

Mach .8, 30,000 ft.
IPCS Autothrottle

Mach 1.2, 30,000 ft.
IPCS Autothrottle

During the acceleration to Mach 2.3 a disturbance was observed on many of the low level PCM channels followed by saturation of the cockpit T4 guage and a rumble shutdown of the A/B. As a result of the indicated overtemperature on the cockpit guage, the pilots shut down the left hand engine and the remainder of the flight was aborted.

Subsequent testing identified the problem as the failure of an IC chip in the PCM data system. The failure put 12 volts on the T3 thermocouple which is common to the cockpit T4, the DPCU and the PCM data system. This resulted in a disturbance in the DPCU T2 and T3 signals causing the A/B fuel flow to increase sufficiently to initiate rumble. Examination of the data shows that the engine did not have a real overtemperature. An oil sample was analyzed and found to be acceptable. As in flight 27 there were no autodisengages.

A.22 Engine Run 34 - March 4, 1976

As a part of the noise measurement study, it was necessary to measure the velocity profiles created by the different afterburner configurations. No DPCU hardware or software changes from the flight 27/28 configuration were made. An exhaust survey rake from NASA/LeRC was used to measure the total temperature and total pressure profile downstream of the nozzle. Profiles were measured for the following conditions:

IDLE, 76%, 82%, 92%, MIL, ZONE1, ZONE2, ZONE3, ZONE4, Max A/B with a normal afterburner configuration, Max ZONE4 with ZONE1 downtrimmed, Max A/B downtrimmed to match Max Zone 4 nozzle area.

A.23 Engine Run 35 - March 5, 1976

The last engine run was devoted to evaluation of an inflight thrust calculation in the DPCU software and attempts to run very fast IPCS accelerations. No hardware changes were made. The following software changes were made: 1) Thrust calculation incorporated, 2) Wf/Pb limit set to +8 ratio units for sense switch 14, and, 3) PLAP rate for A/B accel increased from 15°/sec to 51°sec

The gas generator accels worked well resulting in a 4.8 sec. idle-mil compared to the HMC 5.9 sec. The PLAP rate in the afterburner was too high and resulted in a stall.

Appendix B - Preflight Procedure

IPCS

HANGER PREFLIGHT CHECKLIST

Flight No. _____

11/12/75

A. Equipment Required

1. Test Set Unit (TSU) with Computer Control Unit (CCU) connected.
2. Teletype (TTY)
3. Aircraft Power connected
4. Aircraft Cooling Air connected
5. Ops. Van with Test Point Panel
6. TM Van or Control Room available
7. Required Documents:
   SFCO File
   IPCS Patch Tape Record
   Contractors Engineering Log
   IPCS Interflight Worksheets & Removals
   Software Maintenance Listing

B. Preparation

1. Identify Main Program Tape, and Patch Tapes to be used for flight and check correct identification numbers.
   Program Tape
   Patch Tapes

Loaded in following order:

1. MEDIC, 35000, Copy _____
2. Patch to _____, No. _____, Copy _____
3. Patch to _____, No. _____, Copy _____
4. Patch to _____, No. _____, Copy _____
5. Patch to _____, No. _____, Copy _____

2. Identify SFCO's to be included in any additional patch tape for flight.

_____

3. Prepare Patch Tape Record Form
4. Generate Patch Tape if required
   a. Load Main Program (BOMDIG or IPCS)
   b. Load Medic
   c. Load Patch Tapes

   Note: The following tape loading procedure is used for all tapes.

   1. CCU Pwr ON
   2. DPCU Pwr ON
   3. Selector Sw. to S. I.
      Fetch/Store Sw. to Fetch

Accomplished by: _____ Inspector
_____ Flight Systems Technician
_____ Flight Systems Engineer

4. Press P/Y Button
5. Press MASTER CLEAR, then CLEAR register
6. Enter 1 into P register
7. Press A Register button
8. CLEAR register
9. Selector Sw. to RUN
10. Tape Reader ON (2 min warmup)
11. Press START

Note: If tape fails to transport, reload Bootstrap per included procedure

5. Load contents of SFCO's into memory by TTY using MEDIC. Do not execute IPCS or BOMDIG at this time.

Note: The following procedure is used to execute all programs:

1. Selector Sw. to S.I.
2. Depress P/Y Button
3. Press MASTER CLEAR, then CLEAR
4. Enter program starting address on CCU panel:

   IPCS (Rev. C) - 1215_8

   BOMDIG (Rev. C) - 1174_8

   MEDIC - 35000_8
5. Selector Sw. to RUN
6. Press START

6. Verify that contents of SFCO's have been properly loaded into memory by accessing all locations using the TTY, and comparing the TTY printout with the SFCO's. Date and identify TTY printout.

Type: Memory location then colon (:) for data (numeric mode)
Type: Memory location then slash (/) for instructions (nmenonic mode)

7. Punch patch tape from computer memory. Date and identify each patch as follows:

a. Main Program and Rev.
b. Patch tape load sequence No.
c. Code No. first two digits - year
   second two digits - month
   third two digits - day
   last digit - number that day
   EXAMPLE: 7508281

8. Clear memory using MEDIC, type: (0) 72 - 34777 F
9. Load patch tape, into memory using tape reader
10. Call for memory search of all non-zero locations as data

Type: 123: (for numeric mode)
Type: (0) 72-34777 U

11. Call for memory search of all non-zero locations as in structions

Type: 123/ (for nmenonic mode)
Type: (0) 72-34777 U

12. Load Memory with all One's type: (1) 72-34777 F

13. Load patch tape into memory using tape reader
14. Call for memory search of all zero locations as data

    Type: 123 ;
    Type: (0) 72-34777 S

15. Compare TTY printouts obtained in steps 10, 12 line by line with SFCO contents. Step 14 identifies any zero locations intentionally loaded by patch tape. Date and identify patch tape on leader.

16. Prior to flight all SFCO's incorporated into the new patch tape will be entered and verified in the Software Maintenance Listing

17. If a new patch tape is made a verification engine run will be made prior to a flight utilizing this patch tape.

C. Preflight Operation

1. Clear memory using MEDIC type: (0) 72-34777 F
2. Load Main Program
3. Load MEDIC
4. Load Patch Tapes in correct numerical order

    Note: All tapes should read in smoothly and cease reading at the last punched location. However, the MEDIC tape reads through to the end of the tape. The TTY will make an audible response when tape reading is complete.

    Failure of any tape to load completely indicates a loading error; it is then necessary to reload all tapes in sequence. Direct load into memory from TTY is not permitted after above tape loads.

5. Execute the program using correct starting location. Observe that program runs and note on CMU:

    Track light - ON
    Backup light - OFF
    Fault light - OFF

6. Log loading sequence, tape numbers and any loading failures in the IPCS supplement to the aircraft log (interflight worksheets)

7. Power down system
    a. Selector Sw. to SI
    b. DPCU Pwr. OFF
    c. CCU Pwr. OFF

8. Disconnect CCU cables

9. Connect Test Point Panel cables to connector in nose wheel well

10. Turn on system
    a. DPCU Pwr ON
    b. Check: Track light ON
       Backup light OFF
       Fault light OFF

    Note: Power lever must be less than 8.5° in order to TRACK. It is permissible to cycle power more than once to get the correct light indications.

11. Instrumentation System - ON (Check with Instrumentation Crew)

12. Transducer Static Check
    a. Verify all D/A channels at Test Point Panel:
       set SS = 07 (DUUU), check + 10VDC ± .3 all channels,
       also verify SS01 wired down.
    b. Make checks listed in B-2 and B-3 changing sense switch
       positions as indicated in first column :

13. Verify correct waveform of all Paroscientific Transducers on Test Point Panel
    check: 4 to 6V pp square wave with period 23.2 to 32 microsec.
    (Freq. 43-31 KH_z) (See Table B-1)

14. Verify exhaust nozzle stepper motor not stepping. Verify all stepper
    motors have two coils high and two low.

14a. Engage DPCU
    Check: +28 VDC to

    Engage _____
    SW 12 _____
    SW 07 _____
    Inleaso _____

15. TM Checks
    a. Verify Subcom lockup
    b. Verify all variables correspond to values listed in step 12b

16. DPCU Disengaged

TABLE B-1 PAROS VOLTAGE CHECK

Transducer	Voltage V	Period, MS
PDEM		
PKDA		
PKD3		
PKDC		
PKDD		
PSDEM		
PLM		
PSLM		

17. Aircraft Hydraulics ON

18. Manual Inlet Control Check (if MIC enabled in program).
    a. MIC sw. to MANUAL
    b. Spike control knob CW then CCW, verify spike moves full
       aft then fwd.
    c. Cone Control knob CW then CCW, verify cone expands fully
       then contracts.
    d. MIC Sw to AUTO

Table B-1 Paros Voltage Check (cont)

19. DPCU engage
    check: no movement of inlet
20. IPCS system power down
    a. DPCU - disengage
    b. DPCU pwr - OFF
21. Aircraft Close out (check with crew)
    a. Hydraulics OFF
    b. Cooling Air OFF
    c. Power OFF
    d. Remove Test Point Panel Cables and install caps.

22. Verification engine run if new patch tape has been generated.

Note: If CCU is reconnected for any reason, all tapes must be reloaded and Pre-flight Operation must be repeated

BOOTSTRAP LOADING PROCEDURE

1. CCU Pwr. ON
2. Selector Sw. to MA
3. Press MASTER CLEAR
4. Press P/Y register button
5. Press CLEAR
6. Enter 1 into P register
7. P + 1/P switch to P + 1
8. Fetch/Store switch to Store
9. PFI/PFH switch to PFH
10. ASR/PTR switch to PTR
11. Press M register button
12. Press BOOTSTRAP button
13. Press START
14. Selector Sw. to S.I.
15. Fetch/Store sw. to Fetch
16. ASR/PTR sw. to ASR
17. P + 1/P sw to P

Table B-2 Transducer Preflight Calibration Check Form - Voltage

SENSE SW POSITION	CHANNEL NO.	VARIABLE	NOM VAL. (ENGR UNITS)	LOWER LIM	UPPER LIM	OBSERVED	NOTES
0000	1	P6MS	13.52 psia	2.00	2.32		
	2	PS3S	13.52	.210	.330		
	3	PD3S	0.0	-.08	+.08		
	4	PS3	13.52 psia	.210	.330		
	5	PS22S	13.52 spia	1.002	1.162		
	6	PD22S	0.0	-.08	+.08		
	7	P22S	13.52	1.002	1.162		
	8	T2S	70°F	2.60	2.70		
	9	T3S	70°F	2.60	2.70		
	10	T4S		Not Available		See note B	
	11	T22S	70°F	2.60	2.70		
0001	1	TJBS2A	70°F	1.0	1.8		
	2	AJPS	120°	9.36	9.84		
		"	0°	-.24	0.24		
	3	WFGS		0.202	9.5		
	4	WFZ1S	1200	0.281	0.469		
	5	WFZ2S	1280	0.613	0.988		
	6	WFZ3S	1300	0.625	1.0		
	7	WFZ4S	1550	0.781	1.156		
	8	WFZ5S	2000	1.063	1.438		
	9	AJPV		-6.193	1.290	Nozzle Open	
	10	PLA	0.	-.2	0.2	Nozzle Closed	
	11	(Spare)					
0010	1	P2KDAS	13.52 psia	4.283	4.37		
	2	P2KDBS	13.52 psia	4.283	4.37		
	3	P2KDCS	13.52 psia	4.283	4.37		
	4	P2KDDS	13.52 psia	4.283	4.37		
	5	PDEMS	13.52 psia	4.283	4.37		
	6	PSDEMS	13.52 psia	4.283	4.37		
	7	PLMS	13.52 psia	4.283	4.37		
	8	PSLMS	13.52 psia	4.283	4.37		
	9	XORLS	2.29				
	10	THETAS	8.5°	2.64	2.80		
	11	(Spare)					
0011	1	MNS	0	-.256	+.256		
	2	ALPHAS					Note A
	3	SPKCOM					
	4	CONCOM					
	5	MSPIKE					
	6	MCONE					
	7	IDLTRM					IPCS 5
		IDLTRM					BOMDIG 5
	8	MILTRM					IPCS 5
		MILTRM					BOMDIG 5
	9	ABTRM					IPCS 5
		ABTRM					BOMDIG 5
	10	(Spare)					
	11	(Spare)					

Note A - Angle of Attack Range: + 8.02 V
- .88 V

Note B - Lim=Lim +.005 (OAT-70)

Table B-3 Transducer Preflight Calibration Check Form - Octal

CHANNEL NO	VARIABLE	TM	OCTAL (ENGR UNITS)	LOWER LIM	UPPER LIM	OBSERVED	NOTES
1	P6MS	Channel 3 10-49/50	.15412 B6 13.52 psia	.15000	.16000		
2	PS3S	Channel 4 10-62/63	.01543 B9 13.52	.01240	.02040		Tamb =
3	PD3S	Channel 6 1-7/8	.00000 0.0	177271	.00507		Pamb =
4	P3S	Channel 5 10-72/73	.01543 13.52 psia	.01240	.02040		
5	PS22S	Channel 7 1-22/23	.06605 13.52 psia B7	.06206	.07206		
6	PD22S	Channel 9 1-49/50	0 0.0	177271	.00507		
7	P22S	Channel 8 1-32/33	.06605 13.52 B7	.06206	.07206		
8	T2S	Channel 12 2-7/8	.20440 70°F B11	.20200	.20700		
9	T3S	Channel 10 1-62/63	.20400 70°F B11	.20200	.20700		
10	T4S			Not Available			
11	T22S	Channel 13 2-22/23	.20440 70°F B11	.20200	.20700		
1	TJBS2A	Channel 14 2-32/33	.10600 70°F B9	.06200	.13200		
2	AJPS	Channel 15 2-49/50	.74000 120°	.72400	.75400		Nozzle Open
	AJPS		.0-0 0°	176400	.01400		Nozzle Closed
3	WFGS	Channel 16 2-62/63		.01206	.73300		
4	WFZ1S	Channel 17 2-72/73	.02260 1200 ±300	.01604	.02734		
5	WFZ2S	Channel 18 3-7/8	.05000 1280 pph	.03650	.0613		
6	WFZ3S	3-22/23 Channel 19	.05050 1300	.03720	.06200		
7	WFZ4S	3-23/33 Channel 20	.06034 1550	.04704	.07164		
8	WFZ5S	3-49/50 Channel 21	.07640 2000	.06510	.10770		
9	AJPV	3-62/63 Channel 22		131227	.10040		
10	PLA	3-72/73 Channel 23	0-0	176600	.01200		
11	(Spare)						
1	P2KDAS	4-7/8 Channel 24	.33024 13.52 psia	.32612	.33240		
2	P2KDBS	4-22/23 Channel 25	.33024 13.52 psia	.32612	.33240		
3	P2KDCS	4-32/33 Channel 26	.33024 13.52 psia	.32612	.33240		
4	P2KDDS	4-49/50 Channel 27	.33024 13.52 psia	.32612	.33240		
5	PDEMS	4-62/63 Channel 28	.33024 13.52 psia	.32612	.33240		
6	PSDEMS	4-72/73 Channel 29	.33024 13.52 psia	.32612	.33240		
7	PLMS	5-7/8 Channel 30	.33024 13.52 psia	.32612	.33240		
8	PSLMS	5-22/23 Channel 31	.33024 13.52 psia	.32612	.33240		
9	XORLS	5-32/33 Channel 32	2.29				
10	THETAS	5-49/50 Channel 33	.21000 8.5°	.20400	.21400		
11	(Spare)						
1	MNS	7-49/50 Channel 45	0-0 0.	176315	.01463		
2	ALPHAS	7-62/63 Channel 46	0. ±1.°	+23° on indicator			
3	SPKCOM	5-72/73 Channel 35					MIC Auto
4	CONCOM	6-7/8 Channel 36	8.°				MIC Auto
5	MSPIKE	5-72/73 Channel 35					MIC Manual
6	MCONE	6-7/8 Channel 36	8.°				MIC Manual

APPENDIX C - SUGGESTED IFU HARDWARE REVISIONS

The following paragraphs depict the changes required to implement the recommendations of Section 9.0. All changes should be implemented using flight quality hardware and revision techniques, conformal coating and component mounting, used on previous changes.

C.1 Restrict DMA Address to Locations 400 - 577

As shown in Figure C-1 the DMA address capability can be restricted by grounding the DMA 091 line on the DMA Control Logic Card. The line is isolated by cutting the foil lead as indicated and grounded on the card by use of a jumper.

C.2 Transfer BITE Data to Discrete Input Word

Figures C-2a, b depict a direct approach to the problem in which spare discrete input channels are wired to the BITE signals. Since all signals are TTL the signal conditioners on the A21 card are deleted.

Alternatively the same result can be achieved by using available discrete output buffers as follows:

Wire - PILOIOS1 and WRQOS1 out to spare pins on status and engage card A25 (10048738)

Wire - These two signals and the following three to the spare DISOUT#1 outputs

DISO1 Bit 7	(PILOIOS1)
DISO1 Bit 8	(WRQOS1)
DISO1 Bit 9	(FATRK1)
DISO1 Bit 11	(SAHFO)
DISO1 Bit 12	(ANFO)

Wire - The above five outputs back in to the IFU as inputs

DISIN Bit 2	(PILOIOS1)
DISIN Bit 3	(WRQOS1)
DISIN Bit 4	(FATRK1)
DISIN Bit 12	(SAHFO)
DISIN Bit 13	(ANFO)

C.3 Modify N1, N2 Converters to Clear Prior to Each Sample

This change requires the addition of an I.C. to the A16 card and the use of an existing spare inverter as shown in Figure C-3. The change has the effect of clearing the converter data registers before counting of a new sample commences.

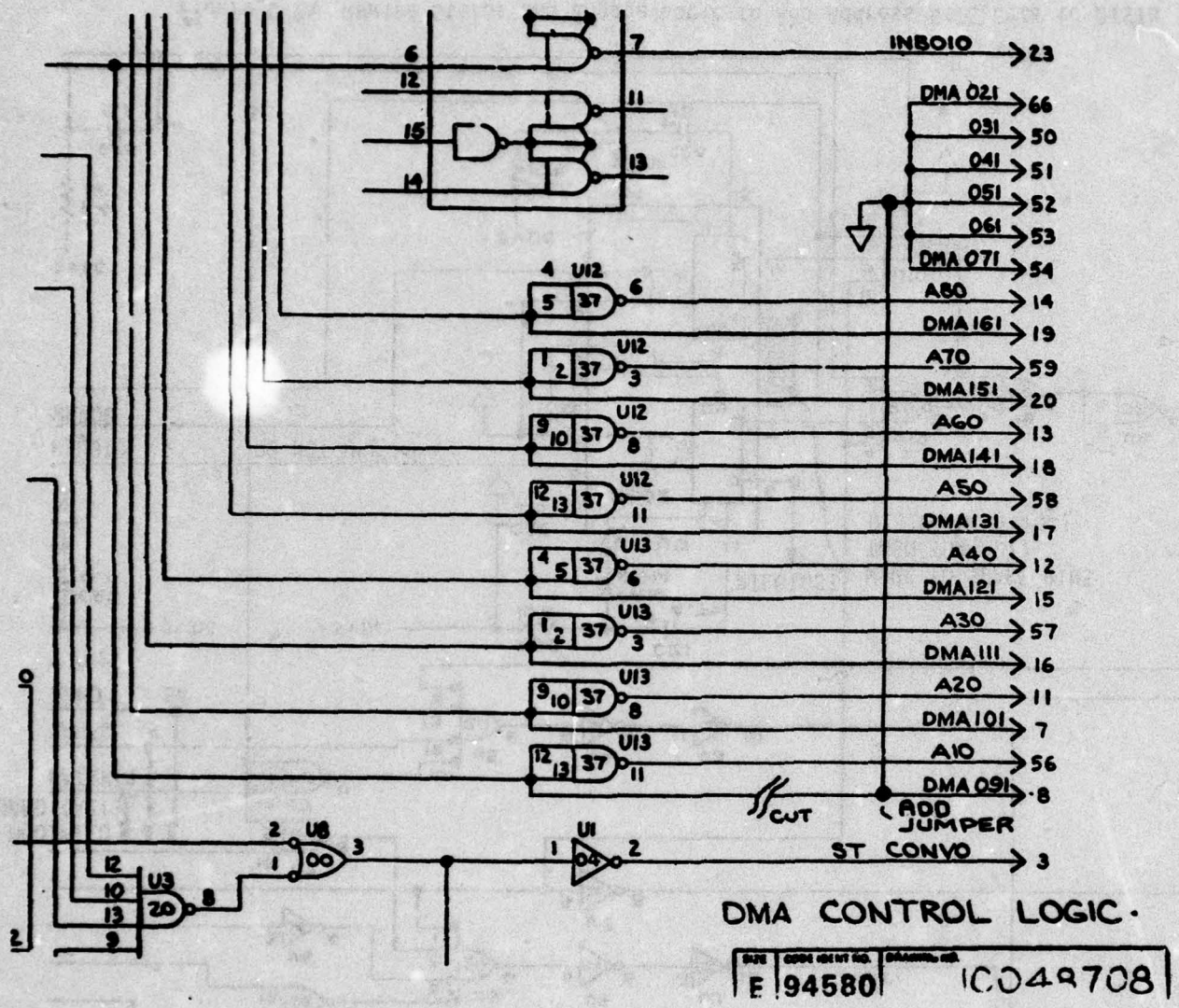

Figure C-1 Restrict DMA Addresses to 400-577

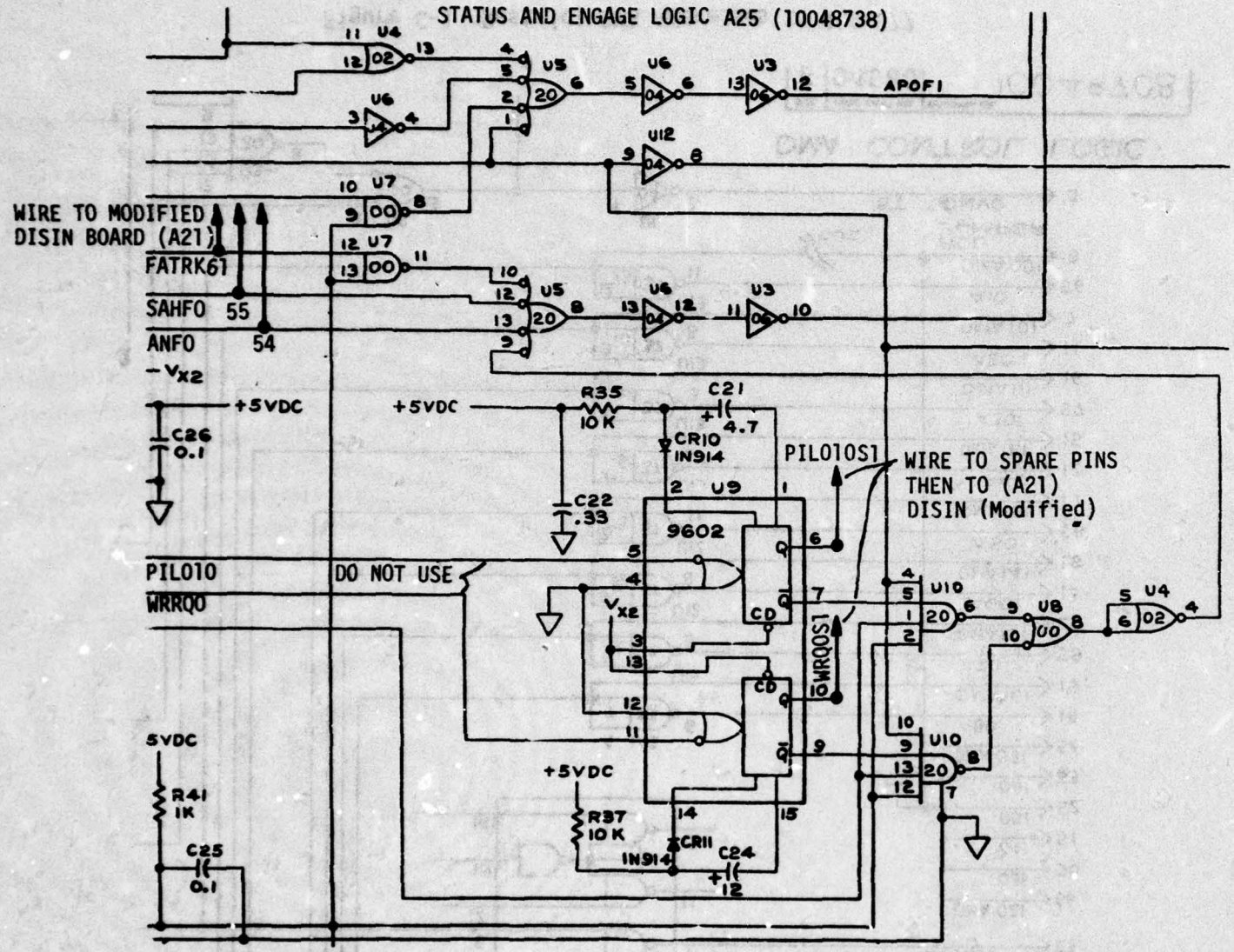

Figure C-2a Rewire Status and Engage Logic to Add Address BITE Data to DISIN

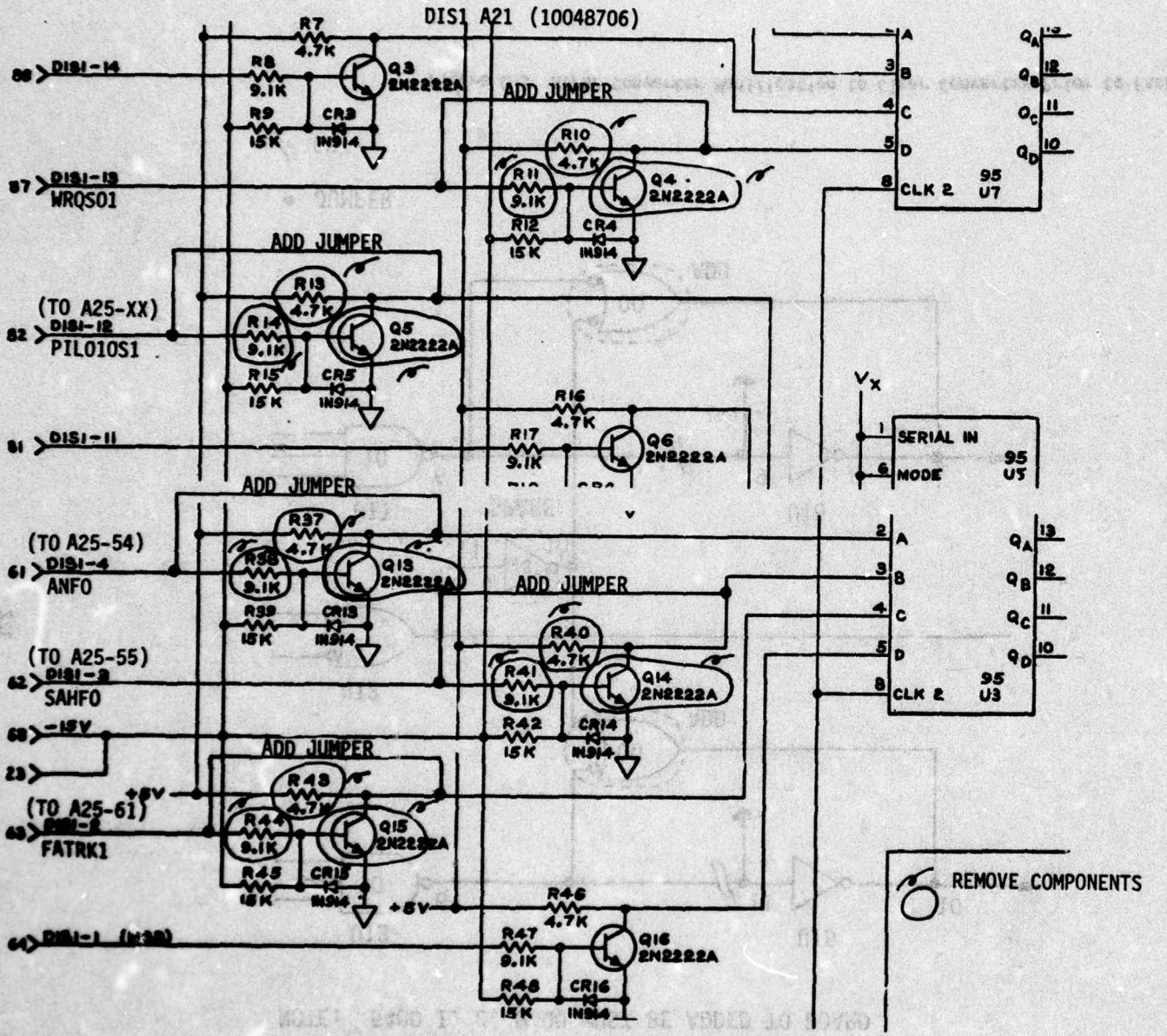

Figure C-2b Modify A21 to Accept Bite Data

MODIFY A16 (10048702) CARD AS SHOWN
NOTE: 5400 I. C. U 00 MUST BE ADDED TO BOARD

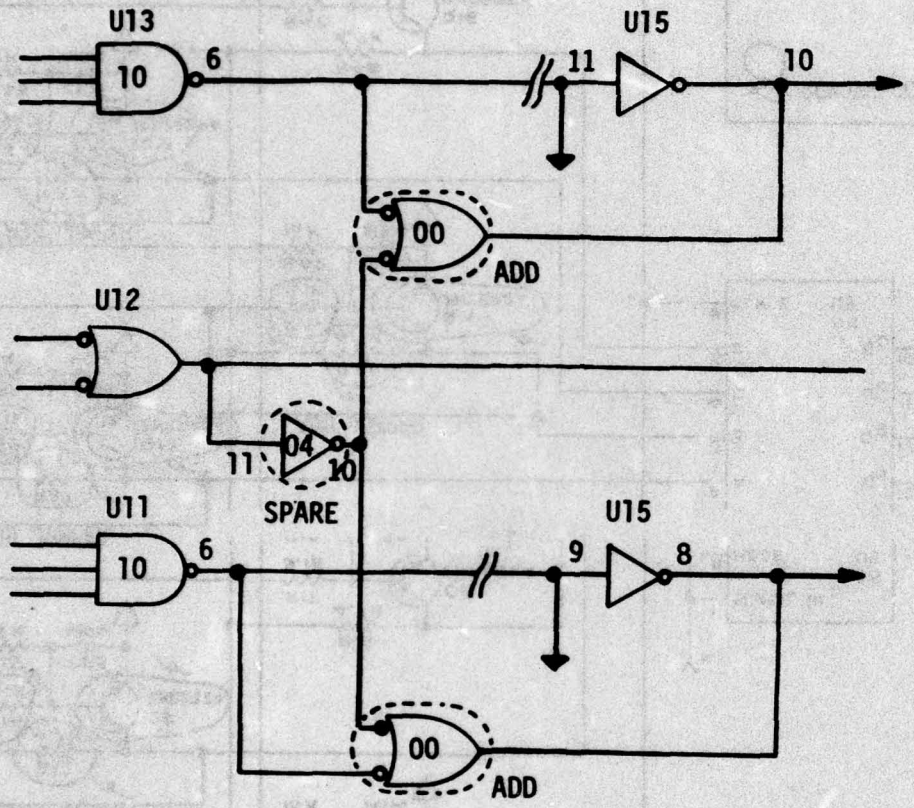

Figure C-3 M1/M2 Converter Modification to Clear Converter Prior to Each Sample

☆ U. S. GOVERNMENT PRINTING OFFICE: 1976 — 757-001/90